Premier Reference Source

AI-Enabled Smart Healthcare Using Biomedical Signals

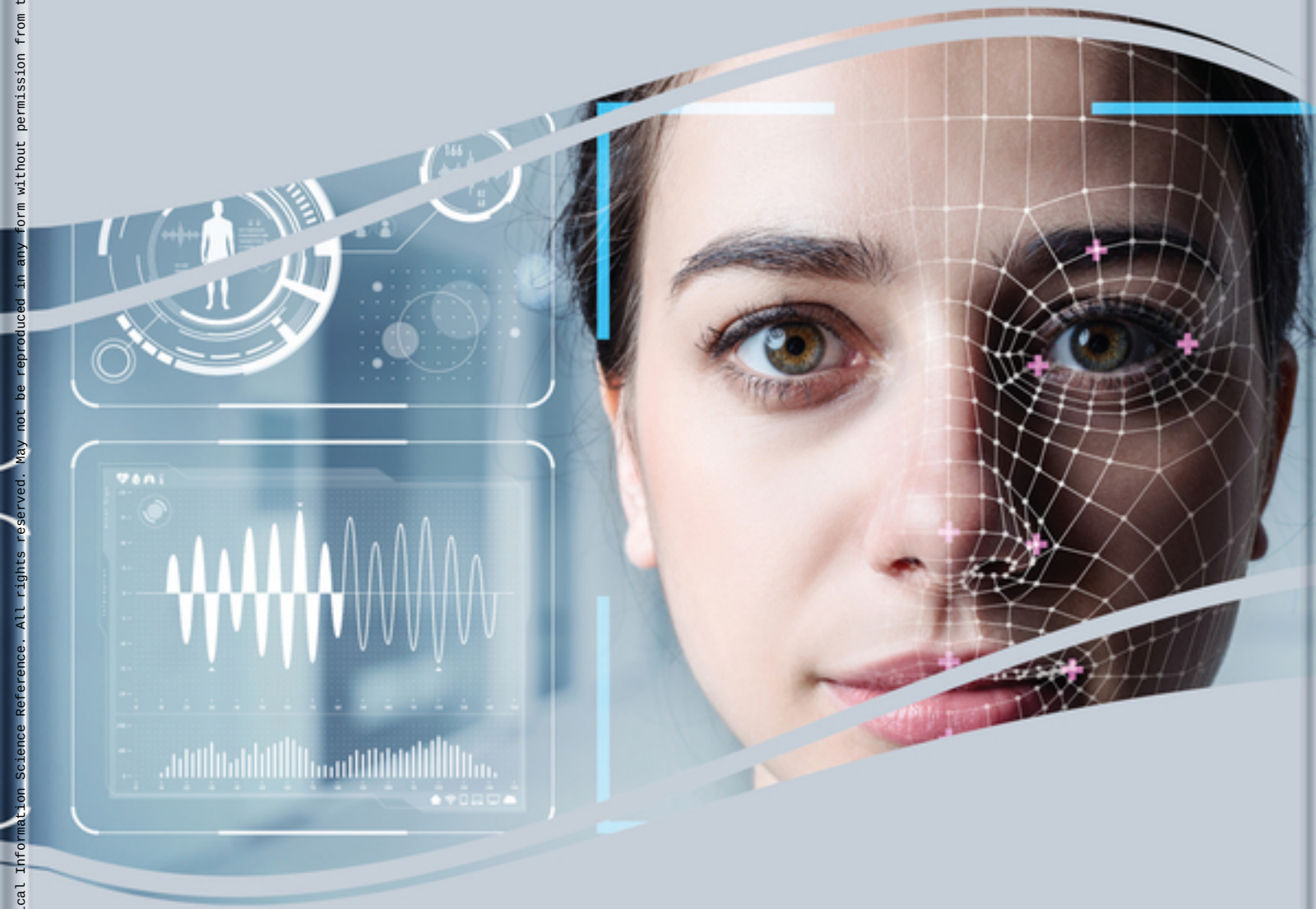

Rahul Kumar Chaurasiya, Dheraj Kumar Agrawal, and Ram Bilas Pachori

IGI Global
PUBLISHER of TIMELY KNOWLEDGE

AI-Enabled Smart Healthcare Using Biomedical Signals

Rahul Kumar Chaurasiya
Maulana Azad National Institute of Technology, Bhopal, India

Dheeraj Agrawal
Maulana Azad National Institute of Technology, Bhopal, India

Ram Bilas Pachori
Indian Institute of Technology, Indore, India

IGI Global
PUBLISHER of TIMELY KNOWLEDGE

A volume in the Advances in Bioinformatics and Biomedical Engineering (ABBE) Book Series

Published in the United States of America by
IGI Global
Medical Information Science Reference (an imprint of IGI Global)
701 E. Chocolate Avenue
Hershey PA, USA 17033
Tel: 717-533-8845
Fax: 717-533-8661
E-mail: cust@igi-global.com
Web site: http://www.igi-global.com

Library of Congress Cataloging-in-Publication Data

Names: Chaurasiya, Rahul (Rahul Kumar), 1987- editor. | Agrawal, Dheraj (Dheraj Kumar), 1979- editor. | Pachori, Ram Bilas, 1979- editor.
Title: AI-enabled smart healthcare using biomedical signals / [edited by] Rahul Chaurasiya, Dheraj Agrawal, Ram Pachori.
Description: Hershey : Medical Information Science Reference, 2022. | Includes bibliographical references and index. | Summary: "The book will not only cover the mathematical description of the AI- and ML-based methods; it will also analyze and demonstrate the usability of different AI methods for a range of biomedical signals"-- Provided by publisher.
Identifiers: LCCN 2022014720 (print) | LCCN 2022014721 (ebook) | ISBN 9781668439470 (hardcover) | ISBN 9781668439487 (ebook)
Subjects: MESH: Signal Processing, Computer-Assisted | Image Processing, Computer-Assisted | Artificial Intelligence
Classification: LCC R855.3 (print) | LCC R855.3 (ebook) | NLM W 26.55.A7 | DDC 610.285--dc23/eng/20220617
LC record available at https://lccn.loc.gov/2022014720
LC ebook record available at https://lccn.loc.gov/2022014721

This book is published in the IGI Global book series Advances in Bioinformatics and Biomedical Engineering (ABBE) (ISSN: 2327-7033; eISSN: 2327-7041)

British Cataloguing in Publication Data
A Cataloguing in Publication record for this book is available from the British Library.

Advances in Bioinformatics and Biomedical Engineering (ABBE) Book Series

Ahmad Taher Azar
Prince Sultan University, Riyadh, Kingdom of Saudi Arabia and Benha University, Egypt

ISSN:2327-7033
EISSN:2327-7041

Mission

The fields of biology and medicine are constantly changing as research evolves and novel engineering applications and methods of data analysis are developed. Continued research in the areas of bioinformatics and biomedical engineering is essential to continuing to advance the available knowledge and tools available to medical and healthcare professionals.

The **Advances in Bioinformatics and Biomedical Engineering (ABBE) Book Series** publishes research on all areas of bioinformatics and bioengineering including the development and testing of new computational methods, the management and analysis of biological data, and the implementation of novel engineering applications in all areas of medicine and biology. Through showcasing the latest in bioinformatics and biomedical engineering research, ABBE aims to be an essential resource for healthcare and medical professionals.

Coverage

- Chemical Structures
- Data Mining
- Robotics and Medicine
- Health Monitoring Systems
- Computational Biology
- Dental Engineering
- DNA Structure
- Biostatistics
- Gene regulation
- Biomedical Sensors

IGI Global is currently accepting manuscripts for publication within this series. To submit a proposal for a volume in this series, please contact our Acquisition Editors at Acquisitions@igi-global.com or visit: http://www.igi-global.com/publish/.

The Advances in Bioinformatics and Biomedical Engineering (ABBE) Book Series (ISSN 2327-7033) is published by IGI Global, 701 E. Chocolate Avenue, Hershey, PA 17033-1240, USA, www.igi-global.com. This series is composed of titles available for purchase individually; each title is edited to be contextually exclusive from any other title within the series. For pricing and ordering information please visit http://www.igi-global.com/book-series/advances-bioinformatics-biomedical-engineering/73671. Postmaster: Send all address changes to above address.

Titles in this Series

For a list of additional titles in this series, please visit: http://www.igi-global.com/book-series/advances-bioinformatics-biomedical-engineering/73671

Advancements in Controlled Drug Delivery Systems
Shekhar Verma (University College of Pharmacy, Pandit Deendayal Upadhyay Memorial Health Science, India & Ayush University of Chattisgarh, India) and Santosh Kumar Verma (Yulin Universit, China)
Medical Information Science Reference • © 2022 • 395pp • H/C (ISBN: 9781799889083) • US $325.00

Polymer-Based Functional Materials for Biomedical Aplications
Nithin Kundachira Subramani (The National Institute of Engineering, India) and D.V. Gowda (JSS College of Pharmacy, India)
Engineering Science Reference • © 2022 • 320pp • H/C (ISBN: 9781799871989) • US $265.00

Emerging Developments and Applications of Low Temperature Plasma
Aamir Shahzad (Government College University, Faisalabad, Pakistan) and Maogang He (Xi'an Jiaotong University, China)
Engineering Science Reference • © 2022 • 239pp • H/C (ISBN: 9781799883982) • US $225.00

Biomedical Computing for Breast Cancer Detection and Diagnosis
Wellington Pinheiro dos Santos (Universidade Federal de Pernambuco, Brazil) Washington Wagner Azevedo da Silva (Universidade Federal de Pernambuco, Brazil) and Maira Araujo de Santana (Universidade Federal de Pernambuco, Brazil)
Medical Information Science Reference • © 2021 • 357pp • H/C (ISBN: 9781799834564) • US $295.00

Deep Neural Networks for Multimodal Imaging and Biomedical Applications
Annamalai Suresh (Department of Computer Science and Engineering, Nehru Institute of Engineering and Technology, Coimbatore, India) R. Udendhran (Department of Computer Science and Engineering, Bharathidasan University, India) and S. Vimal (Department of Information Technology, National Engineering College (Autonomous), Kovilpatti, India)
Medical Information Science Reference • © 2020 • 294pp • H/C (ISBN: 9781799835912) • US $275.00

Biomedical and Clinical Engineering for Healthcare Advancement
N. Sriraam (Ramaiah Institute of Technology, India)
Medical Information Science Reference • © 2020 • 275pp • H/C (ISBN: 9781799803263) • US $285.00

Attractors and Higher Dimensions in Population and Molecular Biology Emerging Research and Opportunities
Gennadiy Vladimirovich Zhizhin (Russian Academy of Natural Sciences, Russia)
Engineering Science Reference • © 2019 • 232pp • H/C (ISBN: 9781522596516) • US $165.00

701 East Chocolate Avenue, Hershey, PA 17033, USA
Tel: 717-533-8845 x100 • Fax: 717-533-8661
E-Mail: cust@igi-global.com • www.igi-global.com

To My Beautiful Wife and Lovely Twin Daughters
Rahul Kumar Chaurasiya

Table of Contents

Detailed Table of Contents

Preface

Medical usage of different biomedical signals including electrocardiograms (ECG), electroencephalograms (EEG), electromyograms (EMG), electrooculogram (EOG), blood pressure, oxygen saturation level, glucose level, skin temperature, galvanic skin response is well known in medical community. These signals can be used to detect several diseases and medical conditions. Recently, the use of artificial intelligence (AI) techniques with biomedical signals has resulted in automatic detection of several health conditions. AI plays a significant role in the modern data processing systems. It is a rapidly growing field and is an essential part of machine learning (ML), pattern recognition, disease detection and signal classification, clustering, and speech recognition etc.

The book entitled *AI-Enabled Smart Healthcare Using Biomedical Signals* covers the basics, history, medical applications, and detailed descriptions of biomedical signals like ECG, EEG, EMG, EOG, blood pressure, oxygen saturation level, glucose level, skin temperature, and galvanic skin response. Along with the basics and descriptions of different biomedical signals, acquisition methodologies of different biomedical signals have also been included. Further, comprehensive information is included on the devices used to acquire different biomedical signals.

For smart healthcare using biomedical signals, state-of-the-art AI and ML methodologies are covered in this book. Mathematical description of different methods is also included. The ML methods have been classified into supervised and unsupervised learning. Mathematical description and employment of different AI-based methods like ANN, SVM, LDA, Bayes classifiers, kNN Classifier, clustering, decision trees & random forests, HMMs, CNN & deep learning, RNN, NLP, reasoning, and statistical approaches on biomedical signals is demonstrated with specific target on healthcare applications. Also, the methods used for segmentation, preprocessing, filtration, signal processing, and feature extraction (from different biomedical signal) are included.

Subsequently, the applications of AI-based methods over biomedical signals for automated and smart healthcare applications are demonstrated in the book. Experimental analysis, applications, and case studies towards smart healthcare using AI-enabled methods applied over biomedical signals are also part of the book. Contributions of the researchers working on AI applications on biomedical signals have also been received and are included. The work presented in this book entitled "AI-Enabled Smart Healthcare Using Biomedical Signals" is divided in 14 chapters. The summary of each chapter is presented in the following paragraphs.

Chapter 1 is titled "Basics and Descriptions of Different Biomedical Signals". The chapter includes basics and description of different biomedical signals in details. Based on different characteristics, categorization of biomedical signals is provided in the chapter. Recent advances in biomedical sensor technology have played an important role in advancing life and information sciences and inventing new

diagnostic and therapeutic tools. The chapter also discusses about the sensors used to acquire biomedical data and to converted the signals into an electrical signal for further processing. As it is known that the human body constantly conveys health information that reflects the condition of organs and general health information, different types biomedical sensors to acquire information related to blood sugar levels, blood pressure, heart rate, nerve condition, and brain activity are described in the chapter.

Chapter 2 is titled "A Comprehensive Review on Brain Simulation Tool and Its Applications". The chapter introduces brain-computer interface (BCI) as a combination of software and hardware that has recently emerged as the tool to control external devices by using human brain signals as commands. In the chapter, various tools that can be used to analyze and perform different functions on the brain signals, create BCI models, and simulations are described. The study also compares the tools and tabulate their usefulness for the user requirements. The real-time implemented of the tools is also illustrated. The experimental analysis presented in the chapter utilizes MAMEM EEG steady-state visually evoked potential (SSVEP) dataset I. Further, different parameters like power spectrum density, power spectrum, and inter-trial coherence (ITC) were analyzed through EEGLAB software.

Chapter 3 is titled "Adaptive Data Analysis Methods for Biomedical Signal Processing Applications". Biomedical signals represent the variation in electric potential due to physiological processes. Authors take the practical assumption that the biomedical signals are complex and non-stationary. This makes adaptive data driven techniques a natural choice for processing of biomedical signals. Data driven methods propose such basis function directly depending on the information content in the signal. The adaptive data analysis methods tend to decompose a signal into individual modes that are present in it, thus separating them from each other. The chapter has presented a detailed review of adaptive data analysis techniques including wavelet transform (WT), empirical mode decomposition (EMD), empirical wavelet transform (EWT), and variational mode decomposition (vmd) with their applications to biomedical signal analysis.

Chapter 4 is titled "A Review for Neuroimaging Techniques in Multimedia Learning: Methodological Framework". The research presented in the chapter attempt to analyze neuroimaging techniques for measurement of cognitive load in multimedia research using a systematic literature review. The literature revie involves state-of-the arts. The observations drawn by the chapter authors indicated that EEGs, functional magnetic resonance imaging (FMRI), functional near-infrared spectroscopy (FNIS), and transcranial doppler ultrasonography (TDU) have been the most preferred neuroimaging tools utilized in cognitive load in multimedia learning research. In the chapter, forty research articles were reviewed based on the techniques that should be known in the field of neuroimaging to study cognitive load in multimedia learning, the analysis methods for neuroimaging, the results related to cognitive load in multimedia research. The findings are evaluated, and many discrepancies in cognitive load research related to multimedia learning are discovered in the chapter.

Chapter 5 is titled "A Review of Automated Diagnosis of ECG Arrhythmia Using Deep Learning Methods". The chapter explains that the arrhythmia is a medical condition in which the heart's normal pumping process becomes irregular. Early identification of the condition essential for diagnosis of the disorder. The chapter than argue that visually assessing the ECG signals can be difficult and time-consuming due to their low amplitudes. However, using an automation process can significantly expedite and increase the accuracy of diagnosis. As the deep learning (DL) developments have made it feasible to extract and classify high-level features automatically, the chapter reviews significant progress in DL approaches for automated arrhythmia diagnosis. The application and category of data input, the modeling architecture, and the performances are also reviewed. The chapter provides detailed knowledge for researchers interested in widening existing knowledge in this area.

Chapter 6 is titled "Quality-Controlled ECG Data Compression and Classification for Cardiac Healthcare Devices". The chapter utilizes ECGs are for the detection of cardiovascular diseases (CVDs). For the detection of CVDs, long-term ECG data is used. The chapter presents a quality-controlled compression method that compresses the ECG data efficiently with retaining its quality up to a certain mark. For this, a distortion measure is used with specifying its value in a tolerable range. MIT-BIH arrhythmia dataset is utilized to measure the compression performance of the proposed algorithm. In performance assessment, it is found that the compression algorithm performs well. The compressed ECG data are also used for arrhythmias beat classification. It denotes the better diagnostic quality of the compressed ECG data.

Chapter 7 is titled "Analogy of Wrist Pulse Signals in the Context of ECG Signals: A Review". The chapter reviews the modern different tools and procedures to observe pulse rate, heart rate variability, speed of pulse, blood pressure (BP), blood flowing rate in arteries, and volume. In past, medical practice like Ayurveda and traditional Chinese medicine (TMC), wrist pulse or radial pulse of the subject in consideration were checked to diagnose the health conditions. Both wrist pulse diagnosis and ECG are the non-invasive methods for health assessment. Wrist pulse is caused by cardiovascular activities and thus it can be correlated with the ECG. The pulse rate is basically a rate of heart beats. The pulse movement is due to flow of blood in vessels. The parameters like rhythm, strength, hardness or softness, transition period, and change in rate of heartbeat can be measured. The chapter presents the pulse rate as a helpful parameter in diagnosis of cardiac and non-cardiac diseases.

Chapter 8 is titled "ECG Signal Analysis for Automated Cardiac Arrhythmia Detection". The chapter presents a study to utilize ECG to detect arrhythmias disease. Irregular heart cycles are collectively known as arrhythmias and may produce sudden cardiac arrest. Frequently, arrhythmia evolves over an extended period. Hence, it requires an AI-enabled continuous ECG monitoring system that can detect irregular heart cycles automatically. In this regard, the chapter presents a methodological analysis of ML and DL-based arrhythmia detection techniques. Focusing on the state of the art, a DL-based technique is implemented in the chapter, that recognizes normal heartbeat and seven different classes of arrhythmias. The technique uses CNN as a classification tool. The performance of the technique is evaluated using ECG records of the MIT-BIH arrhythmia database. This technique performs well in terms of different classification metrics.

Chapter 9 is titled "A Frequency Discrimination Technique for SSVEP-Based BCIs Using Common Feature Analysis and Support Vector Machine". The chapter focuses on BCI as a communication option for those who are suffering from neuromuscular disorders. Steady state visually evoked potentials (SSVEP) are frequency specific responses to visual stimuli. These are extensively used with EEG signals. The chapter presents a method for recognition of SSVEP-based BCIs. The method establishes a processing pipeline where an IIR Butterworth filter is implemented, that filters the signals that are further decomposed into wavelets. Along with the wavelet decomposition, common feature analysis (CFA), canonical correlation analysis (CCA) and MCCA are used to extract features. The best results are obtained from DWT-CFA. The finest classification results are obtained from the RBF kernel-based SVM classifier. In the chapter, the best overall mean accuracy of 94.78% is obtained using DWT-CFA as the feature extraction technique and employing RBF kernel-based SVM as the classifier.

Chapter 10 is titled as A Robust Classification Approach for Character Detection Using P300-Based Brain-Computer Interface". The chapter utilizes BCI with P300 speller paradigm to automatically classify the brain responses by stimulating a subject. This research uses BCI Competition III Dataset II, that consists of a 6×6 character matrix paradigm and EEG data collected from two healthy subjects. The ensemble of SVM method of classification has been employed to overcome the problem of false detection,

which is preceded by empirical mode decomposition (EMD) as the preprocessing technique. The chapter use a stacked autoencoder for feature extraction and covariate shift adaptation by normalized principal components as the feature selection method for better accuracy of the detected character. The experiment yields a better result than many existing methods; and produces an average accuracy of 98.75%.

Chapter 11 is titled "Emotion Identification From TQWT-Based EEG Rhythms". The chapter utilizes EEG rhythms to record different neural dynamics. The EEG rhythms are separated using tunable Q-factor wavelet transform (TQWT). For automatic classification, features like mean, standard deviation, and information potential are extracted from the TQWT-based EEG rhythms. For the purpose, ML classifiers are employed to differentiate various emotional states. The model is validated using a publicly available database. Obtained classification accuracy of 92.9% validates the candidature of the method proposed in the chapter for emotion identification.

Chapter 12 is titled "Empirical Wavelet Transform-based Framework for Diagnosis of Epilepsy Using EEG Signals". The chapter presents a method to classify EEG signals associated with normal and epileptic seizure categories. The method is based on empirical wavelet transform (EWT). The non-stationarities in the EEG signals are captured using EWT, and the common minimum number of modes are determined for each signal. Features based on amplitude envelopes of EEG signals have been computed. The Kruskal-Wallis statistical test has been used to confirm the discrimination ability of feature space. For classification, various classifiers, viz. KNN, SVM, and DT have been employed. The maximum classification accuracy of 98.67% is achieved with the KNN classifier. The approach presented in the chapter has utilized only two features, which makes it simpler. The proposed approach thus can be used in real-time applications.

Chapter 13 is titled "Automated Glaucoma Classification Using Advanced Image Decomposition Techniques From Retinal Fundus Images". The chapter presents Glaucoma as one of the primary reasons for invariant retinal cecity. The chapter investigated automated glaucoma classification methods using advanced image decomposition algorithms such as EWT, DWT, EMD, VMD, and FAWT. The study computes significant texture-based descriptors from the high-frequency descriptors followed by the LS-SVM-based classification. The robustness of the developed CAD system has been tested using the RIM-ONE public database.

Chapter 14 is titled "Deep Learning-Based Approach to Detect Leukemia, Lymphoma, and Multiple Myeloma in Bone Marrow". The chapter focuses on the severity of bone marrow cancer that may even cause death to many individuals. Leukemia, lymphoma, multiple myeloma, and other cancers that form in the blood-forming stem cells of the bone marrow constitute bone marrow cancer. The chapter further argues that the early detection can increase the chance for remission. Accurate and rapid segmentation techniques can assist physicians to identify diseases and provide better treatment at the right time. The usefulness of the CAD systems for the early discovery of bone marrow cancer is presented in the chapter. It features the latest updated algorithm that combines DL with MATLAB for health assessment. This can assist in the early detection of leukemia, lymphoma, and multiple myeloma. For denoising histopathological images, new K-SVD and fast non-local mean filter algorithms are employed. For pre-processing algorithms like multilayer perceptron (MLP) and novel hybrid histogram-based soft covering rough k-means clustering techniques are utilized. Three classifiers, viz. R-CNN, ResNet 50, and LSTM are used to classify and the performance is compared based on the accuracy.

TARGET AUDIENCE

The target audience of this book consists of students, researchers, and professionals working in the field of the applications of AI and ML methods over biomedical signals for better and smart healthcare.

Rahul Kumar Chaurasiya
Maulana Azad National Institute of Technology, Bhopal, India

Dheraj Agrawal
Maulana Azad National Institute of Technology, Bhopal, India

Ram Bilas Pachori
Indian Institute of Technology, Indore, India

Chapter 1
Basics and Descriptions of Different Biomedical Signals

Macha Sarada
https://orcid.org/0000-0003-2910-4623
Jawaharlal Nehru Technological University, Hyderabad, India

ABSTRACT

In the current digital era, many sensor-based devices and application are used for better life. Sensors, which are embedded in touchscreens and touchpads, are tactile in nature. These sensors acquire data from the environment that are converted into an electrical signal for further processing in the sensor system. The main aim of sensors is to estimate a specific quantity and generate a signal for interpretation. The human body constantly conveys health information that reflects the condition of organs and general health information. Such health information is typically collected by physical devices that measure different types of information such as blood sugar levels, blood pressure, heart rate, nerve condition, and brain activity. Doctors use these measurements to make diagnostic and treatment decisions. Engineers are implementing new acquisition devices that noninvasively measure different types of signals for further analysis using mathematical algorithms and formulae to develop models. This chapter includes the basics and description of different biomedical signals.

INTRODUCTION

Monitoring real-time biological data is the key to better chronic illness management, early detection, prediction, and diagnosis, including strokes and heart attacks. Several measured characteristics are unreliable, making it difficult for electrical designers to analyse and deploy these signals. However, despite their variety in terms of environmental circumstances, there are similar characteristics of biomedical signals, such as the design of the equipment, electrode location, and the presence of lipids or blood vessels under which they are collected. Technology advancements, electronic device design/fabrication, and sensors produced more biomedical signals for monitoring, predicting, and detecting various diseases, based on the acquired biomedical signal characteristics from the specific associated sensors, for further signal processing, which is the energetic phase. Multi channels of biomedical signals are created by

DOI: 10.4018/978-1-6684-3947-0.ch001

various sensors attached to the patient in order to get precise information about certain diseases (Okoye G.C, 2008, Nilanjan Dey et.al. 2019).

A sensor is a device that responds to an input by measuring or detecting a certain attribute, record, or condition based on the information received (Eggins V.R 2008). In general, a device that only detects a characteristic or state based on the presence or absence of a physical quantity is neither a detector nor a sensor. Detectors play an important role in medicine, especially in alarms. In biomedical applications, sensors are known as devices that respond to the physical input of the subject and record the associated optical / electrical output. Physical and biomedical inputs include biochemical concentrations / quantities, and medical inputs include biochemical concentrations / quantities and all medical vital signs from the patient.

A sensor system is a device with an electrical output that displays / records or displays electrical signals and is amplified and processed for input to a chart recorder, display monitor, or storage system. However, many of the widely used sensors do not exhibit linear behaviour. Transducer and sensor are both synonyms. Nevertheless, converters are known as devices for converting energy from one format to another. Transducers can be thought of as components of the sensor. B. Microphone diaphragm that converts sound energy into strain energy. Second, a second transducer is essential to convert that energy into recordable electrical energy to create the entire sound sensor. (Graf, R.F. 1999).

The biosensor is an analyser that targets macromolecules or molecules using a biological identification system. They include physicochemical sensors (transducers) that convert biological signals from bio recognition systems into evaluable measurement signals. The biosensor consists of three modules: a detector that identifies the stimulus, a transducer that converts the stimulus into an output, and an output system that amplifies the output and displays it in the appropriate format. Piezoelectricity is a phenomenon that occurs in specific crystals such as: B. Rochelle salt and quartz. Mechanical stress persuades the generation of stress and vice versa (Nilanjan Dey et.al., 2019)

BIOMEDICAL SENSORS

Sensors of biomedical are distinct electronic devices that can convert biomedical impulses into easily quantifiable electric signals. Biomedical sensors are the crucial components in wide range of medical diagnostic tools and equipment. Wide range of inventions and discoveries in biomedical, chemical, physical, acoustic and electronic materials have tremendously gained prominence in biomedical sensor applications such as microstructure, micronano implantable probes, screening sensors, drug analysis and integrated cell molecular detection sensors.. Medical image analysis and diagnostics portable and clinical diagnostics and laboratory analytical applications have all made extensive use of biomedical sensors. Biomedical sensors are classified into biosensor, chemical sensor, and physical sensors as illustrated as Figure 1 (Ronkainen N et.al.,,2010,Scheller F et.al 1989, Rodriguez-Mozaz S et.al 2004).

- Chemical sensors to sense enzymes, hormone, antibody, antigen, microbes and detect biological signals. These sensors are used to identify the concentration and ingredient of liquids in the body.
- Physical sensors to sense to measure mechanical, hydraulic, geometric and thermal variables such as such as muscle displacement, growth velocity, bone growth velocity, blood viscosity, blood flux, blood flow, blood pressure and body temperature.

In general, biosensors a biological identification system for targeting macromolecules or molecules. To do so Converts the signal received from the detection system into a detectable signal. The physicochemical transducer should be included in the biosensor. the most important the components of the biosensor include a detector to identify the stimulus, a transducer to convert the stimulus into an output, and an output system including: Output amplification and display process.

There are various common properties that biomedical sensors should have, such as being gentle, dependable, and safe when they touch the patient's inner organs or skin. Furthermore, an implanted biosensor must be biocompatible with the human body and have a lengthy operating lifespan. As a result, analysing the performance of biomedical sensors and their demanding design standards has a significant influence on correct medical diagnosis.

Several metrics are measured in order to describe the characteristics of the sensor for further selection according to the application. Such metrics include (Rothrock R L et.al., 2000, Herold M et.al.,2002, Gnawali O et.al., 2004; MacRuairi R et.al., 2008; Boccippio D et.al., 2000)

1. Accuracy, which is the difference between the true and actual measured values by the sensor;
2. The sensitivity, which is the relationship between the output change for a given input change;
3. The measurement range, which refers to the expected maximum/minimum operation limits of the sensor;
4. The sensor's frequency response, which represents the sensitivity varia- tion with frequency;
5. The linearity, which refers to the maximum deviance between the calibration and the fitting curves of the sensor's measurements;
6. The signal-to-noise ratio (SNR), which represents the mea- sured signal power ratio to the power of the noise;
7. The hysteresis, which is the measurement's delay due to the variation direction of the measured signal;
8. The response time, which refers to the time reserved by the sensor to reach a percent of its steady state, when its input change;
9. The drift, which is the change in the reading of the sensor with constant input;
10. The offset, which refers to the output value with zero input value and
11. The resolution, which is the smallest detected discernible input change;

Specifically, biosensor can be classified based on the biological sensing component into immune sensors, tissue sensors, cell sensors, microbe sensors, and enzyme sensors. Another classification can be considered in terms of the biosensors' used signal converter, namely, optical biosensors, bio electrode sensors, thermal biosensors, piezoelectric biosensor, and semiconductor biosensor. Biomedical sensors are categorised into catalytic biosensors and affinity biosensors based on the interaction between the measured substance and the sensing component. The fore- most applications of the biomedical sensors are

1. Monitoring biological parameters inside/outside the body, such as the heart sound, the brain activity, and the heart activity.
2. Detecting clinical information, such as the blood pressure and the body temperature; and
3. Detecting control parameters, such as measuring the concentration of enzymes to control the food fabrication;

Figure 1. Biosensors

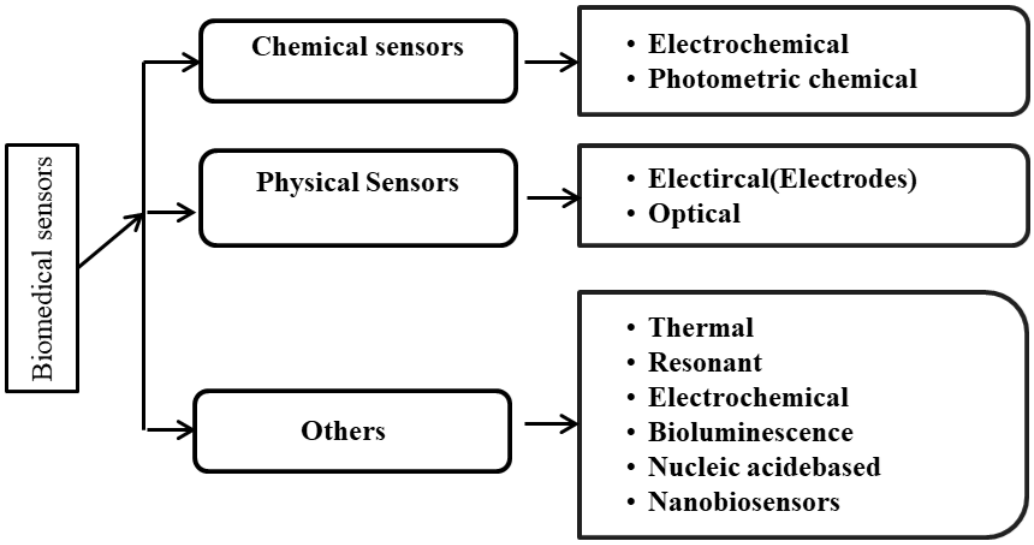

Biomedical signals are recorded as voltages, electrical field strengths, and potentials that are generated by muscles/nerves. Thus, the sensors have an important role within the various biomedical instruments to convert the acquired body signal into an electrical signal, where the electrical components and electrical circuits are wont to detect the bio-signal by different sensors. The bioinstrumentation is then formed after connecting the electrical components and therefore the biosignal sensors. However, the measured biomedical signal has very low voltage levels starting from 1 μV to 100 mV, for instance, the magnitude of the EEG is in microvolt which of the ECG is in millivolts. additionally, a high level noise and high source impedance exist and inter pret the biosignal. Thus, the biosignals require amplification to be compatible with the medical instruments/devices, including the A/D (analog to digital) converters, the recorders, and therefore the displays. so as to perform such task, amplifiers, referred to as biopotential amplifiers, are included to live the biosignals and offer selective amplification to the physiological signal, interference signals, and, the reject super imposed noise (Nagel, J.H., 2000; Zhou,G,et.al., 2015; Nilanjan Dey 2019). Figure 2 illustrates the position of the bio potential amplifier within the instrument .

This assures the biosignal protection from compensations through current and voltage flow for both the equipment and therefore the patient. The accurate design of the biopotential amplifier rejects the signal interferences' large portion, especially the line-frequency interference with strong common-mode signal rejection. additionally, the biopotential amplifier has got to offer suitable gain range and signal-to- noise ratio.

Generally, the operational amplifier is an device including multi- resistors, capacitors, and transistors. it's the inspiration of any bioinstrumentation because it features a significant role to amplify the weak biosignal and adjust the present or voltage within the detecting circuit. so as to retain the present down from the mea- sured, the used amplifiers should have a really high input impedance. The preampli- fier sets the phase for the biosignal quality because it eliminates/minimizes the interfering signals during the measurement of the biopotentials as shown in Figure 2. After pre-amplifying the biosignals, several filters are included, like the high-pass filter (HPF) and low-pass filter (LPF) to eliminate the useless

signal and highlight the beneficial biosignal supported the specified signal frequency range (Estrada E F 2010; Rodrigues F 2015; Cavazzaana L 2012).

Figure 2. Bio-potential amplifier stage sequence

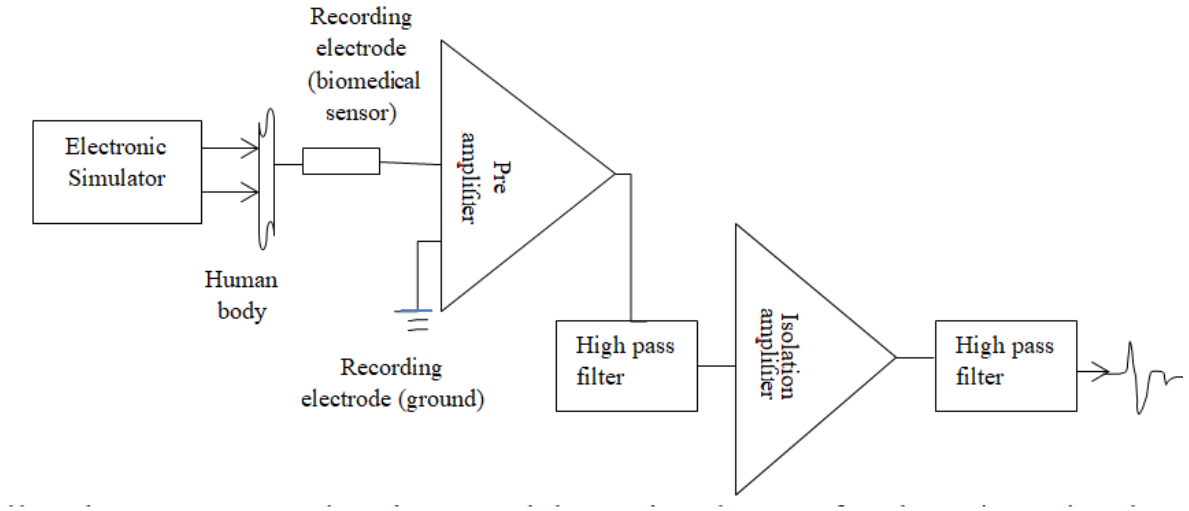

Generally, the sensors require three modules, the element for detection, signal processor, and transducer. Once the source to be detected contacts the detection element, the detection element changes and converted into a sign by the transducer. The signal processor processes the signals. so as to pick the acceptable sensor, the detection element is taken into account the foremost major factor . Thus, for functional biosensor, the sensor should have a discerning detection element consistent with the physical body signal to be detected. Then, the transducers are often thermal, piezoelectric, optical, and electrochemical transducers

BIOSIGNALS

Bio signals are biological signals that can be continuously measured and monitored. The term biomedical signal is often used to refer to bioelectrical signals, but it can also refer to both electrical and non-electrical signals. The usual understanding refers only to time-varying signals, but may also include variations in spatial parameters (eg, nucleotide sequences that determine the genetic code).

Signal is the parameter which is observable from the object. Bio signal is a description of physiological phenomenon of any type or nature. Biosignal is combination of living object, the function that carries the information regarding the state or behaviour. These are the main key objects in biosystems.

Biomedical signals/physiological signals are observations of organisms' physiological processes, such as protein and gene sequences, to cardiac and neural(brain) rhythms, to organ images and tissues. The goal of biomedical impulse processing is to extract valuable information from biological signals.

Biomedical signals/physiological signals are signals (phenomena that carry information) that are primarily utilised to retrieve information from a biological system under examination. Human bodies emit a variety of physiological signals. The ease of access of these signals is vital since these signals:

- Blood pressure (can be internal)
- Infrared radiation (may emanate from the body)
- Blood or tissue biopsy (may be derived from tissue sample)

All biomedical signals/physiological signals can grouped as:

- Bio potential
- Pressure
- Flow
- Dimensions (imaging)
- Displacement (velocity, force, acceleration)
- Impendence
- Temperature respond
- Chemical attention and composition

A transducer converts a biomedical signal into an electrical output. By excluding all other energies transducer should only react to the target form of energy prevailing in the physiological signal. It also needs to be connected to the biological system so that it consumes minimal energy and is non-invasive.

How Are Biological Signals Generated?

Biological signals are generated by the human body by physiological systems when they are functioning. Biological signals consists the information which are resulting from these signals to evaluate the functioning of these physiological systems. The extraction of information may be simple as pulse reading to find the state of heart beats or it can be complex as analysing the structure of internal tissue by ultrasound.

Biomedical / physiological signals are categorized according to where they originated in the body which are shown in Figure 3.

Figure 3. Sources of biomedical signals (biomedical instrumentation system)

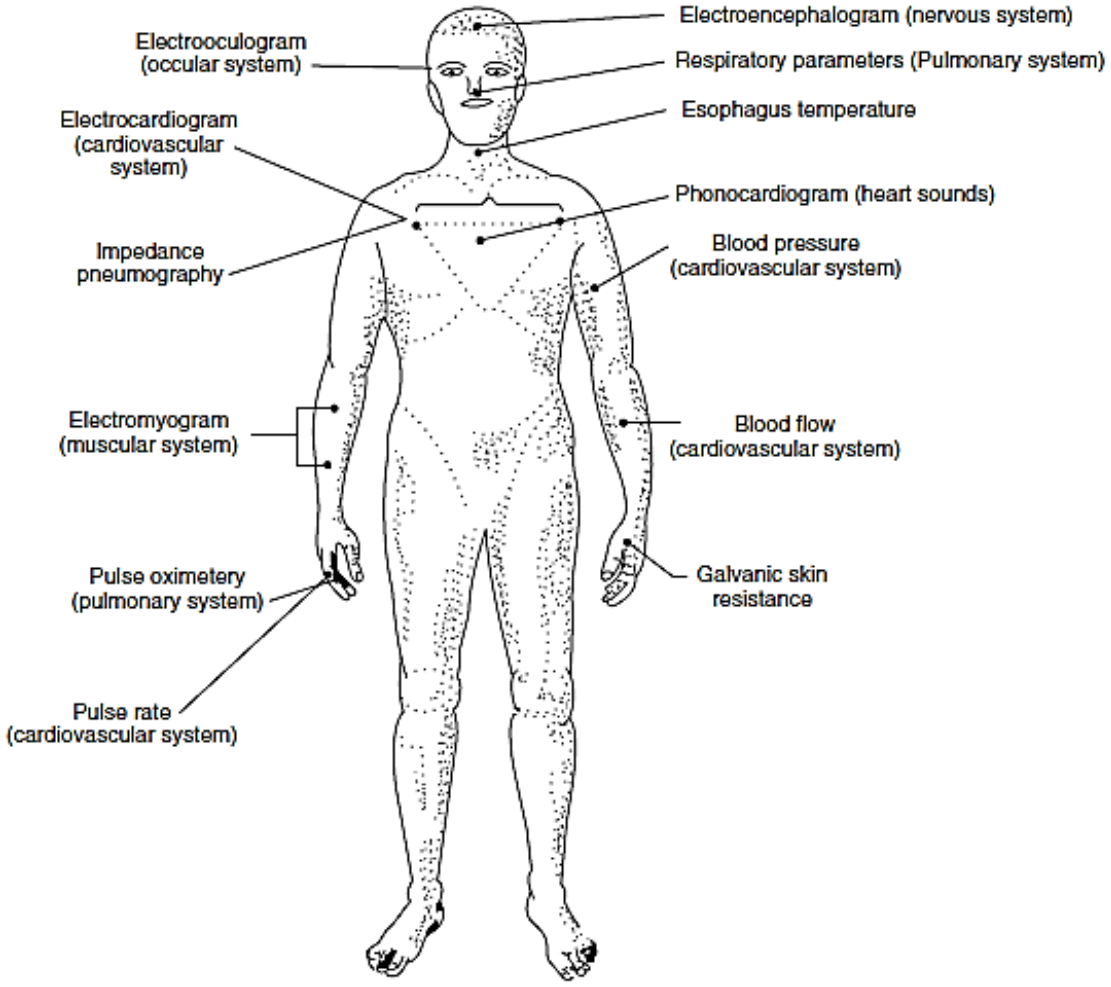

CLASSIFICATION OF BIOSIGNALS

The fundamental biomedical signal types include the signal, electrocardiogram (ECG) signal, speech signals, phonocardiogram (PCG) signal, carotid pulse (CP) signal and electroencephalogram (EEG) signal. Typically, there are 5 sources of noise that affect the biosignals, including the aliasing, interference, instrument noise, sampling noise, thermal noise, and power cable alternative current (AC) [1–10].

Several classifications are raised to categorize the biosignals, consistent with biosignal source, number of channels, dimensionality, biosignal model, and nature.

- Based on the physical nature of the signal: The biosignals are catergorized into optical,chemical, electric,magnetic,acoustic(mechanical),thermal.
- Based on system of the biosignal origin: The orgin of biosignal varies from any other signals in terms of the application as the they originate fro different sources. These are categorized from ner-

vous system, cardiovascular system, auditory system,endocrine system, vision system, circulatory system,gastrointestinal system, respiratory system and musculosketal system.

- Based on the dimensionality: The signals can be onedimesional(1D) as the electrocardiogram (ECG) signal,the electroencephalogram (EEG) and the phonocardiogram(PCG) signal; two dimensional (2D), such as temperature map; three dimensional (3D), suh as the magnetic resonance (MR) images; four dimensional(4D) such as functional magenetic resonanace (fMR) signal.
- Based on the required number of channles: To aquaire a specific biosignal, which can be 1-channel to display pulse wave, 3-channels to display the accelerometer data, or multichannel with the electroencephalography(EEG) signals.
- Based on the signal models: The signals based on analysis approach, the biosignals can be stochastic or deterministic. The stochastic signals is nondeterministic, where the state is determined by predictable acitons and a random element which can be nonstationary or stationary. The deterministic biosignal is either nonperiodic(Transient) or periodic (sinusoidal or complex which can be predictable.

Figure 4. BioSignal classification

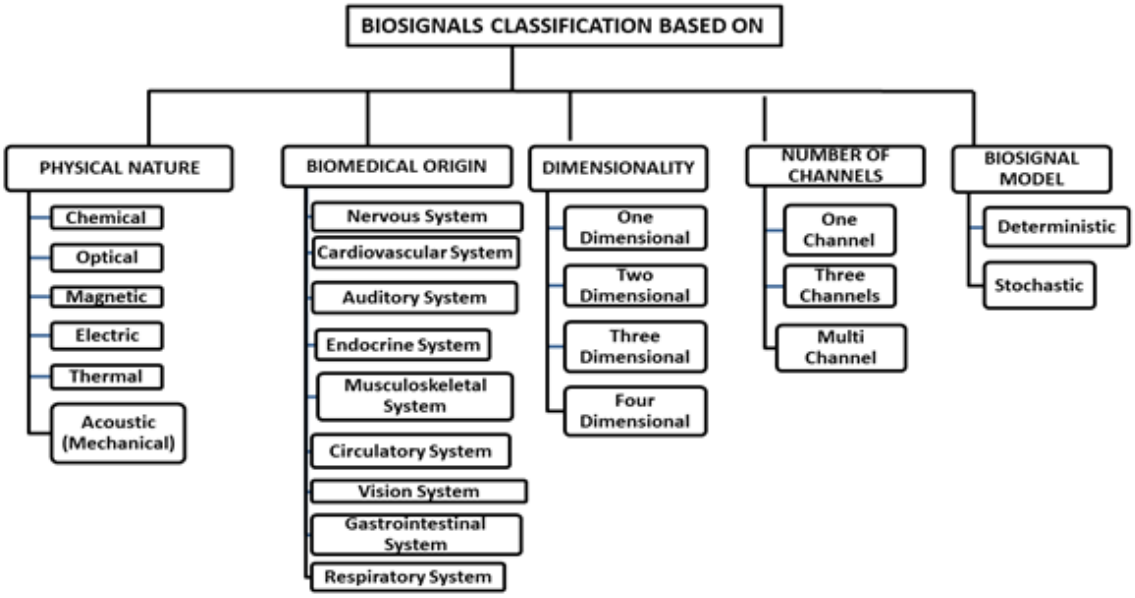

1. Magnetic biosignals are delivered because of the feeble fields of magnetic created by various cells and organs, like the mind, heart and lungs. The estimations of these attractive fields offer critical data. Instances of such biomagnetic signals incorporate the magnetoencephalogram (MEG) signal and the magnetoneurogram (MNG) signal delivered from the brain cells as well as the magnetomyogram (MMG) signal and the magnetocardiogram (MCG) signal, e.g., created from the muscle cells.

2. Chemical biosignals give data about different compound specialists' concentration in the human body, for example, glucose level, gases, the blood oxygen level, and breathing airflow in the blood.
3. Optical biosignals utilize optical ways to deal with sense the biochemical investigations. The biooptical signals mirror the biologic framework's optical capacities blending normally or initiated by the specific estimation. As of late, the advancement of the fiberoptic innovation opened huge uses of the biooptical signals.
4. The electric signs result from the electric field due to the intra-and extracellular ionic flows delivered in the organs or cells (muscle/nerve). This electric bio signal which is called likewise bioelectric signals or bio potentials is produced from the electrochemical instrument in the single ionic channels that creates an activity potential. Such bio signals result from the brain cells, for example, the electroretinogram (ERG) signal, the electroneurogram (ENG) signal, and the electroencephalogram (EEG) signal, or from the muscle cells, like the electromyogram (EMG) and the electrocardiogram (ECG) signal, or from different cells, like the galvanic skin reaction (GSR) signal and the electrooculogram (EOG) signal (Kramme R et.al., 2011, Prutchi D et.al., 2005)
    a. EEG sign mirrors the cerebrum electrical action recorded from the put terminals on the scalp to detect pathologies connected with improvement coordinated execution.
    b. EOG sign is recorded utilizing the electrooculography to quantify the retina resting potential. It records the uniqueness in the electrical charge between the back and front of the eye related with the development of the eyeball. The EOG signal is procured by the terminals situated on the skin close to the eye.
    c. ECG sign is a graphical show of the heart electrical action of additional time, which is recorded by an electrocardiograph. It shows the voltage contrast between the connected cathode sets and the heart muscle action.
    d. EMG sign addresses the muscles' physiologic properties of constriction and rest by identifying the electrical potential created by the muscle cells utilizing the electromyography.

Basic transducers are utilized to gain the bioelectric signals. Microelectrodes are utilized as sensors for single-cell estimations, where the deliberate activity potential addresses the biosignal. In any case, surface anodes are involved as sensors to quantify the electric field created by the many cells' activity for more raw estimations. For the most part, the acquired bioelectric signals from the anodes can be viewed as a point of interaction between the body and the estimation instrument. Because of the particular bioelectric signs' qualities and the gadget related interfer-ences, planning readout circuits for bioelectric signal estimations continuously observing moves a few architects to adapt to different issues and to plan wearable bioelectric obtaining frameworks.

5. The bioimpedance (IMP) signals are additionally created because of the tissue's impedance that passes on data concerning the programmed sensory system action, endocrine action, blood dispersion, and the blood volume. The IMP measure-ment helps the body's properties appraisal by estimating the body tissue's response to an instigated strain. Four cathodes are for the most part used to quantify the IMP estimations. In particular, the place of the estimating cathode (test) on the body surface is testing (Bronzino J 2006, Cacioppo J.T. et.al., 2014, Berntson G et.al., 2007, Soleymani S 2012).

6. Thermal biosignals, including the internal heat level and temperature maps in view of the hotness assimilation and hotness misfortune in the body, or the dissemination of the tem-perature on the body surface (Kaniusas E 2015)
7. Mechanical biosignals repeat the body parts' mechanical capacities, for example, the chest developments during breath process, the pulse, the acceler-ometer signals, and the phonocardiogram (PCG) signal, which mirrors the heart-beats' sounds. Biomechanical signals began from mechanical elements of the biologic framework, including stream signals, strain/pressure signs, and dis-arrangement/movement signals. The biomechanical signs' estimation includes various sensors/transducers, where the mechanical peculiarity doesn't prop-agate the acoustic, attractive, and electric fields (Fay C 2013, Alamdari N.T. 2016, Liu Y et.al., 2016).
8. Acoustic biosignals are characterized as the biosignals created from the respiratory sounds, hack sounds, cackle, wheeze, and wheezing sounds (Safieddine D et.al 2012, Kaniusas E 2012). Commonly, a few biomedical peculiarities create acoustic commotion, which offers critical data about this peculiarity. For instance, the wind current in the lungs favorable to duces acoustic sounds, muscle withdrawal delivers an acoustic clamor, the blood stream in the heart produces acoustic commotion, and the sounds created in the diges-tive plot. These created sounds are widely utilized in medication. For the most part, the acoustic biosignals depict the acoustic sound created by the body (movement/vibration), which is viewed as a subset of the mechanical biosignals. Bioacoustic signals access different body sounds, including gulping and wheezing, respiratory sounds, the cardiovascular sounds (phonocardiography), and the pops of the muscles/joints. This acoustic energy communicates through the bio-rationale medium; accordingly, acoustic transducers, like the accelerometers and miniature telephones, are utilized to secure such bioacoustics signal.

The ceaseless physiological sign obtaining permits the recognition and prevention of the various sicknesses, like the neurological pathologies or the cardiovascular illnesses. To secure any of the former biomedical signs, various kinds of sensors/transducers are involved by the biomedical application as represented in Figure 5. Biosignal procurement is the primary job of any biomedical instrument toward the most thoughtful of the human physiology utilizing equipment, compact, and remote securing transducers/sensors. Nonetheless, the bio-signal procurement is inadequate, where further biomedical sign handling is mandatory to deal with the achieved signal to gain the critical infor-mation from the loud biosignal(Dey N et.al., 2017, Sontakay R 2018, Ashour A et.al., 2016, Soni Y et.al., 2017, Acharya U et.al., 2006,Gospondinova E et.al., 2016).

Figure 5. Acquistion of biosignal

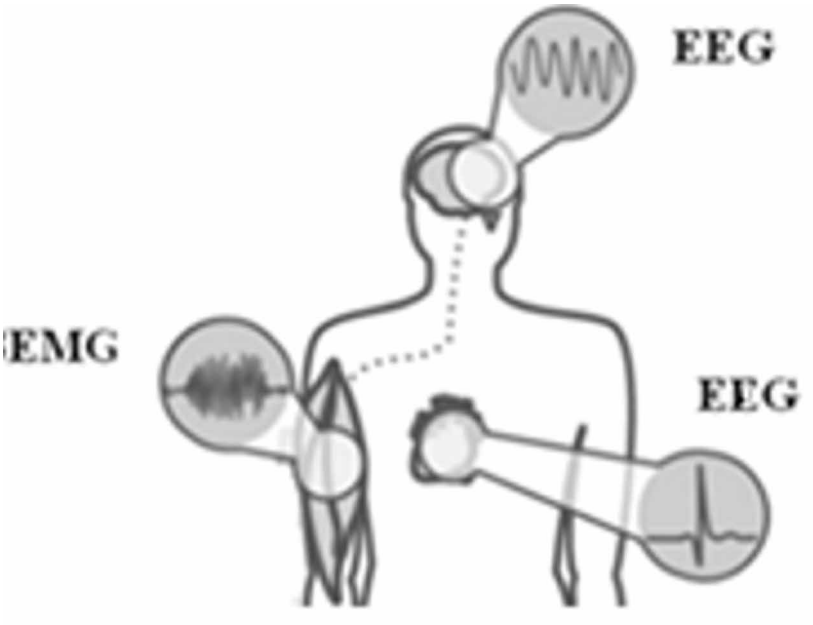

The biomedical sign handling represents an intricacies due to the underly-ing framework's intricacy and the necessary harmless, circuitous estimations. A few biosignal handling strategies are created in view of the fundamental sign's qualities, the point of the biomedical sign handling, and the test conditions. Biosignal handling comprises mostly of the component extraction stage step to extricate the focal points in the biosignal that shows the body conditions, for example, the beginning of the EMG signal and the pulse inconstancy from the ECG signal. Throughout the long term, a few biosignals that mirror the human body conditions have been described and considered to change the ways for different illness analyze. All the former biosignals are procured utilizing transducers/sensors of various kinds as per the required recognized biosignal.

According to the Physical Nature of Bio Signals

1. **Bioelectric signals**: These are produced by muscle and nerve cells. Their primary resource is the cell membrane, which may be stimulated to create an action potential under specific conditions. The bioelectric signal is made up of the electric field created by the activity of numerous cells. ECG (Electrocardiographic) and EEG (Electroencephalographic) signals are the most prevalent types of bioelectric signals.

Types of electrical signals

a. Muscle cells
    - **ECG -** electrocardiogram
    - **EMG –** electromyogram
b. Neural cells

- **ENG-** Electroneurogram
- **EEG**- electroencephalogram
- **ERG-** electroretinogram

c. Other cells
- **EOG -** electrooculogram
- **GSR** - galvanic skin response

2. **Biomechanical signals**: These are created as a result of a mechanical function of a physiological system. In the physiological system, they encompass all sorts of motion and displacement signals, pressure, flow signals, and so on. The respiratory physiological system functions by chest movement. This movement is quantifiable and observable.

Example:

- Blood pressure
- Accelerometer signals describing human movements, gait, balance and pose (Parkinson disease, mobile applications, fitness)
- Chest movements during respiration
- Air flow characteristics during MLV

3. **Bio acoustic signals:** These signals are produced by the physiological system during the movement of blood or air. The movement of blood in the heart, as well as the inspiration and expiration of the lungs, are accompanied by distinct auditory signals.

- Caridiac sounds(phonocariography)
- Snoring (Obstructive sleep apnea detection)
- Swallowing
- Respiratory sounds
- Crackles of joints and muscles

4. **Bio-impedance signals**: The impedance of the skin is determined by the skin's composition, blood distribution, and blood volume through the skin. The measurement of impedance aids in determining the status of the skin and the operation of several physiological systems. A bio-impedance signal is the voltage drop caused by tissue impedance.
5. **Biochemical signal**: A signal acquired as a result of chemical measurements taken from living tissue or samples analysed in the laboratory. Examples include partial pressure of carbon dioxide (pCO2), partial pressure of oxygen (pO2), and the concentration of different ions in the blood.

- pH
- Gases in blood and breathing airflow (anaesthetic gases, carbon dioxide etc)
- Oxygen level in blood (kidney failure, asthma, heart failure and obstructive pulmonary disease)
- Level of glucose(diabetes)
- Blood saturation of gases

SaO2 – arterial blood oxygen saturation, describes the percentage of haemoglobin molecules carrying oxygen.

SvO2 – venous oxygen saturation, describes how much oxygen the body consumes.

SpO2 – it is similar to SaO2 in different in the capillary system - oxygen saturation in peripheral capillary.

SpCO2 – concentration of carboxyhemoglobin in blood.

6. **Bio-optical signals**: These signals are formed by the optical variation caused by the physiological system's operation. The amount of oxygen in the blood may be estimated by measuring the amount of light that is transmitted and reflected from the blood artery.
7. **Bio magnetic signals**: Organs such as the brain, heart, and lungs generate extremely faint magnetic fields. The measurement of these signals offers information that other forms of bio-signals, such as bioelectric signals, do not. Magnetoencephalography, for example, is acquired by recording biomagnetic signals from the brain.

Types of magnetic signals

a. Neural cells
   - **MNG**- Magnetoneurogram
   - **MEG**- Magnetoencephalogram

b. Muscle cells
   - **MCG** - Magnetocardiogram
   - **MMG** – Mageneomyogram

ACCORDING TO THE SYSTEM OF ORIGIN OF BIOSIGNALS

- **Endocrine system**: - It is the collection of glands of an organism that secrete hormones directly into the circulatory system to be carried towards a distant target organ. It uses to control and coordinate body's metabolism, response to injury, energy level, stress, reproduction, growth and development and mood.

Endocrine system is integration of hypothalamus, pituitary, thyroid and parathyroid, pineal body, thymus, pancreas, adrenal gland, testis and, ovary.

- **Hypothalamus:** The hypothalamus is located at the base of the brain, near the optic chiasm where the optic nerves behind each eye cross and meet. The hypothalamus secrets hormones that stimulate or suppress the release of hormones in the pituitary gland, in addition to controlling water balance, temperature m appetite, blood pressure and sleep.
- **Thyroid and Parathyroid:** The thyroid gland and parathyroid glands are located in front of the neck, below the larynx (voice box). The thyroid gland is vital to the body's metabolism. The parathyroid glands are crucial in the control of the body's calcium balance.
- **Pineal body:** The pineal body is located below the corpus callosum, in the middle of the brain. It produces the hormone melatonin, which helps the body know when it's time to sleep.
- **Thymys:** The thymus is located in the upper part of the chest and produces white blood cells that fight infections and destroy abnormal cells.

- **Pancreas:** The pancreas is located across the back of the abdomen, behind the stomach. The pancreas plays a role in digestion, as well as hormone production. Hormones produced by pancreas include insulin and glucagon, which regulate levels of blood sugar.
- **Adrenal gland:** An adrenal gland is located on top of each kidney. The adrenal glands work hand in hand with the hypothalamus and pituitary gland. The adrenal glands produce and release corticosteroid hormones and epinephrine, which control blood pressure and metabolism.
- **Testis:** A man's testis are located in a pouch that hangs suspended outside the male body. The testis produce sperm and testosterone.
- **Ovary**: A woman's ovaries are located on both sides of the uterus, below the opening of fallopian tubes which extended from uterus to the ovaries. In addition to containing the egg cells necessary for reproduction, the ovaries also produce progesterone and estrogen.

Types of signals

- Chemical
- Optical
    - **Nervous System (Central and Peripheral)**: The nervous system is main communicating and controlling system of the body. Every action, thought and emotions reflects its activity. Its cells communicate by electrical and chemical signals, which are specific and rapid, and cause almost immediate responses.
- **Neurons and spinal cord**
    - Electroneruogram(Spike trains)
    - Magnetoneurogram
- **Brain**
    - EEM, MEG
    - Event related potentials (acoustic, visual)
    - Neurovisualization(MRI/fMRI,CT,PET,SPECT)
        - ■
- **Cardiovascular system**: The cardiovascular system has a very important function —— getting oxygen and nutrients to entire body and removing waste. Cells rely on cardiovascular system to obtain the nutrients they require to function properly. That is why it is critical to take care of heart with exercise, a good diet, and blood pressure and cholesterol management.
- **Heart and blood vessels**
    - ECG
    - MCG (current density Maps)
    - Blood pressure
    - Heart rate variablity
- **Visualization**
    - Ultrasonic imaging
    - MRI, Ultrasonic, X-ray
        - **Vision System**:
- EEG (visual cortex)
- VEP(visual evoked potentials)
- EOG(Electrooculogram)

- ERG(Electroretinogry)
    - **Auditory System**: The auditory system is the sensory system for the sense of hearing . It includes both the sensory organs(the ears) and the auditory parts of the sensory system.
- AEP(auditory evoked potentials is type of EEG signal)
- Audiometry
    - **Musculoskeletal system:**
- EMG(Electromyogram)
- Visualization (MRI,X-Ray)
- Reography(myorelaxation)
- Accelerometry(gait)
- Stabilography(Parkinson's) – Analysis of balancing act and postural control
    - **Respiratory system**: The respiratory system is the network of organs and tissues that help to breathe. It includes airways, lungs and blood vessels. The muscles that power the lungs also the respiratory system Is part of. These parts work together to move oxygen throughout the body and clean out waste gases like carbondioxide.
- Chemical signals(gas concentration)
- Mechanical (airflow, pressure, volume)
- Spirometry (flow-volume)
- Plethysmography(volume)
    - **Gastrointestinal system:** The gastrointestinal system includes the mouth, the throat(pharynx, esophagus,stomach, small intestine, large intestine, rectum and anus. It also includes the salivary glands, gallbladder,liver,and pancreas, which make digestive juices and enzymes that help the body digest food and liquids. Also called as digestive system.
- MRI
- X-ray
- Ultrasound imaging
- Chemical signals
- Electrogastrogram
    - **Blood System**
- Chemical signals (concentrations)

Other Classification of Biosignals

Dimensionality

- 1D(ECG)
- 2D(temperature map)
- 3D(MRI image)
- 4D(fMRI image)

Classification According to the Physical Nature of Signal

ECG (electrocardiograms) or EKG (electrocardiograms): An ECG is a basic test that may be performed to examine heart rhythm and electrical activity as a graph that can be presented electronically or

written on paper. Sensors placed on the skin detect the electrical impulses produced by the heart each time it beats. These signals are captured by a machine and analysed by a doctor to determine whether anything unusual is present. An ECG can be used to explore symptoms of potential cardiac abnormalities such as chest discomfort, palpitations (rapid heartbeats), shortness of breath, and dizziness.

- An ECG can aid in the detection of Cardiomyopathy, a condition in which the heart walls thicken or expand.
- Heart attacks occur when the blood supply to the heart is suddenly cut off.
- Arrhythmias are conditions in which the heart beats too slowly, too rapidly, or irregularly.
- Coronary Heart Disease: A condition in which the blood flow to the heart is obstructed or stopped due to a buildup of fatty substances.

An ECG examination often entails attaching a number of tiny, adhesive sensors known as electrodes to the arms, legs, and chest. These are linked to an ECG recording equipment via cables.

ECG Varieties

ECGs are classified into three types:

- A stress or exercise ECG - performed on an exercise bike or treadmill.
- A resting ECG, which is performed while lying down in a comfortable posture.
- An ambulatory ECG (holter monitor) — the electrodes are linked to a tiny portable machine worn around the waist, allowing the heart to be monitored at home for one or more days.

EEG(Electroencephalograms): An EEG (electroencephalogram) is a test that identifies irregularities in brain waves or electrical activity in the brain. Electrodes made of small metal discs connected by thin wires are glued on the scalp during this procedure. The electrodes detect minute electrical charges generated by brain cell activity. These charges are magnified and displayed as a graph on a computer screen or as a recording on paper that can be evaluated and analysed by the healthcare professional.

The EEG is used to assess brain disorders such as epilepsy (seizure), brain lesion (tumour or stroke), brain damage from head injury, brain dysfunction from a variety of causes (encephalopathy), inflammation of the brain (encephalitis), alseimer's disease, certain psychoses, sleep disorder (narcolepsy, during surgical operations, blood flow in the brain is monitored. An EEG is also used to confirm brain death or to determine whether a person is in a coma. A continuous EEG is used to assist in determining the appropriate amount of anaesthetic to identify medically induced coma.

Certain variables or conditions may obstruct the interpretation of an EEG exam. These are some examples:

- Oily or sprayed hair
- Caffeine-containing beverages such as coffee, cola, and tea.
- Sedatives and other medications.
- Light, particularly bright or flashing lights.
- Fasting-induced low blood sugar (hypoglycemia).
- Movement of the body or the eyes during the testing.

Electromyography (EMG): Electromyography is a diagnostic process used to assess the health of muscles and the nerve cells that govern them. These nerve cells (motor neurons) provide electrical signals to the muscles, causing them to contract and relax. An EMG converts these impulses into graphs or data, which aids doctors in making a diagnosis. Numbness, tingling, muscular weakness, and muscle discomfort are examples of muscle or nerve problems (cramping). Paralysis, uncontrollable muscle twitching (tics), and unexplained limb weakness.

In this procedure, a needle electrode inserted directly into a muscle records the electrical activity in that muscle. A nerve conduction study, is another part of an EMG, uses electrode stickers applied to the skin(surface electrodes) to measure the speed and strength of signals travelling between two or more points.

An EMG result can assist a clinician in determining the underlying cause of these symptoms. Possible reasons include

- Nerve problems (amyptrophic latera sclerosis ALS)
- Radiculopathies
- Disorders of the peripheral nerves, which affect the nerves outside the spinal cord (carpal tunnel syndrome)
- Muscle problems (muscular dystrophy or polymyositis).
- Disorders that impair the motor neuron's capacity to deliver electrical impulses to the muscle(myasthenia gravis)

EOG (Electrooculogram): The electroocoulogram is an elecrophysiologic test that measures the existing resting electrical potential between the cornea and brush's membrane. In this procedure patient should be dilated. The amount of light passing through the pupils is measured in a unit called trolands(the product of luminace(cd/m2) and pupil area(mm2). Therefore, the diameter of the pupil can change the brightness needed to have the same effect on the retina.

ERG (Electroretinogry): Electroretinogry is a test to measure the electrical response of light-sensitive eye cells called sticks and caps. These cells form part of the retina (back of the eye). In this procedure, the patient is in a sitting position, and the medical officer puts pain drops in the eye to avoid discomfort during the test. The eyes are kept open by a small device called the mirror. The electrical sensor (electrical) is placed on each eye. The terminal estimates the electrical movement of the retina because of light. The light flares up, and the electrical response is transmitted from electrode to a screen that looks like a TV where you can view it and write it down. A normal sample of the response has waves called A and B. The medical officer will take the readings from the normal light in the room and then again in the dark after the eyes have adapted within 20 minutes.

The following conditions may cause abnormal results"

- Trauma
- Vitamin A deficiency
- Retinal detachment
- Rod-cone dystrophy(retinitis pigmentosa)
- Congenital night blindness
- Giant cells arteritis
- Congential retinoschisis(splitting of the retinal layers)
- Medicines(chloroquine, hydroxychloroquine)

- Arteriscierosis with damage to the retina
- mucopolysaccharidosis

MEG(Magnetoencephalogram): Meg is based on measuring the magnetic field outside the head using an array of very sensitive magnetic field detectros(magnetometers). The signs recorded by EEG and MEG straightforwardly reflect current streams created by neurons inside the cerebrum. The temporal frequency content of these signals ranges from less than 1Hz (one cycle per second) to over 100Hz(100 cycles per second). Because MEG and EEG measure neuronal activity in real time the connections activated either ar rest or during task can be measured, giving us a picture of the dynamic interactions among brain networks. MEG has much greater temporal resolution that fMRI so MEG-based analysis provides high temporal resolution data for analysing the neuromagnetic correlates of fMRI connectivity, its time- frequency content, and temporal interactions.

MCG (Magnetocardiogram): MCG is the measurement of magnetic fields emitted by the human heart from small currents by electrically active cells of the heart muscle.

PCG (Phonocardiogram): PCG reflects sounds of heartbeats, produced by heart sounds corresponding to two consecutive heart valve closures. Indicates closure strength and the valves stiffness.

Respiratory Sounds: Reflect normal breathing sounds superimposed with crackles, cough sounds, rhonchus, snoring, squawk, stridor and wheeze sounds, which are associated with pulmonary disorders

ERG(Electroretinogry): Electroretinography measures the electrical responses of various cell types in the retina, including the photoreceptors (rods and cones), inner retinal cells (bipolar and amacrine cells), and the ganglion cells

BP(Blood Pressure): Blood pressure is the force of blood pushing against the walls of arteries. Each time heart beats, it siphons blood into the veins. Blood pressure is highest when heart beats, pumping the blood. This is called systolic pressure. Whenever heart is at rest, between thumps, pulse falls. This is called diastolic pressure.

Blood pressure reading uses two numbers. Usually the systolic number is above the diastolic number. Ex 120/80 means a systolic of 120 and a diastolic of 80.

High BP usually has no symptoms. Health care provider will use a guage, a stethoscope, or electronic sensor, and BP cuff.

Table 1.

Category of BP	BP – Systolic	BP – Diastolic
Normal	<120	<80
High BP(no other heart risk factors)	>=140	>=90
High BP(with other heart risk factors,according to some providers) >=130 >=80	>=180	>=120
Dangerously high BP – seek		

Types of BP: There are two main types of high BP

- Primary or essential, high blood pressure is the most common type of high blood pressure. It develops over a time of getting older.

- Secondary high blood pressure is caused by another medical condition or use of certain medicines, it usually gets better after stop taking medicines that are causing it.

OSL (Oxygen Saturation Level): A healthy blood oxygen level varies between 75 and 100 mm of mercury (mm Hg).

When arterial blood gas(ABG) test results reveal an oxygen level below 60 mmHg the medical community considers it low. In some cases requires oxygen supplementation.

A blood oxygen level that is too low compared with the average level of a healthy person can be a sign of a condition known as hypoxemia. This develops when the body has difficulty delivering oxygen to all of its cells, tissue, and organs.

Oxygen saturation refers to the percentage of oxygen in blood. Medical professionals often use a device called pulse oxymeter for either a quick test or continuous monitoring. The gadget can connect to the's at the tip of individual's finger.

A healthy oxygen saturation level ranges between 95% and 100%. If a person's level drop below this range, they may experience symptoms associated with a lack of oxygen, such as trouble breathing and confusion.

Table 2.

Observations	Oxygen saturation (SpO2) %	Pulse rate(bpm)	Temp(^{0}C)
Normal reading	>=96%	40-100	3.5-37.5
Acceptable to continue home monitoring	95%	101-109	38
Seek advice from GP	93%-94%	110-130	38.1-39
Need urgent medical advice	<=92%	>=121	>=39

Symptoms of Low Blood Oxygen Levels

Low blood oxygen levels can result in abnormal circulation and cause the following symptoms

- Headaches
- Restlessness
- Shortness of breath
- Dizziness
- Chest pain
- Rapid breathing
- Confusion
- High blood pressure
- Lack of coordination
- Rapid heartbeat
- Visual disorders
- Sense of euphoria

Causes of Low Blood Oxygen (Hypoexemia)

- It causes due to
- Inability of the blood stream to circulate to the lungs, collect oxygen, and transport it around the body
- Insufficient oxygen in the air
- Failure of the lungs to breathe in and send oxygen to all cells and tissues.

Conditions that can Lead to Hypoexemia

- COVID-19
- Heart diseases, including congenital heart disease
- Asthma
- High altitude
- Anemia
- Interstitial lung disease
- Chronic obstructive pulmonary disease(COPD)
- Emphysema
- Acute respiratory stress syndrome(ARDS)
- Pneumonia
- Excess fluid in the lungs
- Impediment of a course in the lung
- Aspiratory fibrosis, or scarring and harm to the lungs
- Presence of air or gas in the chest that makes the lungs collapse
- Certain medications, including some narcotics and pain relievers

GL(Glucose Level): The pancreas usually produces insulin when the blood sugar or glucose levels in the blood It's a signal to the body to absorb glucose until it's back to normal. If a person has diabetes, his or her body does not insulin, i.e. he or she has a disease. Diabetes of type 1 or does not react normally, i.e. type-2 diabetes of It could leave blood sugar too high for too long. Over time, this can damage nerves and blood vessels and lead to heart disease and other problems. This level of blood sugar can be controlled by a special device called a blood glucose monitor. He takes a small sample of blood, usually from the tip of his finger, and measures the amount of glucose in it.
Blood sugar levels for diabetes at age 20 or more:

- Fasting <100 mg/dl
- Before meal 70-130 mg/dl
- After meal <180 mg/dl
- Before exercise 100 mg/dl (if taking insulin)
- Bedtime 100-140 mg/dl
- Three month average hbA1c less than or around 7.0%

ST (Skin Temperature): Skin temperature (thermometer) is the temperature of the outermost surface of the body. Normal human skin temperature on the trunk of the body varies between 33.5 and 36.9^{0}C

(92.3 and 98.4^{0}F) through the skin's temperature is lower over protruding parts, like the nose m and higher over muscles and active organs.

GSR (Galvanic Skin Response): GSR is the category of electrodermal activity (EDA) or skin conductance(SC), which refers to the changes in sweat gland activity that reflective of the intensity of our emotional state, other wise known as emotional arousal which are in response to the environment like scary, joyful, threatening or other type of emotionally relevant activity which increases eccrine sweat gland activity.

MRI (Magnetic Resonance Imaging)

Magnetic resonance imaging (MRI) is a clinical imaging procedure that utilizes an attractive field and PC produced radio waves to make itemized pictures of the organs and tissues in your body.

Most MRI machines are enormous, tube-formed magnets. Whenever you lie inside a MRI machine, the attractive field briefly realigns water particles in your body. Radio waves make these adjusted iotas produce faint transmissions, which are utilized to make cross-sectional MRI pictures - like cuts in a portion of bread.

The MRI machine can likewise create 3D pictures that can be seen from various points.

X-ray is the most often utilized imaging trial of the mind and spinal string. It's often performed to help diagnose:

- Aneurysms of cerebral vessels
- Disorders of the eye and inner ear
- Multiple sclerosis
- Spinal cord disorders
- Stroke
- Tumors
- Brain injury from trauma

An extraordinary sort of MRI is the utilitarian MRI of the mind (fMRI). It produces pictures of blood stream to specific region of the cerebrum. It very well may be utilized to look at the mind's life structures and figure out what portions of the cerebrum are taking care of basic capacities.

This recognizes significant language and development control regions in the minds of individuals being considered for cerebrum medical procedure. Utilitarian MRI can likewise be utilized to evaluate harm from a head injury or from issues like Alzheimer's sickness.

X-ray that spotlights on the heart or veins can evaluate:

- Size and function of the heart's chambers
- Thickness and development of the dividers of the heart
- Extent of damage caused by heart attacks or heart disease
- Primary issues in the aorta, like aneurysms or analyzations
- Inflammation or blockages in the blood vessels

MRI can check for cancers or different anomalies of numerous organs in the body, including the accompanying:

- Liver and bile ducts
- Kidneys
- Spleen
- Pancreas
- Uterus
- Ovaries
- Prostate

MRI of joints and bones can help assess:

- Joint irregularities brought about by awful or monotonous wounds, like torn ligament or tendons
- Bone infections
- Growths of the bones and delicate tissues
- MRI can be utilized with mammography to identify bosom malignant growth, especially in ladies who have thick bosom tissue or who may be at high gamble of the sickness..

CONCLUSION

Biomedical signals are detected by the biomedical sensor, which is the product of the integration of electronic information technology and biomedicine, and have a strong vitality in the development of interdisciplinary interactions for the development of biomedical sensor technology. Now at, the development of medical sensors has changed traditional medical diagnostic methods, forming intelligence, micro, multi-parameter, remote control, and non-invasive development trends and making many technological advances. Other new biomedical sensors, such as DNA, fibre optics, and bio tissue sensors, are also being developed for a variety of biomedical applications. Recent advances in biomedical sensor technology have played an important role in advancing life and information sciences and inventing new diagnostic and therapeutic tools. These advances will ultimately drive the development of modern medicine. Further acquisition of biomedical signals, pre-processing and extracting required data by applying AI and ML techniques which facilitates pre detection of diseases. With the development of cloud storage, IOT technology diseased person can get immediate treatment or suggestion by the physician to extend their life time.

REFERENCES

Okoye, G. C. (2008). Biomedical technology and health human life. *Biomedical Engineering*, ●●●, 1–12.

Dey, A. Mohammed, & Nguyen. (2019). Acoustic Sensors for Biomedical Applications. Academic Press.

Eggins, B. R. (2008). *Chemical sensors and biosensors* (Vol. 28). Wiley.

Graf, R. F. (1999). *Modern dictionary of electronics*. Oxford Newnes.

Ronkainen, N. J., Halsall, H. B., & Heineman, W. R. (2010). *Electrochemical biosensors*. Academic Press.

Ronkainen, N. J., Halsall, H. B., & Heineman, W. R. (2010). Electrochemical biosensors. *Chemical Society Reviews*, *39*(5), 1747–1763. doi:10.1039/b714449k

Scheller, F., Schubert, F., Pfeiffer, D., Hintsche, R., Dransfeld, I., Renneberg, R., Wollenberger, U., Riedel, K., Pavlova, M., Kuhn, M., Muller, H. G., Tan, P., Hoffmann, W., & Movitz, W. (1989). Research and development of biosensors. A review. *Analyst (London)*, *114*(6), 653–662. doi:10.1039/AN9891400653 PMID:2665569

Rodriguez-Mozaz, S., Marco, M. P., de Alda, M. J. L., & Barceló, D. (2004). Biosensors for environmental monitoring of endocrine disruptors: A review article. *Analytical and Bioanalytical Chemistry*, *378*(3), 588–598. doi:10.100700216-003-2385-0 PMID:14647938

Rothrock, R. L., & Drummond, O. E. (2000, July). Performance metrics for multiple-sensor multiple-target tracking. In *Signal and Data Processing of Small Targets 2000* (Vol. 4048, pp. 521–532). International Society for Optics and Photonics. doi:10.1117/12.392004

Herold, M., Scepan, J., & Clarke, K. C. (2002). The use of remote sensing and landscape met- rics to describe structures and changes in urban land uses. *Environment & Planning A*, *34*(8), 1443–1458. doi:10.1068/a3496

Gnawali, O., Yarvis, M., Heidemann, J., & Govindan, R. (2004, October). Interaction of retransmission, blacklisting, and routing metrics for reliability in sensor network routing. In *Sensor and Ad Hoc Communications and Networks, 2004. IEEE SECON 2004. 2004 First Annual IEEE Communications Society Conference on* (pp. 34–43). IEEE.

Mac Ruairí, R., Keane, M. T., & Coleman, G. (2008, August). A wireless sensor network application requirements taxonomy. In *Sensor Technologies and Applications, 2008. SENSORCOMM'08. Second International Conference on* (pp. 209–216). IEEE.

Boccippio, D. J., Koshak, W., Blakeslee, R., Driscoll, K., Mach, D., Buechler, D., Boeck, W., Christian, H. J., & Goodman, S. J. (2000). The Optical Transient Detector (OTD): Instrument characteristics and cross-sensor validation. *Journal of Atmospheric and Oceanic Technology*, *17*(4), 441–458.

Estrada, E. F. (2010). *Computer-aided detection of sleep apnea and sleep stage classification using HRV and EEG signals*. The University of Texas at El Paso.

Rodrigues, F. M. S. (2015). *Establishing a framework for the development of multimodal virtual reality interfaces with applicability in education and clinical practice* (Doctoral dissertation).

Cavazzana, L. (2012). *Integrating an EMG signal classifier and a hand rehabilitation device: Early signal recognition and real time performances*. Academic Press.

Kramme, R., Hoffmann, K. P., & Pozos, R. S. (Eds.). (2011). *Springer handbook of medical technology*. Springer Science & Business Media.

Prutchi, D., & Norris, M. (2005). *Design and development of medical electronic instrumenta- tion: A practical perspective of the design, construction, and test of medical devices*. Wiley.

Bronzino, J. D. (2006). Biomedical signals: Origin and dynamic characteristics; frequency- domain analysis. In *Medical devices and systems* (pp. 27–48). CRC Press.

Bronzino, J. D. (Ed.). (2006). *Medical devices and systems*. CRC Press.

Casaccia, S., Sirevaag, E. J., Richter, E., O'Sullivan, J. A., Scalise, L., & Rohrbaugh, J. W. (2014, May). Decoding carotid pressure waveforms recorded by laser Doppler vibrometry: Effects of rebreathing. In *AIP Conference Proceedings* (Vol. 1600, No. 1, pp. 298–312). AIP.

Berntson, G. G., Quigley, K. S., & Lozano, D. (2007). Cardiovascular psychophysiology. Academic Press.

Cacioppo, J. T., Tassinary, L. G., & Berntson, G. G. (Eds.), *Handbook of psychophysiology* (Vol. 3, pp. 182–210). Cambridge University Press.

Soleymani, S., Borzage, M., Noori, S., & Seri, I. (2012). Neonatal hemodynamics: Monitoring, data acquisition and analysis. *Expert Review of Medical Devices*, *9*(5), 501–511.

Kaniusas, E. (2015). Biomedical signals and sensors II. Springer.

Jeong, J., & Rogers, J. A. (2016). Epidermal mechano-acoustic sensing electronics for cardio- vascular diagnostics and human-machine interfaces. *Science Advances*, *2*(11), e1601185.

Alamdari, N. T. (2016). *A morphological approach to identify respiratory phases of seismo- cardiogram*. The University of North Dakota.

Fay, C. (2013). Investigation into strategies for harvesting chemical based information using digital imaging and infra-red sensors for environmental and health applications (Doctoral dissertation). Dublin City University.

Kaniusas, E. (2012). Fundamentals of biosignals. In Biomedical signals and sensors I (pp. 1–26). Springer.

Acharya, U. R., Joseph, K. P., Kannathal, N., Lim, C. M., & Suri, J. S. (2006). Heart rate vari- ability: A review. *Medical & Biological Engineering & Computing*, *44*(12), 1031–1051.

Safieddine, D., Kachenoura, A., Albera, L., Birot, G., Karfoul, A., Pasnicu, A., Biraben, A., Wendling, F., Senhadji, L., & Merlet, I. (2012). Removal of muscle artifact from EEG data: Comparison between stochastic (ICA and CCA) and deterministic (EMD and wavelet-based) approaches. *EURASIP Journal on Advances in Signal Processing*, *2012*(1), 127.

Dey, N., & Ashour, A. S. (2017). *Direction of arrival estimation and localization of multi-speech sources*. Springer Science and Business Media.

Sontakay, R. (2018). *Real-time signal analysis of the ECG signal for generating an artificial pulse for continuous flow blood pumps using virtual instrumentation* (Doctoral dissertation). California State University, Northridge.

Ashour, A. S., Dey, N., & Mohamed, W. S. (2016). Abdominal imaging in clinical applica- tions: Computer aided diagnosis approaches. In *Medical imaging in clinical applications* (pp. 3–17). Springer.

Dey, N., Hassanien, A. E., Bhatt, C., Ashour, A., & Satapathy, S. C. (Eds.). (2018). *Internet of things and big data analytics toward next-generation intelligence*. Springer.

Gospodinova, E., Gospodinov, M., Dey, N., Domuschiev, I., Ashour, A. S., Balas, S. V., Soni, Y., Jain, J. K., Meena, R. S., & Maheshwari, R. (2017, May). HRV analysis of young adults in pre-meal and post-meal stage. In *Recent Trends in Electronics*. Information.

Olariu, T. (2016, August). Specialized software system for heart rate variability analysis: An implementation of nonlinear graphical methods. In *International workshop soft computing applications* (pp. 367–374). Springer.

Nagel, J. H. (2000). Biopotential amplifiers. In J. D. Bronzino (Ed.), *Biomedical engineering hand book* (2nd ed., pp. 70–71). Springer-Verlag.

Zhou, G., Wang, Y., & Cui, L. (2015). Biomedical sensor, device and measurement systems. In *Advances in Bioengineering*. InTech.

Dickhaus, H., & Heinrich, H. (1996). Classifying biosignals with wavelet networks. *IEEE Engineering in Medicine and Biology Magazine*, *15*(5), 103–111.

Mar, T., Zaunseder, S., Martínez, J. P., Llamedo, M., & Poll, R. (2011). Optimization of ECG classification by means of feature selection. *IEEE Transactions on Biomedical Engineering*, *58*(8), 2168–2177.

Tavakolian, K., Nasrabadi, A. M., & Rezaei, S. (2004, May). Selecting better EEG channels for classification of mental tasks. In *Circuits and Systems, 2004. ISCAS'04. Proceedings of the 2004 International Symposium on* (*Vol. 3*, pp. III–537). IEEE.

Boucsein, W. (2012). *Electrodermal Activity* (2nd ed.). Springer.

Salimpoor, V. N., Benovoy, M., Longo, G., Cooperstock, J. R., & Zatorre, R. J. (2009). The rewarding aspects of music listening are related to degree of emotional arousal. *PLoS One*, *4*, e7487.

Chapter 2
A Comprehensive Review on a Brain Simulation Tool and Its Applications

Ankita Raghuvanshi
Indian Institute of Technology, Gandhinagar, India

Mohit Sarin
National Institute of Technology, Raipur, India

Praveen Kumar Shukla
VIT Bhopal University, India

Shrish Verma
National Institute of Technology, Raipur, India

Rahul Kumar Chaurasiya
Maulana Azad National Institute of Technology, Bhopal, India

ABSTRACT

Brain-computer interface, widely known as BCI, is a relatively new field of research that has emerged as promising field research in the last few decades. It is defined as a combination of software as well as hardware that give us the tool to control external devices by using our brain signals as commands. In this chapter, the authors discuss the various tools that can be used to analyze and perform different functions on the brain signals, create BCI models, simulations, etc. In this study, they compare the tools and tabulate how they might be useful for the user's requirements. Additionally, they have implemented the use of tools for real-time applications. The experimental analysis presented in this work utilizes MAMEM EEG steady-state visually evoked potential (SSVEP) dataset I. Five different frequencies (6.66, 7.50, 8.57, 10.00, and 12.00 Hz) were used for the visual stimulation. The authors have analyzed different parameters like power spectrum density, power spectrum, and inter-trial coherence (ITC) through EEGLAB.

DOI: 10.4018/978-1-6684-3947-0.ch002

INTRODUCTION

Brain-Computer Interface (BCI) is a communication mechanism that does not rely on the normal peripheral nervous and muscular production pathways of the brain. BCI 's ultimate aim is to develop a standardized interface to allow a person with serious motor disabilities to have effective control of devices such as computers, speech synthesizers, prostheses (Dornhege et al., 2007 & Blankertz et al., 2010) and home appliance (Shukla et al., 2020). In other words, BCI describes a system of contact and control between the human brain and computers designed to assist disabled people using their electrical brain activity, which is normally monitored using electroencephalogram (EEG) (Vaid et al., 2015). There are various other ways of recording brain activity like Electrocorticography (ECoG), Near-Infrared chemical analysis (NIRS), practical Resonance Imaging (fMRI), etc. EEG is one of the foremost wide used because of high temporal resolution, ease of use, safe, and high affordability. There are two techniques namely invasive and non-invasive can be used to measure the electrical activities of the brain. In invasive technique, the sensors are placed inside the brain to increase the information in the acquired data. The goal is to target the neurons within a specific brain area and record the high-frequency neural signals. In non-invasive technique (Szafir et al., 2010), the signals are captured without any penetration of the scalp thus avoiding surgery. Recorded signals through noninvasive technique have low frequency and comparatively poor spatial resolution. The non-invasive technique has the chances of localization and the information in addition to low information content.

Our brain generates various types of signals, classified into three main classes, 1) Evoked signals–the signals unconsciously generated to external stimuli, For Example: State Evoked Potentials (SSEP) which are of two types, a) steady-state visually evoked potentials (SSVEP) which occur after looking at a visual stimulus flickering with constant frequency signals, have a frequency range of 3.5–75 Hz and can be divided into bands, according to their frequency (Regan et al., 1975). b) auditory steady-state responses (ASSRs), induced by repetitive auditory stimuli (Galambos et al., 1981); c) Somatosensory steady-state evoked potentials (SSSEPs), observed as a response to a repetitive tactile stimulation; and P300, it is detected with a latency of roughly 300ms after the use of stimuli (Gonzalez et al., 2016); 2)Spontaneous signals-Signals that are generated voluntarily without any external stimuli, It is of two main types, a) Motor and sensorimotor rhythms (8-26 Hz) (Cheyne et al., 2013), b)Slow Cortial Potentials(SCP) (frequency $<$ 1Hz) (Birbaumer et al., 1999); 3)Hybrid signals- Where 2 or more types of brain signals are used as an input to a system (Yin et al., 2015). Brain signals can be used in different application. The detail of the brain signals and its application shown in Table.1

Table 1. Brain signals and its application

S. No.	Brain Signals	Application
1	SSVEP (Li et al., 2013 & Putz et al., 2007)	Wheelchair Control, Control of Electrical Prosthesis
2	P300 (Krusienski et al., 2008 & Seo et al., 2016)	P300 speller, Virtual-Reality based Smart Home.
3	SCP, P300 (Makary et al., 2014)	Improves the signal by removing the superimposed noise
4	Motor and sensorimotor rhythms (Doud et al., 2011)	Virtual helicopter control
5	ERD, NIRS (Cruz et al., 2017)	Double ERP Detection for Automatic Error Correction in BCI Speller
6	SSVEP, P300 (Bi et al., 2014)	Cursor Control system.
7	Motor Imagery, SSVEP (Lin et al., 2006)	Virtual Gaming Paradigm
8	FF-SSMVEP (Zhang et al., 2013)	Improves contrast and has low visual fatigue

Application of BCI isn't solely restricted to medical applications like Brain-Controlled chair, Robotic ligaments, etc., however currently analysis is additionally shown that it is used for day-to-day applications like Home Automation, Game, diversion, and Neuromarketing, etc. A BCI system consists of four consecutive components: (1) signal acquisition (Zhang et al., 2013), (2) Pre-processing and feature extraction (Fatehi et al., 2007, Elsayed et al., 2017 & Lakshmi et al., 2014), (3) feature translation or classification (Hosni et al., 2007 & Lotte et al., 2007), and (4) device output. BCI is a computer-based system that acquires brain signals, analyzes them, and interprets them into commands signals and finally control device will activate. The architecture of BCI- based system is as shown in Figure.1.

Figure 1. General architecture of BCI- based system

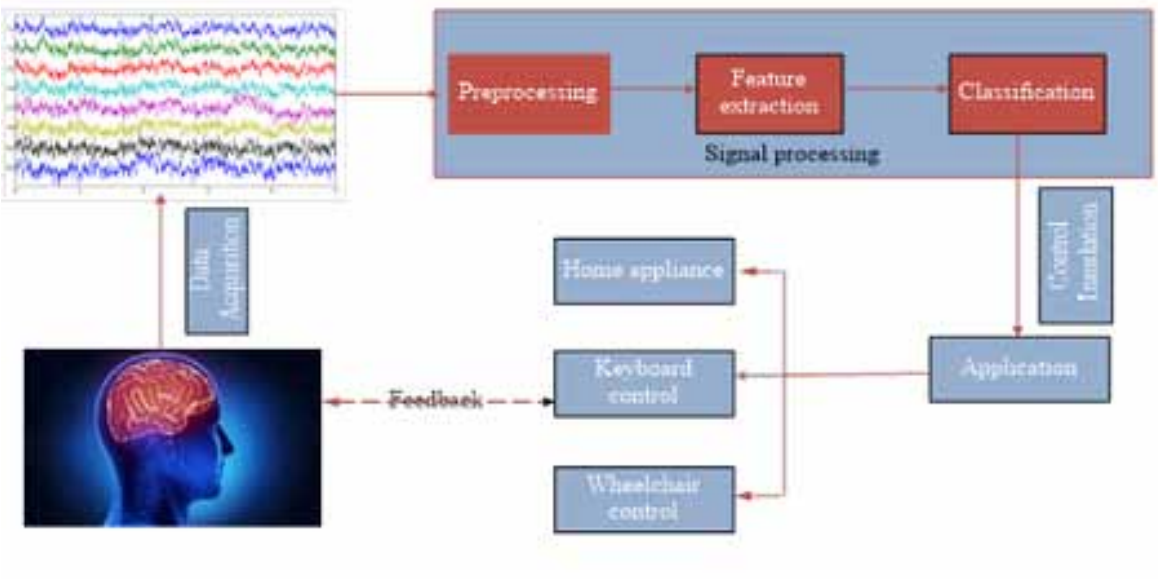

Figure 1, shows the general architecture of a BCI-based system and talks about all the different processes which are used in between. There are many devices are available for data collection/Acquisition such as neurosky, gtech, Acticap etc., after that collected signal pre-processed through different filtering approach such as band pass, Chebyshev etc. (Zhang et al., 2018). These filtered and enhanced signals are then fed to feature extraction algorithms like independent component analysis (ICA), Principal Component Analysis (PCA), Canonical Correlation Analysis (CCA) etc. (Kachenoura et al., 2007), which extract features and information about the signals in the time and frequency domain, after feature extraction these signals are sent to the classification algorithms, like State Vector Machine (SVM), Linear Discriminant Analysis (LDA), Bayes Classifiers etc. (Xu et al., 2009), to classify the extracted features to categories of brain signal patterns for identification of the brain signal. For analysis of these brain signals various toolboxes have been developed like BCILAB, EEGLAB, PyEEG etc. Additionally, several packages were developed specifically for BCI functions, such as BCI++, OPENVibe, etc. (Delorme et al., 2010 & Delorme et al., 2011). The detail description of the brain tools is shown in Table.2.

Table 2. Component of brain signal tools

S. No.	Tool Name	Developed Year	Platform	Website link
1	EEG LAB	1997	MATLAB	https://sccn.ucsd.edu/eeglab/index.php
2	Brainstorm	2004	MATLAB, JAVA	https://neuroimage.usc.edu/brainstorm/Introduction
3	BCI LAB	2008	MATLAB	https://sccn.ucsd.edu/wiki/BCILAB
4	BioSig	2009	MATLAB, Octave	https://www.biosig.com/
5	OpenVIBE	2007	C++	http://openvibe.inria.fr/
6	PsychoPy	2018	Python	https://www.psychopy.org/
7	BCI2000	2001	C++	https://www.bci2000.org
8	BCI++	-	C/C++	http://www.sensibilab.lecco.polimi.it/bci
9	BF++	2003	C++	http://www.brainterface.com/joomla2/bf-toys
10	PyEEG	2010	Python	http://pyeeg.sourceforge.net/
11	OpenMEEG	2006	Python	https://openmeeg.github.io/
12	Tempo	2005	-	https://en.opensuse.org/TEMPO

Motivation and Requirements

About 15% of the world's population suffers from varied disabilities within the world and 1% of them have severe disabilities just like the locked-in syndrome, with the development in BCI, life is created easier for people with such disabilities, also, within the way forward for technology with the rise in understanding and automation of the machines, our day-after-day life activities also can be controlled with the assistance of our brain. Our main necessities for this model are to

- Grasp the fundamentals of a BCI model.
- Spot varied tools for BCI.
- Check and compare the known tools.

LITERATURE REVIEW

Research on brain-computer interfaces (BCIs) started as early as 1973, since then there has been a lot of research going on BCI and varied platforms are being developed for BCI. Many types of software have been developed for easy and efficient visual illustrations of those signals have created a lot of potential for development in the field. Various toolboxes have been developed for platforms like MATLAB and lots of software have been recently developed specifically for BCI Applications. These applications help us in development of a typical BCI system; they assist in the extracting information using different techniques like, Signal Acquisition, Pre-processing, Feature Extraction, Classification, and Feedback Mechanism (Muller et al., 2008). With development in technology and research, many new tools and applications have been developed for BCI; some of them are standalone packages or applications, while others can be found on varied platforms like MATLAB, Spyder (Python), etc. as toolboxes or libraries. Applications in the field of BCI mainly divided into three types; 1) basic analysis such as analysis of brain signals, 2) Clinical/Medical Research such as Automatic Wheelchair Controls, P300 Speller etc. (Muller et al., 2008 & Townsend et al., 2010) 3) Client Products such as Home Automation, Virtual Gaming etc. (Gao et al., 2003 & Goel et al., 2014). While the elemental analysis needs exploration of wide space that might not be potential with the present technology, the other 3 classes still are explored with the restricted resources on the market. Recently, more practical applications like Augmented Reality using BCI, Virtual Gaming have received growing attention (Mohammed et al., 2018), various other real-life applications include spellers, robotic arm, /Automated wheelchair, home automation etc. have gained popularity, and this shows that BCI is now being accepted as a promising field.

The remaining of the paper is organized as follows: Section 2 describes the, detail description of the tools; section 3 describes uses of tool in practical application section 4 provides discussion on tools and its application. Finally, section 6 concludes the paper.

Detailed Study on BCI Tools

In this section, we are describing detail study of the various BCI tools. These tools are useful for the data collection and analysis of the data.

EEGLAB

It is a free open-source MATLAB toolbox for processing data from EEG, MEG, and other electrophysiological signals. EEGLAB runs under Linux, UNIX, Windows, and Mac OS X. The software is available online for free and it can be downloaded from its official website It has a Graphic user interface and multi-format data importing, High-density data scrolling and Interactive plotting functions, the user can easily review and reject data by visual inspection. Other features include Semi-automated artifact removal, ICA & time/frequency transforms, Event & channel location handling, Forward/inverse head/source modelling etc. The EEGLAB comes various plug-ins to provide a vast range of functions and

services to the user, most popular plug-ins include DIPFIT, for source localization of ICA component sources of EEG data; ERPLAB, for deriving measures from average event-related potentials; FASTER, a fully automated, unsupervised method for processing high-density EEG data; NFT, for building electrical forward head models from MR images and/or electrode positions; SIFT, a source information flow toolbox (Delorme et al., 2004).

Figure 2. PSD of sample data

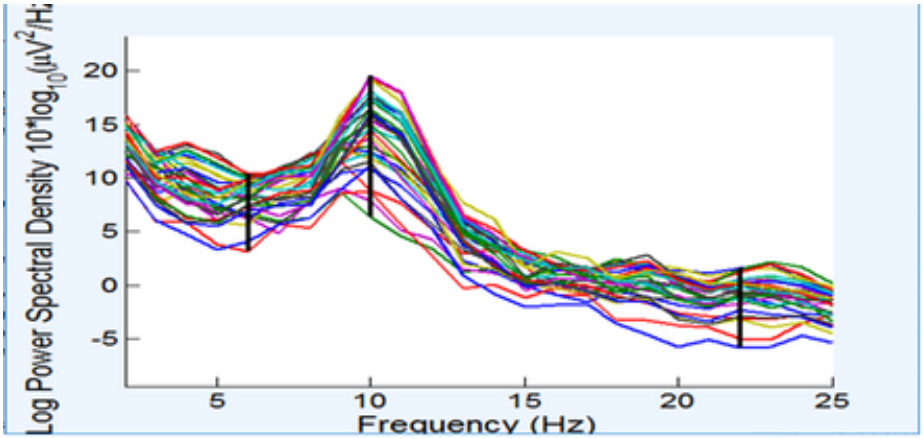

Figure 3. ERP of sample data with Epochs

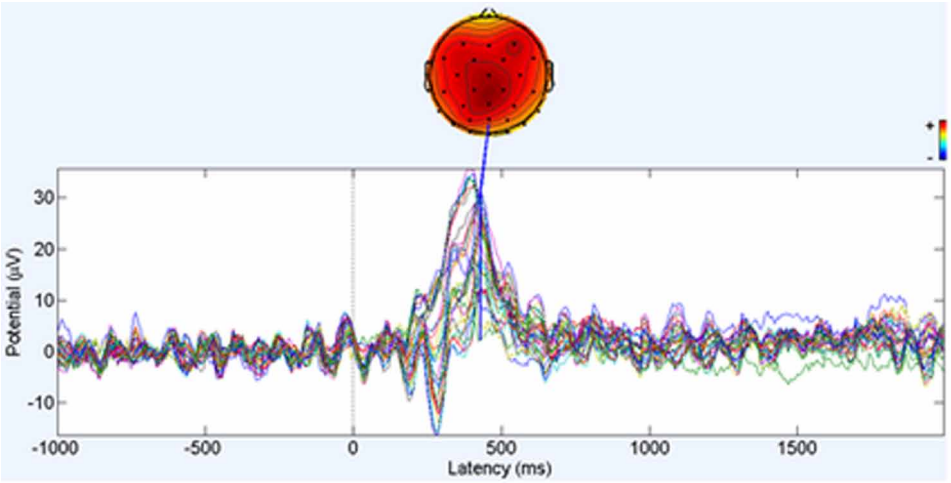

Figure 4. Data scroll

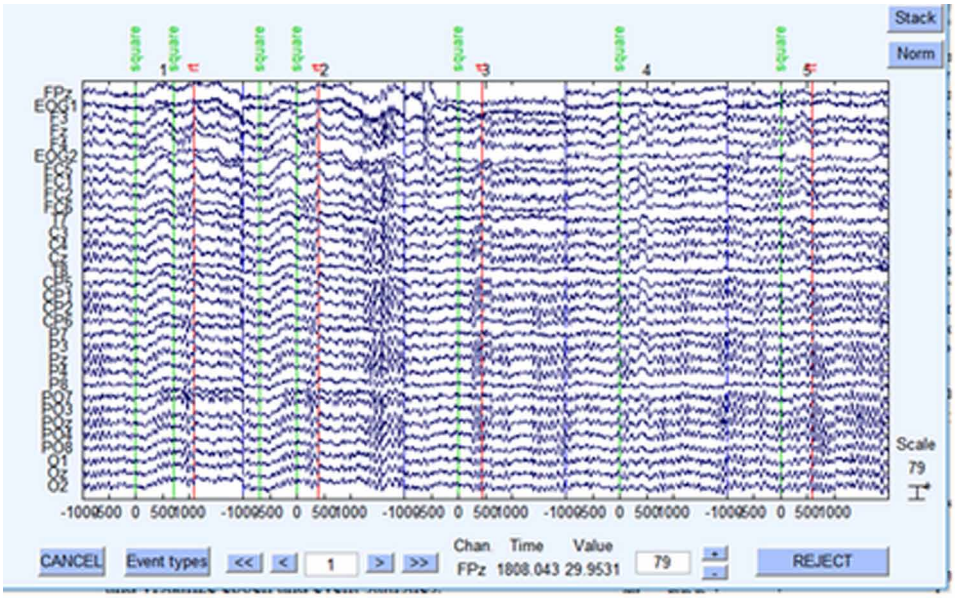

In Figure 2, the Power Spectral Density of the various signals present in the dataset, and it can be inferred that the signals with the frequency of the10-15 Hz have the highest PSD and hence are best suited for extracting information. Figure 3 depicts the Event-related potential that is the brain response to a specific event and from the graph, the position of the epochs where the highest activity is generated can be identified. This further helps us in extracting information about which part of the brain is responsible for the signal generated. In Figure 4 The EEGLAB scrolling data review function, allows the user to review and reject data by visual inspection, we can move the cursor around to scroll through the data and zoom in to find the values at specific times. EEGLAB is widely used as it is free and very easy to use; the various features help in simplifying the process of analyzing the signal. One disadvantage is that it does not have an easy-to-use GUI and does not support .csv files to be used as dataset.

Brainstorm

Brainstorm is a free toolbox and is available easily on the internet, it is used for the analysis of recorded brain signals. It can be used on multiple platforms like MATLAB, Spyder, etc., and also can use languages like python, java, etc. It is a very useful tool as it has many features like Digitization of the position of the EEG electrodes and subject's head shape, it supports multiple modalities and supports multiple file formats, automatically detects well-defined artifacts like eye blinks, heartbeats, it can do Artifact correction and ICA, It Detects bad trials / bad channels. It is also a good platform for Machine Learning implantation (Tadel et al., 2011).

Figure 5. MRI visualization using brainstorm

Figure 6. FFT of the signal

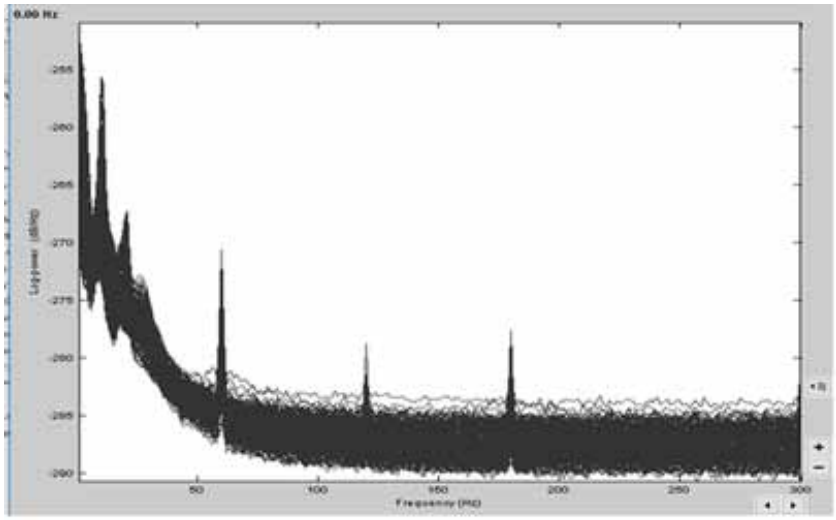

Figure 7. Covariance NxN

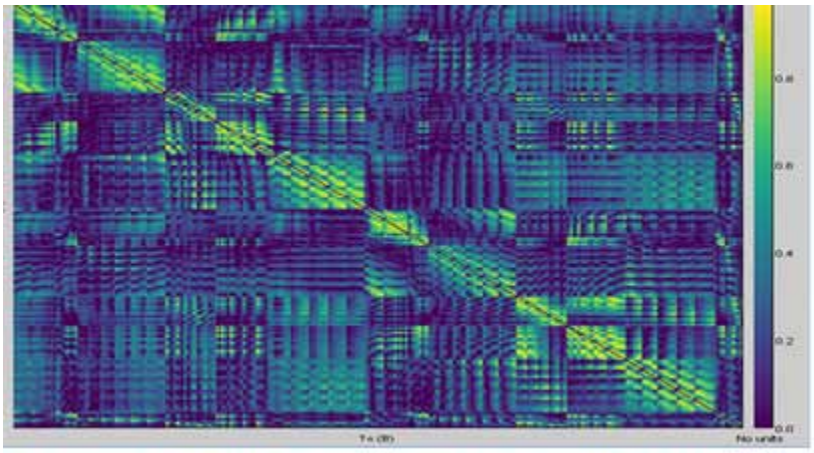

In Figure 5 we can see the MRI of the head using the signals from the epochs, it can be used to easily visualize the data and can tell us about any defects (if exists) in the brain. Figure 6 shows the FFT of the signal which can tell the power of various components at different frequencies and we can select which range of frequency is useful for us and hence help in extracting information. In Figure 7 we can see the covariance matrix of the signal can be used to simplify the signal analysis and is very useful when ML tools such as SVM, LDA are used on it. The brighter spots define the areas with maximum covariance. Brainstorm is a new and very advanced platform for the analysis of brain signals and has various features that are not available in other platforms like EEGLAB, BCILAB, etc.

BCILAB

BCILAB is a MATLAB toolbox and EEGLAB plugin for the design, prototyping, testing, experimentation with, and evaluation of Brain-Computer Interfaces (BCIs), and other systems in the same computational framework. Being a plugin for the EEGLAB toolbox, it has mostly the same features as EEGLAB but has a few extra tools and features which are more directed towards applying various machine learning algorithms on the signal. It has applications for various fields such as Signal Processing, Feature Extraction, Machine Learning, etc. It has a very easy to use GUI and can be used for visualization of signals, Pre-processing of signals for further analysis, etc. (Kothe et al., 2013).

Figure 8. Visualization of model

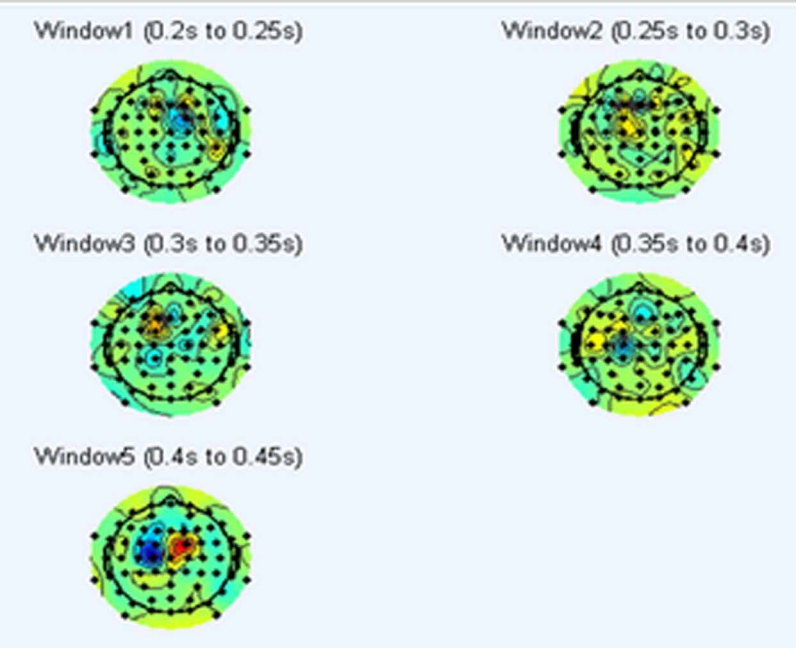

Figure 9. Data summary of model

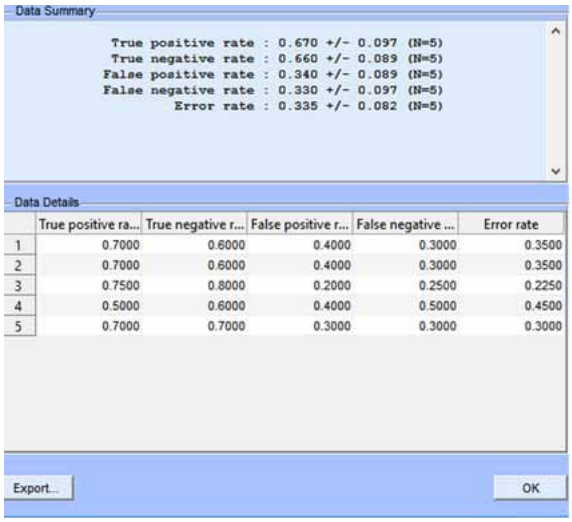

	True positive ra...	True negative r...	False positive r...	False negative ...	Error rate
1	0.7000	0.6000	0.4000	0.3000	0.3500
2	0.7000	0.6000	0.4000	0.3000	0.3500
3	0.7500	0.8000	0.2000	0.2500	0.2250
4	0.5000	0.6000	0.4000	0.5000	0.4500
5	0.7000	0.7000	0.3000	0.3000	0.3000

In Figure 8, we can see the head modelling feature of BCILAB which can be used to find the source of the signal and at which part of the head the signal is being generated. Figure 9 shows the data summary of the BCI model, it tells us about the sensitivity of the model on the basis of its true positive rate

and true negative rate, which is used to measure the percentage of actual positives of negative which have occurred in the dataset.

BioSig

BioSig is an open-source software library for biomedical signal processing, it is a toolbox for Octave, Matlab, python etc. with powerful data import and export filters, feature extraction algorithms, classification methods, and a powerful viewing and scoring software. It is used for the analysis of bio signals such as the EEG, ECG etc. (Guido et al., 2007). It has various features such as easy and simple methods for data acquisition, efficient artifact processing, and quality control, wide range of functions for feature extraction, optimal classification, graphical modelling, and data visualization for better understanding. It can be paired with a viewer provided by it known as the SigViewer which helps in data scrolling and visual analysis of the EEG/MEG signals (Vidaurre et al., 2011).

Figure 10. Data scrolling using the SigViewer

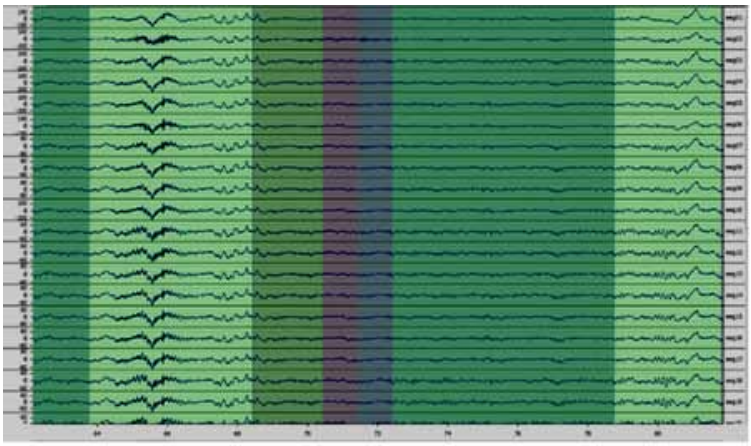

Figure 10, represents the data scrolling feature of the BioSig library, using this we can analyze the signals and select the specific range of frequency that we need.

OpenVIBE

OpenVIBE is a BCI software platform for designing, testing, and analyzing BCI models. The platform contains various tools for creating various BCI models and also contains demo programs to understand the tool. It can run on different operating systems like Linux, UNIX, Windows, and Mac OS X. The software is available online for free and it can be downloaded from the official page of Open Vibe. It can be run easily on various other platforms like Spyder (Python) and MATLAB. It uses visualization techniques to construct the model and hence is easy for designing a paradigm for BCI, it is available for offline analysis and many different operations such as ICA, PSD, and classification, etc. can be easily done without the use of codes (Arrouet et al., 2005).

Figure 11. Graphical commands

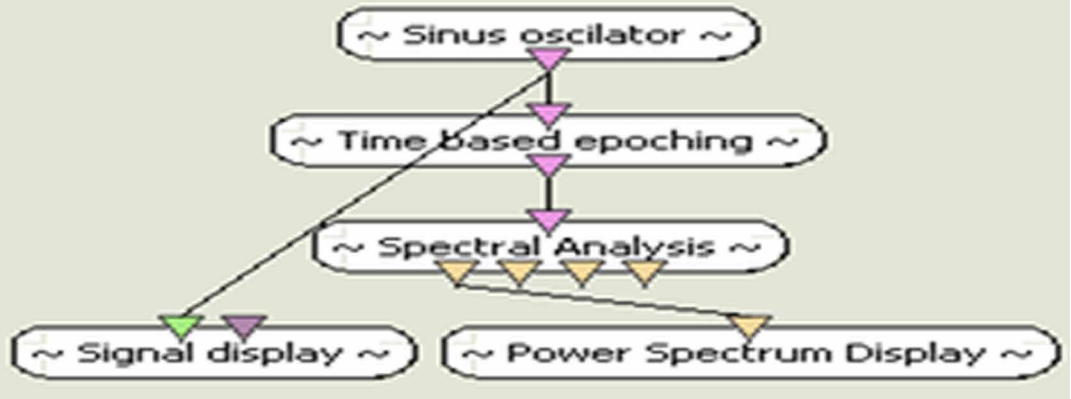

Figure 12. Signal display

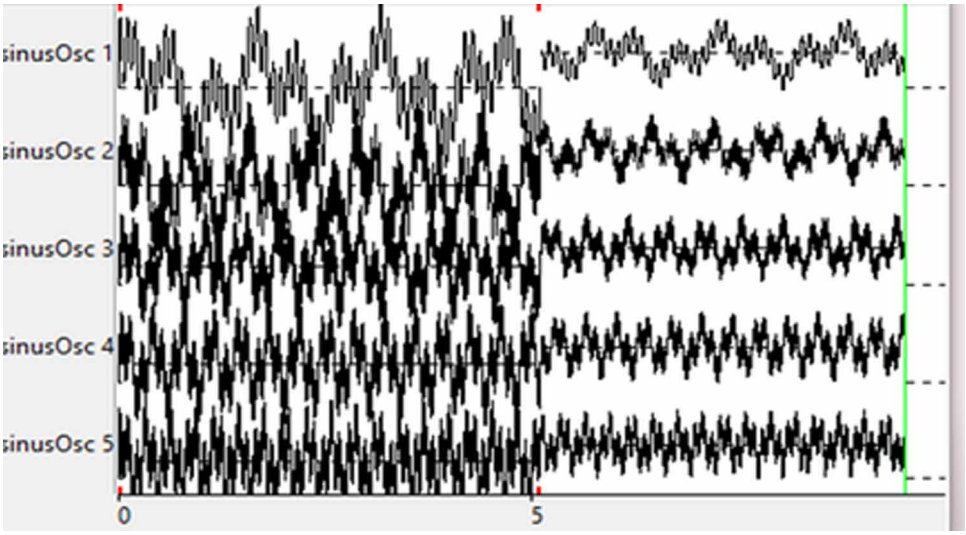

Figure 13. Power spectral display

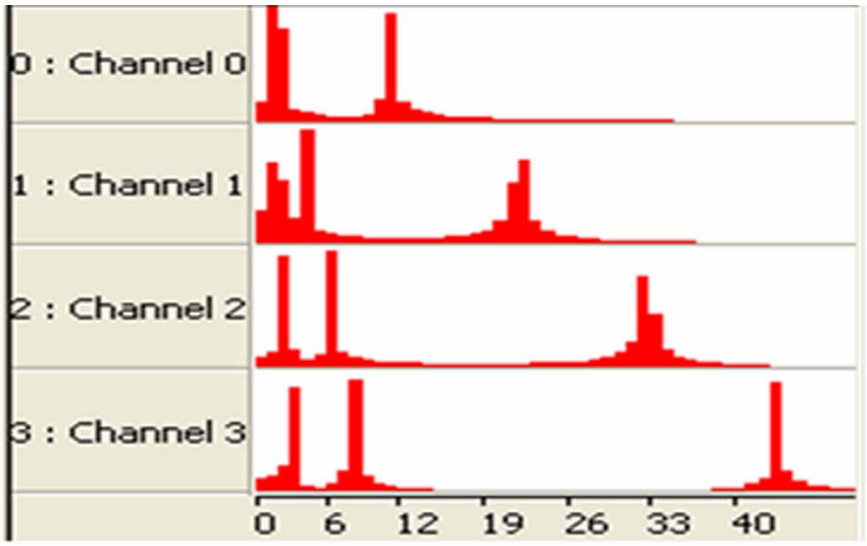

In Figure 11 it is shown how we can use the flowchart/graphical commands method to construct a model for analysis. The various boxes represent the functions and operations to be done on the signals used. Figure 12 shows the signal display function; in this we have displayed the sinus oscillator signals which were available on the GUI. We can easily scroll through the signal and zoom in or zoom out for analysis of the signal at a various range of frequencies. Figure 13 shows the output of the power spectral density of the signal and from it, we can infer which range of frequency of the given signals is of the most useful for us and can be used for further analysis (Congedo et al., 2011).

PsychoPy

PsychoPy is an open-source software package written in the Python programming language primarily for use in neuroscience and experimental psychology research. It is a BCI Designing tool used to design Stimuli for recording brain signals. It is easily available on the internet at its official website and is compatible with Windows as well as Linux. It has a user-friendly GUI and makes it easy to design a stimulus for conducting various experiments. The designer of the experiment can easily insert various media like sounds, images, etc. at various intervals to design a stimulus for generation of a specific brain signal (Bertamini et al. 2018).

Figure 14. Different components of the stimulus

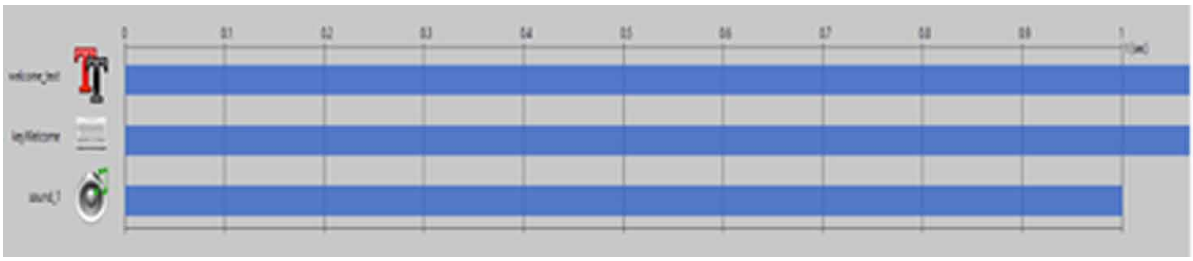

Figure 15. Flowchart for the experiment

In Figure 14 we can see that various component such as sound, text etc. have been added at various different intervals to construct the stimulus. In Figure 15 the flowchart of the experiment can be seen, which tells us how the experiment will proceed (Bertamini et al., 2018). PsychoPy is a very useful tool for designing various experiments for generation of a specific brain signals and is very use friendly as well as easy to use.

BCI2000

BCI2000 is a software suite for brain-computer interface research. It is commonly used for data acquisition, stimulus presentation, and brain monitoring applications. BCI2000 supports a variety of data acquisition systems, brain signals, and study/feedback paradigms. BCI2000 has been written in C++. BCI2000 provides support for writing online signal processing code in MATLAB, and includes an entire layer of Python compatibility. It is compatible in Windows and Mac OS X, though it is currently fully tested and supported on Windows only (Schalk et al., 2009 & Schalk et al., 2004).

BCI++

BCI++ is a software platform that can be used to create prototypes for BCI applications. It is divided into two main modules that communicate through TCP/IP protocol. The first module is HIM (Hardware interface Module) it is used for signal acquisition and visualization, another module is the GUI module which can be used for application-based BCI Modules such as Home Automation interface, etc. HIM and GUI are connected through socket-based TCP/IP Communication (Perego et al., 2009). It is not available for free download and is not provided for public use. It requires various EEG Hardwares and is used solely for Clinical Research.

BF++

The Body Language Framework is a collection of software modules, libraries and tools for the analysis and implementation of BCI modules. It is divided into two main modules,1) NPX LabSuite - used for reviewing, editing, analysis of various brain signals and for performing different functions like filtering etc. on them. (2) BF++ Toys - a group of small applications which are designed for the evaluation, simulation and optimization of BCI modules (Bianchi et al., 2003).

Figure 16. Alphabet builder in the BF++ toys

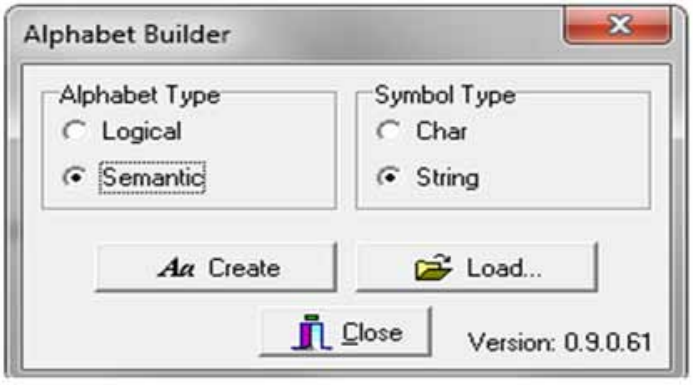

Figure 17. Common spatial pattern maps

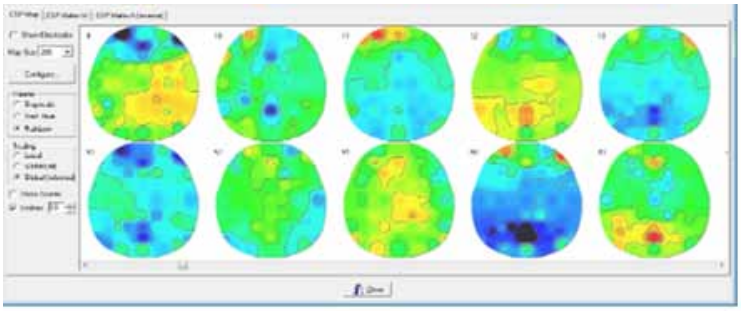

In Figure 16, we can see an alphabet builder BF++ Toy, which allows us to create logical and semantic alphabets for BCI applications. In Figure 17, we can observe a Common Spatial Patter Map, made with the Common Spatial Pattern filter, and can be used as a Feature extraction method for a BCI model.

PyEEG

PyEEG is a Python module which is used to extract EEG features from the brain signals. It uses the standard Python and NumPy data structures. It contains various functions which can be used to calculate parameters like, entropy, Power using FFT, Detrended Fluctuation Analysis, Hjorth Fractal Dimension, and Fisher's information etc., of the signal. (Bao et al., 2011 & Thara et al., 2019) Function like pyeeg. dfa(*X*, *Ave=None*, *L=None*) is used to find the detrended fluctuation analysis of a brain signal. The required parameters are the time series (X) and length of boxes (L). It returns the value of Alpha, which is the slope of the fitting line in the DFA value. The value of alpha should be around 0.5. The value of alpha is directly proportional to the complexity of the signal

Figure 18. Input

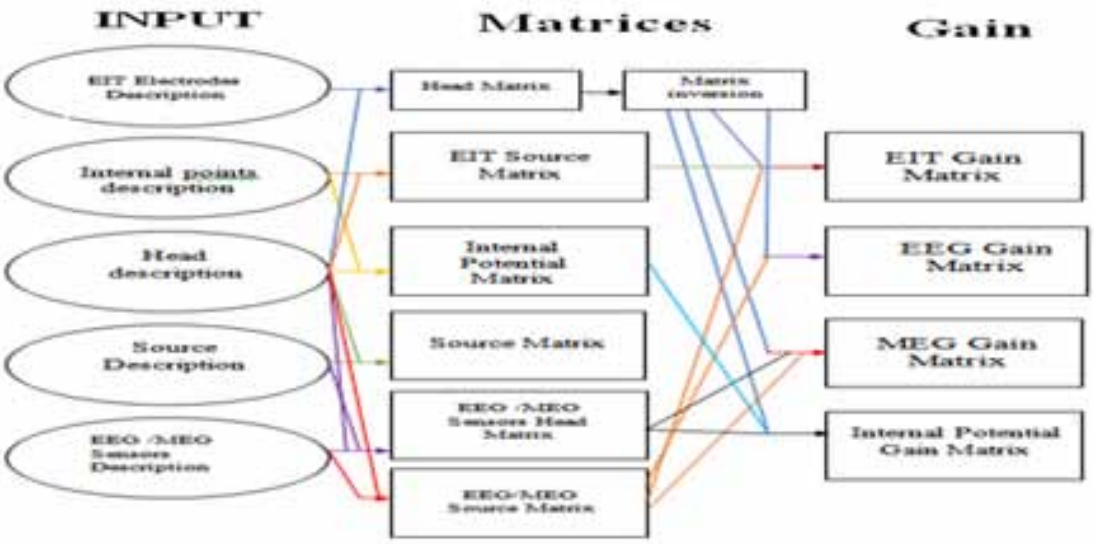

Figure 19. Output

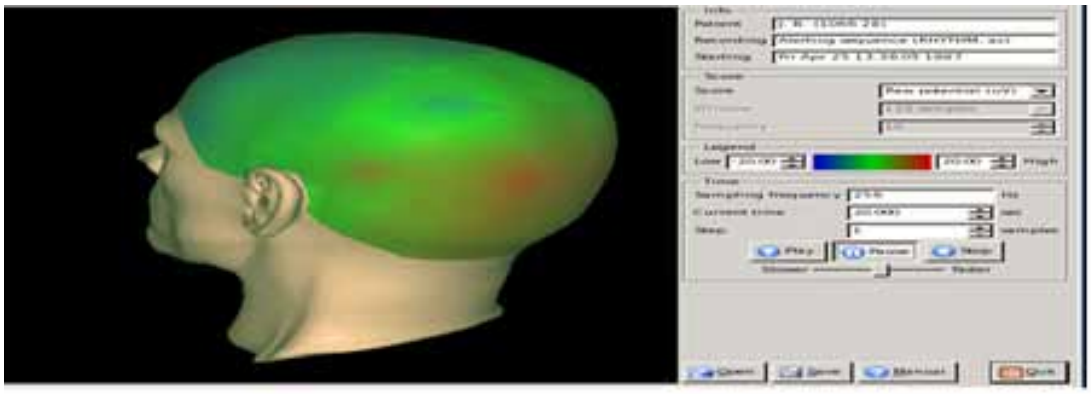

In the above images, we have given imported the PyEEG module from the python library and used it to find the Detrended Fluctuation Analysis of a random signal The required parameters are the time series (X) and length of boxes (L). It returns the value of Alpha, which is the slope of the fitting line in the DFA value. The value of alpha should be around 0.5. The value of alpha is directly proportional to the complexity of the signal.

Open MEEG

OpenMEEG is an open-source brain signal analyzing and processing tool. OpenMEEG is able to provide lead fields for various different brain signals like: Electroencephalography (EEG), Magnetoencephalography (MEG), Electrical Impedance Tomography (EIT) etc. It can be used from MATLAB using brainstorm, and from Python. It has various features such as Source Modelling; various Geometrical features and supports multiple data formats (Kybic et al., 2005 & Gramfort et al., 2010). Low level pipeline of computing fields in the OpenMEEG can be shown in the Figure below.

Figure 20. Low level pipeline of computing fields in the OpenMEEG

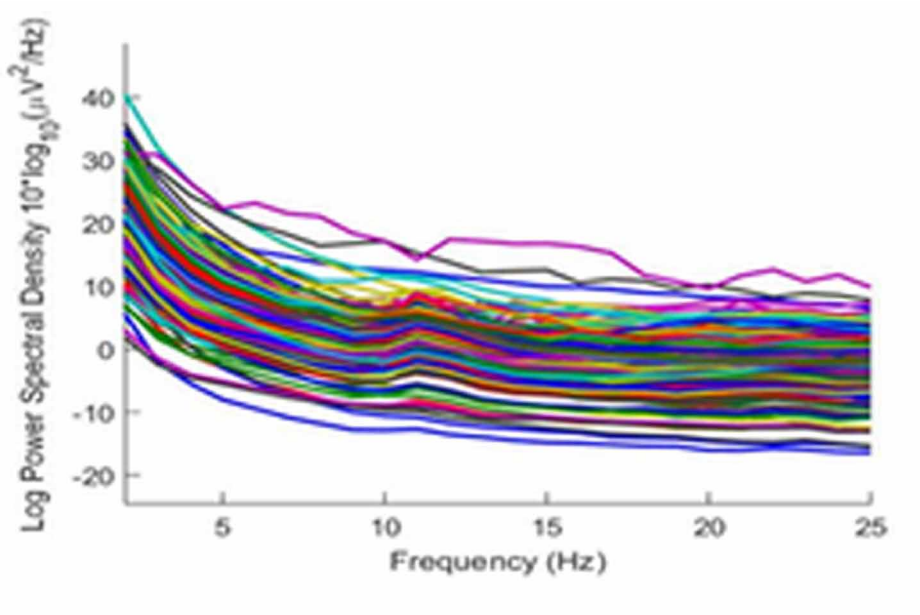

In Figure 20, Low level pipeline of computing fields in the OpenMEEG can be shown.

12. TEMPO is open-source software which is useful for the 3D visualization of the activity in the brain. It used the raw EEG data files and creates topographical maps and animations over the 3-D generated model of the head and user can navigate around it to identify the locations where any sort of brain activity is taking place. These images can be generated as PNG images and can be saved for future observation (Jovanov et al., 1999).

Figure 21. A sample TEMPO modules

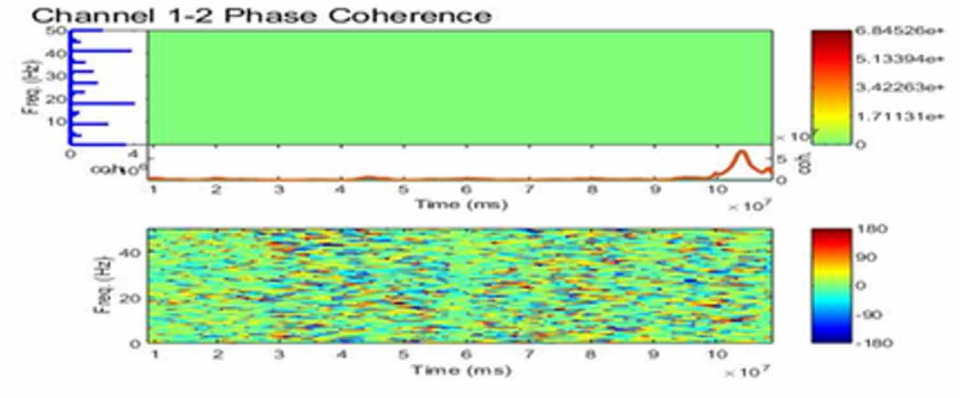

In Figure 21, the 3D Visualization of the brain activity can be seen and we can infer the origin of the signal.

USES OF THE TOOL IN PRACTICAL APPLICATION

The dataset used consists of EEG signals with 256 channels captured from 11 subjects executing a SSVEP-based experimental protocol. Five different frequencies (6.66, 7.50, 8.57, 10.00 and 12.00 Hz) presented in isolation have been used for the visual stimulation. The EGI 300 Geodesic EEG System (GES 300), using a 256-channel HydroCel Geodesic Sensor Net (HCGSN) and a sampling rate of 250 Hz has been used for capturing the signals. This dataset is then imported to MATLAB and then processed so as to later import it as a MATLAB variable in eeglab. We have then found the power Spectral Density of the imported dataset which shows the distribution of frequency in the different channels. Figure 22. Representation of power spectral density of various channels. It can be seen that the PSD is maximum in the frequency range of 2Hz to 15Hz hence the presence of these frequencies is prominent.

Figure 22. Representation of power spectral density of various channels

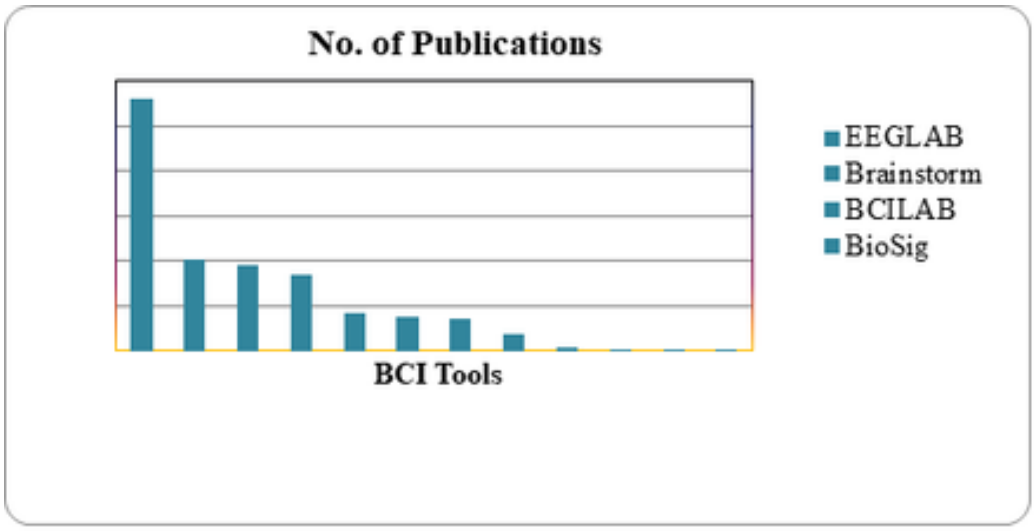

Figure 23. Pictorial diagram of time frequency transform of various channels. To detect transient event-related spectral perturbation, or ERSP, that is event-related shifts in the power spectrum and inter-trial coherence (ITC) in the datasets, Channel time-frequency feature of eeglab is used.

Figure 23. Pictorial diagram of time frequency transform of various channels

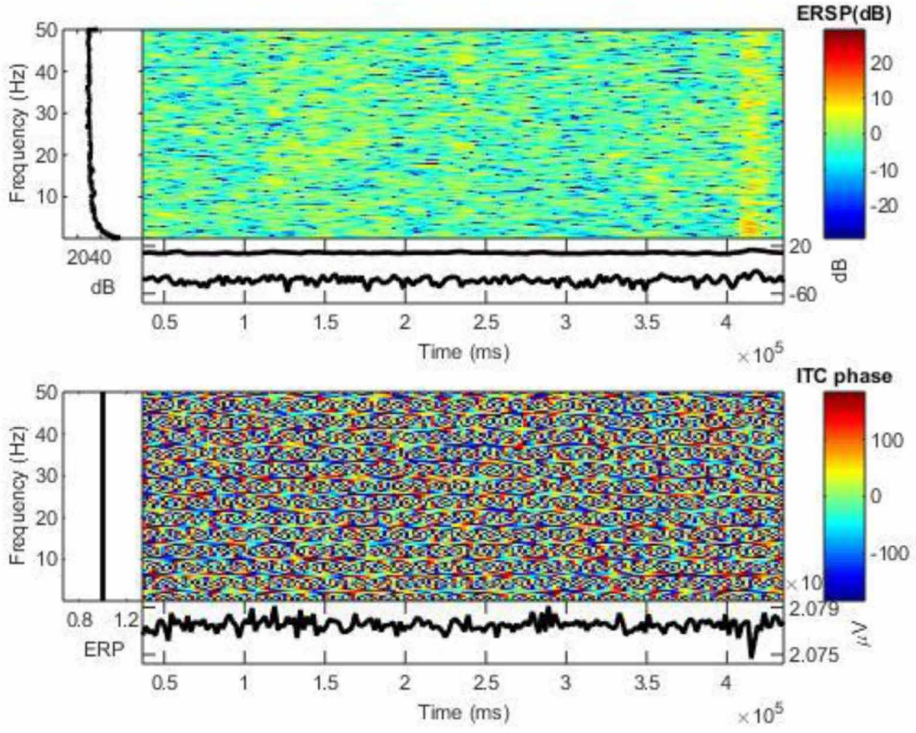

To determine the degree of synchronization between the activations of two channels, we plot their event-related cross-coherence. Figure 24. Channel coherence between channel 1 and channel 2. Even though independent components are (maximally) independent over the whole-time range of the training data, they may become transiently (partially) synchronized in specific frequency bands. We use the channel cross-coherence feature on the dataset.

Figure 24. Channel coherence between channel 1 and channel 2

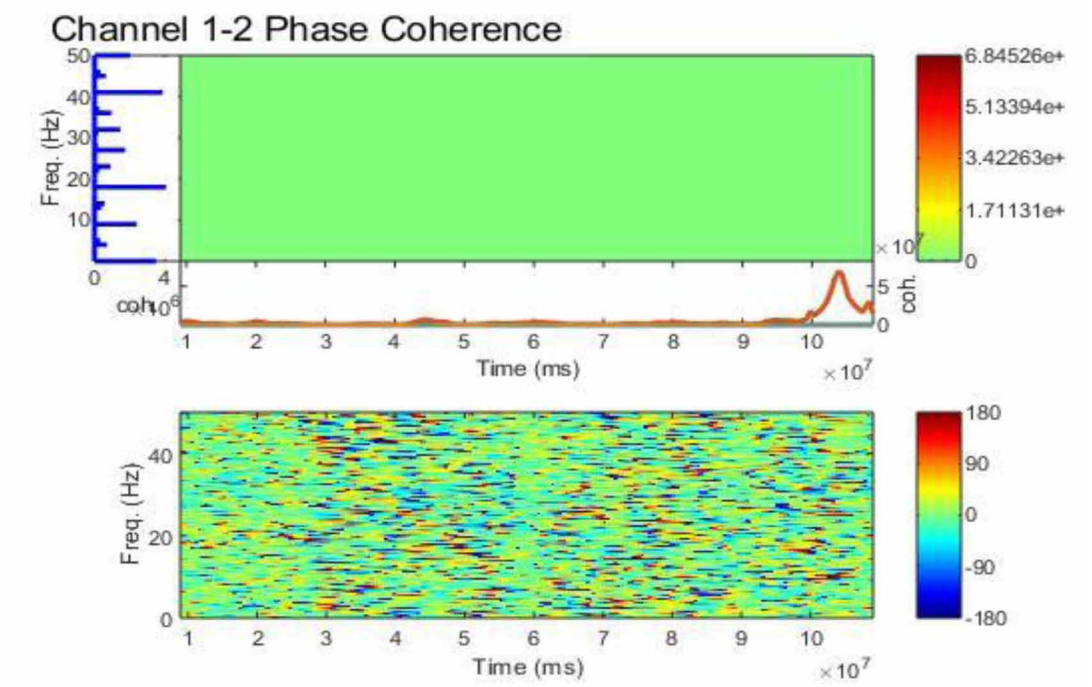

DISCUSSION

Till date many more software has been developed for BCI research and each software has its own advantages and disadvantages, with time some of the software are not as efficient and do not have as many features as other software which was developed much later in time. The following comparison table 3 defines the boundaries between the different software in terms of their features, usability etc.

Table 3. Comparison on different tools and its applications

S. No.	Software	Operating System	Programming Language	Features
1	EEGLAB	Linux, Windows	MATLAB	Easy to use GUI good visualization of signals; Many features such as feature Extraction, filtering etc. are supported Easily available.
2	Brainstorm	Linux, Windows, Mac OS X	MATLAB, Python	Supports multiple modalities and multiple file formats Easy to use GUI Good visualization of signals; Good for Machine Learning implantation due to variety of features. Offline tool for analysis
3	BCILAB	Linux, Windows	MATLAB	Easy to use and readily available Machine Learning Implementation is possible using LDA, SVM etc. Easily Available.
4	BioSig	Linux, Windows, Mac OS X	MATLAB, Python	Features like data acquisition, artifact processing, quality control; feature extraction etc. are available, Classification modelling, and data visualization are possible.
5	OpenVIBE	Linux, Windows	MATLAB, Python	An offline analysis tools. Simplified Implementation of functions like Epoching, Spatial and Temporal filtering; Windowing, Fourier transformations etc.; Supports Classifiers such as LDA, SVM, MLP.
6	PsychoPy	Linux, Windows, Mac OS X	Python	Huge variety of stimuli such as sounds, shapes texts etc.; Automated Monitor Calibration Precise Timing Different types of Interfaces for both coding and drag and drop applications

Continued on following page

Table 3. Continued

S. No.	Software	Operating System	Programming Language	Features
7	BCI2000	Windows	C++	Supports a variety of data acquisition systems, brain signals, and study/ feedback paradigms Contains several tools for data import/conversion Includes tool for timing behavior.
8	BCI++	Linux, Windows, Mac OS X	C++	Modular Structure; High Flexibility; Useful for both in-lab research as well as end-user applications.
9	BF++	Linux, Windows, Mac OS X	Python	Does not depend on any external tools Powerful features for various operations such as ICA, CSP etc. Supports Simulation and optimization.
10	PyEEG	Windows, Linux, Mac OS	Python	Supports various feature extraction methods Can be used to find parameters such as entropy, PSD of signal in specific bands It is a Python module hence is easily programmable.
11	OpenMEEG	Windows, Linux, Mac Os	Matlab, C++, Python	Multiple data formats are supported Various types of brain signals like EEG, MEG etc. can be analyzed
12	TEMPO	Windows, Linux, Mac Os	Standalone Application	3-D Visualization of the model is possible Topographical Maps help in identification of the location where target Signals are being generated.

Hence, different software can be utilized on the basis of the requirement of the user, whichever meets the requirements of the user can be used by him/her. Figure 22. Represent the chart of the number of the publication downloaded with the respect to the tools.

Figure 25. Bar chart depicting no. of publications associated with the EEG tool (Source. Google Scholars)

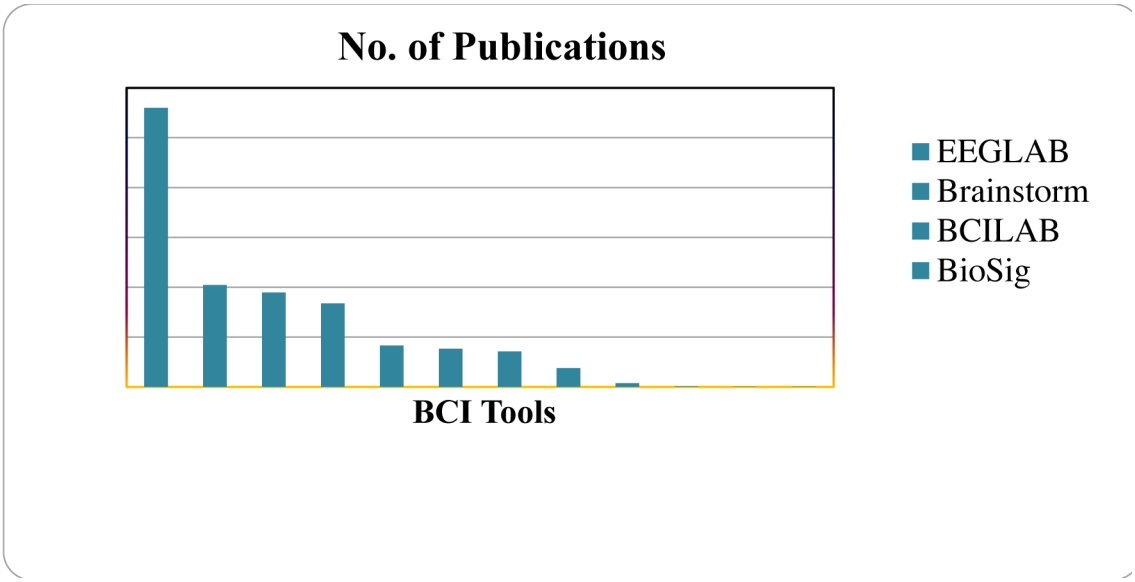

In Figure 25, we have compared the various EEG Tools based on the no. of publications on Google Scholar, which have used the respective tools for realizing their BCI models.

CONCLUSION

BCI is a new field of endless possibilities in terms of research and development, which includes both, software as well as hardware development for BCI. Other than the above-mentioned applications, many other applications also exist which can be used as per the requirement of the user. These applications help us in understanding BCI and how it can be used for our own benefit. The future of BCI depends mainly on the users, industry and research, at present there are several challenges with BCI which are mostly due to the limited technological resources but with advancements in technology in the future, BCI will not just be limited to medical applications, and more day-to-day life activities might involve the use of BCI.

REFERENCES

Alvarado-González, M. (2016). P300 Detection Based on EEG Shape Features. Computational and Mathematical Methods in Medicine.

Arrouët. (2005). Open-ViBE: A Three Dimensional Platform for Real-Time Neuroscience. *Journal of Neurotherapy, 9*, 3-25.

Bao, F. S. (2011). PyEEG: An open source python module for EEG/MEG feature extraction. Computational Intelligence and Neuroscience.

Bertamini, M. (2018). PsychoPy Is Fun. In Programming Visual Illusions for Everyone. Springer.

Bi, L. (2014). A speed and direction-based cursor control system with P300 and SSVEP. *Biomedical Signal Processing and Control*, *14*, 126–133.

Bianchi, L. (2003). Introducing BF++: A C++ framework for cognitive bio-feedback systems design. *Methods of Information in Medicine*, *42*, 104–110.

Birbaumer, N. (1999). Slow cortical potentials: Plasticity, operant control, and behavioral effects. *The Neuroscientist*, *5*, 74–78.

Cheyne, D. O. (2013). MEG studies of sensorimotor rhythms: A review. *Experimental Neurology*, *245*, 27–39.

Congedo. (2011). *"Brain Invaders": A prototype of an open-source P300-based video game working with the OpenViBE platform*. Academic Press.

Cruz, A. (2017). Double ErrP detection for automatic error correction in an ERP-based BCI speller. *IEEE Transactions on Neural Systems and Rehabilitation Engineering*, *26*, 26–36.

Delorme & Makeig. (2014). EEGLAB: An open source toolbox for analysis of single-trial EEG dynamics including independent component analysis. *Journal of Neuroscience Methods, 134*, 9-21.

Delorme, A. (2010). MATLAB-Based Tools for BCI Research. In Brain-Computer Interfaces: Applying our Minds to Human-Computer Interaction. Springer London.

Delorme, A. (2011). EEGLAB, SIFT, NFT, BCILAB, and ERICA: New tools for advanced EEG processing. Computational Intelligence and Neuroscience.

Dornhege. (2010). An introduction to brain-computer interfacing. The Berlin brain–computer interface: non-medical uses of BCI technology. *Frontiers in neuroscience*, *4*, 198. PMID:21165175

Doud, A. J. (2011). Continuous three-dimensional control of a virtual helicopter using a motor imagery based brain-computer interface. *PLoS One*, *6*, e26322.

Elsayed, N. (2017). Brain computer interface: EEG signal preprocessing issues and solutions. *International Journal of Computers and Applications*, *169*, 12–16.

Galambos, R. (1981). A 40-Hz auditory potential recorded from the human scalp. *Proceedings of the National Academy of Sciences of the United States of America*, *78*, 2643–2647.

Gao, X. (2003, June). A BCI-based environmental controller for the motion-disabled. *IEEE Transactions on Neural Systems and Rehabilitation Engineering*, *11*, 137–140.

Goel, K. (2014). Home automation using SSVEP & eye-blink detection based brain-computer interface. *2014 IEEE International Conference on Systems, Man, and Cybernetics (SMC)*, 4035-4036.

Gramfort, A. (2010). OpenMEEG: Opensource software for quasistatic bioelectromagnetics. *Biomedical Engineering Online*, *9*, 45.

Guido, D. (2007). BioSig: An Open-Source Software Library for BCI Research. In Toward Brain-Computer Interfacing. MITP.

Hosni, S. M. (2007). Classification of EEG signals using different feature extraction techniques for mental-task BCI. *2007 International Conference on Computer Engineering & Systems*, 220-226.

Jovanov, E. (1999). Perceptualization of biomedical data. An experimental environment for visualization and sonification of brain electrical activity. *IEEE Engineering in Medicine and Biology Magazine*, *18*, 50–55.

Kachenoura, A. (2007). ICA: A potential tool for BCI systems. *IEEE Signal Processing Magazine*, *25*, 57–68.

Kothe, C. A., & Makeig, S. (2013). BCILAB: A platform for brain–computer interface development. *Journal of Neural Engineering*, *10*, 056014.

Krusienski, D. J. (2008). Toward enhanced P300 speller performance. *Journal of Neuroscience Methods*, *167*, 15–21.

Kybic, J. (2005). A common formalism for the Integral formulations of the forward EEG problem. *IEEE Transactions on Medical Imaging*, *24*, 12–28.

Lakshmi. (2014). Survey on EEG signal processing methods. *International Journal of Advanced Research in Computer Science and Software Engineering, 4*.

Li, Y. (2013). A hybrid BCI system combining P300 and SSVEP and its application to wheelchair control. *IEEE Transactions on Biomedical Engineering*, *60*, 3156–3166.

Lin, Z. (2006). Frequency recognition based on canonical correlation analysis for SSVEP-based BCIs. *IEEE Transactions on Biomedical Engineering*, *53*, 2610–2614.

Lotte, F. (2007). A review of classification algorithms for EEG-based brain–computer interfaces. *Journal of Neural Engineering*, *4*, R1.

Makary, M. M., & Kadah, Y. M. (2014). Improving P300 and SCP-based Brain computer interfacing by spectral subtraction denoising. *2nd Middle East Conference on Biomedical Engineering*, 228-231.

Müller, K.-R. (2008). Machine learning for real-time single-trial EEG-analysis: From brain–computer interfacing to mental state monitoring. *Journal of Neuroscience Methods*, *167*, 82–90.

Muller-Putz, G. R., & Pfurtscheller, G. (2007). Control of an electrical prosthesis with an SSVEP-based BCI. *IEEE Transactions on Biomedical Engineering*, *55*, 361–364.

Muller-Putz, G. R., & Pfurtscheller, G. (2008, January). Control of an electrical prosthesis with an SSVEP-based BCI. *IEEE Transactions on Biomedical Engineering*, *55*, 361–364.

Perego, P. (2009). BCI++: A New Framework for Brain Computer Interface Application. SEDE, 37-41.

Regan, D. (1975). Recent advances in electrical recording from the human brain. Nature, 253, 401-407.

Schalk, G. (2004). BCI2000: A general-purpose brain-computer interface (BCI) system. *IEEE Transactions on Biomedical Engineering*, *51*, 1034–1043.

Schalk, G. (2009). Effective brain-computer interfacing using BCI2000. *2009 Annual International Conference of the IEEE Engineering in Medicine and Biology Society*, 5498-5501.

Seo, D. W. (2016). Hybrid reality-based user experience and evaluation of a context-aware smart home. *Computers in Industry*, *76*, 11–23.

Shukla, P. K., Chaurasiya, R. K., & Verma, S. (2020). Single-Channel Region-Based Speller for Controlling Home Appliances. *International Journal of E-Health and Medical Communications*, *11*(4), 65–89. doi:10.4018/IJEHMC.2020100105

Si-Mohammed, H. (2018). Towards BCI-based interfaces for augmented reality: Feasibility, design and evaluation. *IEEE Transactions on Visualization and Computer Graphics*.

Suleiman, A.-B. R., & Fatehi, T. A.-H. (2007). Features extraction techniques of EEG signal for BCI applications. Faculty of Computer and Information Engineering Department College of Electronics Engineering, University of Mosul, Iraq.

Szafir, D. J. (2010). *Non-Invasive BCI Through EEG* (Unpublished Undergraduate Honors Thesis). Boston College.

Tadel, F. (2011). Brainstorm: A User-Friendly Application for MEG/EEG Analysis. Computational Intelligence and Neuroscience.

Thara & Premasudha. (2019). *Electroencephalogram analysis for Automatic Epileptic Seizure detection method using PyEEG*. Academic Press.

Townsend, G. (2010, July). A novel P300-based brain-computer interface stimulus presentation paradigm: Moving beyond rows and columns. *Clinical Neurophysiology*, *121*, 1109–1120.

Vaid, S. (2015). EEG signal analysis for BCI interface: A review. *2015 fifth international conference on advanced computing & communication technologies*, 143-147. 10.1109/ACCT.2015.72

Vidaurre, C. (2011). BioSig: The free and open source software library for biomedical signal processing. Computational Intelligence and Neuroscience.

Wang, Z. (2019). Towards a hybrid BCI gaming paradigm based on motor imagery and SSVEP. *International Journal of Human-Computer Interaction*, *35*, 197–205.

Xu, Q. (2009). Fuzzy support vector machine for classification of EEG signals using wavelet-based features. *Medical Engineering & Physics*, *31*, 858–865.

Yin, E. (2015). A hybrid brain–computer interface based on the fusion of P300 and SSVEP scores. *IEEE Transactions on Neural Systems and Rehabilitation Engineering*, *23*, 693–701.

Zhang, L. (2013). Low-cost circuit design of EEG signal acquisition for the brain-computer interface system. *2013 6th International Conference on Biomedical Engineering and Informatics*, 245-250.

Zhang, X. (2018). *Neutrosophic filters in pseudo-BCI algebras* (Vol. 8). International Journal for Uncertainty Quantification.

Chapter 3
Adaptive Data Analysis Methods for Biomedical Signal Processing Applications

Haroon Yousuf Mir
National Institute of Technology, Srinagar, India

Omkar Singh
National Institute of Technology, Srinagar, India

ABSTRACT

Biomedical signals represent the variation in electric potential due to physiological processes and are recorded through certain types of sensors or electrodes. In practice, the biomedical signals are typically complex and non-stationary. This makes adaptive data-driven techniques a natural choice for processing biomedical signals. Signal processing methods such as the Fourier transform make use of some pre-defined basic functions designed independent of the signal information. Data-driven methods propose such basic functions directly depending on the information content in the signal. The adaptive data analysis methods tend to decompose a signal into individual modes that are present in it, thus separating them from each other. This chapter presents a detailed review of adaptive data analysis techniques including wavelet transform, empirical mode decomposition, empirical wavelet transform, and variational mode decomposition with their applications to biomedical signal analysis.

INTRODUCTION

Physiological processes are complex phenomena and are characterized by certain biomedical signals revealing their nature and performance. Thus the health status of a physiological system can be evaluated through analysis of the corresponding biomedical signal. Manual analysis of biomedical signals has many limitations and is very subjective. The accuracy and reliability of manual diagnostic processes are limited by several factors including the constraint of humans in extracting and detecting certain features from signals. Thus, computer-based processing and analysis of biomedical signals is necessary since

DOI: 10.4018/978-1-6684-3947-0.ch003

it enables quantitative measurements and thus accurate diagnosis can be provided. Biomedical Signal processing techniques employ the mathematical tools for extracting some key features from a recorded signal based on which a clinical decision is made. The biomedical signal processing applications includes various stages. After signal acquisition by sensors/electrodes, the raw data is pre-processed and filtered. This pre-processing is essential because the measured signals often contain some undesirable noise that is combined with relevant signal information. The next step is to extract features from the processed signal that represent the status and condition of physiological system under consideration. The final step is classification and diagnostics in which clinical decisions are made (Rangayyan et al. 2002). Several techniques for processing of biomedical signals are currently available and many more are being developed for effective analysis and processing of signals. The earlier signal processing techniques were limited to standard linear filters and frequency spectrum based processing. Standard linear filters based analysis techniques have limited utility. In real life, the measured biomedical signals are typically more complex in nature and are often composed of different modes. These modes carry worthy information regarding the originating system and must be studied carefully. Due to nonlinear and non-stationary nature of many biomedical signals, adaptive data analysis techniques become a prime choice. The standard Fourier transform is the most widely used mathematical tool in signal processing but is useful for stationary signals only due to prior selection of sinusoidal basis set (Li, et al. 1995). Wavelet transform is an advanced signal processing method but, its performance is limited by choice of mother wavelet (Unser, 1997; Sharma et al. 2010). A fully adaptive data decomposition technique is Empirical mode decomposition (EMD) which tend to break a signal into a several oscillatory functions termed as intrinsic mode functions (IMF's) and has gained a lot attention in bio-medical signal processing (Huang,et al. 1998). The aim of EMD algorithm is to identify the primary components representing the data, where a component roughly corresponds to a signal having a narrow bandwidth in spectral domain. The EMD algorithm is inherently adaptive and because of its data driven characteristics it can be employed for analyzing non-stationary and non linear signals. However, the major concern with EMD is insufficient mathematical background. In reality, it is an experimental approach and is difficult to model due to its inherent non-linearity. Another adaptive and data driven analysis technique is Empirical wavelet transform (EWT). EWT is relatively a new technique and decompose a time series into its various modes using adaptively designed filter banks (Gilles, J. 2013). The EWT technique first computes frequency spectrum of signal followed by its segmentation and then extraction of mode using adaptively designed wavelets. EWT is relatively a new mathematical technique that is still being researched and applications for it are being found. Variational mode decomposition (VMD) is another adaptive method used to break a signal into separate sub-signals (Dragomiretskiy et al 2013). In the next section, these techniques are discussed with their contemporary applications for biomedical signals.

WAVELET THEORY

The Fourier transform is perhaps the most commonly applied mathematical tool for processing of biomedical signals. It provides the frequency information of a function $g(t)$ by converting it from time to frequency domain. The French mathematician Joseph Fourier, in 1807 discovered that a periodic signal satisfying certain conditions, can be written as a weighted linear combination of complex exponential functions or a sum of sine and cosine functions. In 1822, in his book entitled, "The Analytical Theory of Heat" (Fourier, J. 1878), Fourier described that an aperiodic signal can also be written by a weighted

integral of a series of complex exponentials. This integral is called the Fourier transform. Later in 1965, the computationally efficient implementation of FT, termed as fast Fourier transform (FFT) algorithm was developed the FT became even more popular (Cooley et al 1965).

The wavelet transform was first introduced in 1982 by Morlet et al., who utilized it for seismic data processing (Morlet et al. 1982). As compared to the Fourier transform, which uses pre-defined basis functions, many basis functions are available in the wavelet transform. A wavelet function ψ(t) represents a small oscillatory wave, in order to discriminate between different frequencies (Daubechies, I. 1988). The wavelet function forms the basis function and also serves as the window function in wavelet transform. The wavelets are localized in time and frequency and this feature, results in various applications such as signal denoising, signal compression, Detecting features in signals and images. The wavelet transform uses a variable window for signal analysis. Wavelet analysis pertains to use wider window for low frequency content, and narrow window for high frequency content. Thus, for isolating the signal discontinuities, short-duration wavelets are desired, and to obtain detailed frequency analysis; very long basis functions are indeed required. Wavelet transform does not have fixed basis functions like the Fourier transform, rather a family of wavelets is available. Thus wavelet analysis can provide more detailed information than that can be obscured by Fourier analysis. Wavelet theory is therefore a natural choice in biomedical signal processing (Garget al., 2012;Goldberger et al.2000).

J. R. P., & Mittal, A. P. (2012) developed a computationally efficient wrapper-based Wavelet Feature Optimization (WFO) algorithm. The algorithm was developed for the classification of high dimensional EEG signals which may suffer from the curse of dimensionality and sub-optimal feature selection. Their design of the algorithm was based on three phases Feature Transformation, Feature Extraction, and Selecting the optimal subset of the RWE (Relative Wavelet Energy) features. Feature Transformation of the original EEG signals was done by using Discrete Wavelet Transform, Feature Extraction by using the concept of Relative Wavelet Energy (RWE) and finally optimal subset was selected using wrapper approach by them. Goldberger et al. (2000) introduced PhysioNet as a resource to the biomedical research community. Researchers at different universities inaugurated a new resource for the biomedical research community, under the auspices of the National Center for Research Resources of the US National Institutes of Health. This resource, intended to stimulate current research and new investigations in the study of complex biomedical signals, discussed physiotoolkit, PhysioNet and PhysioBank .these all are large collection data in software for viewing, analyzing, and simulating physiologic time series and signals.

Discrete Wavelet Transform

A function *f(t)* can be better described, processed or analyzed if it can be written as a weighted linear summation of some other basic functions $\phi k(t)$

$$f(t) = \sum_{k} a_k \phi_k(t) \tag{2.1}$$

where *k* is an integer index, a_k are expansion coefficients with $\phi k(t)$ compose a set of functions termed as expansion set. If this representation is unique, the collection of functions $\phi k(t)$ is called Ba**sis f**or the signals which can be decomposed so (Burrus, C. S. 1997). If the functions in basis set posses orthogonality (Inner product of two functions in the set is zero) i.e.

$$\left\langle \phi_m(t), \phi_n(t) \right\rangle = \int \phi_m(t)\phi_n(t)dt = 0 \; m \neq n \tag{2.2}$$

In that case, expansion coefficient a_k are computed using the inner product of signal *f(t)* with the basis function.

$$a_k = \int f(t)\phi_k(t)dt \tag{2.3}$$

Equation (2.3) provides a single coefficient using equation (2.1) and the orthogonal property in equation (2.2).

For example, In Fourier series, a periodic function *f(t)* (which satisfies Dirichlet conditions) is decomposed using complex exponentials in the form of equation (2.4)

$$f(t) = \sum_k a_k e^{j\omega_o kt} \tag{2.4}$$

The basis functions are complex exponentials and form an orthogonal set. The expansion coefficients (Fourier series coefficients) are computed using the inner product of function *f(t)* with basis function $e^{-j\omega_o kt}$

$$a_k = \frac{1}{T}\int f(t)e^{-j\omega_o kt}dt \tag{2.5}$$

Wavelet expansion is similar to Fourier series in which a signal *f(t)* is decomposed as a linear weighted summation using basis function which are wavelets. For a wavelet expansion, a two dimensional system is constructed so that equation (2.1) turns into

$$f(t) = \sum_j \sum_k a_{j,k}\psi_{j,k}(t) \tag{2.6}$$

Here *j,k* are integers and $\psi j_{,k}(t)$ are time scaled and shifted wavelets. The collection of coefficients $aj_{,k}$ is defined as (DWT) of f*(t)* and (2.6) is becomes inverse discrete wavelet transform(IDWT).

Whereas in Fourier series, a 1-D signal is mapped to a 1-D set of coefficients, the wavelet system maps a 1-D signal into 2-D set of coefficients. Due to two dimensional representations, wavelet analysis provides a time frequency localization of signal. Fourier series coefficients localize a signal in frequency only and localization in time is given by time domain representation itself. Wavelet analysis provides localization in time and frequency concurrently. In wavelet expansion, all basis functions $\psi j_{,k}(t)$ are computed from a prototype function namely mother wavelet $\psi(t)$ using scaling and translation.

$$\psi_{j,k}(t) = 2^{j/2}\psi(2^j t - k) \; j,k \in z \tag{2.7}$$

The scaling factor $2^{j/2}$ provides constant norm at each scale. Index *k* represents the translation operation which simply shifts position of wavelet on time axis. Index *j* represents scaling operation and as *j* changes, the wavelet is stretched or compressed by a factor of 2^j thus changing the frequency of wavelet. Thus $\psi j_{,k(}t)$ for j=*2, k=1* is obtained from mother wavelet by first compressing it by a factor of 2 and then shifting by 0.25. It is narrow wavelet and slight translation that capture details or high resolution information in signal. Unlike in Fourier series where the basis function is fixed, this is not the case with wavelets. There is family of wavelets which one can use of signal expansion. Due to time –frequency localization of wavelets, they are well suited for transient signals or time changing phenomenon. This property of wavelets ensures transient signals to be denoted with few coefficients which is very interesting for biomedical signal applications. The size of DWT coefficients drops off quickly with j and k for a most of the signals. That is why wavelets are very useful in various signal processing applications including compression and denoising.

The wavelet systems also satisfy multiresolution condition. It means if a set of signals can be represented by a weighted linear combination of ϕ(t–*k)*, then a larger set including the original can be represented by ϕ(2t–*k).* For multi resolution formulation of wavelets system, another function called scaling function is used and a signal is expanded in terms of scaling and wavelet functions. In fact, the scaling function is defined first and then the wavelet is derived from the scaling function.

Let $\upsilon j_{\,b}$e the space of all functions spanned by $\phi_{j,k}(t) = 2^j\phi(2^j t - k)$. Thus any signal f*(*t*)*$\in\upsilon j_{\,c}$an be expressed as $f(t) = \sum_k a_k\phi_k(t)$. For formulation of multi resolution analysis, nesting of spanned spaces is required such that $.....\upsilon_0 \subset \upsilon_1 \subset \upsilon_2 \subset \upsilon_3....$ as illustrated in Figure 1. From the nesting of spaces, it is clear that if ϕ(t*)* is in υ0, it is also in υ1 ($_s$pace spanned by ϕ(2t)) *w*hich means ϕ(t) ca*n* be expressed as linear combination of shifted ϕ(2t)

$$\phi(t) = \sum_n h(n)\sqrt{2}\phi(2t - n), n \in z \qquad (2.8)$$

Where the coefficients h(n*) ar*e called scaling filter coefficients and $\sqrt{2}$ maintains the norm of scaling function with scale of 2. For Haar scaling function ϕ(t)=ϕ(2t)+ϕ*(*2t–1) *wh*ich gives

$$h(0) = \frac{1}{\sqrt{2}},\ h(1) = \frac{1}{\sqrt{2}}$$

Figure 1. Nesting of spaces spanned by scaling functions

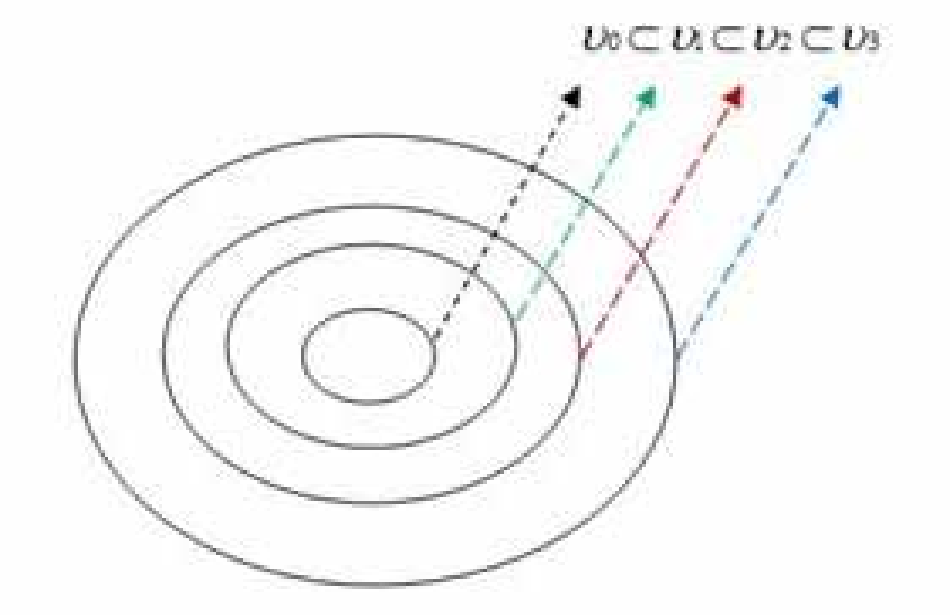

The wavelet functions $\psi_{j,k}(t) = 2^{j}\psi(2^{j}t - k)$ span the differences between spaces spanned by various scales of scaling functions. Thus if $\varphi 0$ is the space spanned by $\psi 0_{,k(t}$) then $\upsilon 1 = \upsilon 0 \oplus \varphi 0$ which extends to $\upsilon 2 = \upsilon 0 \oplus \varphi 0 \oplus \varphi 1$ and so on. Thus we use a single scaling function and rest is taken care by the wavelets. The scale of initial space is arbitrary in scaling function and could be chosen at higher resolution ($j \neq 0$). Since wavelets reside in space spanned by the next scale scaling function, Thus wavelet can also be expressed by linear weighted combination of scaling functions.

$$\psi(t) = \sum_{n} h_1(n)\sqrt{2}\phi(2t - n), n \in z \tag{2.9}$$

Where the coefficients $h_j(n)$ are called wavelet filter coefficients and $\sqrt{2}$ maintains the norm of wavelet function with scale of 2. For haar wavelet, $\phi(t) = \phi(2t) - \phi(2t - 1)$

$$h_1(0) = \frac{1}{\sqrt{2}},\ h_1(1) = -\frac{1}{\sqrt{2}}$$

Thus using scaling and wavelet functions, a function may be decomposed as

$$f(t) = \sum_{k=-\infty}^{\infty} c_{jo}(k)\phi_{jo,k}(t) + \sum_{k=-\infty}^{\infty}\sum_{j=jo}^{\infty} d_j(k)\psi_{j,k}(t) \tag{2.10}$$

Where scaling function is used at any arbitrary scale j_0 (Generally j_0 is set to zero). The coefficients in this expansion are called discrete wavelet transform (DWT) of *f(t).* The scaling function represents the coarse information whereas the wavelets provide the detailed information in the signal.

Finally in DWT, the lower resolution coefficients are computed from higher resolution coefficients using filter banks, and one has never to deal directly with scaling or wavelet function. Only the coefficients (scaling and wavelet filters) and the expansion coefficients *c(k), dj(k)* to be considered.

The scaling coefficients (approximate coefficients) and wavelet coefficients (detailed coefficients) at a scale *j* are computed from scaling coefficients are a scale *j+1* using filter banks.

$$c_j(k) = \sum_m h(m-2k)c_{j+1}(m) \tag{2.11}$$

$$d_j(k) = \sum_m h_1(m-2k)c_{j+1}(m) \tag{2.12}$$

Mathematically, in equation (2.11) the coefficients at scale c_{j+1} are first passed through a filter with time reversed coefficients *h(-n)* and the output is then down sampled by a factor of 2 to provide c_j as shown in figure 2. Likewise c_{j+1} are first passed through a filter with time reversed coefficients $h_1(-n)$ and the output is then down sampled by a factor of 2 to provide d_j. The approximate coefficients at scale *j* (c_j) are further decomposed using the same mechanism to give coefficients (c_{j-1} and d_{j-1}) at scale j-1and so on. The reconstruction of coefficients at scale j is given by

$$c_{j+1}(k) = \sum_m c_j(m)h(k-2m) + \sum_m d_j(m)h_1(k-2m) \tag{2.13}$$

The input coefficients for the first stage are taken samples of signals (above the nyquist rate).

Figure 2. Calculation of low resolution coefficients from high resolution coefficients

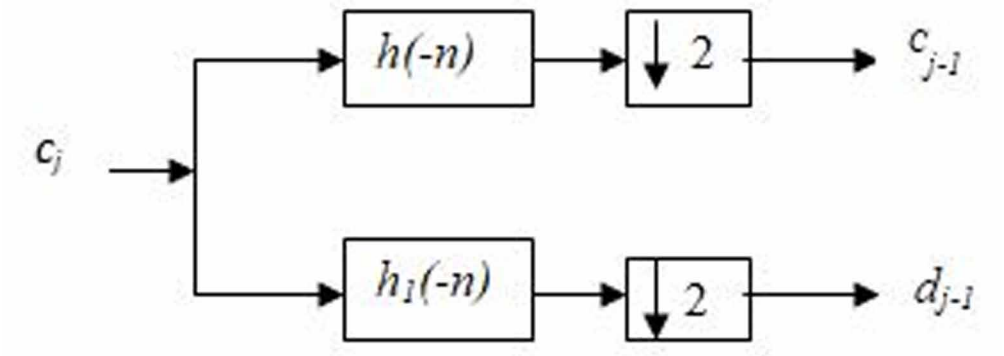

In DWT, the signal is filtered using a combination of and low pass and high pass filters For any given input signal *s* of length *N*, the DWT algorithm can have log2*N* stages. At first stage the input *s*, is

filtered through a low pass filter and high pass filter, followed by down sampling by a factor of 2 thus producing approximation coefficients $a1$, and detail coefficients $d1$ respectively as shown in Figure 3. The operation of low pass filtering is equivalent to the convolution of the signal s with a scaling function ϕ(t), having Fourier spectrum similar to a low pass filter and operation of high pass filtering is equivalent to the convolution of the signal s with a wavelet function ψ(t), having Fourier spectrum similar to a high pass filter. The second stage decomposes the approximation coefficients $a1$ into two bands using the same approach, where *s is replaced* by $a1$ and this stage produces $a2$ and $d2$, as output and so on. So the signal s, analyzed using DWT upto level j has the following structure: [aj, dj, ..., $d1$]. Conversely, the IDWT algorithm starts from aj and dj by up sampling and then convolving the outputs with the reconstruction filters and summing at each stage till start.

Figure 3. Implementation of discrete wavelet transform (DWT)

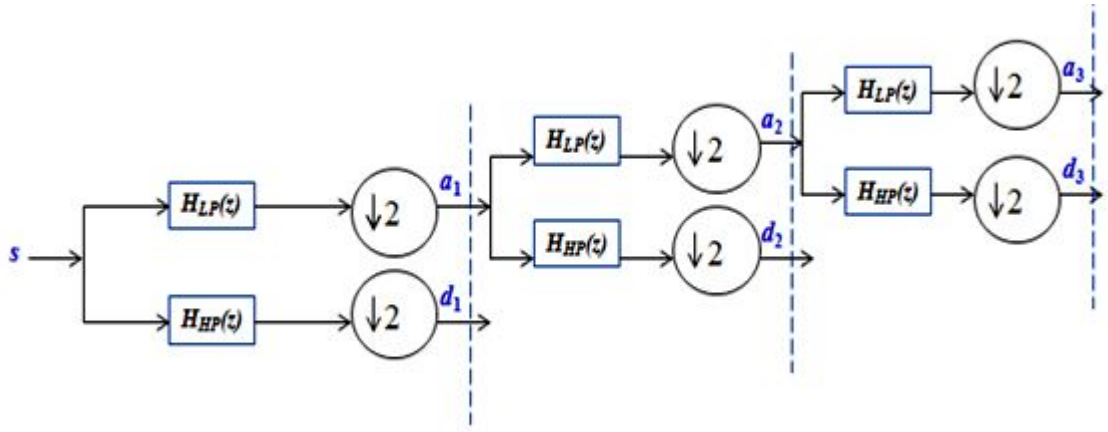

In wavelet based biomedical signal processing applications, the signal is decomposed upto certain levels using a mother wavelet and then detailed coefficients are threshold after which the signal is recovered in time via IDWT using the modified coefficients (Mamun, M., Al-Kadi, M., & Marufuzzaman, M 2013; Rahman et al. 2019 ; Sharmaet al. 2010 ; Poornachandra, S. 2008 ;Gokgoz, E., & Subasi, A. 2015 ; Sharma, S., & Kumar, G. 2012 ;Tunce et al. 2020)

Electroencephalogram (EEG) has been long utilized to diagnose different disorders of the nervous system such as epilepsy, classifying stages of sleep in patients, seizures and brain damage. EEG is the electrical activity recorded from the scalp surface, which is picked up by conductive media and electrodes. Analyzing Electroencephalogram (EEG) signal is a challenge due to the various artifacts they found that present de-noising techniques based on the frequency-selective filtering suffer from a substantial loss of the EEG data and they used wavelets. They found that noise removal using wavelet has the characteristic of preserving signal uniqueness even if noise is going to be minimized. Mamun, et al. (2013) employed discrete wavelet transform to remove noise from EEG signal and Root mean square difference was used to find the usefulness of the noise elimination. They employed four different discrete wavelet functions to remove noise from the Electroencephalogram signal taken from two different types of patients (healthy and epileptic). The result obtained by them showed that the WF orthogonal Meyer was perfect for noise

elimination from the EEG signal of epileptic subjects and the WF Daubechies 8 (db8) was excellent for noise elimination from the EEG signal on healthy subjects.

Rahman et al. (2019) analyzed focal and non-focal EEG signals by using variational mode decomposition (VMD) and discrete wavelet transform (DWT) domain and features such as refined composite multiscale dispersion entropy, refined composite multiscale fuzzy entropy, and autoregressive model (AR) coefficients were extracted by using VMD, DWT and VMD-DWT domain.

Sharma et al. (2010) proposed a novel denoising method based on analysis of higher-order statistics at distinct Wavelet bands for an electrocardiogram (ECG) signal. Higher-order statistics at separate Wavelet bands provide significant information about the statistical nature of the data in the time and frequency domain. The fourth-order cumulant, Kurtosis, and the Energy Contribution Efficiency (ECE) of signal in a Wavelet subband were combined to assess the noise content in the signal.

Poornachandra, S. (2008) study presents a framework for classification of EMG signals using multiscale principal component analysis (MSPCA) for de-noising, discrete wavelet transform (DWT) for feature extraction and decision tree algorithms for classification. These results exhibit that the proposed approach has the capability for the classification of EMG signals with good precision.

Gokgoz, E., & Subasi, A. (2015) introduced a framework for classifying EMG signals using multiscale principal component analysis (MSPCA) for de-noising, discrete wavelet transform (DWT) for feature extraction along with decision tree algorithms for classification. Sharma, S., & Kumar, G. (2012) concludes the usefulness of multiple level wavelet transforms decomposition for EMG feature extraction. The results shown by them prove that it provides better class separability and can be used for machine learning algorithms.

Tuncer et al. (2020) defines a novel ternary pattern and discrete wavelet (TP-DWT) based iterative feature extraction method. By employing the proposed TP-DWT-based feature extraction network, and sEMG (surface electromyography) signal recognition method was introduced. The proposed TP-DWT-based sEMG signal recognition method is comprised of channel concatenation, feature extraction using TP-DWT network, feature selection by using 2 leveled feature selection method and classification using conventional classifiers.

EMPIRICAL MODE DECOMPOSITION

In the previous section, the theory of wavelets was described in brief. Although WT has become a natural choice for many applications in bio-electric signal processing, the performance of WT based methods is somehow affected by the choice of mother wavelet used in the signal analysis. The measured bio-electric signals are generally non –stationary in nature and certain pathologies in physiological systems alter the morphology of these signals. Thus choosing a mother wavelet for a specific signal is a critical task as the wavelet may not be suitable for a wide variety of signals corresponding to same originating system. This makes adaptive data analysis techniques as a natural choice for processing of bio-electric signals. Such an adaptive data analysis technique is the Empirical Mode Decomposition (EMD) proposed by Huang et al. (1998). This technique has gained a lot of attention in signal processing since its inception as method is highly adaptive in nature and separates the stationary and non-stationary components from an original signal. Because of its data driven characteristics, it is being widely used for the processing of non-linear and non-stationary signals. The uniqueness of EMD method is based on the fact that it does not require any prior basis function but is self adaptable depending on the signal being analyzed.

EMD algorithm aims to decompose a signal as a (finite) sum of Intrinsic Mode Functions (IMF) that must satisfy the two conditions: (i) the no of local extrema and the zero crossing must be equal or differ by at most one, (ii) at any point of the time, the mean value of the upper envelope (local maxima) and the lower envelope (local minima) must be zero. Moreover, the EMD method for extracting IMFs is a pure algorithmic approach without any detailed mathematical theory. In order to extract an IMF, the algorithm starts finding maxima and minima of the signal x(t) and then constructs upper envelope u(t) & and lower envelope *l*(t) from detected maxima and minima respectively via cubic spline interpolation. Next the mean *m*(*t*) of the upper and lower envelope is computed and is subtracted from the original signal x(t) to obtain first component $h_1(t)$

$$m(t) = [u(t) + l(t)] / 2 \tag{3.1}$$

$$h_1(t) = x(t) - m(t) \tag{3.2}$$

The component $h_1(t)$ is then subjected to the condition of being an IMF and normally, it does not fulfill the conditions of an IMF. An IMF can be obtained by iterating the same procedure to $h_1(t)$ and the subsequent components. This iterative process of finding the IMF is termed as the sifting process. This sifting process is to be repeated for subsequent $h_k(t)$, the first IMF I1(t), is then retained. The next IMF is computed by the same sifting process applied on $r_1(t) = x(t) - I_1(t)$ where $r_1(t)$ is the residue. Thus after obtaining the first IMF, the residue is treated as original signal and is subjected to same algorithm as mentioned above. This process is further repeated on all subsequent $r_k(t)$, as follows:

$$\begin{aligned} r_1(t) &= I_2(t) + r_2(t) \\ &\vdots \\ r_{N-1}(t) &= I_N(t) + r_N(t) \end{aligned}$$

Finally, the iterative sifting procedure is stopped when the residue, $r_N(t)$, becomes a constant, monotonic function or a function with only one extremum from which no more IMF can be extracted. Thus, the EMD algorithm decomposes a signal *x*(t) into sum of different IMFs and a residue as shown below:

$$x(t) = \sum_{k=1}^{N} I_k(t) + r_N(t) \tag{3.3}$$

Where $I_k(t)$ is the kth IMF and $r_N(t)$ is the final residue. The EMD is being widely used for many applications in biomedical signal including signal enhancement, denoising and feature extraction.

Kabir, M. A., & Shahnaz, C. (2012) introduced a new ECG denoising method builds on noise reduction algorithms in empirical mode decomposition (EMD) and discrete wavelet transform (DWT) domains. they proposed to perform windowing in the EMD domain so that noise can be reduced from the initial IMFs instead of removing them completely thus retaining the QRS complex and allowing a relatively cleaner ECG signal. The signal obtained was transformed in the DWT domain, where an adaptive soft thresholding-based noise reduction algorithm was employed. Kopsinis, Y., & McLaughlin, S. (2009)

used the wavelet thresholding principle in the decomposition modes resulting from applying EMD to a signal. They used principles of hard and soft wavelet thresholding, including translation-invariant denoising, which were appropriately modified to develop denoising methods suitable for thresholding EMD modes. The novel techniques presented by them exhibit an enhanced performance compared to wavelet denoising in the cases where the signal SNR is low and/or the sampling frequency is high.

Krishna, P. K. M., & Ramaswamy, K. (2017) discussed the unsupervised separation of two speakers from single microphone recording using empirical mode decomposition (EMD) and Hilbert transform (HT). A two-stage was done using EMD, HT and instantaneous frequencies. EMD decomposes the mixed signal into oscillatory functions known as intrinsic mode functions (IMFs). Suitable IMFs were selected using successive EMD decomposition and HT was applied to extract the instantaneous frequencies.

Pal, S., & Mitra, M. (2012) proposed Empirical Mode Decomposition (EMD) based ECG signal enhancement and QRS detection algorithm. Being a non-invasive measurement, ECG is prone to various high and low-frequency noises causing baseline wander and power line interference. Here, the first baseline wander was corrected by selective reconstruction-based slope minimization technique from IMFs and then high-frequency noise was removed by eliminating a noisy set of lower order IMFs with a statistical peak correction.

EMPIRICAL WAVELET TRANSFORM

The EMD algorithm tends to break a signal into several components contained in it using a recursive approach. A relative new method for signal decomposition is Empirical Wavelet Transform which builds adaptively designed scaling and wavelet functions to break a signal into constituent components. Empirical wavelet transform is based on design of a wavelet family adapted to the signal. Empirical wavelet transform employs empirical wavelets and scaling function to decompose any given signal into different modes. Based on Fourier theory, the spectrum of a mode has a compact support around a precise frequency and thus design of an adaptive wavelet filter bank relies on detection of frequencies where the information in the spectrum of is located. The adaptability of EWT in reference to a signal relies on segmentation of its Fourier Transform.
The steps in EWT are as follows:

1. Find Fourier Transform (FFT) of signal *s(t),* to get its spectrum *S(ω).* Locate maxima in *S(ω)* along with their related frequencies. Suppose spectra *S(ω)* have *M* maxima with frequencies ω_i, i =1, 2……*M*. Arrange all maxima in descending order.
2. Next, the Fourier spectrum is segmented. If, we choose to split *S(ω)*{0, π} into *N (N ≤ M)* frames, then only (*N-1*) maxima are required (excluding *0* and *π*). The boundary of each frame is made as mod point between two successive maxima. Thus if each frame is represented as $\Lambda_n = [\omega_{n-1,}\ \omega_n]$, then $\bigcup_{n=1}^{N} \Lambda n = [0\ \pi]$. A transition band is created around centre of each ω_n .
3. An adaptively designed filter bank comprising a scaling function and *(N−1)* wavelet functions is created. In Fourier domain, empirical wavelets appear as band pass filters on each Λ_n. The empirical scaling and wavelet functions are given by equation (3.1) and (3.2) respectively (Huang et al. 1998) .

$$\Phi_n(\omega)=\begin{cases}1 & if\ |\omega|\le(1-\gamma)\omega_n \\ \cos\left[\frac{\pi}{2}\beta\left(\frac{1}{2\gamma\omega_n}\left(|\omega|-(1-\gamma)\omega_n\right)\right)\right] & if(1-\gamma)\omega_n\le|\omega|\le(1+\gamma)\omega_n \\ 0 & otherwise\end{cases} \tag{3.1}$$

$$\Psi_n(\omega)=\begin{cases}1 & if\quad(1+\gamma)\omega_n\le|\omega|\le(1-\gamma)\omega_{n+1} \\ \cos\left[\frac{\pi}{2}\beta\left(\frac{1}{2\gamma\omega_{n+1}}\left(|\omega|-(1-\gamma)\omega_{n+1}\right)\right)\right] & if\,(1-\gamma)\omega_{n+1}\le|\omega|\le(1+\gamma)\omega_{n+1} \\ \sin\left[\frac{\pi}{2}\beta\left(\frac{1}{2\gamma\omega_n}\left(|\omega|-(1-\gamma)\omega_n\right)\right)\right] & if\,(1-\gamma)\omega_n\le|\omega|\le(1+\gamma)\omega_n \\ 0 & otherwise\end{cases} \tag{3.2}$$

4. After defining the empirical scaling function and empirical wavelets, the empirical EWT, $W_s(n,t)$ of function $s(t)$ is same like wavelet transform. The iner product of function with empirical wavelets generates detailed coefficients

$$W_s(n,t) = \langle s,\Psi_n\rangle = \int s(\tau)\psi_n(\tau-t)d\tau = f^{-1}\left[(s(\omega)\psi_n(\omega))\right] \tag{3.3}$$

f^1 is inverse fourier transform . The iner product of function with scaling function generates approximte coefficients.

$$W_s(0,t) = \langle s,\Phi_1\rangle = \int s(\tau)\Phi_1(\tau-t)d\tau = f^{-1}\left[(s(\omega)\Phi_1(\omega))\right] \tag{3.4}$$

The reconstructed signal is given by

$$s(t)=w_s(0,t)*\Phi_1(t)+\sum_{n=1}^{N}w_s(n,t)*\Psi_n(t) \tag{3.5}$$

Figure 4 shows the results of applying empirical wavelet transform on a signal which is a superposition of three sinusoidal functions with frequencies (2 Hz, 8 Hz and 16 Hz). The EWT has been used for various applications in biomedical signal processing applications. (Anuragi, A., & Sisodia, D. S. 2020; Singh, O., & Sunkaria, R. K. 2017, 2015; Oung, et al. 2018; Xu et al 2019; He et al 2020)

Anuragi, A., & Sisodia, D. S. (2020) introduced a novel empirical wavelet transform (EWT) based machine learning framework for the classification of alcoholic and normal subjects using EEG signals. In the framework, adaptive filtering was used to draw out Time–Frequency-domain features from Hil-

bert–Huang Transform (HHT). The empirical wavelets transform (EWT) using Hilbert–Huang transforms (HHT) was used to extract the statistical characteristics such as mean, standard deviation, variance, skewness, kurtosis, Shannon entropy, and log entropy from each of the intrinsic mode functions.

Singh, O., & Sunkaria, R. K. (2017) proposed new methods for baseline wander correction and powerline interference contraction in electrocardiogram (ECG) signals was employed by using empirical wavelet transform (EWT). A new approach was used to refine baseline wander and power line interference from the ECG signal. Its performance as a filter was correlated to the standard linear filters and empirical mode decomposition. The results showed that EWT delivers better performance. Singh, O., & Sunkaria, R. K. (2015) presents novel methods for the reduction of powerline interference in ECG signals by applying empirical wavelet transform (EWT) and adaptive filtering.

Oung et al. (2018) proposed a multiclass classification with three classes of PD (Parkinson's disease) severity level (mild, moderate, severe), and healthy control. The focus was to detect and classify PD using signals from wearable motion and audio sensors drew on both empirical wavelet transform (EWT) and empirical wavelet packet transform (EWPT) respectively.

Xu et al. (2019)developed an ECG motion artifact removal approach based on empirical wavelet transform (EWT) and wavelet thresholding (WT) was proposed. Their method consists of five steps, namely, spectrum preprocessing, spectrum segmentation, EWT decomposition, wavelet threshold denoising, and EWT reconstruction. He et al. (2020) present a study for an automated break-up of respiratory and heartbeat signals by using empirical wavelet transform (EWT) for multiple people.

VARIATIONAL MODE DECOMPOSITION

Variational Mode Decomposition (VMD) is a relative new technique which adaptively decomposes a signal into its principal modes. The mode estimations is such that (1) they are able to reconstruct the signal either exactly or in the mean square sense (2) each mode is band-limited around an certain estimated center frequency (Dragomiretskiy et al 2013). InVMD, the mode centre frequencies are initialized and are updated along with the spectrum of modes directly in the Fourier domain. The VMD method is being used by various researchers in biomedical signal analysis (Mert, A. 2016; Liu, et al. 2016; Wu, et al. 2018; Singh, P., & Pradhan, G. 2018; Dora, C., & Biswal, P. K. 2020; Dora, C., & Biswal, P. K. 2020; Ma, Y., & Cao, S. 2019 ; Lahmiri, S. (2014);Wang et al. 2017**;** Kaur et al. 2021). The algorithm of VMD is described here.
If we tend to split a signal into "K" modes, the VMD has following steps:

VMD algorithm:

1. Find the unilateral spectrum ($\hat{f}$) of signal *f(t)* using Hilbert transform
2. Initialize ($\hat{u}^{1}{}_{k}, \hat{\omega}_k^1, \hat{\lambda}^1$)

Where $\hat{u}_k^1$ is the Fourier transform of kth mode u_k. Initially all u_k for k=0, 1……..K are set to zeros. $\hat{\omega}_k^1$ are the initial estimated frequencies which are generally uniformly distributed between {0 0.5}. Thus if we decompose a signal into K=3 modes, $\hat{\omega}_k^1$ = {0,0.33.0.66}.The frequencies and modes are updates with each iteration subsequently in next step.

3. Update $\hat{u}_k$ for all $\omega \geq 0$

$$\hat{u}_k^{n+1} = \left(\hat{f} - \sum_{i \neq k} \hat{u}_i + \frac{\hat{\lambda}}{2}\right) \frac{1}{1 + 2\alpha(\omega - \omega_k)^2}$$

4. Update ωk

$$\omega_k^{n+1} = \frac{\int_0^\infty \omega \left|\hat{u}_k(\omega)\right|^2 d\omega}{\int_0^\infty \left|\hat{u}_k(\omega)\right|^2 d\omega}$$

5. Update λ:

$$\hat{\lambda}^{n+1} = \hat{\lambda}^n + \tau\left(\hat{f} - \sum_k \hat{u}_k{}^{n+1} \right)$$

6. For a given discrimination accuracy $\varepsilon > 0$, if

$$\sum_k \left\|\hat{u}_k^{n+1} - \hat{u}_k^n\right\|_2^2 / \left\|\hat{u}_k^n\right\|_2^2 < \varepsilon$$

Stop the iteration. Otherwise, return to step (2).

Figure 5 shows the spectrum of signal and figure 6 shows the convergence of mode frequencies with iterations. Finally in Figure 7, the original signal and extracted modes are represented in Mert, A. (2016) obtained the bandwidth properties of the modes by using variational mode decomposition (VMD) is used to classify arrhythmia electrocardiogram (ECG) beats. VMD is an enhanced version of the empirical mode decomposition (EMD) algorithm for analyzing non-linear and non-stationary signals. It decomposes the signal into a set of band-limited oscillations called modes. Liu, et al. (2016) proposed a novel signal denoising method that combines variational mode decomposition (VMD) and detrended fluctuation analysis (DFA), named DFA–VMD. The noisy signal was first broken down into a given number K band-limited intrinsic mode functions (BLIMFs) by VMD. Singh, P., & Pradhan, G. (2018). introduced a novel electrocardiogram (ECG) denoising approach based on variational mode decomposition (VMD). Their work also incorporates the efficacy of the non-local means (NLM) estimation and the discrete wavelet transform (DWT) filtering technique.

Figure 4. An example of empirical wavelet transform

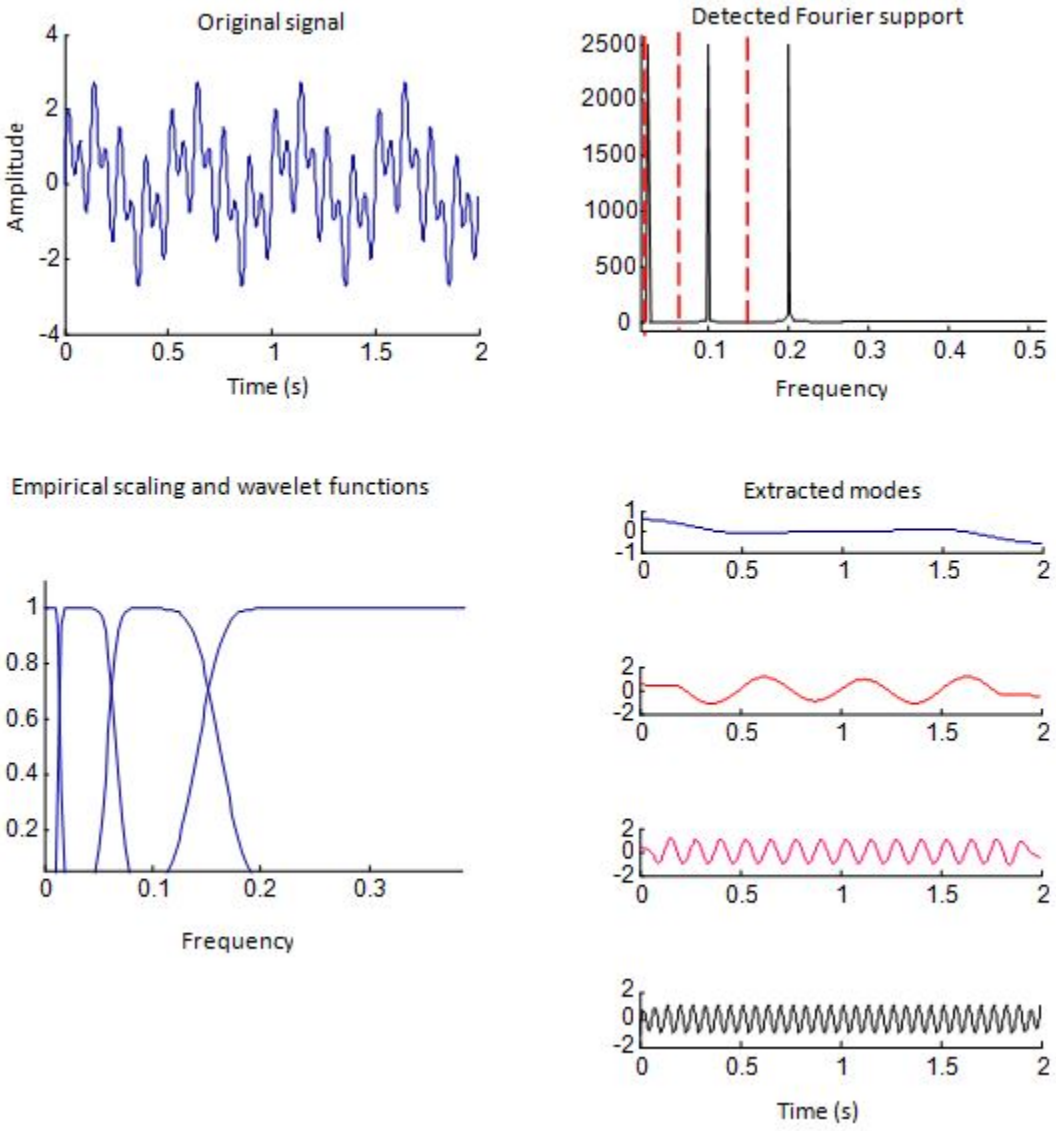

Figure 5. Spectrum of signal (a) in terms of Hz (b) in terms of radians/sample

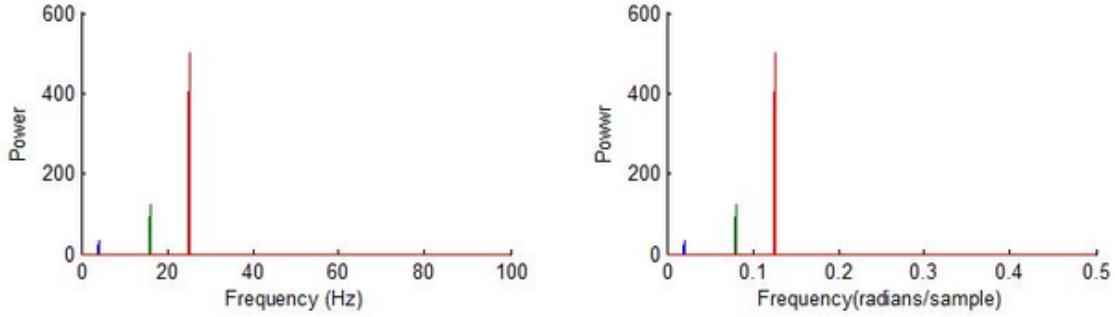

Figure 6. Estimation of centre frequencies

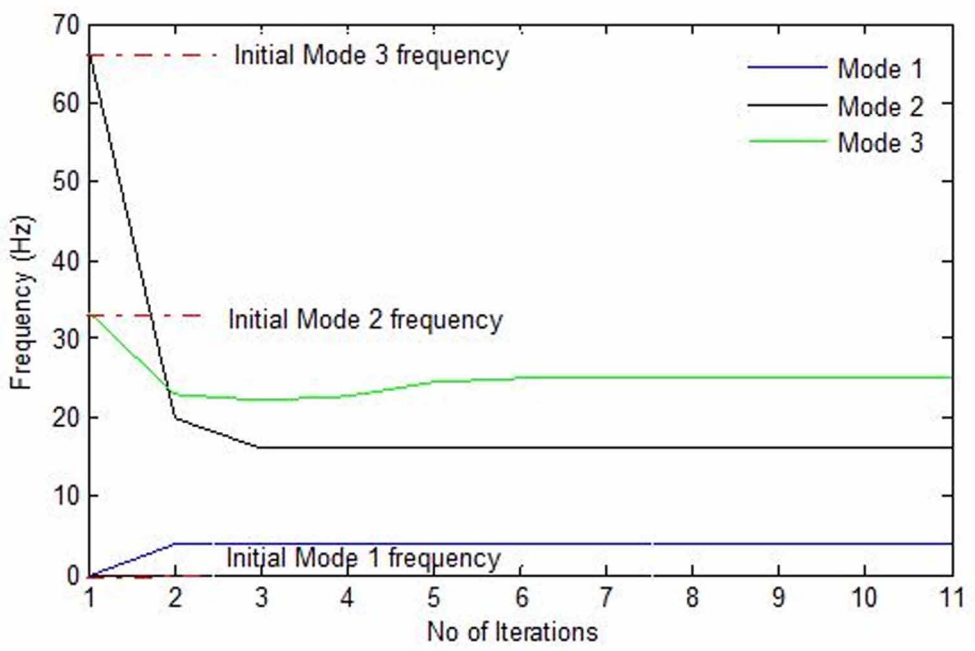

Figure 7. (a) Original signal (b) 1st mode (Original and reconstructed) (c) 2nd mode (Original and reconstructed) (d) 3rd mode (Original and reconstructed)

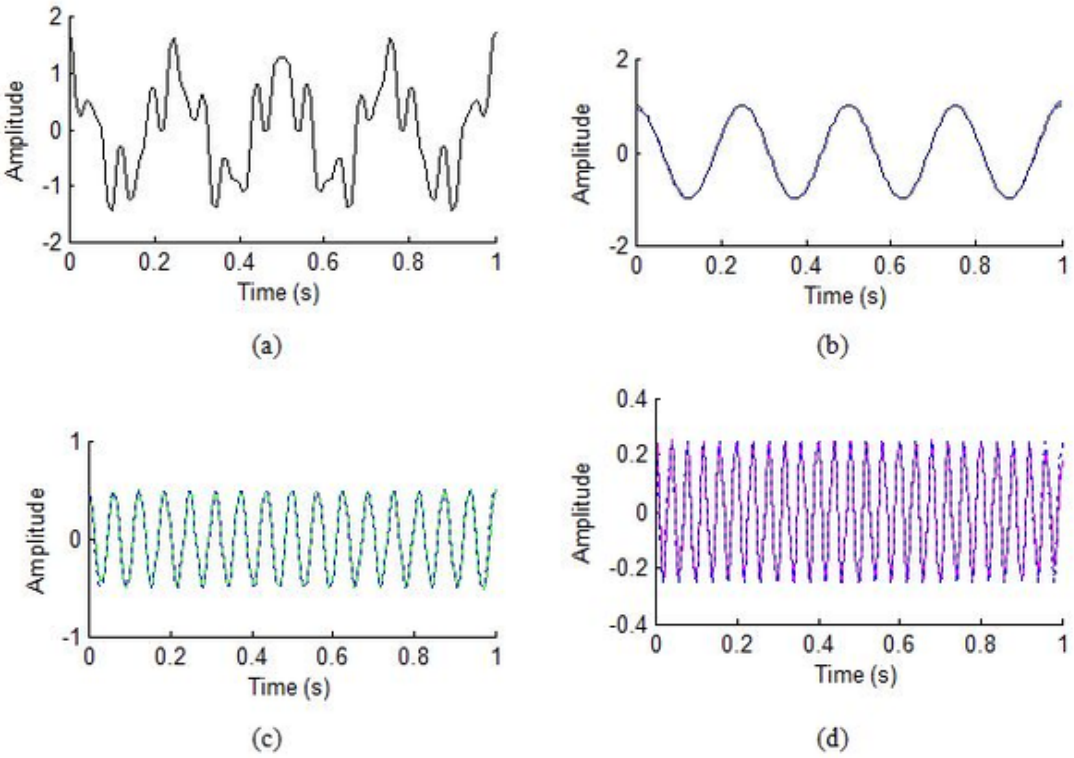

CONCLUSION

This chapter presented a review of several adaptive data analysis techniques with their applications in biomedical signal processing. The wavelet theory was discussed in detail followed by several new methods such as Empirical wavelet transform and Variational mode decomposition. These are relative new techniques in signal processing for decomposing a signal into various components and are still being researched. The reader can further explore the applications of these methods in various filed of biomedical signal and image processing including detection of event, estimation of clinical parameters, denoising and compression.

REFERENCES

Rangayyan, R. M., & Reddy, N. P. (2002). Biomedical signal analysis: A case-study approach. *Annals of Biomedical Engineering*, *30*(7), 983–983. doi:10.1114/1.1509766

Li, C., Zheng, C., & Tai, C. (1995). Detection of ECG characteristic points using wavelet transforms. *IEEE Transactions on Biomedical Engineering*, *42*(1), 21–28. doi:10.1109/10.362922 PMID:7851927

Unser, M. A. (1997, October). Ten good reasons for using spline wavelets. In *Wavelet Applications in Signal and Image Processing V* (Vol. 3169, pp. 422–431). International Society for Optics and Photonics. doi:10.1117/12.292801

Sharma, L. N., Dandapat, S., & Mahanta, A. (2010). ECG signal denoising using higher order statistics in Wavelet subbands. *Biomedical Signal Processing and Control*, *5*(3), 214–222. doi:10.1016/j.bspc.2010.03.003

Huang, N. E., Shen, Z., Long, S. R., Wu, M. C., Shih, H. H., Zheng, Q., . . . Liu, H. H. (1998). The empirical mode decomposition and the Hilbert spectrum for nonlinear and non-stationary time series analysis. *Proceedings of the Royal Society of London. Series A: Mathematical, Physical and Engineering Sciences, 454*(1971), 903-995. 10.1098/rspa.1998.0193

Gilles, J. (2013). Empirical wavelet transform. *IEEE Transactions on Signal Processing*, *61*(16), 3999–4010. doi:10.1109/TSP.2013.2265222

Dragomiretskiy, K., & Zosso, D. (2013). Variational mode decomposition. *IEEE Transactions on Signal Processing*, *62*(3), 531–544. doi:10.1109/TSP.2013.2288675

Fourier, J. (1878). *The analytical theory of heat*. The University Press.

Cooley, J. W., & Tukey, J. W. (1965). An algorithm for the machine calculation of complex Fourier series. *Mathematics of Computation*, *19*(90), 297–301. doi:10.1090/S0025-5718-1965-0178586-1

Morlet, J., Arens, G., Fourgeau, E., & Giard, D. (1982). Wave propagation and sampling theory—Part II: Sampling theory and complex waves. *Geophysics*, *47*(2), 222–236. doi:10.1190/1.1441329

Daubechies, I. (1988). Orthonormal bases of compactly supported wavelets. *Communications on Pure and Applied Mathematics*, *41*(7), 909–996. doi:10.1002/cpa.3160410705

Garg, G., Singh, V., Gupta, J. R. P., & Mittal, A. P. (2012). Wrapper based wavelet feature optimization for EEG signals. *Biomedical Engineering Letters*, *2*(1), 24–37. doi:10.100713534-012-0044-0

Goldberger, A. L., Amaral, L. A., Glass, L., Hausdorff, J. M., Ivanov, P. C., Mark, R. G., ... Stanley, H. E. (2000). PhysioBank, PhysioToolkit, and PhysioNet: Components of a new research resource for complex physiologic signals. *Circulation*, *101*(23), e215–e220.

Burrus, C. S. (1997). *Introduction to wavelets and wavelet transforms: A primer*. Academic Press.

Mamun, M., Al-Kadi, M., & Marufuzzaman, M. (2013). Effectiveness of wavelet denoising on electroencephalogram signals. *Journal of Applied Research and Technology*, *11*(1), 156–160. doi:10.1016/S1665-6423(13)71524-4

Rahman, M. M., Bhuiyan, M. I. H., & Das, A. B. (2019). Classification of focal and non-focal EEG signals in VMD-DWT domain using ensemble stacking. *Biomedical Signal Processing and Control*, *50*, 72–82. doi:10.1016/j.bspc.2019.01.012

Sharma, L. N., Dandapat, S., & Mahanta, A. (2010). ECG signal denoising using higher order statistics in Wavelet subbands. *Biomedical Signal Processing and Control*, *5*(3), 214–222. doi:10.1016/j.bspc.2010.03.003

Poornachandra, S. (2008). Wavelet-based denoising using subband dependent threshold for ECG signals. *Digital Signal Processing*, *18*(1), 49–55. doi:10.1016/j.dsp.2007.09.006

Gokgoz, E., & Subasi, A. (2015). Comparison of decision tree algorithms for EMG signal classification using DWT. *Biomedical Signal Processing and Control*, *18*, 138–144. doi:10.1016/j.bspc.2014.12.005

Sharma, S., & Kumar, G. (2012). Wavelet analysis based feature extraction for pattern classification from Single channel acquired EMG signal. *Elixir Online Journal, 50*, 320-1.

Tuncer, T., Dogan, S., & Subasi, A. (2020). Surface EMG signal classification using ternary pattern and discrete wavelet transform based feature extraction for hand movement recognition. *Biomedical Signal Processing and Control*, *58*, 101872. doi:10.1016/j.bspc.2020.101872

Kabir, M. A., & Shahnaz, C. (2012). Denoising of ECG signals based on noise reduction algorithms in EMD and wavelet domains. *Biomedical Signal Processing and Control*, *7*(5), 481–489. doi:10.1016/j.bspc.2011.11.003

Kopsinis, Y., & McLaughlin, S. (2009). Development of EMD-based denoising methods inspired by wavelet thresholding. *IEEE Transactions on Signal Processing*, *57*(4), 1351–1362. doi:10.1109/TSP.2009.2013885

Krishna, P. K. M., & Ramaswamy, K. (2017). Single channel speech separation based on empirical mode decomposition and Hilbert transform. *IET Signal Processing*, *11*(5), 579–586. doi:10.1049/iet-spr.2016.0450

Pal, S., & Mitra, M. (2012). Empirical mode decomposition based ECG enhancement and QRS detection. *Computers in Biology and Medicine*, *42*(1), 83–92. doi:10.1016/j.compbiomed.2011.10.012 PMID:22119222

Anuragi, A., & Sisodia, D. S. (2020). Empirical wavelet transform based automated alcoholism detecting using EEG signal features. *Biomedical Signal Processing and Control*, *57*, 101777.

Singh, O., & Sunkaria, R. K. (2017). ECG signal denoising via empirical wavelet transform. *Australasian Physical & Engineering Sciences in Medicine*, *40*(1), 219–229.

Singh, O., & Sunkaria, R. K. (2015). Powerline interference reduction in ECG signals using empirical wavelet transform and adaptive filtering. *Journal of Medical Engineering & Technology*, *39*(1), 60–68.

Oung, Q. W., Muthusamy, H., Basah, S. N., Lee, H., & Vijean, V. (2018). Empirical wavelet transform based features for classification of Parkinson's disease severity. *Journal of Medical Systems*, *42*(2), 1–17.

Xu, X., Liang, Y., He, P., & Yang, J. (2019). Adaptive motion artifact reduction based on empirical wavelet transform and wavelet thresholding for the non-contact ECG monitoring systems. *Sensors (Basel)*, *19*(13), 2916.

He, M., Nian, Y., Xu, L., Qiao, L., & Wang, W. (2020). Adaptive separation of respiratory and heartbeat signals among multiple people based on empirical wavelet transform using uwb radar. *Sensors (Basel)*, *20*(17), 4913.

Mert, A. (2016). ECG feature extraction based on the bandwidth properties of variational mode decomposition. *Physiological Measurement*, *37*(4), 530.

Liu, Y., Yang, G., Li, M., & Yin, H. (2016). Variational mode decomposition denoising combined the detrended fluctuation analysis. *Signal Processing*, *125*, 349–364.

Wu, Y., Shen, C., Cao, H., & Che, X. (2018). Improved morphological filter based on variational mode decomposition for MEMS gyroscope de-noising. *Micromachines*, *9*(5), 246.

Singh, P., & Pradhan, G. (2018). Variational mode decomposition based ECG denoising using non-local means and wavelet domain filtering. *Australasian Physical & Engineering Sciences in Medicine*, *41*(4), 891–904.

Dora, C., & Biswal, P. K. (2020). An improved algorithm for efficient ocular artifact suppression from frontal EEG electrodes using VMD. *Biocybernetics and Biomedical Engineering*, *40*(1), 148–161.

Dora, C., & Biswal, P. K. (2020). Correlation-based ECG artifact correction from single channel EEG using modified variational mode decomposition. *Computer Methods and Programs in Biomedicine*, *183*, 105092.

Ma, Y., & Cao, S. (2019). An improved robust threshold for variational mode decomposition based denoising in the frequency-offset domain. *Journal of Seismic Exploration*, *28*(3), 277–305.

Lahmiri, S. (2014). Comparative study of ECG signal denoising by wavelet thresholding in empirical and variational mode decomposition domains. *Healthcare Technology Letters*, *1*(3), 104–109.

Wang, Y., Liu, F., Jiang, Z., He, S., & Mo, Q. (2017). Complex variational mode decomposition for signal processing applications. *Mechanical Systems and Signal Processing*, *86*, 75–85.

Kaur, C., Bisht, A., Singh, P., & Joshi, G. (2021). EEG Signal denoising using hybrid approach of Variational Mode Decomposition and wavelets for depression. *Biomedical Signal Processing and Control*, *65*, 102337.

Chapter 4
A Review for Neuroimaging Techniques in Multimedia Learning: Methodological Framework

Pınar Ozel
Nevsehir Hacı Bektas Veli University, Turkey

Duygu Mutlu Bayraktar
https://orcid.org/0000-0002-2276-3768
Hasan Ali Yucel Faculty of Education, Turkey

Tugba Altan
Faculty of Education, Kahramanmaras Sutcu Imam University, Turkey

Veysel Coskun
Faculty of Education, Hatay Mustafa Kemal University, Turkey

Ali Olamat
Faculty of Engineering, Istanbul University-Cerrahpasa, Turkey

ABSTRACT

This research analyzed neuroimaging techniques for measuring cognitive load in multimedia research using a systematic literature review on all related papers published until April 2020. The most striking observation to emerge from the analysis is that electroencephalography, functional magnetic resonance imaging, functional near-infrared spectroscopy, and transcranial doppler ultrasonography have been the most preferred neuroimaging tools utilized in cognitive load in multimedia learning research. Forty articles were reviewed based on the techniques that should be known in the field of neuroimaging to study cognitive load in multimedia learning, the analysis methods for neuroimaging, the results related to cognitive load in multimedia research. The study's findings were evaluated, and many discrepancies in cognitive load research related to multimedia learning were discovered.

DOI: 10.4018/978-1-6684-3947-0.ch004

INTRODUCTION

Cognitive load theory (CLT) aims to explain the effects of cognitive processing load due to learning tasks during new cognitive processing and information processing in long-term memory (Sweller et al., 2019). The heart of the CLT depends on the necessity of processing information in working memory before being stored in long-term memory in an information processing model (Anmarkrud et al., 2019). But, working memory which processes limited information at a time, limits information processing (Sweller, 2010). For this reason, the instructional design must decrease the unnecessary cognitive load in working memory. Otherwise, if working memory capacity exceeds and cognitive overload occurs, it may cause learning to be obscured (Leppink et al., 2013).

According to CLT, three types of cognitive load affect working memory during learning tasks; intrinsic cognitive load, extraneous cognitive load, and germane cognitive load (Paas & Sweller, 2014, p. 37). Intrinsic cognitive load refers to the inherent difficulty and complexity of every learning task. Extraneous load deals with when the learner has to process unnecessary interactive elements due to inappropriate instructional design. Germane cognitive load refers to the load occurring in working memory by learning, as when relating information between long-term memory and new information construction process. On the other hand, in their recent update of cognitive load theory, Sweller et al. (2011) preferred the term "germane resources'' because, unlike intrinsic and extraneous cognitive load, the germane load is not imposed by nature or structure of the learning material.

Measuring cognitive load is very important to provide guidelines and implications for successful instructional design (Korbach et al., 2017). Because implications for CL research allow determining possibility levels of CL in the early design phase (Paas et al., 2003). CL is measured with two different instruments, subjective measures for CL and objective measures for CL. Neuroimaging is an objective and direct type of measure for CL (Chang et al., 2016; A. Dan & Reiner, 2017; M. Mazher et al., 2017).

In recent years, a range of highly sensitive scanning technologies has been developed for computer imaging researchers to monitor human brain processing. By benefiting from the literature, current brain imaging techniques are grouped into three types:

Structural; Computerized Tomography (CT) (Schlorhaufer et al., 2012), Magnetic Resonance Imaging (MRI) (Juanes et al., 2015)

Functional; Electroencephalography (EEG) (Castro-Meneses et al., 2020), Positron emission tomography (PET) (Ruisoto Palomera et al., 2014), Functional magnetic resonance imaging (fMRI) (C. Liu et al., 2020), Functional near-infrared spectroscopy(fNIRS) (Uysal, 2016), Magnetoencephalography (MEG) (C.-J. Liu & Chiang, 2014), Infrared Thermography (IT) (Jenkins & Brown, 2014), Transcranial Magnetic Stimulation (TMS) (Hilbert et al., 2019) and, Transcranial Doppler Ultrasonography (TCD) (J. J. Loftus et al., 2018).

Metabolic; Magnetic Resonance Spectroscopy (MRS) (Ross & Sachdev, 2004).

Neuroimaging techniques may provide opportunities to measure CL and different types of CL accurately (Whelan, 2007) because fMRI and PET techniques use blood flow to collect data for CL during brain activity (Antonenko et al., 2010). fMRI can be effective in measuring intrinsic CL (Whelan, 2007). An alternative device to fMRI is fNIRS due to its smaller size to measure brain activity while collecting cortical blood flow data (Antonenko et al., 2010). EEG collects data as electrical activity occurs in brain regions (Jan-Louis Kruger & Doherty, 2016). Studies measure extraneous CL with EEG in the literature (e.g., Dan & Reiner, 2017; Örün & Akbulut, 2019).

METHOD

A literature review identifies, selects, and synthesizes the chosen research studies to summarize the research subject based on established research (Oakley, 2012). To answer the research questions, this review uses a systematic examination of the literature. The systematic evaluation process was used in three stages: (1) preparation, (2) performing the review, and (3) reporting the results. The indexes for searching for research studies were chosen during the preparation stage, and the inclusion and exclusion criteria, as well as the categories for study, were specified. Research studies were chosen and explored during the second stage of the study. Data was processed, synthesized, and coded after that. The study results, discussion of observations, tendencies, and conclusions of the evaluation were all recorded in the final stage.

Search Strategy

Following the definition of the study's research questions, the research's parameters, such as general, specific, and exclusive, are decided.

Inclusive Criteria

General Criteria:

- The studies should be published as articles or conference papers.
- The studies should have appeared in the databases Web of Science (WOS), Education Resources Information Center (ERIC), Scopus, and EBSCO.
- Full texts of the studies should be chosen.
- Articles and conference papers should be written in English.

Specific Criteria:

- A multimedia learning environment should be included in the studies.
- Neuroimaging techniques should be used to measure CL in the studies.
- Keywords such as "Multimedia," "Cognitive load," "Multimedia learning," "fMRI," "EEG," "Magnetoencephalography," "MEG," "fNIRS," "TDCS," "Transcranial doppler," "Transcranial electrical stimulation," "Transcranial magnetic stimulation," and "TMS" should be used to search studies.

Exclusive Criteria:

- A review, meta-analysis, or commentary article should not be included in the research. No books, theses, or book chapters should be chosen.

Study Selection Process

The study took place in April 2020, focused on the keywords in chosen databases, which yielded a total of 892 studies. The outcomes of the research were entered into an excel spreadsheet and saved. This list was updated to delete 12 duplicate studies that were indexed in several databases. The list of 880 records was evaluated using inclusive and exclusive criteria. 773 research were ineligible for the research because they did not follow the study's requirements. The remaining 107 research were examined using the research questions as a guide. During this stage, 65 studies that did not satisfy the review criteria were removed from the report, and one study did not have a full text available. As a result, 40 articles were chosen for this comprehensive analysis. There were 23 journal articles and 17 conference papers among these.

Categories for Analysis and Data Coding

Each of the research questions was divided into several categories. The researchers then encoded the study data using these categories before analyzing it. Furthermore, the investigation's findings were discussed under the following research questions:

- RQ1. Which analysis methods are used for neuroimaging data on CL in multimedia learning research?
- RQ2. Which results were acquired in CL in multimedia learning research using neuroimaging methods?

RESULTS

RQ1: Which analysis methods are used for neuroimaging data on CL in multimedia learning research?

All the methods, time, frequency, and time-frequency analysis methods and machine learning methods can be used all together or separately. While signal processing methods are generally used as EEG pre-processing steps and feature extraction methods, more statistical analyzes have been studied in fNIRS, fMRI, and TCD methods. Accordingly, the detailed explanation of the findings we obtained is as follows. The EEG section has been described in detail as there are many more studies on EEG utilization on the issue. Figure 1 shows the classical examination methodology for processing and classifying EEG data.

Analysis Techniques of EEG

1. Pre-processing Step:

Researchers have used different methods to remove noise for the same reasoning. Only components related to brain activity are demanded to retain for further analysis. According to our research, thirty-three EEG-related publications were relevant to our study, but in eleven of these publications, detailed information about pre-processing was not provided in the studies presented in (N. Al Madi & Khan, 2019; Bertolo et al., 2014; Cao et al., 2019; Chang et al., 2016; Crk & Kluthe, 2014; Alex Dan & Reiner, 2017; Díaz et al., 2015; J.-L. Kruger et al., 2014; Lee, 2014; Qayyum, Khan, et al., 2018; Zhang & Liu,

2017). Table 1 summarizes the methods for pre-processing step using EEG signal for neuroimaging data on CL in multimedia learning research.

Figure 1. The classical examination methodology for processing and classifying EEG data

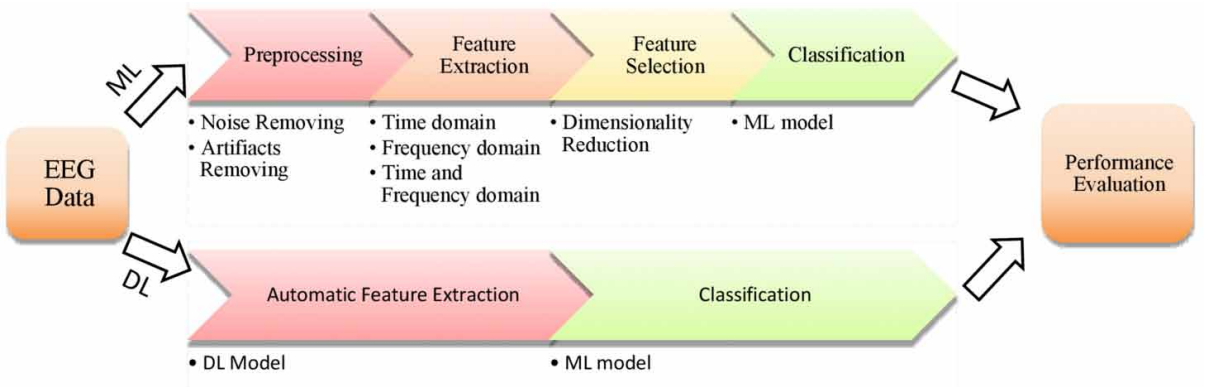

Based on the WinEEG software program for filtering and noise reduction (Alex Dan & Reiner, 2017a) used the independent component analysis (ICA) artifact correction algorithm due to its reliability. Fernandez Rojas et al. (2020) carried out EEG pre-processing via MATLAB (version 2018b, MathWorks Inc.) by utilizing customized software and the EEGLAB toolbox. Baseline adjustment was carried out by subtracting the matching mean from pre-trial duration EEG signals were then processed through the band-pass filter between 2 and 43 Hz utilizing the FIR filter. Artifacts from blinking and motions were cleared up utilizing the Multiple Artifact Rejection Algorithm (MARA), which assessed ICA components. Castro-Meneses et al. (2020) pre-processed EEG signals online with a high-pass filter of 16 Hz, a low-pass filter of 43 Hz, and two 50 and 60 Hz notch filters before being digitalized at 2048 Hz. The data were downsampled to 256 Hz and transferred to the computer that used the integrated SensoMotoric Instruments (SMI) Experiment Centre software program. The EEG signal was processed offline using version 13.6.5b of EEGLAB and version R2016b of MATLAB. Thus, the data were filtered to maintain the theta power with a cut-off frequency of 4 and 7 Hz. Similarly, Wang et al. (2020) had written the customized EEGLAB scripts to clean and pre-process the EEG signal. The researchers also applied the ICA method to purify the EEG signal from muscle actions and eyeblinks artifacts. Balamurugan et al. (2020) used eight bands gathered from NeuroSkymindwaves as pre-processing features for the EEG phase. The raw EEG signals were pre-processed with two separate normalization methods, using local and global normalization techniques to scale the signal. In Eldenfria & Al-Samarraie's (2019) study, the pre-processing step was summarized in four different stages: re-reference, filter, artifact rejection, and running the ICA. The MARA algorithm was used to streamline the processing of hand marking independent components for rejecting artifacts in the artifact rejection step. Removing the sources of noise did not satisfy enough activation. Therefore, the unconstrained ICA was implemented by using Runica Algorithm. Makransky et al. followed a more traditional way in the pre-processing step (Guido Makransky et al., 2019). EEG signals were filtered via a band-pass filter between 0.5 Hz and 100 Hz and were re-referenced to an average reference to arrange the EEG outputs for PSD. A notch filter was performed at 50 Hz to decrease the line noise noticeable in the spectrum plot. Even after the manual

rejection of the visual artifact, ICA was particularly conducted to erase components, including eye blinks and horizontal eye movement artifacts. These analyses were carried out utilizing the EEGLAB toolbox. Bernhardt et al. (2019) just mentioned in their pre-processing step that the EEG signals were downsampled at 256 Hz and processed online with notch filters as 50, 60, 100, and 120 Hz via low-pass FIR filters while data gathering process. Makransky et al. (2019) analyzed and cleaned up EEG signals per second by ABM's proprietary software for extra muscle acts, slow and fast eye blinks, and movement artifact declinations. Örün & Akbulut (2019) analyzed the EEG signals in MATLAB, utilizing EEGLAB. The signals were filtered via a high-pass filter at 1 Hz and a low-pass filter at 30 Hz for a better ICA. An FIR filter algorithm was used to implement the band-pass filter. The signals were eventually re-referenced to an average reference, and large artifacts were first discarded by visual inspection. Then via ICA, eye movements and muscle artifacts were eliminated. Dan & Reiner (2018) utilized WinEEG software to analyze the recorded signals to obtain a PSD curve, epoch length was set to 1s in each period, and the ICA algorithm was implemented. Hanning time window smoothed every epoch to suppress energy penetration by input filter sidelobes, and the chosen very low (0.25 Hz) limits of low-frequency signal range values were provided to eliminate the artifacts. In another study, using notch filters of 50, 60, 100, and 120 Hz and high-pass and median-pass filters (Reinerman-Jones et al., 2017) filtered the EEG signals automatically via ABM software. In a study presented by Mazher et al. (2017), the frequencies ranging from 0 and 100 Hz were extracted based on a band-pass filter. The ECG signal was collected utilizing the EGI Polygraph input box (PIB), and the EOG signal was collected utilizing the defined electrodes in the 128-channel mounting EGI. The objective of ECG and EOG signals recordings was to identify artifacts (heartbeats, eye movements, eye blinks) to pre-process EEG signals. Ortiz De Guinea et al. (2013) decontaminated and externalized one second period signal included artifact via B-alert x10 software. Gerlič & Jaušovec (2001) segmented epochs as 2 seconds (1024 data points) and automatically scanned for artifacts. Exempts were all epochs displaying amplitudes greater than ± 100 μV. Mazher et al. (2017) mentioned as a pre-processing step that the frequency band of gathered data ranged from 0–100 Hz utilizing a band-pass filter. Preprocessing EEG data was implemented by removing the artifacts and the EEG device's internal impedance fluctuations. Similarly, in another study, similar steps were followed (Mazher et al., 2015a). The artifacts, as stated before, were extracted from the raw EEG data to produce the real task-related data by utilizing BESA (6) Software (Mazher et al., 2015b). Walter et al. (2013) pre-processed the EEG signal using a Common Average Reference Filter and a detrend function algorithm, utilizing the FieldTrip toolbox running with MATLAB. All task and subject EEG channels that included excessive noise were eliminated from all databases after visual inspection for further study. Qayyum et al. (2018) utilized BESA software to decontaminate the signal by extracting the artifacts' raw EEG data. To clean artifacts, Zhou et al. (2017) implemented an auto ICA-based ADJUST algorithm, which recognized and erased components related to artifacts resulting from the integrated use of spatial and temporal features in their context. Accordingly, it was removed the confusing components that the motor activities create. Conrad and Bliemel (2016) followed up using libMuse applications to uncover blink and jaw clench events.

Table 1. The methods for pre-processing step using EEG signal for neuroimaging data on CL in multimedia learning research

Authors	Pre-processing Step Methods
A. Dan & Reiner (2017)	WinEEG software program, the independent component analysis (ICA)
Fernandez Rojas et al. (2020)	MATLAB (version 2018b), EEGLAB toolbox, Band-pass filter between 2 and 43 Hz, Multiple Artifact Rejection Algorithm (MARA)
Castro-Meneses et al. (2020)	A high-pass filter of 16 Hz, a low-pass filter of 43 Hz, and two 50 and 60 Hz notch filters, the software program of the integrated SensoMotoric Instruments (SMI) Experiment Centre, MATLAB (version 2016b), EEGLAB toolbox
Wang et al. (2020)	EEGLAB scripts, ICA
Balamurugan et al. (2020)	Local and global normalization techniques
Eldenfria & Al-Samarraie (2019)	Re-reference, filter, artifact rejection, and running the ICA, MARA algorithm, Runica Algorithm
Makransky et al. (2019b)	Band-pass filter between 0.5 Hz and 100 Hz, Re-reference, a notch filter, ICA, EEG toolbox
Bernhardt et al. (2019)	Notch filters as 50, 60, 100, and 120 Hz via low-pass FIR
Makransky et al. (2019a)	ABM's proprietary software
Örün & Akbulut (2019)	MATLAB, EEGLAB toolbox, a high-pass filter at 1 Hz and a low-pass filter at 30 Hz, an FIR filter algorithm, re-reference, ICA
A. Dan & Reiner (2018)	WinEEG software, ICA
Reinerman-Jones et al. (2017)	Notch filters of 50, 60, 100, and 120 Hz and high-pass and median-pass filters, ABM software
M. Mazher et al. (2017)	A band-pass filter (0-100 Hz) (the objective of ECG and EOG signals recordings was to identify to pre-process EEG signals)
Ortiz De Guinea et al. (2013)	B-alert x10 software
Gerlič & Jaušovec (2001)	segmented into epochs as 2 seconds (1024 data points) and automatically scanned for artifacts
Moona Mazher et al. (2016)	the frequency band of gathered data ranged from 0–100 Hz utilizing a band-pass filter.
Moona Mazher et al. (2015a)	BESA (6) Software
Walter et al. (2013)	A Common Average Reference Filter and a detrend function algorithm, utilizing the FieldTrip toolbox running with MATLAB
Qayyum, Faye, et al. (2018)	BESA Software
Zhou et al. (2017)	an auto ICA based ADJUST algorithm
Conrad and Bliemel (2016)	libMuse applications

2. Feature Extraction Step:

The feature extraction used in machine learning, pattern recognition, and image processing creates derived values using the input's measured data. Looking at the literature, 28 of 33 publications on the review issue utilizing EEG signals provide detailed information about feature extraction, while six of them do not share information about the process. Accordingly, in some of the studies (Bertolo et al., 2014; Cao et al., 2019; Conrad & Bliemel, 2016; Díaz et al., 2015; Jan-Louis Kruger et al., 2013; J.-L.

Kruger et al., 2014), there was no clear knowledge about the feature extraction process. Meanwhile, only Fernandez Rojas et al. (2020) performed the feature selection process to minimize the number of features and construct a more accurate learning model. The selection criteria were dependent on the Joint Mutual Information Algorithm (JMI), which currently ranked the features with the largest Mutual Information (MI) between the class label and the vector. Table 2 summarizes the methods for feature extraction step using EEG signal for neuroimaging data on CL in multimedia learning research.

Accordingly, Dan and Reiner (2017a) utilized it to figure out the cognitive load index (CLI). Power spectra were measured with WinEEG using Fernandez Rojas et al. (2020), conducted the feature extraction step utilizing spectral analysis. Firstly, each channel's power distribution was analyzed by converting the EEG into PSD, performing a Fast-Fourier transform (FFT), and operating 10-s windows with 50 percent overlapping windows estimated by the Hamming function to decrease spectral leakage. Furthermore, EEG channels were already decomposed from each window into subbands: delta (2–4 Hz), theta (4–8 Hz), alpha (8–12 Hz), beta (12–30 Hz), and gamma (30–40 Hz). Additionally, PSD findings of each frequency band were normalized (1 / f) to get each band's relative PSD to the baseline period. Lastly, the following PSD measurements were averaged in each band to get the power spectral features utilized classification. Castro-Meneses et al. (2020) squared each time point in the theta band to get the power. Only for four electrodes, over each video and baseline, the mean theta power was calculated. The four electrodes were separated into two interest regions, and after that averaged for the regions as right frontal (AF4, F4) and left frontal (AF3, F3). For each video, Wang et al. (2020) examined the EEG signal. Every video was 240 seconds long, and thus the EEG files were split into 120 segments. Power spectral analysis was therefore performed on EEG data utilizing FFT in EEGLAB. The mean power values in the alpha and theta waves (μV2) in related regions of interest were measured and evaluated between the teacher presence and the teacher absence video versions. Balamurugan et al. (2020) acquired the features via NeuroSkymindwaves software as eight frequency bands (1-theta, 2-alpha (high, low), 2-beta (high, low), 2-gamma (high, low)). Eldenfria and Al-Samarraie (2019) investigated the implications mentioned in their research hypotheses utilizing linear regression and ANOVA. The data were calculated as formalization presented in their study for engagement, emotion, CL, and concentration. Makransky et al. (2019) executed the Neurospec toolbox to derive the frequency-domain metrics of EEG signals via a Discrete Fourier Transform (DFT) with a 2000 ms Hanning window length defined as a 256-sample rate and a 2-9 segment length. The EEG signals were normalized and log-transformed to minimize the possible unit variance and distribution skew and measure the log-spectral density measures. The mean estimates were thus calculated for the theta and alpha bands (decibel power / Hz). Bernhardt et al. (2019) estimated PSD automatically via (Advanced Brain Monitoring; B-Alert Live, 2009) by utilizing FFT on raw EEG signals and computing the sinusoidal component amplitudes, second by second, for specified frequency bins. FFT analyses were conducted with and without applying a Kaiser window for data smoothing after applying a 50 percent overlay between two sequential epochs. Then, the chosen 1-Hz bins were automatically averaged and logged through five bandwidths to establish standard EEG bands: delta (1–2 Hz), theta (3–7 Hz), alpha (8–13 Hz), beta (13–29 Hz), and gamma (25–40 Hz). Makransky et al. (2019) obtained the relative and absolute power spectra parameters from the channels as Cz-PO, C3-C4, Fz-C3, F3-Cz, and Fz-PO, utilizing regression step by step. Örün and Akbulut (2019) calculated average spectral power (ASP) for the alpha and beta bands by FFT for each electrode. The brain waves within 8–13 Hz and 13–30 Hz were used to measure alpha and beta power. Dan and Reiner (2018) estimated alpha waves (8–12 Hz) and theta waves (4–8 Hz) from all channels and averaged the spectra power over periods for each electrode, participant, time window, and experi-

mental condition. Moreover, theta spectral power of Fz electrode values and the Pz electrode values' alpha spectra power was measured. The average wave potential for each channel for each period was assessed as the mean of sessional intervals. The CLI was quantified using the ratio of theta Fz to alpha Pz (Holm et al., 2009). For the observation sessions, it was evaluated theta Fz, alpha Pz, and the average CLI for each participant. Reinerman-Jones et al. (2017) calculated via EEG signals' PSDs based on FFT, each including 1 s of data (256 decontaminated EEG samples), with a 50 percent overlap smoothed with a Kaiser window via ABM software. Mazher et al. (2017) implemented discrete wavelet transformation (DWT) to extract the spectral feature on the EEG data for the first part of the study. The approximate entropy, spectral entropy, and sample entropy were extracted for features. For every three learning phases, the second part of the study intended to evaluate the effective connectivity based on the Partial Direct Coherence. Lee (2014) calculated beta power while watching the video and evaluated CL's mean differences for Korean and English classes and CL indicator relationships. The statistical analyses of results were performed in IBM SPSS 18.0 utilizing correlation analysis and t-tests. Guinea et al. (2013) formed EEG engagement and workload indexes ranging from 1 to 40 Hz of EEG signal utilizing absolute and relative power spectra. To calculate the absolute spectral power (μV) in different brain waves, Gerlič and Jaušovec (2001) operated FFT on artifact-free 2-second chunks of data for each condition. The reported analyzes concentrated on lower and upper alpha band metrics. A spectral power average (μV) was determined for each problem and scalp location. Coherence values were conducted for all electrode pairs in both the lower and upper alpha bands. In this form, 171 measurements of coherence were calculated for each analyzed variable. Alex Dan and Reiner (2017b) measured spectral power (μV2) from the central parietal (Pz) and mid-frontal (Fz) electrodes and averaged the power of the spectra for electrode, time window, each participant, an experimental condition over all periods. The Cognitive Load Index (CLI) was assessed using the theta Fz ratio to alpha Pz, and the average CLI per observation session for each participant (n = 1,2,3,4) was evaluated. In another study, the theta/alpha ratio was estimated by Chang et al. (2016) as brain workload during the learning tasks. Qayyum et al. (2018a) derived the various brain waves utilizing DWT from the EEG resting data set and the EEG multimedia learning data set utilizing a distinct number of segments of each EEG dataset. Mazher et al. (2017) generated alpha waves, theta, and delta waves based on DWT, and FFT was used to quantify the frequency domain of the chosen channels. Depending on the spectral power density (PSD), the intensity weighted mean frequency (IWMF), its bandwidth (IWBW), the set of spectral features used for analysis were utilized for the analysis. Al Madi and Khan (2016) measured the average spectral density of power based on chosen channels and assessed the intensity-weighted mean frequency and intensity-weighted bandwidth. Moona Mazher et al. (2015a) obtained spectral PSD of the demanded frequency bands via FFT and DWT. In the study presented by Moona Mazher et al. (2015b), a frequency domain analysis utilizing FFT was conducted on processed channels to acquire the required frequencies for alpha waves. After that, PSD of alpha waves was obtained for each channel, and then the PSD was averaged for each brain region. Walter et al. (2013) calculated Event-Related Synchronization/Event-Related Desynchronization (= ERS/ERD), which estimates the percentage amount of band power increase (ERS) or decrease (ERD) from a reference interval to an activation interval in a frequency band. For each overlapping window, the power spectra were determined to utilize autoregressive models based on Burg's maximum entropy method utilizing a sample order of 64, estimated using the MATLAB, ARMASA Toolbox. Afterward, it was averaged for all sub-power spectra per trial with a frequency resolution of 1 Hz bins, consisting of one power spectrum for each trial. Qayyum et al. (2018) segmented EEG signals into equal numbers of segments to analyze CL measurement's deep temporal knowledge. The brain oscillations were obtained

utilizing DWT for each segment and fed those segments to the suggested classification and CL assessment model. Zhou et al. (2017) performed the FFT on the cleaned EEG signal and acquired theta and alpha bands. The linear feature extraction takes less time to compute; it uses six linear features such that mean square, mean absolute amplitude, activity, complexity, mobility, and variance. Zhang and Liu (2017) utilized the MindWave headset, which monitors the wearers' mental state in the context of the patented mediation and attention values of NeuroSky and the raw brain activity and EEG power spectrums. Thus, in the dual-screen condition, they measured the level of attention to reflect the participants' CL. Crk and Kluthe (2014) first modified the EEG signal based on predicted ranges of the theta to alpha bands via a band-pass filter. Estimates of the PSD were achieved by utilizing the Welch method. The gravity frequency was reported for each participant for the range 7 Hz to 13 Hz and then employed to compute the theta range. Then, the ERD parameters were acquired based on the rest and trial periods divided into windows of 125ms. Averaged over the windows, the rest period's power was utilized as a reference for measuring the ERD of the subsequent trial period.

Table 2. The methods for feature extraction step using EEG signal for neuroimaging data on CL in multimedia learning research

Authors	Feature Extraction Step Methods
A. Dan & Reiner (2017)	Cognitive load index (CLI), power spectra, WinEEG
Fernandez Rojas et al. (2020)	Power Spectral Density (PSD) findings of each frequency band were normalized (1 / f)
Castro-Meneses et al. (2020)	the mean theta power was calculated
Wang et al. (2020)	PSD was performed on EEG data utilizing Fast Fourier Transform (FFT) in EEGLAB
Balamurugan et al. (2020)	NeuroSkymindwaves software as eight frequency bands.
Eldenfria & Al-Samarraie (2019)	linear regression and ANOVA.
Makransky et al. (2019b)	the Neurospec toolbox was used via Discrete Fourier Transform (DFT), normalization, and log transformation
Bernhardt et al. (2019)	PSD automatically via (Advanced Brain Monitoring; B-Alert Live) by utilizing FFT
Makransky et al. (2019a)	the relative and absolute power spectra parameters utilizing regression
Örün and Akbulut (2019)	Average spectral power (ASP) by FFT
A. Dan & Reiner (2018)	ASP
Reinerman-Jones et al. (2017)	PSDs based on FFT via ABM software
M. Mazher et al. (2017)	Discrete wavelet transform (DWT), the approximate entropy, spectral entropy, and sample entropy, the Partial Direct Coherence
Lee (2014)	The statistical analyses of results were performed in IBM SPSS 18.0 utilizing correlation analysis and t-tests.
Guinea et al. (2013)	absolute and relative power spectra
Gerlič and Jaušovec (2001)	the absolute spectral power via FFT, Coherence values
Alex Dan and Reiner (2017)	spectral power, CLI was assessed using the theta Fz ratio to alpha Pz
Chang et al. (2016)	the theta/alpha ratio
Qayyum, Faye, et al. (2018)	DWT
M. Mazher et al. (2017)	DWT, and FFT. PSD, the intensity weighted mean frequency (IWMF), its bandwidth (IWBW), the set of spectral features
Al Madi and Khan (2019)	the average spectral density, (IWMF), (IWBW)

Continued on following page

Table 2. Continued

Authors	Feature Extraction Step Methods
Moona Mazher et al. (2015)	PSD of the demanded frequency bands via FFT and DWT.
Moona Mazher et al. (2015b)	FFT, PSD
Walter et al. (2013)	Event-Related Synchronization/ Desynchronization (ERS/ERD), PSD MATLAB, ARMASA Toolbox.
Qayyum, Khan, et al. (2018)	DWT
Zhou et al. (2017)	FFT, mean square, mean absolute amplitude, activity, complexity, mobility, and variance
Zhang and Liu (2017)	MindWave headset, power spectrums.
Crk and Kluthe (2014)	the theta to alpha bands via a band-pass filter, PSD was achieved by utilizing Welch method, the ERD parameters

3. Classification Step:

Classification approaches are utilized to identify the characteristics of signals or images obtained via different techniques. Researchers use many popular algorithms to classify EEG signals. However, in our literature review, it is realized that only 9 out of 33 studies found on the theme of evaluating the multimedia measurements of CL with EEG signals performed a classification process and summarized them as follows. Rojas et al. (2020) utilized the linear discriminant analysis (LDA) to identify the four mental effort levels as offline analysis. The data was separated into two parts to estimate the classifier's performance, with 70 percent for training and the remaining 30 percent utilized to test and evaluate generalization performance. Balamurugan et al. (2020) implemented it to the machine learning algorithms (SVM, k-nearest neighbors (kNN), and random forest) for the classification and decision making of learner's mental effort via 10-fold cross-validation in MOOC platforms. Within this study, the classifier efficiency was measured using the metrics as mentioned: sensitivity, specificity, F-measure, precision, and overall accuracy, which were evaluated with true positive (TP) and negative (TN), false positive (FP), and negative (FN) rates. Subsequently, experimental research suggested that random forest classifiers, including the non-Markovian process, obtained more than the other two models in F-measure (99.21%) and overall accuracy (99.15%). Makransky et al. (2019) assessed and trained the classification process designed by Berka et al. (2007) utilizing a linear discriminant function analysis with two classes based on data acquired from testing various integrations of high and low complexity levels of starting grid, trail making, mental arithmetic, and digital tasks. These tasks were utilized as capacitors for a neuropsychological evaluation of working memory, and workload metrics were designed explicitly to be adaptive to working memory executive processes. For classification, Mazher et al. (2017) employed three kinds of classifiers (Linear Kernel, Naïve Bayes, and RBF Kernel) and three entropy-based spectral features. SVM generated better outcomes in a complex application, practice, implementations of the brain modality and obtained satisfying findings in mental and cognitive task activities. In the study presented by Qayyum et al. (2018), the time-frequency spectrogram images were generated utilizing alpha and other brain waves from windowed EEG signals and were transferred to a pre-trained CNN model for the classification of EEG data. The extracted features from the pre-trained VGG networks offered the EEG dataset better classification functionality for CL. Mazher et al. (2016) compared machine learning algorithms (SVM, LDA, Naïve Bayes, Random Forest, ANN) on the extracted features to determine the similarity and dis-

similarity between various brain oscillations. The alpha frequency band demonstrated more accuracy in L1 utilizing the SVM model, 85% that used PSD features, 86% using IWFM, and 78.4% using the IBWB feature. Walter et al. (2013) comparatively assigned a within-task classification and a cross-task classification to create effective classification methods that individually distinguish each subject's working load levels. SVMs with Radial-Basis-Function (RBF) kernel were used in both classification processes to classify working load states in EEG data during simple and challenging tasks. Qayyum et al. (2018b) fed the partitioned data into the 1D-CNN network to classify. The suggested 1D-CNN was composed of various layers referred to as pooling, convolutional, and fully connected layers. The suggested CNN model outlines the seven layers, given the small input data size. The Kappa Coefficients (KC) were then used to assess a classification's accuracy. Zhou et al. (2017) executed SVM to classify EEG data based on statistical learning theory. Concerning the kernel function, the linear kernel was utilized as it works much better with EEG data than the polynomial and the radial base function kernel (RBF). Table 3 summarizes the methods for the classification step using EEG signal for neuroimaging data on CL in multimedia learning research.

Table 3. The methods for classification step using EEG signal for neuroimaging data on CL in multimedia learning research

Authors	Classification Step Methods
Fernandez Rojas et al. (2020)	linear discriminant analysis (LDA), with 70 percent for training and the remaining 30 percent utilized to test
Balamurugan et al. (2020)	SVM, k-nearest neighbors (kNN), and random forest via 10-fold cross-validation in MOOC platforms
Makransky et al. (2019a)	a linear discriminant function analysis with two classes
M. Mazher et al. (2017)	Linear Kernel, Naïve Bayes, and RBF Kernel
Qayyum, Faye, et al. (2018)	a pre-trained CNN (Convolutional Neural Network) model, the pre-trained VGG networks
Moona Mazher et al. (2016)	Support Vector Machines (SVM), LDA, Naïve Bayes, Random Forest, Artificial Neural Network (ANN)
Walter et al. (2013)	SVMs with Radial-Basis-Function (RBF) kernel
Qayyum, Khan, et al. (2018)	1D-CNN network, The Kappa Coefficients (KC)
Zhou et al. (2017)	SVM, the linear kernel

Analysis Techniques of TCD

J. Loftus et al. (2016) and J. J. Loftus et al. (2017) directed examining performance outcomes and alterations in cerebral blood velocity (CBV) utilizing a one-way ANOVA. Baseline physiological measurements for low and high spatial ability comparisons were conducted using a t-test. Similarly, J. J. Loftus et al. (2018) evaluated their findings using statistical tests. Apart from these, there are studies in which CL in multimedia learning is not studied, but it tells about TCD analysis methods to give researchers ideas and encouragement. Sejdić et al. (2013) investigated both the raw and the envelope CBV signals using time-domain features as standard deviation, the skewness, the kurtosis of the signal amplitude, cross-correlation coefficient, and nonlinear methods as The Lempel-Ziv complexity, entropy, cross-entropy,

and frequency-domain features as the peak frequency, the centroid frequency, the bandwidth of spectrum, and lastly time-frequency features a wavelet entropy, the relative energy in distinct time-frequency bands estimated based on wavelet transform(WT). In summary, many time, frequency, and time-frequency methods mentioned in the literature can be used to examine the TCD signal.

Analysis Techniques of fMRI

fMRI ensures a capability to learn neuronal activity in the human brain in a noninvasive way because it shifts in near real-time. Most fMRI studies calculate the oxygen-level-dependent (BOLD) signal in the blood, which rises to a peak several seconds after an active brain region. In fMRI research, various experimental designs are widespread. Block alternate designs periods in which subjects conduct some tasks with rest periods, while event-related designs display a set of discrete trials to the subject. Following the completion of the fMRI experiment, pre-processing analysis prepares the data for task-related assessments. The far more prevalent task-related analysis utilizes the General Linear Model to correlate the predicted BOLD response with the activity observed in each brain region. Regions with a high degree of this correlation are marked as task-related. Connectivity analysis then aims to understand active areas belonging to the same functional network. On the other hand, multivariate methods, including independent component analysis and multi-voxel pattern analysis, recognize event-related regions' networks rather than single regions to address functional connectivity issues concurrently (Ashby, 2015).

Analysis Techniques of fNIRS

Zahabi et al. (2020) utilized the COBI software for the baseline signal values to measure the oxygenations and report them as output data. Afterward, the testing and analysis software filtered the artifacts via a low-pass filter to obtain the filtered data. Finally, some of the data were eliminated due to disruption (equipment noise, breathing, and body movement artifacts), and the exact data was collected in new text files for each participant. Each of these files has been converted to a spreadsheet to measure the participant's accumulated oxygenation modifications. The data were then aggregated to a single value representing the average alteration in oxygenation and the participants' total cognitive response. Finally, they were incorporated into the statistical analysis procedures program SPSS v.18. To further explain the relationship between mental effort and performance, Uysal (2016) used an efficiency metric based on neural efficiency theory to measure alterations in neural resources requirements. Neural efficiency was measured via the normalized (z-score) of neural or cognitive effort and behavioral performance. Therefore, separate ANOVAs of the AF7, FP1, FP2, and AF8 regions of interest were performed on mean HbO. Behavioral performance (P) was assessed in terms of time to activate ACC or LKAS features to calculate neural efficiency, and cognitive effort (CE) for brain-derived measurements was evaluated utilizing summative HbO activation from the four regions of interest. Except for these studies, time-domain features, frequency domain features, and time-frequency features can be extracted as stated for EEG signals.

RQ2: Which results were acquired in CL in multimedia learning research using neuroimaging methods?

The Evaluation of EEG Utilization in CL in Multimedia Learning

The EEG studies found in the literature have many satisfied evaluation comments with explicit expressions. And it has been expressed these comments below, respectively. A. Dan & Reiner (2017) evaluated CL correlated with a simple and complex paper folding (origami) learning task by visualizing 2D or stereoscopic 3D displays. The results have important implications for comprehending cognitive processing related to the 2D and 3D environments while also using stereoscopic 3D technology over 2D displays. For better processing, the stereo 3D mode was considered superior to 2D. Under 2D conditions, the theta Fz power decrease was higher than under 3D conditions.

Fernandez Rojas et al. (2020) aimed to define a collection of measures used in a multitasking environment to analyze cognitive workload effectively. They built a simulation system that controls the tasks' complexity by changing the simulation's information quality. Ultimately, they intended to define EEG indicators that could be used to activate performance-conserving technical support. Nineteen specific EEG features gave a differential control of the four high-classification accuracy workloads (82.23 percent). The defined collection of features reflects EEG metrics for objective assessment of the cognitive workforce across participants. Castro-Meneses et al. (2020) tested a group of students seeking postgraduate study as a second language through the English medium to stimulate CL. As a result, the subjective scale of linguistic complexity at all three levels was substantially dissimilar. The power of theta and recall differed considerably between the two most different levels. Although the result indicates that theta power might not be as susceptible as the subjective scale for intrinsic CL for average CL, correlation analysis revealed that theta power was correlated with self-reported CL. The study suggests that theta power can be established into a reliable objective assessment of average CL. Wang et al. (2020) investigated how online videos with and without teachers influence learning and CL through subjective and objective measurements. The study looked at how teacher-present video impacts the learning results, self-reported, brainwave-inferred CL of the learner compared with teacher-absent video, and the extent to which the EEG-derived CL prediction estimates learning from the video. The findings showed that the teacher-present video enhanced the learners' ability to pass knowledge and was correlated with a lower self-reported extraneous and intrinsic load. Additionally, event-related alterations in theta wave demonstrated lower CL with the teacher present.

Through Balamurugan et al.'s (2020) study, a brain-computer interface was created to collect data and detect the mental condition by monitoring massive open online course (MOOC) videos and EEG signals based on the Cognitive Load Theory by John Sweller. Subsequently, experimental research revealed that the non-Markovian random forest classifier accomplished more than the other two classifiers in accuracy (99.15%) and F-measure (99.21%). Eldenfria & Al-Samarraie (2019) aimed to study the idea that implementing an online continuous adaptation mechanism (OCAM) of learning content to control the presentation of learning content according to variations in the learner's level promotes a better cognitive and emotional response among students, encouraging their engagement. The findings showed that the OCAM positively affected the levels of concentration and CL of the learners, which greatly improved their engagement. Makransky et al. (2019b) examined the spatial contiguity effect's basic processes and utilized self-reports, eye-tracking, post-tests, and EEG for measuring CL. As a result, it was found that post-testing, perceived difficulty, and eye-tracking were relevant to extraneous CL. The behavior of the EEG-derived alpha band and the perceived difficulty were indicative of intrinsic CL. Bernhardt et al. (2019) assessed the validity of commercially available EEG cognitive workload state metrics and engagement in students with differentially experienced air traffic control (ATC). It was indicated that

for less experienced students, the engagement was greater than in more experienced students. There were no differences in scenario performance between the experiential groups. Neurological workload measures ranged across task requirements, not levels of experience.

Makransky et al. (2019a) discussed the impacts of adding immersive VR to simulation. The effect of immersion degree on the redundancy principle was researched. The students showed a significantly greater presence but got to learn less in the condition of immersive VR. In the immersive VR condition, students even had a higher CL based on EEG. Örün & Akbulut (2019) investigated the connection among content retention, working memory capacity, and subjective CL; apart from these, they examined the relationship between objective and subjective CL and the degree-specific conditions of multitasking and surrounding environment impact retention and CL. And, it was examined whether the use of EEG harms retention and CL for learners or not. Accordingly, there were lower retention rankings for the simultaneous multitaskers. The perceived mental effort expanded among simultaneous multitaskers in the cafeteria. The retention was forecasted by perceived mental effort and working memory. EEG members and non-EEG members did not vary concerning dependent variables. The perceived mental effort was directly linked to beta frequency (F7). A. Dan & Reiner (2018) evaluated learning in two virtual learning scenarios on 2D displays and the same 3D stereoscopic (3DS) virtual learning environment. In a 3DS virtual environment, CL derived from EEG was lower compared to a flat-screen. Evaluations revealed an essential difference in two-dimensional (2D) outcomes compared to 3D ones in the folding test scores, CL measures, and self-assessment questionnaires. 3DS virtual learning environment teaching sessions were more convincing than traditional 2D training sessions, resulting in higher learning. Reinerman-Jones et al. (2017) assessed the impact of varying tactile information forms (i.e., directional indications vs. static indications vs. dynamic indications) on objective performance and perceived workload in a human-robot collaborative task. As a second experiment, they measured the effect of task load and type of information message (i.e., single words vs. clustered phrases) on the same collaborative task. The relation of personal attributes (spatial ability and attentional control) to efficiency and workload was also evaluated in both experiments. It was also tested various physiological responses in each experiment and self-report of CL and objective performance. Even though EEG indicators were partly related to performance, they appeared to have limited utility as workload measurements connected with tactile displays.

M. Mazher et al. (2017) executed EEG to analyze CL in multimedia learning tasks via different frequency bands and partial direct coherence (PDC) in the three learning states (L1, L2, L3). The study revealed that alpha frequency bands had a high accuracy in classification for each of the three spectral features. These findings indicated that alpha bands were the strongest brain waves to differentiate between various states of learning. The analysis also demonstrated that L3 produced a greater CL than L2 or L1, while L2 produced a greater CL than L1. The second part of the study aimed to evaluate the effective connectivity utilizing PDC for each of the three learning states. During L3, more connections were revealed than during L2 or L1, while for all described brain signals, L2 had a higher number of connections than L1. Lower CL has been shown to suggest a higher number of connections. Therefore, both investigations demonstrate that L3 demands less CL or mental effort. Lee (2014) assessed a credible and accurate tool for estimating CL during learning by evaluating different types of metrics of CL such as EEG, self-reporting, and learning outcome via participants viewing a documentary supplied in English or Korean. First of all, the English class registered higher difficulty scores than the Korean class. Based on the findings, it might be concluded that English as a foreign language video had a higher CL than Korean as a first-language video. Secondly, the English class indicated less mental effort than the Korean class. The finding showed that capturing all the information in the English video was more

complicated than in the first language video; thus, English team participants made less effort than Korean team participants to produce cognitive processes. Participants who viewed the English video encountered serious problems, and their learning motivation might have been decreased. Thirdly, it was found that various delivery languages influenced the beta band in the regions of T3 and F7. The beta oscillations of T3 and F7 were more reflected in the team viewing the English video than those viewing the Korean video. It was also carried out that the beta band in channel T3 was positively correlated with the level of difficulty but never with learning effectiveness. Finally, the analysis indicated that the difficulty rating was negatively correlated with the comprehension test and the mental effort rating but was positively correlated with the beta band in T3 channel. J.-L. Kruger et al. (2014) examined the distribution of visual attention between subtitles and other information sources through eye-tracking. They applied to academic understanding and CL as assessed by self-report questionnaires and EEG, providing impressive outcomes for utilizing first and second language subtitles in academic contexts.

Ortiz De Guinea et al. (2013) ensured a comprehensive evaluation of the construct validity of information systems (ISs) through a multitrait-multimethod (MTMM) matrix by estimating IS constructs as CL, arousal, and engagement. It was found that the results support a connection between self-reported measures and neurophysiological metrics. Gerlič & Jaušovec (2001) assessed the students ' cognitive processes through the EEG technique when learning physics. The findings obtained altogether indicate that learning information between areas of the brain had no favorable effect on the amount of learned material. A further result was that physics experts learned more than novices did, regardless of the form of presentation. The indicators of EEG differentiated primarily in the lower alpha band, thereby attempting to point to the superior expert supervision of attention processes. Alex Dan & Reiner (2017) evaluated how near-online measurements could enhance Education Data Mining in the process of learning technologies in comparison to two conditions – flat 2D video and 3D immersive VR demonstrations, utilizing EEG and a relative CL statistical model- and then they correlate with learning. When looking at the learning scenario, it was found that two sessions (the second and the fourth) were considerably dissimilar in the mean relative CLI observed for all participants.

Chang et al. (2016) carried out a systematic examination into the correlations between learners' EEG-based workload and their self-reported CL in a multimedia learning approach. The findings demonstrated that CL was significant, but the theta/alpha ratio was not significant. Given the initial correlations, no significant difference was identified between the theta/alpha and CL ratios. Qayyum, Faye, et al. (2018) proposed the deep learning algorithm using the pre-trained convolutional neural network (CNN) as a transfer learning method to classify resting states and cognitive states and evaluated CL-based brain signals, especially alpha waves. The findings indicated that the alpha band generated reasonable activity for all cognition tasks depending on pre-trained CNN models for classification and CL evaluation.

M. Mazher et al. (2017) described the rehearsal impact based on the data obtained by EEG. Three frequency-based features were used to differentiate between the three learning states, referred to as L1, L2, and L3 utilizing machine learning algorithms in which L1 is defined as the first learning state, while L2 and L3 are the rehearsal states of L1. The analysis findings indicated that alpha waves induced desynchronization from resting-state to the learning process relative to other EEG measured waves. This desynchronization was a product of a mental effort forced by working memory during a learning experience. The alpha band demonstrated more precision in L1 based on the SVM classifier, 85 percent using PSD features, 86 percent for IMFM, and 78.4 percent using the IBWB features. The findings also showed that L3 shows less precision for each of the three derived features than L2 and L1. The results demonstrated that L3 needs less mental effort while learning. The studies have shown the rehearsal

to be a reasonable mechanism of long-term memorized learning. Al Madi & Khan (2019) focused on learning output and cognitive abilities through text comprehension and multimedia perception. The findings revealed significant variations in the alpha and beta waves' power between text and multimedia presentations. As anticipated, measures of observed emotions showed that multimedia comprehension produced a higher magnitude of positive emotions than text. At the same time, text comprehension produced higher CLs than multimedia presentations. Moona Mazher et al. (2015a) aimed at a statistical analysis of learning and nonlearning mental states focused on EEG-reported brain waves. The ANOVA statistical test outcomes showed that the alpha frequency band had more discriminatory behavior from nonlearning to mental learning than other frequency bands. These findings also demonstrated that DWT was a superior form of spectral analysis to FFT. Moona Mazher et al. (2015b) provided a comprehensive study of four brain regions focusing on CL (mental effort) dictated by working memory throughout 2D multimedia animation learning. The findings demonstrated a decrease in PSD of the alpha brain waves in all regions of the brain. Specific responses were reported along with all four brain areas. Parietal and occipital areas were concerned with the processing and perception of visual information such that significant suppression of alpha wave power had been observed during the 2D multimedia aid. Walter et al. (2013) intended to develop an EEG-derived learning system that adapts to online learners' workloads. Therefore, the research focused on cross-task classification performance for SVMs trained on EEG data, registered during participants 'performing three work memory tasks. Accordingly, although within-task classification performance was higher for working memory tasks (average: 95 per cent-97 percent), cross-task classification accuracy was not meaningful over the chance level. Cao et al. (2019) examined the impact of different lecture videos on student learning utilizing eye-tracking and EEG methodologies together. The outcomes of eye-tracking and EEG records indicated that teachers' presence affected learners' concentration and attention to lecture video learning. Besides, the perceived satisfaction of learners was often linked to the learning of students.

Qayyum, Khan, et al. (2018) suggested that the deep learning algorithm based on the 1D CNN model classify resting states, cognitive states, and CL was evaluated utilizing brain waves, especially alpha waves. The findings demonstrated that the alpha brain wave showed reasonable attitudes through the 1D-CNN methodology for CL analysis and offered an important alternative in the EEG signal for learning and resting-state tasks. Zhou et al. (2017) developed a real-time sensitive Brain-Computer Interface device to track cognitive workloads using an EEG-based headset, used in an interactive online environment like MOOC. The designed prototype, based on two layers, which utilized classifying machine learning approaches, could record EEG signals and classify CL levels while students watch online course videos. This research aimed to explore students' reading comprehension and CL improvement in the multi-display presentation system in an experimental environment Zhang & Liu (2017). The findings demonstrated that the level of attention to the dual-screen system was increased. Reading forms of text-only or text images provided further fixation time and attracted more attention to both the single-and dual-screen system. They stated that the multi-display design system might positively impact Chinese reading comprehension and raise students' attention levels. Conrad & Bliemel (2016) provided the basis for extending a model that explains the role of CL on Knowledge Gained to the development of a neuroadaptive learning system. An experiment was described that utilizes noninvasive tools to validate this model and investigate the viability of off-the-shelf EEG data collection in e-learning experimentation. Their preliminary findings indicated a relationship between sessions' EEG signal and variance in the flow of self-report. Díaz et al. (2015) presented an experiment with participants' exposure to videos about various kinds of open software licenses, intended to observe the implications of utilizing a talking

head in educational videos often utilized in video-based learning processes. The outcomes showed an enhancement in the CL in the mixed condition.

Crk & Kluthe (2014) presented information on the direct evaluation of cognitive ability consistent with programming tasks by a deliberately designed observational analysis utilizing a cross-section of undergraduate students in computer science and a low-cost off-the-shelf brain-computer interface. This research introduced a correlation between expertise and programming language comprehension concludes the cognitive ability measures obtained utilizing recent cognitive theories. Bertolo et al. (2014) explored the effects of utilizing an innovative iPad application (named FINGERS ©) on cognitive workload while viewing 3D geometry problems. The cognitive workload (evaluated with EEG) based on three supports (paper-and-pencil / polyhedrons / FINGERS ©) was compared while viewing 3D geometry problems. The research findings demonstrated, in particular, that the utilization of their application drastically reduces CLs while viewing 3D geometry problems, for the most difficult geometry problems. Jan-Louis Kruger et al. (2013) assessed CL by eye-tracking EEG, frustration, self-reported mental effort ratings, engagement, and comprehension effort in addition to performance measurements (comprehension test). Negative psychological states could be triggered by higher CL (or cognitive overload) conditions resulting in learning frustration and dissatisfaction with learning activities and self-performance.

The Evaluation of TCD Utilization in CL in Multimedia Learning

The actions in respiration can affect CBV. Thus, researchers are required to determine a benchmark value for end-tidal CO2 (EtCO2) concentrations as a means of verifying that alterations in cerebral blood velocity resulted from cognitive demands but rather changes in respiration rhythms during testing. During the learning of individuals with low and high spatial ability, Loftus et al. investigated the effect from the outlook of CBV in the brain with both dynamic (J. Loftus et al., 2016; J. J. Loftus et al., 2018) and statistic images (J. J. Loftus et al., 2017). Their findings demonstrated for static images that there was a modest enhancement in baseline values of CBV in individuals with high spatial ability. Conversely, during the learning task, individuals with low spatial ability resulted in a decrease from baseline. Similarly, individuals with high spatial ability tended to be better at interacting with complex images, such as dynamic images moving in time and space. These findings showed that spatial ability alleviates CL and effectively impacts visual learning tasks on learner performance in all three mentioned studies.

The Evaluation of fMRI Utilization in CL in Multimedia Learning

In the reviewed studies, only one study focused on CL's multimedia environment using fMRI modality. In this study, two experimental stages were carried out. The first experiment study used three different encoding modes, including text reading, story listening, and video watching. After learning naturalistic events, participants took recall tests. The outcomes indicated that, at immediate recall, the participants made fewer errors in the conditions of the text reading and video watching than the condition of the story listening; at delayed recall, these distinctions vanished.

Similarly, Experiment 2, participants carried out the same process and experienced an fMRI scan during a recall task. The fMRI analysis suggests stronger activation in the right angular gyrus to retrieve bimodal naturalistic events (i.e., video watching) than unimodal ones (i.e., story listening and text reading). Participants conduct better in bimodal encoding mode than unimodal ones. Consequently, the right

AG (angular gyrus (AG)) was triggered more powerfully to retrieve bimodal events than unimodal ones (C. Liu et al., 2020).

The Evaluation of fNIRS Utilization in CL in Multimedia Learning

Remarkably, the results were provided by the two separate hemodynamic activities to comprehend the physiological value and its cognitive context (decreases and increases in the mean concentration levels of oxygenated hemoglobin) (Uysal, 2016). The mental workload was assessed using just the prefrontal cortex oxygenated hemoglobin (Oxy-Hb) obtained via fNIRS. With an increased mental workload, the amount of hemoglobin oxygenated found in the prefrontal cortex was raised. Thus, lower HbO rates suggested the most effective usage of neural resources (Zahabi et al., 2020). On the other hand, Uysal (2016) states that their results contradicted León-Carrion et al. (2008) outcomes regarding the task complexity in fNIRS experiments. These findings indicated how much the cognitive task and its complexity level affected the fNIRS evaluations were, and however, supporting evidence is still needed.

CONCLUSION

CL is a variable that has been used to investigate learners' cognitive processes in a number of multimedia studies. On the other hand, in most CL studies, subjective measurement methods were used (Mutlu-Bayraktar et al., 2019). CL was investigated in multimedia learning studies that used neuroimaging methods in this research. It displays the findings of 40 systematic articles that matched the search criteria and were discovered due to an index search conducted in April 2020. Among the peer-reviewed articles, the first published one was in 2001.

In the pre-processing step, the use of band-pass filters and MATLAB-EEGLAB programs are predominantly preferred. It is seen that the program used in the feature extraction step is usually EEGLAB running on MATLAB again. Although different methods are used, it is seen that the most preferred method in feature extraction is PSD. The classification step is quite less preferred in CL measurement in the multimedia environment. Of the nine studies with the classification step, only two used the Deep Learning method, and the others focused more on conventional machine learning methods.

Although the content of CL studies using EEG signals is generally different, we can say that they have intersections at a few points. The results have important implications for understanding cognitive processing related to 2D and 3D environments and the effects of adding immersive VR to the simulation. Also, studies suggest that theta, alpha, and beta waves can be established in a reliable and objective assessment of average CL. And, whether the use of EEG harms retention and CL for learners or not was examined. The studies have demonstrated the rehearsal to be a plausible mechanism of long-term memorized learning. For TCD, the findings showed that spatial ability attenuates CL and effectively influences learner performance on visual learning tasks. In fMRI, right AG (angular gyrus (AG)) was triggered more powerfully to retrieve bimodal events (i.e., video watching) than unimodal ones (i.e., story listening and text reading). On the other hand, the mental workload was evaluated using prefrontal cortex oxygenated hemoglobin (Oxy-Hb) obtained only with fNIRS. With increasing mental workload, the amount of oxygenated hemoglobin in the prefrontal cortex increased. The mental workload was assessed using just the prefrontal cortex oxygenated hemoglobin (Oxy-Hb) obtained via fNIRS. With an

increased mental workload, the amount of hemoglobin oxygenated found in the prefrontal cortex was raised.

SUGGESTIONS

As it is noticed, brain imaging studies are mostly focused on EEG signals. However, this area is very exciting and open to new developments. It will contribute to many new fields of study in terms of the proposed method and different modalities. Especially in the literature, hybrid modality studies such as fNIRS-EEG, fMRI-EEG, Hybrid PET-fMRI attract attention. It is thought that such studies will make a difference in CL research in multimedia environments. The details of the experimental process, parameters, and methodological differences are important in terms of the study's contribution. A list of criteria, operations, methodologies, or parameters should be created that are satisfied.

As a result, this paper concludes with a call for more research using more precise brain imaging approaches and CL t measure knowledge in multimedia environments. This study is expected to build on previous studies by using new methods and strategies for evaluating multimedia learning environments.

REFERENCES

Al Madi, N., & Khan, J. I. (2019). Is a picture worth a thousand words? A computational investigation of the modality effect. *International Journal of Computational Science and Engineering, 19*(3), 440–451. doi:10.1504/IJCSE.2019.101351

Al Madi, N. S., & Khan, J. I. (2016). Measuring learning performance and cognitive activity during multimodal comprehension. *2016 7th International Conference on Information and Communication Systems (ICICS)*, 50–55. 10.1109/IACS.2016.7476085

Anmarkrud, Ø., Andresen, A., & Bråten, I. (2019). Cognitive Load and Working Memory in Multimedia Learning: Conceptual and Measurement Issues. *Educational Psychologist*, *54*(2), 1–23. doi:10.1080/00461520.2018.1554484

Antonenko, P., Paas, F., Grabner, R., & van Gog, T. (2010). Using Electroencephalography to Measure Cognitive Load. *Educational Psychology Review*, *22*(4), 425–438. doi:10.100710648-010-9130-y

Ashby, F. G. (2015). An Introduction to fMRI. In B. U. Forstmann & E.-J. Wagenmakers (Eds.), *An Introduction to Model-Based Cognitive Neuroscience* (pp. 91–112). Springer. doi:10.1007/978-1-4939-2236-9_5

Balamurugan, B., Mullai, M., Soundararajan, S., Selvakanmani, S., & Arun, D. (2020). *Brain-computer interface for assessment of mental efforts in e-learning using the nonmarkovian queueing model. Computer Applications in Engineering Education*. Scopus. doi:10.1002/cae.22209

Bernhardt, K. A., Poltavski, D., Petros, T., Ferraro, F. R., Jorgenson, T., Carlson, C., Drechsel, P., & Iseminger, C. (2019). The effects of dynamic workload and experience on commercially available EEG cognitive state metrics in a high-fidelity air traffic control environment. *Applied Ergonomics, 77*, 83–91. doi:10.1016/j.apergo.2019.01.008

Bertolo, D., Dinet, J., & Vivian, R. (2014). Reducing cognitive workload during 3D geometry problem solving with an app on iPad. *2014 Science and Information Conference*, 896–900. 10.1109/SAI.2014.6918292

Cao, X., Cheng, M., Xue, X., & Zhu, S. (2019). Effects of Lecture Video Types on Student Learning: An Analysis of Eye-Tracking and Electroencephalography Data. In F. Xhafa, S. Patnaik, & M. Tavana (Eds.), *Advances in Intelligent, Interactive Systems, and Applications* (pp. 498–505). Springer International Publishing. doi:10.1007/978-3-030-02804-6_66

Castro-Meneses, L. J., Kruger, J.-L., & Doherty, S. (2020). Validating theta power as an objective measure of cognitive load in educational video. *Educational Technology Research and Development, 68*(1), 181–202. doi:10.1007/s11423-019-09681-4

Chang, H.-C., Hung, I.-C., Chew, S. W., & Chen, N.-S. (2016). Yet Another Objective Approach for Measuring Cognitive Load Using EEG-Based Workload. *2016 IEEE 16th International Conference on Advanced Learning Technologies (ICALT)*, 501–502. 10.1109/ICALT.2016.145

Conrad, C., & Bliemel, M. (2016). Psychophysiological Measures of Cognitive Absorption and Cognitive Load in E-Learning Applications. *ICIS 2016 Proceedings*. https://aisel.aisnet.org/icis2016/HumanComputerInteraction/Presentations/9

Crk, I., & Kluthe, T. (2014). Toward using alpha and theta brain waves to quantify programmer expertise. *2014 36th Annual International Conference of the IEEE Engineering in Medicine and Biology Society*, 5373–5376. 10.1109/EMBC.2014.6944840

Dan, A., & Reiner, M. (2017). Real Time EEG Based Measurements of Cognitive Load Indicates Mental States During Learning. *Journal of Educational Data Mining, 9*(2), 31–44. doi:10.5281/zenodo.3554719

Dan, A., & Reiner, M. (2017). EEG-based cognitive load of processing events in 3D virtual worlds is lower than processing events in 2D displays. *International Journal of Psychophysiology, 122*, 75–84. doi:10.1016/j.ijpsycho.2016.08.013

Dan, A., & Reiner, M. (2018). Reduced mental load in learning a motor visual task with virtual 3D method. *Journal of Computer Assisted Learning*, *34*(1), 84–93. doi:10.1111/jcal.12216

Díaz, D., Ramírez, R., & Hernández-Leo, D. (2015). The Effect of Using a Talking Head in Academic Videos: An EEG Study. *2015 IEEE 15th International Conference on Advanced Learning Technologies*, 367–369. 10.1109/ICALT.2015.89

Eldenfria, A., & Al-Samarraie, H. (2019). Towards an Online Continuous Adaptation Mechanism (OCAM) for Enhanced Engagement: An EEG Study. *International Journal of Human-Computer Interaction, 35*(20), 1960–1974. doi:10.1080/10447318.2019.1595303

Fernandez Rojas, R., Debie, E., Fidock, J., Barlow, M., Kasmarik, K., Anavatti, S., Garratt, M., & Abbass, H. (2020). Electroencephalographic Workload Indicators During Teleoperation of an Unmanned Aerial Vehicle Shepherding a Swarm of Unmanned Ground Vehicles in Contested Environments. *Frontiers in Neuroscience, 14*. doi:10.3389/fnins.2020.00040

Gerlič, I., & Jaušovec, N. (2001). Differences in EEG power and coherence measures related to the type of presentation: Text versus multimedia. *Journal of Educational Computing Research, 25*(2), 177–195. doi:10.2190/YDWY-U3FJ-4LY4-LYND

Hilbert, S., McAssey, M., Bühner, M., Schwaferts, P., Gruber, M., Goerigk, S., & Taylor, P. C. J. (2019). Right hemisphere occipital rTMS impairs working memory in visualizers but not in verbalizers. *Scientific Reports*, *9*(1), 6307. doi:10.103841598-019-42733-6 PMID:31004125

Jenkins, S. D., & Brown, R. D. H. (2014). A correlational analysis of human cognitive activity using Infrared Thermography of the supraorbital region, frontal EEG and self-report of core affective state. *Proceedings of the 2014 International Conference on Quantitative InfraRed Thermography*. 10.21611/qirt.2014.131

Juanes, J. A., Ruisoto, P., Obeso, J. A., Prats, A., & San-Molina, J. (2015). Computer-Based Visualization System for the Study of Deep Brain Structures Involved in Parkinson's Disease. *Journal of Medical Systems*, *39*(11), 151. doi:10.100710916-015-0348-6 PMID:26370536

Korbach, A., Brünken, R., & Park, B. (2017). Measurement of cognitive load in multimedia learning: A comparison of different objective measures. *Instructional Science*, *45*(4), 515–536. doi:10.100711251-017-9413-5

Kruger, J.-L., Hefer, E., & Matthew, G. (2013). Measuring the impact of subtitles on cognitive load: Eye tracking and dynamic audiovisual texts. *Proceedings of the 2013 Conference on Eye Tracking South Africa*, 62–66. 10.1145/2509315.2509331

Kruger, J-L., & Doherty, S. (2016). *Measuring cognitive load in the presence of educational video: Towards a multimodal methodology*. doi:10.14742/ajet.3084

Kruger, J.-L., Hefer, E., & Matthew, G. (2014). Attention distribution and cognitive load in a subtitled academic lecture: L1 vs. L2. *Journal of Eye Movement Research, 7*(5). https://www.scopus.com/inward/record.uri?eid=2-s2.0-84921875042&partnerID=40&md5=37f8408445395de5b8087cb794e90925

Lee, H. (2014). Measuring cognitive load with electroencephalography and self-report: Focus on the effect of English-medium learning for Korean students. *Educational Psychology, 34*(7), 838–848. doi :10.1080/01443410.2013.860217

León-Carrion, J., Damas-López, J., Martín-Rodríguez, J. F., Domínguez-Roldán, J. M., Murillo-Cabezas, F., Barroso y Martin, J. M., & Domínguez-Morales, M. R. (2008). The hemodynamics of cognitive control: The level of concentration of oxygenated hemoglobin in the superior prefrontal cortex varies as a function of performance in a modified Stroop task. *Behavioural Brain Research*, *193*(2), 248–256. doi:10.1016/j.bbr.2008.06.013 PMID:18606191

Leppink, J., Paas, F., Van der Vleuten, C. P. M., Van Gog, T., & Van Merriënboer, J. J. G. (2013). Development of an instrument for measuring different types of cognitive load. *Behavior Research Methods*, *45*(4), 1058–1072. doi:10.375813428-013-0334-1 PMID:23572251

Liu, C., Wang, R., Li, L., Ding, G., Yang, J., & Li, P. (2020). Effects of encoding modes on memory of naturalistic events. *Journal of Neurolinguistics, 53*. doi:10.1016/j.jneuroling.2019.100863

Liu, C.-J., & Chiang, W.-W. (2014). Theory, Method And Practice Of Neuroscientific Findings In Science Education. *International Journal of Science and Mathematics Education*, *12*(3), 629–646. doi:10.100710763-013-9482-0

Loftus, J., Jacobsen, M., & Wilson, T. D. (2016). Spatial Ability Mitigates Cognitive Load during Learning with Dynamic Images: A Transcranial Doppler Ultrasonography Study. AERA Online Paper Repository.

Loftus, J. J., Jacobsen, M., & Wilson, T. D. (2017). Learning and assessment with images: A view of cognitive load through the lens of cerebral blood flow. *British Journal of Educational Technology, 48*(4), 1030–1046. doi:10.1111/bjet.12474

Loftus, J. J., Jacobsen, M., & Wilson, T. D. (2018). The relationship between spatial ability, cerebral blood flow and learning with dynamic images: A transcranial Doppler ultrasonography study. *Medical Teacher, 40*(2), 174–180. doi:10.1080/0142159X.2017.1395401

Makransky, G., Terkildsen, T. S., & Mayer, R. E. (2019a). Adding immersive virtual reality to a science lab simulation causes more presence but less learning. *Learning and Instruction*, *60*, 225–236. doi:10.1016/j.learninstruc.2017.12.007

Makransky, G., Terkildsen, T. S., & Mayer, R. E. (2019b). Role of subjective and objective measures of cognitive processing during learning in explaining the spatial contiguity effect. *Learning and Instruction*, *61*, 23–34. doi:10.1016/j.learninstruc.2018.12.001

Mazher, M., Aziz, A. A., Malik, A. S., & Qayyum, A. (2015a). A statistical analysis on learning and nonlearning mental states using EEG. *2015 IEEE Student Symposium in Biomedical Engineering Sciences (ISSBES)*, 36–40. 10.1109/ISSBES.2015.7435889

Mazher, M., Aziz, A. B. A., Malik, A. S., & Qayyum, A. (2015b). A comparison of brain regions based on EEG during multimedia learning cognitive activity. *2015 IEEE Student Symposium in Biomedical Engineering Sciences (ISSBES)*, 31–35. 10.1109/ISSBES.2015.7435888

Mazher, M., Aziz, A. A., & Malik, A. S. (2016). Evaluation of rehearsal effects of multimedia content based on EEG using machine learning algorithms. *2016 6th International Conference on Intelligent and Advanced Systems (ICIAS)*, 1–6. 10.1109/ICIAS.2016.7824134

Mazher, M., Abd Aziz, A., Malik, A. S., & Ullah Amin, H. (2017). An EEG-Based Cognitive Load Assessment in Multimedia Learning Using Feature Extraction and Partial Directed Coherence. *IEEE Access, 5*, 14819–14829. doi:10.1109/ACCESS.2017.2731784

Mutlu-Bayraktar, D., Cosgun, V., & Altan, T. (2019). Cognitive load in multimedia learning environments: A systematic review. *Computers & Education*, *141*, 103618. doi:10.1016/j.compedu.2019.103618

Oakley, A. (2012). Foreword. In D. Gough, S. Oliver, & J. Thomas (Eds.), *An Introduction to Systematic Reviews* (pp. 7–10). SAGE Publications.

Ortiz De Guinea, A., Titah, R., & Léger, P.-M. (2013). Measure for Measure: A two study multi-trait multi-method investigation of construct validity in IS research. *Computers in Human Behavior, 29*(3), 833–844. doi:10.1016/j.chb.2012.12.009

Örün, Ö., & Akbulut, Y. (2019). Effect of multitasking, physical environment and electroencephalography use on cognitive load and retention. *Computers in Human Behavior*, *92*, 216–229. doi:10.1016/j.chb.2018.11.027

Paas, F., & Sweller, J. (2014). Implications of Cognitive Load Theory. In *The Cambridge Handbook of Multimedia Learning* (2nd ed., pp. 27–43). Cambridge University Press. doi:10.1017/CBO9781139547369.004

Paas, F., Tuovinen, J. E., Tabbers, H., & Van Gerven, P. W. (2003). Cognitive load measurement as a means to advance cognitive load theory. *Educational Psychologist*, *38*(1), 63–71. doi:10.1207/S15326985EP3801_8

Qayyum, A., Faye, I., Malik, A. S., & Mazher, M. (2018). Assessment of Cognitive Load using Multimedia Learning and Resting States with Deep Learning Perspective. *2018 IEEE-EMBS Conference on Biomedical Engineering and Sciences (IECBES)*, 600–605. 10.1109/IECBES.2018.8626702

Qayyum, A., Khan, M. K. A. A., Mazher, M., & Suresh, M. (2018). Classification of EEG Learning and Resting States using 1D-Convolutional Neural Network for Cognitive Load Assessment. *2018 IEEE Student Conference on Research and Development (SCOReD)*, 1–5. 10.1109/SCORED.2018.8711150

Reinerman-Jones, L., Barber, D. J., Szalma, J. L., & Hancock, P. A. (2017). Human interaction with robotic systems: Performance and workload evaluations. *Ergonomics, 60*(10), 1351–1368. doi:10.1080/00140139.2016.1254282

Ross, A. J., & Sachdev, P. S. (2004). Magnetic resonance spectroscopy in cognitive research. *Brain Research. Brain Research Reviews*, *44*(2), 83–102. doi:10.1016/j.brainresrev.2003.11.001 PMID:15003387

Ruisoto Palomera, P., Juanes Méndez, J. A., & Prats Galino, A. (2014). Enhancing neuroanatomy education using computer-based instructional material. *Computers in Human Behavior*, *31*, 446–452. doi:10.1016/j.chb.2013.03.005

Schlorhaufer, C., Behrends, M., Diekhaus, G., Keberle, M., & Weidemann, J. (2012). Implementation of a web-based, interactive polytrauma tutorial in computed tomography for radiology residents: How we do it. *European Journal of Radiology*, *81*(12), 3942–3946. doi:10.1016/j.ejrad.2012.07.006 PMID:22883533

Sejdić, E., Kalika, D., & Czarnek, N. (2013). An Analysis of Resting-State Functional Transcranial Doppler Recordings from Middle Cerebral Arteries. *PLoS One*, *8*(2), e55405. doi:10.1371/journal.pone.0055405 PMID:23405146

Sweller, J. (2010). Element Interactivity and Intrinsic, Extraneous, and Germane Cognitive Load. *Educational Psychology Review*, *22*(2), 123–138. doi:10.100710648-010-9128-5

Sweller, J., Ayres, P., & Kalyuga, S. (2011). *Cognitive Load Theory*. Springer. doi:10.1007/978-1-4419-8126-4

Sweller, J., van Merriënboer, J. J. G., & Paas, F. (2019). Cognitive Architecture and Instructional Design: 20 Years Later. *Educational Psychology Review*, *31*(2), 261–292. doi:10.100710648-019-09465-5

Uysal, M. P. (2016). Evaluation of learning environments for object-oriented programming: Measuring cognitive load with a novel measurement technique. *Interactive Learning Environments*, *24*(7), 1590–1609. doi:10.1080/10494820.2015.1041400

Walter, C., Schmidt, S., Rosenstiel, W., Gerjets, P., & Bogdan, M. (2013). Using Cross-Task Classification for Classifying Workload Levels in Complex Learning Tasks. *2013 Humaine Association Conference on Affective Computing and Intelligent Interaction*, 876–881. 10.1109/ACII.2013.164

Wang, J., Antonenko, P., Keil, A., & Dawson, K. (2020). *Converging Subjective and Psychophysiological Measures of Cognitive Load to Study the Effects of Instructor-Present Video. In Mind, Brain, and Education*. Scopus., doi:10.1111/mbe.12239

Whelan, R. R. (2007). Neuroimaging of cognitive load in instructional multimedia. *Educational Research Review, 2*(1), 1–12. doi:10.1016/j.edurev.2006.11.001

Zahabi, M., Abdul Razak, A. M., Shortz, A. E., Mehta, R. K., & Manser, M. (2020). Evaluating advanced driver-assistance system trainings using driver performance, attention allocation, and neural efficiency measures. *Applied Ergonomics, 84*. doi:10.1016/j.apergo.2019.103036

Zhang, X., & Liu, S. (2017). Understanding Reading Comprehension in Multi-display Presenting System: Visual Distribution and Cognitive Effect. In C. Stephanidis (Ed.), *HCI International 2017 – Posters' Extended Abstracts* (pp. 207–214). Springer International Publishing. doi:10.1007/978-3-319-58753-0_32

Zhou, Y., Xu, T., Cai, Y., Wu, X., & Dong, B. (2017). Monitoring Cognitive Workload in Online Videos Learning Through an EEG-Based Brain-Computer Interface. In P. Zaphiris & A. Ioannou (Eds.), *Learning and Collaboration Technologies. Novel Learning Ecosystems* (pp. 64–73). Springer International Publishing. doi:10.1007/978-3-319-58509-3_7

APPENDIX: ABBREVIATIONS

CLT: Cognitive load theory
CT: Computerized Tomography
MRI: Magnetic Resonance Imaging
TMS: Transcranial Magnetic Stimulation
TCD: Transcranial Doppler Ultrasonography
MEG: Magnetoencephalography
EEG: Electroencephalography
fNIRS: Functional near-infrared spectroscopy
fMRI: Functional magnetic resonance imaging
PET: Positron emission tomography
MRS: Magnetic Resonance Spectroscopy
LDA: Linear discriminant analysis
kNN: K-nearest neighbors
SVM: Support Vector Machines
ANN: Artificial Neural Network
RBF: Radial-Basis-Function kernel
KC: The Kappa Coefficients
CNN: Convolutional Neural Network
CLI: Cognitive load index
PSD: Power Spectral Density
FFT: Fast Fourier Transform
ASP: Average spectral power
DFT: Discrete Fourier Transform
DWT: Discrete wavelets transform
IWMF: The intensity weighted mean frequency
IWBW: its bandwidth
ERS/ERD: Event-Related Synchronization/ Desynchronization
CBV: Cerebral blood velocity
WT: Wavelet transform
CE: Cognitive effort
MOOC: Massive open online course
OCAM: Online continuous adaptation mechanism
MTMM: Multitrait-multimethod matrix
AG: Angular gyrus

Chapter 5
A Review of Automated Diagnosis of ECG Arrhythmia Using Deep Learning Methods

Praveen Kumar Tyagi
Maulana Azad National Institute of Technology, Bhopal, India

Neha Rathore
Maulana Azad National Institute of Technology, Bhopal, India

Deepak Parashar
IES College of Technology, Bhopal, India

Dheeraj Agrawal
Maulana Azad National Institute of Technology, Bhopal, India

ABSTRACT

Arrhythmia is a medical condition in which the heart's normal pumping process becomes irregular. Early identification of arrhythmia is one of the essential phases in diagnosing the disorder. However, due to the relatively low amplitudes, visually assessing the electrocardiogram signals can also be difficult and time-consuming. Using an automation process from a clinical perspective can significantly expedite and increase the accuracy of diagnosis. Conventional machine learning algorithms have gained significant progress. Such methods depend on customized feature extraction, which requires in-depth knowledge. Deep learning (DL) developments have made it feasible to extract and classify high-level features automatically. This study reviewed recent significant progress in DL approaches for automated arrhythmia diagnosis and some critical areas of the dataset used, the application and category of data input, the modeling architecture, and the performance. Overall, this study provides extensive and detailed knowledge for researchers interested in widening existing knowledge in this area.

DOI: 10.4018/978-1-6684-3947-0.ch005

INTRODUCTION

Heart disorders, also known as Cardiovascular Diseases (CDs), are the leading causes of increased mortality rates. They are caused by a lack of blood in the coronary artery, which also supplies blood to the heart. CDs cause arrhythmia, or irregular heartbeats, and depending on the severity of the arrhythmia issue, sudden death can occur (Dahe & Sodini, 2014). The electrocardiogram/electrokardiogram (ECG/EKG) depicts the electrical activity of the human heart, and the ECG pulse morphologies reveal particular types of arrhythmia based on various heart diseases. Arrhythmia identification from the ECG signal that is precise and efficient can save billions of lives and save healthcare costs throughout the world (Chen et al., 2017). This prompted us to conduct a detailed ECG analysis review and respond in the form of a method model based on many phases in order to further describe and categorize the flow and relevance of each stage of ECG signal analysis. With the massive effects of an efficient ECG signal analysis on public health and the economy, providing a worldview of hardware and software components, as well as real-time data collection using wearable and portable technologies to analyze an ECG signal as a function of the stage-based method, is another motivating factor that led us to conduct this research (Luz et al., 2016).

Figure 1. Arrhythmia detection process (a) Machine learning (b) Deep learning framework (Parvanesh et al., 2019)

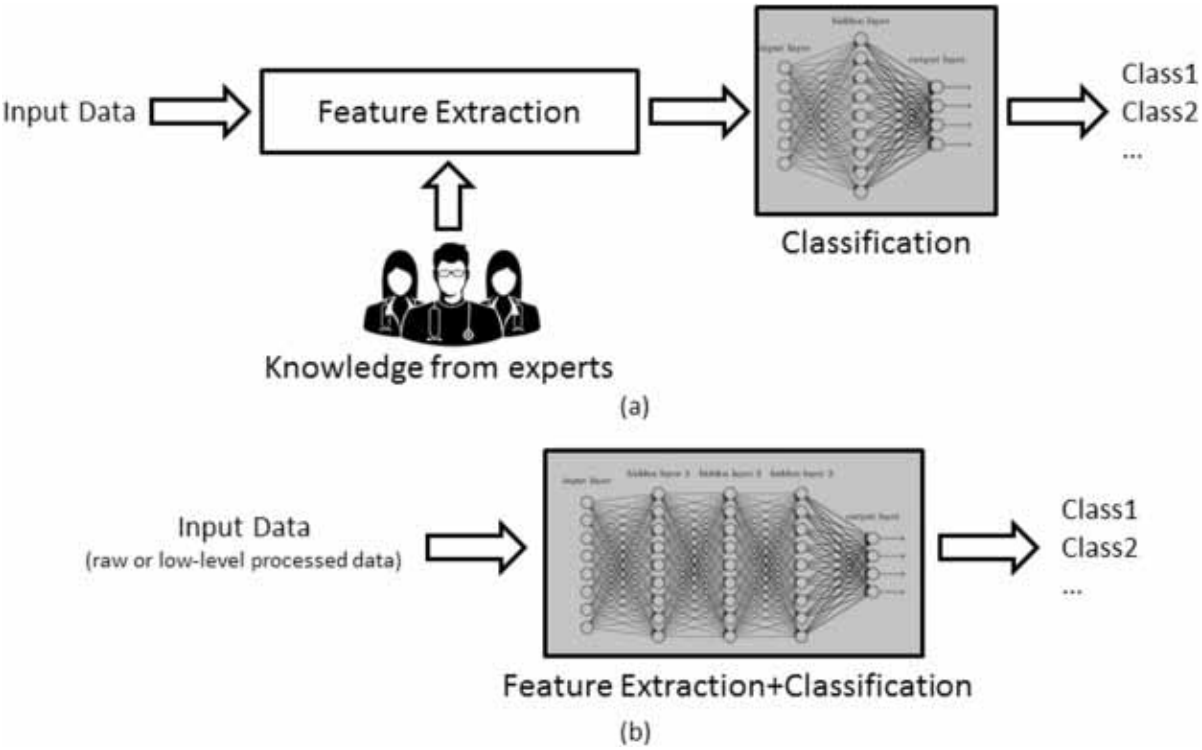

The conventional CDs diagnostic paradigm relies on the medical history and clinical evaluations of each patient. Such observations are analyzed using a set of quantitative medical characteristics to identify individuals according to medical disease taxonomy. In many conditions, the conventional rule-based diagnostic approach is inefficient because of handling the large amounts of data sources, and it requires extensive analysis and specialized knowledge to reach appropriate diagnostic performance. The challenge will become increasingly acute in areas where medical specialists and clinical equipment are few, particularly in developing nations. Due to its simplicity and modest cost, analyzing an Electrocardiogram is the more used method for identifying cardiac arrhythmia. A large size of ECG data collected every day, at residence and in hospitals, could limit human operators/technicians from reviewing the data (Hannun et al., 2019). As a result, numerous strategies for totally automated arrhythmia identification or event selection for subsequent validation by human specialists have been presented. Conventional machine learning to deep learning and their combinations are among the machine learning-based approaches for ECG observation and interpretation (Parvaneh & Rubin, 2018). In conventional machine learning (ML) algorithms Fig. 1, input such as ECG and RR series data is identified to a collection of features such as morphological properties or any ECG characteristic, the presence of a P wave, vector cardiogram, entropy measures, vector cardiogram, Poincare section-based features, coefficients derived with wavelets and heartbeat interval (Parvanesh et al., 2019; Zhang et al., 2014; Parashar & Agrawal, 2020) and then a classification model is used to classify the data as a neural network, learning vector quantization, support vector machine (Parashar & Agrawal, 2021; Llamedo & Martínez, 2010). Expertise knowledge is used to identify features that are commonly depictions of cardiac arrhythmia. In recent years, conventional machine learning algorithms have made substantial progress. They depend on hand-crafted feature identification, which needs significant domain expertise and signal data preprocessing. Furthermore, due to the wide variation in wave shape across subjects and the background noise, computerized interpretation is hard to obtain high accuracy.

Deep learning (DL) has recently advanced to the point where it is now able to extract high-level features automatically and classify them. Raw or low-level processed data is input into a deep network architecture made up of many different hidden layers in deep learning methods Fig. 1. In contrast to classical ML, the deep network does feature extraction, selection, and classification automatic DL-based algorithms outperformed conventional methods on a variety of data sets (Acharya et al., 2017; Sannino & De Pietro, 2018). Convolutional neural networks (CNNs) in particular have been effectively employed for performing complicated image processing tasks on the both non-medical (Li et al., 2018) and medical (Ullah et al., 2021) problems. Deep neural networks (DNN) have recently been developed or modified for the processing of 1-D bio-signals in time series (Shen et al., 2021; Zarei et al., 2022).

The remainder of the paper is structured according to as follows. In the Section 2 provides a methodology and database used in this study. Section 3 and 4 briefly describe the types of arrhythmia and performance metrics, respectively. Literature review of deep learning in arrhythmia presented in section 5. Finally, Section 6 concludes the paper.

METHODOLOGY AND DATABASE

This paper aims to evaluate the work on ECG interpretation that has been published in the literature over the last few decades, including signal preprocessing to feature selection to real-time classification. From 2011 to 2021, relevant papers were obtained from a variety of sources and publishers, including IEEE,

SENSORS, MDPI, ELSEVIER, SPRINGER, and IOP. To find the relevant articles, different keywords were used, such as "deep learning'', "DNN", with the "ECG classification of Arrhythmia signal", "real-time detection systems for ECG", and "cardiac arrhythmia". Starting with the data acquisition source, feature selection, and eventually classification, the analysis covers the various phases that ECG data goes through. Different transformations and DL techniques are used to detect centroid points such as R-peaks and QRS complex. The motive guides for dataset collection for ECG signal processing for feature extraction and/or beat classification based on various arrhythmias. The ECG signal's properties aid in determining the features that can be extracted or examined further. This stage discusses the different ECG data acquisition sources that can be used as input to the stages-based model, with a focus on the data source. The dataset referenced are MITDB ECG, MIT-BIH database, BIDMC, Fantasia database, challengeDB 2017 (Moody, 2001, 2008; Goldberger et al.,2000; Penzel et al., 2000; Clifford et al., 2017). Each database does have its own set of properties, such as the set of records, duration of time, sample size, ECG channel counts, frequency label, age category, and purpose of arrhythmia. There are several EGC databases that can be accessed for free online. For EGC classification, numerous current systems have been trained on such databases. Table 1 summarizes the ECG recording characteristics for various databases. It also presents the time window which is used to classify the details. Various morphological profiles for registered ECG signals can be found in these databases. In such recording environments, certain databases used telehealth sensors to capture certain ECG signals. According to research, ECG classification based on a single-lead record can be as accurate as twelve-lead ECG recordings in some conditions.

Table 1. ECG database specifications

Database	Number of Recording	Records time duration	Sampling frequency	Disease
Physio Net, The ECG-ID Database (Goldberger et al., 2000)	310	20s	500hz	Normal sinus rhythm (NSR) AF
Physikalisch-Technische Bundesanstalt (PTB) (Goldberger et al., 2000)	549	2 min	1Khz	MI
MIT-BIH Supraventricular Arrhythmia Database (SVDB) (Moody et al., 2001)	48	30 min	128Hz	VEB SVEB
Creighton University VT Database (CUDB) (Goldberger et al., 2000)	35	8 min	250Hz	VT VF VFib
The DNNIH Arrhythmia Database MITDB (Goldberger et al., 2000)	48	30 min	360 Hz	Arrhythmia Abnormalities
Fantasia Database- Physio Bank (Goldberger et al., 2000)	40	120 min	250 Hz	NSR
BIDMC PPG and Respiration Dataset (Goldberger et al., 2000)	53	8 min	125 Hz	Congestive heart failure
Physionet Apnea ECG (Penzel et al., 2000)	70		100Hz	Sleep Apnea NSR
ChallengeDB2017 (Clifford et al. (2017)	3658	6-60 sec	500 Hz	NSR AF

TYPES OF ECG ARRHYTHMIA

Cardiac arrhythmias are irregular heartbeats caused by abnormal electrical impulses. ECG characterization indicates the heart's condition. ECG readings are affected by any disturbance in the electrical activity of cardiac nerve cells. The heart's electrical signals are expressed by the ECG signal. The ECG record, as shown in the fig. 2, is generally a periodic signal. One period of the blood transformation process from the heart of the arteries constitutes one phase of the Heart rhythm. P-QRS-T waves make up one cardiac cycle in the ECG. A reduced voltage displacement away from its baseline induced by atrial depolarization would be a P-wave (Wasimuddin et al., 2020). The QRS complex is the greatest portion of the magnitude of the ECG induced by vertical depolarization, thereby training the heart muscles for the next ECG period. Many of the ECG's clinically valuable knowledge is found in the cycles and amplitudes identified by the characteristics of the ECG (Luz et al., 2016). Particularly for large recording research, the advancement of an accurate and rapid method for automated ECG extracting features is of significant importance. This research is made possible by the vast number of known wavelet families and functions (Hoffmann et al., 2020). The ECG function extraction method offers basic features for use in analysis (magnitude and periods). Because of the time-varying structure of the signal as it is influenced by noise and under many physiological environments, the development of an algorithm for the identification of the P-wave, QRS complex, and T-wave in ECG is a challenging problem. A series of methods have recently been used to detect their characteristics. QRS identification in the ECG series is one of the basic problems of ECG signal processing. During one cardiac cycle, the QRS complex is comprised of 3 characteristic points, defined as Q, R, and S. The biggest amplitude component of the ECG signal has been the QRS complex. There are various algorithms for identification, such as wavelet transformation, filtering methods, artificial neural networks, Markov models, etc. The key objective of the paper is to use methods of wavelet transformation to derive different features such as R max, QRS estimation (Annam et al., 2020; Diker et al., 2020).

Arrhythmia is divided into two categories. The first category includes Bradyarrhythmias, which are characterized by low heart rates of lower than 60 beats per minute. Tachyarrhythmia with a heart rate of more than 100 beats per minute, is further subdivided into two categories. The first form is supraventricular tachycardia (SVT), which includes AV nodal and AV junctional tachycardia. The second category is ventricular arrhythmia, which includes premature ventricular beats, ventricular tachycardia (VT), and ventricular fibrillation (VF) (Wasimuddin et al., 2020). A brief description of the most frequent forms of arrhythmia.

Figure 2. Electrocardiograph waveform over a one cardiac rhythm (Diker et al., 2020)

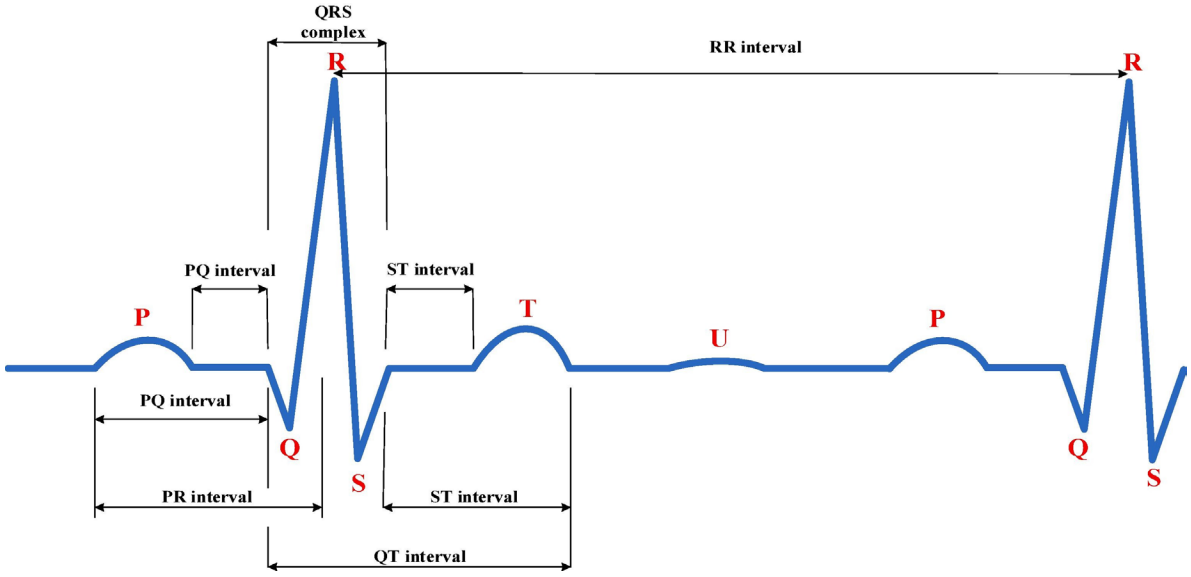

- Atrial Fibrillation (AF) is a condition in which electrical impulses in the atrium fire very frequently, resulting in a fast atrial rhythm.
- Myocardial Infarction (MI) occurs when blood circulation to a region of the cardiovascular reduces or ceases, causing irreversible damage to the ventricular arteries (Ebrahimi et al., 2020).
- Ventricular fibrillation (VFib) is a cardiovascular irregularity wherein the heart quivers instead of pumping because of disordered electrophysiological impulses in the ventricles, that is characterized by irregular indistinct QRS complexes and no discernible P-waves (Ebrahimi et al., 2020).
- Atrial flutter (AFL) is a common irregular cardiac rhythm that begins in the heart's atrial chambers.
- A ventricular ectopic beat (VEB) is an additional heartbeat that originates in the heart's lower chamber. This pulse, also known as a premature ventricular contraction (PVC), happens before the usual heartbeat (Gale Encyclopedia of Medicine, 2008).
- Supraventricular Ectopic Beats (SVEB) are irregular heartbeats that occur shortly before a typical beat. Ectopic heartbeats are common and normally do not cause worry, however, they might induce anxiety.

PERFORMANCE METRICS

Table 2. Parameters for evaluating performance metrics

Parameters	Calculation
accuracy (Acc)	$\frac{TP+TN}{TP+FP+TN+FN}$
Specificity (Spe)	$\frac{TN}{TN+FP}$
Sensitivity (Sen)	$\frac{TP}{TP+FN}$
Precision (Pre)	$\frac{TP}{TP+FP}$
Recall (Rec)	$\frac{TP}{TP+FN}$
Positive- predictive value (PPV)	$\frac{TP}{TP+FP}$
negative-predictive value (NPV)	$\frac{TN}{TN+FN}$
F_1	$2\frac{PPV*Sen}{PPV+Sen}$

A number of metrics are used to test performance of sleep apnea prediction algorithms. Table 2 presents the parameters and calculations used to determine the metrics. The true positive (TP), true negative (TN), false positive (FP), and false negative (FN) values have been used to measure some most similar parameters defined across most studies. The receiver operating characteristic (ROC) has been used to assess apnea detection efficiency of various classification thresholds, and the area under the ROC curve (AUC) is measured to assess overall performance. Positive- predictive value and sensitivity are used to calculate the F-measure, also defined as the F1 Score.

DEEP LEARNING TECHNIQUE IN ARRHYTHMIA DETECTION

DL relates to research on extracting knowledge, forecasts, intelligent decision processing, or, in that other phrase, identifying complicated patterns using a collection of data known as training data. DNNs are much more scalable than conventional learning methods, as improved performance is frequently gained

by expanding the length of the structure or the training set. The deficiencies and insufficiency of several shallow models, such as Support vector machines (SVMs) and decision trees, notably since applied to advanced solutions, since its limits emerge in various ways, along with the necessity for a majority of human labor and the availability of a vast amount of data (Loni et al., 2020). Various models, including the CNN, Multilayer Preceptor (MLP), Deep Belief Network (DBN), and, Recurrent Neural Network (RNN), have recently been presented to enhance and develop accuracy in DL techniques. The late neural network evolved into the expanding neural network, which was described as a novel learning theory as time passed. Table 3 summarizes the various DL technique literature that has been studied.

CONVOLUTIONAL NEURAL NETWORK (CNN)

CNN is a common DNN structure that is often trained using a gradient-based evaluation approach. For classifying, CNNs employ single or multiple convolutional and max pooling, succeeded by a fully linked layer. Acharya et al. (2017) presented an 11-layer deep CNN-based technique for autonomously diagnosing MI. The obtained R-peaks are used to divide all the ECG signals, except the beginning and final beats. Each episode is normalized with Z-score standardization to fix the issue of amplitude scaling and eliminate the offset effect. For ECG signals without noise, the average Acc, Sen, and Spe were 95.22 percent, 95.49 percent, and 94.19 percent, respectively. In another study, the Acharya et al. (2019) method to detect CHF automatically utilizing ECG data, this study used an 11-layer deep CNN model. The suggested model is totally automated and does not need R-peak detection. In addition, the CNN model was trained and tested using four distinct data sets of Physio Bank. Wang et al. (2019a) proposed diagnosis system network structure was built using the long short-term memory (LSTM) and CNN to identify CHF automatically. Also suggested a deep learning-based end-to-end system for CHF identification using short-term RR intervals, utilizing five open-source datasets comprising all-class CHF data and obtained Acc and Sen of 99.2 respectively.

Fu et al. (2020) presented the identify and detect MI using 12-lead ECG recordings using the multi-lead attention (MLA) technique combined with CNN and a bidirectional gated recurrent unit (BiGRU) architecture. The MLA system calculates and distributes weights to distinct leads based on their value automatically. The 2-D CNN subsystem obtains discriminative spatial information by exploiting the interconnected features among leads. In addition, the BiGRU subsystem collects important temporal information from each lead. This proposed technique obtained Acc and Sen of 99.9 percent each and Sen of 99.6 percent.

MULTILAYER PERCEPTRON (MLP)

MLP is the most widely use the supervised network, and it has been shown to be successful at learning complex models. The MLP design varies, but it typically comprises of multiple levels of neurons coupled in a feed-forward method. Lou et al. (2017) Presented a time-frequency representation and a DL architectural model for patient-specific pulse categorization Time-frequency technology is an effective technique for characterizing biosignals. Li et al. (2018) suggested a technique for detecting Obstructive Sleep Apnea (OSA) using a solitary ECG data that is based on DNN and the Hidden Markov model (HMM). They computed the RR interval period and interpolated the RR interval data into 100

points using the validated R-peaks position. The characteristics were retrieved by DNN. The SVM and Artificial Neural Network classifier are used to feature classification. To address the aforementioned issues, Hammad et al (2020) propose a DNN technique where a learning stage technique involves using a strong feature extraction method to increase classification performance. The optimal combination of data extraction and categorization is then aggregated using a genetic algorithm (GA) approach. This technique comprises putting the ECG data into a DNN model that extracts deep information from each patient. The characteristics are then put into a GA, which calculates the best combination of them. The feature is then classified using a variety of classifiers, including SVM, and MLP.

Table 3. Summary of various Arrhythmia classification deep learning model performance analysis

Reference (year)	Analysis model	Appli-cation	Dataset	Performance metrics (%)
				Acc Spe Sen Pre Rec Others
Luo et al. (2017)	MLP	VEB SVEB	MITDB	99.1 99.5 93.3 - - PPV- 93.3 98.8 99.8 71.4 - - PPV- 94.4
Acharya et al. (2017)	CNN	MI	PTB	95.2 94.1 95.5 - - -
Sujadevi et al. (2017)	RNN GRU	NSR AF	MITDB	95.0 - - 100 88.9 F_1 - 94.1 100 - - 100 100 F_1 - 100
Taji et al. (2018)	DBN-RBM	AF	MITDB AFDB	81.0 85.0 - 65.0 68.1 -
Faust et al. (2018)	BiLSTM	AF	MITDB	98.5 98.6 98.3 - - PPV-98.3
Li et al. (2018)	MLP	OSA	Physionet	100 100 100 - - -
Acharya et al. (2019)	CNN+ FCN	CHF	BIDMC Fantaisa	95.8 95.7 96.5 - - - 98.3 98.1 98.5 - - -
Wang et al. (2019a)	CNN+ LSTM	CHF	BIDMC-MITBIH	99.2 99.7 99.2 - - -
Wang et al. (2019b)	GRNN	VEB SVEB	MITDB SVDB	97.4 98.3 85.7 - - - 97.2 99.2 77.2 - - -
Fu et al. (2020)	CNN+ BiGRU	MI	PTB	99.9 99.6 99.9 - - -
Hammed et al. (2020)	MLP+ GA	CDs	MIT-BIH	97.3 93.4 99.6 - - PPV- 98.5
Gourisaria et al. (2021)	DBN-LR	VEB	MIT-BIH	96.7 99.0 - 93.0 0.98 F_1 - 95.0
Jiang et al. (2021)	Resnet+BiLSTM	AF	Phydionet	86.7 - - 86.6 85.9 F_1 -88.0

DEEP BELIEF NETWORK (DBN)

In an unsupervised configuration, a DBN composed of layered restricted Boltzmann machines (RBM) is employed to learn a relevant feature representation of the data waveform. The DBN is developed in an unsupervised and greedy layer-by-layer approach, with data input without labeled and each layer learned one at a moment. When one layer has been trained, the following layer can be learned because the input of every hidden layer is, as stated previously, the output of the preceding layer. The objective is to extract a feature hierarchy from the set of data. Afterward, the completed set of features learned by the networks is produced by the last layer, and this feature set is employed by classification for supervised learning.

Taji et al. (2017) developed an approach to minimize the false alarm rate for AF diagnosis due to poor ECG measurements. They developed a DBN model with 3 RBM layers. The first 2 RBMs had generated RBMs that did not require labels, while the last level featured discriminative RBMs that categorized the data input user information with their labels. The outcomes demonstrate that for ECGs with lower SNR, gating, a data-remembering method, considerably enhanced AF diagnosis ability. With gating, Pre, Rec, Acc and Spe improved significantly, increasing to 65 percent, 68.1 percent, 81 percent, and 85 percent.

Gourisaria et al. (2021) proposed a deep learning technique to create a fully automated classification heartbeat system using various ECG pulse signals. An unsupervised DBN cascaded onto a basic logistic regression (LR) algorithm extracts useful features from ECG data for model performance optimization. The analysis showed significant feature enhancement is essential for correctly classifying the data, as performance-enhanced from 86 percent to 96 percent using extraction of features. Similar outcomes were obtained, with the DBN-Logistic approach outperforming 1D convolution.

RECURRENT NEURAL NETWORK (RNN)

RNN is the optimal learning method for learning sequential data inputs and time-series data processing since its feedback and current value are feeding back across that network as well as the output includes the addition of variables in memory. For each stage in the process, the RNN collects an information, updated its hidden layer, and made the prediction. The analyzed works used two forms of RNN: LSTM and gated recurrent unit (GRU).

RNNs can do a similar equivalent task for each element of an input signal, whereas the output is reliant on the preceding calculation. This system design includes a memory that stores knowledge regarding input history and previous estimates. Sujadevi et al. (2017) used DL algorithms such as RNN, LSTM, and GRU to identify AF in ECG traces very efficiently. Their method does not necessitate the use of any de-noising, filter, or preprocessing techniques. The data was classified as NSR or AF by the systems. They used the MIT-BIH PhysioNet database, which is open to the public. The experimental findings show that RNN, LSTM, and GRU attain accuracy of 95.0 percent, 100 percent, and 100 percent, respectively. To identify AF pulses, Faust et al. (2018) suggested a DL algorithm. A sliding window spanning 100 pulses has been used to split the data. The LSTM data blocks then were set up ahead of an RNN. With 10-fold cross-validation, it obtained 98.51 percent accuracy, and blindfold validation produced 99.77 percent accuracy. The suggested structure was simple because there was no requirement of data minimization by extraction of features.

Wang et al. (2019b) developed the Global Recurrent Neural Network, a globally and editable categorization framework (GRNN). First, based on GRNN's massive capacities and ability to fit. Second, when training and test samples come from different databases, the GRNN increases generalization performance. Finally, GRNN learns the significant distinctions between data from various categories automatically. There are four levels in all in the GRNN. To store a longer track record, LSTM units were used rather than typical RNN units in the morphology section. That after the next LSTM layer, a 20-node fully-connected outer layer was constructed.

To develop the classification method, Jiang et al (2021) presented three DL techniques. The classification algorithm includes the residual network (ResNet) and Bi-LSTM networks. The ResNet portion extracts local characteristics by superimposing 16 residual blocks, while the Bi-LSTM extracts global features simultaneously. Additionally, the fused characteristics, that can retrieve various aspects of the

source Data sets, were the global characteristic of Bi-LSTM as well as the localized characteristic from ResNet. The Pulse is classified into four categories without compromise of generalization: AF, noise, other, and normal signals.

CONCLUSION

The paper presented the findings of an evaluation of several approaches for identifying arrhythmia using ECG data signals. The review framework aimed to examine the best effective DL algorithms for diagnosing different forms of arrhythmia. The fundamental aspects of the most frequent approaches were examined in detail. AF, SVT, VF, SVEB, MI, and VFib were correctly classified using the MLP, CNN, DBN, GRU, and LSTM, respectively. The forms of inputs data signal utilized to learn and execute deep neural networks can indeed be different. ECG. This research examined how deep learning can also be utilized to identify physiological information and compared it to existing approaches. The outcomes of the ECG Classification research can get utilized by medical experts in the detection and interpreting of arrhythmias, and also in the implementation of technologies that automatically interconnect distant health professionals to the patient. Based on the outcomes of these literature studies, deep learning, namely CNN and DBN approach, has now been established as a potential approach for biological signal assessment. As a consequence, the review study's limited form will contribute modestly to the current amount of literature while simultaneously shining a light on research issues and prospective prospects in the field of biological signal processing. Then it is stated that using the right combination of the DL approach may significantly increase the performance of the classifier for the relevant application.

REFERENCES

Acharya, U. R., Fujita, H., Lih, O. S., Hagiwara, Y., Tan, J. H., & Adam, M. (2017). Automated detection of arrhythmias using different intervals of tachycardia ECG segments with convolutional neural network. *Information Sciences*, *405*, 81–90. doi:10.1016/j.ins.2017.04.012

Acharya, U. R., Fujita, H., Oh, S. L., Hagiwara, Y., Tan, J. H., & Adam, M. (2017). Application of deep convolutional neural network for automated detection of myocardial infarction using ECG signals. *Information Sciences*, *415*, 190–198.

Acharya, U. R., Fujita, H., Oh, S. L., Hagiwara, Y., Tan, J. H., Adam, M., & Tan, R. S. (2019). Deep convolutional neural network for the automated diagnosis of congestive heart failure using ECG signals. *Applied Intelligence*, *49*(1), 16–27.

Annam, J. R., Kalyanapu, S. Ch. S., Somala, J., & Raju, S. B. (2020). Classification of ECG heartbeat arrhythmia: A review. *Procedia Computer Science*, *171*, 679–688.

Chen, Z., Luo, J., Lin, K., Wu, J., Zhu, T., Xiang, X., & Meng, J. (2017). An energy-efficient ECG processor with weak-strong hybrid classifier for arrhythmia detection. *IEEE Transactions on Circuits and Wystems. II, Express Briefs*, *65*(7), 948–952. doi:10.1109/TCSII.2017.2747596

Clifford, G. D., Liu, C., Moody, B., Li-wei, H. L., Silva, I., Li, Q., . . . Mark, R. G. (2017, September). AF classification from a short single lead ECG recording: The PhysioNet/computing in cardiology challenge 2017. In 2017 Computing in Cardiology (CinC) (pp. 1-4). IEEE.

Da He, D., & Sodini, C. G. (2014). A 58 nW ECG ASIC with motion-tolerant heartbeat timing extraction for wearable cardiovascular monitoring. *IEEE Transactions on Biomedical Circuits and Systems*, *9*(3), 370–376. PMID:25252285

Diker, A., Avci, E., Tanyildizi, E., & Gedikpinar, M. (2020). A novel ECG signal classification method using DEA-ELM. *Medical Hypotheses*, *136*, 109515.

Ebrahimi, Z., Loni, M., Daneshtalab, M., & Gharehbaghi, A. (2020). A review on deep learning methods for ECG arrhythmia classification. *Expert Systems with Applications: X, 7*, 100033.

Faust, O., Shenfield, A., Kareem, M., San, T. R., Fujita, H., & Acharya, U. R. (2018). Automated detection of atrial fibrillation using long short-term memory network with RR interval signals. *Computers in Biology and Medicine*, *102*, 327–335.

Fu, L., Lu, B., Nie, B., Peng, Z., Liu, H., & Pi, X. (2020). Hybrid network with attention mechanism for detection and location of myocardial infarction based on 12-lead electrocardiogram signals. *Sensors (Basel)*, *20*(4), 1020.

Goldberger, A. L., Amaral, L. A., Glass, L., Hausdorff, J. M., Ivanov, P. C., Mark, R. G., ... Stanley, H. E. (2000). PhysioBank, PhysioToolkit, and PhysioNet: Components of a new research resource for complex physiologic signals. *Circulation*, *101*(23), e215–e220.

Gourisaria, M. K., Harshvardhan, G. M., Agrawal, R., Patra, S. S., Rautaray, S. S., & Pandey, M. (2021). Arrhythmia Detection Using Deep Belief Network Extracted Features From ECG Signals. *International Journal of E-Health and Medical Communications*, *12*(6), 1–24. https://doi.org/10.4018/IJEHMC.20211101.oa9

Hammad, M., Iliyasu, A. M., Subasi, A., Ho, E. S., & Abd El-Latif, A. A. (2020). A multitier deep learning model for arrhythmia detection. *IEEE Transactions on Instrumentation and Measurement*, *70*, 1–9.

Hannun, A. Y., Rajpurkar, P., Haghpanahi, M., Tison, G. H., Bourn, C., Turakhia, M. P., & Ng, A. Y. (2019). Cardiologist-level arrhythmia detection and classification in ambulatory electrocardiograms using a deep neural network. *Nature Medicine*, *25*(1), 65–69. doi:10.103841591-018-0268-3 PMID:30617320

Hoffmann, J., Mahmood, S., Fogou, P. S., George, N., Raha, S., Safi, S., . . . Hübner, M. (2020, September). A Survey on Machine Learning Approaches to ECG Processing. In 2020 Signal Processing: Algorithms, Architectures, Arrangements, and Applications (SPA) (pp. 36-41). IEEE.

Jiang, M., Gu, J., Li, Y., Wei, B., Zhang, J., Wang, Z., & Xia, L. (2021). HADLN: Hybrid attention-based deep learning network for automated arrhythmia classification. *Frontiers in Physiology*, 12.

Li, J., Qiu, T., Wen, C., Xie, K., & Wen, F. Q. (2018). Robust face recognition using the deep C2D-CNN model based on decision-level fusion. *Sensors (Basel)*, *18*(7), 2080. doi:10.339018072080 PMID:29958478

Li, K., Pan, W., Li, Y., Jiang, Q., & Liu, G. (2018). A method to detect sleep apnea based on deep neural network and hidden Markov model using single-lead ECG signal. *Neurocomputing*, *294*, 94–101.

Llamedo, M., & Martínez, J. P. (2010). Heartbeat classification using feature selection driven by database generalization criteria. *IEEE Transactions on Biomedical Engineering*, *58*(3), 616–625. doi:10.1109/TBME.2010.2068048 PMID:20729162

Loni, M., Sinaei, S., Zoljodi, A., Daneshtalab, M., & Sjödin, M. (2020). DeepMaker: A multi-objective optimization framework for deep neural networks in embedded systems. *Microprocessors and Microsystems*, *73*, 102989.

Luo, K., Li, J., Wang, Z., & Cuschieri, A. (2017). Patient-specific deep architectural model for ECG classification. *Journal of Healthcare Engineering*.

Luz, E. J. D. S., Schwartz, W. R., Cámara-Chávez, G., & Menotti, D. (2016). ECG-based heartbeat classification for arrhythmia detection: A survey. *Computer Methods and Programs in Biomedicine*, *127*, 144–164. doi:10.1016/j.cmpb.2015.12.008 PMID:26775139

Luz, E. J. D. S., Schwartz, W. R., Cámara-Chávez, G., & Menotti, D. (2016). ECG-based heartbeat classification for arrhythmia detection: A survey. *Computer Methods and Programs in Biomedicine*, *127*, 144–164. doi:10.1016/j.cmpb.2015.12.008 PMID:26775139

Moody, G. B. (2008, September). The physionet/computers in cardiology challenge 2008: T-wave alternans. In 2008 Computers in Cardiology (pp. 505-508). IEEE.

Moody, G. B., & Mark, R. G. (2001). The impact of the MIT-BIH arrhythmia database. *IEEE Engineering in Medicine and Biology Magazine*, *20*(3), 45–50. doi:10.1109/51.932724 PMID:11446209

Parashar, D., & Agrawal, D. (2021). 2-D Compact Variational Mode Decomposition-Based Automatic Classification of Glaucoma Stages From Fundus Images. *IEEE Transactions on Instrumentation and Measurement*, *70*, 1–10. doi:10.1109/TIM.2021.3071223

Parashar, D., & Agrawal, D. K. (2020). Automated classification of glaucoma stages using flexible analytic wavelet transform from retinal fundus images. *IEEE Sensors Journal*, *20*(21), 12885–12894. doi:10.1109/JSEN.2020.3001972

Parvaneh, S., & Rubin, J. (2018, September). Electrocardiogram monitoring and interpretation: from traditional machine learning to deep learning, and their combination. In *2018 Computing in Cardiology Conference (CinC)* (Vol. 45, pp. 1-4). IEEE. 10.22489/CinC.2018.144

Parvaneh, S., Rubin, J., Babaeizadeh, S., & Xu-Wilson, M. (2019). Cardiac arrhythmia detection using deep learning: A review. *Journal of Electrocardiology*, *57*, S70–S74. doi:10.1016/j.jelectrocard.2019.08.004 PMID:31416598

Penzel, T., Moody, G. B., Mark, R. G., Goldberger, A. L., & Peter, J. H. (2000, September). The apnea-ECG database. In Computers in Cardiology 2000. Vol. 27 (Cat. 00CH37163) (pp. 255-258). IEEE.

Sannino, G., & De Pietro, G. (2018). A deep learning approach for ECG-based heartbeat classification for arrhythmia detection. *Future Generation Computer Systems*, *86*, 446–455. doi:10.1016/j.future.2018.03.057

Shen, Q., Qin, H., Wei, K., & Liu, G. (2021). Multiscale deep neural network for obstructive sleep apnea detection using RR interval from single-lead ECG signal. *IEEE Transactions on Instrumentation and Measurement*, *70*, 1–13. doi:10.1109/TIM.2021.3062414

Sujadevi, V. G., Soman, K. P., & Vinayakumar, R. (2017, September). Real-time detection of atrial fibrillation from short time single lead ECG traces using recurrent neural networks. In *The International Symposium on Intelligent Systems Technologies and Applications* (pp. 212-221). Springer.

Taji, B., Chan, A. D., & Shirmohammadi, S. (2017). False alarm reduction in atrial fibrillation detection using deep belief networks. *IEEE Transactions on Instrumentation and Measurement*, *67*(5), 1124–1131.

Ullah, A., Tu, S., Mehmood, R. M., & Ehatisham-ul-haq, M. (2021). A hybrid deep CNN model for abnormal arrhythmia detection based on cardiac ECG signal. *Sensors (Basel)*, *21*(3), 951. doi:10.339021030951 PMID:33535397

Ventricular Ectopic Beats. (n.d.). *Gale Encyclopedia of Medicine*. Retrieved March 10 2022 from https://medical-dictionary.thefreedictionary.com/Ventricular+Ectopic+Beats

Wang, G., Zhang, C., Liu, Y., Yang, H., Fu, D., Wang, H., & Zhang, P. (2019). A global and updatable ECG beat classification system based on recurrent neural networks and active learning. *Information Sciences*, *501*, 523–542.

Wang, L., & Zhou, X. (2019). Detection of congestive heart failure based on LSTM-based deep network via short-term RR intervals. *Sensors (Basel)*, *19*(7), 1502.

Wasimuddin, M., Elleithy, K., Abuzneid, A. S., Faezipour, M., & Abuzaghleh, O. (2020). Stages-based ECG signal analysis from traditional signal processing to machine learning approaches: A survey. *IEEE Access: Practical Innovations, Open Solutions*, *8*, 177782–177803. doi:10.1109/ACCESS.2020.3026968

Wasimuddin, M., Elleithy, K., Abuzneid, A. S., Faezipour, M., & Abuzaghleh, O. (2020). Stages-based ECG signal analysis from traditional signal processing to machine learning approaches: A survey. *IEEE Access: Practical Innovations, Open Solutions*, *8*, 177782–177803.

Zarei, A., Beheshti, H., & Asl, B. M. (2022). Detection of sleep apnea using deep neural networks and single-lead ECG signals. *Biomedical Signal Processing and Control*, *71*, 103125.

Zhang, Z., Dong, J., Luo, X., Choi, K. S., & Wu, X. (2014). Heartbeat classification using disease-specific feature selection. *Computers in Biology and Medicine*, *46*, 79–89. doi:10.1016/j.compbiomed.2013.11.019 PMID:24529208

Chapter 6
Quality-Controlled ECG Data Compression and Classification for Cardiac Healthcare Devices

Chandan Kumar Jha
Indian Institute of Information Technology, Bhagalpur, India

ABSTRACT

Electrocardiogram (ECG) signals are widely used by cardiologists for the early detection of cardiovascular diseases (CVDs). In the early detection of CVDs, long-term ECG data is used for analysis. Healthcare devices used for the acquisition of long-term ECG data require an efficient ECG data compression algorithm. But compression of ECG signal with maintaining its quality is a challenge. Hence, this chapter presents a quality-controlled compression method that compresses the ECG data efficiently with retaining its quality up to a certain mark. For this, a distortion measure is used with specifying its value in a tolerable range. The compression performance of the proposed algorithm is evaluated using ECG records of the MIT-BIH arrhythmia database. In performance assessment, it is found that the compression algorithm performs well. The compressed ECG data are also used for normal and arrhythmia beat classification. The classification performance for ECG beats obtained from the compressed ECG data is good. It denotes the better diagnostic quality of the compressed ECG data.

INTRODUCTION

In cardiology, electrocardiogram (ECG) signals are widely used as a non-invasive diagnostic tool to detect abnormal behavior of heart. In hospitals, usually, ECG signals are recorded using 12-lead ECG acquisition machine. These ECG signals are analyzed by cardiologist to diagnose cardiovascular diseases (CVD's). In early detection of CVD's, ECG signals are recorded for long-term which may vary from 12-72 hours (Jha & Kolekar, 2021a). ECG data acquired in this duration requires large memory space for storage. Large ECG data also consumes large bandwidth to transmit it from one terminal to other. It results in increased transmission cost. An ECG data acquisition and transmission model used in remote healthcare is shown in Figure 1. This model is used for cardiac patient monitoring from remote. In am-

DOI: 10.4018/978-1-6684-3947-0.ch006

bulatory monitoring of cardiac patients, wearable ECG devices are used which can acquire ECG data during normal activity of patients. These ECG devices use wireless ECG sensors for which handling of large ECG data increases power consumption. For efficient performance of these devices, compression of ECG data size is essential to reduce the memory space requirement, transmission cost and power consumption (Lee et al., 2011), (Jha & Kolekar, 2016).

Figure 1. Cardiac patient monitoring model in remote healthcare

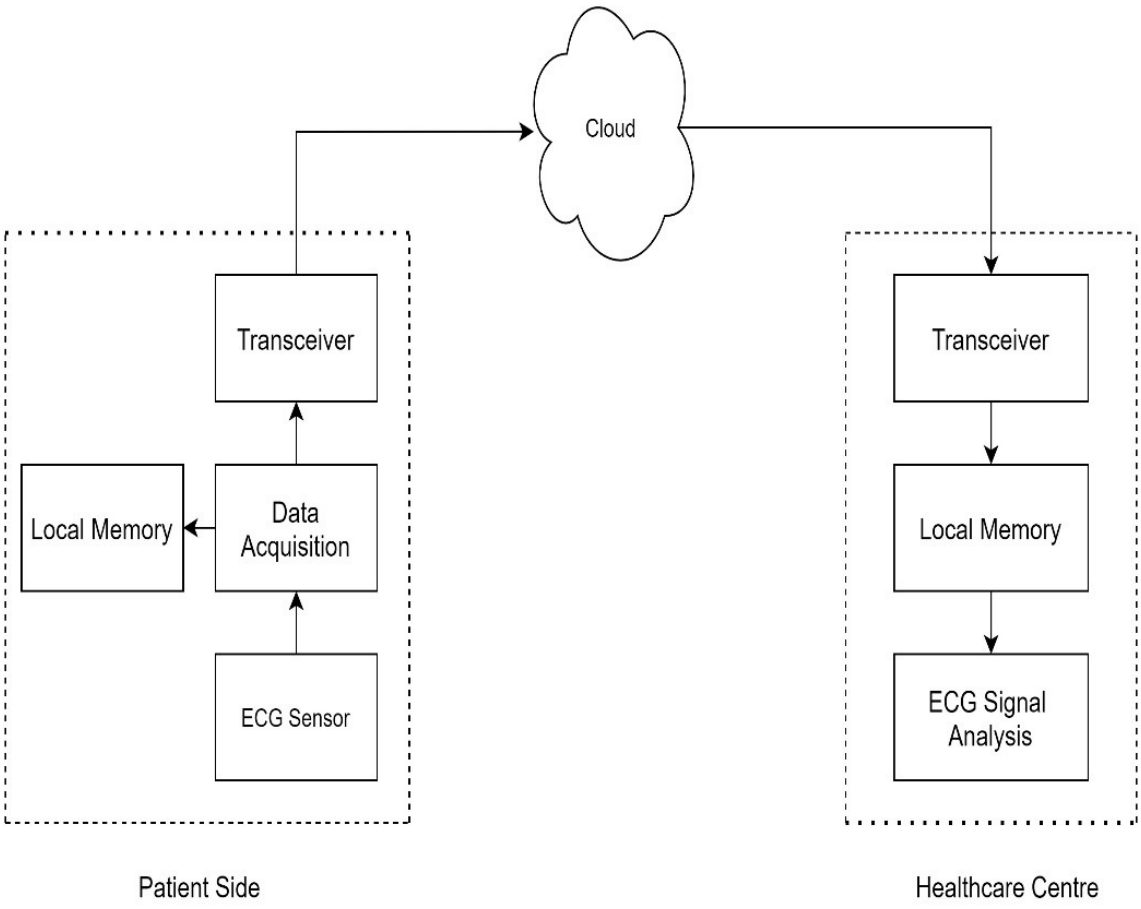

In past, several techniques have been developed for ECG data compression. These techniques are broadly categorized into two types (Manikandan & Dandapat, 2014): lossless and lossy. Lossless ECG data compression techniques offer no any distortion of signal, but compression ratio obtained by these techniques are very low. Examples of lossless ECG data compression techniques are Huffman encoding, run-length encoding, entropy coding, and linear prediction. In order to achieve higher compression ratio, lossy techniques have been developed with more focus. Further, lossy compression techniques are classified into three types. These types are (Jalaleddine et al., 1990): direct-time domain, parameter extraction and transform domain.

In direct time-domain techniques, ECG data is analyzed and compressed directly without changing it in another domain (Alvarado et al., 2012) For ECG data, many direct time-domain techniques have been developed such as turning-point (TP), scan along polynomial approximation (SAPA), amplitude zone time epoch coding (AZTEC), coordinate reduction time encoding system (CORTES), differential pulse code modulation (DPCM) and entropy coding. These techniques involve simple steps to implement but achieved compression ratio by these techniques are poor. In parameter extraction techniques, important features of ECG signals are extracted and based on those features ECG signals are reconstructed again. Examples of parameter extraction techniques are neural network-based method, peak picking and linear prediction method (Deepu & Lian, 2014), (Adamo et al., 2015). Transform domain compression methods analyze energy distribution of signal by converting it to another domain.

In past, many ECG data compression techniques have been developed based on transform domain methods. These techniques widely use discrete Fourier transform (DFT) (Sadhukhan et al., 2015), discrete cosine transform (DCT) (Jha & Kolekar, 2017), (Lee et al., 2011) and discrete wavelet transform (DWT) (Hossain, 2011), (Abo-Zahhad et al., 2013; Jha & Kolekar, 2015, 2019a, 2019c, 2021c, 2021b; Kolekar et al., 2021; Motinath et al., 2016). An ECG data compression technique is proposed in (Sadhukhan et al., 2015) which uses adaptive bit encoding of DFT coefficients. In this technique, DFT coefficients are calculated using sine and cosine basis functions. It avoids to get complex coefficients values. Further, DFT coefficients are encoded using fixed and adaptive strategies. In (Lee et al., 2011), an ECG data compression algorithm based on DCT is proposed. It utilizes DCT to compact energy of the signal. This algorithm is suitable for real-time compression and transmission of ECG data between e-health terminals. A DCT based ECG data compression algorithm along with dual encoding technique is proposed in (Jha & Kolekar, 2017). It compresses ECG data very well and it is suitable for tele-monitoring of cardiac patients.

Among transform-domain methods, wavelet transform based techniques are very popular as it offers promising compression performance. An ECG data compression algorithm based on mother wavelet parametrization is proposed in (Brechet et al., 2007) which selects wavelet filters optimally for improvement of compression performance. However, this technique is computationally expensive. Brechlet *et al.* proposed a compression technique for ECG data which uses discrete wavelet packet transform (Abo-Zahhad et al., 2013). In this technique, mother wavelet optimization is used to get good compression performance. In addition to this, basis of wavelet packets are also optimized followed by encoding of wavelet coefficients using modified embedded zerotree coding. In (Jha & Kolekar, 2021b), (Wang et al., 2016), wavelet transform is combined with empirical mode decomposition for ECG data compression. A wavelet-based ECG data compression technique is proposed in (Jha & Kolekar, 2019b) which selects most suitable wavelet filter from a set wavelet-filter family to get better compression performance. In (Jha & Kolekar, 2021c), tunable Q-wavelet transform technique is proposed which performs well for ECG data compression. This technique is validated using cardiac arrhythmia classification.

Although, many wavelet-based ECG data compression techniques have been developed in past, but these techniques lack with respect to quality constrained compression. In compression methods, preserving the quality of ECG signal is essential so that the reconstructed signals can be used for diagnostic purposes. Hence, this chapter reports a wavelet-based quality-controlled ECG data compression technique which controls quality of the compressed signal using a mathematical performance measure called normalized percent root-mean square difference (PRD_1). In this technique, quality of the reconstructed ECG signal is maintained using a predefined value of PRD_1. The proposed technique compacts energy

of the signal using wavelet transform. Further, dead-zone quantization and run-length encoding is used to get the compressed version of ECG data.

METHODOLOGY

The proposed compression technique is implemented by following the steps which are shown in Figure 2 using a block diagram. First, ECG signals are acquired from the MIT-BIH arrhythmia database (Moody & Mark, 2001). These ECG signals are pre-processed to eliminate high-frequency noises. After pre-processing, ECG signals are decomposed using wavelet transform which serves well to compact maximum energy of the signal to a few coefficients. The obtained transform coefficients are further processed through dead-zone quantization. It converts small-valued coefficients to zero. After quantization, run-length coding is applied to transform coefficients which provides the compressed form of ECG data.

Figure 2. Block diagram of the proposed compression technique

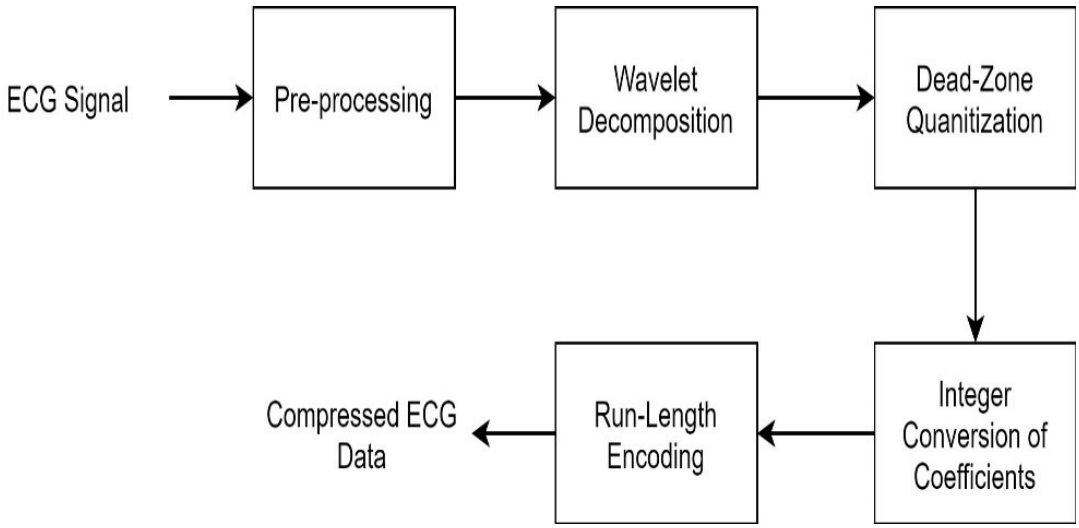

Figure 3. Quality-control procedure in the proposed technique

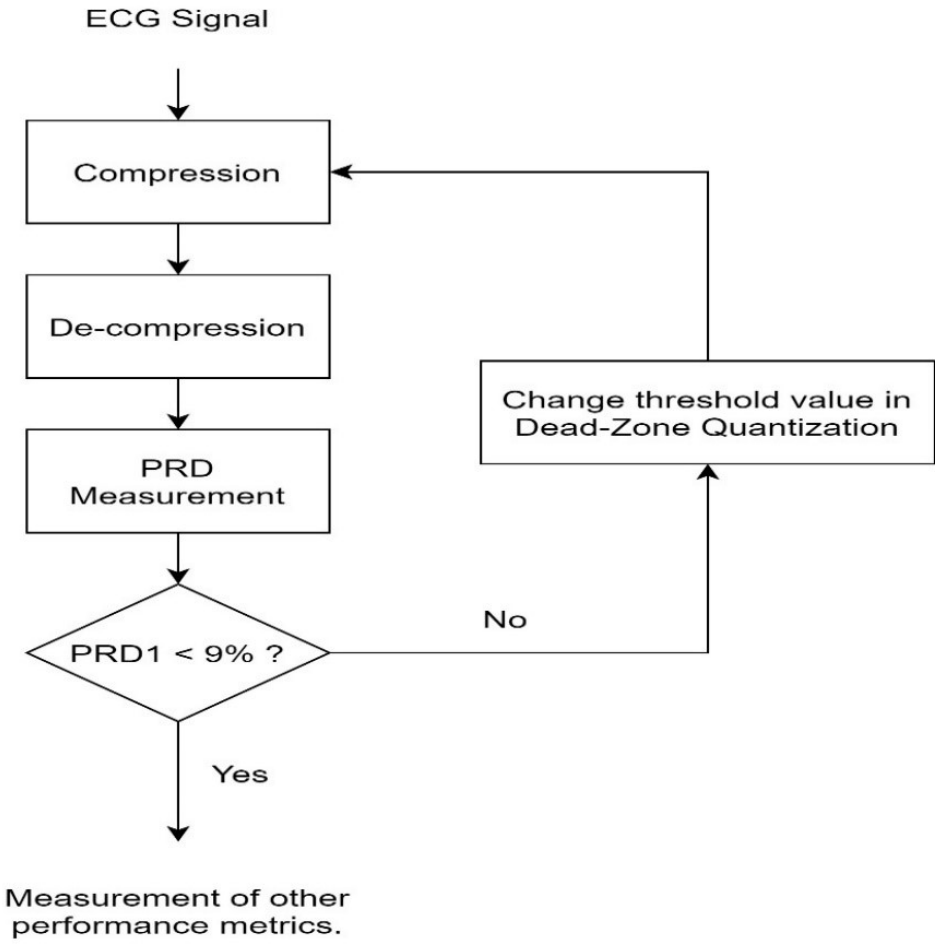

ECG Signal

The proposed technique is experimented using ECG signals of the MIT-BIH arrhythmia database. The MIT-BIH arrhythmia database consists of 48 ECG records obtained from 47 subjects. These records are sampled at the sampling frequency of 360 Hz with the resolution of 11-bits per sample (Moody & Mark, 2001). In the proposed technique, all 48 ECG records of the database are used to evaluate the performance.

Pre-Processing

ECG signals of the MIT-BIH arrythmia database contain different high-frequency noises. In pre-processing, high-frequency noises of the acquired ECG signals are removed using Savitzky-Golay (SG) filter (Jha & Kolekar, 2019b). In SG filtering, window dimension 3 and order 17 are chosen. These parameters of the SG-filter are selected empirically.

Wavelet Decomposition

After pre-processing, ECG signals are decomposed using DWT. Wavelet decomposition of signal, compacts maximum energy of the signal to few transform coefficients. In decomposition, number of levels N_L is chosen by the equation (Manikandan & Dandapat, 2014):

$$N_L = \left\lfloor \log_2 f_s - 2.96 \right\rfloor \tag{1}$$

Here, f_s denotes sampling frequency of the signal. Since sampling frequency of the ECG signal of the MIT-BIH arrhythmia database is 360 Hz, number of decomposition level for the proposed technique is 5. In wavelet decomposition, "bior4.4" wavelet family is chosen which is considered as suitable for ECG data compression. After wavelet decomposition, the obtained data is the combination of approximate coefficients and detail coefficients.

Dead-Zone Quantization

Among transform coefficients obtained after wavelet decomposition, many coefficients have small values. These coefficients are discarded using dead-zone quantization. In dead-zone quantization, the decision intervals I_n for the input data sample and quantized output data samples O_n are defined by following equations (J. Chen et al., 2008):

$$I_n = \begin{cases} \left(-3\alpha, T\right]; \text{ if n = -1} \\ \left(-T, T\right); \text{ if n = 0} \\ \left[T, 3\alpha\right); \text{ if n =1} \\ \left(2k-1\right)\alpha, \left(2k+1\right)\alpha; \text{ Otherwise} \end{cases} \tag{2}$$

$$O_n = \begin{cases} 0; \text{ if n = 0} \\ \pm\delta; \text{ if n = } \pm 1 \\ n\delta; \text{ Otherwise} \end{cases} \tag{3}$$

Here, n denotes sample index. T is threshold value of the dead-zone quantization. Quantization step size and half of the quantization step size are denoted by α and δ respectively. In dead-zone quantization, all the transform coefficients lying in the interval (-T,*T)* are converted to zero. Hence, the interval (-T,*T)* is called dead-zone which has 2T *w*idth, where 2T<δ. For an ECG signal, if P is maximum value of amplitude and Q is minimum value then threshold value T is determined by the relation:

$$T = \frac{P - Q}{2^4.t - 1} \tag{4}$$

where, t=1,2,3,4,… . Quantization step size α and threshold value T are related by the equation, $\delta=\gamma T$. *H*ere, γ is a parameter which value should lie in the range 1.20 to 1.80. In the proposed technique, the taken value of γ is 1.60. It is selected empirically and it offers good performance for all ECG records of the MIT-BIH arrhythmia database.

Integer Conversion of Coefficients

Since transform coefficients are in decimal values which require a greater number of bits to store. Hence, after dead-zone quantization, transform coefficients are multiplied by hundred and rounded-off to nearest integer values. Here, transform coefficients are multiplied by hundred to minimize the information loss due to rounding-off process.

Run-Length Encoding

After integer-conversion, it is observed that the approximate coefficients of the wavelet decomposition contain very less repetition of data instances while the detail coefficients consist of many repeated data instances. This repetition of detail coefficients is exploited using run-length encoding. It represents the data instances in terms of values and their number repetition. After run-length encoding, the resulting data is the compressed version of ECG signal.

The ECG signal is reconstructed again from the compressed version of data using the inverse steps of compression. After reconstruction of the ECG signal, distortion is measured by calculating PRD_1. It is considered that the PRD_1 value less than 9% offers quality of the reconstructed ECG signal in tolerable range. Hence, If PRD_1 value is greater than 9% then the threshold value of dead-zone quantization is changed to make it low. The quality-control process of the proposed compression technique is shown in Figure 3 using signal flowgraph. Performance of the proposed compression technique is evaluated using some mathematical measures which are discussed in next section.

Performance Measures

For assessment of performance of the proposed compression technique, following performance metrics are used (Lee et al., 2011):

- Compression ratio (CR):

$$CR = \frac{\text{Original signal size (in bytes)}}{\text{Compressed signal size (in bytes)}} \tag{5}$$

- Percent root mean square difference (PRD):

$$PRD = \sqrt{\frac{\sum_{i=1}^{N}(X_i - X_i^r)^2}{\sum_{i=1}^{N} X_i^2}} \times 100\% \tag{6}$$

Here, X_i is original ECG signal, X_i^r is reconstructed ECG signal, and i is sample index of data.

- Normalized PRD (PRD_1):

$$PRD = \sqrt{\frac{\sum_{i=1}^{N}(X_i - X_i^r)^2}{\sum_{i=1}^{N}\left(X_i - \bar{X}\right)^2}} \times 100\% \tag{7}$$

Here, $\bar{X}$ is mean of the original ECG signal.

- Quality score (QS):

$$QS = \frac{CR}{PRD} \tag{8}$$

$$QS_1 = \frac{CR}{PRD_1} \tag{9}$$

- Signal to noise ratio (SNR):

$$SNR = 10 \log \left(\frac{\sum_{i=1}^{N}(X_i - \bar{X})^2}{\sum_{i=1}^{N}\left(X_i - X_i^r\right)^2} \right) \tag{10}$$

Performance of the compression technique depends on values of abovementioned metrics. For a good compression technique CR value should be high. Since PRD and PRD_1 are distortion measures, it should be low. Quality score is the ratio of CR and PRD. There is another version of quality score also which is QS_1. High quality score denotes good performance. Lastly, high SNR value indicates good compression quality.

RESULTS AND DISCUSSION

The proposed compression technique is evaluated using 48 single channel ECG records of the MIT-BIH arrhythmia database. Compression performance in terms of six performance metrics as mentioned in eqns. (5)-(10) is shown in Table 1. The average CR for 48 ECG records is 24.19 while average PRD, PRD_1, QS, QS_1, and SNR are 5.58, 8.04, 4.34, 3.02 and 21.92 dB respectively. The average performance of the proposed technique is good which can be generalized for all ECG records. The variation in performance for different records is observed due to different morphology of different ECG signals. Since, threshold value T of dead-zone quantization varies for different ECG signals, hence it offers different compression performance. For all ECG signals, distortion measure PRD is less than 2% which assures good quality of reconstructed ECG signal. For quality-control, threshold value T is varied till the point up to which PRD value less 2% is obtained.

Figure 4 displays the original and reconstructed ECG signal od ECG record nos. 105. It is quite clear that the reconstructed signal is very much similar to original ECG signal.

Figure 4. Original and reconstructed ECG signal of ECG record no. 101

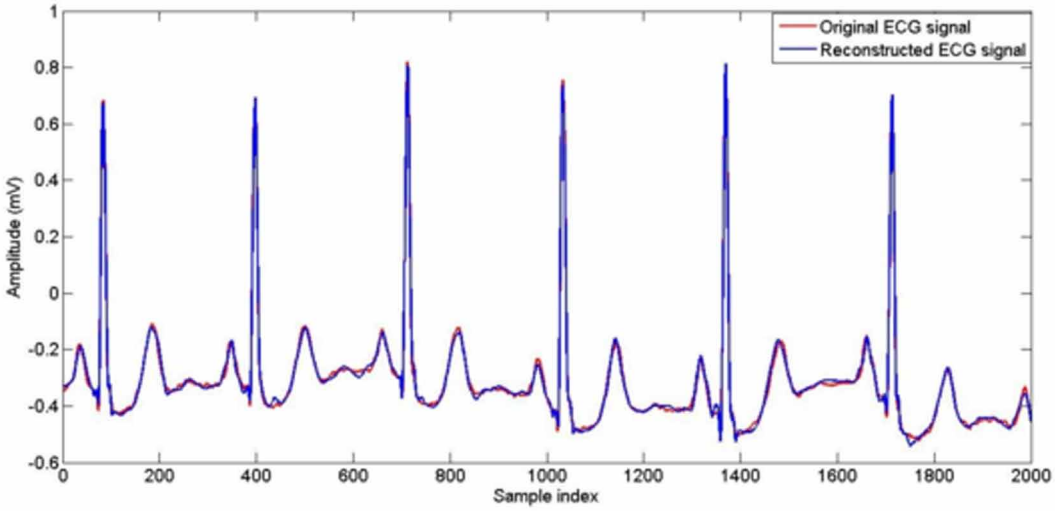

Table 1. Compression performance of the proposed technique

ECG Record No.	CR	PRD	PRD_1	QS	QS_1	SNR (dB)
100_MLII	22.50	3.93	8.57	5.72	2.63	21.34
101_MLII	20.72	4.37	7.49	4.75	2.77	22.51
102_V5	21.80	4.18	7.56	5.22	2.88	22.43
103_MLII	24.43	6.17	7.60	3.96	3.21	22.38
104_V5	24.41	6.48	8.39	3.76	2.91	21.52
105_MLII	26.37	7.20	8.76	3.66	3.01	21.15
106_MLII	20.70	6.09	6.99	3.40	2.96	23.11
107_MLII	23.89	6.76	7.01	3.54	3.41	23.09
108_MLII	24.26	4.83	8.43	5.03	2.88	21.48
109_MLII	24.71	6.21	7.49	3.98	3.30	22.52
111_MLII	22.43	5.84	7.54	3.84	2.97	22.45
112_MLII	22.80	1.83	8.31	12.47	2.74	21.61
113_MLII	25.46	7.48	8.13	3.41	3.13	21.80
114_MLII	23.56	4.35	8.11	5.42	2.91	21.82
115_MLII	25.07	3.78	7.61	6.63	3.30	22.37
116_MLII	24.91	4.45	8.60	5.59	2.90	21.31
117_MLII	30.04	2.38	8.88	12.61	3.38	21.03
118_MLII	24.63	3.38	8.86	7.29	2.78	21.05
119_MLII	26.20	4.40	7.79	5.95	3.36	22.17
121_MLII	37.88	2.89	8.58	13.10	4.41	21.33
122_MLII	24.94	2.88	7.74	8.67	3.22	22.23
123_MLII	25.70	2.82	8.21	9.12	3.13	21.71
124_MLII	29.63	2.81	7.06	10.53	4.20	23.03
200_MLII	22.73	7.79	8.35	2.92	2.72	21.57
201_MLII	20.83	5.83	7.76	3.57	2.68	22.20
202_MLII	31.10	7.59	8.79	4.10	3.54	21.12
203_MLII	21.94	8.56	8.95	2.56	2.45	20.96
205_MLII	23.29	3.66	8.49	6.36	2.74	21.42
207_MLII	33.30	7.49	7.88	4.45	4.22	22.07
208_MLII	21.43	7.90	8.02	2.71	2.67	21.92
209_MLII	22.04	6.90	8.78	3.20	2.51	21.13
210_MLII	24.31	7.38	8.69	3.29	2.80	21.22
212_MLII	18.83	6.74	7.61	2.79	2.47	22.37
213_MLII	20.47	6.38	7.71	3.21	2.66	22.26
214_MLII	27.57	7.01	7.75	3.93	3.56	22.21
215_MLII	19.19	7.68	8.50	2.50	2.26	21.41
217_MLII	28.82	7.91	8.13	3.65	3.54	21.80
219_MLII	23.72	4.75	8.40	4.99	2.83	21.52

Continued on following page

Table 1. Continued

ECG Record No.	CR	PRD	PRD_1	QS	QS_1	SNR (dB)
220_MLII	23.72	3.85	8.39	6.17	2.83	21.53
221_MLII	23.93	6.58	7.86	3.64	3.04	22.09
222_MLII	21.93	5.62	7.72	3.90	2.84	22.25
223_MLII	26.81	4.52	7.83	5.93	3.42	22.12
228_MLII	24.80	7.11	7.77	3.49	3.19	22.19
230_MLII	20.84	6.50	7.44	3.20	2.80	22.56
231_MLII	22.21	5.82	7.06	3.82	3.14	23.02
232_MLII	13.99	3.97	8.15	3.52	1.72	21.78
233_MLII	21.83	8.30	8.62	2.63	2.53	21.29
234_MLII	24.49	6.68	7.52	3.67	3.26	22.47
Avg.	24.19	5.58	8.04	4.34	3.02	21.92

Performance of the proposed compression technique is compared with recent techniques developed in this field. Table 2 shows this comparison in terms CR, PRD, and QS. In comparison, it is found that the proposed technique provides better performance than techniques based on DCT based discrete orthogonal Stockwell transform (DOST), DWT, combination of empirical mode decomposition (EMD) and DWT. In comparison with beta wavelet-based technique, the proposed technique offers higher CR an QS but PRD is also higher. In this, comparison of QS decides the better method. Since offered QS is higher than beta wavelet-based technique, hence performance of the proposed technique is better.

Table 2. Comparison of compression performance

Technique	CR	PRD	QS
DCT based DOST (Jha & Kolekar, 2018)	6.27	5.37	1.49
DWT (Jha & Kolekar, 2019b)	22.62	5.66	4.00
EMD+DWT (Jha & Kolekar, 2021b)	23.02	6.11	3.77
Proposed	24.19	5.58	4.34

COMPRESSED ECG BEATS CLASSIFICATION

Further, diagnostic qualities of compressed ECG signals are evaluated using classification performance analysis of arrhythmia ECG beats. For this, normal beats and seven different arrhythmias beats are acquired from compressed ECG signals taken from the MIT-BIH arrhythmia database. Methodology of acquisition and classification ECG beats obtained from compressed ECG data is discussed in next section. These ECG beats are classified using convolutional neural network (CNN) (C. Chen et al., 2020; Rahul & Sharma, 2022).

Acquisition and Classification of Compressed ECG Beats

Different steps of acquisition and classification of ECG beats obtained from compressed ECG data are shown in Figure 5 using a block diagram. First, compressed ECG data is pre-processed to remove different kinds of noises associated in ECG signal due to different artifacts. In pre-processed ECG signals, R-peaks are detected using the standard Pan-Tompkins algorithm. R-peaks detection followed by beat segmentation by selecting 89 samples before the R-peak and 162 samples after the R-peak (Jha & Kolekar, 2020). Thus, total 45702 ECG beats obtained from the compressed ECG signals. These ECG beats included normal (N) and seven different types of arrhythmias which are Left bundled branch block (LBBB), Right bundled branch block (RBBB), Atrial premature contraction (APC), Paced (P), Premature ventricular contraction (PVC), Fusion of normal and paced beat (FNPB), Fusion of ventricular and normal beats (FVNB). Number of different types of ECG beats and their distribution among training, testing and validation sets are shown in Table 3. The training and validation sets are used to build a classifier model based on convolutional neural network (CNN).

Figure 5. Acquisition and classification of compressed ECG beats

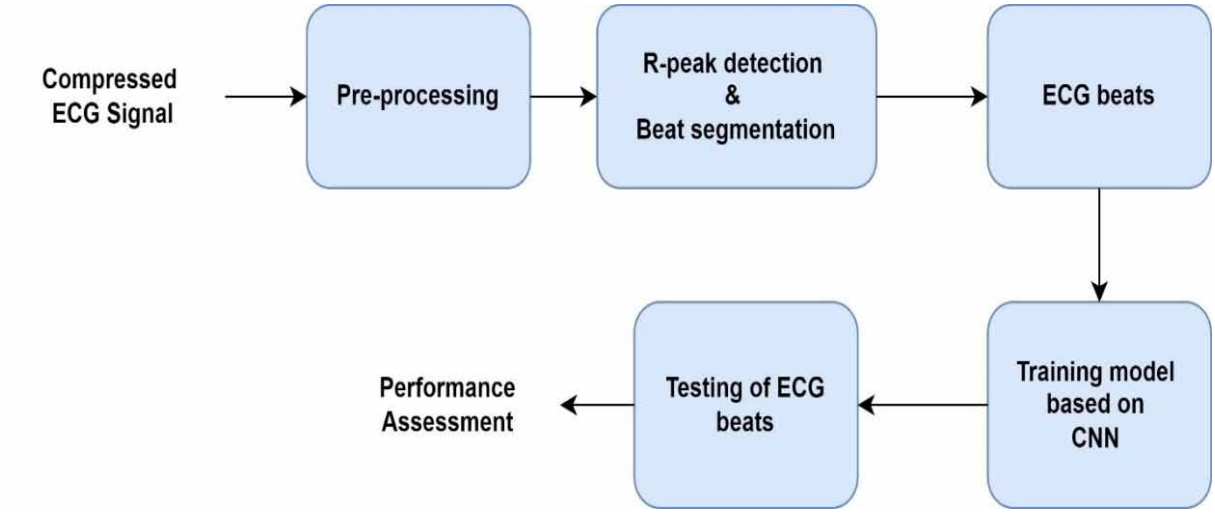

Table 3. Distribution of different types of ECG beats in training, testing and validation sets

Types	Training Set	Validation Set	Testing Set
Normal	12951	2873	2813
Left bundled branch block (LBBB)	6863	1455	1533
Right bundled branch block (RBBB)	5715	1202	1174
Atrial premature contraction (APC)	1403	299	317
Paced (P)	7091	1489	1457
Premature ventricular contraction (PVC)	1172	234	232
Fusion of normal and paced beat (FNPB)	1020	213	231
Fusion of ventricular and normal beats (FVNB)	767	160	168
Total	36982	7925	7925

Convolutional Neural Network

Convolutional neural network (CNN) is a form of deep neural network which consists of one or more convolutional layers. In comparison with the multi-layer perceptron, CNN is more advantageous as it features a set of convolutional layers along with the normal hidden layers which contains smaller number of weights and these weights are shared. In CNN, layers are sparsely connected rather than fully connected as MLP. It contains fewer parameters than MLP with the same number of hidden layers. It is self-learned and self-organized network which does not require supervision. In bio-medical signal and image processing, CNNs are widely used to distinguish different classes of data. Hence it is used as a powerful tool to provide automated disease diagnosis in medical field. The classifier model based on CNN is build using the training and validation sets of ECG beats. Further, testing set is used to evaluate the classification performance.

Classification Performance Assessment

Performance of the CNN classifier for testing ECG beats is evaluated using following performance metrics accuracy, sensitivity, specificity (Jha & Kolekar, 2020).
Accuracy is defined as the total number of true events detected by the classifier.

$$Accuracy = \frac{TP + TN}{P + N} \times 100\% \tag{11}$$

Sensitivity is also called true positive rate. It is defined as the ability of the classifier to detect true positive events.

$$Sensitivity = \frac{TP}{TP + FN} \times 100\% \tag{12}$$

Specificity is also called true negative rate. It is defined as the ability of the classifier to detect true negative events.

$$Specificity = \frac{TN}{TN + FP} \times 100\% \tag{13}$$

Where, *P*, *N*, *TP, TN*, *FP,* and *FN* indicates total positive, total negative, true positive, true negative, false positive and false negative events respectively.

The classification results in terms of accuracy, sensitivity and specificity are shown in Table 4 for compressed ECG beats. The classification results denote the compressed ECG beats are distinguished by the classifier properly. The overall classification results for eight different compressed ECG beats are 98.22%, 97.38% and 98.25% in terms of accuracy, sensitivity and specificity respectively.

Table 4. Performance of the CNN classifier for compressed ECG beats

Classes	Accuracy (%)	Sensitivity (%)	Specificity (%)
N	96.81	96.49	97.99
LBBB	98.89	99.18	96.84
RBBB	97.91	98.83	98.92
APC	98.02	97.02	97.88
P	98.73	98.33	98.82
PVC	98.86	98.78	98.89
FPNB	97.65	94.59	97.80
FVNB	98.89	95.85	98.87
Overall	98.22	97.38	98.25

CONCLUSION

This chapter presents a compression technique which controls quality of the reconstructed ECG signal by employing a PRD_1 criteria. The proposed technique utilize wavelet transform to compact energy of the signal. Dead-zone quantization and run-length encoding also play a prominent role to achieve a good compression performance. Average compression performance of the proposed technique is good for 48 single channel ECG records obtained from the MIT-BIH arrhythmia database. In visual inspection of the original and reconstructed ECG signals, it is found that the compression technique provides good reconstruction quality which signifies benefit of the quality-control criteria. This compression method offers better performance than many techniques recently developed in this area. Apart from this, the normal and seven different arrhythmias ECG beats are obtained from the compressed data which further classified using the convolutional neural network. The classification results are good for eight different classes of compressed ECG beats. It denotes that the information contained by the compressed ECG beats are quiet enough to distinguished as different classed. This compression and classification technique can be used for cardiac healthcare devices.

REFERENCES

Abo-Zahhad, M., Al-Ajlouni, A. F., Ahmed, S. M., & Schilling, R. J. (2013). A new algorithm for the compression of ECG signals based on mother wavelet parameterization and best-threshold levels selection. *Digital Signal Processing*, *23*(3), 1002–1011. doi:10.1016/j.dsp.2012.11.005

Adamo, A., Grossi, G., Lanzarotti, R., & Lin, J. (2015). ECG compression retaining the best natural basis k-coefficients via sparse decomposition. *Biomedical Signal Processing and Control*, *15*, 11–17. doi:10.1016/j.bspc.2014.09.002

Alvarado, A. S., Lakshminarayan, C., & Principe, J. C. (2012). Time-based compression and classification of heartbeats. *IEEE Transactions on Biomedical Engineering*, *59*(6), 1641–1648. doi:10.1109/TBME.2012.2191407 PMID:22453601

Brechet, L., Lucas, M.-F., Doncarli, C., & Farina, D. (2007). Compression of biomedical signals with mother wavelet optimization and best-basis wavelet packet selection. *IEEE Transactions on Biomedical Engineering*, *54*(12), 2186–2192. doi:10.1109/TBME.2007.896596 PMID:18075034

Chen, C., Hua, Z., Zhang, R., Liu, G., & Wen, W. (2020). Automated arrhythmia classification based on a combination network of CNN and LSTM. *Biomedical Signal Processing and Control*, *57*, 101819. doi:10.1016/j.bspc.2019.101819

Chen, J., Wang, F., Zhang, Y., & Shi, X. (2008). ECG compression using uniform scalar dead-zone quantization and conditional entropy coding. *Medical Engineering & Physics*, *30*(4), 523–530. doi:10.1016/j.medengphy.2007.06.008 PMID:17693118

Deepu, C. J., & Lian, Y. (2014). A joint QRS detection and data compression scheme for wearable sensors. *IEEE Transactions on Biomedical Engineering*, *62*(1), 165–175. doi:10.1109/TBME.2014.2342879 PMID:25073164

Hossain, M. S. (2011). ECG signal compression using energy compaction based thresholding of the wavelet coefficients. *Duet Journal, 1*(2).

Jalaleddine, S. M. S., Hutchens, C. G., Strattan, R. D., & Coberly, W. A. (1990). ECG data compression techniques-a unified approach. *IEEE Transactions on Biomedical Engineering*, *37*(4), 329–343. doi:10.1109/10.52340 PMID:2186997

Jha, C. K., & Kolekar, M. H. (2015). Performance analysis of ECG data compression using wavelet based hybrid transform method. *2015 International Conference on Microwave, Optical and Communication Engineering (ICMOCE)*, 138–141. 10.1109/ICMOCE.2015.7489709

Jha, C. K., & Kolekar, M. H. (2016). Efficient ECG data compression and transmission algorithm for telemedicine. *2016 8th International Conference on Communication Systems and Networks (COMSNETS)*, 1–6.

Jha, C. K., & Kolekar, M. H. (2017). ECG data compression algorithm for tele-monitoring of cardiac patients. *International Journal of Telemedicine and Clinical Practices*, *2*(1), 31–41. doi:10.1504/IJTMCP.2017.082106

Jha, C. K., & Kolekar, M. H. (2018). Electrocardiogram data compression using DCT based discrete orthogonal Stockwell transform. *Biomedical Signal Processing and Control*, *46*, 174–181. doi:10.1016/j.bspc.2018.06.009

Jha, C. K., & Kolekar, M. H. (2019a). Arrhythmia ECG beats classification using wavelet-based features and support vector machine classifier. In *Advanced Classification Techniques for Healthcare Analysis* (pp. 74–88). IGI Global. doi:10.4018/978-1-5225-7796-6.ch004

Jha, C. K., & Kolekar, M. H. (2019b). Diagnostic quality assured ECG signal compression with selection of appropriate mother wavelet for minimal distortion. *IET Science, Measurement & Technology*, *13*(4), 500–508. doi:10.1049/iet-smt.2018.5217

Jha, C. K., & Kolekar, M. H. (2020). Cardiac arrhythmia classification using tunable Q-wavelet transform based features and support vector machine classifier. *Biomedical Signal Processing and Control*, *59*, 101875. doi:10.1016/j.bspc.2020.101875

Jha, C. K., & Kolekar, M. H. (2021a). Electrocardiogram data compression techniques for cardiac healthcare systems: A methodological review. *IRBM*. Advance online publication. doi:10.1016/j.irbm.2021.06.007

Jha, C. K., & Kolekar, M. H. (2021b). Empirical mode decomposition and wavelet transform based ECG data compression scheme. *IRBM*, *42*(1), 65–72. doi:10.1016/j.irbm.2020.05.008

Jha, C. K., & Kolekar, M. H. (2021c). Tunable Q-wavelet based ECG data compression with validation using cardiac arrhythmia patterns. *Biomedical Signal Processing and Control*, *66*, 102464. doi:10.1016/j.bspc.2021.102464

Kolekar, M. H., Jha, C. K., & Kumar, P. (2021). ECG Data Compression Using Modified Run Length Encoding of Wavelet Coefficients for Holter Monitoring. *IRBM*. Advance online publication. doi:10.1016/j.irbm.2021.10.001

Lee, S., Kim, J., & Lee, M. (2011). A real-time ECG data compression and transmission algorithm for an e-health device. *IEEE Transactions on Biomedical Engineering*, *58*(9), 2448–2455. doi:10.1109/TBME.2011.2156794 PMID:21606020

Manikandan, M. S., & Dandapat, S. (2014). Wavelet-based electrocardiogram signal compression methods and their performances: A prospective review. *Biomedical Signal Processing and Control*, *14*, 73–107. doi:10.1016/j.bspc.2014.07.002

Moody, G. B., & Mark, R. G. (2001). The impact of the MIT-BIH arrhythmia database. *IEEE Engineering in Medicine and Biology Magazine*, *20*(3), 45–50. doi:10.1109/51.932724 PMID:11446209

Motinath, V. A., Jha, C. K., & Kolekar, M. H. (2016). A novel ECG data compression algorithm using best mother wavelet selection. *2016 International Conference on Advances in Computing, Communications and Informatics (ICACCI)*, 682–686. 10.1109/ICACCI.2016.7732125

Rahul, J., & Sharma, L. D. (2022). Automatic cardiac arrhythmia classification based on hybrid 1-D CNN and Bi-LSTM model. *Biocybernetics and Biomedical Engineering*, *42*(1), 312–324. doi:10.1016/j.bbe.2022.02.006

Sadhukhan, D., Pal, S., & Mitra, M. (2015). Electrocardiogram data compression using adaptive bit encoding of the discrete Fourier transforms coefficients. *IET Science, Measurement & Technology*, *9*(7), 866–874. doi:10.1049/iet-smt.2015.0013

Wang, X., Chen, Z., Luo, J., Meng, J., & Xu, Y. (2016). ECG compression based on combining of EMD and wavelet transform. *Electronics Letters*, *52*(19), 1588–1590. doi:10.1049/el.2016.2174

Chapter 7
Analogy of Wrist Pulse Signals in the Context of ECG Signals: A Review

Neha Rathore
Maulana Azad National Institute of Technology, Bhopal, India

Praveen Kumar Tyagi
Maulana Azad National Institute of Technology, Bhopal, India

Deepak Parashar
IES College of Technology, Bhopal, India

Dheraj Agrawal
Maulana Azad National Institute of Technology, Bhopal, India

ABSTRACT

Modern medical practices use different tools and procedures to observe pulse rate, heart rate variability, speed of pulse, blood pressure (BP), blood flowing rate in arteries, volume, etc. Years ago, in ancient medical practice like Ayurveda and traditional Chinese medicine (TMC), wrist pulse or radial pulse of the subject in consideration is checked to diagnose health conditions. Both wrist pulse diagnosis and ECG are non-invasive methods for assessing the health of a person. Wrist pulse is caused by cardiovascular activities, and thus, it can be correlated with the electrocardiography (ECG). In biomedical signals, ECGs represent electric activity of the heart. The rate at which a heart beats is pulse rate. The pulse movement is due to flow of blood in vessels. The parameters like rhythm, strength, hardness or softness, transition period, and change in rate of heartbeat can be measured. This may be helpful in diagnosis of cardiac and non-cardiac diseases.

DOI: 10.4018/978-1-6684-3947-0.ch007

INTRODUCTION

As per stated by World Health Organization, Cardiovascular diseases (CVDs) are the one of the main reason of mortality around worldwide. Around 17.9 million individuals died from CVDs in 2019, accounting 32% of all deaths globally. Out of these fatalities, 85% were due to heart attacks and strokes. Early diagnose of cardiovascular disease is important so that medicines and counselling can be provided on time to reduce the death risk.

Today, different techniques are available to examine the pulse of a subject. Their clinical methods, concepts and practices are also differing. In modern medical science, the tools which is used to determine the signs of heart disease is an electrocardiogram (ECG) measuring device. The ECG signal is an electrical signal from the heart, which can be used to indicate abnormality of the heart by pulse shape and the analysis of heart rate. These signals are produced by heart contraction and relaxation, reaches to all around the body.

While in the Ancient times, in Ayurveda and in Traditional Chinese medicine, the palpation at wrist pulse of an individuals is examined for disease diagnose. The palpation is obtained at three accurate position on wrist at radial artery. Signals obtained are named as Vatta (V), Pitta (P) and Kapha(K). The signals felt from these particular points are not only due to the contraction and relaxation of blood vessels but also a result of movement of blood through the artery. The specialist of nadi diagnosis, use their meditation skill and experience, to feel signals on the subject's wrist. The palpation also occurs when blood flows through the artery. The pulse is very weak and minute and only a highly skilled practitioner (Nadi Vaidya) can detect it accurately. (Upadhyaya et el. 2005)

Wrist pulse signal, unlike ECG, is a bloodstream signal that is impacted by a variety of physiological and pathological elements, including artery walls, blood parameters, nerves, muscles, and skin. The process is less costly, Eco friendly and painless. In Ayurveda, it is, mention that the three nadis are the manifestation of human body which contains five elements namely Air, water, earth, fire and space. Vata is combination of air and space. Imbalance of its components causes problems related to abdomen, hemorrhoids, rectum malfunctioning, nerves disorder etc. Water and fire are the components of Pitta. High pitta generally causes metabolism disorder, constipation and indigestion. The components of Kapha are Water and Earth. It causes cold, allergies, problems related to lungs and respiration system. (Rhyner H.H. 1998, Suguna GC, Veerabhadrappa 2019)

According to literature, it is proved that wrist pulse signal can be used not only for the detection of cardiovascular diseases but also successfully daigonesd disease like Diabetes, Gastrointestinal disorders, Hypertension, Cancer, Arthritis, Infertility, Paralysis, Mental disorder etc. Hence radial pulse is appropriate for the investigation of non-cardiac disorders. (Rajani et el. 2012, Zhang Z 2018).

A review on the basis of literature is presented to show the analogy between wrist pulse signal and ECG signal.

Pattern of Signals

Both ECG signal and Radial pulse signal occurs due to cardiac activity. The PQRST pattern of ECG signal pattern can be correlated with the PTVD pattern of wrist pulse. Hence the parameters of ECG signal are somehow similar to pulse signal. (David Zhang et el. 2019, Chaiwisood et el. 2012)

ECG Signal

An electrocardiogram (ECG) is a test that measures the intensity and timing of electrical activity in your heart. Each phase of signal is represented on graph which has a P, Q, R, S, and T wave pattern.

Figure 1 shows an ECG signal. As the signal goes through this node, it slows down, enabling the ventricles to fill with blood. Between P wave and the Q wave, this slowing signal appears on the ECG as a flat line (PR segment).

The electrical signal originates in the sinoatrial node (SA) that is present in right atrium's and goes to the right and left atria, which contract and pump blood into the ventricles. On the ECG, this electrical impulse is recorded as the P wave. The PR Interval is the time duration between the P wave and the QRS complex.

Figure 1. PQRST pattern of ECG signal

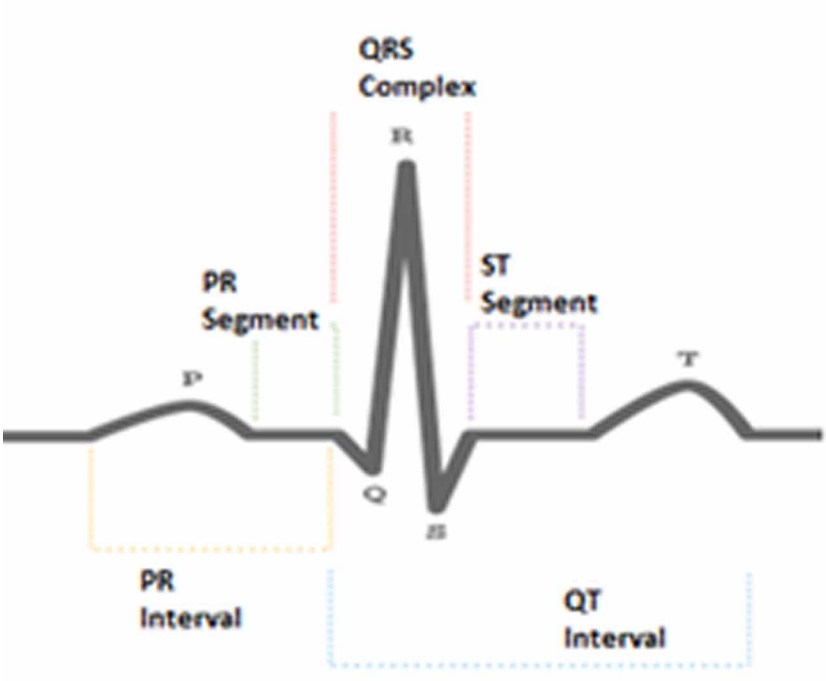

The signal passes through the ventricles of the heart, prompting them to contract and pump blood to the lungs and the rest of the body. On the ECG, this signal is captured as QRS waves. These waves are commonly referred to as the QRS complex because they occur in quick succession The T wave represents the return of the ventricles to their normal electrical condition. With each pulse, the muscles relax and cease contracting, enabling the atria to fill with blood, and the process continues itself. (Gholam-Hosseini and Nazeran, 1998) (Alivecor, n.d.).

Wrist Pulse Signal

Wrist pulse signal is a type of circulatory signal that is mostly created by the depolarization and repolarization of the heart. When heart pushes blood, it impacts on the wall of artery and a pressure is created along the artery. The radial artery pulse wave is a periodic signal and it can be sensed over an artery that lies near the surface of the skin.

Figure 2 shows the technique to feel pulse. Doctors use three fingers (index, middle, and ring fingers) to take pulses at a patient's wrist. The sensations on the fingertips helps doctors to determine patients' physiological conditions. Although, pulse signal results as the heart pumping action the pattern on of wrist pulse is slightly changed due to variability and the functionality of all the other organ. It is difficult to sense the rhythm accurately. Only the experienced practitioners can accurately sense it (Abhinav et el. 2009, Goyal et el. 2017).

Figure 2. Pulse sensing with index, middle and ring finger

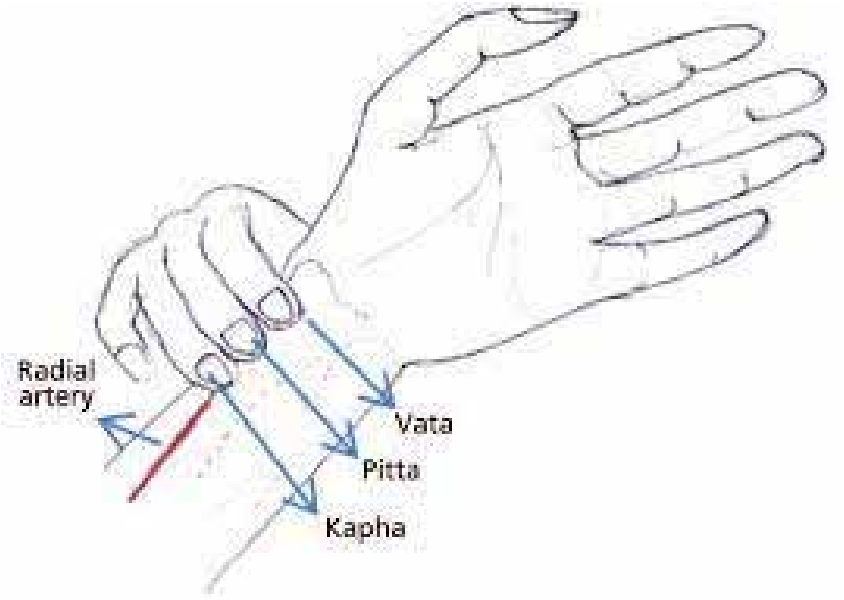

The Radial pulse can be measured from both the hands. Pulses from each hand, on applying different amount of pressure, provides information about the different organs of the body. Such as disfunctioning of small intestine, bladder, lungs can be detected from left hand whereas information about large intestine, stomach can be detected from right hand. Applying more pressure on the point of left hand detects disorder related to heart, liver and kidney. (Yoon et el. 2000)

Figure 3. Wrist pulse signal pattern (https://www.naditarangini.com)

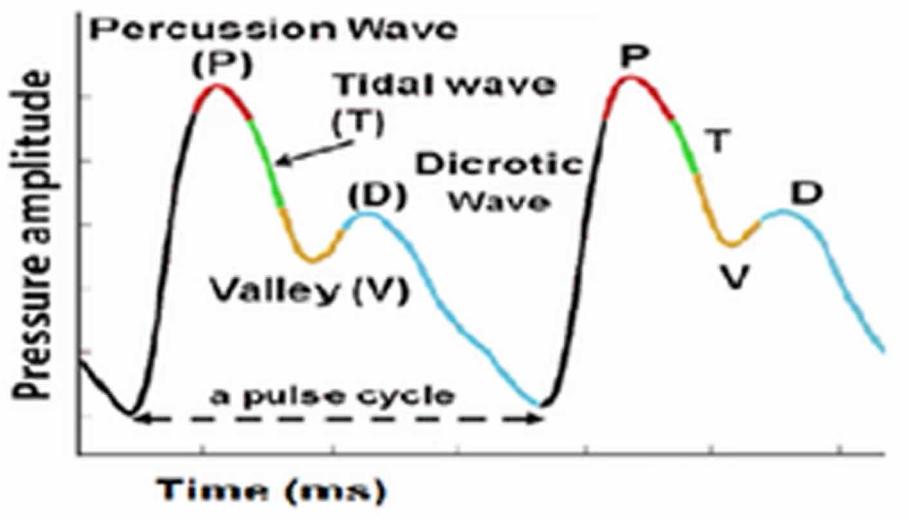

But with the advancement of technology like pattern recognition, AI and computer vision it is now possible to sense the pulse accurately and can be displayed on monitor and the data is stored for future also. Various researchers have already designed the devices like Nadi tarangini, Nadi Swara, Nadi nidan, Nadi parikshan yantra etc to capture the pulse signal.

Figure 3 shows the wrist pulse signal pattern. When we feel the pulse, it feels like high and lows. These highs and lows (or ups and downs) are in rhythmic pattern as hearts beats in rhythm. Every pulse beat is comprising of four subwaves, the Percussion wave(P), a tidal wave(T), the valley (V) and dicrotic wave(D) which are very much similar to the PQRST pattern of ECG signal. The Doctors can correlate these signal with the inter variability and intra variability of the sensed pulse. (https://www.naditarangini.com)

Signal Acquisition and Processing System

Figure 4 shows a basic building block a wrist pulse signal acquisition system. Both ECG and Radial pulse system requires sensors for capturing signals. Different types of sensors (e.g. Optical pulse sensors, Piezo resistive pressure sensors, piezoelectric sensors, (Kalange, Gangal 2007) pressure transducer gauge, Ultrasound, flexible MEMS sensors and biosensors. etc.) with different working principle are used to measure pressure.

In contemporary Pulse detection technologies, piezoresistive pressure sensors are commonly employed. When pushed against the wrist, this sensor has the benefit of detecting the dynamic pulse pressure and rejecting the static pulse pressure operating on it. Proper positioning of sensors is important. If sensors are not positioned correctly it will indicate false output. A proper amount of pressure is applied to the wrist so that the sensor's diaphragm comes into contact with the radial artery and the pressure or vibration of blood flow may be monitored. (Peng Fang et el. 2021, Goyal, and Agarwal 2008)

While in ECG signal capturing ultrasonic sensor and graphene is widely used. The physical, electrochemical, and electrical characteristics of a graphene-based ECG sensor are all outstanding. Graphene

is a two-dimensional carbon-based material whose electrical conductivity has expanded its usage in electronics, particularly in sensors.

Figure 4. Signal Acquisition and Processing system

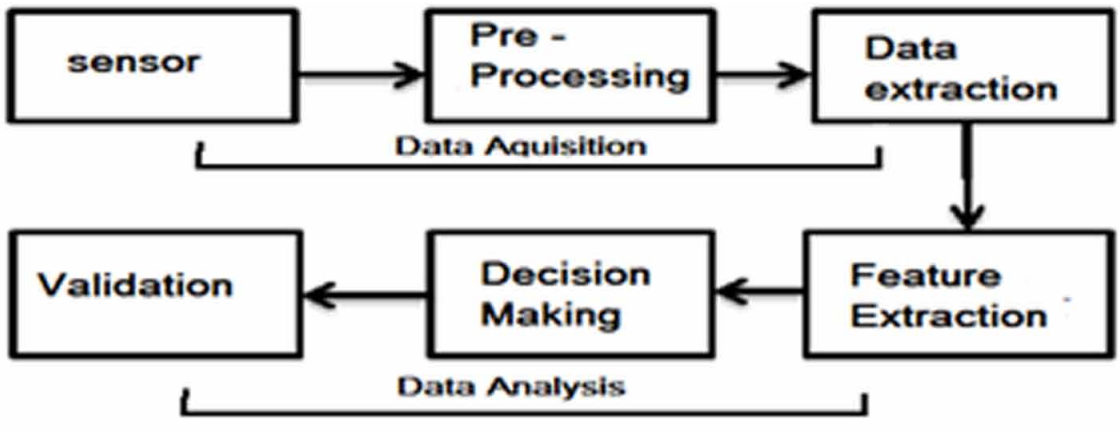

After capturing signals, it is important to Pre-processing the acquired signals as the received pulse signals contains noise. The noise occurred due to interaction of the pulse signals with the skin and muscles during acquisition. Hence, the design of suitable filter like low pass, Butterworth (order of 8 or 16) is required for noise removal. [2,3]. Also the acquired signal is of very low strength < 20 Hz, it must be amplified and sampled before analysis. (Zeli Gao et el. 2012)

After preprocessing, various pattern recognition and machine learning algorithm are applied to decode the missed and errored pattern for error free decision making.

Wrist signal

Figure 5 shows a hardware set up and arrangement of sensor and acquisition system. One or more pressure sensors are placed on the wrist with the help of Velcro to sense three location pulses either one at a time or collectively. The pressure is slowly increased on the wrist until one of the three Pulse waveforms start to take the form of a typical Pulse wave.

Figure 5. Hardware set up for wrist pulse capturing (https://www.nadiparikshan.com/)

The sampling frequency is kept around about 500Hz or 1000Hz. (Thakkar S, Thakker B. 2015, Parikhrt K, Thakker B, 2015) The pressure is then kept constant to record of that particular Pulse waveform that can be used for further computation. The microcontroller is attached to the pulse sensor. The pulse sensor data is acquired using a microcontroller in the form of analogue voltage. The electrical signal proportional to the pressure is then digitized using the 32-bit or 16- bit data acquisition card that is interfaced with the personal computer. Data Acquisition software (MATLAB, LAB View) is used to acquire samples at a particular rate. Extraction: A Data base will be created with the help of trained practitioners. Data is then splitted in training and testing data for feature extraction and testing is done using Machine learning and Artificial Neural Network. (S. Joshi, P.Bajaj 2012)

ECG Signal

Normally an ECG machine has 12 sensors connected to each lead. Out of which six of the leads are attached to the arms and/or legs of patient and referred as “limb leads”. The remaining six leads are attached to the chest as illustrated in the diagram. To get an ECG signal, we must first arrange the electrodes on the patient’s body in the right placements. The voltage between a pair of electrodes may then be recorded for each ECG lead. The obtained signals are amplified using an instrumentation amplifier and then it is filtered using a bandpass of Butterworth filter.

Signal Analysis

Many researchers have proposed different methods to analyze and to extract Several hemodynamic parameters from the acquired pulse waveform. Parameters obtain from the analysis of signal in time domain as well as in frequency domain provide a useful information about the health of patients. To determine the irregularities is the signal data, nonlinear method like sample entropy and approximation entropy algorithm can also be applied and is correlated with the existing pattern.

Time Domain Analysis

Signals in the time domain are in their raw form. It is a function of time and the plot is time -amplitude representation of signal. The pulse shape and patterns are examined using time domain analysis. The pressure pulse consists of P wave (Percussion), T wave (tidal), Valley and D (Dichotic) wave. Peak amplitude, slope, notch, and associated time are typical indicators that are used to assess human health. The amplitudes of tidal and dichotic waves in an unhealthy subject are relatively low. In sick participants, larger changes in pulse shape were found when static pressure increased. Sometimes, due to irregularities in the pulse waveform, it is difficult to measure parameters (Wang et el. 2003). So it can also be measured from first order derivative. (Thakkar S, Thakker B. 2015, Parikhrt K, Thakker B, 2015) Radial signal variability can be calculated with the Approximation entropy, recurrence plot and multiscale entropy. (Wang et el. 2003)

Figure 6. Time domain analysis

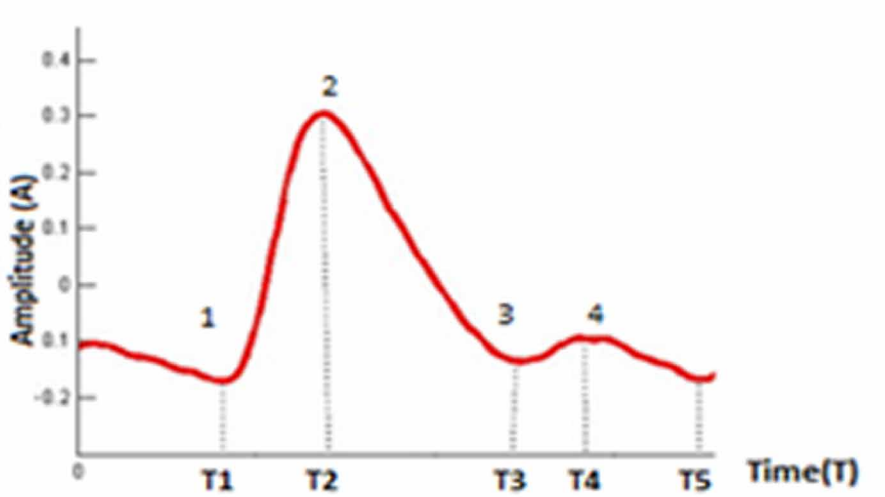

Figure 6 shows the time domain representation of parameters and their duration. Pulse amplitude is distance between onsets of point 1 and 2. Total pulse duration (T5 – T1) is Pulse time, Time (T2 – T1) is notch time, Time between top notch and valley (Notch minimum) is Fall Time (T3 – T2). Pulse width is total width of pulse. Pulse transit Time is the time between the Peaks of two pulses. Notch amplitude is the distance from the onset of the pulse point 1 to the notch minimum during the cycle. Slope of the pulse is the ratio of pulse amplitude to pulse rise time.

Similarly, many other statistical parameters like mean, variance, standard deviation, Root mean square value, etc can be calculated and correlated with human physiological condition for disease diagnosis. (Chung et el. 2013)

Frequency Domain Analysis

The pulse's resonance frequency, energy, and spectrum are investigated using frequency domain analysis. Distinct organs have varying resonance frequencies and harmonics that provide pathological and physical information. Deviation in harmonic frequencies determines vascular stiffness. Several study groups computed the Band Energy Ratio (BER) for healthy and sick participants. The energy distribution in case of healthy person is in band between 0- 4 Hz and for unhealthy person it is above 4 Hz. (Chaiwisood, 2012)

Moving average estimator and Autoregressive, moving average estimators., Fast Fourier transform, DFT, Wavelet transform etc can be use obtain parameters like PSD, Band energy ratio, frequency shift, energy, phase shift, and pulse repetition frequency. The presence of wavy, toughness, rigidity, and normal pulses depending on the frequency and phase components in the spectrum can be estimated. (Wei LY and Chow P 1983)

The wrist pulse signal gradually changes over time. Amplitude, frequency, PSD, variances changes with time and hence time-frequency analysis is found to be more accurate. Wavelet transform and STFT (short time FT) are used to compute the frequency parameters that are time dependent. (Su ZY et el 2008)

CONCLUSION

The electrical activity that is created by cardiac activity and travels throughout the body is recorded as wrist pulse signal and an ECG. The scientific knowledge of abnormalities of human organism can be acquire precisely by studying the wrist pulse. Finding its interrelation with the social, environmental and seasonal effect and then improve dietary habits and nutrition to maintain the health and prevention of disease. Pulse signal analysis has sparked renewed attention as a result of latest research on non-invasive ways for prior detection and a better understanding of cardiac issues. Biological or pathological aspects, such as blood pressure, rate of flow, and visidity and nerves, would also impact pulse signal (Lee CT and Wei LY 1983) making pulse signal useful for non-cardiac illness detection. The Ayurvedic treatment is mainly based on plants and herbs. It best utilizes the natural resources for daily usage and for making drug. Hence it will be beneficial to understand the health issues with nadi signals similar to ECG analysis

REFERENCES

Rajani, Nawsupe, & Wangikar. (2012). Automatic detection of pulse morphology patterns & cardiac risks. *Journal of Biomedical Science and Engineering*, *5*(6).

Chaiwisood, Wongkittisuksa, & Phukpattaranont. (2012). Comparison of Signal Quality between Electrocardiograms Measured from the Chest and the Wrist. *The 10th International PSU Engineering Conference*.

Joshi, S., & Bajaj, P. (2012). Design & Development of Portable Vata, Pitta & Kapha [VPK] Pulse Detector to Find Prakriti of an Individual using Artificial Neural Network. *6th International Conference for Convergence in Technology (I2CT)*.

Lee, C. T., & Wei, L. Y. (1983). Spectrum analysis of human pulse. *IEEE Transactions on Biomedical Engineering*, *BME-30*(6), 348–352. doi:10.1109/TBME.1983.325136 PMID:6873965

Wei, L. Y., & Chow, P. (1985). Frequency distribution of human pulse spectra. *IEEE Transactions on Biomedical Engineering*, *BME-32*(3), 245–246. doi:10.1109/TBME.1985.325537 PMID:3997182

Suguna, G. C., & Veerabhadrappa, S. T. (2009). A review of wrist pulse analysis. *Biomedical Research*, *30*(4).

Goyal, K., & Agarwal, R. (2017). Pulse based sensor design for wrist pulse signal analysis and health diagnosis. *Biomedical Research (Aligarh)*, *28*, 5187–5195.

Tang, A. C. Y. (2012). Review of traditional Chinese medicine pulse diagnosis quantification. *Complementary Ther. Contemp. Healthcare*, *2012*, 61–80.

Gao, Z., Wu, J., Zhou, J., & Jiang, W. (2012). Design of ECG Signal Acquisition and Processing System. *International Conference on Biomedical Engineering and Biotechnology.* 10.1109/iCBEB.2012.128

Abhinav, M. S., Kumar, M., Santhosh, J., Salhan, A., & Anand, S. (2009). Nadi Yantra: A Robust System Design to Capture the Signals from the Radial Artery for NonInvasive Diagnosis. *Journal of Biomedical Science and Engineering*, *2*(7).

Kwang-Sup Soh, Myeong-Hwa Lee, & Young-Zoon Yoon. (2000, November-December). Pulse type classification by varying contact pressure. *IEEE Engineering in Medicine and Biology Magazine*, *19*(6), 106–110. doi:10.1109/51.887253 PMID:11103713

Fang, P., Peng, Y., Lin, W.-H., Wang, Y., Wang, S., & Zhang, X. (2021). Wrist Pulse Recording with a wearable Piezo resistor – Piezoelectric Compound Sensing system and Its Applications in Health Monitoring. *IEEE Sensors Journal*.

Gholam-Hosseini & Nazeran. (1998). Detection an Extraction of the ECG signal Parameters. *Proceedings of the 20th Annual International Conference the IEEE Engineering in Medicine and Biology Society*, 20(1).

Thakker, B., & Vyas, A. L. (2009). Outlier pulse detection and feature extraction for wrist pulse analysis. *International Conference on Biological Science and Technologies (ICBST 2009)*.

Kalange, A.E., & Gangal, S.A. (2007). Piezoelectric sensor for human pulse detection. *Defense Sci Journals, 57*, 109-114.

Su, Z.Y., Wang, C.C., Wu, T., Wang, Y.T., & Tang, F.C. (2008). Instantaneous Frequency-Time analysis of physiology signals: The application of pregnant Women's Radia l Artery Pulse Signals. *Physica A: Statistical Mechanics and its Application, 387*, 485-494.

Thakkar, S., & Thakker, B. (2015). Wrist pulse acquisition and recording system. *Communication on Applied Electronics.*, *1*(6), 20–24. doi:10.5120/cae-1568

Parikhrt, K., & Thakker, B. (2015). Wrist pulse classification system for healthy and unhealthy subjects. *International Journal of Computers and Applications*, *1*, 120–124.

Zhang, Z., Zhang, Y., Yao, L., Song, H., & Kos, A. (2018). A sensor-based wrist pulse signal processing and lung cancer recognition. *Journal of Biomedical Informatics*, *79*, 107–116. doi:10.1016/j.jbi.2018.01.009 PMID:29428411

Thakker, B., & Vyasn, A. L. (n.d.). Wrist (pulse signal classification for health diagnosis. *4th International Conference on Biomedical Engineering and Informatics (BMEI)*. 10.1109/BMEI.2011.6098759

Luo, C. H., Chung, Y. F., Yeh, C. C., Si, X. C., Chang, C. C., Hu, C. S., & Chu, Y.-W. (2012). String like pulse quantification study by pulse wave in 3D pulse mapping. *Journal of Alternative and Complementary Medicine (New York, N.Y.)*, *18*(10), 924–931. doi:10.1089/acm.2012.0047 PMID:23057481

Wang, K., Xu, L., Li, Z., Zhang, D., Li, N., & Wang, S. (2003). Approximate entropy based pulse variability analysis. *16th IEEE Symposium Computer-Based Medical Systems*.

Zhang, D., Zuo, W., & Wang, P. (2019). *Comparision Between Pulse and ECG signal*. Computational Pulse Signal Analysis.

Chung, C. Y., Chung, F. Y., Chu, Y. W., & Luo, C. H. (2013). Spatial feature extraction from wrist pulse signals. *1st International Conference on Orange Technologies Tainan*.

Upadhyaya & Deva. (2003). *Nadi Vijnana: Ancient pulse science*. Chaukhamba Sanskrit Pratishthan.

Rhyner, H. H. (1998). *Ayurveda: The gentle health system*. Motilal Banarsidass Publishers Pvt. Ltd.

Nanyue, W., Youhua, Y., Dawei, H., Bin, X., Jia, L., Tongda, L., Liyuan, X., Zengyu, S., Yanping, C., & Jia, W. (2015). Pulse diagnosis signals analysis of fatty liver disease and cirrhosis patients by using machine learning. *TheScientificWorldJournal*.

Alivecor. (n.d.). *What is an ECG?* Retrieved from https://www.alivecor.com/education/ecg.html

Chapter 8
ECG Signal Analysis for Automated Cardiac Arrhythmia Detection

Chandan Kumar Jha
Indian Institute of Information Technology, Bhagalpur, India

ABSTRACT

The graphical recordings of electrical stimuli generated by heart muscle cells are known as an electrocardiogram (ECG). In cardiology, ECG is widely used to detect different cardiovascular diseases among which arrhythmias are the most common. Irregular heart cycles are collectively known as arrhythmias and may produce sudden cardiac arrest. Many times, arrhythmia evolves over an extended period. Hence, it requires an artificial-intelligence-enabled continuous ECG monitoring system that can detect irregular heart cycles automatically. In this regard, this chapter presents a methodological analysis of machine-learning and deep-learning-based arrhythmia detection techniques. Focusing on the state of the art, a deep-learning-based technique is implemented which recognizes normal heartbeat and seven different classes of arrhythmias. This technique uses a convolutional neural network as a classification tool. The performance of this technique is evaluated using ECG records of the MIT-BIH arrhythmia database. This technique performs well in terms of different classification metrics.

INTRODUCTION

As per the report of the world health organization (WHO), cardiovascular diseases (CVDs) are the leading cause of death globally. In this report, it is stated that 17.9 million people die annually due to CVDs which constitutes an estimated 32% of all deaths worldwide (World Health Organization, Cardiovascular Diseases). For the diagnosis of CVDs, electrocardiogram (ECG) signals are widely used by cardiologists. It provides a non-invasive diagnostic method that is most preferable to medical experts. Abnormal heart rhythms generate irregular ECG waveforms which are collectively known as arrhythmias. There are different types of arrhythmias that evolve during an extended period of time. Early diagnosis of arrhythmias requires continuous monitoring of cardiac patients. For this purpose, Holter monitors are used which

DOI: 10.4018/978-1-6684-3947-0.ch008

continuously records ECG signals for 24 to 48 hours (Jha & Kolekar, 2020, 2021). Manual analysis of these long-term ECG records is difficult for cardiologists. Hence, artificial intelligence (AI) enabled continuous ECG monitoring systems are essential to reduce the burden of cardiologists in arrhythmia detection. In these systems, machine learning/ deep learning-based methods are used to recognize normal heart rhythm and arrhythmias using ECG signal analysis. In Figure 1, the ECG waveform of a normal heart cycle is shown which has different components: P-wave, QRS-complex, T-wave, PR-Segment, QT-Segment, and ST-segment. Morphology of ECG waveforms changes in the case of arrhythmias which corresponds to abnormal cardiac activities. There are different types of arrhythmias which are broadly categorized into five classes as per the recommendation by the Association for the Advancement of Medical Instrumentation (AAMI).

These five classes of ECG beat as per AAMI are non-ectopic beat, supra-ventricular ectopic beat, ventricular ectopic beat, fusion beat, and an unknown beat. The class of non-ectopic beats includes normal (N), left-bundled branch block (LBBB), and right-bundled branch block (RBBB) ECG beats. The class of

Figure 1. ECG waveform of a normal heart cycle

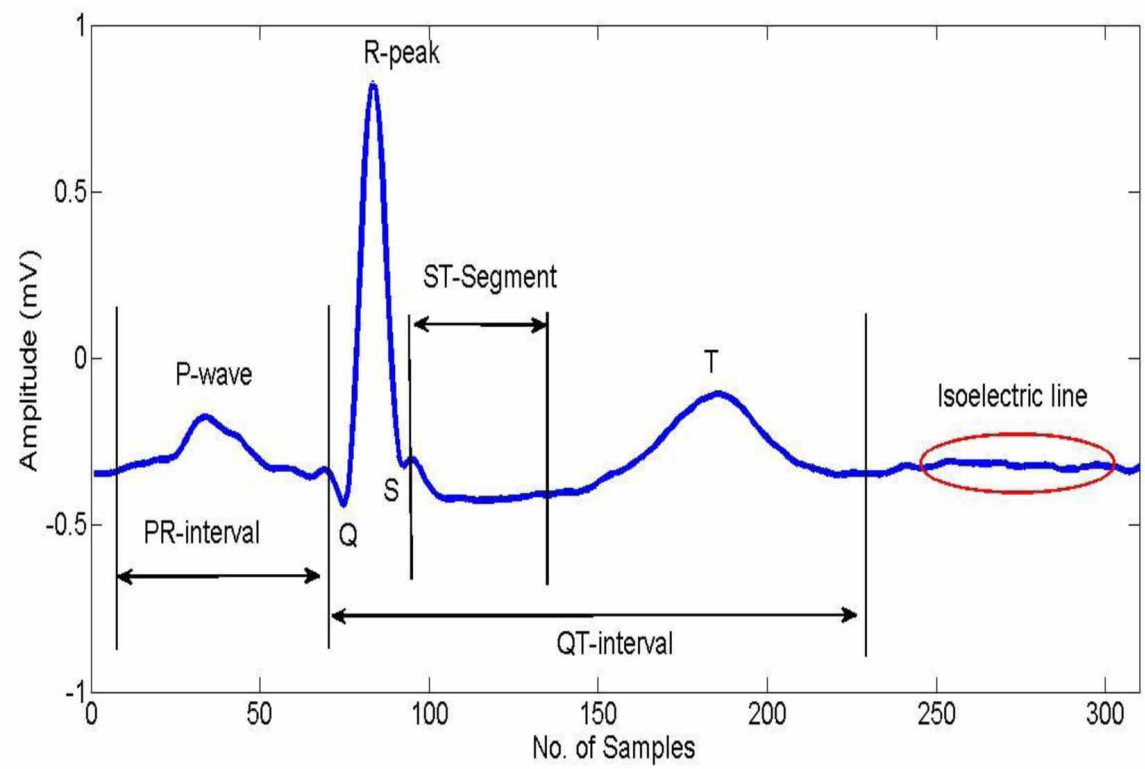

supra-ventricular ectopic beat includes atrial-premature contraction (APC) beats while the class of ventricular ectopic beat includes premature ventricular contraction (PVC) beats. The fusion of normal and paced beat (FNPB) comes in the class of fusion beats while the fusion of normal and paced beat (FNPB) and paced (P) beats are associated in the class of unknown beat. The automated arrhythmia

detection technique distinguishes different classes of arrhythmias based on different features of ECG beats which include time-domain features, frequency domain features, and statistical features.

In past, many arrhythmia detection techniques have been developed which are based on machine learning-based methods. Generally, machine learning-based methods use a support vector machine (SVM) (Khalaf et al., 2015; Qin et al., 2017), artificial neural network (ANN) (Li et al., 2017; Melin et al., 2014), probabilistic neural network (PNN) (Gutiérrez-Gnecchi et al., 2017), and ensemble classification tools (Mondéjar-Guerra et al., 2019; Rajesh & Dhuli, 2018). These machine-learning-based methods utilize different kinds of features which are used as inputs to the training model of the classifier. These features of ECG beats are extracted separately and among these features, efficient features are selected. The features extraction and selection steps are important in machine-learning-based methods which affect the classification performance. In recent few years, many deep-learning-based methods have been developed which are based on convolutional neural network (CNN), recurrent neural network (RNN), and long short-term memory network (LSTM). These are different architectures of deep-neural networks which extract features of ECG beats as weights of the network. Hence, features extraction and selection steps are not required separately in deep-learning-based methods. General methodologies of machine-learning and deep-learning-based techniques are discussed in the next section.

BACKGROUND

Machine-learning-based arrhythmia detection technique employs a general methodology which is shown in Figure 2. The first step in this technique is the acquisition of ECG data which may be contaminated by different artifacts. The pre-processing step removes different artifacts of ECG signal noise using different filtering methods. The presence of artifacts corrupts features of ECG beats and affects classification performance. Hence, ECG artifacts removal is essential to achieve good classification performance. The pre-processing step is followed by R-peak detection and beat segmentation. In an ECG signal, R-peak is detected at a certain location in terms of time or sample index, and choosing a time window around that sample index results in the segmented ECG beat. After segmentation, different features are extracted from the ECG beat which may be based on time-domain, frequency-domain and statistical characteristics. Features of different ECG beats are partitioned into two groups: the training group and the testing group. Features of the training group are used to train the model of the classifier while the testing group is used to test the classification and recognition capability of the classifier model. Based on this general methodology, many machine-learning methods have been developed for arrhythmia detection. These techniques widely used SVM, ANN, PNN, and ensemble classifiers to classify different types of ECG beats.

Figure 2. General methodology of machine-learning based arrhythmia detection technique

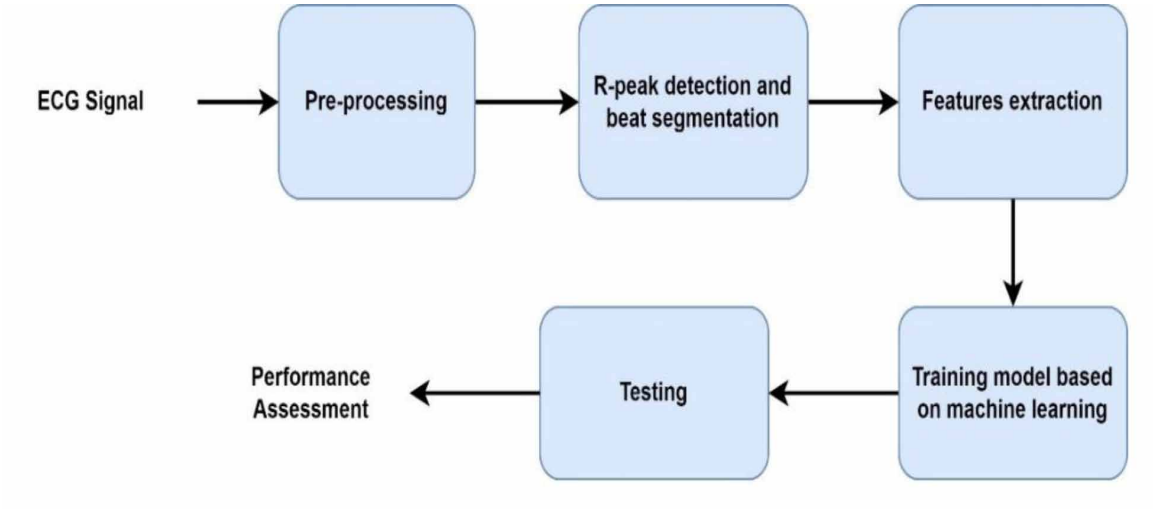

Recently, neural networks have emerged as a powerful classifier for ECG arrhythmia classification (Moavenian & Khorrami, 2010). For example, a fuzzy C-mean (FCM) probabilistic neural network-based classification method was proposed by (Haseena et al., 2011) which can discriminate eight types of ECG beats. The overall accuracy of 97.54% was achieved by this method. Osowski et. al (Osowski & Linh, 2001) utilized a fuzzy hybrid neural network to recognize different types of ECG beats representing arrhythmia. A type-2 fuzzy clustering neural network was employed by Ceylan et. al (Ceylan et al., 2009) to classify ten types of arrhythmic ECG beats. The classifier utilized in this method has consisted of type-2 fuzzy C means clustering and backpropagation learning. A novel neural network with an adaptive function was implemented by Ozbay (Özbay & Tezel, 2010) to classify ECG beats with an average accuracy of 98.19%. Yu et. al (Yu & Chen, 2007) proposed a probabilistic neural network-based ECG beats classification scheme to discriminate six types of ECG beats with an overall classification accuracy of about 99%. A combined neural-network-based ECG beat classification method was developed by Guler et. al (Güler & Übeyl, 2005). It classifies four types of ECG beats with an accuracy of 96.4%. Melgani et. al (Melgani & Bazi, 2008) utilized a support vector machine classifier with particle swarm optimization to recognize six types of arrhythmic ECG beats.

In (Khalaf et al., 2015), an SVM-based arrhythmia classification technique is reported which uses spectral correlation and statistical features of ECG beats to classify it into five classes. This technique selects features using principal component analysis (PCA) and achieves 99.20% classification accuracy. Ensemble decision trees are used to classify common arrhythmias (Afkhami et al., 2016). This technique uses morphological, statistical and time-domain (RR-interval) features of ECG beats. Apart from it, skewness, kurtosis, and fifth moment are also used as features. In (Rajesh & Dhuli, 2018), an Adaboost ensemble classifier is used to classify five types of arrhythmia ECG beats using ensemble empirical mode decomposition, high order statistics, and entropy as features. In (Vafaie et al., 2014), a dynamic model of ECG beat is used for the early detection of an abnormal heartbeat using a classifier based on fuzzy logic. A modular neural network with a learning vector quantization algorithm is used (Melin et al., 2014) to classify five different types of arrhythmias. Again, a backpropagation neural network (BPNN) is used to classify arrhythmia ECG beats using coefficients obtained after wavelet packet decomposition

and their statistical characteristics. In this technique, a genetic algorithm (GA) is used to decrease the dimension of the feature set (Li et al., 2017).

Table 1. Machine learning based arrhythmia classification methods

Literature	Features	Classifier
Khalaf et al., 2015	Spectral correlation, statistical	SVM
Afkhami et al., 2016	Morphological, statistical & RR-intervals	Ensemble of decision trees
Rajesh & Dhuli, 2018	Ensemble empirical mode decomposition, high order statistics, entropy	Ada-boost ensemble classifier
Vafaie et al., 2014	Dynamic model of ECG beats	Fuzzy logic
Melin et al., 2014	Learning vector quantization	Modular neural network
Li et al., 2017	WPD and statistical characteristics	GA-BPNN
Sahoo et al., 2017	Multi-resolution wavelet transform	ANN, SVM
Mondéjar-Guerra et al., 2019	Temporal, morphological, wavelet and higher order statistics	SVM
Jha & Kolekar, 2020	Tunable Q-wavelet transform	SVM
Marinho et al., 2019	Fourier, Goertzel, higher order statistics, and structural co-occurrence matrix	SVM, ANN
Elhaj et al., 2016	Linear and non-linear features	SVM, ANN
Gutiérrez-Gnecchi et al., 2017	Wavelet transform	PNN
Qin et al., 2017	Wavelet transform	SVM

In (Sahoo et al., 2017), ANN and SVM classifier is used to distinguish five different types of arrhythmias using wavelet-based features. In the analysis of classification performance, it is found that SVM offers better performance than ANN for the same feature sets of ECG beats. An SVM-based approach is developed by (Mondéjar-Guerra et al., 2019) which utilizes temporal, morphological, wavelet, and higher-order statistics to classify 0four types of normal and abnormal ECG beats. In(Jha & Kolekar, 2020a), tunable Q-wavelet transform-based features are used to classify eight different types of ECG beats using multi-class SVM. In (Marinho et al., 2019), a novel features extraction method based on Fourier, higher-order statistics, and structural co-occurrence matrix are used to classify four different types of arrhythmias using SVM and ANN. In (Elhaj et al., 2016), linear features such as discrete wavelet transform coefficients and non-linear features such as higher-order statistics are used to classify five different types of ECG beats using ANN and SVM. In this technique, independent component analysis and principal component analysis are used to reduce the dimension of feature sets. In (Gutiérrez-Gnecchi et al., 2017), wavelet transform-based features are used to classify eight classes of ECG beats using a probabilistic neural network (PNN). Again, wavelet transform-based features are utilized to distinguish six different classes of ECG beats using an SVM classifier (Qin et al., 2017). In this technique, the dimension of the feature set is reduced using principal component analysis. Table 1 shows the different features and classifiers used by researchers in machine-learning-based arrhythmia detection techniques.

Machine-learning-based arrhythmia detection techniques developed in recent years widely use the wavelet transform to extract features. Further, efficient features are selected using different dimensionality

reduction tools such as principal component analysis and independent components analysis. Different classifier models based on SVM, ANN & PNN use the selected features to classify different ECG beats. Wavelet transform, SVM, ANN, and PNN are briefly discussed in the next section.

WAVELET TRANSFORM

In ECG signal analysis, wavelet-transform is widely used due to its good time-frequency localization at different scales. Wavelet transform provides multi-resolution analysis from which efficient features are extracted and used for classification. In wavelet transform, a mother wavelet $\chi(t)$ is used to generate different basis functions based on the dilation (scaling) parameter m and translational (shifting) parameter n. The scaled and shifted version of the mother wavelet is expressed by:

$$\chi_{m,n}(t) = \left|m\right|^{-\frac{1}{2}} \chi\left(\frac{t-n}{m}\right); m \neq 0 \tag{1}$$

A basis function of a mother wavelet may be expanded or compressed based on the choice of the scaling parameter *m*. Using the expression of the wavelet basis function, continuous wavelet transform of a signal $x(t)$ is obtained using the expression

$$X^{\chi}{}_{CWT}(m,n) = \frac{1}{\left|m\right|^{\frac{1}{2}}} \int_{-\infty}^{+\infty} x(t).\chi * \left(\frac{t-n}{m}\right) \tag{2}$$

where the asterisk denotes the complex conjugate. Further, the scaling and translational parameters are discretized as: $a = a_0{}^{j}$ and $b = kb_0a_0{}^{j}$, where a_0 and b_0 are constants and $j,k \in Z$. The discrete form of scaling and translational parameters are used to represent the discrete wavelet function

$$\chi_{j,k}(t) = \frac{1}{\sqrt{\left|a_0{}^{j}\right|}} \chi * \left(\frac{t - kb_0a_0{}^{j}}{a_0{}^{j}}\right) \tag{3}$$

Using the discrete wavelet function, discrete wavelet transform of a signal $x(t)$ can be written as:

$$X^{\chi}{}_{DWT}(j,k) = \frac{1}{\sqrt{\left|a\right|}} \int_{-\infty}^{+\infty} x(t)\chi^{*}{}_{j,k}(t)dt \tag{4}$$

In discrete wavelet transform, values of a_0 and $b_0$are chosen in such a way that the wavelet family constitutes an orthonormal basis $L^2(R)$. For this, values of a_0 and b_0 are taken as 1 and 2 respectively. Using these values, the discrete wavelet family is represented as

$$\chi_{j,k}(t) = \frac{1}{\sqrt{2^j}} \chi\left(2^{-j} t - k\right) \tag{5}$$

The wavelet transform based on this wavelet family is called dyadic wavelet transform which satisfies almost all properties of continuous wavelet transform such as linearity, scale and shift invariance etc. The wavelet transform also provides multi-resolution analysis which is used to extract features of ECG beats.

FEATURES EXTRACTION USING WAVELET MULTI-RESOLUTION ANALYSIS

Features of each ECG beat are extracted using multi-resolution wavelet transform (MRWT). For multi-resolution analysis, scaling function ϕ(t) and wavelet function χ(t) are required with the low-pass coefficients {gk} and high-pass filter coefficients {hk}. The scaling function ϕ(t) and the wavelet function χ(t) satisfy the following difference equations:

$$\chi(t) = \sqrt{2} \sum_k g_k \chi(2t - k) \tag{6}$$

$$\phi(t) = \sqrt{2} \sum_k h_k \phi(2t - k) \tag{7}$$

The above-mentioned functions associated with low-pass and high-pass filter coefficients are used to implement the wavelet-transform that decomposes a given signal up to the desired number of decomposition levels. At each decomposition level, approximate and detail coefficients are obtained that can be used as features (Jha & Kolekar, 2019). A three-level decomposition of a given signal $x(k)$ is shown in Figure 3 which shows approximate coefficients $A_1(k)$, $A_2(k)$, $A_3(k)$ and detail coefficients $D_1(k)$, $D_2(k)$, $D_3(k)$ at different decomposition levels.

Figure 3. ECG signal decomposition and feature extraction using wavelet multi-resolution analysis

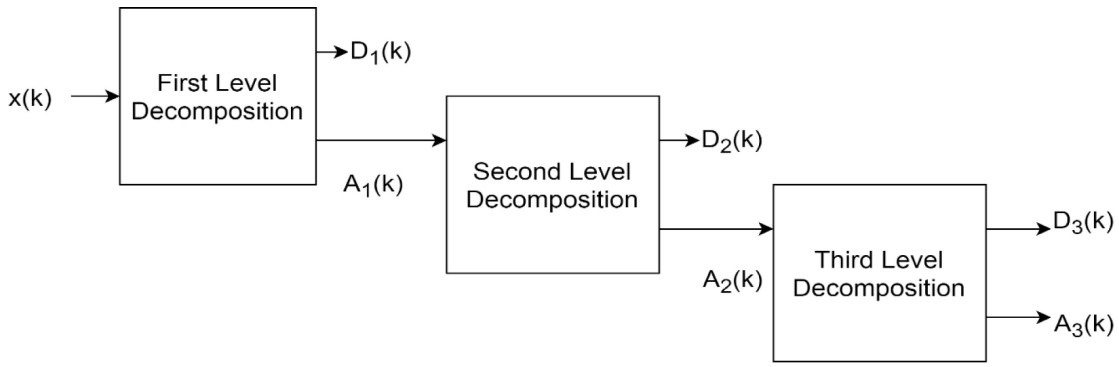

SUPPORT VECTOR MACHINE

In pattern recognition problems, support vector machine (SVM) is widely used that works on supervised learning models. SVM performs binary classification by constructing a hyper-plane between two classes. However, multi-class pattern recognition problems can also be solved by SVM using a decision function that considers all classes once. For fair classification between two classes, the distance between the hyperplane and the nearest point is maximized by employing the dual-solution of the optimization problem. The SVM can perform linear as well as non-linear classification of two classes. In non-linear classification, a kernel function is used to achieve optimization. There are different types of kernel functions such as linear, sigmoid, and radial-basis functions. In different applications, these kernel functions offer different classification performances. In the case of multi-class arrhythmia ECG beats classification Gaussian radial basis function is used.

Artificial Neural Network

Artificial neural network (ANN)/ Multi-layer perceptron (MLP) is also known as a neural network as it imitates the working of brain neurons. The architecture of neural networks is based on the human brain. It consists of at least 3 layers: input layer, hidden layer, and output layer. Each of these layers is built up of many nodes which are called perceptrons. In the architecture of a neural network, many hidden layers may exist. At the input layer, the number of input features determines the number of input nodes. These nodes are connected to the hidden layer through the synaptic weights. The hidden layer is connected to the output layer which contains the output dimension as same as the number of classes being predicted. In MLP, the backpropagation technique is used to train the classification model. In the case of linearly separable data, MLP uses a linear activation function while non-linear activation functions such as sigmoidal or logistic are used for non-linearly separable data. MLP is widely used in different fields such as biomedical signal and image processing, speech processing, and machine translation software.

PROBABILISTIC NEURAL NETWORK

The PNN was first proposed by Specht (Specht, 1990). It is a special type of radial basis-function networks. In PNN (Mao et al., 2000), (Wang et al., 2018) outputs can be represented as the estimation of probability of class membership and the training rule is based on estimation of probability density functions (pdf) of classes. Figure 4 illustrates the architecture of the PNN which consists of an input layer, a pattern layer, a summation layer and an output layer. Neurons of the input layer distributes the input features to the neurons of the pattern layer directly. In the pattern layer, the neuron $X_{i,j}$ computes its output using the received pattern X from the input layer. Multi-dimensional Gaussian function is utilized to calculate output of the neuron $X_{i,j}$:

$$\phi_{i,j}(X) = \frac{1}{\left(2\pi\right)^{\frac{d}{2}}} e^{\left\{-\frac{\left(X-X_{i,j}\right)\left(X-X_{i,j}\right)^{T}}{2\sigma^{2}}\right\}} \tag{8}$$

where, $X_{i,j}$ denotes the neuron vector of the pattern layer, σ the smoothing parameter and d *t*he dimension of the pattern vector X *r*eceived from the input layer. Neurons of the summation layer calculate the maximum likelihood of the pattern vector X *b*eing classified into class C*i* by averaging the output of all the pattern layer neurons that belong to the same class:

$$p_i(X) = \frac{1}{N_i \left(2\pi\right)^{\frac{d}{2}} \sigma^2} \sum_{i=1}^{N} e^{\left\{-\frac{\left(X-X_{i,j}\right)\left(X-X_{i,j}\right)^T}{2\sigma^2}\right\}} \tag{9}$$

where, N_i is the total number of samples in a class C_i. In the decision layer, the class belongingness of the pattern X is determined by Equation (16) which is in accordance with Baye's decision rule. It satisfies the two conditions: first, the a priori probability for each class is same and second, the losses associated with misclassification for each class are the same:

$$C\left(X\right) = \arg\max\left(p_i\left(X\right)\right), i = 1,2,3,4,...,m \tag{10}$$

where, C_X is the estimated class of the pattern X and m denotes the total number of classes in the training samples.

Figure 4. Architecture of PNN

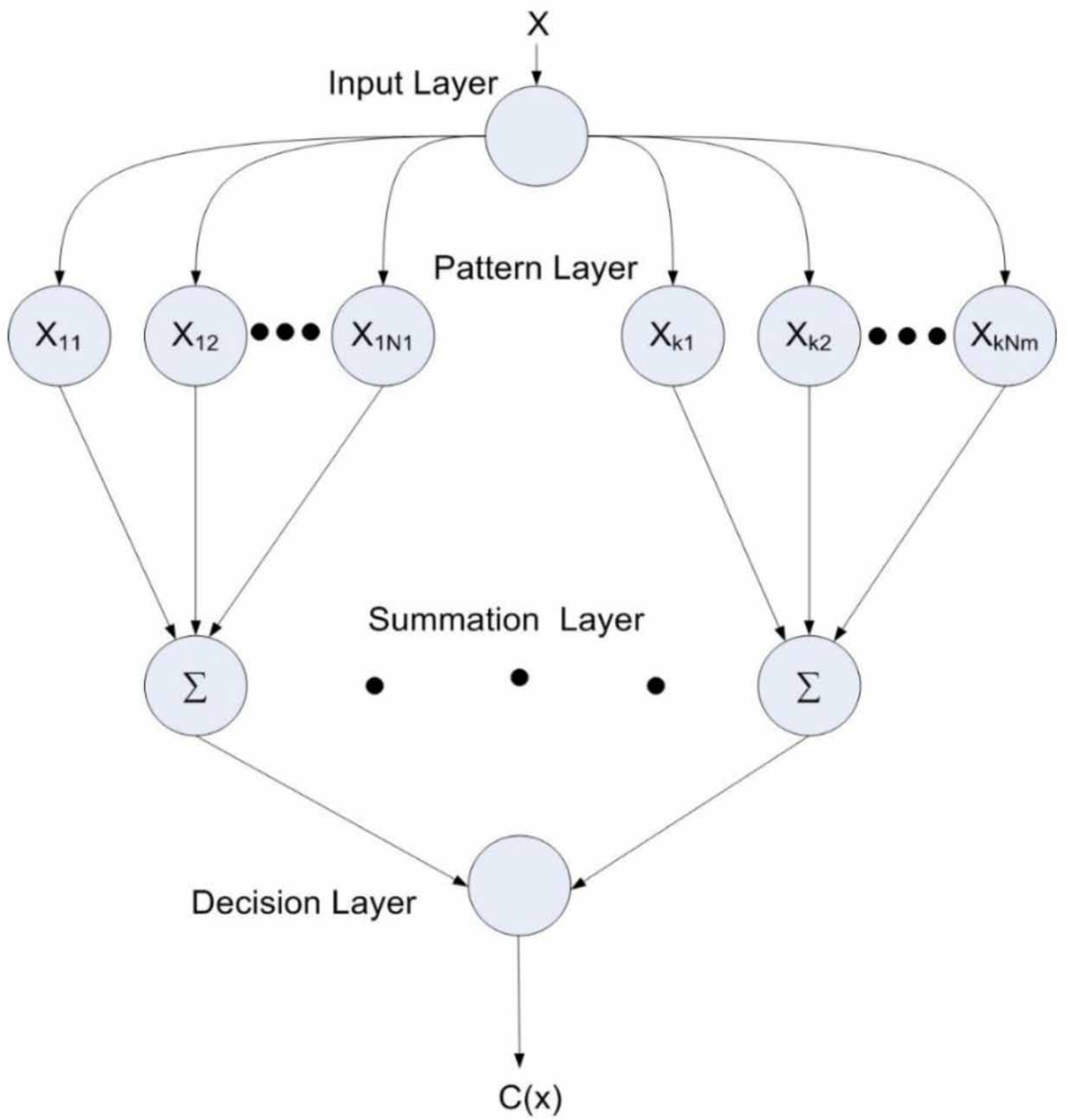

DEEP LEARNING BASED METHODS

In recent years, many deep-learning-based methods have been developed for automated arrhythmia detection. These methods utilize convolutional neural network (CNN) (Chen et al., 2020; Rahul & Sharma, 2022), recurrent neural network (RNN) (Chen et al., 2020; Wang et al., 2018a), long-short term memory network (LSTM) (Yildirim et al., 2019), bi-directional LSTM (Rahul & Sharma, 2022), etc., to classify different types of arrhythmia ECG beats. The deep learning-based methods do not require features extraction and selection steps because the deep networks are able to distinguish different patterns of ECG

beats by themselves. This is the most advantageous point of the deep-learning-based methods. Figure 5 shows the general methodology of the deep learning-based methods. In a similar way as machine-learning-based techniques, it consists of steps such as ECG signal acquisition, pre-processing, R-peak detection & beat segmentation which produces ECG beats. These beats are given as input to the training model of the classifier. Later, the trained model is used for testing different patterns of ECG beats, and the performance of the classifier is assessed.

Figure 5. General methodology of deep-learning based arrhythmia detection techniques

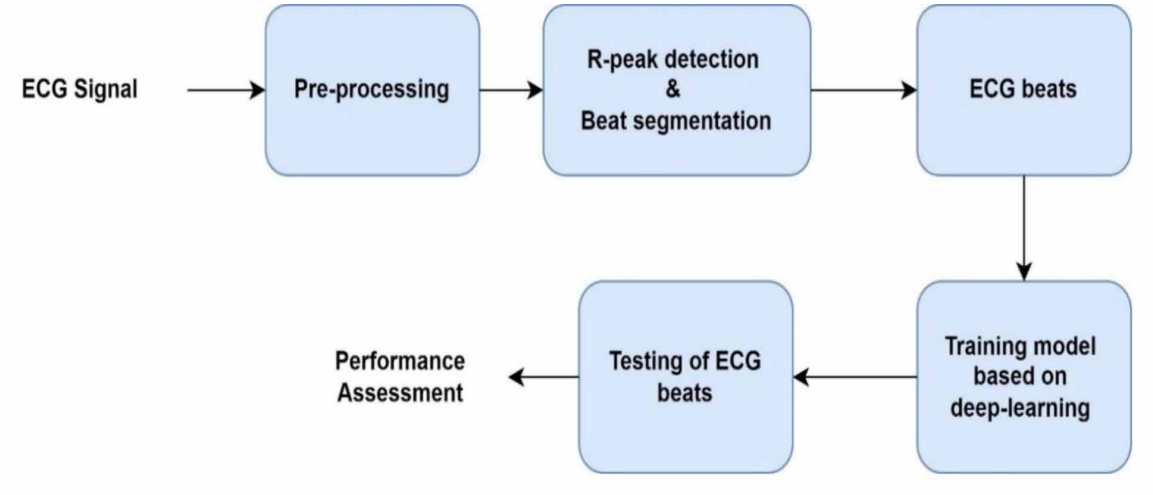

The deep-learning-based methods widely used CNN, RNN, and LSTM networks for classification which have different architectures. Brief introductions of CNN, RNN, and LSTM networks are included in the next section.

Convolutional Neural Network

A CNN (Chen et al., 2020) is a type of artificial neural network that performs convolution operation instead of matrix multiplication among its layers. CNN is also considered as the regularized version of MLP. CNN is more advantageous than conventional MLP because it contains a shared weight architecture. The number of weights shared among convolutional layers along with hidden layers is also lesser than MLP. The input layer, hidden layer, and output layer of the CNN are sparsely connected to each other while the MLP follows the fully connected architecture. CNN requires lesser pre-processing of signals/ images than MLP. In addition to this, it does not require manual features extraction and selection steps which makes it convenient to use as a powerful classification. Hence, it is widely used in pattern recognition problems related to biomedical signals and images to develop automated diagnostic tools.

Recurrent Neural Network

Recurrent neural network (RNN) (Wang et al., 2018b) is the extended version of MLP which is considered as the most suitable machine learning tool for the classification of sequential time-varying data. Parameters of the RNN are shared across the network with time. At every time step, the RNN updates its hidden states for every input and distinguishes the class. In the training model of the RNN, a gradient descent algorithm is used for the training of weights. Apart from this, the RNN uses a non-linear activation function due to which it provides highly dynamic behavior. One of the specific types of RNN is the bi-directional RNN which uses a cyclic graph structure for forwarding and backward propagation. It allows the network to learn features from both past and future values while also being sensitive to the given input data sequence.

Long Short-Term Memory Network

In the case of long-range sequential data, RNN is not suitable due to its vanishing gradient problem which interrupts the network's ability to backpropagate. This problem is also called the long-term dependency problem (Yildirim et al., 2019). This problem is resolved using a long short-term memory network (LSTM) in which the vanishing gradient problem is handled by remembering the long-term dependency. In LSTM, memory blocks are used with memory cells which are called "gates". In the recurrent hidden layer of LSTM, gates control the new information states and determine the output. The input information flow is controlled by the input gate for which the output gate works conditionally to produce the controlled output stream. Combination of LSTM gates in bi-directional RNN (Wang et al., 2018) yields a bi-directional LSTM network which is assumed to produce the best classification result for time-varying sequential data.

In this chapter, a CNN model is used for the classification of normal and seven different arrhythmia ECG beats. The stepwise procedure of the developed technique is discussed next sections.

ECG Signal

For arrhythmia beats classification, ECG records of the MIT-BIH arrhythmia database (MIT-BIH Arrhythmia Database) are used for the acquisition of different classes of ECG beats. The database consists of 48 ECG records sampled at 360 Hz with a resolution of 11-bits per sample. ECG records of this database contain normal beats and different arrhythmia beats. Examples of a few arrhythmia beats are left bundle-branch block (LBBB), right bundled-branch block (RBBB), atrial premature contraction (A), premature ventricular contraction (V), and paced (P). Since ECG signals are contaminated with different types of artifacts it generates different noise. Hence, pre-processing is essential to remove these noises.

PRE-PROCESSING

In pre-processing, different filtering techniques are used to remove noises which generates due to different artifacts of the ECG signal. Savizky-Golay (SG) filter is used to remove high-frequency noises. In SG filtering, polynomial order and length of the window is selected as 5 and 21 respectively. Low frequency noises which generate due to muscular contraction, electrode movement and many more

reasons are removed using a third order Butterworth filter. Since it removes low-frequency noises, it is a high-pass Butterworth filter. After pre-processing, R-peaks in ECG signals are detected and beat segmentation is performed.

R-PEAKS DETECTION AND BEAT SEGMENTATION

For ECG beats acquisition, R-peaks detection is essential. For this, a well-known Pan-Tompkins algorithm (Pan & Tompkins, 1985) is used. Different steps of the Pan-Tompkins algorithm are shown in Figure 6. First, the pre-processed ECG signal is passed through a band-pass filter that is implemented using a low-pass filter and a high-pass filter. It removes all the insignificant information that is not required for R-peaks detection. Slopes of the QRS-complexes of ECG beats are recognized using derivative operation. For this, a five-point differentiation operation is performed on the filtered ECG signal. Again, the squaring operation enhances the slope information. The moving window integration operation followed by adaptive thresholding locates the R-peaks in the ECG signal. After R-peaks detection, 256 samples are selected around a R-peak (102 samples before and 153 samples after) to segment an ECG beat. In Figure 7, R-peaks detection and beat segmentation is shown for an ECG signal of the MIT-BIH arrhythmia database.

Figure 6. Steps of R-peaks detection in ECG signal

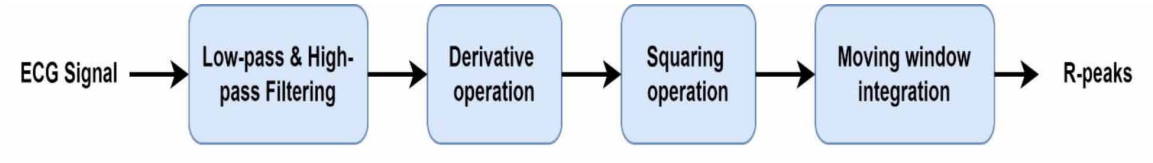

Figure 7. Detection of R-peaks and beat segmentation in ECG signal

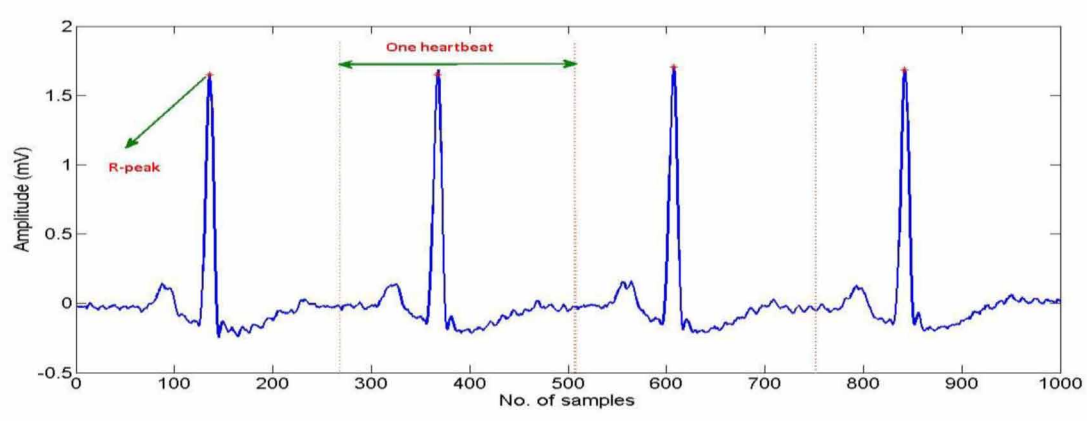

CLASSIFICATION USING CNN

For classification using a CNN model, a total of 52832 ECG beats of eight different classes are acquired from different ECG records of the MIT-BIH arrhythmia database. These ECG records are numbered as 100, 103, 112, 113, 114, 117, 121, 109, 111, 207, 214, 118, 124, 212, 231, 209, 220, 222, 232, 102, 104, 107, 217, 219, 221, 228, 233, 104, 208, 213 as per details available in the database. Eight different classes of chosen ECG beats are normal (N), Left bundled branch block (LBBB), right bundled branch block (RBBB), atrial premature contraction (APC), premature ventricular contraction (PVC), paced (P), the fusion of ventricular and normal beats (FVNB), and fusion of normal and paced beat (FNPB). The distributions of ECG beats for training, testing, and validation sets are shown in Table 2.

In CNN implementation, batch size and number of epochs are 32 and 15 respectively. In the classification model "softmax" library is used with "relu" activation model. The confusion matrix obtained after classification is shown in Table 3.

Table 2. Distribution of different types of ECG beats in training validation and testing sets

Types	Training Set	Validation Set	Testing Set
Normal	12951	2873	2813
Left bundled branch block (LBBB)	6863	1455	1533
Right bundled branch block (RBBB)	5715	1202	1174
Atrial premature contraction (APC)	1403	299	317
Paced (P)	7091	1489	1457
Premature ventricular contraction (PVC)	1172	234	232
Fusion of normal and paced beat (FNPB)	1020	213	231
Fusion of ventricular and normal beats (FVNB)	767	160	168
Total	36982	7925	7925

Table 3. Confusion matrix of the CNN classification of arrhythmia ECG beats

	Predicted values								
	Classes	**N**	**LBBB**	**RBBB**	**APC**	**P**	**PVC**	**FPNB**	**FVNB**
True values	N	2737	1	3	7	0	1	2	0
	LBBB	1	1511	0	0	0	0	1	1
	RBBB	0	0	1221	0	1	0	1	0
	APC	0	5	0	294	2	0	2	0
	P	0	0	0	1	1486	2	7	0
	PVC	0	2	0	0	1	244	0	0
	FPNB	0	2	2	1	7	0	210	0
	FVNB	0	0	0	0	0	5	2	162

PERFORMANCE METRICS

Performance of the CNN classifier is evaluated using following performance metrics: accuracy, sensitivity, and specificity (Jha & Kolekar, 2019, 2020, 2021).

$$Accuracy = \frac{TP + TN}{P + N} \times 100\% \tag{11}$$

$$Sensitivity = \frac{TP}{TP + FN} \times 100\% \tag{12}$$

$$Specificity = \frac{TN}{TN + FP} \times 100\% \tag{13}$$

In all these formulae, P and N denotes total positive and total negative predictions. TP and TN denote true positive and true negative predictions while FP and FN indicate false positive and false negative predictions.

CLASSIFICATION RESULTS

After classification, the performance of the classifier for each class is determined. Table 4 depicts the performance for eight different classes in terms of accuracy, sensitivity, and specificity. Overall accuracy, sensitivity, and specificity of eight different classes of beats are 99.80%, 98.08%, and 99.88% respectively. Hence, the CNN classification model performs well to distinguish eight different types of ECG beats.

Table 4. Performance of the CNN classifier

Classes	Accuracy (%)	Sensitivity (%)	Specificity (%)
N	99.81	99.49	99.99
LBBB	99.83	99.80	99.84
RBBB	99.91	99.83	99.92
APC	99.77	97.02	99.88
P	99.73	99.33	99.82
PVC	99.86	98.78	99.89
FPNB	99.65	94.59	99.80
FVNB	99.89	95.85	99.87
Overall	99.80	98.08	99.88

CONCLUSION

This chapter presents automated ECG analysis methods for arrhythmia beats detection. Broadly, these analysis methods are based on machine-learning and deep-learning techniques. A general methodology of machine learning and deep-learning-based techniques are discussed in detail. In the methodological analysis, it is found that the deep-learning-based technique does not require the features extraction and selection step. It is considered as a prime advantage of the deep-learning-based method. Further, eight different classes of ECG beats are distinguished using a deep-learning method based on the CNN model. The CNN model performs the convolution operation in its layers. Using the CNN-based deep-learning technique, eight different classes of ECG beats are selected to be classified that are N, LBBB, RBBB, PVC, P, PVC, FPNB, and FVNB. It is observed that the CNN classification model performs well in classification. The overall classification performance obtained in terms of accuracy, sensitivity, and specificity is 99.80%, 98.08%, and 99.88% respectively. This classification technique can be used in artificial intelligence-enabled cardiac healthcare devices for the assistance of cardiologists.

REFERENCES

Afkhami, R. G., Azarnia, G., & Tinati, M. A. (2016). Cardiac arrhythmia classification using statistical and mixture modeling features of ECG signals. *Pattern Recognition Letters*, *70*, 45–51. doi:10.1016/j.patrec.2015.11.018

Ceylan, R., Özbay, Y., & Karlik, B. (2009). A novel approach for classification of ECG arrhythmias: Type-2 fuzzy clustering neural network. *Expert Systems with Applications*, *36*(3), 6721–6726. doi:10.1016/j.eswa.2008.08.028

Chen, C., Hua, Z., Zhang, R., Liu, G., & Wen, W. (2020). Automated arrhythmia classification based on a combination network of CNN and LSTM. *Biomedical Signal Processing and Control*, *57*, 101819. doi:10.1016/j.bspc.2019.101819

Elhaj, F. A., Salim, N., Harris, A. R., Swee, T. T., & Ahmed, T. (2016). Arrhythmia recognition and classification using combined linear and nonlinear features of ECG signals. *Computer Methods and Programs in Biomedicine*, *127*, 52–63. doi:10.1016/j.cmpb.2015.12.024 PMID:27000289

Güler, İ., & Übeylı˙, E. D.Güler. (2005). ECG beat classifier designed by combined neural network model. *Pattern Recognition*, *38*(2), 199–208. doi:10.1016/j.patcog.2004.06.009

Gutiérrez-Gnecchi, J. A., Morfin-Magana, R., Lorias-Espinoza, D., del Carmen Tellez-Anguiano, A., Reyes-Archundia, E., Méndez-Patiño, A., & Castañeda-Miranda, R. (2017). DSP-based arrhythmia classification using wavelet transform and probabilistic neural network. *Biomedical Signal Processing and Control*, *32*, 44–56. doi:10.1016/j.bspc.2016.10.005

Haseena, H. H., Mathew, A. T., & Paul, J. K. (2011). Fuzzy clustered probabilistic and multi layered feed forward neural networks for electrocardiogram arrhythmia classification. *Journal of Medical Systems*, *35*(2), 179–188. doi:10.100710916-009-9355-9 PMID:20703571

Jha, C. K., & Kolekar, M. H. (2018). Classification and compression of ECG signal for holter device. In *Biomedical signal and image processing in patient care* (pp. 46–63). IGI Global. doi:10.4018/978-1-5225-2829-6.ch004

Jha, C. K., & Kolekar, M. H. (2019). Arrhythmia ECG Beats Classification Using Wavelet-Based Features and Support Vector Machine Classifier. In *Advanced Classification Techniques for Healthcare Analysis* (pp. 74–88). IGI Global. doi:10.4018/978-1-5225-7796-6.ch004

Jha, C. K., & Kolekar, M. H. (2020). Cardiac arrhythmia classification using tunable Q-wavelet transform based features and support vector machine classifier. *Biomedical Signal Processing and Control*, *59*, 101875. doi:10.1016/j.bspc.2020.101875

Jha, C. K., & Kolekar, M. H. (2021). Tunable Q-wavelet based ECG data compression with validation using cardiac arrhythmia patterns. *Biomedical Signal Processing and Control*, *66*, 102464. doi:10.1016/j.bspc.2021.102464

Khalaf, A. F., Owis, M. I., & Yassine, I. A. (2015). A novel technique for cardiac arrhythmia classification using spectral correlation and support vector machines. *Expert Systems with Applications*, *42*(21), 8361–8368. doi:10.1016/j.eswa.2015.06.046

Li, H., Yuan, D., Ma, X., Cui, D., & Cao, L. (2017). Genetic algorithm for the optimization of features and neural networks in ECG signals classification. *Scientific Reports*, *7*(1), 1–12. doi:10.1038rep41011 PMID:28139677

Mao, K. Z., Tan, K.-C., & Ser, W. (2000). Probabilistic neural-network structure determination for pattern classification. *IEEE Transactions on Neural Networks*, *11*(4), 1009–1016. doi:10.1109/72.857781 PMID:18249828

Marinho, L. B., Nascimento, N. M. M., Souza, J. W. M., Gurgel, M. V., Rebouças Filho, P. P., & de Albuquerque, V. H. C. (2019). A novel electrocardiogram feature extraction approach for cardiac arrhythmia classification. *Future Generation Computer Systems*, *97*, 564–577. doi:10.1016/j.future.2019.03.025

Melgani, F., & Bazi, Y. (2008). Classification of electrocardiogram signals with support vector machines and particle swarm optimization. *IEEE Transactions on Information Technology in Biomedicine*, *12*(5), 667–677. doi:10.1109/TITB.2008.923147 PMID:18779082

Melin, P., Amezcua, J., Valdez, F., & Castillo, O. (2014). A new neural network model based on the LVQ algorithm for multi-class classification of arrhythmias. *Information Sciences*, *279*, 483–497. doi:10.1016/j.ins.2014.04.003

Moavenian, M., & Khorrami, H. (2010). A qualitative comparison of artificial neural networks and support vector machines in ECG arrhythmias classification. *Expert Systems with Applications*, *37*(4), 3088–3093. doi:10.1016/j.eswa.2009.09.021

Mondéjar-Guerra, V., Novo, J., Rouco, J., Penedo, M. G., & Ortega, M. (2019). Heartbeat classification fusing temporal and morphological information of ECGs via ensemble of classifiers. *Biomedical Signal Processing and Control*, *47*, 41–48. doi:10.1016/j.bspc.2018.08.007

Osowski, S., & Linh, T. H. (2001). ECG beat recognition using fuzzy hybrid neural network. *IEEE Transactions on Biomedical Engineering*, *48*(11), 1265–1271. doi:10.1109/10.959322 PMID:11686625

Özbay, Y., & Tezel, G. (2010). A new method for classification of ECG arrhythmias using neural network with adaptive activation function. *Digital Signal Processing*, *20*(4), 1040–1049. doi:10.1016/j.dsp.2009.10.016

Pan, J., & Tompkins, W. J. (1985). A real-time QRS detection algorithm. *IEEE Transactions on Biomedical Engineering*, *32*(3), 230–236. doi:10.1109/TBME.1985.325532 PMID:3997178

Qin, Q., Li, J., Zhang, L., Yue, Y., & Liu, C. (2017). Combining low-dimensional wavelet features and support vector machine for arrhythmia beat classification. *Scientific Reports*, *7*(1), 1–12. doi:10.103841598-017-06596-z PMID:28729684

Rahul, J., & Sharma, L. D. (2022). Automatic cardiac arrhythmia classification based on hybrid 1-D CNN and Bi-LSTM model. *Biocybernetics and Biomedical Engineering*, *42*(1), 312–324. doi:10.1016/j.bbe.2022.02.006

Rajesh, K. N., & Dhuli, R. (2018). Classification of imbalanced ECG beats using re-sampling techniques and AdaBoost ensemble classifier. *Biomedical Signal Processing and Control*, *41*, 242–254. doi:10.1016/j.bspc.2017.12.004

Sahoo, S., Kanungo, B., Behera, S., & Sabut, S. (2017). Multiresolution wavelet transform based feature extraction and ECG classification to detect cardiac abnormalities. *Measurement*, *108*, 55–66. doi:10.1016/j.measurement.2017.05.022

Specht, D. F. (1990). Probabilistic neural networks. *Neural Networks*, *3*(1), 109–118. doi:10.1016/0893-6080(90)90049-Q PMID:18282828

Vafaie, M. H., Ataei, M., & Koofigar, H. R. (2014). Heart diseases prediction based on ECG signals' classification using a genetic-fuzzy system and dynamical model of ECG signals. *Biomedical Signal Processing and Control*, *14*, 291–296. doi:10.1016/j.bspc.2014.08.010

Wang, G., Zhang, C., Liu, Y., Yang, H., Fu, D., Wang, H., & Zhang, P. (2018a). A global and updatable ECG beat classification system based on recurrent neural networks and active learning. *Information Sciences*.

Wang, G., Zhang, C., Liu, Y., Yang, H., Fu, D., Wang, H., & Zhang, P. (2018b). A global and updatable ECG beat classification system based on recurrent neural networks and active learning. *Information Sciences*.

World Health Organization. (n.d.). *Cardiovascular Diseases*. Author.

Yildirim, O., Baloglu, U. B., Tan, R.-S., Ciaccio, E. J., & Acharya, U. R. (2019). A new approach for arrhythmia classification using deep coded features and LSTM networks. *Computer Methods and Programs in Biomedicine*, *176*, 121–133. doi:10.1016/j.cmpb.2019.05.004 PMID:31200900

Yu, S.-N., & Chen, Y.-H. (2007). Electrocardiogram beat classification based on wavelet transformation and probabilistic neural network. *Pattern Recognition Letters*, *28*(10), 1142–1150. doi:10.1016/j.patrec.2007.01.017

Chapter 9
A Frequency Discrimination Technique for SSVEP-Based BCIs Using Common Feature Analysis and Support Vector Machine

Akshat Verma
National Institute of Technology, Raipur, India

Shrish Verma
National Institute of Technology, Raipur, India

Praveen Kumar Shukla
VIT Bhopal University, India

Rahul Kumar Chaurasiya
Maulana Azad National Institute of Technology, Bhopal, India

ABSTRACT

BCI is a communication option that has come up as a very radical tool for those who are suffering from neuromuscular disorders. BCI provide a way for the brain to communicate with the outer world without the use of any outlying nerves. Steady state visually evoked potentials (SSVEP) are frequency-specific responses to visual stimuli. These are extensively used with EEG signals. This research projects an innovative method for recognition of SSVEP-based BCIs. The method establishes a processing pipeline where an IIR Butterworth filter is implemented which filters the signals that are further decomposed into waveforms also known as wavelets. Along with the wavelet decomposition, common feature analysis (CFA), canonical correlation analysis (CCA), and MCCA are used to extract features. The best result is obtained from DWT-CFA. The finest classification results are obtained from the RBF kernel-based SVM classifier. The best overall mean accuracy of 94.78% is obtained using DWT-CFA as the feature extraction technique and employing RBF kernel-based SVM as the classifier.

DOI: 10.4018/978-1-6684-3947-0.ch009

INTRODUCTION

Brain-Computer Interface (BCI) is a technology that enables the brain and the world outside to communicate directly. This is a powerful technology because it directly translates the recorded neuromuscular abilities and disabilities into control signals for peripheral devices. Electroencephalogram (EEG) is an activity which is electrical in nature that are generated by the events in the brain which are logged from the scalp surface using metallic electrodes and a media which is conducting type (Sarin, Verma, Mehta, Shukla, & Verma, 2020). The most prevalent noninvasive systems are the EEG based BCIs (Nicolas-Alonso, F., & Gomez-Gil, 2012), and these BCIs depend on different types of electrophysiological sources: slow cortical potentials (SCPs), event-related de-synchronization, synchronization (ERD/ERS), event-related potentials (like P300), or Steady-State Visually Evoked Potentials (SSVEPs) (Mondini, Mangia, Talevi, & Cappello, Sinc-Windowing and Multiple Correlation Coefficients Improve SSVEP Recognition Based on Canonical Correlation Analysis, 2018). The most interesting amongst these sources are the SSVEPs because they higher accuracies even without any training by the user.

SSVEPs are periodic brain activities that are provoked at the equivalent frequencies as the flicker frequencies. The SSVEPs are strongest when the flicker frequency is around 15 Hz. Generally, SSVEP based BCIs employ different flicker frequencies at which the data is recorded. This system can be used to control a large range of peripherals. This can help in improving the lives of those who are suffering from Neuromuscular disorders or can be employed as a means of entertainment in video games. The main advantage of using SSVEP based BCI lies in the interpretation of EEG data that is recorded using BCI. The recorded data is transformed into computer instructions by recognizing the SSVEP.

Figure 1. Block diagram of a SSVEP based BCI system

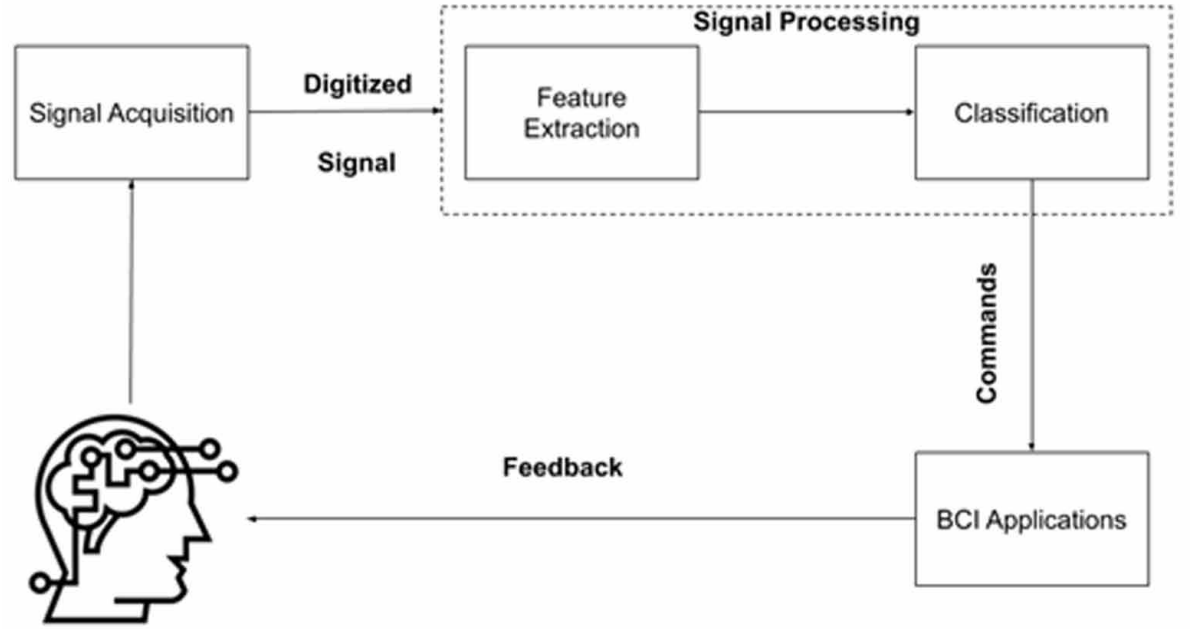

In SSVEP frequency recognition many types of methods have been applied over the years. The most common methods of SSVEP frequency recognition are the Power Spectral Density Analysis (PSDA) (Lin, Zhang, Wu, & Gao, Frequency recognition based on canonical correlation analysis for SSVEP-based BCIs, 2007). Though the methods built on PSDA are noise-sensitive if single or bipolar channels are acquired and needs comparatively longer window of time in the evaluation of the spectrum (e.g., >3s) with adequate determination of frequency (Z & D, 2008). Due to these drawbacks, the accuracy of the SSVEP recognition falls very much when the window is smaller (i.e., <3s) (Wu, et al., 2011).

Recent developments in the field of SSVEP-based BCIs have led to Canonical Correlation Analysis (CCA) that can determine and explore the hidden correlation between two types of datasets (Hotelling, 1936). This technique has been magnificently applied to the recognition of SSVEP. Exceptional accuracy for the recognition has been obtained by the CCA method that has surpassed the PSDA method (Lin, Zhang, Wu, & Gao, Frequency recognition based on canonical correlation analysis for SSVEP-based BCIs, 2007), (Bin, Gao, Yan, Hong, & Gao, 2009). This method has also proven its dominance over the PSDA method in terms of computational load, speed and accuracy (Hakvoort, Reuderink, & Obbink, 2011). This led to several types of CCA over the years. Each new method tended to increase the accuracy of SSVEP recognition but it also caused the increase in complexity of a simple algorithm. The CCA method is now one of the most commonly used method in the recognition of SSVEPs. However, when the method is applied to a shorter time window (i.e., <1s), it is expected to come across overfitting (Müller-Putz, Scherer, Christian, & Gert, 2005). This is because of the adopted reference signals which are sine-cosine waves that incorporate no features from the data that consist of training sets (Mondini, Mangia, Talevi, & Cappello, Sinc-Windowing and Multiple Correlation Coefficients Improve SSVEP Recognition Based on Canonical Correlation Analysis, 2018).

For the classification of EEG signals, there have been many researches which have established that a thoroughly described process for feature extraction can radically increment the accuracy (Li & Guan, 2008). A newer and more recent method for the analysis of SSVEPs called the Multiway Extension of CCA (MCCA) (Zhang Y., et al., 2011) has been introduced. The MCCA method draws collaborative correlation maximization in several proportions of a multiway array of data with a specified order which is the number of dimensions (Cichocki, 2009). In the case of EEG tensor data, it creates a correlation between data and sine-cosine waves that are pre-constructed to acquire more efficient reference signals. This optimization in reference signals has made MCCA to perform better than CCA in case of SSVEP recognition (Zhang Y., et al., 2011). In case of MCCA also, the model parameters were learnt by implementing pre-constructed sine-cosine reference signals. A more recent method of Common Feature Analysis (CFA) deals with this modelling of parameters. The Common Feature Analysis (CFA) is built on the certitude that EEG trials on a subject are performed and are grouped at a specific stimulus frequency, they have a natural link and share some mutual features (Zhang Y., Zhou, Jin, Wang, & Cichocki, 2015). The CFA method depends on these common features and deals with their utilization in the form of the reference signals for the recognition of SSVEP. The CFA method greatly enhanced the accuracy and speed and also reduced the computational load.

BACKGROUND

Many of the researcher worked for the SSVEP based brain computer interface system like (Li & Guan, 2008), (Cong, et al., 2012), (Zhang Y., Zhou, Jin, Wang, & Cichocki, 2014) have proven that selecting

a good processing pipeline can drastically enhance the performance of recognition from SSVEP-based BCIs and help in increasing the accuracy of the SSVEP recognition.

(Li & Guan, 2008) proposed a method for the joint feature re-extraction and classification using a semi-supervised support vector machine (SVM) where the re-extraction of features is based on the extraction of features from the previous iteration. (Mondini, Mangia, Talevi, & Cappello, Sinc-Windowing and Multiple Correlation Coefficients Improve SSVEP Recognition Based on Canonical Correlation Analysis, 2018) proposed a sinc-windowing filter in the pre-processing step along with the count of the number of canonical correlations used which resulted in an increase in the classification accuracy. (Lin, Zhang, Wu, & Gao, Frequency recognition based on canonical correlation analysis for SSVEP-based BCIs, 2007) proposed an innovative method of using Canonical Correlation Analysis for the analysis of SSVEP based BCIs which proved to be a drastic improvement over the traditional method of FFT. (Zhang Y., Zhou, Jin, Wang, & Cichocki, 2014) projected a method that used Multiset CCA (MsetCCA) for the optimization of the pre-constructed signals developed in CCA method. (Zhang Y., Zhou, Jin, Wang, & Cichocki, 2014) had proven that selecting a good processing pipeline can drastically boost the recognition process from SSVEP-based BCIs and help in increasing the accuracy of the SSVEP recognition.

Talwar's work on the Discrete Wavelet Transform discusses the use of DWT method in the extraction of features from the given EEG data. But DWT alone is not subjected to provide the best accuracy. (Lin, Zhang, Wu, & Gao, Frequency recognition based on canonical correlation analysis for SSVEP-based BCIs, 2007) work on the Canonical Correlation Analysis (CCA) is a powerful tool which results in a more accurate method for the recognition of SSVEP. Canonical Correlation Analysis is a renowned multivariate statistical method that is able to determine and explore the hidden correlation between two datasets. (Zhang Y., et al., 2011) work on the Multiway extension of Canonical Correlation Analysis (MCCA) and Common Feature Analysis (CFA) proved the dominance of MCCA and CFA over CCA. The MCCA technique draws maximized correlations that are collaborative in the multiple dimensions of data that has multiway array with a specified order equivalent to the number of dimensions (Cichocki, 2009). The CFA method depends on these common features and deals with their utilization as the reference signals for the recognition of SSVEP.

(Lotte, Congedo, Lécuyer, Lamarche, & Arnaldi, 2007) provided the EEG signal cataloging using various Machine Learning Techniques. In this research, the focus was given on a number of classification techniques which are as follows: k-Nearest Neighbors (k-NN), Neural Networks (NN), Linear Discriminant Analysis (LDA), Multilayer Perceptron (MLP), Support Vector Machine (SVM), Hidden Markov Model (HMM).

(Rashid, and Sulaiman, and Mustafa, and Khatun, & and Bari, 2019) also provided research on the classification techniques like: SVM, K-NN and LDA. Standard deviation, Average power spectral density, entropy, and spectral centroid of the EEG alpha and beta band were considered in this research. In this research, the authors have taken the above methods into consideration to establish a processing pipeline to obtain an increase in the accuracy, speed and a decrease in computational load obtained by SSVEP-based BCIs.

MAIN FOCUS OF THE CHAPTER

1. To define a pipeline for the that could easily pre-process the raw EEG SSVEP data.
2. To extract the features from this data using a wavelet decomposition method.

3. To correctly select the features and identify the best method for the selection of features.
4. To determine the classifier that is best suitable to obtain the accuracy of the extracted features.
5. To increase the detected accuracy.

In this study, the authors have proposed a processing pipeline consisting of the Butterworth bandpass Filter and the Discrete Wavelet Transform to analyze and further deduct the changes in the three types of analysis methods mentioned above. This study is performed on MAMEM SSVEP EEG Dataset 1. The dataset consists of EEG data that is recorded from eleven healthy subjects which is implemented to verify the performance of CFA, CCA and MCCA after the given processing.

SOLUTIONS AND RECOMMENDATIONS

Dataset Description

In this research, the authors have used the data which is already available as open-source. The dataset used in MAMEM (Multimedia Authoring and Management Using your Eyes and Mind) EEG SSVEP Dataset 1. This dataset consists of EEG signals from 256 channels taken from 11 subjects implementing SSVEP-based experimental protocol. The visual stimulation has been performed at five different frequencies which have been presented in isolation to each other. These frequencies are (6.66, 7.50, 8.57, 10.00 and 12.00 Hz). The data has been collected using EGI 300 Geodesic EEG System (GES 300), by means of a 256-channel HydroCel Geodesic Sensor Net (HCGSN). Signals were captured at a sampling rate of **250 Hz**. The details of the subjects in the dataset are as follows:

Table 1. General description of the subjects

Subject Id	Age	Gender	Hair type	Handedness
S001	24	Male	Regular	Right
S002	37	Male	Regular	Right
S003	39	Male	Thick	Right
S004	31	Male	Thick	Right
S005	27	Female	Thick	Left
S006	28	Female	Thick	Right
S007	26	Male	Regular	Right
S008	31	Female	Thick	Right
S009	29	Male	Short	Right
S010	37	Male	Regular	Right
S011	25	Male	Regular	Right

A major tactic in recognizing Steady State Visually Evoked Potentials (SSVEP) is the Canonical Correlation Analysis (CCA). Yet, there are two more approaches: Common Features Analysis (CFA)

and Multiway extension of Canonical Correlation Analysis (MCCA) which have achieved higher recognition accuracy than CCA in SSVEP signals. The CCA method outdoes the commonly used power spectral density investigation properties but it has certain drawbacks. In this research, many methods for the recognition of SSVEP have been compared using the EEG SSVEP Dataset 1 provided by. This dataset contains SSVEP based EEG signals having 256 channels which have been recorded for 11 different subjects. This dataset contains 5 different frequencies (6.66 Hz, 7.50 Hz, 8.57 Hz, 10.00 Hz and 12.00 Hz). The EEG signals provided from this dataset is processed using the following apparatuses: Butterworth Bandpass Filter for pre-processing, Discrete Wavelet Transform for feature extraction, which is further analyzed using Common Feature Analysis, Canonical Correlation Analysis, and a Multiway extension of Canonical Correlation Analysis.

Figure 2. Flowchart of method employed

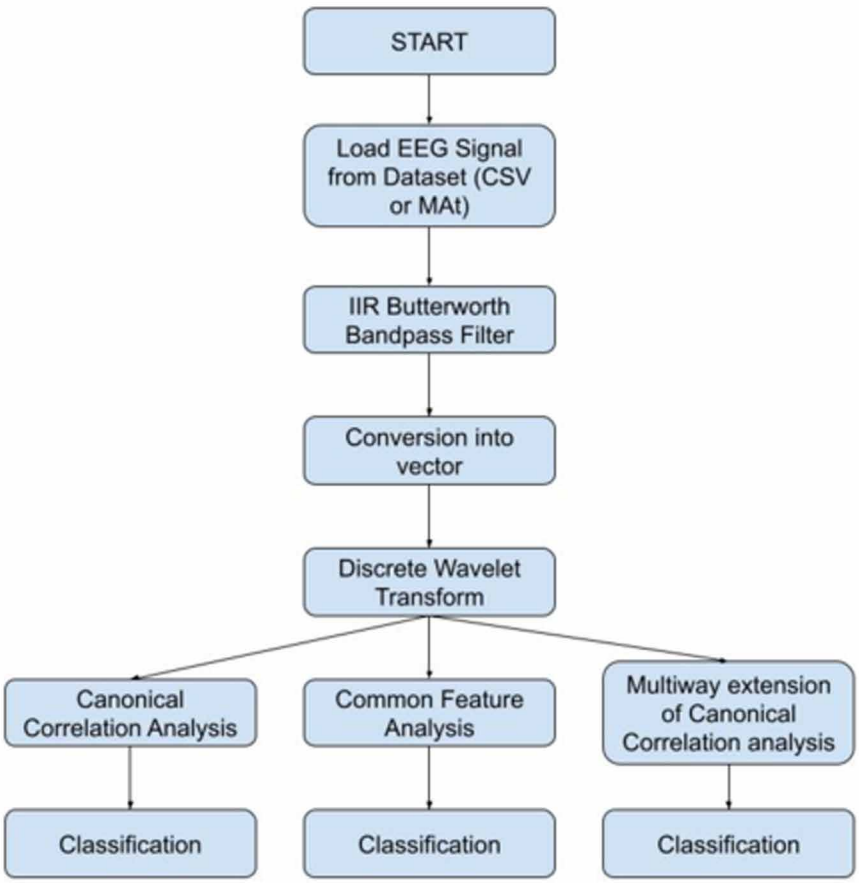

Pre-Processing

The dataset provided by MAMEM consist of 256 channels and therefore has 257 columns of signals. The last column being 0. Data has been collected from the subjects from a minimum of 3 sessions to

a maximum of 5 sessions. The dataset also contains the age, hair type, handedness, sampling rate etc. related to the experiment conducted on the subject. The initial analysis of the data helps us to visualize the following:

Figure 3. Plot of EEG signals from the 40 components

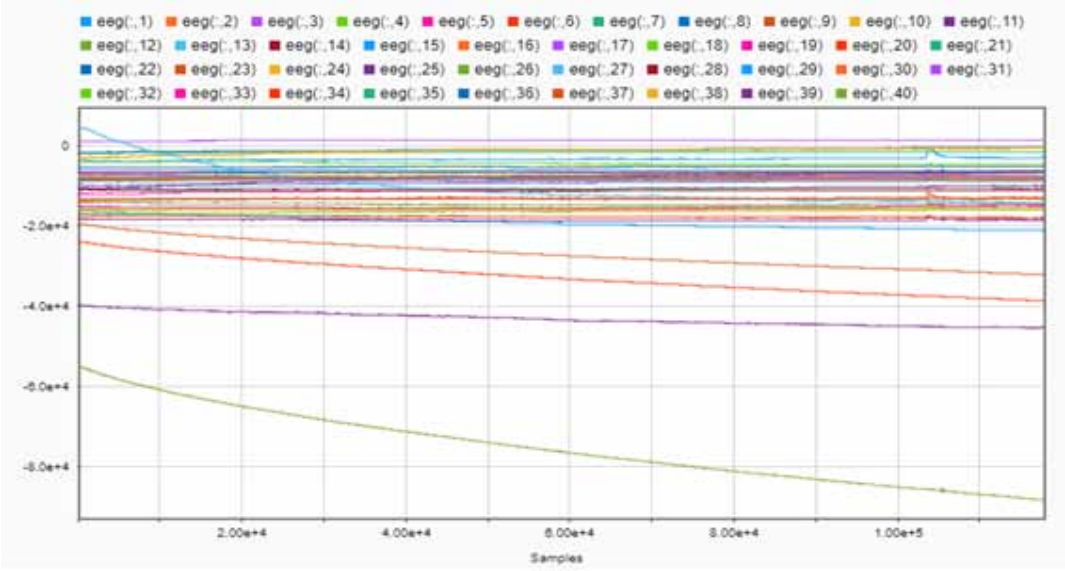

Figure 4. Plot of power spectrum vs. normalized frequency curve of EEG signals from the 40 components

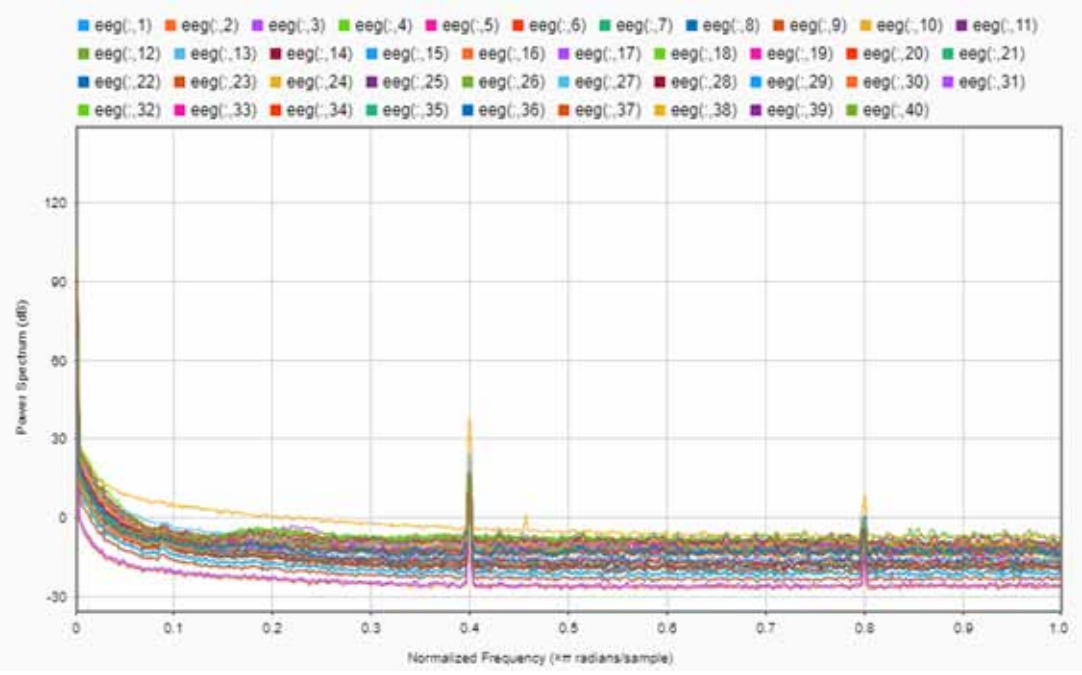

Figure 5. 256-channel sensor net plot and determination of the channels lying in the occipital (Vangelis, et al., 2016)

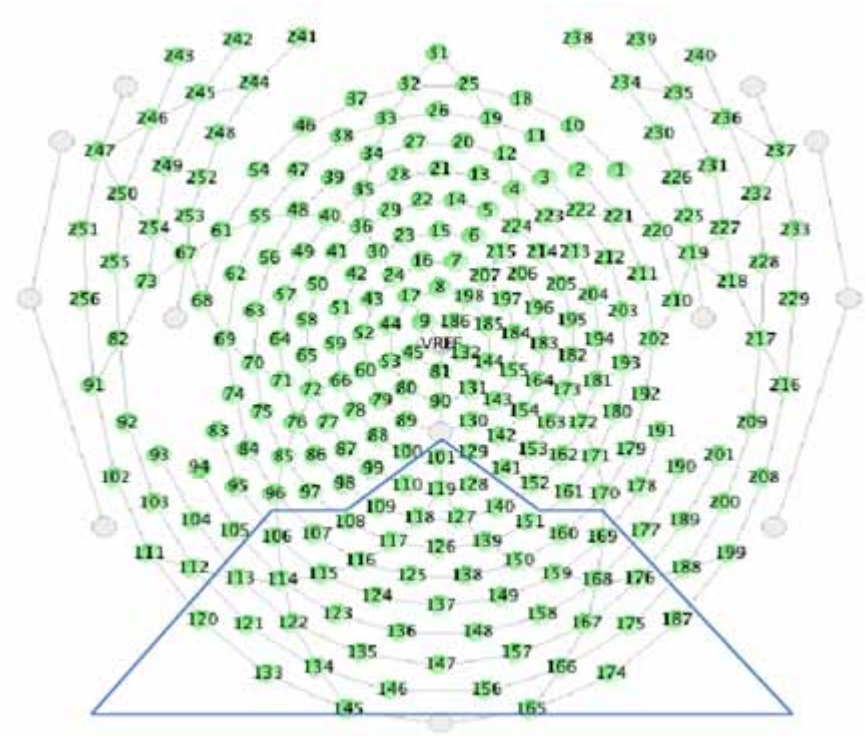

The above analysis shows us how the EEG signals behave and help us to determine the occipital area by identifying the important channels that lie there. The 40 channels have been identified which are close to the bounding boxes close as shown in the figure and explained in (Vangelis, et al., 2016).

IIR Butterworth Bandpass Filter

In this study, after properly analyzing the dataset, an IIR Butterworth Bandpass filter is implemented. The filter has been designed using the DSP System Toolbox (v. 9.8) and the analysis of the filter has been performed using the Signal Processing Toolbox (v. 8.2) of MATLAB R2019a. These toolboxes have been used for the designing of the Butterworth bandpass filter in the pre-processing stage. The Butterworth filter has been used to cutoff frequencies lower than 6 Hz and higher than 30 Hz at a sampling rate which is same as the sampling rate of the EEG dataset in consideration. The Impulse response of this filter is chosen to be IIR and the filter type as single-rate. The stopband attenuation of this filter is chosen to be 60 dB and the passband ripple to be 1. The design used in Butterworth with exact match of Stopband and the structure of Direct-form II SOS. SOS filter coefficients are scaled to reduce the chances of overflow. A filter which is designed so well that it can have the frequency response to be as flat as imaginable in the passband is known as Butterworth filter. The magnitude of this type of filter is considered to be maximally flat (Butterworth, 1930).

Figure 6. Magnitude (dB) V/s Normalized Frequency (x π rad/sample), Phase (radians) V/s Normalized Frequency (x π rad/sample) and Magnitude (dB) and Phase (radians) V/s Normalized Frequency (x π rad/sample) and Group Delay (in samples) V/s Normalized Frequency (x π rad/sample) and Phase Delay (in samples) V/s Normalized Frequency (x π rad/sample) and the Impulse Response, Step Response and Pole Zero Plot of the Filter

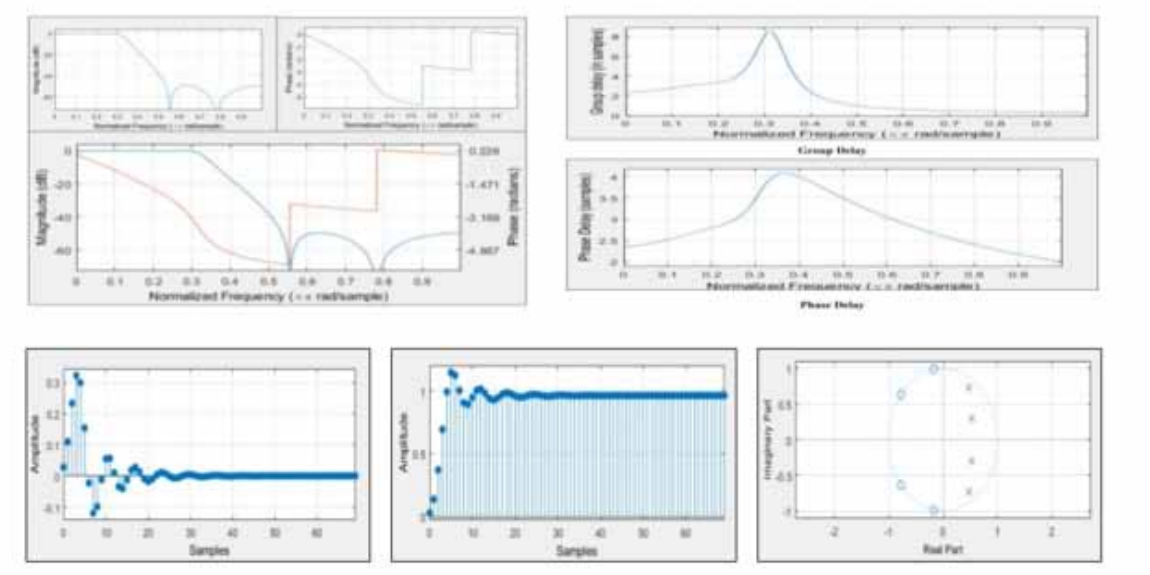

The application of Butterworth Filter on the 11 subjects helps in obtaining the analysis of the signals before and after the application of the filter which is very useful when the decomposition into wavelets is performed.

Figure 7. Amplitude V/s Time (mins) Butterworth plot of the signals from subject 7 (various colors representing various channels after the application of Butterworth Filter, and violet color representing the overall signal after the filter application), subject 3 (green color representing the overall signal after the filter application), and subject 1 (blue color representing the overall signal after the filter application)

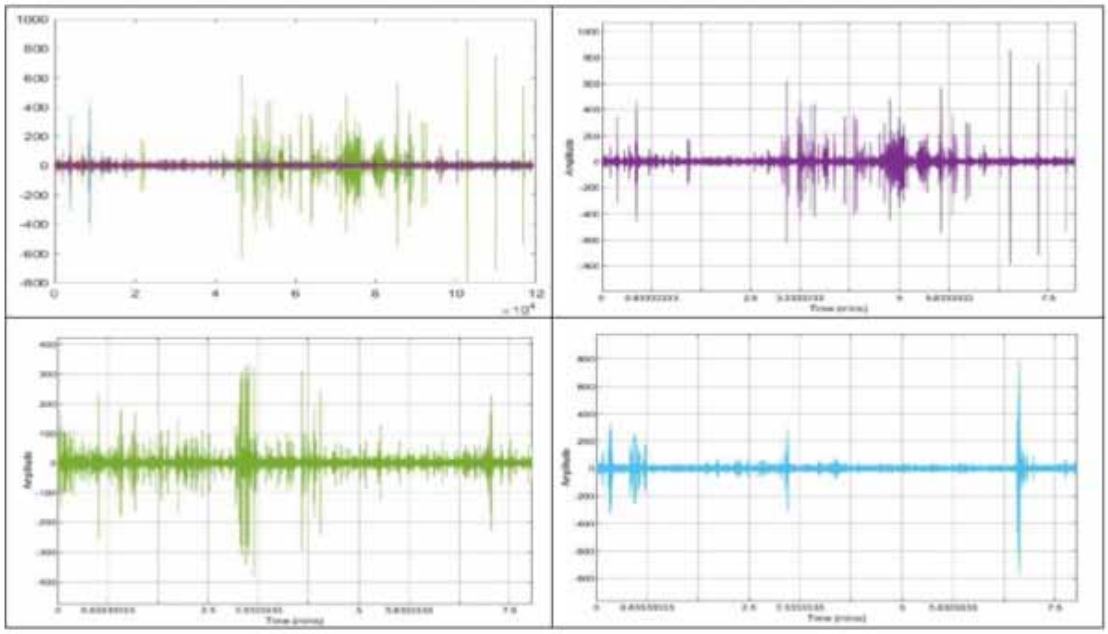

Discrete Wavelet Transform

The data processed through this filter is further passed through a discrete wavelet transform. The discrete wavelet transforms or the DWT decomposes the given input signal into a set of rudimentary waveforms which are known as "wavelets" it also delivers a route of investigating the coefficients (weights) of these wavelets. The wavelet transform method is a reasonably suitable method in examining of the non-stationary signals (Talwar & Matharu, 2016). The wavelet functions used for the designing of the wavelet transform are the Daubechies wavelets, which are a collection of orthogonal wavelets that define the discrete wavelet transform and that are identified by vanishing moments. This class of wavelets involve of a scaling function known as the father wavelet that produces the orthogonal multiresolution analysis. The Daubechies wavelets are selected such that they contain *A* number of vanishing moments where *A* is determined by the width *2A-1*. The naming scheme which is commonly used is the *dbA* naming scheme. Therefore, a *db2* wavelet function means two vanishing moments. This also suggests that the total number of taps or the length used is 4 (Daubechies, 1992).

Figure 8. Scaling and wavelet functions of the db2 or the D4 wavelets and their spectrums [24]

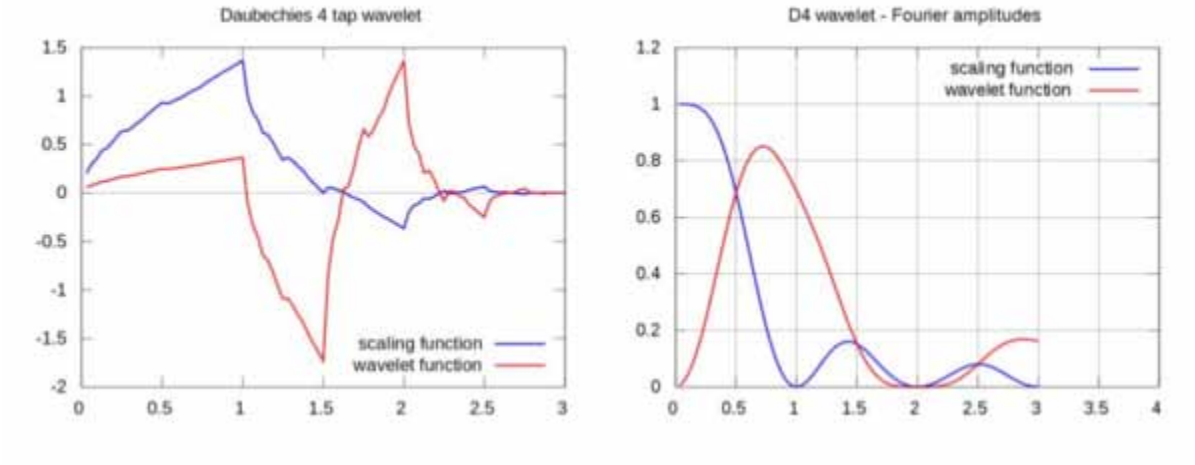

After setting the above parameters, the multilevel 1-D wavelet decomposition is performed. The decomposition is performed using the wavedec function which takes a signal vector as the input at a specified level. The outputs from the decomposition are the decomposition vector C and the bookkeeping vector L. A level of 5 is selected for the wavelet decomposition.

Figure 9. Five Level Wavelet Decomposition

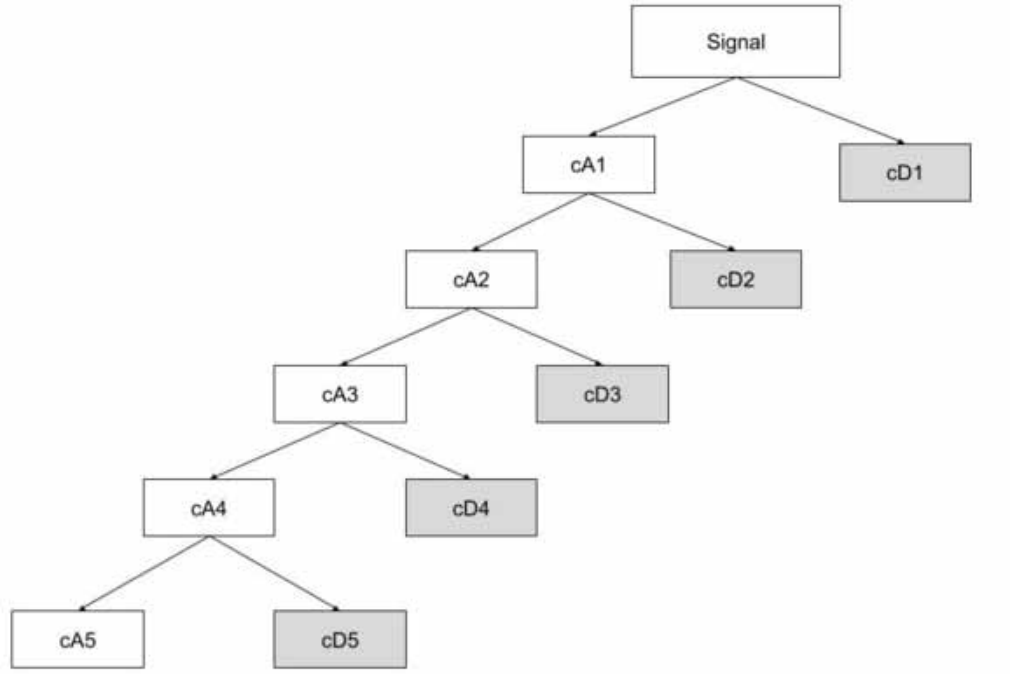

Figure 10. The bookkeeping vector L and the decomposition vector C

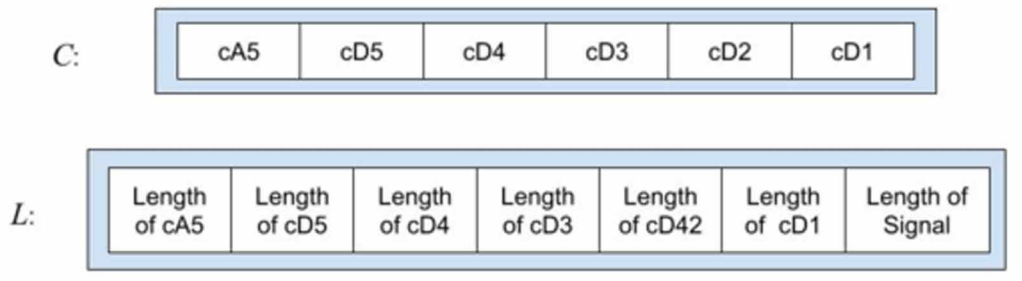

This decomposition helps in obtaining the approximation coefficients and the detail coefficients. The reconstruction of the coefficients of a one-dimensional signal is performed thereafter based on the assembly of decomposition. The below analysis of detail coefficients, approximation coefficients, reconstruction coefficients is performed with respect to subject 05.

Figure 11. Plot of the decomposition vector C and bookkeeping vector L

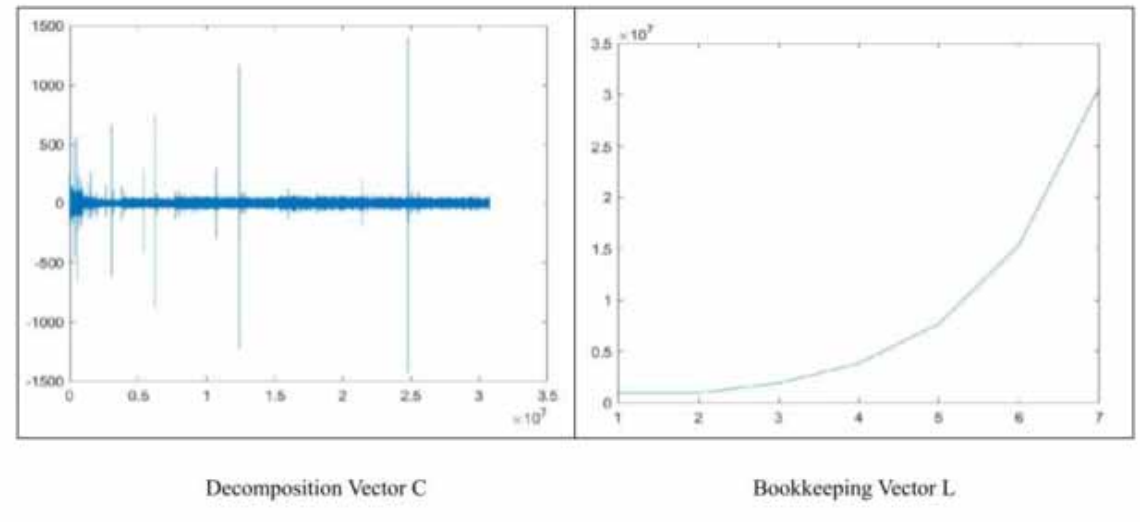

Figure 12. Plot of detail coefficient of alpha sub band or 3rd wavelet (D3) and plot of detail and approximation coefficients of Delta sub band or 5th wavelet (D5 and A5)

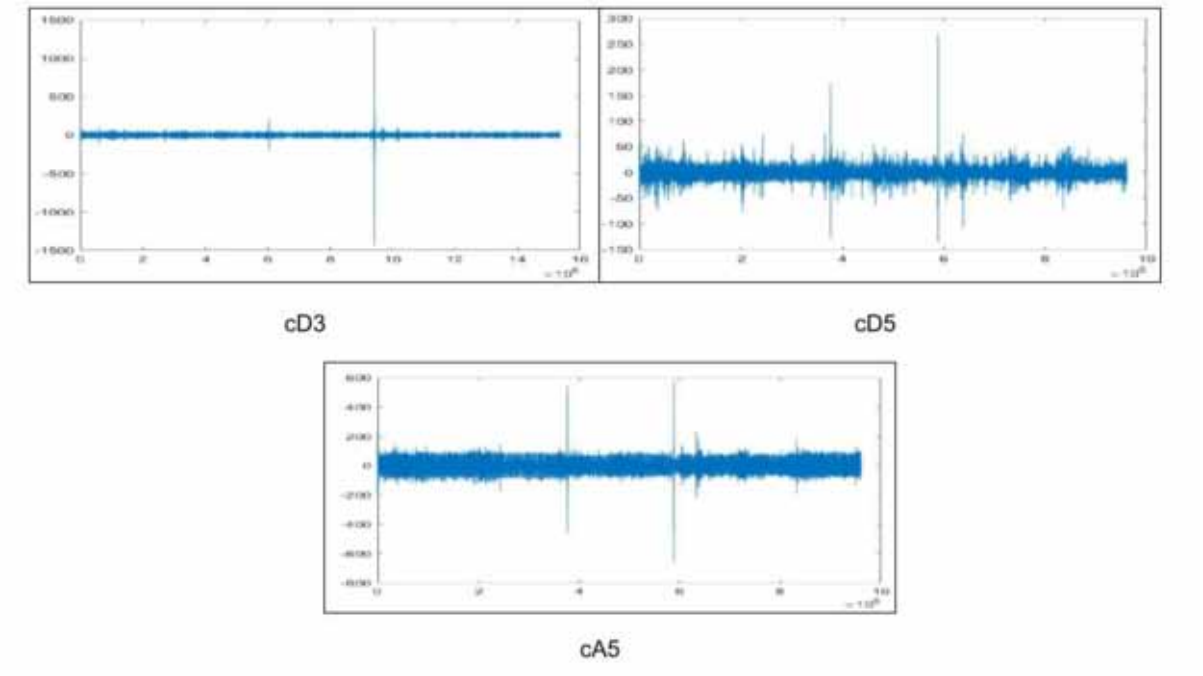

Canonical Correlation Analysis (CCA)

Canonical Correlation Analysis stands as a multivariable statistical method, implemented to determine unknown correlation belonging to the 2 sets of data. CCA determines a pair of linear combinations such that results in the maximization of correlation between the two variables. Consider two sets of multidimensional variables, X and Y such that X = (x_1,x_2,…,x_n) and Y = (y_1,y_2,…,y_n). CCA determines the direction or the weight vectors w_x and w_y such that after projecting X on w_x and Y on w_y, two new samples (X_{w_x} and Y_{w_y}) with newer coordinates are found and display maximum correlation ρ. The equation is as explained in (Kalunga, Djouani, Hamam, Chevallier, & Monacelli, 2013):

$$\rho = \max_{w_x, w_y} corr\left(Xw_x, Yw_y\right)$$
$$= \max_{w_x, w_y} \frac{\left(Xw_x, Yw_y\right)}{\left\|Xw_x\right\|\left\|Yw_y\right\|}$$

$$\rho = \max_{w_x, w_y} \frac{w_x^{'} C_{xy} w_y}{\sqrt{w_x^{'} C_{xx} w_x w_y^{'} C_{yy} w_y}}$$

Where C_{xx} and C_{yy} are the within-sets covariance matrix and C_{xy} is the between-sets covariance matrix. The solution of equation (1) has similar effect as that of maximizing the numerator to 1, i.e,

$$w_x^{'} C_{xx} w_x = 1 \text{ and } w_y^{'} C_{yy} w_y = 1.$$

CCA is a powerful technique and its application to SSVEP helps in determining the supreme correlation between the EEG samples logged from the Y channels which are passed through the Discrete wavelet transform to obtain various sub-bands and their reconstruction coefficients. These reconstruction coefficients that contains the vector of the signals. So effectively, the CCA determines the maximum correlation between the reconstruction coefficients R and the reference signals Z. The reference signals are nothing but the pre-constructed sine-cosine signals which are generated as in [27]:

$$Y = \begin{bmatrix} sin\left(2\Delta \text{ x1 x f}\right) \\ \cos\left(2\Delta \text{ x1 x f}\right) \\ sin\left(2\Delta \text{x2 x f}\right) \\ cos\left(2\Delta \text{ x2 x f}\right) \\ \vdots \\ sin\left(2\Delta \text{ x n x f}\right) \\ cos\left(2\Delta \text{ x n x f}\right) \end{bmatrix}$$

Where n represents the number of harmonics considered and f is the fundamental frequency according to the flash stimuli (Kalunga, Djouani, Hamam, Chevallier, & Monacelli, 2013). When the 5 level DWT analysis is performed, the reference signals to be used are limited to the third harmonic only (i.e., *m3*). CCA is the most common method that is currently adopted for the recognition of SSVEP based BCIs (Lin, Zhang, Wu, & Gao, Frequency recognition based on canonical correlation analysis for SSVEP-based BCIs, 2007). The execution of CCA is comparatively better than the performance obtained using PSDA. This is because CCA enhances Signal to Noise Ratio using multi-channel optimization (Bin, Gao, Yan, Hong, & Gao, 2009).

Multiway Extension of Canonical Correlation Analysis (MCCA)

A multiway array of data is called a tensor and the quantity of dimensions which are also called as ways or models are the order of this tensor (Zhang Y., et al., 2011). The order plays a vital part in the tensor. The change in order can lead to the change in the dimension of how the data is interpreted. The order basically represents the dimensions of the tensor. A tensor of order N is denoted by $X = \left(X\right)_{t_1 t_2 \ldots t_n} \epsilon \ \mathbb{R}^{I_1 x I_2 x \ldots x I_N}$ (Zhang Y., et al., 2011). The n-mode product of the tensor with the vector $\mathbf{y} \epsilon \ \mathbb{R}^{I_N x 1}$ is:

$$\left(X\mathbf{y}^{\mathrm{T}}\right)_{t_1 \ldots t_{n-1} t_{n+1} \ldots t_N} = \sum_{t_n=1}^{I_n} x_{t_1 t_2 \ldots t_N} w_{t_n}$$

Where (Xy^T) denotes the nth way projection of the tensor with a vector.

The practice of using the reference signals on the basis of pre-constructed sine-cosine functions in CCA method may not always produce optimum results and may outcome in a decrement of the overall correctness because of the absence of features from the data that is used for training. This may be overcome by application of a Multiway extension of the traditional Canonical Correlation Analysis which optimizes the reference signal used. This maximization is performed using collaboratively maximizing the multiple dimensions between the pre-constructed signals used for reference and the tensor data consisting of EEG (Zhang Y., Zhou, Jin, Wang, & Cichocki, 2015).

$$\left(X\mathrm{x}_1\mathbf{y}^{\mathrm{T}}\right)_{t_2,t_3} = \sum_{t_1=1}^{s} x_{t_1,t_2,t_3} w_{t_1} for\, k = 1$$

$$\left(X\mathrm{x}_3\mathbf{y}^{\mathrm{T}}\right)_{t_1,t_2} = \sum_{t_3=1}^{N} x_{t_1,t_2,t_3} w_{t_3} for\, k = 3$$

The maximization is done as mentioned in (Zhang Y., et al., 2011) which is given by:

$$\underset{w_1, w_3, v}{max} \frac{E\left[\overline{\boldsymbol{xy}}^{\boldsymbol{T}}\right]}{\sqrt{E\left[\overline{\boldsymbol{xx}}^{\boldsymbol{T}}\right] E\left[\overline{\boldsymbol{yy}}^{\boldsymbol{T}}\right]}}$$

where $\overline{\boldsymbol{x}} = X\mathrm{x}_3 w_1^{\mathrm{T}}$, $\overline{y} = v^T$ and $v \epsilon\, \mathbb{R}^{2H}$.

This results in the determination of maximal correlation which helps in the determination of classification scores for the recognition of SSVEP.

Common Feature Analysis (CFA)

The common problem that is encountered in both CCA and MCCA is that the reference signals that are used for the analysis are learnt by still going back to the sine-cosine waves that are pre-constructed. This leads to the elimination of the possibility of completely using the training data. In (Zhang Y., Zhou, Jin, Wang, & Cichocki, 2015) a new technique is introduced which learns the reference signals based on the consideration that the trials on the same subject at a certain stimulus frequency should be connected and share some features that are common. This method first splits the given data matrix to a certain number of group of matrices. A certain stimulus frequency is used to extract common features by this method from the group of matrices. Let $\boldsymbol{X}_n$ (n= 1, 2, …, N) denote a multiple group of data matrices that is obtained by splitting the original data matrix $\boldsymbol{X}$. Consider a set of latent variables $\boldsymbol{Y}_k$ (sources) from $\boldsymbol{X}_n$ and $\boldsymbol{Z}_k$(loading). Then,

$$\boldsymbol{Y}_n = \left[\overline{Y} \quad \overline{Y}_n\right], \;\; n = 1, 2, \ldots, N$$

Where $\bar{Y}$ consists of the shared common features and $\bar{Y}_n$ consists the individual information in Y_n. The matrix factorization therefore is:

$$\boldsymbol{X_n} = \begin{bmatrix} \bar{Y} & \breve{Y}_n \end{bmatrix} \begin{bmatrix} \bar{Z}_n^T \\ \breve{Z}_n^T \end{bmatrix} = \bar{Y}\bar{Z}_n^T + \breve{Y}_n\breve{Z}_n^T, n = 1, 2, \ldots, N$$

Therefore, the extraction of common features can be performed using simultaneous matrix factorization mentioned below.

$$\min_{\boldsymbol{Y}} \sum_{n=1}^{N} \left\| \boldsymbol{X_n} - \left(\bar{\boldsymbol{Y}}\bar{\boldsymbol{Z}}_{\boldsymbol{n}}^{\boldsymbol{T}} + \breve{Y}_{\boldsymbol{n}}\breve{Z}_{\boldsymbol{n}}^{\boldsymbol{T}} \right) \right\|_F^2$$

Figure 13. Plot of the preconstructed sine-cosine reference signals and a final representation of all the pre-constructed signals on the same plot

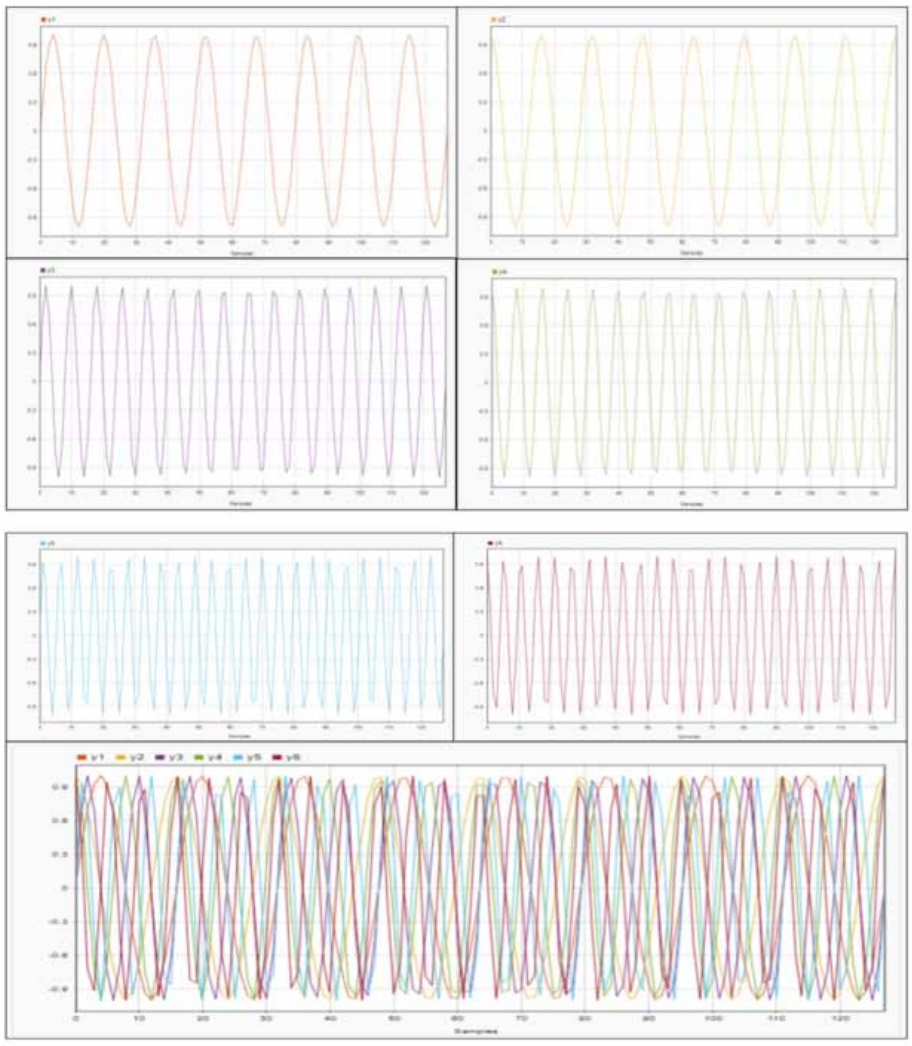

CLASSIFICATION

Linear Discriminant Analysis (LDA)

The application of LDA results in finding the combinations that are linear and are of the feature vectors which are used to evaluate the characteristics belonging to a particular signal. The objective of LDA is to separate two or more class of objects that represent various classes. This is achieved by the use of hyperplanes. An isolated hyperplane is assimilated such that the forecast of the distance between the classes' means is maximized. The main advantage of this practice is that it has very small computational needs and it is user friendly (Rashid, and Sulaiman, and Mustafa, and Khatun, & and Bari, 2019). However, LDA also considers the margin b/w the classes. This means that the covariance matrix of the two classes is assumed to be equal and of full rank (Vangelis, et al., 2016).

Support Vector Machine (SVM)

SVMs are undoubtedly the most popular classification algorithms. The aim of SVM and LDA is somewhat similar as both of these algorithms try to determine a hyper-plane. The difference lies in the fact that in SVM, these hyper-planes are the ones that maximize the distance between the between the training points (Rashid, and Sulaiman, and Mustafa, and Khatun, & and Bari, 2019). This hyper-plane which is optimal is embodied by a bias parameter and vector. Both of these are learnt during the training phase. SVM is one of the most powerful and popular classifiers. However, the problem occurs when the assumption of linearity in training data is taken into account. In case of real-world data like that of EEG signal taken from BCIs is considered. Here, the definition of linearly separable is not applicable and therefore the trick of using kernels was introduced. The kernel that has shown the most promising results in case of EEG based BCIs is a Function which is also Gaussian or Radial Basis and known as RBF kernel (Jian & Tang, 2014). This was achieved by the projection of data that is fed as the input to a dimensional space with a greater number of dimensions using a kernel function.

K-Nearest Neighbors (K-NN)

This method focuses on appointing a hidden point from the main class in the k-nearest neighbors from the training set. When models consisting of the Brain Computer Interfaces are considered, a metric distance is considered in order to obtain these neighbors (Rashid, and Sulaiman, and Mustafa, and Khatun, & and Bari, 2019). If the value of k is taken to be adequately high and plenty training samples are provided, K-NN can be used to create nonlinear decision boundaries for any function. The KNN has the meekest and the simplest approach in the classification category.

RESULTS AND DISCUSSIONS

Application of IIR Butterworth filter and Discrete Wavelet Transform greatly affects the overall result of the performance of the three types of recognition of SSVEP analysis methods. The performance of these three methods is classified over the SVM, LDA and K-NN classification methods. For the SVM method, RBF kernel has been used which has been performed using the LIBSVM whereas for the other

two classification methods, the authors have used the Statistics and Machine Learning Toolbox (v. 11.5) of MATLAB R2019a. The mean of the classification accuracy from the 11 subjects with the different number of runs belonging to a particular subject are as mentioned below.

Table 2. Table of mean classification accuracies in %

Classification	CCA	MCCA	CFA
SVM	88.62	91.43	94.78
LDA	87.57	89.74	90.81
K-NN	85.13	87.91	88.30

The best performance is observed from the feature selection using Common Feature Analysis and the classifier SVM. The table also helps us to observe various sections for improvement in other methods. This also helps us conclude that the selection of pre-processing method greatly affects the final output in case of SSVEP-based BCIs. It is observed that the performance of CCA+LDA is very close to the performance of MCCA+K-NN and differs by nearly 0.34%. Similarly, the performance of MCCA+SVM and CFA+LDA are very close and differ by nearly 0.38%.

The CFA method uses the latent common features as the reference signals which are observed assumed to be present if a data matrix is split into a group of matrices (Zhang Y., Zhou, Jin, Wang, & Cichocki, 2015). The CCA method used the pre-constructed sine-cosine signals for this purpose (Lin, Zhang, Wu, & Gao, Frequency recognition based on canonical correlation analysis for SSVEP-based BCIs, 2007). The MCCA method refined these pre-constructed but still depended on using pre-constructed reference signals (Zhang Y., et al., 2011). The DWT method implemented for the extraction of features helped in the conversion of the vector signals to discrete wavelets which were then passed through the above-mentioned feature selection methods. The SVM classifier implemented with RBF kernel outperformed other methods of classification in all the three types of classification methods in the respective category of the feature selection methods. When the three feature selection methods are compared, it is observed that the CFA method surpassed the MCCA and CCA methods. The combination of CFA as a feature selection method and the RBF kernel based SVM is therefore outperformed the other methods mentioned above which can also be seen from TABLE 2.

CONCLUSION

This study presents a pipeline for the recognition of SSVEP based BCIs where the best process implemented was concluded to be the DWT based CFA that gave an accuracy of 94.78% when RBF kernel based SVM was used. EEG data used for this study is open-source and has been readily provided by MAMEM. The dataset used for this study is the EEG SSVEP Dataset 1. The dataset has been pre-processed by implementing an IIR Butterworth Bandpass Filter. This data is then passed through a five-level discrete wavelet transform where the extraction of features into wavelets is performed. These wavelets are then subjected to three types of classification techniques, viz, CCA, MCCA and CFA. The best performance is obtained from the CFA method of feature selection which is then classified using three types of clas-

sifiers. The best result is obtained using the RBF kernel SVM classifiers. The BCI technology is a relatively newer technology. In the previous 15-20 years, there have been many developments in the field of interaction between the brain and computer. This is because of the BCI and owing to the easiness with which this technology can be used. The BCI technology also has very important applications in the of persons suffering from neuromuscular disorders and it focuses on helping these people to improve their quality of life. The method suggested in this research can be used to help these people and can also be implemented in the home automation systems. The only catch in this application is that it may not be suitable for the patients with impaired eyesight as this method focuses on the subject's ability to focus their eye gaze at a particular target. This research can further be extended to a home automation system where embedded systems and/or other systems can also be implemented alongside SSVEP signals and a real-time SSVEP based BCI can be obtained.

REFERENCES

Bin, G., Gao, X., Yan, Z., Hong, B., & Gao, S. (2009). An online multi-channel SSVEP-based brain-computer interface using a canonical correlation analysis method. *Journal of Neural Engineering*, *6*(4), 046002. doi:10.1088/1741-2560/6/4/046002 PMID:19494422

Butterworth, S. (1930). On the Theory of Filter Amplifiers. *Experimental Wireless and the Wireless Engineer*, *7*, 536–541.

Cichocki, A. Z. (2009). Nonnegative Matrix and Tensor Factorizations - Applications to Exploratory Multi-way Data Analysis and Blind Source Separation. *IEEE Signal Processing Magazine*, 142–145.

Cong, F., Phan, A. H., Zhao, Q., Huttunen-Scott, T., Kaartinen, J., Ristaniemi, T., Lyytinen, H., & Cichocki, A. (2012). Benefits of multi-domain feature of mismatch negativity extracted by non-negative tensor factorization from EEG collected by low-density array. *International Journal of Neural Systems*, *22*(06), 1250025. doi:10.1142/S0129065712500256 PMID:23186274

Daubechies, I. (1992). *Ten Lectures on Wavelets.* Academic Press.

Hakvoort, G., Reuderink, B., & Obbink, M. (2011). *Comparison of PSDA and CCA detection methods in a SSVEP-based BCI-system.* Centre for Telematics and Information Technology (CTIT).

Hotelling, H. (1936). Relations Between Two Sets of Variates. *Biometrika*, *28*(3-4), 321–377. doi:10.1093/biomet/28.3-4.321

Jian, H., & Tang, K.-T. (2014). Improving classification accuracy of SSVEP based BCI using RBF SVM with signal quality evaluation. *2014 International Symposium on Intelligent Signal Processing and Communication Systems (ISPACS)*, 302-306. 10.1109/ISPACS.2014.7024473

Kalunga, E., Djouani, K., Hamam, Y., Chevallier, S., & Monacelli, E. (2013). *SSVEP enhancement based on Canonical Correlation Analysis to improve BCI performances. In IEEE AFRICON*. IEEE.

Li, Y., & Guan, C. (2008). Joint feature re-extraction and classification using an iterative semi-supervised support vector machine algorithm. *Machine Learning*, *71*(1), 33–53. doi:10.100710994-007-5039-1

Lin, Z., Zhang, C., Wu, W., & Gao, X. (2007). Frequency recognition based on canonical correlation analysis for SSVEP-based BCIs. *IEEE Transactions on Biomedical Engineering*, *54*(6), 1172–1176. doi:10.1109/TBME.2006.889197 PMID:17549911

Lotte, F., Congedo, M., Lécuyer, A., Lamarche, F., & Arnaldi, B. (2007). A review of classification algorithms for EEG-based brain-computer interfaces. *Journal of Neural Engineering*, *4*(2), R1–R13. doi:10.1088/1741-2560/4/2/R01 PMID:17409472

Mondini, V., Mangia, A., Talevi, L., & Cappello, A. (2018). Sinc-Windowing and Multiple Correlation Coefficients Improve SSVEP Recognition Based on Canonical Correlation Analysis. *Computational Intelligence and Neuroscience*, *2018*, 1–11. doi:10.1155/2018/4278782 PMID:29849546

Müller-Putz, R. G., Scherer, R., Christian, B., & Gert, P. (2005). Steady-state visual evoked potential (SSVEP)-based communication: Impact of harmonic frequency components. *Journal of Neural Engineering*, *2*(4), 123–130. doi:10.1088/1741-2560/2/4/008 PMID:16317236

Nicolas-Alonso, F. L., & Gomez-Gil, J. (2012). Brain computer interfaces, a review. *Sensors (Basel)*, *12*(2), 1211–1279. doi:10.3390120201211 PMID:22438708

Rashid, M., Sulaiman, N., Mustafa, M., Khatun, S., & Bari, B. S. (2019). The Classification of EEG Signal Using Different Machine Learning Techniques for BCI Application. *Robot Intelligence Technology and Applications*, 207-221.

Sarin, M., Verma, A., Mehta, D. H., Shukla, P. K., & Verma, S. (2020). Automated Ocular Artifacts Identification and Removal from EEG Data Using Hybrid Machine Learning Methods. In *7th International Conference on Signal Processing and Integrated Networks (SPIN)* (pp. 1054-1059). Noida: IEEE. 10.1109/SPIN48934.2020.9071360

Talwar, T. S., & Matharu, S. S. (2016). Classification of SSVEP Based Brain Signals using Discrete Wavelet Transform. *International Journal for Research in Applied Science and Engineering Technology*, 421–426.

Vangelis, P. O., Georgios, L., Kostantinos, G., Elisavet, C., Katerina, A., Spiros, N., & Ioannis, K. (2016). Comparative evaluation of state-of-the-art algorithms for SSVEP-based BCIs. *Clinical Orthopaedics and Related Research*.

Wu, C. H., Chang, H. C., Lee, P. L., Li, K. S., Sie, J. J., Sun, C. W., Yang, C.-Y., Li, P.-H., Deng, H.-T., & Shyu, K. K. (2011). Frequency recognition in an SSVEP-based brain computer interface using empirical mode decomposition and refined generalized zero-crossing. *Journal of Neuroscience Methods*, *196*(1), 170–181. doi:10.1016/j.jneumeth.2010.12.014 PMID:21194547

Z, W., & D, Y. (2008). Frequency detection with stability coefficient for steady-state visual evoked potential (SSVEP)-based BCIs. *J Neural Eng*, 36-43.

Zhang, Y., Zhou, G., Jin, J., Wang, X., & Cichocki, A. (2014). Frequency recognition in SSVEP-based BCI using multiset canonical correlation analysis. *International Journal of Neural Systems*, *24*(04), 1450013. doi:10.1142/S0129065714500130 PMID:24694168

Zhang, Y., Zhou, G., Jin, J., Wang, X., & Cichocki, A. (2015). SSVEP recognition using common feature analysis in brain-computer interface. *Journal of Neuroscience Methods*, *244*, 8–15. doi:10.1016/j.jneumeth.2014.03.012 PMID:24727656

Zhang, Y., Zhou, G., Zhao, Q., Onishi, A., Jin, J., Wang, X., & Cichocki, A. (2011). Multiway Canonical Correlation Analysis for Frequency Components Recognition in SSVEP-Based BCIs. *Neural Information Processing*, 287-295.

Chapter 10
A Robust Classification Approach for Character Detection Using P300-Based Brain-Computer Interface

Deepthi Hitesh Mehta
National Institute of Technology, Raipur, India

Shrish Verma
National Institute of Technology, Raipur, India

Mohit Sarin
National Institute of Technology, Raipur, India

Rahul Kumar Chaurasiya
Maulana Azad National Institute of Technology, Bhopal, India

Praveen Kumar Shukla
VIT Bhopal University, India

ABSTRACT

Researchers have been contributing to the brain-computer interface (BCI), which acts as a direct connection between the human brain and the computer that uses the P300 speller paradigm to decode the response of the brain by stimulating a subject, involving no muscular movements. This research uses BCI Competition III Dataset II, which uses a 6x6 character matrix paradigm for data collection purposes for two healthy subjects. The ensembles of support vector machine (SVM) method of classification has been proposed to surpass the problem of false detection, which is preceded by empirical mode decomposition (EMD) as the preprocessing technique and the use of a stacked autoencoder for feature extraction and covariate shift adaptation by normalized principal components as the feature selection method for better accuracy of the detected character. The experiment yields a better result than many existing methods; it produces an average accuracy of 98.75%.

DOI: 10.4018/978-1-6684-3947-0.ch010

INTRODUCTION

Brain-Computer Interface (BCI) is direct communication between the human brain and the computer machine. BCI involves the decoding of brain responses without any involvement of muscular motions. BCI is a proven excellent mode of communication for people with neurological disorders who cannot communicate their emotions and feelings through handwriting, speaking, or typing (R.K. Chaurasiya et al., 2016). One of the primarily used techniques among all the BCI techniques is Electroencephalographic(EEG) because of its non-invasive recording technique and cost-benefit ratio. The communication in EEG is based on an event-related potential (ERP)which is generated, recorded, and analyzed, resulting in the event that visually stimulates a subject. An elicited component that is the response to ERP is the P300 signal. P300 ERP is a natural endogenous response that varies with stimulation type, subject matter, and expectations, but it is independent of stimulation's physical characteristics. P300 speller consists of the following technical aspects-recording of EEG signals, preprocessing, feature extraction, and classification (Akcakaya M et al., 2014).

P300 potential is observed when rare, and expected events occur at the central locations of EEG measurement. P300 is the user's brain signature which typically happens around 300 ms after the unusual occurrence (Wolpaw JR et al., 2002). A 6x6 matrix of characters is shown in the P300 speller. The job of the user is to focus his attention on the characteristics of a predefined sentence, one character at a time. But due to the proposed paradigm, the user faces problems with crowding, exhaustion, and thus resulting in false detection. So, to surpass this problem, the Ensembled Support Vector Machine (ESVM) method of classification has been proposed in this research which is preceded by Empirical Mode Decomposition (EMD) as the preprocessing technique and use of a stacked autoencoder and have applied Covariate Shift Adaptation by normalized principal components as an optimization technique for selection of extracted features for better accuracy after classification.

LITERATURE REVIEW

This research uses BCI Competition III Dataset II, which consists of P300 signals, and for the feature extraction, the research makes use of an autoencoder. Any autoencoder takes input in the form of images, so there is a need to convert the P300 signals into an image. In their paper (Azad et al., 2019), has converted the 1D signals/ vibrational signals to 2-D signals using Empirical Mode Decomposition (EMD) and utilizing the energy esteems. The main reasons for the use of EMD for the conversion are because of its adaptive nature and since it allows the projection of a non-stationary signal onto a time-frequency plane using mono-component signals.

There are many ways to extract features; this research uses an autoencoder for feature extraction as the autoencoder is capable of removing redundant information. It doesn't require labeled information of the data to create a model for feature extraction (Md Shopon et al., 2016). There are many autoencoders available for feature extraction. In their research (S. Kundu et al., 2019), have used sparse and stacked sparse autoencoder for feature extraction, which yielded good results but took more time for training and had less consistency. (Minmin Chen, 2014) proposed a Marginalized Denoising autoencoder that learns the mapping from input to the output but doesn't learn representation. This autoencoder can only modify the domain but cannot be used for representational learning and related problems. Stacked Autoendocer has recently evolved to provide a version of the raw data with very comprehensive and promising fea-

tures to train a classifier in a particular context and find more consistency than raw information training (Venkata Krishna Jonnalagadda, 2018).

To increase the accuracy, this research uses Principal Component Analysis (PCA) along with Covariate Shift Adaption (CSA). PCA is used for extracting the principal components (Jolliffe, I. T et al., 2016). (Spüler, M et al., 2012) paper has made use of the mentioned technique and has described that the technique extracts principle components using PCA and CSA is used to normalize extracted components to the effect of non-stationarity by displacing the window over the results. There are various covariate shift adaption methods. A. Satti in (A. Satti et al., 2010) proposed a covariate shift adaption method that uses a polynomial function to adapt the data accordingly resulting from the estimation of the covariate shift of the subsequent trial, for that it uses a polynomial of order 3.

(Chaurasiya et al., 2015) have proposed an efficient P300 speller. They have performed their experiments on the Devnagiri script. The design and architecture of the speller are much similar to that of BCI Competition III Dataset II. Classification of P300 signals was performed using Ensembles of SVM in this research. They were successful in minimizing problems related to multi-trial. Taking it one step further, (G. B. Kshirsagar et al., 2020) proposed a Single-trial Character Detection using the Ensembles of a Deep Convolutional Network. They have achieved an accuracy of 96.2% on Devnagiri based P300 speller.

DATASET DESCRIPTION

The dataset used is the BCI Competition III Dataset II. It is a complete record of P300 evoked potentials, recorded with BCI20001 by Donchin et al. in 2000 and originally Farwell and Donchin in 1988 using a paradigm. The dataset contained data collected from 2 subjects collected in 5 sessions. The user was shown a 6x6 matrix of English alphabets and digits (0-9) and was asked to focus on the single character out of the 36 characters. The frequencies were increased successively and at random at 5.7Hz, for all rows and columns on this matrix. Out of the 12 intensified rows and columns, a particular row and column contain the desired character. The reactions evoked by these two of the 12 stimuli which contain the desired character differ from the stimuli which did not contain the desired character and are similar to those described in Farwell and Donchin, 1988; (Donchin et al., 2000).

The data was collected in 5 sessions, each having many runs. The subject focuses on a series of characters in each run. The user display was as follows for the run of each character epoch: the matrix was seen for 2.5 s, and each character had the same intensity during that time. Each row and column was intensified for 100ms, and then the matrix was left blank for 75ms. There were a total of 12 intensifications; each of them was repeated 15 times for each character epoch, so there were a total of 180 intensifications (12 x 15=180) for each character epoch. An epoch of each character followed for a period of 2.5sec, and then the matrix was kept blank. During this period, the user was told of the completion of this character, and the emphasis was on the next character in the word on the top of the screen. The dataset had 4 data, two for each subject, one of two was training data, and the other was the test data of that subject. The training data was used to predict the character sequence in the test data. In the end, the signals were passed through a bandpass filter from 0.1-60 Hz (Farwell LA et al., 1988).

Figure 1. The P300 speller paradigm for data collection

PROPOSED METHODOLOGY

The research makes use of BCI Competition III Dataset II, which consists of data with signals in binary matrix form which need to be converted into 2-D grayscale images; thus, the research makes use of Empirical Mode Decomposition (EMD) as the preprocessing technique. The application of EMD results in Intrinsic Mode Functions (IMFs); out of all the IMFs, those with higher frequencies are only considered. Then the energy of the signals used for converting into 2-D images is calculated. Then the energy values are normalized, and the energy spectrum is converted into a 2-D image. The research uses a stacked autoencoder for feature extraction from 2-D images, and classification is done using the Support Vector Machine (SVM) method.

FILTERING AND PREPROCESSING

To avoid noise and to restrict our observation to a particular range of frequencies, we have used the 8th order Chebyshev Bandpass filter with a lower cut-off frequency of 0.1 Hz and a higher cut-off frequency of 10 Hz. We have chosen this range because, as the study (Zhihua Yang et al., 2006) suggests, the P300 signal lies predominantly in this range of frequencies.

Figure 2. Proposed method

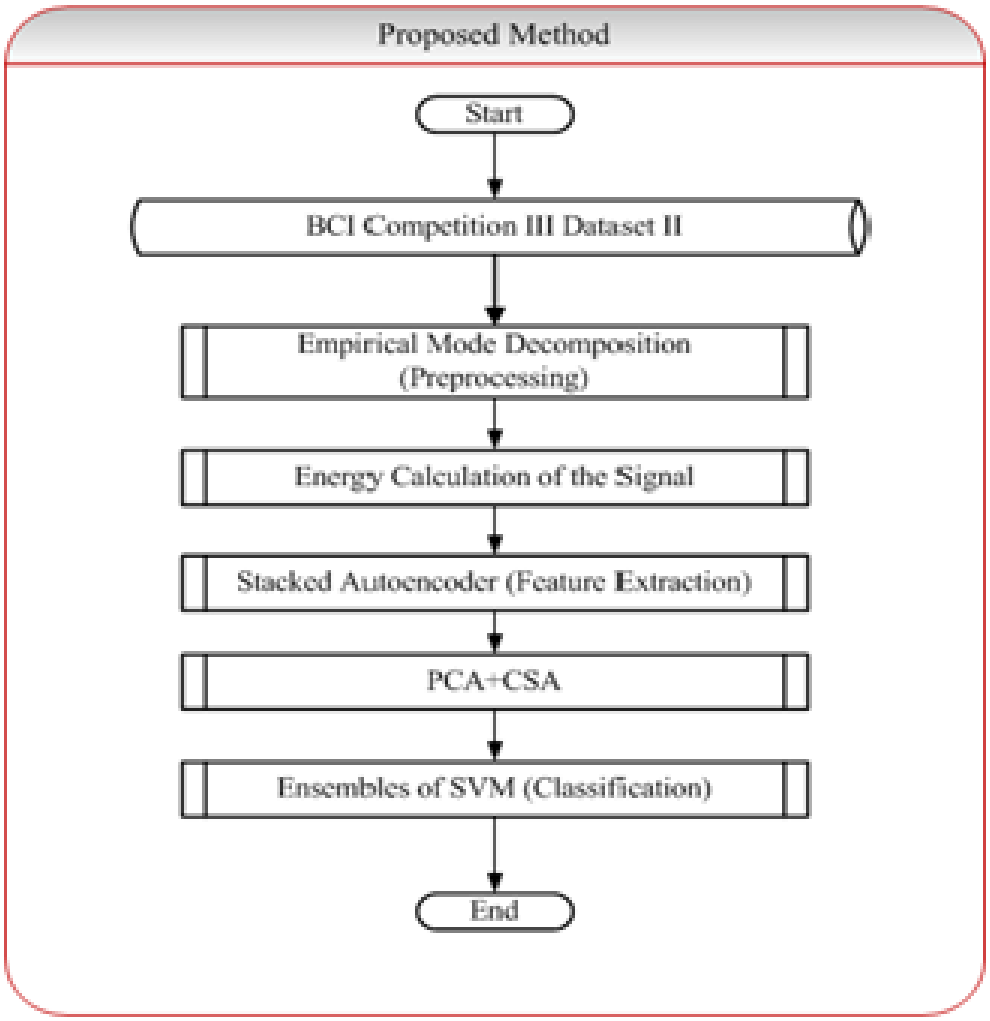

EMD

This research makes use of autoencoders which take inputs only in the form of images. The dataset used for the study is the BCI Competition III Dataset II which consists of the data in the form of signals which is not suitable as an input for the autoencoder. So, there arises a need to preprocess the data to make that suitable as an input for the autoencoder.

EMD is a time-space adaptive analysis approach suitable for non-stationary, non-linear, and stochastic signal processing. EMD involves breaking down a signal without leaving the time domain and was proposed as an integral part of the Hilbert–Huang transform (HHT). Hilbert-Huang transform (HHT) works in two stages. In the first stage, EMD breaks up non-linear and non-stationary data into a band-limited component summary called Intrinsic Mode Functions (IMF). The second stage involves producing an instantaneous frequency spectrum by applying the Hilbert transform to the results obtained in the first stage.

The energy of the wave signal has then been used to describe the essence of the signal more effectively than using the numerical values of the time field of the signal. Then the energy values are used to convert into a 2-D image.

1. Segmentation of the signal into subparts called Frames.
2. Calculating the size of the frame which is the multiplication of duration of the frame and signal's frequency rate.
   Size of the frame= frame duration x Frequency rate of the signal.
   Defining the size of the matrix-
   The height of the matrix is equal to the size of the frame (M) and width equates to the number of frames (N) produced after segmentation.
   Size of the matrix= M x *N*
3. Keeping the energy values into the cells of the matrix and transferring the frame values vertically to the matrix. The first column holds the energy values of the first frame, the first frame value is transferred to the first cell of the first row, the second frame value is transferred to the first cell of the second row and so on, and the last frame value of the first frame is transferred to the first cell of the last row. This process continues for further frames. Since the height of the matrix equates to the size of the frame, all the frame values get fit in the matrix and since the width of the matrix is equal to the number of frames produced after segmentation, all the energy values get fit in the matrix.
4. The values in the matrix are normalized in the range 0-255, thus reducing the noise.

2-D representation preserves time-domain signal characteristics, and even 2-D signal texture characteristics can be extracted to detect the signal [4].

Figure 3. Conversion into a 2-D matrix with the energy values of the sample

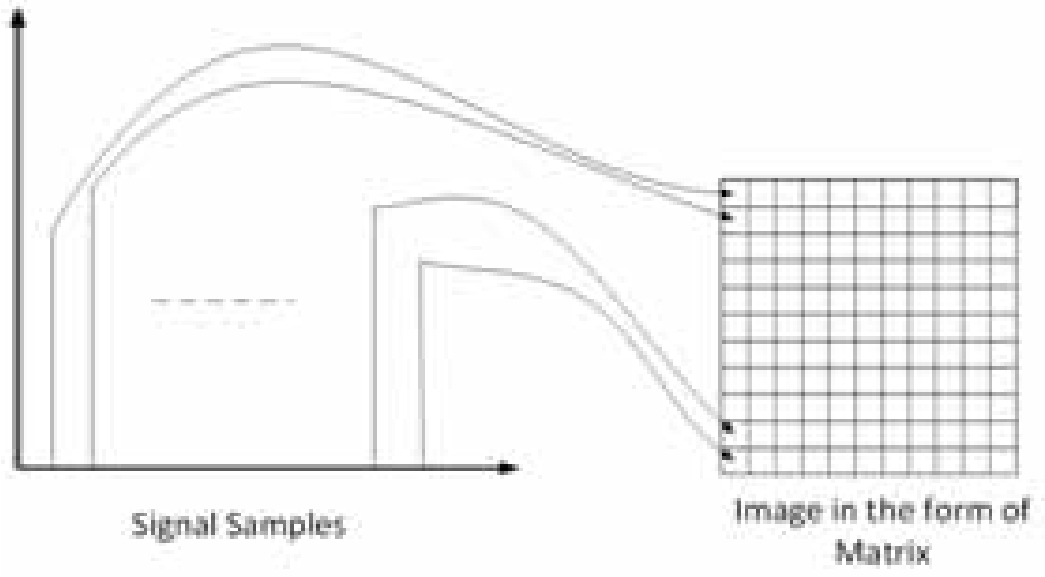

Figure 4. Producing an image from the 2-D matrix

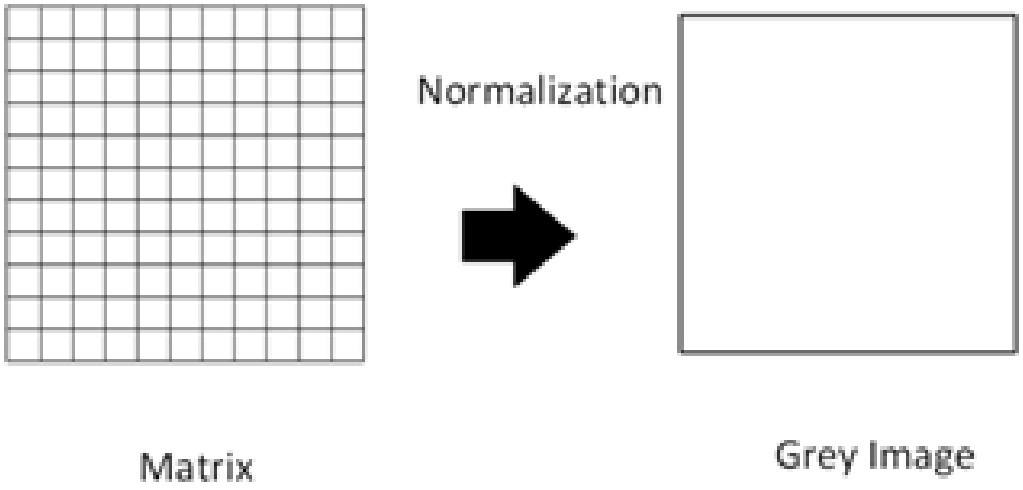

Figure 5. Conversion of signal into a grey image

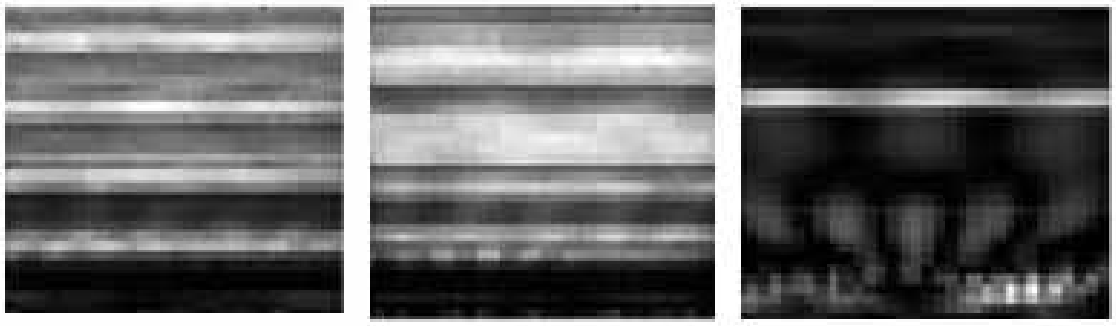

Feature Extraction Autoencoder

Stacked Autoencoder is prominently used for denoising images and compression of extracted features to a minimum so that only the most important features will remain. It is a feed-forward network that is used to reproduce the result in the output.

The hidden layer will maintain all the useful information, as the bottleneck part is much smaller than the input layer; hence it is used for data compression. The weights between the hidden layer and the reconstructed output layer, which is weighted towards the decoder side, are tied to the weights used in encoder sides. “Tied” means that the weights towards the decoder side are the transpose of weights used for the encoder side.

In this research, the output obtained after converting the P300 signals into a 2-D grayscale image is given as input to the stacked autoencoder. Initially, 30 percent of the features for the test and 70 percent for training were chosen to analyze classification problems better. This was achieved to ensure that the model knows the P300 stimulus and can develop the parameters. And then, all the training sets were passed together for better learning levels and precision after the parameters and the model had been found.

MATLAB neural network was used to implement this project. Parameters such as the number of iterations, number of layers, and neurons of the stacked autoencoders were set empirically. Initially, the project began with two layers and 1000 iterations. Still, as the work continued, the layers were increased to improve the accuracy, and the iterations were reduced to 300 after examination to face the over-fitting condition. The investigation resulted in an optimum number of layers as follows:

1. The inputs with 420 features were passed to the autoencoder's first layer.
2. The inputs with 420 features were shortened to 210 by the first layer of autoencoder, which was trained to 210.
3. Next, there was a 100 neuron autoencoder.
4. The 100 features were passed on to the next autoencoder with 50 neurons.
5. And then, the 50 features were passed on to the next autoencoder with 20 neurons.
6. The 20 features were passed to the last autoencoder with ten neurons.

This clearly shows that to reduce the features from 420 to 10 there were 5 layers which were a combination of 5 autoencoders. Besides, other parameters such as L2Weight Regularization and Sparsity Regularization were set in the MATLAB default configuration.

Further, the ten features were passed on to the softmax matrix with 200 iterations. So, stacked autoencoders with the structure: 420-210-100-50-10 were achieved at the end (Vařeka et al., 2017)

Figure 6. Architecture of stacked autoencoder

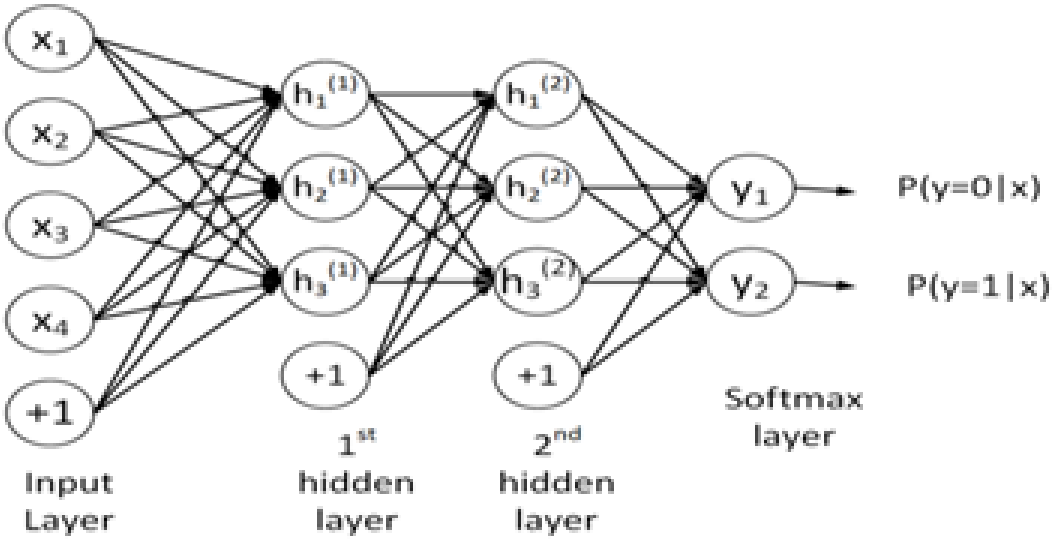

CSA and PCA

The uncorrelated variables obtained by orthogonal transformation of correlated variables are called principal components, and this method is called the PCA method (Andrzej Maćkiewicz et al., 1993). The sorting of the principal components depends on the variance, and the first major component reflects the highest variance of the original data. After extracting the features, when the power spectrum has been estimated for each channel, the normalization method is applied. The dataset contains a matrix D with dimensions n to p in the case of n testing of training, and the numbers of p= (channels. bins) and D (i, j) features are the value of tests i and j.

Firstly, a PCA is employed to minimize dimensionality and remove non-stationary components for the covariate shift adaptation, followed by the selection of m principal components with the highest variance, thus resulting in a transformation matrix W(pxm) and a P=D.W matrix representing the principal components of m. Further, a rectangular window is defined with length w, which moves through the data and normalizes the value of P (i, j) in the previous w trial with-

$$\widehat{P_{(ij)}} = P_{(ij)} - mean(P_{(i-w,j)},...,P_{(w,j)})$$

$(P_{(1,j)},\ldots,P_{(w,j)})$ is used for all $\widehat{P_{(ij)}}$ with $i \leq w$

ESVM

In this research work, the features extracted are applied to the ensembles of the SVM classifier (Marc Claesen et al., 2014) as the input, and the final output is the sum of the results from each classifier which are normalized using min-max normalization. Different types of features selected for evaluation are then concatenated to represent the signal in a much better way in terms of the ratio of information it holds.

Min-Max

If f_p is the score for test data assigned by the pth classifier then the min-max normalization (Patro et al., 2015) function is given as follows-

$$f_{pnorm} = \frac{f_p - \min(f_p)}{\max(f_p) - \min(f_p)}$$

f_p is the normalized score.

The scaling takes place between 0 and 1 because of the min-max normalization. The final output of the classifier is given as-

$$s = \frac{1}{j}\frac{1}{p}\sum_{j=1}^{J}\sum_{p=1}^{P} f_{pnorm}$$

J-number of epochs.
P-number of classifiers.

The intersection of the row and column gives the desired character.

RESULTS

For every subject, they have provided test data that consists of 85 characters and training data that consists of 100 characters. So, we have approximately 46% training data and 54% testing data individually for both the subjects. Hence, in total, they have provided four .mat files in single-precision format. As we have worked on a newer version of MATLAB, we have converted a single-precision format to a double-precision format.

In this research, we used EMD as a preprocessing technique; and extracted features using stacked autoencoders. We have optimized the obtained results using PCA- Corporate Shift Analysis. For the final classification, we have used Ensembles of SVM. Further, we have used two different architectures of the model. The first is preprocessing, feature extraction using a stacked autoencoder, and classification using ESVM. In the second method, we have applied PCA+ CSA for effective feature selection and to improve the performance of our proposed model.

Figure 7 summarizes the results using the first architecture obtained after every epoch. For simplification, results are rounded off to the nearest one's place. It is evident from the results that classification accuracy for subject A is significantly lower for the first epoch, but it gained faster than subject B. At the end of 1st, 5th, 10th, 15th, and 18th epoch we have obtained the subject wise accuracies of A as 19.5%, 71.6%, 85.2%, 95.5%, and 98.0%, whereas for subject B the results are 32.0%, 76.9%, 89.0%, 95.0%, and 97.5% respectively. The average accuracy obtained after 18 epochs is 97.75%.

Figure 7 also compares results we have obtained after including PCA +CSA for feature selection before the classification using Ensembles of SVM with those obtained without CSA. We can see the results obtained using this architecture is around 1-1.5% better than the first architecture of the proposed model. Using PCA+ CSA, we have obtained subject-wise classification accuracies for Subject A for epochs 1st, 5th, 10th, 15th, and 18th as 21.0%, 72.1%, 93.2%,98.4%, and 99.3%. Similarly for Subject B it is 36.3%, 78.3%, 91.2%, 96.8%, and 98.2%respectively. We can see that the average classification accuracy here is increased to 98.75%.

Table 1. Confusion after 18 epochs without CSA

Subjects	Expected	Output
A	H	Z
	Q	P
B	T	Z

Table 2. Confusion after 18 epochs with CSA

Subjects	Expected	Output
A	Q	P
B	T	Z

Mainly, the alphabets misclassified after 18 epochs lie in the same row or same columns. It means either row or column is detected correctly for these misclassified symbols. This may be because some of the signals which have been recorded using different subjects are co-related.

In Table 1, H, which is misclassified as Z, is in the same column, Q, which is misclassified as P, is in the same row, similarly for T, which is misclassified as Z, by subject B. On the contrary, Table 4 summarizes the classification result obtained using the architecture that consists of feature selection using PCA + CSA. It's clear from the results that the feature selection technique helps to improve the model accuracy.

Figure 7. Graph showing results with CSA and without CSA

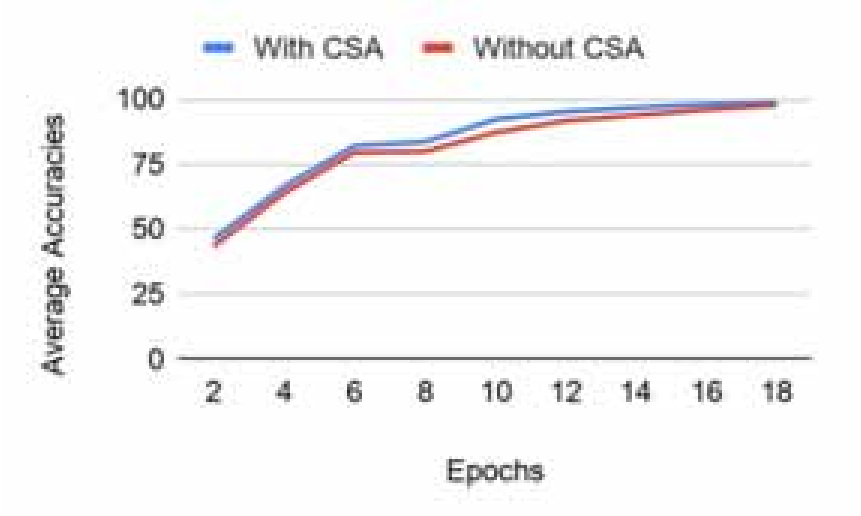

Table 3. Paired T-test

Method	P-value
CNN-1 (H. Cecotti et al., 2011)	$8.735\ 10^{-6}$
MCNN-1 (F. Reza et al.,2012)	$4.255\ 10^{-5}$
Temporal-ESVM (S. Kundu et al., 2018)	$2.78\ 10^{-3}$
PCA-EWSVM (V. Guigue, 2008)	$5.669\ 10^{-6}$
ESVM (M. J. Idaji et al., 2017)	$4.89\ 10^{-4}$

Hypothesis testing is one of the oldest procedures for checking data validity. The T-test is one of those statistical methods. In the beginning, the t-test implies a null hypothesis meaning the two data set means are identical. Based on the test's predefined method, specific values are calculated and compared with standard values, and the null hypothesis is finally accepted or rejected depending on the calculated values. If the null hypothesis appears to be dismissed, the collection of evidence is solid and is therefore not by mistake.

In this data, we have applied, paired T-test, and checked the value p-value. As it is clear from Table 3, that all of the results of the paired t-test give the p-value, which is significantly less than 0.05. Hence this set of data passes the t-test. This test also validates the performance of our model, as it shows improvement in character recognition compared to earlier reported techniques by other researchers.

DISCUSSIONS

For further analysis of the results obtained, we have compared our results with the results of our fellow researchers. Many great researchers have worked in this field and specifically on this dataset, they have used various methods for pre-processing, feature extraction, channel selection, and classification. Some have reported average classification accuracy, whereas few reported subject-wise accuracy. A few experiments have targeted artifact removal in pre-processing, whereas others targeted proper channel selection. In this section, we have compared feature extraction techniques, channel selection techniques, and classification methods.

Table 4 provides a detailed comparison of different methods that different researchers used to solve the proposed classification problem for BCI Competition III dataset II. Authors [25] used ensembles of SVM to classify this data; they have extracted features using a proposed deep neural network. He (H. Cecotti et al., 2011) has used CNN with 16 hidden layers, extracted deep features using CNN, and performed classification using the CNN network.

He (S. Kundu et al., 2018) used PCA as a feature extraction method and ensembles of SVM as a classification method and has obtained a classification accuracy of 99% & 97% for subjects A & B, respectively. In the (Mina Jamshidi Idaji, 2017) applied LDA for classification of these signals, and the results were comparatively less accurate than deep neural networks. Deep neural networks are more effective in this classification problem as they extract more relevant features. Moreover, the results are much more optimized because of the use of autoencoders for extracting features, as this would also include temporal features, and hence much better feature extraction. Autoencoders have already been used by (Liu et al., 2017) & (S. Kundu et al., 2019, and they have reported an average classification accuracy of 98% & 98.5%. We have extended his (S. Kundu et al., 2019) thoughts of using autoencoder but with autoencoder, we have also applied PCA+CSA for effective feature selection to improve classification results.

Table 4. Comparison of classification accuracy

Method	Subject A	Subject B	Mean
Proposed Method	99.3	98.2	98.75
CNN-1(H. Cecotti et al., 2011)	97.0	92.0	94.5
MCNN-1(H. Cecotti et al., 2011)	97.0	94.0	95.5
Temporal-ESVM (F. Reza et al., 2012)	99.0	97.0	98.0
PCA-EMSVM (V. Guigue et al., 2008)	99.0	97.0	98.0
ESVM (Mina et al.,2017)	97.0	96.0	96.5
HOSRDA&LDA (Mina et al.,2017)	96.0	97.0	96.5
GsBLDA (T. Yu et al., 2015)	99.0	95.0	97.0
BN3 (Liu et al., 2017)	98.0	95.0	96.5
SSAE-ESVM (S. Kundu et al., 2019)	99.0	98.0	98.5

CONCLUSION AND FUTURE SCOPE

In this set of experiments, we have improved the classification accuracy of BCI Competition III dataset II. For this, we have implemented a stacked autoencoder for the extraction of features and PCA +CSA for feature selection and the classification was performed using the ensemble of SVM and the overall results are represented in normalized form using min-max normalization. Feature extraction using a Stacked autoencoder, we have obtained an average accuracy of 98.75% when we have used this model architecture, compared to the accuracy of 97.75% when PCA +CSA is not included in the architecture of the model. Approximately an increase of [1-1.5] % is recorded when we have used the feature selection compared to when not. Paired t-test with other proposed methods was also performed, and the results are satisfactory as all of them give a p-value less than 0.05. A detailed comparison of results obtained and that obtained by other research has been done, in terms of classification method and preprocessing techniques which they have used. Those alphabets are also identified, which have been misclassified after 18 epochs and have been listed in Table 4.

In the future, we can try improving the accuracy close to 100% by using different channel selection algorithms to reject those channels that have more noise. We will also try to extend this research to more than two subjects and compare the performance of our model in that case. Further, we plan to implement our proposed model in an online system. Also, we are working to improve accuracy using lower sequences r trails.

CONFLICT OF INTEREST

The authors declare that there is no conflict of interest regarding this work.

ACKNOWLEDGMENT

The authors extend their appreciation and gratitude to the Electronics and Communication Department, National Institute of Technology, Raipur, for supporting this research work.

REFERENCES

Akcakaya, M., Peters, B., Moghadamfalahi, M., Mooney, A. R., Orhan, U., Oken, B., Erdogmus, D., & Fried-Oken, M. (2014). Noninvasive brain-computer interfaces for augmentative and alternative communication. *IEEE Reviews in Biomedical Engineering*, *7*, 31–49. doi:10.1109/RBME.2013.2295097 PMID:24802700

Azad, M., Khaled, F., & Pavel, M. I. (2019). A novel approach to classify and convert 1D signal to 2D grayscale image implementing support vector machine and empirical mode decomposition algorithm. *International Journal of Advanced Research*, *7*(1), 328–335. doi:10.21474/IJAR01/8331

Cecotti, H., & Graser, A. (2011). Convolutional Neural Networks for P300 Detection with Application to Brain-Computer Interfaces. *IEEE Transactions on Pattern Analysis and Machine Intelligence*, *33*(3), 433–445.

Chaurasiya, R. K., Londhe, N. D., & Ghosh, S. (2015). An efficient P300 speller system for Brain-Computer Interface. *International Conference on Signal Processing, Computing and Control (ISPCC).*

Chaurasiya, R. K., Londhe, N. D., & Ghosh, S. (2016). Binary DE-Based Channel Selection and Weighted Ensemble of SVM Classification for Novel Brain–Computer Interface Using Devanagari Script-Based P300 Speller Paradigm. *International Journal of Human-Computer Interaction*, *32*(11), 861–877. doi: 10.1080/10447318.2016.1203047

Chen, Weinberger, Sha, & Bengio. (2014). Marginalized Denoising Auto-encoders for Nonlinear Representations. *Proceedings of the 31st International Conference on Machine Learning, 32*(2), 1476-1484.

Claesen, M., De Smet, F., Suykens, J. A. K., & De Moor, B. (2014). EnsembleSVM: A Library for Ensemble Learning Using Support Vector Machines. *Journal of Machine Learning Research*, 141–145.

Farwell, L. A., & Donchin, E. (1988). Talking off the top of your head: Toward a mental prosthesis utilizing event-related brain potentials. *Electroencephalography and Clinical Neurophysiology*.

Idaji, Shamsollahi, & Sardouie. (2017). Higher order spectral regression discriminant analysis (HOSRDA): A tensor feature reduction method for ERP detection. *Journal of Pattern Recognition.*

Jolliffe, I. T., & Cadima, J. (2016). Principal component analysis: a review and recent developments. *Philosophical Transactions. Series A, Mathematical, Physical, and Engineering Sciences, 374*(2065).

Jonnalagadda. (2018). *Sparse, Stacked and Variational Autoencoder*. https://medium.com/

Kshirsagar, G. B., & Londhe, N. D. (2020). Weighted Ensemble of Deep Convolution Neural Networks for Single-Trial Character Detection in Devanagari-Script-Based P300 Speller. *IEEE Transactions on Cognitive and Developmental Systems*, *12*(3), 551–560.

Kundu, S., & Ari, S. (2018). P300 Detection Using Ensemble of SVM for Brain-Computer Interface Application. *9th International Conference on Computing, Communication and Networking Technologies (ICCCNT).*

Kundu, S., & Ari, S. (2019). P300 based character recognition using sparse autoencoder with ensemble of SVMs. *Biocybernetics and Biomedical Engineering*, *39*(4), 956–966. doi:10.1016/j.bbe.2019.08.001

Kundu, S., & Ari, S. (2019). P300 based character recognition using sparse autoencoder with ensemble of SVMs. *Biocybernetics and Biomedical Engineering*.

Liu, Wu, Gu, & Yu, Qi, & Li. (2017). Deep Learning Based on Batch Normalization for P300 Signal Detection. *Neurocomputing*, *275*, 288–297.

Lukáš & Pavel. (2017). Stacked Autoencoders for the P300 Component Detection. *Frontiers in Neuroscience.*

Maćkiewicz, A., & Ratajczak, W. (1993). Principal components analysis (PCA). *Computers & Geosciences*, *19*(3), 303–342.

Patro, Sahu, & Kumar. (2015). Normalization: A Preprocessing Stage. *International Advanced Research Journal in Science, Engineering and Technology.*

Rakotomamonjy, A., & Guigue, V. (2008). BCI Competition III: Dataset II- Ensemble of SVMs for BCI P300 Speller. *IEEE Transactions on Biomedical Engineering*, *55*(3), 1147–1154.

Reza, F.-R., Brendan, A., Christoph, G., Eric, S., Sonja, K., & Andrea, K. (2012). P300 brain computer interface: Current challenges and emerging trends. *Frontiers in Neuroengineering*.

Satti, A., Guan, C., Coyle, D., & Prasad, G. (2010). A Covariate Shift Minimisation Method to Alleviate Non-stationarity Effects for an Adaptive Brain-Computer Interface. *20th International Conference on Pattern Recognition.*

Shopon, Mohammed, & Abedin. (2016). Bangla handwritten digit recognition using autoencoder and deep convolutional neural network. *International Workshop on Computational Intelligence*, 64-68. 10.1109/IWCI.2016.7860340

Spüler, M., & Rosenstiel, W., & Bogdan, M. (2012). Principal component based covariate shift adaption to reduce non-stationarity in a MEG-based brain-computer interface. *EURASIP Journal on Advances in Signal Processing*.

Thulasidas, M., Guan, C., & Wu, J. (2006). Robust classification of EEG signal for brain-computer interface. *IEEE Transactions on Neural Systems and Rehabilitation Engineering*.

Wadsworth. (2004). *B. C. I. Dataset (P300 Evoked Potentials), Data Acquired Using BCI2000's P3 Speller Paradigm*. http://www.bci2000.org

Wolpaw, J. R., Birbaumer, N., McFarland, D. J., Pfurtscheller, G., & Vaughan, T. M. (2002). Brain-computer interfaces for communication and control. *Clinical Neurophysiology*, *113*(6), 767–791. doi:10.1016/S1388-2457(02)00057-3 PMID:12048038

Yang, Z., Yang, L., Qi, D., & Suen, C. Y. (2006). An EMD-based recognition method for Chinese fonts and styles. *Pattern Recognition Letters*, *27*.

Yu, T., Yu, Z., Gu, Z., & Li, Y. (2015). Grouped Automatic Relevance Determination and Its Application in Channel Selection for P300 BCIs. *IEEE Transactions on Neural Systems and Rehabilitation Engineering*, *23*(6), 1068–1077.

Chapter 11
Emotion Identification From TQWT-Based EEG Rhythms

Aditya Nalwaya
Indian Institute of Technology Indore, Indore, India

Kritiprasanna Das
Indian Institute of Technology Indore, Indore, India

Ram Bilas Pachori
Indian Institute of Technology Indore, Indore, India

ABSTRACT

Electroencephalogram (EEG) signals are the recording of brain electrical activity, commonly used for emotion recognition. Different EEG rhythms carry different neural dynamics. EEG rhythms are separated using tunable Q-factor wavelet transform (TQWT). Several features like mean, standard deviation, information potential are extracted from the TQWT-based EEG rhythms. Machine learning classifiers are used to differentiate various emotional states automatically. The authors have validated the proposed model using a publicly available database. Obtained classification accuracy of 92.9% proves the candidature of the proposed method for emotion identification.

INTRODUCTION

Emotion plays a vital role in human life, as it influences human behavior, mental state, decision making, etc. (Šimić et al., 2021). In human beings, overall intelligence is generally measured by logical and emotional intelligence (Picard et al., 2001; Salovey & Mayer, 1990). In recent years artificial intelligence (AI) and machine learning (ML) have helped computers to achieve higher intelligence particularly, in numerical computing and logical reasoning. But still, there are some limitations in its ability to understand, comprehend, and respond according to the emotional state of persons, interacting with a computer. To address these shortcomings, research in the domain of affective computing is going on. Affective computing is a field that aims to design machines that can recognize, interpret, process, and stimulate

DOI: 10.4018/978-1-6684-3947-0.ch011

the human experience of feeling or emotion. Recognizing a person's emotional state can help a computer to interact with humans in a better way.

In order to get more customized and user-centric information and communications technology solutions, an emotion recognition system could play an important role. In the absence of emotional intelligence, computers lag understanding and making a decision according to the situation. Thus, instead of making decisions logically, computers can be made aware of the human emotional state and then make any decision. Emotion recognition may be also helpful in upcoming new entertainment systems such as virtual reality systems for enhancing user experience (Gupta et al., 2020). Emotion recognition systems can also be used in understanding the health condition of patients with mental disabilities or infant patients (Hassouneh et al., 2020). Emotion detection can be used to monitor students learning and create personalized educational content for students (Kołakowska et al., 2014). Also, a software developer can examine user experience by using the emotion recognition system. Emotion recognition system has a vast area of application such as health care, brain-computer interface (BCI), education, smart entertainment system, smart rooms, intelligent cars, psychological study, etc. (Kołakowska et al., 2014).

Emotions are revealed by a human through either facial expression, verbal expression, or several physiological signals such as variability in heart rate, skin conductance, brain electrical activity, etc. These are generated by the human body in response to the emotion evoked (Egger et al., 2019).

In an emotion recognition system, emotions can be evoked or elicited either in a passive way or in an active way. In the case of passive emotion elicitation, the subject's emotions are evoked by exposing them to targeted emotion elicitation material. Some of the publicly available elicitation materials are the international affective picture system (IAPS) (Lang et al., 1997); it is a library of photographs used extensively for emotion elicitation, Nencki affective picture system (NAPS); is another database for visual stimulus. The Montreal affective voices and the international affective digitized sounds (IADS) are some of the acoustic stimulus databases used for passive emotion elicitation (Yang et al., 2018). In the case of active emotion elicitation, subjects will be asked to actively participate in a certain task that leads to emotion elicitation. Participants may be asked to play video games (Martínez-Tejada et al., 2021) or engage in conversation with another participant (Boateng et al., 2020); thus, by actively participating in the experiment subject's emotions can be evoked. Emotion elicited can be labelled either through explicit assessment by the subject itself, where the subject tells about his/her feeling, or by an implicit assessment, where the subject's emotional state is evaluated externally by some other person. Some standard psychological questionnaires, used for the emotion evaluation, are self-assessment manikin (SAM) (Bradley et al., 1994), the positive and negative affective (PANA) scheme (Watson et al., 1988), and differential emotion scale (DES) (Gross & Levenson, 1995), where subjects will answer according to their feelings. Both implicit and explicit methods of assessment are approximate evaluations of elicitation. Therefore in (Correa et al., 2018), to ensure the correctness of the label, both techniques are used in combination. Thus, in order to get physiological signals for a targeted emotion, the elicitation or stimulus of a particular emotion must be chosen carefully.

Signals which are interpretable such as facial expressions, speech expressions, etc., can be collected easily as the subject is not required to wear any equipment for recording such signals. Most facial emotion recognition (FER) approaches have three main stages: preprocessing, feature extraction, and emotion classification.

Preprocessing involves operations related to face detection and face alignment. There are many face detection techniques available such as Viola-Jones (Viola & Jones, 2001), normalized pixel difference (NPD) feature-based face detection (Liao et al., 2015), and facial image threshing machine (Kim et al.,

2021). Zhang et al. proposed an algorithm that can detect faces as well as perform a face alignment operation (Zhang et al., 2016). Face alignment is an important operation for making a non-frontal face image to a frontal image. An active appearance model (AAM) matches the statistical appearance model iteratively to get new face aligned images (Cootes et al., 2001). Another face alignment technique is constrained local models (CLM), which has more smooth image alignment due to the use of linear filters (Saragih et al., 2009).

The next task to preprocessing step is feature extraction. It is a process of extracting useful information from any given image or video. The process of identifying information from a given image is called data registration (Sariyanidi et al., 2014). It can be either from a full facial image, part of a facial image, or a point-based method. The full facial image is generally used when one is looking for every single detail of variation across the face. Whereas in the case of the part-based method, only a part of the facial image, such as eye, nose, etc., is considered. The point-based method is useful in getting information related to shape. Both part-based and point-based hold low-level feature information. Different low-level features are local binary pattern (LBP) (Jabid et al., 2010), local phase quantisation (LPQ) (Ojansivu & Heikkilä, 2008), histogram of gradients (HOG) (Dalal & Triggs, 2005), etc. Such low-level feature generates high dimensional feature vectors. Therefore, for removing redundancy from the obtained feature vector pooling methods are used. Next, facial expressions are classified into different emotional classes using the feature vector obtained.

In (Bendjillali et al., 2019), authors have used discrete wavelet transform (DWT) to extract features from a face image and then convolutional neural network (CNN) is used for determining the class of emotion. In (Zhang et al., 2016), authors have extracted multiscale features using biorthogonal wavelet entropy from the face image and then a fuzzy support vector machines (SVM) classifier is used for recognizing emotion. In (Kumar et al., 2021), authors have calculated features using a multilevel wavelet gradient transform, then using Pearson kernel principal component analysis pooling is done. The classification of different types of emotion is done using a fuzzy SVM classifier. In (Chowdary et al., 2021), the authors have used pre-trained CNN that were trained using the ImageNet database. Using such a transfer learning approach facial emotions have been recognized. Such FER systems have been found in applications related to video analytics for monitoring people (Gautam & Thangavel, 2021), e-learning to identify student engagement (De Carolis et al., 2019), reducing fatigue during video conferencing (Rößler et al., 2021), etc.

Another popular approach for recognizing a person's emotions is a speech analysis. Speech emotion recognition (SER) estimates the emotional state of a speaker from a voice signal. The SER has the same stages as the FER system had; the only difference is in the kind of features been extracted from the input signal. Preprocessing stage helps in extracting the speech signal of the target speaker and removing the voice of the non-target speaker as well as background noise and reverberation. Frequently used features for emotion recognition through speech are the Teager-energy operator (TEO) (Kaiser, 1993, pp. 149-152), prosodic features (Ingale & Chaudhari, 2012), voice quality features (Guidi et al., 2019), and spectral features (Gupta et al., 2018). TEO features find stress in the speech. It has been observed that speech is produced due to the nonlinear airflow from the human vocal tract, which is directly related to change in muscle tension. Thus, TEO can be used to analyze the pitch contour to detect emotions such as neutral, angry, etc. Prosodic feature highlights pitch-related information such as stress, tone, pause in between words, etc. The voice quality feature represents voice level, voice pitch for a particular emotion, i.e., the amplitude and the duration of the speech. Spectral features give information related to frequency distribution over the audible frequency range. Linear predictive cepstral coefficients (LPCC),

mel frequency cepstral coefficients (MFCC), modulation spectral features, etc., are some of the popular spectral features used for emotion recognition (Gupta et al., 2018).

In (Vasquez-Correa et al., 2016), the energy content in the speech signal is computed using wavelet-based time-frequency distribution for the classification of emotions. In (Li et al., 2010), authors have used empirical mode decomposition (EMD) based signal reconstruction method for feature extraction. (Daneshfar et al., 2020) have proposed hybrid spectral-prosodic features of a speech signal. Then, using quantum-behaved particle swarm optimization (QPSO) dimensionality of the feature vector has been reduced. The reduced feature vector is then passed to a neural network classifier having a Gaussian elliptical basis function (GEBF) for detecting speech emotion. In (Palo & Mohanty, 2018), LPCC and MFCC features have been extracted using wavelet decomposition. These features are then reduced using the vector quantization method and using the radial basis function neural network (RBFNN) classifier emotions were classified. Compared to biological signals, facial expressions and speech signals can be acquired comfortably and economically. Although such signals can be controlled or fabricated by the subject, thus are less reliable when compared with physiological signals (Zhang & Song, 2021)

The autonomous nervous system (ANS) regulates different parameters of our body. Emotions cause a change in the activity of ANS (McCraty, 2015). Thus, to analyze changes in the emotional state of a person, its heart rate, body temperature, respiration rates, and other physiological signals are often used. There are many physiological signals such as electroencephalogram (EEG) (Zheng, 2016), electrocardiogram (ECG) (Jing et al., 2009), phonocardiogram (PCG) (Xiefeng et al., 2019), galvanic skin response (GSR) (Wu et al., 2010), respiration (Philippot, 2002), etc. which have been used for emotion recognition.

The ECG signal represents the heart's electrical activity due to cardiac contraction and expansion. The sympathetic system in the ANS stimulates differently for different emotions. Emotions influence the ANS activity, which causes changes in the heartbeat rhythm. Using standard procedure ECG signals can be recorded by placing electrodes at some specified parts of the chest (Jing et al., 2009).

Similar to FER and SER systems, here also features are extracted for emotion recognition. Three different approaches of feature extraction from ECG are: first; PQRST detection, second; heart rate (HR) and within beat (WIB), and third; heart rate variability (HRV), and inter-beat interval (IBI) (Hasnul et al., 2021). HRV is a time-domain feature and is most widely used for the purpose of emotion recognition (Ferdinando et al., 2016). It measures variation in the heartbeats interval. The time between beats is called an IBI or RR interval. There are three domains of features that are generally extracted from the HRV, namely: time domain, frequency domain, and nonlinear domain feature.

Emotion recognition using ECG signal is done in (Dissanayake et al., 2019). ECG signal features such as WIB mean, standard deviation, median, etc., are calculated, and various time and frequency domain parameters have been calculated using EMD. This feature vector is then passed to extra tree, a random forest classifier for recognizing emotion. In (Chen et al., 2019), the signal is decomposed using DWT, and different features have been calculated, and then using the feature vector, signals have been classified into different emotional labels with the help of an SVM classifier.

GSR measures the conductivity of the skin, which is also known as electrodermal activity (EDA). Like heartbeat is regulated by ANS, sweating is also regulated by the ANS. Due to stress or fear emotions, the nervous system gets stimulated, and sweat is generated. Thus EDA signals can be used for the purpose of emotion detection. The conductivity of the skin increases when the subject is active and decreases when a subject is in a relaxed state. EDA signals can be recorded by placing electrodes over the fingers (Wu et al., 2010). In (Panahi et al., 2021), fractional Fourier transform (FrFT) is used for feature extraction from GSR signal, then feature selection is done using Wilcoxon test. In the end, SVM

is used for classification. Generally, for emotion recognition purposes, GSR is used in combination with other physiological signals such as ECG, EEG, etc (Li et al., 2021).

Respiration rate is defined as the number of times a person breathes per unit time. The breathing pattern of a person varies with changes in the physical and emotional state. Due to an increase in physical workload, respiration may increase. Similarly, a decreased respiration rate indicates a relaxed state. Thus respiration rate indicates the affective state of the ANS with respect to a particular emotional response and mental workload. Fast and deep breathing indicates anger or a happy emotional state. Momentary interruption of respiration indicates tension. Irregular respiration may also indicate a depressed or fearful emotional state (Philippot et al., 2002). In (Zhang et al., 2017), a deep learning-based sparse auto-encoder is used to extract features for recognizing emotional information from respiratory signals. Then logistic regression is used for the identification of the emotional state of a person.

An EEG signal is generated due to electrical activities inside the brain. EEG signals can be recorded both invasively and non-invasively. A non-invasive way of EEG signal recording is popularly used in the case of human brain study. An international 10-20 EEG electrode standard cap of multiple electrodes is placed over the scalp to record the EEG signal, and the potential difference among the electrodes captures any electrical activity inside the brain. Here 10–20 refers to the distance between the adjacent electrodes i.e., 10% or 20% distance from front to back or from right to the left of the skull. A professionally trained person can only understand such nonstationary EEG signals like a doctor uses these signals in diagnosing different brain disorders.

Various signal processing algorithms can help to extract information from such nonstationary signals to automate this manual process. Before applying any signal processing algorithm, a signal must be preprocessed. Preprocessing stage makes the signal suitable for further processing. Preprocessing includes operations such as artifact removal, noise filtering, and resampling the signal. The signal is generally recorded at a higher sampling rate, and then the signal is downsampled before further processing to reduce the computational complexity. Downsampling helps in reducing the number of samples used while still maintaining the needed information. Several artifact removal techniques based on independent component analysis (ICA), bandpass filtering, deep learning, etc., will further improve the signal quality (Li et al., 2021). The preprocessed signal is then analyzed using advanced signal decomposition techniques. Then certain features are extracted from the decomposed signal. Various features which help in characterizing signals are spatial features, spectral features, temporal features, statistical features, etc. can be extracted from the oscillatory components. Spatial information helps in finding out the source of information in the brain. In the case of EEG signal, this feature will help in selecting specific EEG channels or focusing more on the signal coming from a specific region of the brain. The spectral feature can be helpful in describing signal power distribution in different frequency bands. While mean, variance, standard deviation, skewness, kurtosis etc., are some of the widely used statistical features.

EEG signals are very useful physiological signals for the study of human emotion recognition, as EEG signals have a high temporal resolution (Zheng, 2016). Also, they are generated from the human brain; these signals have more important emotion-related information. EEG signals consist of different rhythms such as delta (δ) (0.5–4 Hz), theta (θ) (4–8 Hz), alpha (α) (8–13 Hz), beta (β) (13–30 Hz) and gamma (γ) (more than 30 Hz) (Das & Pachori, 2021). The study of these EEG rhythms may give useful information about the user's mental and emotional state.

Several methods have been proposed for emotion recognition using EEG signals. In (Lin, 2010), feature extraction from EEG signal is done using short-time Fourier transform (STFT). Then, F-score is used for feature selection then using SVM based classification is performed to estimate the emotional

state of the subject was done. In (Li, 2017), the author has extracted rational asymmetry (RASM), which describes the frequency-space domain characteristic of EEG signal, then using long short-term memory (LSTM) recurrent neural networks; different emotional states were classified with an accuracy of 76%. In (Li et al., 2017), multivariate synchrosqueezing transform (MSST) is used for time-frequency representation. The high-dimensional extracted feature is reduced using ICA. Gupta et al. decomposed EEG signals using flexible analytic wavelet transform (Gupta et al., 2018). Information potential (IP) using Reyni's quadratic entropy is computed from each sub-band. The obtained feature is smoothed using a moving average filter. The classification is done using a random forest classifier. In (Ullah, 2019), the authors have divided an EEG signal into small segments. For each segment, statistical parameters such as mean, median, Fisher information ratio, standard deviation, variance, maximum, minimum, range, skewness, kurtosis, entropy, and Petrosian fractal dimension are calculated. The feature vector of the above computed statistical parameter is passed to a classifier called sparse discriminative ensemble learning (SDEL) for the classification of the different emotional states of a person. In (Bhattacharyya et al., 2020), Fourier-Bessel series expansion (FBSE) based empirical wavelet transform (FBSE-EWT) is used for computing K-nearest neighbour (K-NN) and spectral Shannon entropies. The extracted features are smoothed and then given to the sparse autoencoder-based random forest (ARF) classifier for the identification of human emotion.

In (Zhang & Song, 2021), various multimodal emotion recognition approaches are explained. In a multimodal-based approach, different signals are captured from the subject, and a separate feature vector is formed from each signal. These feature vectors of different signals are combined either at the feature level or at the decision level.

The proposed methodology uses EEG signals for human emotion recognition. The EEG signal is analysed using tunable Q-factor wavelet transform (TQWT) based signal decomposition technique. TQWT sub-bands obtained after decomposing the EEG signal are separated into different EEG rhythms. Information potential features are extracted from each rhythm which is then used for the identification of the emotional state of a person. The performance of the proposed method is evaluated using a publically available database consisting of EEG signals of different participants.

The remaining chapter is arranged as follows. Section 2 (proposed framework) describes all the steps of the proposed emotion recognition system. Section 3 (results and discussion) presents the obtained results. The last section concludes the study.

Proposed Framework

This section explains the proposed methodology. The flow chart of the proposed emotion recognition system is shown in Figure 1.

Figure 1. Flow chart of the proposed methodology

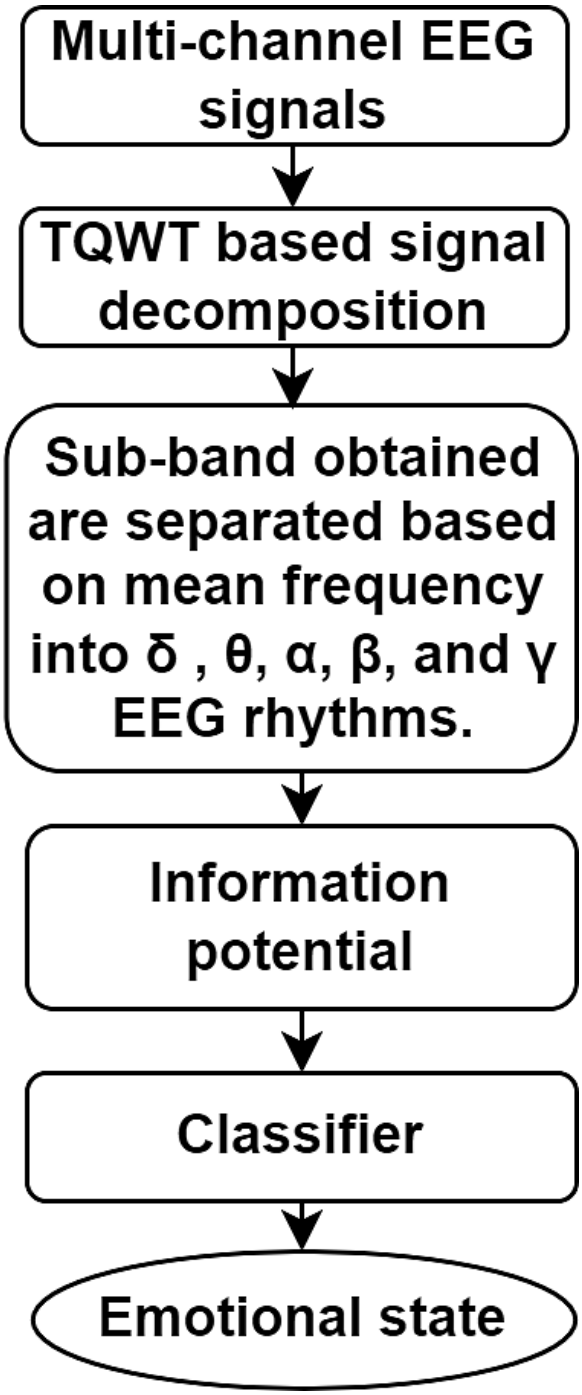

1. Database description:

A publically available database called SJTU Emotion EEG Dataset (SEED) is used for validating the proposed model (Zheng & lu, 2015). It contains recording of 15 subjects for three classes of emotions, i.e., neutral, sad, and happy. Each subject has participated in three sessions. The SEED database includes the Chinese movie clips used to elicit emotion, a list of subjects, and recorded EEG data. The Chinese movie clips used for eliciting emotion were selected based on certain criteria: 1) to avoid fatigue among subjects during the trial, clips are chosen as short as possible, 2) the subject must easily understand the clip, and 3) only desired emotion must get elicited. Clips were then shown to twenty participants, and among those, only 15 were selected finally with an equal number of clips for evoking each emotion. The time interval of each movie clip was approximately 4 minutes duration.

2. TQWT based signal decomposition (Selesnick, 2011):

In this stage, the signal is decomposed into different sub-bands. DWT is the most widely used time-frequency analysis technique for analyzing nonstationary signals (Daubechies, 1992). DWT has a constant Q-factor, which is not suitable for different varieties of signals, i.e. if the signal is highly oscillatory then it should have a high Q-factor. On the other hand, if the signal is less oscillatory then it should have a low Q-factor. TQWT is a more advanced version of the wavelet transform. Using TQWT multi-component EEG signals can be decomposed into several sub-band signals. TQWT is more flexible than the original DWT as the Q factor of the filter can be adjusted. It provides good time-frequency localization. TQWT has three main parameters Q, r, and J, where Q represents the Q-factor it is a dimensionless quantity, J is a parameter that represents the levels of decomposition, which varies from 1 to N integer values and r represents the oversampling rate. Wavelet oscillations are adjusted by Q, whereas r controls temporal localization while conserving its form. By increasing the value of Q, frequency response becomes narrower resulting in more levels of decompositions for the same frequency range span. For the fixed value of Q, if r is increased then overlap between the adjacent frequency responses will in turn increase the levels of decomposition for the same frequency range. TQWT contains a chain of two-channel high pass and low pass filter banks. The output of low pass filter is connected to the input of the next stage of the filter bank. Fig. 2 (a) shows the process of decomposition and reconstruction of a given input EEG signal using TQWT based approach. Fig. 2 (b) shows the process of iterative signal decomposition up to N levels. For the N level of decomposition, the number of sub-bands will be (N+1) i.e., one low pass sub-band and N high pass sub-bands. In Fig. 2 (a) α represents low pass scaling factor, it preserves the low-frequency components of the signal. Similarly, β represents the high pass scaling factor it preserves the high-frequency components of the signal.

Figure 2. (a) TQWT decomposition and reconstruction. (b) Multi-stage filter bank

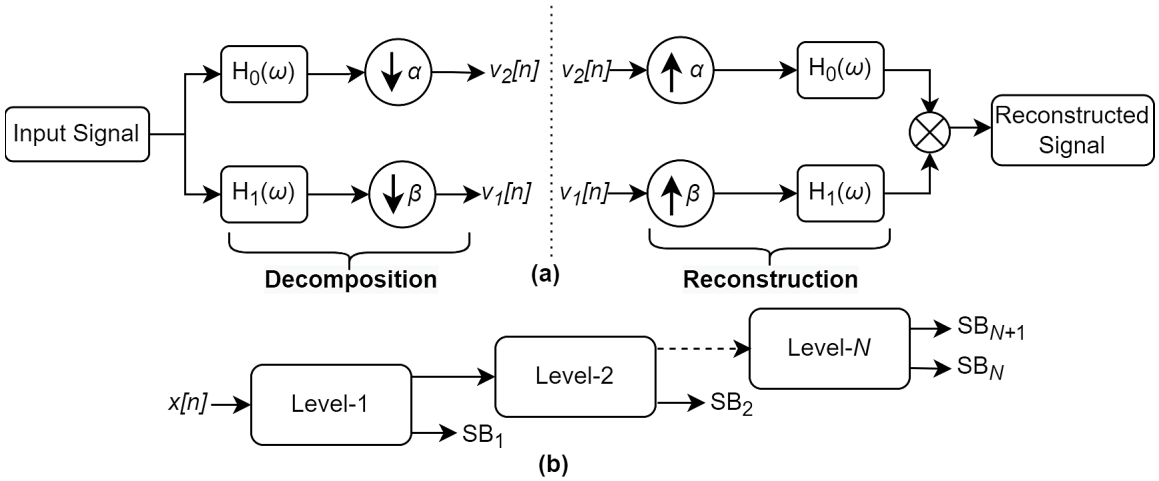

Equivalent frequency response of low pass ($\mathrm{H}_0^N\left(\omega\right)$) and high pass ($\mathrm{H}_1^N\left(\omega\right)$) filter bank is given as follows (Selesnick, 2011):

$$\mathrm{H}_0^N\left(\omega\right)=\begin{cases}\prod_{k=0}^{N-1}\mathrm{H}_0\left(\frac{\omega}{\alpha^k}\right), & \left|\omega\right|\leq\alpha^N\pi\\ 0, & \alpha^N\pi\ \leq\left|\omega\right|\leq\pi\end{cases}$$

$$\mathrm{H}_1^N\left(\omega\right)=\begin{cases}\mathrm{H}_1\left(\frac{\omega}{\alpha^{N-1}}\right)\prod_{k=0}^{N-2}\mathrm{H}_0\left(\frac{\omega}{\alpha^k}\right), & \left(1-\beta\right)\alpha^{N-1}\pi\leq\left|\omega\right|\leq\alpha^{N-1}\pi\\ 0, & \omega\in\left[-\pi,\pi\right]\end{cases}$$

For perfect reconstruction $\alpha + \beta > 1$, and for $\alpha + \beta = 1$, TQWT is critically sampled with no transition width. For getting the desired Q-factor wavelet filter bank parameters α & β are given by [68]:

$$\beta=\frac{2}{\mathrm{Q}+1},\qquad\alpha=1-\frac{\beta}{r}$$

3. Rhythm separation:

Rhythms from decomposed EEG signals are separated by calculating the mean frequency of the sub-bands signals. If the mean frequency value lies between 0.5 to 4 Hz then delta rhythm is obtained. Similarly, alpha, beta, and gamma rhythm's mean frequency values lie between 4 to 8 Hz, 8 to 13 Hz, 13 to 30 Hz, 30 to 75 Hz, respectively.

Sub-bands of decomposed EEG signal are grouped to separate rhythms according to their mean frequency (μ_k) calculated as follows (Das & Pachori, 2021):

$$\mu_k = \frac{\sum_{i=0}^{\frac{N}{2}-1} f_i \left|Y_k\left(i\right)\right|^2}{\sum_{i=0}^{\frac{N}{2}-1} \left|Y_k\left(i\right)\right|^2}$$

Where $f_i = \frac{f_s\, i}{N}$, here f_s is the sampling frequency, N is the length of the signal and Y_k is the discrete Fourier transform (DFT) of sub-band. As only a one-sided spectrum is considered, therefore, the range for i is between 0 to (N/2)-1.

4. Feature extraction:

IP of the obtained rhythm is then calculated using Reyni's quadratic entropy (Xu & Erdogmuns, 2010). For adaptation and learning of the information, Renyi derived a group of estimators which use entropy and divergences as a cost function. Since entropy is a scalar quantity, for calculating the entropy of random data, first its probability density function (PDF) must be estimated. But for high dimensional spaces, it is difficult to calculate. Using quadratic Renyi's entropy and the IP (i.e. H(x)) requirement of estimating PDF can be relaxed. Where H(x) is a Gaussian kernel with σ as variance, $\mathrm{IP}_{\sigma}(x)$ is a quadratic IP estimator which depends on σ, x_m, and x_n are sample pairs and the total number of samples is given by N. The mathematical expression for IP is as follows:

$$\mathrm{IP}_{\tilde{\mathrm{A}}}\left(x\right) = \frac{1}{N^2}\sum_{m=1}^{N}\sum_{n=1}^{N} H_{\sigma}\left(x_n - x_m\right)$$

5. Classification:

SVM is a supervised machine learning algorithm. It is mainly used for finding decision boundaries or support vectors which are then used for classification. SVM classifier learns from the training data that are projected into a higher-dimensional space, where data is separated into two classes by a hyperplane (Cortes & Vapnik, 1995). The user-defined kernel function helps in transforming the original feature space into a higher-dimensional space. It finds support vectors to maximize the separation between the two classes. Margin is the total separation between the hyperplanes. Once hyperplanes are defined, SVM iteratively optimizes in order to maximize the margin. SVM can perform both linear and nonlinear classification. In the case of a nonlinear classifier, the kernels are complex polynomial, homogenous polynomial, Gaussian radial basis function, and hyperbolic tangent function. In this work SVM classifier, with a cubic kernel is used. Hyperplane of SVM classifier can be expressed mathematically as follows (Suykens & Vandewalle, 1999):

$$y\left(x\right) = \text{sign}\left[\sum_{n-1}^{N} a_n y_n \phi\left(x, x_n\right) + c\right]$$

where a_n is a positive real constant, c is a real constant, ϕ(x,xn_j is a kernel or feature space, xn and yn are nt^{h} input and output vector. For a linear feature space $\phi\left(x, x_n\right) = x_n^T x$, for polynomial SVM of order d feature space is given by $\phi\left(x, x_n\right) = \left(x_n^T x + 1\right)^d$ i.e., for quadratic polynomial (d=2) and cubic polynomial (d=3).

RESULTS AND DISCUSSION

The proposed methodology for the recognition of human emotion using EEG signals is evaluated using a publically available database. TQWT decomposes EEG signal into several sub-bands. Different parameters related to TQWT were chosen as Q = 5, r = 3, and J = 18. One second epoch of the EEG signal is chosen for decomposing it into (J+1) sub-bands. EEG signals and sub-band signals (SB_1 to SB_N) corresponding to happy, neutral, and sad emotional states are shown in Figs. 3, 4, and 5, respectively.

Figure 3. EEG (happy emotion) and its corresponding sub-band signals obtained using TQWT

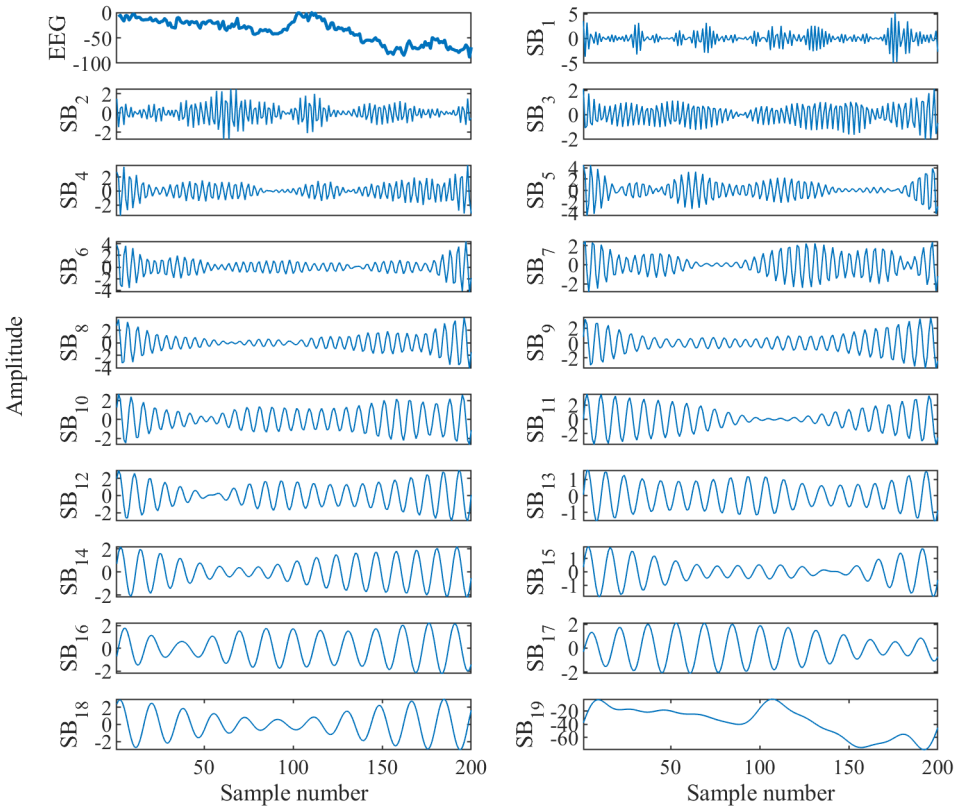

Figure 4. EEG (neutral emotion) and its corresponding sub-band signals obtained using TQWT

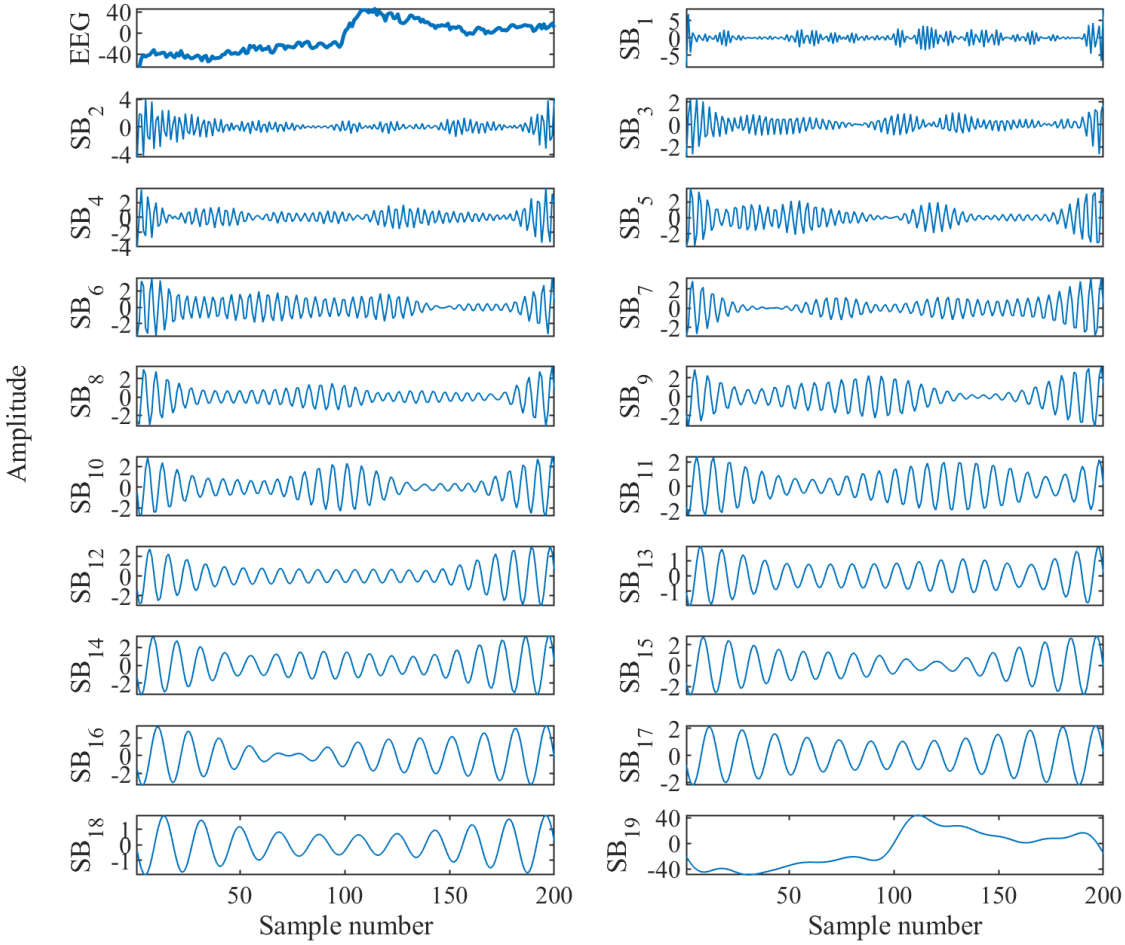

Figure 5. EEG (sad emotion) and its corresponding sub-band signals obtained using TQWT

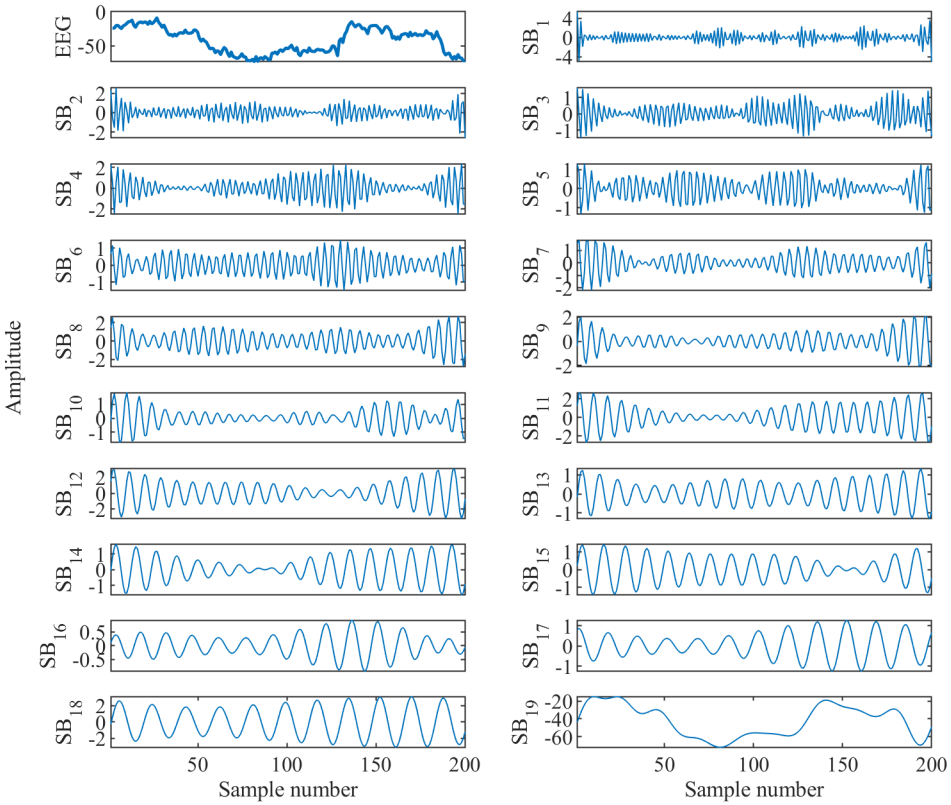

Figure 6. EEG signal and its rhythms for happy emotion

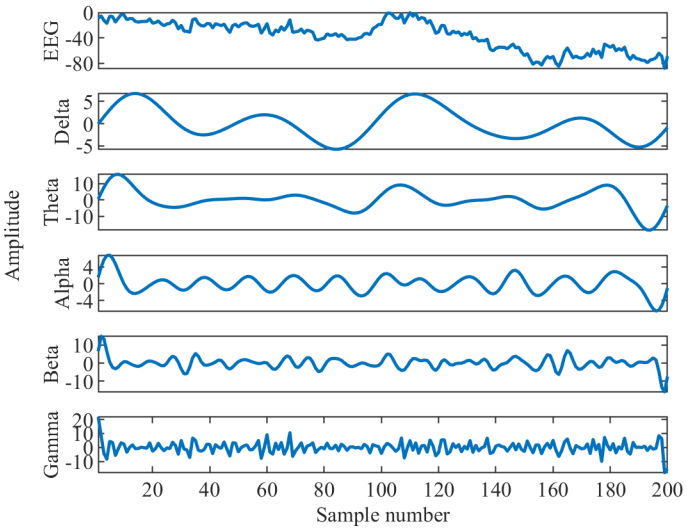

Figure 7. EEG signal and its rhythms for neutral emotion

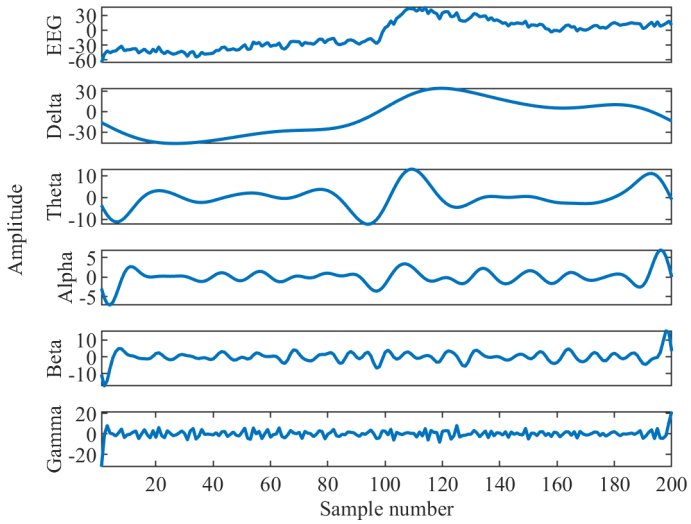

Figure 8. EEG signal and its rhythms for sad emotion

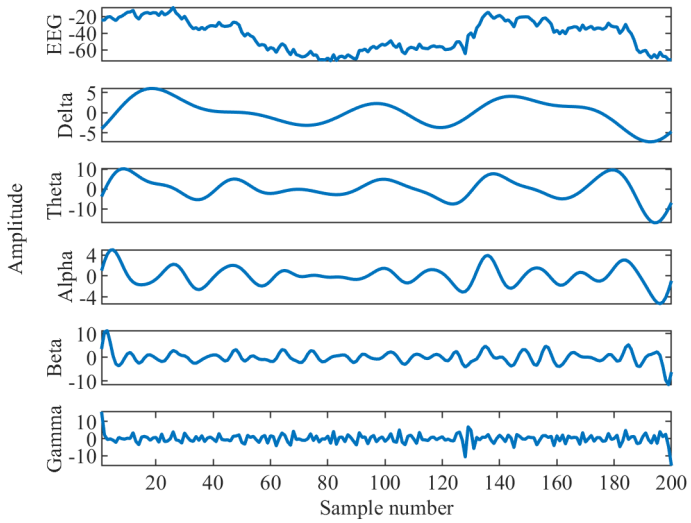

Then mean frequency of each sub-bands are calculated, and based on its value, EEG rhythms were extracted by grouping the sub-bands. Thus, all sub-bands with a mean frequency value between 1 to 4 Hz are summed together to obtain delta rhythm. In a similar way, all other EEG rhythms were obtained as shown in Figs. 6, 7, and 8, respectively. Then information potential for each rhythm is calculated, and a feature vector corresponding to a particular emotion was formed. Several machine learning classifiers are trained using the feature vector.

SVM classifier with cubic kernel outperforms other classifiers. The performance of the classifier is compared based on the statistical parameters: true positive rate and overall accuracy which are defined as follows:

$$\text{True Positive rate} = \frac{\text{True Positive}}{\text{True Positive} + \text{False Negative}}$$

$$\text{Overall accuracy} = \frac{\text{True Positive}}{\text{True Positive} + \text{True Negative} + \text{False Positive} + \text{False Negative}}$$

All simulations are done using MATLAB 2021b, installed on a system having an Intel i5 processor and 8 GB RAM. Table 1 shows the accuracy of the classifier for an individual subject. The overall average accuracy for the subject-dependent emotion recognition task is 92.9%.

Table 1. SVM (cubic) classifier performance for subject dependent emotion recognition

Subject	True positive rate (in %)			Overall accuracy (in %)
	Sad (-1)	Neutral (0)	Happy (1)	
Subject 1	91.7	93.7	95.9	93.8
Subject 2	93.6	94.7	94.2	94.2
Subject 3	86.8	88.7	94.2	90.0
Subject 4	99.1	99.5	99.6	99.4
Subject 5	93.8	93.0	92.7	93.2
Subject 6	93.8	92.4	97.9	94.7
Subject 7	82.1	87.7	88.4	86.1
Subject 8	89.0	90.2	92.5	90.6
Subject 9	88.8	87.2	95.2	90.5
Subject 10	92.1	92.8	97.5	94.2
Subject 11	89.0	91.8	91.5	90.8
Subject 12	93.0	94.8	92.9	93.6
Subject 13	91.4	92.6	94.8	93.0
Subject 14	93.6	94.6	96.5	94.9
Subject 15	93.1	95.5	93.2	93.9
Average	**91.4**	**92.6**	**94.5**	**92.9**

In the case of subject independent classification, MATLAB classifier learner application is used, and five different classifiers are trained. Table 2 shows a comparison of different classifiers' performance in the case of subject independent emotion recognition. Ensemble bagged trees provides the highest overall accuracy of 86.8%.

Table 2. Classification performance for subject independent emotion recognition

Classifier	True positive rate (in %)			Overall Accuracy (in %)
	Sad (-1)	Neutral (0)	Happy (1)	
Fine tree	51.8	68.9	80.1	67.1
SVM (cubic)	81.8	83.1	90.9	85.4
KNN (cubic)	58.2	61.4	73.4	64.4
Ensemble boosted trees	50.0	59.4	80.3	64.2
Ensemble bagged trees	85.0	85.2	90.0	**86.8**

TQWT based emotion recognition using EEG signal requires less amount of training data compared to the deep neural network-based emotion recognition system. Comparative performance of different emotion recognition methods is shown in Table 3.

Table 3. Performance comparison of the different existing methods with the proposed method

Author	Dataset	Methodology	Accuracy
(Li et al., 2017)	DEAP	CNN + LSTM, RNN	75.21%
(W. Zhang et, al. 2019)	SEED	CNN and DDC	82.1%
(Zhong et al., 2020)	SEED	RGNN	85.3%
(Yucel et al., 2020)	SEED	Pretrained CNN	78.34%
(Wang et al., 2020)	SEED	CNN, EFDMs, and STFT	90.59%
(Wei et al., 2020)	SEED	Dual-tree complex wavelet transform and simple recurrent units network	80.02%
(Khateeb et al., 2021)	DEAP	Multi-domain features extraction using wavelet (entropy, energy) and SVM classifier	65.92%
(Haqque et al., 2021)	SEED	Wavelet filters and CNN	83.44%
Proposed work	**SEED**	**TQWT based feature extraction, and SVM with cubic kernel-based classification**	**92.9%**

CNN: convolutional neural network, LSTM: long short-term memory, RNN: recurrent neural network, DDC: deep domain confusion, EFDMs: electrode-frequency distribution maps, STFT: short-time Fourier transform, SVM: support vector machine.

CONCLUSION

This study recognized human emotions using EEG signals by applying advanced signal processing techniques. TQWT decomposes EEG signal into several sub-bands. Depending on the mean frequency, sub-bands are grouped together in order to obtain EEG rhythms. Statistical feature from each rhythm is computed and used for classification using an SVM classifier with the cubic kernel. SEED emotion database is used for evaluation of the proposed methodology. For subject-dependent and independent

emotion recognition, 92.9% and 86.8% accuracy, respectively, are obtained. The proposed technique may be helpful in creating a more user-friendly interactive system. Also, the complexity of such a system will be less compared to deep learning methods. Therefore, it can be easily deployed in real-time applications.

ACKNOWLEDGMENT

This study is supported by the Council of Scientific & Industrial Research (CSIR) funded Research Project, Government of India, Grant number: 22(0851)/20/EMR-II.

REFERENCES

Bendjillali, R. I., Beladgham, M., Merit, K., & Taleb-Ahmed, A. (2019). Improved facial expression recognition based on DWT feature for deep CNN. *Electronics (Basel)*, *8*(3), 324. doi:10.3390/electronics8030324

Bhattacharyya, A., Tripathy, R. K., Garg, L., & Pachori, R. B. (2020). A novel multivariate-multiscale approach for computing EEG spectral and temporal complexity for human emotion recognition. *IEEE Sensors Journal*, *21*(3), 3579–3591. doi:10.1109/JSEN.2020.3027181

Boateng, G., Sels, L., Kuppens, P., Lüscher, J., Scholz, U., & Kowatsch, T. (2020, April). *Emotion elicitation and capture among real couples in the lab. In 1st Momentary Emotion Elicitation & Capture workshop (MEEC 2020). ETH Zurich*. Department of Management, Technology, and Economics.

Bradley, M. M., & Lang, P. J. (1994). Measuring emotion: The self-assessment manikin and the semantic differential. *Journal of Behavior Therapy and Experimental Psychiatry*, *25*(1), 49–59. doi:10.1016/0005-7916(94)90063-9 PMID:7962581

Chen, G., Zhu, Y., Hong, Z., & Yang, Z. (2019). EmotionalGAN: generating ECG to enhance emotion state classification. *Proceedings of the 2019 International Conference on Artificial Intelligence and Computer Science*, 309-313. 10.1145/3349341.3349422

Chowdary, M. K., Nguyen, T. N., & Hemanth, D. J. (2021). Deep learning-based facial emotion recognition for human–computer interaction applications. *Neural Computing & Applications*, 1–18. doi:10.100700521-021-06012-8

Cimtay, Y., & Ekmekcioglu, E. (2020). Investigating the use of pretrained convolutional neural network on cross-subject and cross-dataset EEG emotion recognition. *Sensors (Basel)*, *20*(7), 2034. doi:10.339020072034 PMID:32260445

Cootes, T. F., Edwards, G. J., & Taylor, C. J. (2001). Active appearance models. *IEEE Transactions on Pattern Analysis and Machine Intelligence*, *23*(6), 681–685. doi:10.1109/34.927467

Correa, J. A. M., Abadi, M. K., Sebe, N., & Patras, I. (2018). Amigos: A dataset for affect, personality and mood research on individuals and groups. *IEEE Transactions on Affective Computing*.

Cortes, C., & Vapnik, V. (1995). Support-vector networks. *Machine Learning*, *20*(3), 273–297. doi:10.1007/BF00994018

Dalal, N., & Triggs, B. (2005). Histograms of oriented gradients for human detection. In *2005 IEEE Computer Society Conference on Computer Vision and Pattern Recognition (CVPR'05)* (Vol. 1, pp. 886-893). 10.1109/CVPR.2005.177

Daneshfar, F., Kabudian, S. J., & Neekabadi, A. (2020). Speech emotion recognition using hybrid spectral-prosodic features of speech signal/glottal waveform, metaheuristic-based dimensionality reduction, and Gaussian elliptical basis function network classifier. *Applied Acoustics*, *166*, 107360. doi:10.1016/j.apacoust.2020.107360

Das, K., & Pachori, R. B. (2021). Schizophrenia detection technique using multivariate iterative filtering and multichannel EEG signals. *Biomedical Signal Processing and Control*, *67*, 102525. doi:10.1016/j.bspc.2021.102525

Daubechies, I. (1992). *Ten lectures on wavelets*. Society for Industrial and Applied Mathematics.

De Carolis, B., D'Errico, F., Macchiarulo, N., & Palestra, G. (2019). "Engaged Faces": Measuring and Monitoring Student Engagement from Face and Gaze Behavior. In *IEEE/WIC/ACM International Conference on Web Intelligence-Companion Volume* (pp. 80-85). 10.1145/3358695.3361748

Dissanayake, T., Rajapaksha, Y., Ragel, R., & Nawinne, I. (2019). An ensemble learning approach for electrocardiogram sensor based human emotion recognition. *Sensors (Basel)*, *19*(20), 4495. doi:10.339019204495 PMID:31623279

Egger, M., Ley, M., & Hanke, S. (2019). Emotion recognition from physiological signal analysis: A review. *Electronic Notes in Theoretical Computer Science*, *343*, 35–55. doi:10.1016/j.entcs.2019.04.009

Ferdinando, H., Seppänen, T., & Alasaarela, E. (2016). Comparing features from ECG pattern and HRV analysis for emotion recognition system. *IEEE Conference on Computational Intelligence in Bioinformatics and Computational Biology (CIBCB)*, 1-6. 10.1109/CIBCB.2016.7758108

Gautam, K. S., & Thangavel, S. K. (2021). Video analytics-based facial emotion recognition system for smart buildings. *International Journal of Computers and Applications*, *43*(9), 858–867. doi:10.1080/1206212X.2019.1642438

Gross, J. J., & Levenson, R. W. (1995). Emotion elicitation using films. *Cognition and Emotion*, *9*(1), 87–108. doi:10.1080/02699939508408966

Guidi, A., Gentili, C., Scilingo, E. P., & Vanello, N. (2019). Analysis of speech features and personality traits. *Biomedical Signal Processing and Control*, *51*, 1–7. doi:10.1016/j.bspc.2019.01.027

Gupta, D., Bansal, P., & Choudhary, K. (2018). The state of the art of feature extraction techniques in speech recognition. *Speech and Language Processing For Human-Machine Communications*, 195-207.

Gupta, K., Lazarevic, J., Pai, Y. S., & Billinghurst, M. (2020). AffectivelyVR: Towards VR Personalized Emotion Recognition. *26th ACM Symposium on Virtual Reality Software and Technology*, 1-3.

Gupta, V., Chopda, M. D., & Pachori, R. B. (2018). Cross-subject emotion recognition using flexible analytic wavelet transform from EEG signals. *IEEE Sensors Journal*, *19*(6), 2266–2274. doi:10.1109/JSEN.2018.2883497

Haqque, R. H. D., Djamal, E. C., & Wulandari, A. (2021). Emotion Recognition of EEG Signals Using Wavelet Filter and Convolutional Neural Networks. In *2021 8th International Conference on Advanced Informatics: Concepts, Theory and Applications (ICAICTA)* (pp. 1-6). 10.1109/ICAICTA53211.2021.9640279

Hasnul, M. A., Alelyani, S., & Mohana, M. (2021). Electrocardiogram-Based Emotion Recognition Systems and Their Applications in Healthcare—A Review. *Sensors (Basel)*, *21*(15), 5015. doi:10.339021155015 PMID:34372252

Hassouneh, A., Mutawa, A. M., & Murugappan, M. (2020). Development of a real-time emotion recognition system using facial expressions and EEG based on machine learning and deep neural network methods. *Informatics in Medicine Unlocked*, *20*, 100372. doi:10.1016/j.imu.2020.100372

Ingale, A. B., & Chaudhari, D. S. (2012). Speech emotion recognition. *International Journal of Soft Computing and Engineering*, *2*(1), 235–238.

Jabid, T., Kabir, M. H., & Chae, O. (2010). Local directional pattern (LDP) for face recognition. *Digest of Technical Papers International Conference On Consumer Electronics (ICCE)*, 329-330.

Jing, C., Liu, G., & Hao, M. (2009). The research on emotion recognition from ECG signal. *International Conference on Information Technology and Computer Science*, 1, 497-500. 10.1109/ITCS.2009.108

Kaiser, J. F. (1993). Some useful properties of Teager's energy operators. *IEEE International Conference on Acoustics, Speech, and Signal Processing*, 3, 149-152. 10.1109/ICASSP.1993.319457

Khateeb, M., Anwar, S. M., & Alnowami, M. (2021). Multi-Domain Feature Fusion for Emotion Classification Using DEAP Dataset. *IEEE Access: Practical Innovations, Open Solutions*, *9*, 12134–12142. doi:10.1109/ACCESS.2021.3051281

Kim, J. H., Poulose, A., & Han, D. S. (2021). The extensive usage of the facial image threshing machine for facial emotion recognition performance. *Sensors (Basel)*, *21*(6), 2026. doi:10.339021062026 PMID:33809352

Kołakowska, A., Landowska, A., Szwoch, M., Szwoch, W., & Wrobel, M. R. (2014). Emotion recognition and its applications. In *Human-Computer Systems Interaction: Backgrounds and Applications 3* (pp. 51–62). Springer.

Kumar, R., Sundaram, M., & Arumugam, N. (2021). Facial emotion recognition using subband selective multilevel stationary wavelet gradient transform and fuzzy support vector machine. *The Visual Computer*, *37*(8), 2315–2329. doi:10.100700371-020-01988-1

Lang, P. J., Bradley, M. M., & Cuthbert, B. N. (1997). International affective picture system (IAPS): Technical manual and affective ratings. NIMH Center for the Study of Emotion and Attention, 1(39-58), 3.

Li, W., Zhang, Z., & Song, A. (2021). Physiological-signal-based emotion recognition: An odyssey from methodology to philosophy. *Measurement*, *172*, 108747. doi:10.1016/j.measurement.2020.108747

Li, X., Li, X., Zheng, X., & Zhang, D. (2010). EMD-TEO based speech emotion recognition. In *Life System Modeling and Intelligent Computing* (pp. 180–189). Springer. doi:10.1007/978-3-642-15597-0_20

Li, Y., Huang, J., Zhou, H., & Zhong, N. (2017). Human emotion recognition with electroencephalographic multidimensional features by hybrid deep neural networks. *Applied Sciences (Basel, Switzerland)*, *7*(10), 1060. doi:10.3390/app7101060

Li, Z., Tian, X., Shu, L., Xu, X., & Hu, B. (2017, August). Emotion recognition from EEG using RASM and LSTM. *In International Conference on Internet Multimedia Computing and Service* (pp. 310-318). Springer.

Liao, S., Jain, A. K., & Li, S. Z. (2015). A fast and accurate unconstrained face detector. *IEEE Transactions on Pattern Analysis and Machine Intelligence*, *38*(2), 211–223. doi:10.1109/TPAMI.2015.2448075 PMID:26761729

Lin, Y. P., Wang, C. H., Jung, T. P., Wu, T. L., Jeng, S. K., Duann, J. R., & Chen, J. H. (2010). EEG-based emotion recognition in music listening. *IEEE Transactions on Biomedical Engineering*, *57*(7), 1798–1806. doi:10.1109/TBME.2010.2048568 PMID:20442037

Martínez-Tejada, L. A., Puertas-González, A., Yoshimura, N., & Koike, Y. (2021). Exploring EEG Characteristics to Identify Emotional Reactions under Videogame Scenarios. *Brain Sciences*, *11*(3), 378. doi:10.3390/brainsci11030378 PMID:33809797

McCraty, R. (2015). *Science of the heart: Exploring the role of the heart in human performance*. HeartMath Institute.

Mert, A., & Akan, A. (2018). Emotion recognition based on time–frequency distribution of EEG signals using multivariate synchrosqueezing transform. *Digital Signal Processing*, *81*, 106–115. doi:10.1016/j.dsp.2018.07.003

Mühl, C., Allison, B., Nijholt, A., & Chanel, G. (2014). A survey of affective brain computer interfaces: Principles, state-of-the-art, and challenges. *Brain-Computer Interfaces*, *1*(2), 66–84. doi:10.1080/2326263X.2014.912881

Ojansivu, V., & Heikkilä, J. (2008). Blur insensitive texture classification using local phase quantization. In *International Conference On Image And Signal Processing*. Springer. 10.1007/978-3-540-69905-7_27

Palo, H. K., & Mohanty, M. N. (2018). Wavelet-based feature combination for recognition of emotions. *Ain Shams Engineering Journal*, *9*(4), 1799–1806. doi:10.1016/j.asej.2016.11.001

Panahi, F., Rashidi, S., & Sheikhani, A. (2021). Application of fractional Fourier transform in feature extraction from electrocardiogram and galvanic skin response for emotion recognition. *Biomedical Signal Processing and Control*, *69*, 102863. doi:10.1016/j.bspc.2021.102863

Philippot, P., Chapelle, G., & Blairy, S. (2002). Respiratory feedback in the generation of emotion. *Cognition and Emotion*, *16*(5), 605–627. doi:10.1080/02699930143000392

Picard, R. W., Vyzas, E., & Healey, J. (2001). Toward Machine Emotional Intelligence: Analysis of Affective Physiological State. *IEEE Transactions on Pattern Analysis and Machine Intelligence*, *23*(10), 1175–1191. doi:10.1109/34.954607

Rößler, J., Sun, J., & Gloor, P. (2021). Reducing Videoconferencing Fatigue through Facial Emotion Recognition. *Future Internet*, *13*(5), 126. doi:10.3390/fi13050126

Salovey, P., & Mayer, J. D. (1990). Emotional intelligence. *Imagination, Cognition and Personality*, *9*(3), 185–211. doi:10.2190/DUGG-P24E-52WK-6CDG

Saragih, J. M., Lucey, S., & Cohn, J. F. (2009). Face alignment through subspace constrained mean-shifts. In *2009 IEEE 12th International Conference on Computer Vision* (pp. 1034-1041). 10.1109/ICCV.2009.5459377

Sariyanidi, E., Gunes, H., & Cavallaro, A. (2014). Automatic analysis of facial affect: A survey of registration, representation, and recognition. *IEEE Transactions on Pattern Analysis and Machine Intelligence*, *37*(6), 1113–1133. doi:10.1109/TPAMI.2014.2366127 PMID:26357337

Selesnick, I. W. (2011). Wavelet transform with tunable Q-factor. *IEEE Transactions on Signal Processing*, *59*(8), 3560–3575. doi:10.1109/TSP.2011.2143711

Šimić, G., Tkalčić, M., Vukić, V., Mulc, D., Španić, E., Šagud, M., & ... & R Hof, P. (. (2021). Understanding Emotions: Origins and Roles of the Amygdala. *Biomolecules*, *11*(6), 823. doi:10.3390/biom11060823 PMID:34072960

Suykens, J. A., & Vandewalle, J. (1999). Least squares support vector machine classifiers. *Neural Processing Letters*, *9*(3), 293–300. doi:10.1023/A:1018628609742

Tuncer, T., Dogan, S., & Subasi, A. (2021). A new fractal pattern feature generation function based emotion recognition method using EEG. *Chaos, Solitons, and Fractals*, *144*, 110671. doi:10.1016/j.chaos.2021.110671

Ullah, H., Uzair, M., Mahmood, A., Ullah, M., Khan, S. D., & Cheikh, F. A. (2019). Internal emotion classification using EEG signal with sparse discriminative ensemble. *IEEE Access: Practical Innovations, Open Solutions*, *7*, 40144–40153. doi:10.1109/ACCESS.2019.2904400

Vasquez-Correa, J. C., Arias-Vergara, T., Orozco-Arroyave, J. R., Vargas-Bonilla, J. F., & Noeth, E. (2016, October). Wavelet-based time-frequency representations for automatic recognition of emotions from speech. In *Speech Communication; 12. ITG Symposium* (pp. 1-5). VDE.

Viola, P. A., & Jones, M. J. (2001). Rapid object detection using a boosted cascade of simple features. *Proceedings of the 2001 IEEE Computer Society Conference on Computer Vision and Pattern Recognition*, *1*, I-I. 10.1109/CVPR.2001.990517

Wang, F., Wu, S., Zhang, W., Xu, Z., Zhang, Y., Wu, C., & Coleman, S. (2020). Emotion recognition with convolutional neural network and EEG-based EFDMs. *Neuropsychologia*, *146*, 107506. doi:10.1016/j.neuropsychologia.2020.107506 PMID:32497532

Watson, D., Clark, L. A., & Tellegen, A. (1988). Development and validation of brief measures of positive and negative affect: The PANAS scales. *Journal of Personality and Social Psychology*, *54*(6), 1063–1070. doi:10.1037/0022-3514.54.6.1063 PMID:3397865

Wei, C., Chen, L. L., Song, Z. Z., Lou, X. G., & Li, D. D. (2020). EEG-based emotion recognition using simple recurrent units network and ensemble learning. *Biomedical Signal Processing and Control*, *58*, 101756. doi:10.1016/j.bspc.2019.101756

Wu, G., Liu, G., & Hao, M. (2010). The analysis of emotion recognition from GSR based on PSO. In *International Symposium on Intelligence Information Processing and Trusted Computing* (pp. 360-363). IEEE. 10.1109/IPTC.2010.60

Xiefeng, C., Wang, Y., Dai, S., Zhao, P., & Liu, Q. (2019). Heart sound signals can be used for emotion recognition. *Scientific Reports*, *9*(1), 1–11. doi:10.103841598-019-42826-2 PMID:31019217

Xu, D., & Erdogmuns, D. (2010). Renyi's entropy, divergence and their nonparametric estimators. In *Information Theoretic Learning* (pp. 47–102). Springer. doi:10.1007/978-1-4419-1570-2_2

Yang, W., Makita, K., Nakao, T., Kanayama, N., Machizawa, M. G., Sasaoka, T., Sugata, A., Kobayashi, R., Hiramoto, R., Yamawaki, S., Iwanaga, M., & Miyatani, M. (2018). Affective auditory stimulus database: An expanded version of the International Affective Digitized Sounds (IADS-E). *Behavior Research Methods*, *50*(4), 1415–1429. doi:10.375813428-018-1027-6 PMID:29520632

Zhang, K., Zhang, Z., Li, Z., & Qiao, Y. (2016). Joint face detection and alignment using multitask cascaded convolutional networks. *IEEE Signal Processing Letters*, *23*(10), 1499–1503. doi:10.1109/LSP.2016.2603342

Zhang, Q., Chen, X., Zhan, Q., Yang, T., & Xia, S. (2017). Respiration-based emotion recognition with deep learning. *Computers in Industry*, *92*, 84–90. doi:10.1016/j.compind.2017.04.005

Zhang, W., Wang, F., Jiang, Y., Xu, Z., Wu, S., & Zhang, Y. (2019). Cross-subject EEG-based emotion recognition with deep domain confusion. In *International Conference On Intelligent Robotics And Applications* (pp. 558-570). Springer. 10.1007/978-3-030-27526-6_49

Zhang, Y. D., Yang, Z. J., Lu, H. M., Zhou, X. X., Phillips, P., Liu, Q. M., & Wang, S. H. (2016). Facial emotion recognition based on biorthogonal wavelet entropy, fuzzy support vector machine, and stratified cross validation. *IEEE Access: Practical Innovations, Open Solutions*, *4*, 8375–8385. doi:10.1109/ACCESS.2016.2628407

Zheng, W. (2016). Multichannel EEG-based emotion recognition via group sparse canonical correlation analysis. *IEEE Transactions on Cognitive and Developmental Systems*, *9*(3), 281–290. doi:10.1109/TCDS.2016.2587290

Zheng, W. L., & Lu, B. L. (2015). Investigating critical frequency bands and channels for EEG-based emotion recognition with deep neural networks. *IEEE Transactions on Autonomous Mental Development*, *7*(3), 162–175. doi:10.1109/TAMD.2015.2431497

Zhong, P., Wang, D., & Miao, C. (2020). EEG-based emotion recognition using regularized graph neural networks. *IEEE Transactions on Affective Computing*, 1. doi:10.1109/TAFFC.2020.2994159

Chapter 12
Empirical Wavelet Transform-Based Framework for Diagnosis of Epilepsy Using EEG Signals

Sibghatullah I. Khan
Sreenidhi Institute of Science and Technology, Hyderabad, India

Ram Bilas Pachori
Indian Institute of Technology, Indore, India

ABSTRACT

In the chapter, a novel yet simple method for classifying EEG signals associated with normal and epileptic seizure categories has been proposed. The proposed method is based on empirical wavelet transform (EWT). The non-stationarity in the EEG signal has been captured using EWT, and subsequently, the common minimum number of modes have been determined for each EEG signal. Features based on amplitude envelopes of EEG signals have been computed. The Kruskal-Wallis statistical test has been used to confirm the discrimination ability of feature space. For classification, various classifiers, namely K-nearest neighbor (KNN), support vector machine (SVM), and decision tree (DT), have been used. The maximum classification accuracy of 98.67% is achieved with the K-nearest neighbor (KNN) classifier. The proposed approach has utilized only two features, which makes the proposed approach simpler. The proposed approach thus can be used in real-time applications.

INTRODUCTION

Epileptic seizures are human brain disorders that can affect individuals form all ages. Globally, approximately 45.9 million people have epilepsy (Beghi et al., 2019). To access neurological activities, electroencephalogram (EEG) signals are used. The EEG signal's spikes are frequently considered as the indicator of brain disorders like epilepsy (Mukhopadhyay & Ray, 1998; Ray, 1994). The classical strategy to diagnose epilepsy from EEG signals involves the expert's visual inspection, which is often

DOI: 10.4018/978-1-6684-3947-0.ch012

time-consuming and cumbersome. Therefore, various methods to process EEG signals have been reported for detecting epileptic seizures automatically in the literature.

Broadly, these methods make use of time-domain analysis, frequency domain analysis, and time-frequency analysis (Acharya et al., 2013). Line length and energy features have been used to detect epileptic seizures from EEG signals (Tessy et al., 2017). Features based on linear prediction (LP) have been proposed to detect epileptic seizures from EEG signals (Altunay et al., 2010). In (Ghosh-Dastidar et al., 2008), principal component analysis (PCA) has been used for the detection of epileptic seizures from EEG signals. With the presumption of stationarity in the EEG signals, authors in (Polat & Güneş, 2007; Srinivasan et al., 2005), have proposed time-domain and frequency-domain features to classify epileptic seizures from EEG signals. The EEG signals have non-stationary behavior (Boashash et al., 2003; Nishad & Pachori, 2020).

Taking the non-stationarity behavior of EEG signals into consideration, authors in (Tzallas et al., 2007, 2009) have developed time-frequency-based techniques to analyze and classify epileptic seizures from EEG signals. Numerous approaches based on wavelet and multi-wavelet transform have been developed to classify epileptic seizures from EEG signals (Akut, 2019; Anuragi et al., 2021; Khan et al., 2020; Nishad & Pachori, 2020; Sharan & Berkovsky, 2020; Uthayakumar & Easwaramoorthy, 2013; Zeng et al., 2020). Moreover, wavelet coefficients with phase space reconstruction (PSR) based features have been utilized to construct feature space to detect epileptic seizures from EEG signals (Lee et al., 2014). Various non-linear features inspired from chaotic signal processing, like, correlation dimension (Silva et al., 1999), Lyapunov exponent (Swiderski et al., 2005), and approximate entropy (ApEn) (Gupta & Pachori, 2019), are effective in detecting epileptic EEG signals (Srinivasan et al., 2007). Additionally, the Lyapunov exponent has been used to describe EEG signal's chaotic nature; consequently, the Lyapunov exponent has been used to discriminate epileptic seizure and seizure-free EEG signals (Swiderski et al., 2005). To quantify the neural functioning during interictal (seizure-free) and ictal (seizure) activities, the correlation dimension from the EEG signal has been used (Lehnertz & Elger, 1995). Furthermore, the human brain's ictal and interictal activities have been successfully discriminated against using fractal dimension parameters (Accardo et al., 1997). The higher-order spectral (HOS) analysis of EEG signals has been carried out to classify normal, ictal, and interictal activities in the human brain (Chua et al., 2007). Authors in (Acharya et al., 2011) have proposed features obtained from recurrence quantification analysis (RQA) to classify normal, ictal, and interictal EEG signals. To discriminate EEG signals in normal, pre-ictal, and epileptic seizure categories, authors in (Acharya et al., 2009) have used Hurst exponent, correlation dimension, and ApEn as features, and promising results were obtained. In (Wang et al., 2010), the ApEn parameter was computed, and a significant difference in ApEn values has been observed for epileptic seizures and normal EEG signals. In (Liang et al., 2010), the authors have used the spectral features with ApEn to classify EEG signals in normal, ictal, and interictal categories. Empirical mode decomposition (EMD) has been found to be useful in the analysis of EEG signals (Oweis & Abdulhay, 2011). In (Oweis & Abdulhay, 2011), it has been found that the weighted mean frequency of intrinsic mode functions (IMFs) differs significantly for EEG signals associated with normal and epileptic seizure categories. In (de la O Serna et al., 2020), the authors have suggested the filter bank approach based on the Tylor-Fourier series for analyzing EEG signals.

Identification of patterns in the ictal EEG signals is carried out in (Li et al., 2013) using fluctuation index and coefficients of variation, computed from the IMFs of the EEG signals. In (Akbari & Esmaili, 2020), the EEG signals associated with ictal, interictal, and normal categories have been analyzed and subsequently classified using two-dimensional phase space reconstruction-based geometrical features.

Recently, various deep learning approaches have been used to classify the EEG signals (Craik et al., 2019; Sharma et al., 2020). A deep learning method based on long short-term memory (LSTM) has been used to detect epileptic seizures from EEG signals (Tsiouris et al., 2018).

In the present study, the key contribution is the feature extraction process of EEG signals using EWT followed by taking the product of maximum and mean value of the amplitude envelope of intrinsic modes (IMs). To obtain the geometrical characteristics of IMs, first, the maximum and mean value amplitude envelopes of IMs have been computed. Finally, the product of maximum and mean values have been taken for each mode to obtain the feature set. This procedure resulted in two-dimensional feature space, over which various basic classifiers to classify EEG signals into normal and epileptic seizure categories have been used. The proposed methodology is presented in Fig. 1.

METHODOLOGY

Dataset

The dataset described in (Andrzejak et al., 2001) is used in this study. This dataset is provided by the University of Bonn, and it is available publicly online. There are five subsets in the dataset, namely, Z, O, N, F, and S. The dataset has 100 EEG recordings for each subset which have been recorded from healthy and epilepsy subjects. The duration of each EEG signal is 23.6 seconds. These EEG signals were sampled at a rate of 173.61 Hz. The subsets N, F, and S correspond to the EEG signals of epileptic subjects. The subset N and F contains recordings in seizure-free intervals pertaining to five subjects. The signals in subset F have been recorded from the epileptogenic zone, whereas the signals in the N subset are recorded from hippocampal formation. Subset S contains seizure activities in the EEG signal. The EEG signals in subset Z and O are recorded from five healthy subjects with surface EEG using the standard electrode placement scheme (Andrzejak et al., 2001). In the present chapter, the subsets Z, O, and S have been used to evaluate the proposed approach's performance.

Figure 1. The proposed methodology to classify EEG signals in normal and epileptic seizure categories

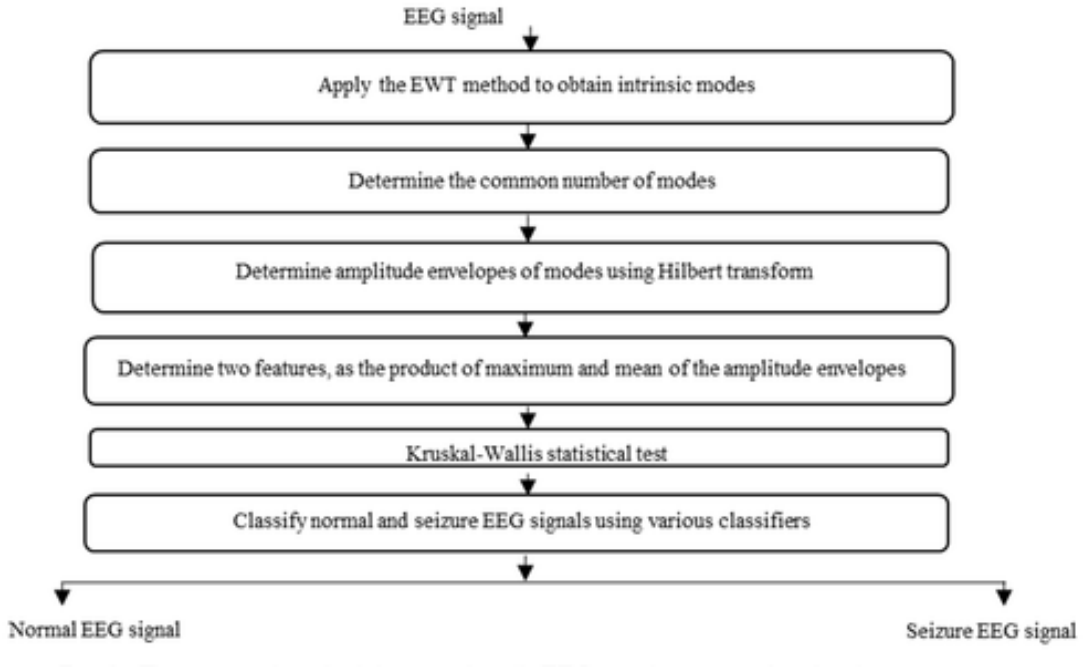

Moreover, subset S which constitutes the seizure class of EEG signals has been included, whereas subsets Z and O have been combined to constitute the normal class of EEG signals. Furthermore, each EEG signal for the window size of 500, 1000, 2000, and 4000 samples has been segmented and consequently, they have been processed.

Empirical Wavelet Transform (EWT)

The empirical wavelet transform (EWT) is an adaptive type of decomposition method wherein the signal's amplitude modulated-frequency modulated (AM-FM) components are extracted [45]. The EWT utilizes compact Fourier support in obtaining an adaptive wavelet filter bank. Following are the important steps required to obtain EWT of the signal (Gilles, 2013):

Step 1: Obtain the frequency spectrum of discrete signal $s(t)$ using Fourier transform, where, $t=\{t_i\}$, $i=1,2,3,\ldots,n$, and n is the total number of samples in $s(t)$. The frequency range of the spectrum is $[0,\pi]$.

Step 2: The frequency spectrum is then segmented into N adjoining segments. EWT boundary detection algorithm (Gilles, 2013) is used to segment the frequency spectrum. This procedure determines the boundary frequencies $\left\{\xi_i\right\}_{i=0\ldots N}$. The boundary frequencies are $\xi 0$ and ξN, respectively (Gilles, 2013). The segments of frequency spectrum are $[0,\xi 0], [\Omega 1,\xi_2],\ldots,[\xi_{N-1}\pi]$.

S**tep 3: O**ver each segment, apply the Littlewood-Paley and Meyer's wavelets as the bandpass filters to generate the empirical wavelet-based filter (Daubechies, 1992). The empirical scaling and wavelet function can be respectively expressed by (1) and (2), (Gilles, 2013) as,

$$\Psi_i\left(\xi\right)=\begin{cases}1, & if\left|\xi\right|\le\left(1-\theta\right)\xi_i\\ \cos\left[\dfrac{\pi\Theta(\theta,\xi_i}{2}\right], & if\left(1-\theta\right)\xi_i\le\left|\xi\right|\le\left(1+\theta\right)\xi_i\\ 0, & otherwise\end{cases}\tag{1}$$

$$\Omega_i\left(\xi\right)=\begin{cases}1,\\ if\left(1+\theta\right)\xi_i\le\left|\xi\right|\le\left(1-\theta\right)\xi_{i+1}\\ \cos\left[\dfrac{\pi\Theta(\theta,\ \xi_{i+1}}{2}\right],\\ if\left(1-\theta\right)\xi_{i+1}\le\left|\xi\right|\le\left(1+\theta\right)\xi_{i+1}\\ \sin\left[\dfrac{\pi\Theta(\theta,\ \xi_i}{2}\right],\\ if\left(1-\theta\right)\xi_i\le\left|\xi\right|\le\left(1+\theta\right)\xi_i\\ 0,\ otherwise\end{cases}\tag{2}$$

where,

$$\Theta\left(\theta,\xi_i\right)=\alpha\left[\frac{\left(\left|\xi\right|-\left(1-\theta\right)\xi_i\right.}{2\theta\xi_i}\right]\tag{3}$$

In the above expression, the parameter θ ensures the tight framing of empirical wavelet and scaling function in $L^2\left(\mathfrak{R}\right)$. The expression for the condition of the tight frame is given as (Gilles, 2013),

$$\theta<\min_i\left(\frac{\xi_{i+1}-\xi_i}{\xi_{i+1}+\xi_i}\right)\tag{4}$$

The definition of an arbitrary function $\alpha(z)$ is given as (Gilles, 2013),

$$\alpha\left(z\right)\begin{cases}0, & if\ z\le 0\\ and\,\alpha\left(z\right)+\alpha\left(1-z\right)=1,\ \forall z\in\left[0\ 1\right] & \\ 1, & if\ z\ge 1\end{cases}\tag{5}$$

The approximation and detail coefficients of applied signal $s(t)$ were found by taking the inner product of $s(t)$ with the wavelet and scaling functions.

By applying the Hilbert transform, the signal can be represented in the time-frequency domain. The next section provides the details of the envelope extraction process using the Hilbert transform.

Envelope Extraction using Hilbert Transform

To compute the envelope of modes, the Hilbert transform has been used. The Hilbert transform of a real, band limited signal $s(t)$ is defined as (Huang, 2014),

$$\hat{s}\left(t\right) = H\left[s\left(t\right)\right] = \frac{1}{\pi} C \int_{-\infty}^{+\infty} \frac{s\left(\tau\right)}{t-\tau} d\tau \tag{6}$$

where C denotes Cauchy principal value. The complex-valued signal $m(t)$ is given as,

$$m\left(t\right) = s\left(t\right) + j\hat{s}\left(t\right) \tag{7}$$

Additionally, the signal $m(t)$ in its analytic form can be written as,

$$m\left(t\right) = \left|m\left(t\right)\right| e^{-j\varnothing\left(t\right)} \tag{8}$$

where,

$$\varnothing\left(t\right) = \arctan \frac{\hat{s}\left(t\right)}{s\left(t\right)} \tag{9}$$

$$\left|m\left(t\right)\right| = \left[s^2\left(t\right) + \hat{s}^2\left(t\right)\right]^{\frac{1}{2}} \tag{10}$$

The $|m(t)|$ is the envelope of signal $s(t)$. In this study, the mean and maximum values of the envelope have been computed for each mode obtained through EWT. Hereafter, the amplitude envelope will be represented by A_E.

Let the maximum value of the p^{th} mode's envelope is $A_{\text{max}p}$. For each envelope, maximum and mean values have been computed as A_{max1}, $\max\{A_{E1}\}$, A_{max2}, $\max\{A_{E2}\}$, A_{max3}, $\max\{A_{E3}\}$, $A_{\text{max}p}$, $\max\{A_{EP}\}$ where $A_{\text{max1}},\ldots,A_{\text{max}p}$ are the maximum values of the amplitude envelopes of respective modes from $A_{E1}\ldots A_{EP}$.

Similarly, the mean value of amplitude envelopes for each mode has been computed as A_{mean1}, $\text{mean}\{A_{E1}\}$, A_{mean2}, $\text{mean}\{A_{E2}\}$, A_{mean3}, $\text{mean}\{A_{E3}\}$, $A_{\text{mean}p}$, $\text{mean}\{A_{EP}\}$ where, $A_{\text{mean1}},\ldots,A_{\text{mean}p}$ are the mean values of the amplitude envelopes of respective modes from $A_{E1}\ldots A_{EP}$. The P is the common number of modes for the studied EEG signals.

Finally, the product of these values has been computed as follows:

$$F_{\max} = \prod_{p=1}^{P} A_{\max p} \tag{11}$$

$$F_{\text{mean}} = \prod_{p=1}^{P} A_{\text{mean}p} \tag{12}$$

Classification

Several factors influence the efficiency of conventional classifiers. Hence, it should be addressed both during the development of the mathematical model and the generalization of actual data analysis. The distribution of data in the feature space, the balance of class data samples, variability, the diversity of training data, and the existence of noise are the most significant considerations. In addition, relative benefits and drawbacks compared to others arise for each classifier. For e.g., a memory-based learning method is K-nearest neighbor (KNN) (Xu et al., 2013), wherein, the availability of train and test data is necessary. The support vector machine (SVM) classifier has been effective in classifying linear and non-linear features space (Axelberg et al., 2007). The decision tree classifier has been proven effective in classifying noisy data (Mantas & Abellán, 2014).

In the present work, using the cross-validation methodology, the output of various typical classifiers has been checked on the features extracted from the dataset.

Figure 2. First 14 IMs of normal EEG signal

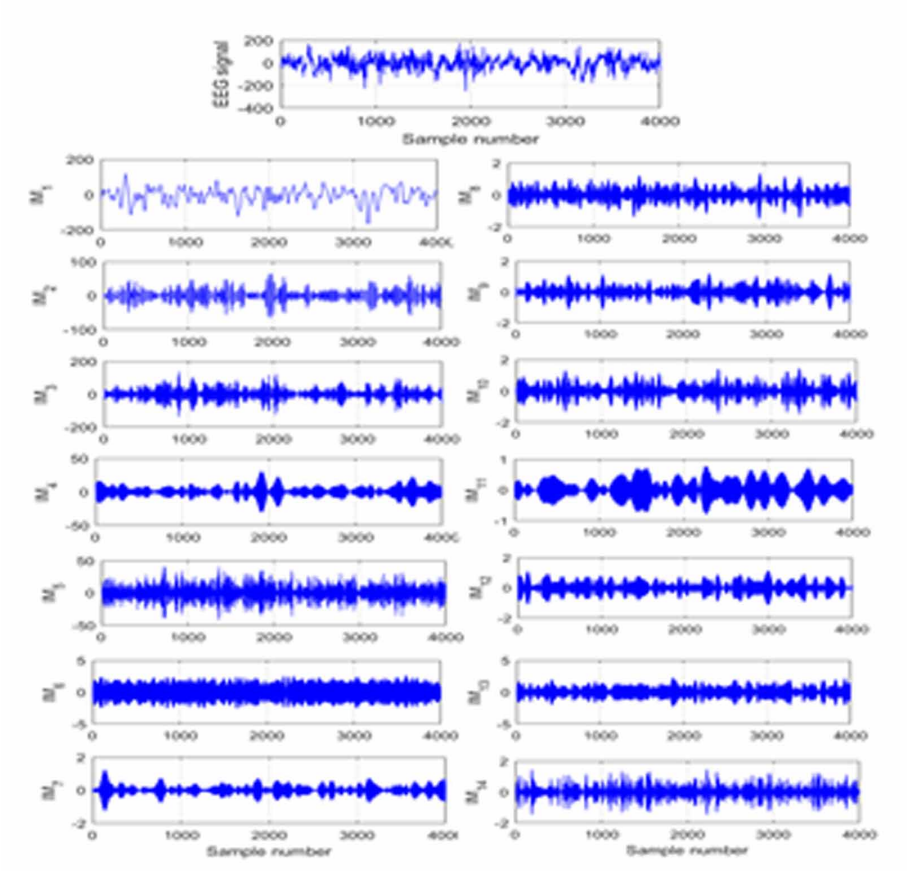

Figure 3. Amplitude envelopes of first 14 IMs for normal EEG signal

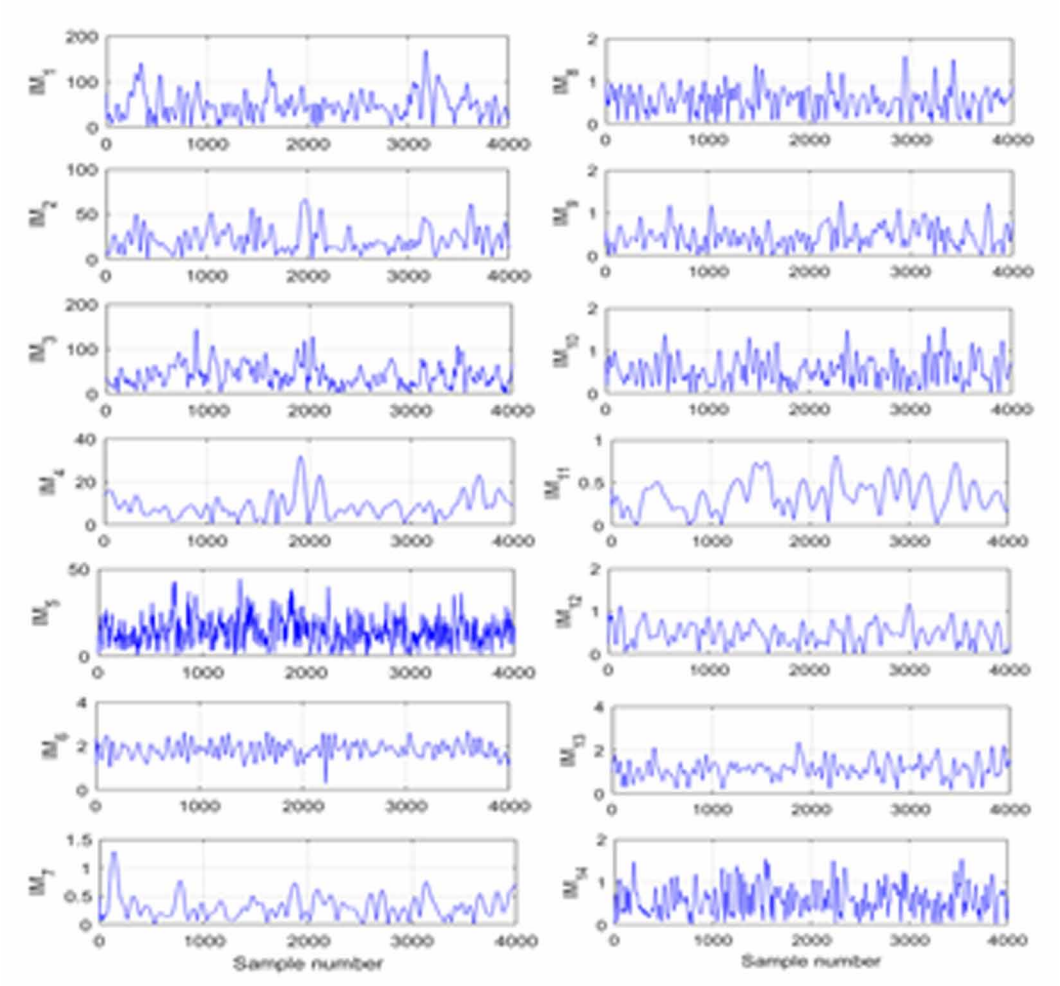

Figure 4. First 14 IMs of epileptic seizure EEG signal

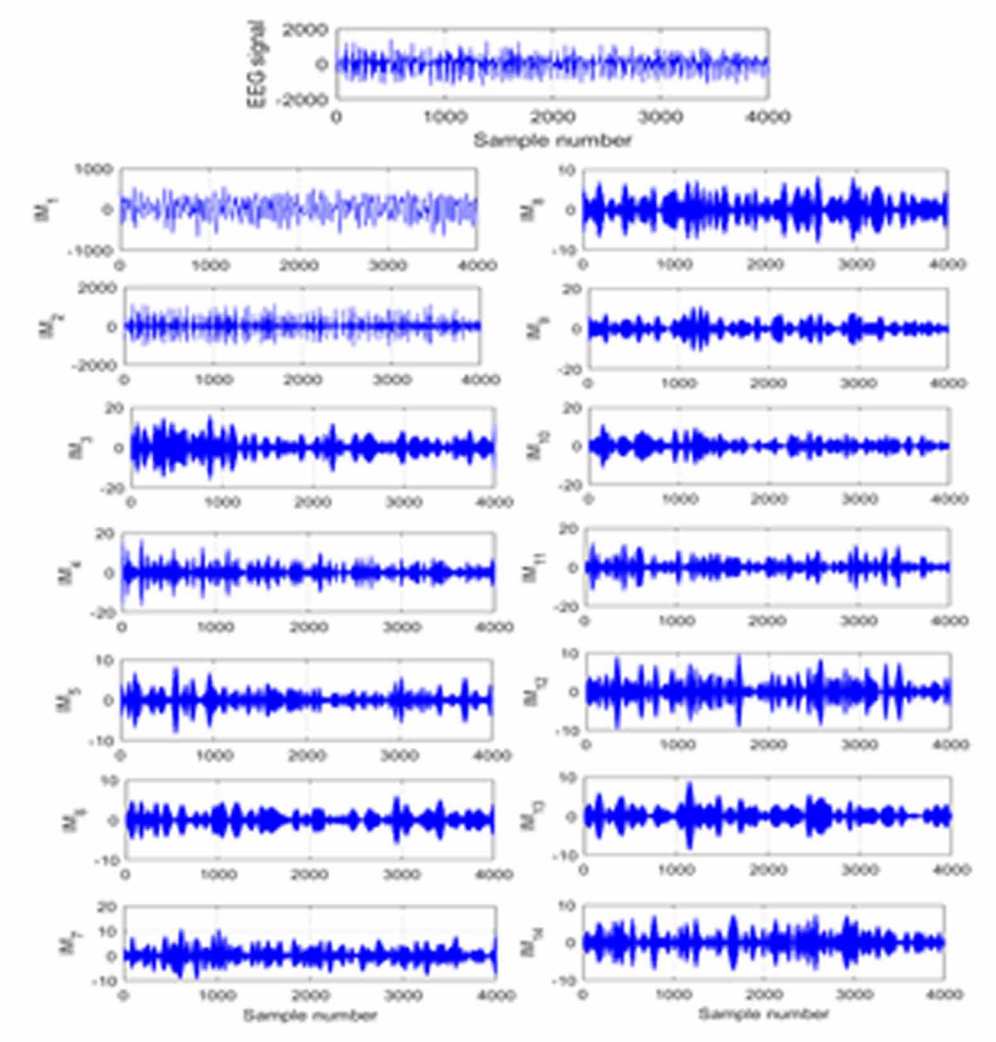

Figure 5. Amplitude envelopes of first 14 IMs for epileptic seizure EEG signal

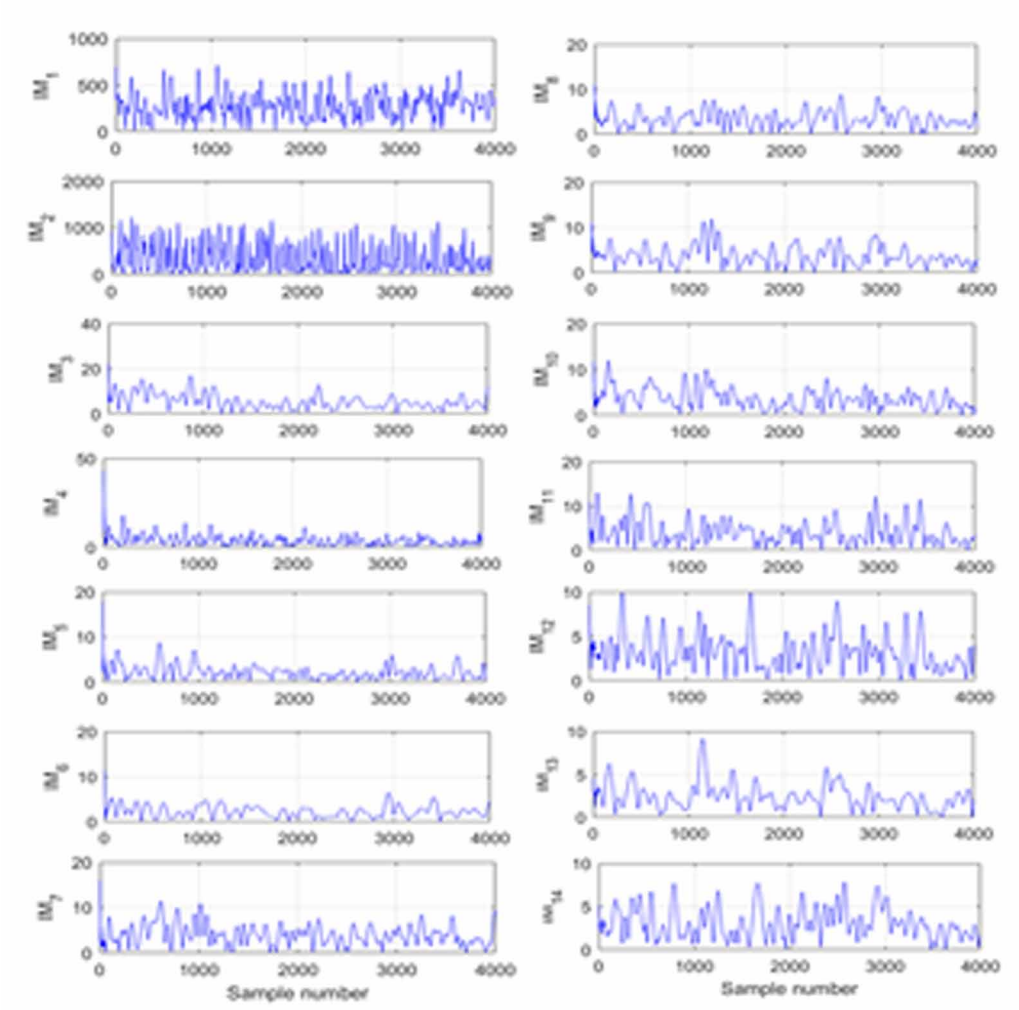

In the present study, the performance of the classifier has been evaluated using various performance measures. The definitions of these performance measures are given below:

1. Sensitivity (SEN)- It is given as,

$$\mathrm{SEN} = \frac{\mathrm{TP}}{\mathrm{TP} + \mathrm{FN}} \times 100\% \tag{13}$$

where, TP denotes correctly identified positive instances and FN denotes the incorrectly identified negative instances. The SEN measures the classifiers ability to predict the correct positive class labels (Wong & Lim, 2011).

2. Specificity (SPE)- It can be defined by,

$$\mathrm{SPE} = \frac{\mathrm{TN}}{\mathrm{TN} + \mathrm{FP}} \times 100\% \tag{14}$$

where, TN denotes the true positive labels and FP denotes the false positive labels. The SPE measures the classifier's ability to correctly predict the negative instances (Wong & Lim, 2011).

3. Accuracy (ACC)- It is stated as follows (Wong & Lim, 2011):

$$\mathrm{ACC} = \frac{\mathrm{TP} + \mathrm{TN}}{\mathrm{TP} + \mathrm{TN} + \mathrm{FP} + \mathrm{FN}} \times 100\% \text{ (15).}$$

The ACC quantifies the classifiers' overall ability to classify the positive and negative instances correctly.

4. Positive predictive value (PPV)- It is expressed as,

$$\mathrm{PPV} = \frac{\mathrm{TP}}{\mathrm{TP} + \mathrm{FP}} \times 100\% \tag{16}$$

It quantifies the classifier model's ability to identify positive instances out of total positive samples (Wong & Lim, 2011).

5. Negative predictive value (NPV)- Mathematically, it can be defined as,

$$\mathrm{NPV} = \frac{\mathrm{TP}}{\mathrm{TP} + \mathrm{FN}} \times 100\% \tag{17}$$

Contrary to PPV, it quantifies the classifier's ability to identify negative instances from total negative space (Gorodkin, 2004).

6. Mathew's correlation coefficient (MCC)- It is the weighted harmonic mean of the PPV and SEN (Chicco & Jurman, 2020). It is expressed as,

$$\mathrm{MCC} = \frac{\mathrm{TP} \times \mathrm{TN} - \mathrm{FN} \times \mathrm{FP}}{\sqrt{\big(\mathrm{TP} + \mathrm{FN}\big)\big(\mathrm{TP} + \mathrm{FP}\big)\big(\mathrm{TN} + \mathrm{FN}\big)\big(\mathrm{TN} + \mathrm{FP}\big)}} \tag{18}$$

Table 1. Description of the classifiers used in this study

Classifier		Parameter
KNN (Xu et al., 2013)	Euclidian	K=5, Euclidian distance, equal distance weight.
	Cosine	K=5, cosine distance, equal distance weight.
	Cubic	K=5, cubic distance, equal distance weight.
SVM (Axelberg et al., 2007)	Linear	Linear kernel, box constraint level =1, Sequential minimal optimization (SMO) solver.
	Gaussian	Gaussian kernel, box constraint level =1, SMO solver.
	Quadratic	Quadratic kernel, box constraint level =1, SMO solver.
DT (Mantas & Abellán, 2014)	Gini diversity index	Split criterion = Gini diversity index, maximum number of splits= 2.

RESULTS

At first, all the EEG signals were passed through the EWT process. To ensure the feasibility and uniformity in the feature extraction process, the common number of modes were determined using the EWT process. The resultant common minimum number of modes for a window size of 500, 1000, 2000, and 4000 samples are 2, 4, 8, and 14, respectively. Following equation (10), modes of EEG signals have been computed, which is followed by the computation of amplitude envelope using Hilbert transform. The amplitude envelopes of EEG signals for normal and epileptic seizure categories with a window size of 4000 samples are illustrated in Fig. 3 and Fig. 5, respectively. From Figs 3 and 5, a significant difference between the amplitude envelopes associated with normal and epileptic seizure EEG signals is observed, hence to quantify the difference in the envelopes, two features from the amplitude envelope, namely, the maximum value and the mean value have been erected. The process is repeated for all the modes of a particular window size. Finally, the features were obtained by taking product as mentioned in equations (11) and (12). The graphical representation of these two features have been depicted in Fig. 6. From Fig. 6, the scatter plots show the separability between the two-feature set. The feature set's ability to discriminate EEG signals has been confirmed using the Kruskal-Wallis statistical test. The results of the Kruskal-Wallis statistical test are shown in Figs 7 and 8. From the Kruskal-Wallis statistical test, the significance (p) value for both the features obtained is 4.7×10^{-47} and 3.6×10^{-39} confirming the said feature set's discrimination ability. For the classification of a normal and epileptic seizure, EEG signals using computed feature sets, three types of classifiers, namely, KNN, SVM, and DT have been employed. The details of classifiers along with their parameter is given in Table 1. The experimental results of the classification task are tabulated in Table 2. The proposed method's effectiveness has been evaluated using the aforementioned performance measures.

Figure 6.

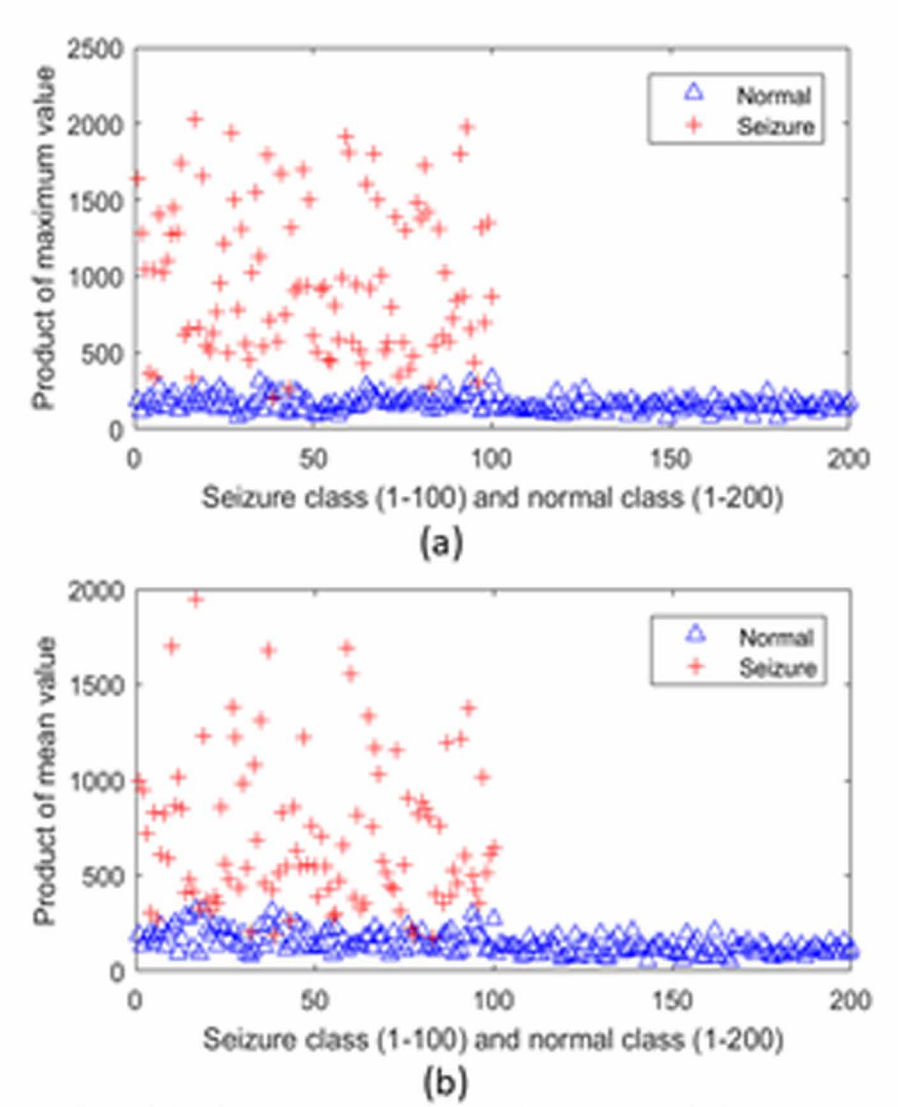

It can be observed from Table 2 that the performance of SVM reduces with the increase in kernel order. The higher-order kernels of the SVM are highly non-linear. As the feature space is linearly separable, the non-linear kernels tend to deviate, and hence decrease in the performance is observed. The sensitivity and PPV value in the case of the SVM classifier with a window size of 4000 samples gives the maximum value of 100%, which indicates the maximum separability for the two categories of EEG signals. The MCC quantifies the effectiveness of the classifier and its values range from -1 to +1, wherein, the -1 indicates the total disagreement in prediction and observation and vice versa (Chicco & Jurman, 2020). As with the increase in window size, the classifier performance has increased, hence the MCC has a high value for the higher value of window size. In Table 2, the entries highlighted in bold letters indicate the highest performance. The KNN classifier with Euclidian and cubic distance results

in the maximum classification ACC of 98.67% with SEN and SPE of 98% and 99%, respectively. The proposed methodology has been compared with existing methods in terms of classification accuracy, and it is listed in Table 3. It is evident from Table 3 that the proposed methodology is comparable and outperforms in some cases to the existing methods in terms of classification ACC over the same dataset.

Figure 7. Comparison of the normalized maximum value of amplitude envelope for a window size of 4000 samples ($p<0.05$)

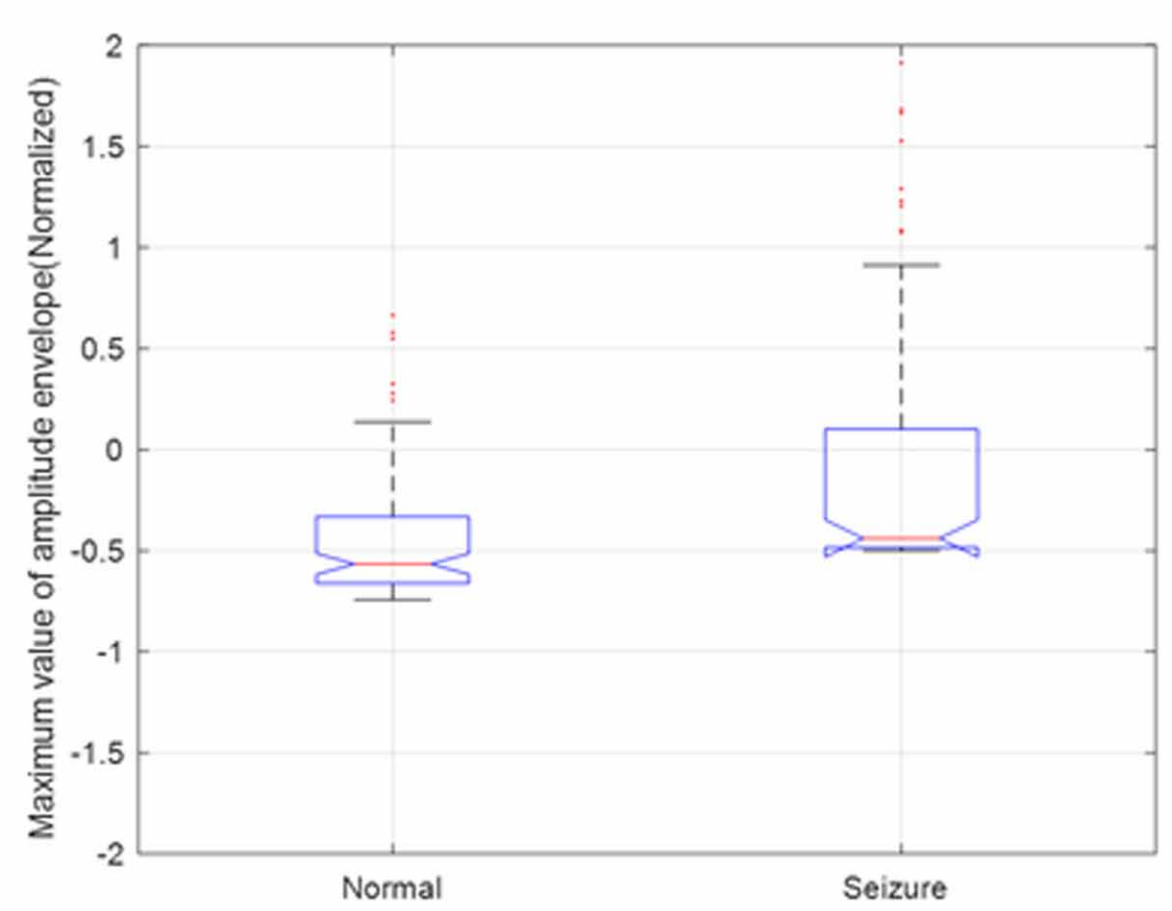

Figure 8. Comparison of the normalized mean value of amplitude envelope for a window size of 4000 samples ($p<0.05$)

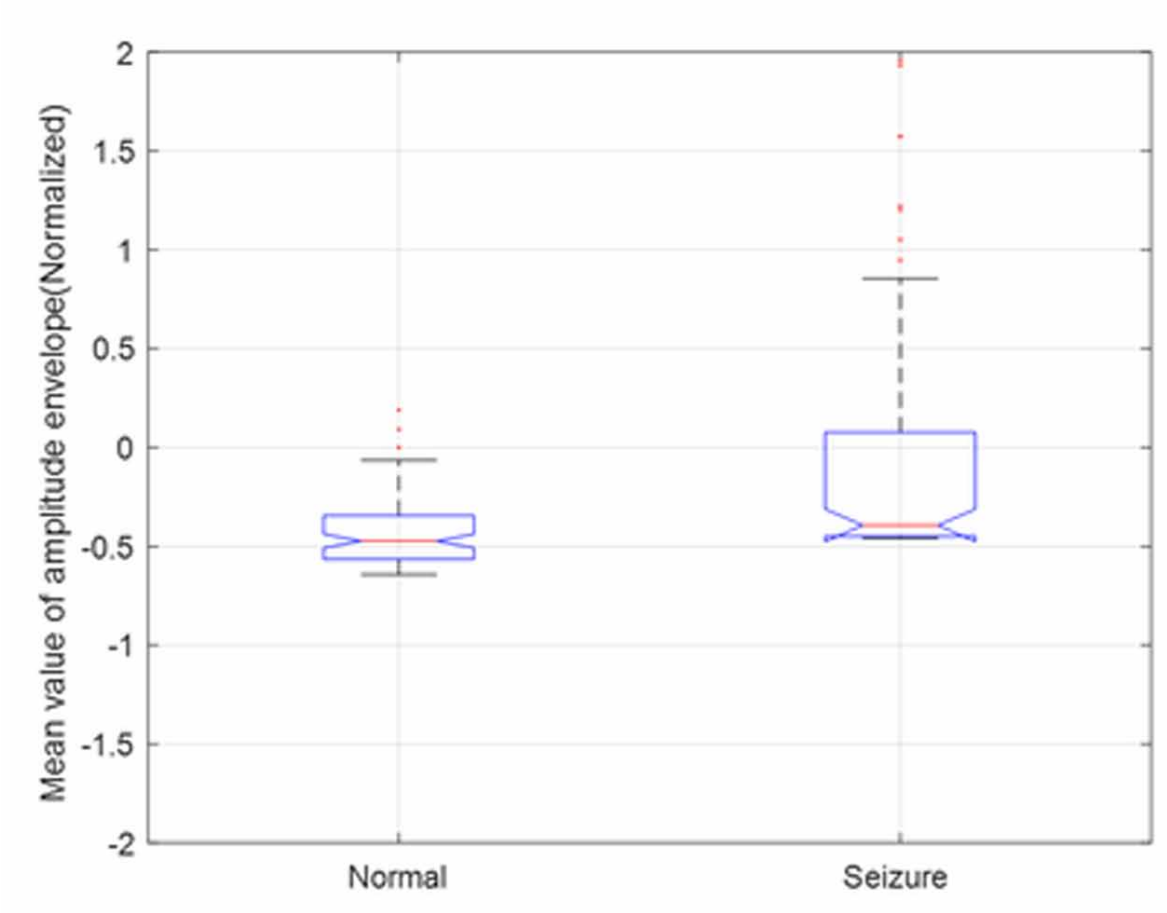

DISCUSSION

The EWT method is suitable for analyzing nonstationary signals (Bhattacharyya et al., 2018); hence, EWT's use to analyze nonstationary EEG signals is justified. The EWT process decomposes the EEG signals into the oscillatory and symmetric modes. The process of EWT can be considered as the adaptive sub-band filtering (Biju et al., 2017; Yang et al., 2007). The modes extracted through the EWT process have been placed in the ascending order of frequency, which means that the lower frequency modes are placed at top level. As each EEG signal contains various frequency components, it is not compelling to have the same number of modes for all EEG signals. Hence, it is important to determine the common minimum number for entire EEG dataset. The resultant common minimum number of modes for a window size of 500, 1000, 2000, and 4000 samples are 2, 4, 8, and 14, respectively. Figs 2 and 4 show all 14 IMs of normal and epileptic seizure EEG signals. Figs 3 and 5 depict the envelopes corresponding to the window size of 4000 samples for normal and epileptic seizure EEG signals. Figs 4 and 5 show an increase in amplitude for the seizure class of EEG signals. Hence, to quantify the shape of the envelope, its maximum and mean value have been computed. The amplitude envelope obtained the through

Hilbert transform has proven to be effective for extracting features (Kohavi, 1995). Moreover, due to higher amplitudes of IMs of seizure EEG signals, the mean and maximum value of amplitude envelopes are well suited to classify the EEG signals. The computed features, which have been obtained by taking the product improves the classification ability of the feature set. The significance and effectiveness of the computed feature set is confirmed using the Kruskal-Wallis statistical test ($p < 0.05$). To avoid the overfitting, the commonly used procedure is to use the k-fold cross validation strategy. In the k-fold cross validation, the data is divided randomly into k subsets of equal size (Kohavi, 1995). Now, the training and testing is carried out for k times, while considering each data subset as testing and remaining (k-1) data subsets as training. Finally, the results of all k iterations are averaged to measure the final performance of the classifier. For real world dataset, the k-fold cross validation has been widely used in the existing literature (Kohavi, 1995). In the present study, with k=10, ten-fold cross validation is used to assess the classifier performance.

The comparison of various classifiers has been carried out, and it has been found that the KNN classifier gives the maximum value of ACC along with other performance measures. KNN with a neighborhood distance of 5 has been used in this study. The robustness of the classifier has been tested using 10-fold cross-validation (Liu et al., 2020). From Table 2, it is observable that the KNN classifier with Euclidian and cosine distance parameters has resulted in maximum classification ACC. Similarly, significant improvement in the other performance measures has

been observed for the KNN classifier employing Euclidian and cosine distance. In the present work, different window sizes for EEG signals have been used. From Table 2, it is noticeable that the proposed analysis with a window size of 4000 samples has resulted in better classification ACC as compared to the window sizes of 500, 1000, and 2000 samples. Table 3 shows the comparison of some existing methods that have been used to classify EEG signals. Authors in (Liu et al., 2020) have used ordinal pattern-based feature extraction and KNN classifier for the classification of EEG signals. The maximum ACC attended by the study in (Liu et al., 2020) is 96%. In (Xue et al., 2020), the researchers carried out auto-weighted multi-view discrimination-based feature extraction to classify EEG signals into normal and seizure categories. In (Xue et al., 2020) the authors have reported the maximum classification ACC of 97%. In (Akyol, 2020), the authors have used a stacking ensemble-based deep learning approach to classify EEG signals in normal and seizure categories.

The author in (Akyol, 2020) have reported the classification ACC of 97.17%. In (Thara et al., 2021), the authors employed bidirectional long short-term memory (LSTM) based deep learning approach for classifying EEG signals into normal and seizure categories. The authors in (Thara et al., 2021) have achieved a classification ACC of 97.65%.

Reconstructed phase space images with convolution neural networks (Ilakiyaselvan et al., 2020) have been used to classify the EEG signals into normal and seizure categories.

Table 2. Performance of the classifiers for different window sizes

Window size (samples)	Classifier	Classifier parameter	ACC	SEN	SPE	NPV	PPV	MCC
500	KNN	Euclidian	80.33	74.70	82.49	62.00	89.50	0.54
		Cosine	69.33	54.55	75.47	48.00	80.00	0.29
		Cubic	80.33	75.00	82.87	63.00	89.50	0.55
	SVM	Linear	66.67	50.00	66.89	1.00	99.50	0.03
		Gaussian	51.00	28.83	64.02	32.00	60.50	-0.07
		Quadratic	48.67	34.30	67.97	59.00	43.50	0.02
	DT	Gini diversity index	83.33	85.71	82.61	60.00	95.00	0.61
1000	KNN	Euclidian	85.33	80.43	87.50	74.00	91.00	0.66
		Cosine	78.33	73.97	79.74	54.00	90.50	0.49
		Cubic	86.00	82.22	87.62	74.00	92.00	0.68
	SVM	Linear	66.67	50.00	66.78	1.00	99.50	0.03
		Gaussian	87.00	96.92	84.26	63.00	99.00	0.71
		Quadratic	43.00	28.22	60.58	46.00	41.50	-0.12
	DT	Gini diversity index	84.67	85.53	84.38	65.00	94.50	0.64
2000	KNN	Euclidian	91.00	92.94	90.23	79.00	97.00	0.80
		Cosine	87.67	81.82	90.55	81.00	91.00	0.72
		Cubic	90.67	92.86	89.81	78.00	97.00	0.79
	SVM	Linear	66.00	25.00	66.55	1.00	98.50	-0.02
		Gaussian	91.33	100.00	88.50	74.00	100.00	0.81
		Quadratic	65.00	47.75	75.13	53.00	71.00	0.23
	DT	Gini diversity index	92.67	100.00	90.09	78.00	100.00	0.84
4000	KNN	**Euclidian**	**98.67**	**98.00**	**99.00**	**98.00**	**99.00**	**0.97**
		Cosine	96.33	95.88	96.55	93.00	98.00	0.92
		Cubic	**98.67**	**98.00**	**99.00**	**98.00**	**99.00**	**0.97**
	SVM	Linear	92.33	100.00	89.69	77.00	100.00	0.83
		Gaussian	93.67	100.00	91.32	81.00	100.00	0.86
		Quadratic	93.00	100.00	90.50	79.00	100.00	0.85
	DT	Gini diversity index	98.00	97.96	98.02	96.00	99.00	0.95

Table 3. Comparison of the proposed method with existing methodologies to classify normal and epileptic seizure EEG signals on the same dataset

Authors	year	Approach used	ACC (%)
(Liu et al., 2020)	2020	Ordinal pattern with KNN classifier	96.00%
(Xue et al., 2020)	2020	Auto-weighted multi-view discriminative metric learning method	97.00%
(Akyol, 2020)	2020	Stacking ensemble-based deep neural networks	97.17%
(Thara et al., 2021)	2020	Bidirectional LSTM	97.65%
(Ilakiyaselvan et al., 2020)	2020	Reconstructed phase space images and CNN	98.50%
(Ravi Kumar & Srinivasa Rao, 2019)	2019	VMD	94.10%
Proposed method		EWT, amplitude envelope-based feature extraction, and KNN classifier	98.67%

The authors in (Ilakiyaselvan et al., 2020) have reported the classification ACC of 98.50%. In (Ravi Kumar & Srinivasa Rao, 2019), semantic variational mode decomposition (VMD) based features have been used to classify EEG signals. The authors in (Ravi Kumar & Srinivasa Rao, 2019) have reported a classification ACC of 94.10%. In (Bhattacharyya et al., 2017), the authors have used EWT followed by the computation of Hilbert marginal spectrum-based features such as spectral energy, Shannon entropy, and Renyi entropy for classifying EEG signals into seizure-free and seizure categories. In (Bhattacharyya et al., 2017), three features have been used, in contrast, in the present study, only two features are used. The authors in (Bhattacharyya et al., 2017) have achieved the classification ACC of 99.3% with 50% training and testing split of the data. In present work, 0.66% less ACC compared to (Bhattacharyya et al., 2017), but it is worth to note here that, we have used two features and classifier performance has been evaluated with 10-fold cross validation.

In the present study, EWT has been used followed by extraction of amplitude envelopes of respective IMs. From the amplitude envelopes, only two features (maximum and mean) have been extracted, thus, making it a simple yet effective approach to classify EEG signals into normal and seizure categories. Moreover, the proposed analysis involves EWT, which is well-suited for analysis of signals like EEG. Related to noise in the EEG dataset, the EEG signal which have been used in the present study are already denoised (Gupta & Pachori, 2019). Moreover, the external noise can be added to test the efficiency of EEG classification algorithms (Gupta & Pachori, 2019). In future studies, it will be of interest to add the external noise to the present dataset for development of robust EEG classification algorithm. Furthermore, in present work, the window size of 4000 samples provides better performance compared to smaller window sizes. The features extracted from EWT based decomposition fits better with window size of 4000 samples. Moreover, in the previous studies, it has been observed that the window size of 4000 samples with empirical mode decomposition provides better results. Thus, the result obtained in the present study is in the accordance with the previous ones (Nishad & Pachori, 2020).

However, the proposed approach is tested over limited dataset. Before applying the proposed approach in clinical practice, the methodology must be tested on a large dataset.

CONCLUSION

In the present chapter, a novel approach to classify epileptic seizure EEG signal is presented using EWT-based decomposition. The EWT of EEG signal resulted in IMs. The resultant modes were used for extraction of features. The modes obtained through EWT show the higher amplitude for the EEG signals of seizure class. In this study, features based on the Hilbert envelope of computed modes have been used for the classification of EEG signals into normal and epileptic seizure categories. Two features, namely, maximum value and mean values, were computed for all the modes from the envelopes. Finally, the product of these values has been taken to form the feature space. The two-dimensional feature space is then used to classify the EEG signals. The KNN classifier performs better as compared to SVM and DT. The proposed approach has resulted in maximum classification ACC of 98.70% with a KNN classifier employing Euclidian and cosine distance parameters. The sensitivity and specificity obtained are 98% and 99%, respectively. However, the present approach uses limited dataset. In future work, the proposed approach can be integrated with various time and frequency domain features for improving the classification accuracy with diverse datasets.

REFERENCES

Accardo, A., Affinito, M., Carrozzi, M., & Bouquet, F. (1997). Use of the fractal dimension for the analysis of electroencephalographic time series. *Biological Cybernetics*, *77*(5), 339–350. doi:10.1007004220050394 PMID:9418215

Acharya, U. R., Chua, C. K., Lim, T. C., Dorithy, & Suri, J. S. (2009). Automatic identification of epileptic EEG signals using nonlinear parameters. *Journal of Mechanics in Medicine and Biology*, *9*(4), 539–553. doi:10.1142/S0219519409003152

Acharya, U. R., Sree, S. V., Chattopadhyay, S., Yu, W., & Ang, P. C. A. (2011). Application of recurrence quantification analysis for the automated identification of epileptic EEG signals. *International Journal of Neural Systems*, *21*(3), 199–211. doi:10.1142/S0129065711002808 PMID:21656923

Acharya, U. R., Vinitha Sree, S., Swapna, G., Martis, R. J., & Suri, J. S. (2013). Automated EEG analysis of epilepsy: A review. *Knowledge-Based Systems*, *45*, 147–165. doi:10.1016/j.knosys.2013.02.014

Akbari, H., & Esmaili, S. (2020). A Novel Geometrical Method for Discrimination of Normal, Interictal and Ictal EEG Signals. *Traitement Du Signal*, *37*(1), 59–68. doi:10.18280/ts.370108

Akut, R. (2019). Wavelet based deep learning approach for epilepsy detection. *Health Information Science and Systems*, *7*(1), 1–9. doi:10.100713755-019-0069-1 PMID:31019680

Akyol, K. (2020). Stacking ensemble based deep neural networks modeling for effective epileptic seizure detection. *Expert Systems with Applications*, *148*, 113239. doi:10.1016/j.eswa.2020.113239

Altunay, S., Telatar, Z., & Erogul, O. (2010). Epileptic EEG detection using the linear prediction error energy. *Expert Systems with Applications*, *37*(8), 5661–5665. doi:10.1016/j.eswa.2010.02.045

Andrzejak, R. G., Lehnertz, K., Mormann, F., Rieke, C., David, P., & Elger, C. E. (2001). Indications of nonlinear deterministic and finite-dimensional structures in time series of brain electrical activity: Dependence on recording region and brain state. *Physical Review E: Statistical Physics, Plasmas, Fluids, and Related Interdisciplinary Topics*, *64*(6), 8. doi:10.1103/PhysRevE.64.061907 PMID:11736210

Anuragi, A., Sisodia, D. S., & Pachori, R. B. (2021). Automated FBSE-EWT based learning framework for detection of epileptic seizures using time-segmented EEG signals. *Computers in Biology and Medicine*, *136*, 104708. doi:10.1016/j.compbiomed.2021.104708 PMID:34358996

Axelberg, P. G., Gu, I. Y.-H., & Bollen, M. H. (2007). Support vector machine for classification of voltage disturbances. *IEEE Transactions on Power Delivery*, *22*(3), 1297–1303. doi:10.1109/TPWRD.2007.900065

Beghi, E., Giussani, G., Abd-Allah, F., Abdela, J., Abdelalim, A., Abraha, H. N., Adib, M. G., Agrawal, S., Alahdab, F., Awasthi, A., Ayele, Y., Barboza, M. A., Belachew, A. B., Biadgo, B., Bijani, A., Bitew, H., Carvalho, F., Chaiah, Y., Daryani, A., ... Murray, C. J. L. (2019). Global, regional, and national burden of epilepsy, 1990–2016: A systematic analysis for the Global Burden of Disease Study 2016. *Lancet Neurology*, *18*(4), 357–375. doi:10.1016/S1474-4422(18)30454-X PMID:30773428

Bhattacharyya, A., Gupta, V., & Pachori, R. B. (2017). Automated identification of epileptic seizure EEG signals using empirical wavelet transform based Hilbert marginal spectrum. *2017 22nd International Conference on Digital Signal Processing (DSP)*, 1–5.

Bhattacharyya, A., Singh, L., & Pachori, R. B. (2018). Fourier–Bessel series expansion based empirical wavelet transform for analysis of non-stationary signals. *Digital Signal Processing: A Review Journal, 78*, 185–196. doi:10.1016/j.dsp.2018.02.020

Biju, K. S., Hakkim, H. A., & Jibukumar, M. G. (2017). Ictal EEG classification based on amplitude and frequency contours of IMFs. *Biocybernetics and Biomedical Engineering*, *37*(1), 172–183. doi:10.1016/j.bbe.2016.12.005

Boashash, B., Mesbah, M., & Colitz, P. (2003). Time-Frequency Detection of EEG Abnormalities. In B. Boashash (Ed.), *TIme-Frequency Signal Analysis and Processing: A Comprehensive Reference* (pp. 663–670). Elsevier Ltd. https://eprints.qut.edu.au/21351/https://espace.library.uq.edu.au/view/UQ:167080

Chicco, D., & Jurman, G. (2020). The advantages of the Matthews correlation coefficient (MCC) over F1 score and accuracy in binary classification evaluation. *BMC Genomics*, *21*(1), 6. doi:10.118612864-019-6413-7 PMID:31898477

Chua, K. C., Chandran, V., Aeharya, R., & Lim, C. M. (2007). Higher order spectral (HOS) analysis of epileptic EEG signals. *Annual International Conference of the IEEE Engineering in Medicine and Biology - Proceedings*, 6495–6498. 10.1109/IEMBS.2007.4353847

Craik, A., He, Y., & Contreras-Vidal, J. L. (2019). Deep learning for electroencephalogram (EEG) classification tasks: A review. *Journal of Neural Engineering*, *16*(3), 031001. doi:10.1088/1741-2552/ab0ab5 PMID:30808014

Daubechies, I. (1992). *Ten Lectures on Wavelets*. Society for Industrial and Applied Mathematics. doi:10.1137/1.9781611970104

de la O Serna, J. A., Paternina, M. R. A., Zamora-Mendez, A., Tripathy, R. K., & Pachori, R. B. (2020). EEG-Rhythm Specific Taylor–Fourier Filter Bank Implemented With O-Splines for the Detection of Epilepsy Using EEG Signals. *IEEE Sensors Journal*, *20*(12), 6542–6551. doi:10.1109/JSEN.2020.2976519

Ghosh-Dastidar, S., Adeli, H., & Dadmehr, N. (2008). Principal component analysis-enhanced cosine radial basis function neural network for robust epilepsy and seizure detection. *IEEE Transactions on Biomedical Engineering*, *55*(2), 512–518. doi:10.1109/TBME.2007.905490 PMID:18269986

Gilles, J. (2013). Empirical wavelet transform. *IEEE Transactions on Signal Processing*, *61*(16), 3999–4010. doi:10.1109/TSP.2013.2265222

Gorodkin, J. (2004). Comparing two K-category assignments by a K-category correlation coefficient. *Computational Biology and Chemistry*, *28*(5–6), 367–374. doi:10.1016/j.compbiolchem.2004.09.006 PMID:15556477

Gupta, V., & Pachori, R. B. (2019). Epileptic seizure identification using entropy of FBSE based EEG rhythms. *Biomedical Signal Processing and Control*, *53*, 101569. doi:10.1016/j.bspc.2019.101569

Huang, N. E. (2014). Introduction to the Hilbert–Huang transform and its related mathematical problems. In *Hilbert–Huang transform and its applications* (pp. 1–26). World Scientific. doi:10.1142/9789814508247_0001

Ilakiyaselvan, N., Khan, A. N., & Shahina, A. (2020). Deep learning approach to detect seizure using reconstructed phase space images. *Journal of Biomedical Research*, *34*(3), 240–250. doi:10.7555/JBR.34.20190043 PMID:32561702

Khan, K. A., P. P., S., Khan, Y. U., & Farooq, O. (2020). A hybrid Local Binary Pattern and wavelets based approach for EEG classification for diagnosing epilepsy. *Expert Systems with Applications*, *140*, 112895. doi:10.1016/j.eswa.2019.112895

Kohavi, R. (1995). A study of cross-validation and bootstrap for accuracy estimation and model selection. *Proceedings of the 14th International Joint Conference on Artificial Intelligence*, 2, 1137–1143.

Lee, S. H., Lim, J. S., Kim, J. K., Yang, J., & Lee, Y. (2014). Classification of normal and epileptic seizure EEG signals using wavelet transform, phase-space reconstruction, and Euclidean distance. *Computer Methods and Programs in Biomedicine*, *116*(1), 10–25. doi:10.1016/j.cmpb.2014.04.012 PMID:24837641

Lehnertz, K., & Elger, C. E. (1995). Spatio-temporal dynamics of the primary epileptogenic area in temporal lobe epilepsy characterized by neuronal complexity loss. *Electroencephalography and Clinical Neurophysiology*, *95*(2), 108–117. doi:10.1016/0013-4694(95)00071-6 PMID:7649002

Li, S., Zhou, W., Yuan, Q., Geng, S., & Cai, D. (2013). Feature extraction and recognition of ictal EEG using EMD and SVM. *Computers in Biology and Medicine*, *43*(7), 807–816. doi:10.1016/j.compbiomed.2013.04.002 PMID:23746721

Liang, S.-F., Wang, H.-C., & Chang, W.-L. (2010). Combination of EEG Complexity and Spectral Analysis for Epilepsy Diagnosis and Seizure Detection. *EURASIP Journal on Advances in Signal Processing*, *15*(1), 853434. Advance online publication. doi:10.1155/2010/853434

Liu, Y., Lin, Y., Jia, Z., Ma, Y., & Wang, J. (2020). Representation based on ordinal patterns for seizure detection in EEG signals. *Computers in Biology and Medicine*, *126*, 104033. doi:10.1016/j.compbiomed.2020.104033 PMID:33091826

Mantas, C. J., & Abellán, J. (2014). Credal-C4.5: Decision tree based on imprecise probabilities to classify noisy data. *Expert Systems with Applications*, *41*(10), 4625–4637. doi:10.1016/j.eswa.2014.01.017

Mukhopadhyay, S., & Ray, G. C. (1998). A new interpretation of nonlinear energy operator and its efficacy in spike detection. *IEEE Transactions on Biomedical Engineering*, *45*(2), 180–187. doi:10.1109/10.661266 PMID:9473841

Nishad, A., & Pachori, R. B. (2020). Classification of epileptic electroencephalogram signals using tunable-Q wavelet transform based filter-bank. *Journal of Ambient Intelligence and Humanized Computing*, 1–15. doi:10.100712652-020-01722-8

Oweis, R. J., & Abdulhay, E. W. (2011). Seizure classification in EEG signals utilizing Hilbert-Huang transform. *Biomedical Engineering Online*, *10*(1), 1–15. doi:10.1186/1475-925X-10-38 PMID:21609459

Polat, K., & Güneş, S. (2007). Classification of epileptiform EEG using a hybrid system based on decision tree classifier and fast Fourier transform. *Applied Mathematics and Computation*, *187*(2), 1017–1026. doi:10.1016/j.amc.2006.09.022

Ravi Kumar, M., & Srinivasa Rao, Y. (2019). Epileptic seizures classification in EEG signal based on semantic features and variational mode decomposition. *Cluster Computing*, *22*(S6), 13521–13531. doi:10.100710586-018-1995-4

Ray, G. C. (1994). An Algorithm to Separate Nonstationary Part of a Signal Using Mid-Prediction Filter. *IEEE Transactions on Signal Processing*, *42*(9), 2276–2279. doi:10.1109/78.317850

Sharan, R. V., & Berkovsky, S. (2020). Epileptic Seizure Detection Using Multi-Channel EEG Wavelet Power Spectra and 1-D Convolutional Neural Networks. *2020 42nd Annual International Conference of the IEEE Engineering in Medicine & Biology Society (EMBC)*, 545–548.

Sharma, R., Pachori, R. B., & Sircar, P. (2020). Seizures classification based on higher order statistics and deep neural network. *Biomedical Signal Processing and Control*, *59*, 101921. doi:10.1016/j.bspc.2020.101921

Silva, C., Pimentel, I. R., Andrade, A., Foreid, J. P., & Ducla-Soares, E. (1999). Correlation dimension maps of EEG from epileptic absences. *Brain Topography*, *11*(3), 201–209. doi:10.1023/A:1022281712161 PMID:10217444

Srinivasan, V., Eswaran, C., & Sriraam, A. N. (2005). Artificial neural network based epileptic detection using time-domain and frequency-domain features. *Journal of Medical Systems*, *29*(6), 647–660. doi:10.100710916-005-6133-1 PMID:16235818

Srinivasan, V., Eswaran, C., & Sriraam, N. (2007). Approximate entropy-based epileptic EEG detection using artificial neural networks. *IEEE Transactions on Information Technology in Biomedicine*, *11*(3), 288–295. doi:10.1109/TITB.2006.884369 PMID:17521078

Swiderski, B., Osowski, S., & Rysz, A. (2005). Lyapunov exponent of EEG signal for epileptic seizure characterization. *Proceedings of the 2005 European Conference on Circuit Theory and Design*, 153–156. 10.1109/ECCTD.2005.1523016

Tessy, E., Muhammed Shanir, P. P., & Manafuddin, S. (2017). Time domain analysis of epileptic EEG for seizure detection. *2016 International Conference on Next Generation Intelligent Systems, ICNGIS 2016*. 10.1109/ICNGIS.2016.7854034

Thara, D. K., Premasudha, B. G., Nayak, R. S., Murthy, T. V., Prabhu, G. A., & Hanoon, N. (2021). Electroencephalogram for epileptic seizure detection using stacked bidirectional LSTM_GAP neural network. *Evolutionary Intelligence*, *14*(2), 823–833. doi:10.100712065-020-00459-9

Tsiouris, K., Pezoulas, V. C., Zervakis, M., Konitsiotis, S., Koutsouris, D. D., & Fotiadis, D. I. (2018). A Long Short-Term Memory deep learning network for the prediction of epileptic seizures using EEG signals. *Computers in Biology and Medicine*, *99*, 24–37. doi:10.1016/j.compbiomed.2018.05.019 PMID:29807250

Tzallas, A. T., Tsipouras, M. G., & Fotiadis, D. I. (2007). Automatic seizure detection based on time-frequency analysis and artificial neural networks. *Computational Intelligence and Neuroscience*, *2007*(18), 1–13. doi:10.1155/2007/80510 PMID:18301712

Tzallas, A. T., Tsipouras, M. G., & Fotiadis, D. I. (2009). Epileptic seizure detection in EEGs using time–frequency analysis. *IEEE Transactions on Information Technology in Biomedicine*, *13*(5), 703–710. doi:10.1109/TITB.2009.2017939 PMID:19304486

Uthayakumar, R., & Easwaramoorthy, D. (2013). Epileptic seizure detection in eeg signals using multifractal analysis and wavelet transform. *Fractals*, *21*(2), 1350011. Advance online publication. doi:10.1142/S0218348X13500114

Wang, C., Zou, J., Zhang, J., Wang, M., & Wang, R. (2010). Feature extraction and recognition of epileptiform activity in EEG by combining PCA with ApEn. *Cognitive Neurodynamics*, *4*(3), 233–240. doi:10.100711571-010-9120-2 PMID:21886676

Wong, H. B., & Lim, G. H. (2011). Measures of diagnostic accuracy: Sensitivity, specificity, PPV and NPV. *Proceedings of Singapore Healthcare*, *20*(4), 316–318. doi:10.1177/201010581102000411

Xu, Y., Zhu, Q., Fan, Z., Qiu, M., Chen, Y., & Liu, H. (2013). Coarse to fine K nearest neighbor classifier. *Pattern Recognition Letters*, *34*(9), 980–986. doi:10.1016/j.patrec.2013.01.028

Xue, J., Gu, X., & Ni, T. (2020). Auto-Weighted Multi-View Discriminative Metric Learning Method With Fisher Discriminative and Global Structure Constraints for Epilepsy EEG Signal Classification. *Frontiers in Neuroscience*, *14*, 586149. doi:10.3389/fnins.2020.586149 PMID:33132835

Yang, Y., Yu, D., & Cheng, J. (2007). A fault diagnosis approach for roller bearing based on IMF envelope spectrum and SVM. *Measurement: Journal of the International Measurement Confederation*, *40*(9–10), 943–950. doi:10.1016/j.measurement.2006.10.010

Zeng, W., Li, M., Yuan, C., Wang, Q., Liu, F., & Wang, Y. (2020). Identification of epileptic seizures in EEG signals using time-scale decomposition (ITD), discrete wavelet transform (DWT), phase space reconstruction (PSR) and neural networks. *Artificial Intelligence Review*, *53*(4), 3059–3088. doi:10.100710462-019-09755-y

Chapter 13
Automated Glaucoma Classification Using Advanced Image Decomposition Techniques From Retinal Fundus Images

Deepak Parashar
IES College of Technology, Bhopal, India

Dheraj Kumar Agrawal
Maulana Azad National Institute of Technology, Bhopal, India

Praveen Kumar Tyagi
Maulana Azad National Institute of Technology, Bhopal, India

Neha Rathore
Maulana Azad National Institute of Technology, Bhopal, India

ABSTRACT

Glaucoma is one of the main reasons for invariant retinal cecity. Several approaches have been developed to screen glaucoma based on fundus photographs. This chapter investigated automated glaucoma classification methods using advanced image decomposition algorithms such as EWT, DWT, EMD, VMD, and FAWT. This study computed significant texture-based descriptors from the high-frequency descriptors followed by the LS-SVM classifier classification. The robustness of the developed CAD system has been tested using the RIM-ONE public database.

DOI: 10.4018/978-1-6684-3947-0.ch013

INTRODUCTION

The World Health Organization (WHO) estimates that, after cataracts, glaucoma is the second leading cause of cecity (Stella Mary, 2016). Glaucoma is the leading cause of cecity in older people, but it may affect people of all ages worldwide. Worldwide, almost 12.3% of cases of blindness were declared because of glaucoma (Dervisevic, 2016). About 64.3 million people suffered due to this disease in 2013. This number is tends to increase by 111.8 million in 2040 (Hagiwara, 2018, Greany, 2002, Parashar, 2021). Glaucoma is a constant ocular infection that prompts perpetual visual impairment, anticipated to influence roughly 85 million individuals by 2021(Pachiyappan, 2012).

Glaucoma is a condition in which the ONH is damaged (Dervisevic, 2016). It generally occurs when fluid accumulates in the front of the eye. The excess fluid in the eye raises the pressure inside it, damaging the optic nerve (Hagiwara, 2012). Glaucoma is a severe eye disorder that can damage the ONH due to advanced fluid pressure within the eye, called Intraocular Pressure (IOP) (Greany, 2002). The leading indicator of glaucoma progression is the ONH cupping. The fundus photo of a standard retinal image is shown in Figure 1. The most crucial measure for glaucoma measurement is the Cup-to-Disc Ratio (CDR) that is calculated using vertical and horizontal disc diameter (VDD) and vertical and horizontal cup diameter (VCD) measurement (Parashar, 2020). When a nerve is viewed through the eye's pupil, it looks like a cup in top view. The amount of cupping is known as the CDR (Rewri & M. Kakkar, 2014). In the case of glaucoma, the cup becomes larger. The CDR ratio in healthy patients can range from 0.0 to 0.3. While for glaucoma patients, the CDR ratio can range from 0.3 to 1.0 (Sung, 2011, Naithani, 2007). As a result, eyes that depart from the ISNT rule may require glaucoma screening. According to the ISNT rule, the width of the neuro-retinal rim with the dominant meridians of the optic disc reduced in the sequence Inferior (I); > Superior (S); > Nasal (N); > Temporal (T) in normal eyes. The lower value of ISNT indicates the presence of glaucoma (Essock, 2000). It is conceivable that the loss of retinal nerve fibers and weakening of the former tissue causes the shift in retinal vasculature seen in glaucoma (Yousefi, 2014).

Glaucoma is a disease that can affect anybody, although it is more common among elderly individuals. Persons over 60, family members of those already diagnosed, and people with diabetes are all high-risk categories. Many forms of glaucoma have no warning signs (Lim, 2012). The effect is so gradual that it cannot be identified until the condition is advanced. It is essential to have regular eye checkups that include eye pressure measurements to diagnose its early stage (Fellman, 2011). People can avoid permanent blindness by detecting glaucoma in the early stage and appropriate treatment. According to the ICD-9 staging definitions, the 365.70 code denotes an unspecified stage of glaucoma. The 365.71 code represents mild or early-stage glaucoma, whereas the moderate-stage glaucoma condition is given with Code 365.72. And code 365.73 is defined for severe or advanced-stage glaucoma condition (Li, 2019). The implications of vision loss at various stages are shown in Figure 2.

The conventional diagnostic instruments such as Tonometers, Goniolens, Corneal Pachymeters, OCT, SLP, and SLO are used in ophthalmology clinics. Most instrument-based techniques' working principle is based on optical and mechanical approaches (Balazsi, 1983). Here we conclude that the instrument-based systems are time-consuming and laborious. Hence, a computer-aided diagnosis (CAD) method is required for fast and accurate detection.

LITERATURE REVIEW

In recent work, many researchers proposed automated methods for screening glaucoma employing fundus images in recent work. Most of the methodologies are implemented for binary classification, and these methods are used for glaucoma screening utilizing the information captured from retinal fundus photographs.

In related studies, (Acharya, 2011) investigated an automated diagnostic network for glaucoma classification using Higher-Order Spectra (HOS). This approach utilized 60 fundus photographs (30 healthy and 30 POAG photos). Then, histogram equalization is used to increase the picture's dynamic range. Further, radon transform (RT) is employed to capture meaningful information. They reported 91% accuracy using the RF classifier. The performance of the developed framework can be improved using feature optimization.

(Dua, 2012) proposed wavelet-based energy features to classify glaucoma images. This technique used first-level discrete wavelet transform (DWT) for image decomposition. The dataset consists of 60 (30 healthy and 30 glaucomatous) retinal fundus images.

Figure 1. Anatomy of a normal and glaucoma affected eye

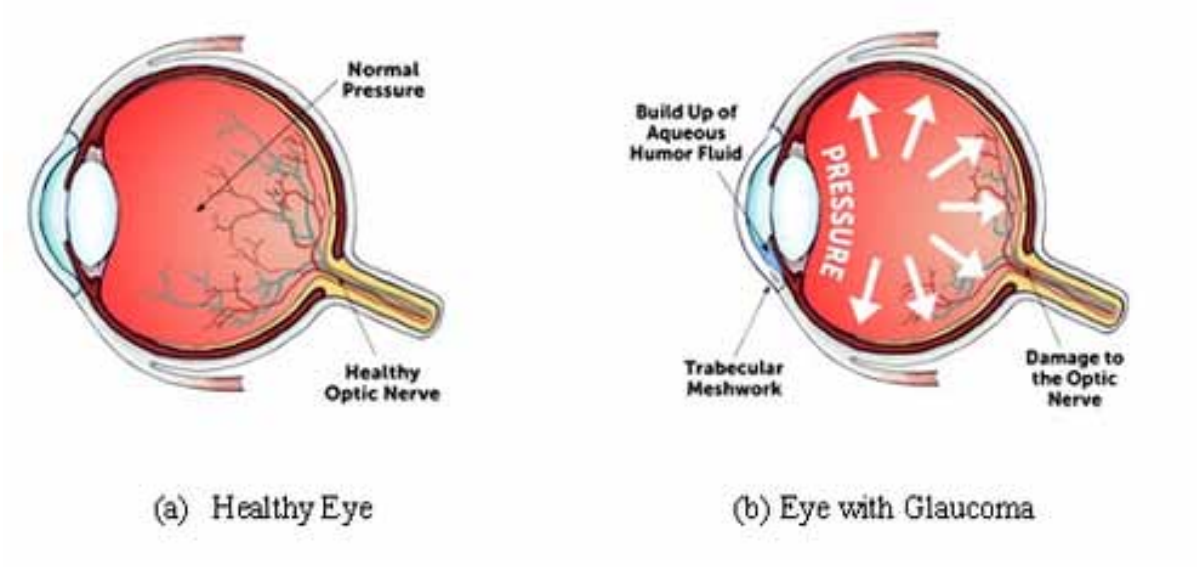

Figure 2. Vison loss effects at different stages of glaucoma, (a) Normal Vision, (b) Early-stage, and (c) Advanced-stage

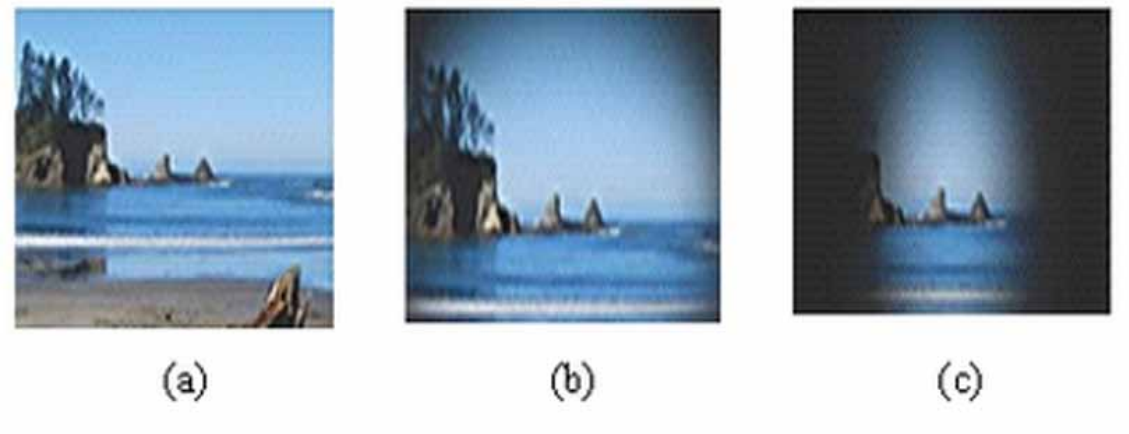

(Noronha, 2014) proposed an automatic framework for classifying glaucoma classes using radon transform higher-order cumulant features extracted from preprocessed retinal fundus photographs for multiclass classification. Then, Naïve Bayesian (NB) and SVM classifiers are utilized to classify different classes. They used the database of 272 retinal pictures, including 72 mild glaucomatous, 100 severe glaucomatous, and 100 healthy. They reported the highest classification accuracy of 92.65% with the NB classifier.

(Acharya, 2016) developed a CAD method to classify normal and glaucoma. All 800 input images (400 healthy and 400 unhealthy) were resized and preprocessed to reduce the computational time. Bi-Dimensional Empirical Mode Decomposition (BD-EMD) is applied to preprocessed images. BD-EMD decomposed components into intrinsic mode functions (IMFs). Various types of entropies, namely Shannon, Renyi, Vajda, Fuzzy, Yager, and Kapur, were extracted from IMFs. Then, t-test, Kullback-Leibler divergence, Bhattacharyya distance algorithm, Wilcoxon, and Chernoff bound test were applied to rank and select robust features. They choose 17 powerful components, which are used to classify images into normal or abnormal categories. The reported maximum glaucoma detection accuracy was 88.63% using 10 FCV.

(Maheshwari, 2017) used 505 retinal fundus photos (255 healthy and 250 glaucomatous) from the RIM-ONE database. 2D-EWT is applied to preprocessed images. 2D-EWT was used separately on each red, green, blue, and grey component. In this work, they exacted correntropy features. The t-test was applied to rank and select robust features. Using the least-squares SVM (LS-SVM), they used only six elements to classify images into healthy or glaucoma classes.

(Lahmiri, 2017) investigated a variational mode decomposition technique to classify color fundus photos. Variational mode decomposition (VMD) is used for image analysis. Ahn et al. [81] proposed a deep learning framework to detect advanced and early glaucoma. They used input retinal fundus images from the Harvard Dataverse V1 repository. The performance of the developed model can be improved using a new approach of data augmentation and advanced deep learning models.

(Kirar & Agrawal, 2019) proposed a mixed approach for computer-aided glaucoma diagnosis using a concatenation of DWT and EWT image decomposition techniques. 255 healthy and 250 glaucomatous photographs for implementation purposes.

(Agrawal, 2019) proposed an improved framework for glaucoma screening using QB-VMD image decomposition techniques. They used the RIM-ONE database of 255 healthy and 250 glaucomatous for performance evaluation. In this method, they used a combined feature set of the pictures. Then ReliefF algorithm is applied to select robust features from the collection of all extracted features. Finally, they reported 86.13% of accuracy. They also reported specificity and sensitivity of 87.43% and 84.8%, respectively.

(Sharma, 2019) investigated an automated system for glaucoma classification using a center slice of higher-order statistics. This paper uses private and public databases from KMC hospital Manipal, India, and RIM-ONE release 2. In this method, preprocessed images are used to extract the center slice of the bispectrum. These spectrums are used to extract features energy, mean, variance, skewness, and kurtosis. Further, they used a zero-cross normalization approach for feature normalization followed by locality sensitive discriminant analysis (LSDA) data reduction, and an SVM was used for classification. They reported 98.8% and 95% classification accuracy on the KMC and public databases, respectively.

(Pinto, 2018) proposed a methodology for glaucoma assessment using semi-supervised learning with the synthesis of the retinal image. This work used the Deep Convolutional Generative Adversarial Network (DC-GAN) framework for glaucoma detection. The proposed method is evaluated on an extensive glaucoma database consisting of 86926 images. They reported obtained results in sensitivity, specificity, AUC, and F-score of 79.86%, 82.90%, 0.9017, and 84.29%, respectively. The researchers can use the developed framework to classify color fundus images with hemorrhages to diagnose diabetic retinopathy and other ocular disorders.

(Li, 2020) proposed a deep learning methodology. In this method, they used an improved convolutional neural network model to identify glaucoma. The LAG database is composed of 11760 images collected from two different resources. The method proposed in this paper will also be tested using the RIM-ONE database. The reported results in specificity, accuracy, sensitivity, AUC, and F2-score is 85.50%, 85.2%, 84.80%, 0.9160, 83.70%, respectively. The proposed CNN-based deep learning model can be employed for multiclass glaucoma classification.

(Orlando, 2020) developed a glaucomatous diagnosis model from fundus images called retinal fundus glaucoma challenge (REFUGE). This paper proposed many deep learning algorithms using the REFUGE glaucoma database for automatic glaucoma classification and optical disc/cup segmentation. REFUGE released a large dataset of 1200 images. Twelve teams with 12 different methods participated in this challenge's online challenge.

The summary of the literature review is given in Table 1. It can be seen from the literature that the existing computerized approaches have been used for glaucoma screening using retinal fundus photographs. However, we cannot use most of the current methodologies to classify glaucoma stages. The main contributions of our research work are as follows. (1) To study and analyze existing methods for glaucoma classification. (2) To investigate a suitable image decomposition technique for feature extraction from fundus images. (3) To classify the glaucoma stages with high accuracy using different machine learning algorithms.

Table 1. Summary of latest methods used for automated glaucoma classification

Authors (Year)	Database/ Number of Images	Method/Features/Classifier	Shortcoming/Scope for Future Work
(Acharya, 2011)	KMC/60	HOS and texture feature, SVM (RBF)	The performance of the proposed framework can be improved using feature optimization.
(Dua, 2012)	KMC/60	DWT, chi-square, gain ratio, ReliefF, SMO	The effectiveness of the method can be tested on the diverse public glaucoma database.
(Noronha, 2014)	KMC/272	RT and HOS cumulants, LDA, NB	We can test the performance of the proposed system on the public database.
(Acharya, 2016)	KMC/800	BD-EMD, entropies and energy features, SVM	The performance of the developed model can be improved using the VMD algorithm.
(Maheshwari, 2017)	RIM-ONE r12/505	EWT, correntropy, LS-SVM	This method can be extended to the diagnosis of other diseases like DR and AMD.
(Kirar, 2019)	RIM-ONE r12/505	Concatenation of EWT and DWT, combined set of features, LS-SVM	The developed hybrid concatenation approach can be used for multiclass glaucoma classification.
(Agrawal, 2019)	RIM-ONE r12/505	QB-VMD, combined set of features, LS-SVM	The proposed framework can be evaluated to diagnose early-stage glaucoma.
(Sharma, 2019)	RIM-ONE r2/455	Center slice of HOS, SVM	The performance of the proposed framework can be improved using deep learning models.

IMAGE DECOMPOSITION TECHNIQUES

In this chapter, we present different image decomposition techniques (IDTs) such as Two-Dimensional DWT (2D-DWT), Bi-Dimensional Empirical Mode Decomposition (BD-EMD), Two-Dimensional FAWT (2D-FAWT), Two-Dimensional Tensor EWT (2D-T-EWT), and Two-Dimensional Compact VMD (2D-C-VMD).

Recently, image decomposition techniques have been used in medical imaging to decompose the fundus photos into different images. In particular, the high-frequency components are used for feature extraction to capture helpful information for glaucoma classification. Then the irregularities in the retinal images by statistical texture features are classified into normal and abnormal classes using different classification algorithms [Acharya, 2016, Maheshwari, 2017, Lahmiri, 2017).

Two-Dimensional Discrete Wavelet Transform (2D-DWT)

A DWT is a transform with discretely sampled wavelets (Dua, 2012). The temporal resolution, which captures both frequency and position information, significantly benefits the Fourier transform (Dua, 2012, Yoshida, 2011). The 2D-DWT decomposes input images into an approximation and detailed sub-band images (SBIs). The approximation coefficient of an image is further used for second-level decomposition. In this approach, frequency and time resolutions are doubled and halved, respectively, after each decomposition level. The fundamental, one-level, two-dimensional DWT method is shown in Figure 3.

Figure 3. A flow chart of first level, 2D-DWT (Dua, 2012)

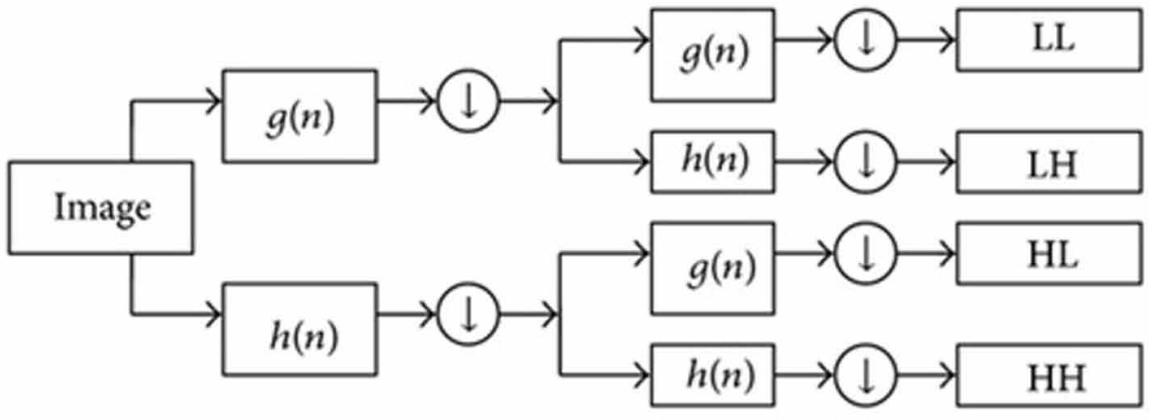

Bi-Dimensional Empirical Mode Decomposition (BD-EMD)

The EMD is an adaptive approach for analyzing non-stationary signals generated by nonlinear systems (Acharya, 2016). With the capacity to distinguish superposed spatial frequencies locally, the EMD utilized in the Hilbert-Huang transform (HHT) was expanded into two-dimensional applications. The EMD decomposes the signal into intrinsic mode functions inherent to the functions (IMFs). The original signal, represented as the sum of amplitude and frequency modulated (AM-FM) functions, is an IMF (Acharya, 2016, Huang, 1998). The flowchart of the iterative EMD is shown in Figure 4.

A signal must meet two criteria to be classified as an IMF. (1) The number of extrema and zero crossings in the entire data set must be identical or deviate by no more than one. (2) Local mean, defined as the mean of the lower and upper envelope, must be zero (Huang, 1998, Mishra, 2017).
The complete empirical mode decomposition technique is described below.

1. Find all of a signal's local minima and maxima.
2. To produce the upper and lower envelopes, interpolate all indicated maxima and minima.
3. Take the mean of the upper and lower envelopes.
4. Subtract the original signal from the mean.
5. Repeat steps 1–4 until the stop condition is met, resulting in the IMF.

Iterate steps 1 to 5 using the residual difference signal until the last residual becomes a monotonic function.

Figure 4. A flow chart of Empirical mode decomposition iterative process (Huang, 1998)

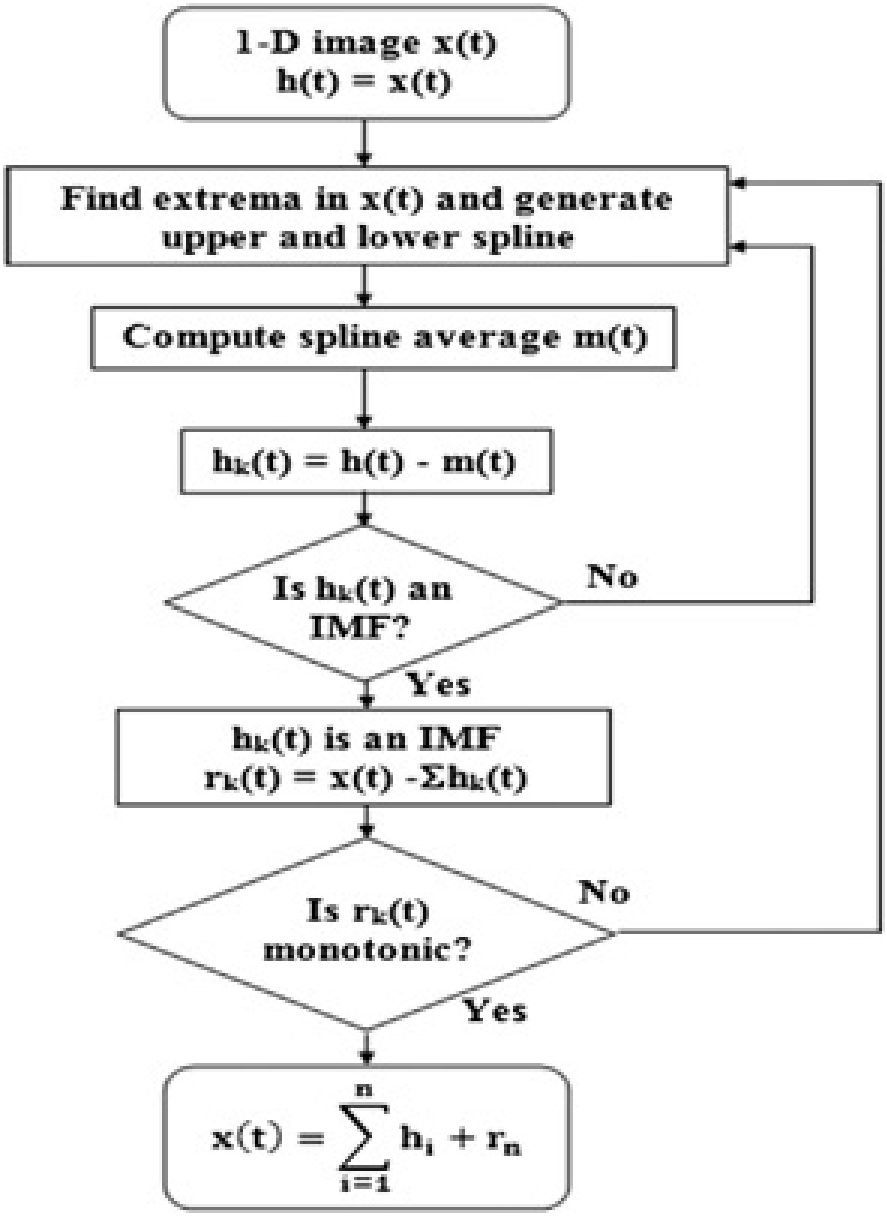

Two-Dimensional Flexible Analytic Wavelet Transform (2D-FAWT)

FAWT is improved form of DWT and a helpful wavelet transform for medical image analysis (Bayram, 2013). FAWT's most crucial characteristic is its time-frequency covering. Figure 5 shows the transform is composed of iterated FBs (Parashar, 2020).

Figure 5. The transform is composed of an iterated filter bank (Bayram, 2013)

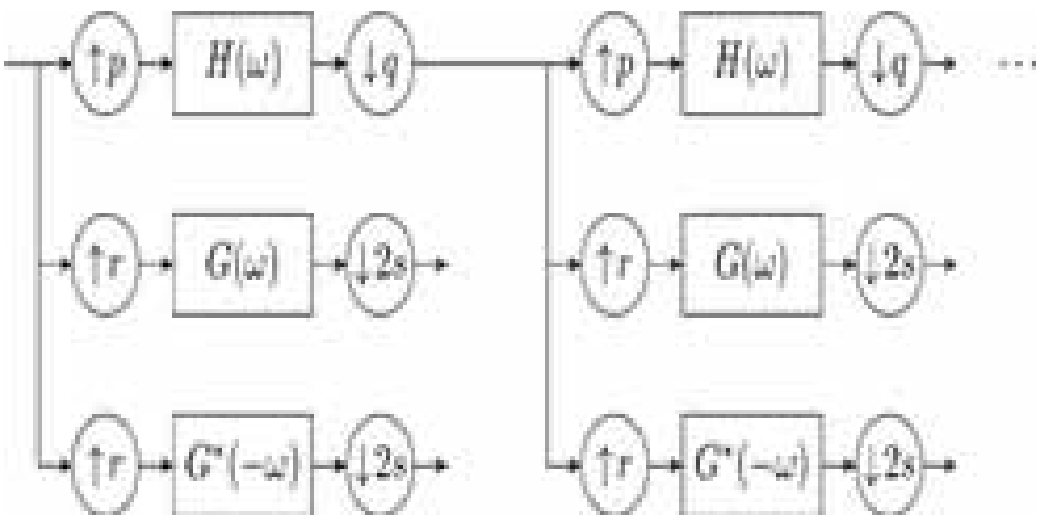

Two-Dimensional Tensor Empirical Wavelet Transform (2D-T-EWT)

EWT is a signal-dependent algorithm. This technique cannot use predetermined basis functions like Fourier transform (Gilles, 2013). Figure 6 shows the EWT basis structure and the Fourier line decomposition concept (Gilles, 2014).

Figure 6. The EWT basis structure and the Fourier line decomposition concept (Gilles, 2013)

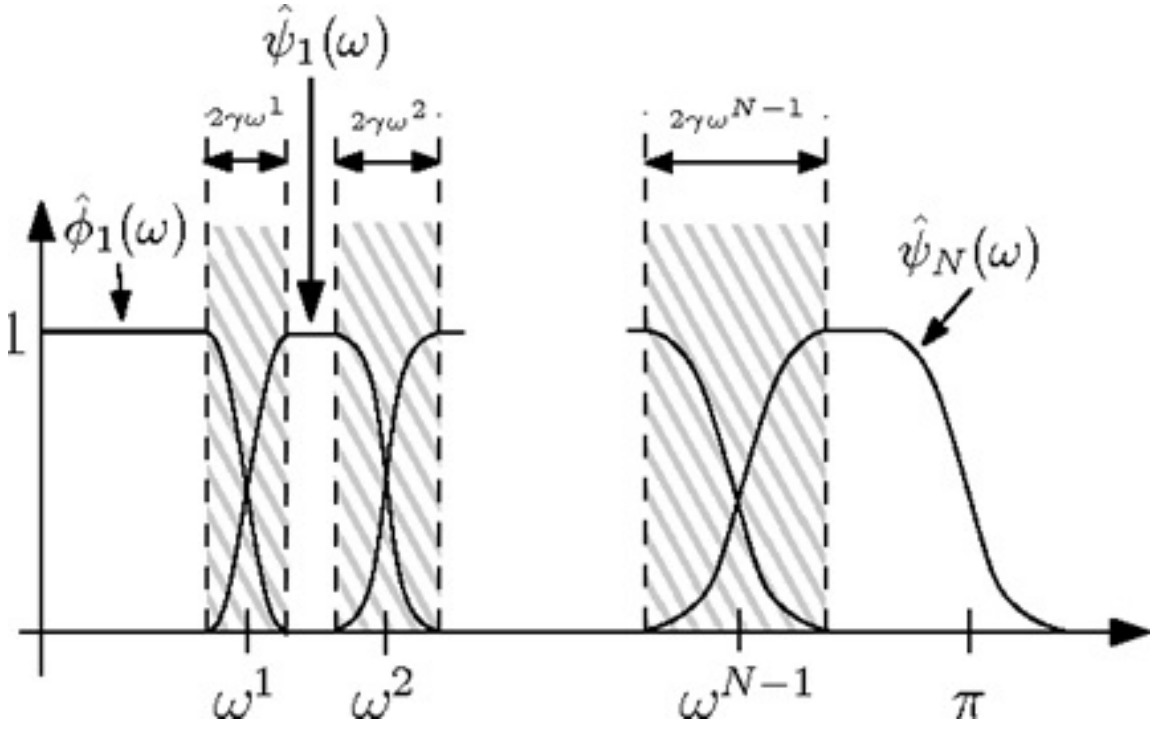

Two-Dimensional Compact Variational Mode Decomposition (2D-C-VMD)

VMD is an advanced version of empirical mode decomposition (Dragomiretskiy, 2015). It can be employed to decompose an original signal into a fixed number of band-limited IMFs (BLIMFs) (Zosso, 2017). The image decomposition procedure using the 2D-C-VMD algorithm is shown in Figure 7. It can be seen from the literature that the newly developed 2D-C-VMD algorithm is more suitable for digital image analysis. In particular, the high-frequency variational modes (VMs) are used for feature extraction to capture useful information for image classification.

Figure 7. Image decomposition procedure employing the 2D-C-VMD

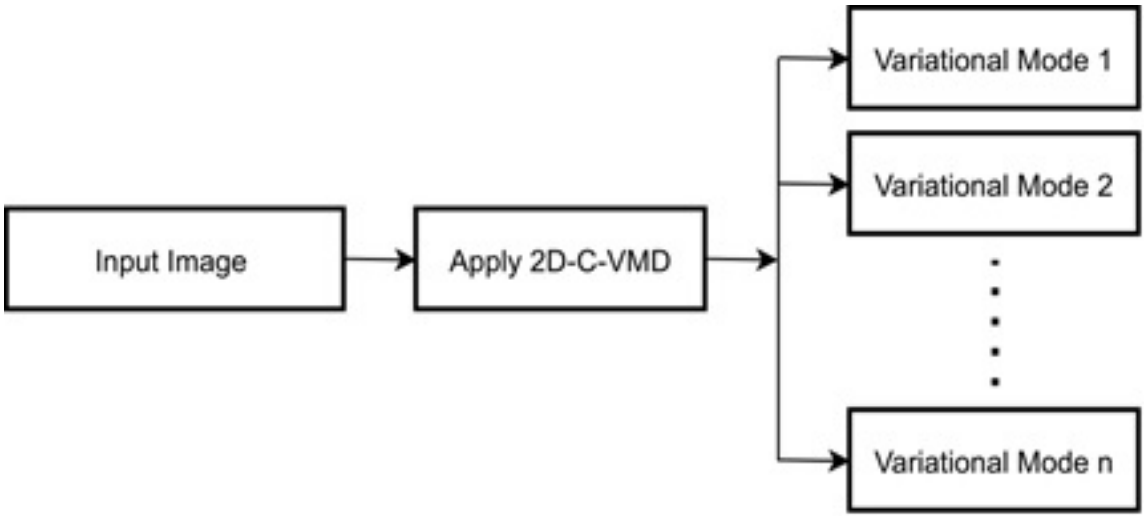

PROPOSED METHODOLOGY

We proposed an improved method for glaucoma identification in fundus images using image decomposition techniques. This research aims to investigate an automated system for computer-aided diagnosis (CAD) of glaucoma using the information extracted from retinal fundus photographs. The performance of the proposed methodology is improved using suitable image decomposition techniques. This work applies image-preprocessing operations on input fundus images to improve image quality. The preprocessed images are down-streamed into sub-bands employing the 2D-C-VMD algorithm. The high-frequency decomposed components are helpful for feature extraction to capture important detail for glaucoma classification. Figure. 8 depicts the block diagram of the proposed method (PM).

Figure 8. The block diagram of the proposed CAD system

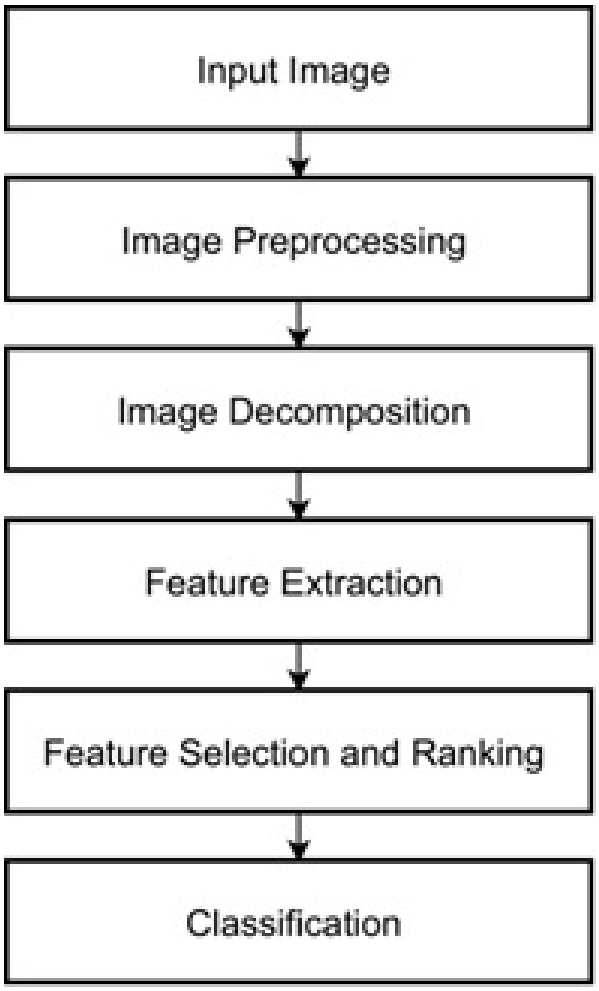

Retinal Fundus Image Database

We used publicly available glaucoma database RIM-ONE (Fumero, 2011). These glaucoma datasets are used to evaluate image-processing algorithms for automated glaucoma classification. The RIM-ONE (Parashar, 2021) is a publicly accessible retinal fundus image dataset with optic nerve head (ONH) accurate gold standards given by various specialists. The medical image analysis group (MIAG) produced the RIM-ONE database for automated retinal image analysis. It includes fundus images of normal eyes as well as images of glaucoma in various stages. In this work, 505 fundus images (Maheshwari, 2017, Kirar, 2019, Agrawal, 2019) (255 healthy and 250 glaucomatous) have been collected from RIM-ONE database.

Feature Extraction

The information extracted from the decomposed components is helpful for glaucoma classification (Maheshwari, 2017). Feature extraction has been used to obtain important information from the high-frequency variational modes (Kirar, 2019). For glaucoma classification, texture-based features are helpful to measure coarseness, smoothness, and pixel regularities (Agrawal, 2019). In this work, various entropy and Fractal dimension (FD) features have been extracted from high frequency decomposed components.

Feature Selection and Classification

The ReliefF algorithm has been used to select the full features from all extracted features in the proposed research work (Kirar, 2019). The ReliefF feature selection algorithm employs a statistical technique to identify statistically essential features instead of a heuristic search (Agrawal, 2019). The feature vectors to the proportional class labels are the input to the ReliefF algorithm. Twenty-two robust features are selected from 48 extracted features, computed from six different texture feature sets using the ReliefF algorithm. Further, in this work, for the glaucoma classification task, we use an SVM-based machine learning method (Maheshwari, 2017).

Figure 9. A glaucomatous retinal fundus image (a) Input image, (b) Preprocessed image

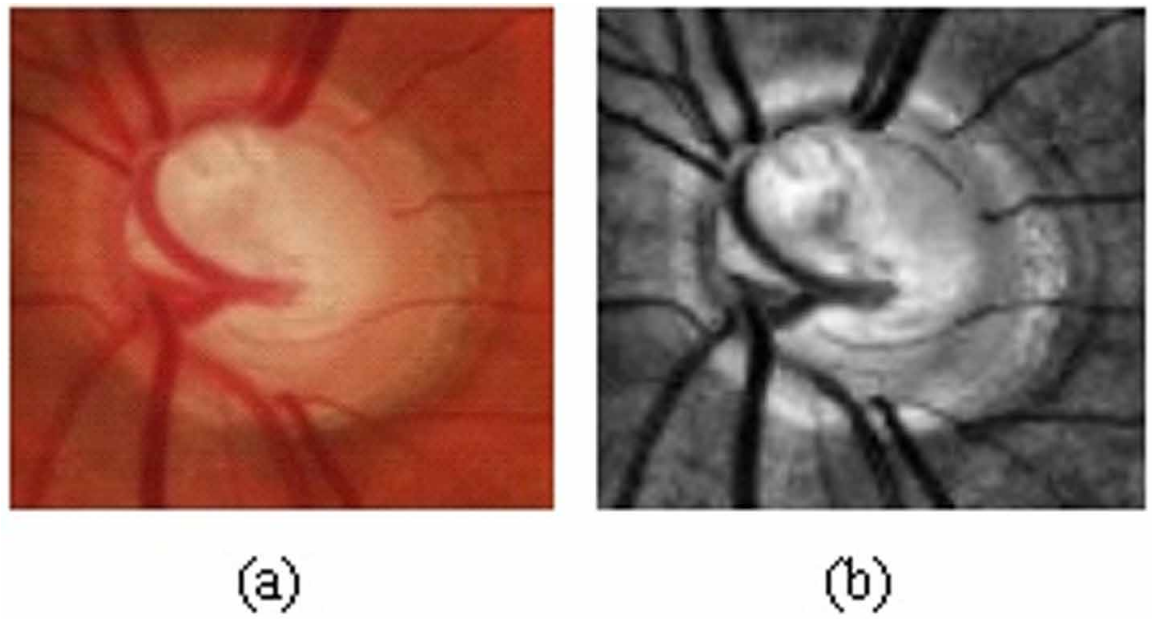

Figure 10. Extraction of different channels from RGB color image, (a) RCI, (b) GCI, and (c) BCI

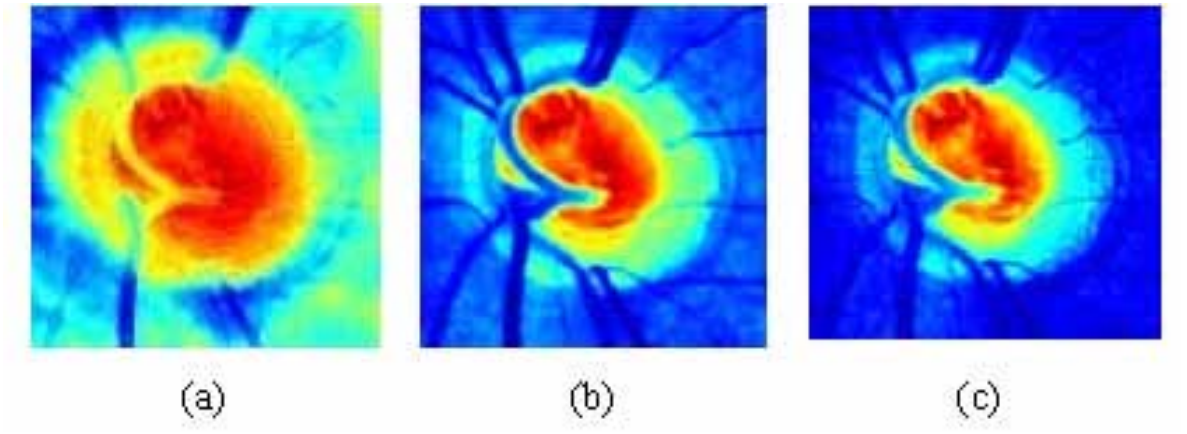

RESULTS AND DISCUSSION

A glaucomatous r Input image and its preprocessed image are shown in Figure 9. Figure 10. Shows the extraction of different channels from RGB color image. Further green image components have been used for feature extraction and classification. The classification performance of the proposed methodology has been measured using different measures Accuracy (Ac), Sensitivity (Sn), and Specificity (Sp) (Kirar, 2019). Generally, the effectiveness of the classifier can be measured with classification accuracy. Ideally, the accuracy of machine learning models is close to 100%. The accuracy is widely considered for performance evaluation parameters, which is also used to compute the performance of the proposed method. The plots of features versus performance indicators and kernel parameter versus performance parameters are shown in Figures 11 and 12, respectively. As shown in these plot, we varied the value of the RBF Kernel parameter (σ) from 0.1 to 2 with an increment of 0.1. The 2D-C-VMD-based approach achieved a far better classification accuracy of 96.23% on the RIM-ONE dataset.

The performance of the various image decomposition methods has been evaluated on the same database. The obtained results using different image decomposition techniques on the RIM-ONE r12 database are shown in Table 2. The achieved results of accuracies for different algorithms 2D-DWT, 2D-FAWT, BD-EMD, 2D-T-EWT, and 2D-C-VMD are 88.71%, 90.76%, 91.88%, 92.47%, and 96.23%, respectively. As shown in Table 2, the 2D-C-VMD-based method achieved the highest classification accuracy of 96.23%. A plot of performance comparison in the accuracy of different image decomposition techniques is shown in Figure 13. In sum, the experimental results show that the proposed method using the 2D-C-VMD technique outperformed other image decomposition techniques such as 2D-DWT, BD-EMD, 2D-FAWT, and 2D-T-EWT. We present a comparative summary on the same database in Table 3.

Figure 11. A plot of the number of features versus performance parameters after 10 FCV using the 2D-C-VMD

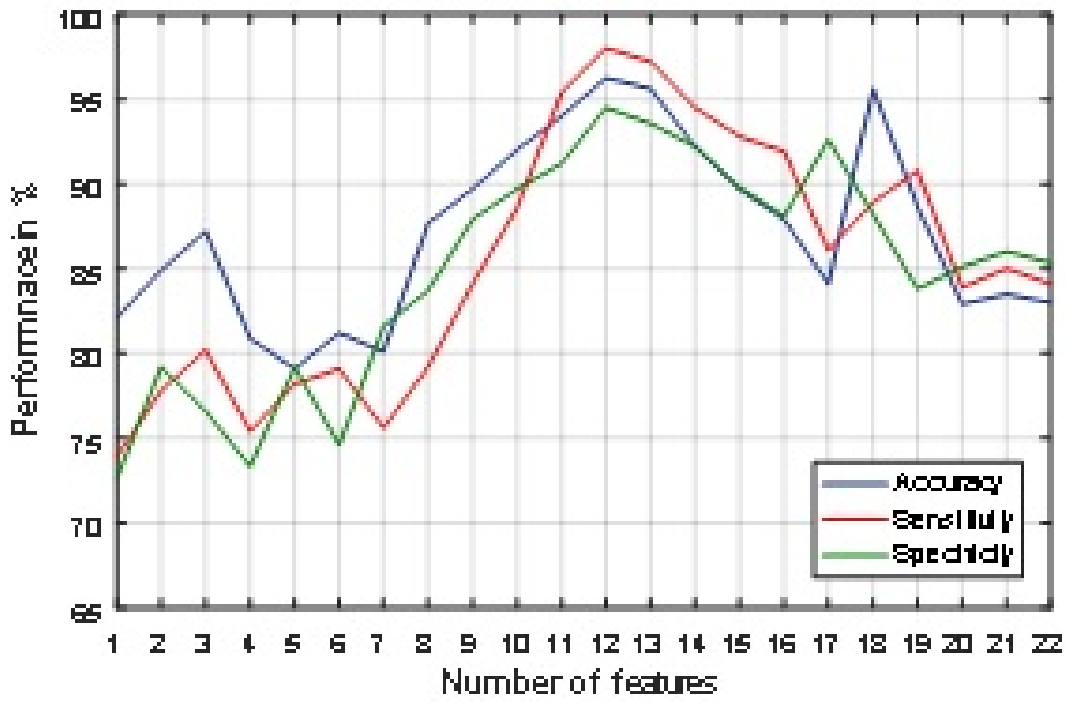

Figure 12. A plot of performance parameters versus RBF kernel parameter after 10 FCV using the 2D-C-VMD

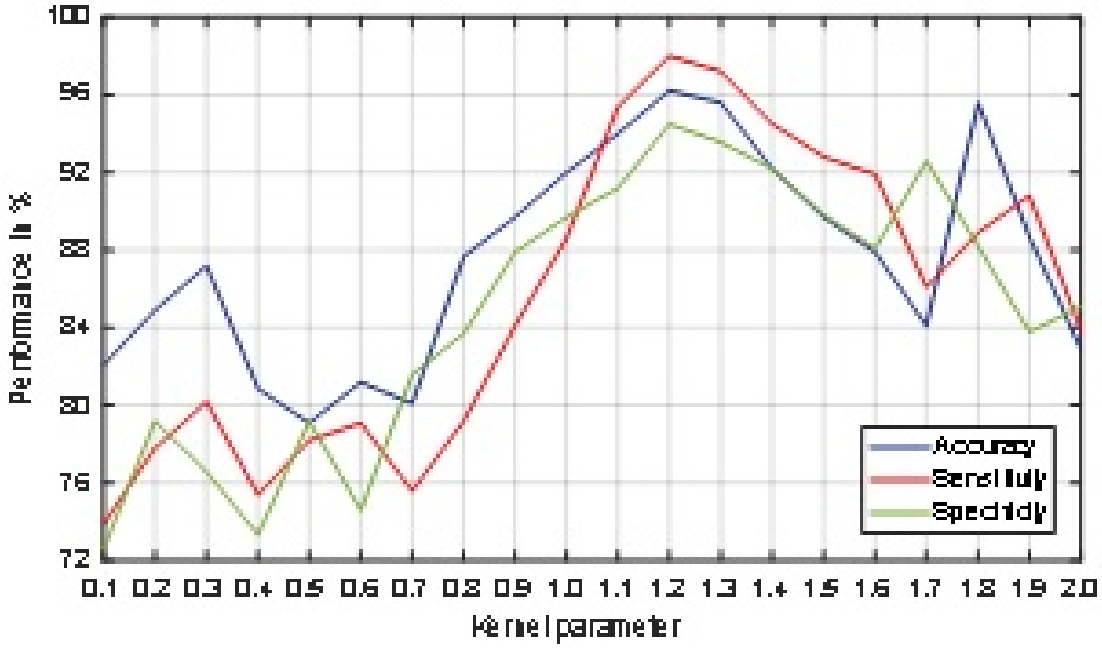

Table 2. The obtained results of the proposed method using different image decomposition techniques (IDTs) on RIM-ONE database

Database	IDTs used	Ac (%)	Sn (%)	Sp (%)
RIM-ONE	2D-DWT	88.71	89.92	88.23
	2D-FAWT	90.76	94.5	87.84
	BD-EMD	91.88	91.20	92.54
	2D-T-EWT	92.47	93.20	91.67
	2D-C-VMD	**96.23**	98	94.50

Figure 13. A plot of performance comparison of different IDTs

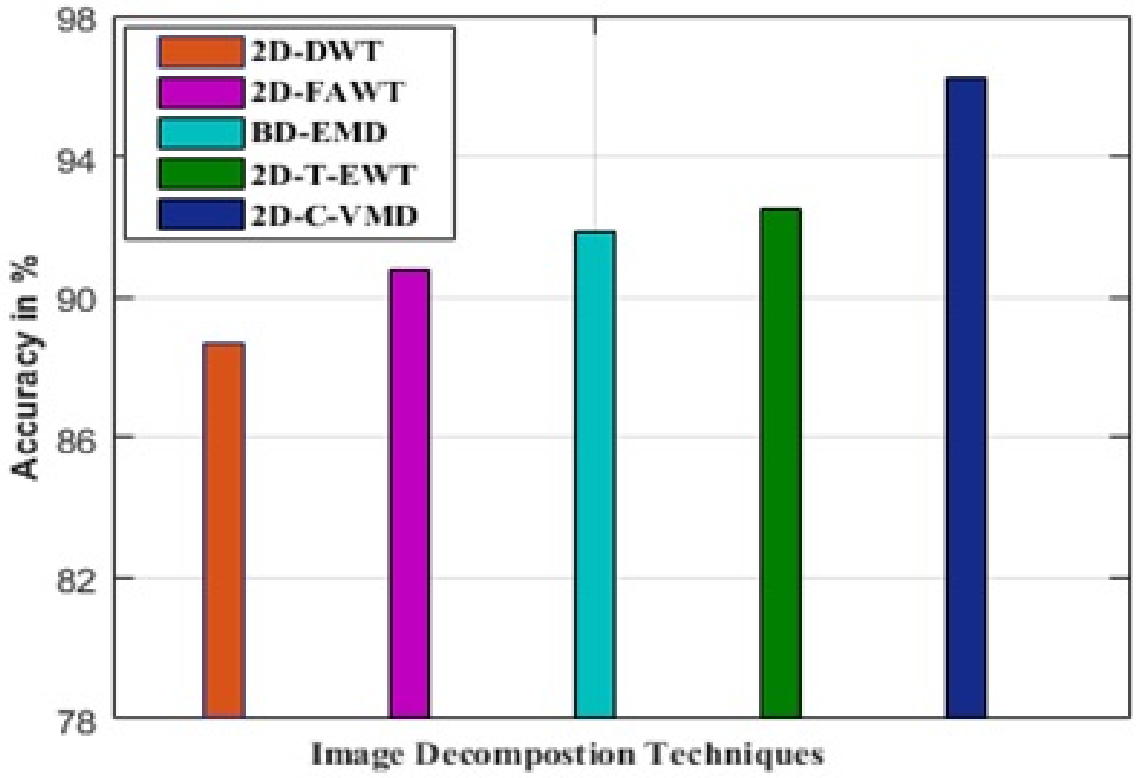

Table 3. Comparison of the proposed method with the existing methods on the same database

Database/Number of images	Method/Reference	IDTs	Ac (%)	Sn (%)	Sp (%)
RIM-ONE/505	(Maheshwari, 2017)	2D-LP-EWT	80.66	78.00	88.23
	(Kirar, 2019)	EWT and DWT	83.60	86.4	80.80
	(Agrawal, 2019)	QB-VMD	86.13	84.8	87.43
	(Proposed Method)	2D-C-VMD	**96.23**	98	94.50

CONCLUSION

The conventional diagnostic instruments such as Tonometers, Goniolens, Corneal Pachymeters, OCT, SLP, and SLO are used in ophthalmology clinics. Most instrument-based techniques' working principle is based on optical and mechanical approaches. Here we conclude that the instrument-based tools are time-consuming and laborious. Hence, a computer-aided diagnosis (CAD) method is required for fast and accurate detection.This chapter presents an improved CAD method for glaucoma classification using the information extracted from retinal fundus images. In the proposed research work, different image decomposition techniques; 2D-DWT, 2D-FAWT, 2D-T-EWT, BD-EMD, and 2D-C-VMD have been used to evaluate the performance of the proposed approach. A plot of performance comparison in the accuracy of different image decomposition techniques is shown in Figure 13. As shown in Figure 13, the 2D-C-VMD image decomposition technique-based method obtained better accuracy than other decomposition algorithms. The proposed method using 2D-C-VMD achieved the highest classification accuracy of 96.23%. We compare the performance with the existing glaucoma classification on the same database with an equal number of images. The obtained parameters show that the proposed method outperformed other image decomposition techniques on the same database.

REFERENCES

Acharya, U. R., Dua, S., Du, X., Sree S, V., & Chua, C. K. (2011). Automated diagnosis of glaucoma using texture and higher order spectra features. *IEEE Transactions on Information Technology in Biomedicine*, *15*(3), 449–455. doi:10.1109/TITB.2011.2119322 PMID:21349793

Acharya, U. R., Mookiah, M. R. K., Koh, J. E. W., Tan, J. H., Bhandary, S. V., Rao, A. K., Fujita, H., Hagiwara, Y., Chua, C. K., & Laude, A. (2016). Automated screening system for retinal health using bi-dimensional empirical mode decomposition and integrated index. *Computers in Biology and Medicine*, *75*(1), 54–62. doi:10.1016/j.compbiomed.2016.04.015 PMID:27253617

Agrawal, D. K., Kirar, B. S., & Pachori, R. B. (2019). Automated glaucoma detection using quasi-bivariate mode decomposition from fundus images. *IET Image Processing*, *13*(13), 2401–2408. doi:10.1049/iet-ipr.2019.0036

Balazsi, G. (1983). Relationship between baring of circumlunar vessels of the optic disc and glaucomatous visual field loss. *Canadian Journal of Ophthalmology*, *18*(7), 333–336. PMID:6671152

Bayram, I. (2013). An analytic wavelet transform with a flexible time-frequency covering. *IEEE Transactions on Signal Processing*, *61*(5), 1131–1142. doi:10.1109/TSP.2012.2232655

Dervisevic, E., Pavljasevic, S., Dervisevic, A., & Kasumovic. (2016). Challenges in early glaucoma detection. *Medicinski Arhiv*, *70*(3), 203–207. doi:10.5455/medarh.2016.70.203-207 PMID:27594747

Dragomiretskiy, K., & Zosso, D. (2015). Two-dimensional variational mode decomposition. In Energy Minimization Methods in Computer Vision and Pattern Recognition (Lecture Notes in Computer Science). Springer. doi:10.1007/978-3-319-14612-6_15

Dua, S., Acharya, U. R., Chowriappa, P., & Sree, S. V. (2012). Wavelet-Based Energy Features for Glaucomatous Image Classification. *IEEE Transactions on Information Technology in Biomedicine*, *16*(1), 80–87. doi:10.1109/TITB.2011.2176540 PMID:22113813

Essock, E. A., Sinai, M. J., Fechtner, R. D., Srinivasan, N., & Bryant, D. F. (2000). Fourier analysis of nerve fiber layer measurements from scanning laser polarimetry in glaucoma: Emphasizing shape characteristics of the 'double-hump' pattern. *Journal of Glaucoma*, *9*(6), 444–452. doi:10.1097/00061198-200012000-00005 PMID:11131750

Fellman, R. L. (2011). Know the New Glaucoma Staging Codes. *American Academy of Ophthl., EyeNet Magazine*, 65-66. https://www.aao.org/eyenet/article/know-new-glaucoma-staging-codes

Fumero, F. (2011). RIM-ONE: An open retinal image database for optic nerve evaluation. *24th IEEE Int. Symposium on Comput. Med. Syst. (CBMS),* 1-6.

Gilles, J. (2013). Empirical wavelet transform. *IEEE Transactions on Signal Processing*, *61*(16), 3999–4010. doi:10.1109/TSP.2013.2265222

Gilles, J., Tran, G., & Osher, S. (2014). 2D empirical transforms: Wavelets, ridgelets, and curvelets revisited. *SIAM Journal on Imaging Sciences*, *7*(1), 157–186. doi:10.1137/130923774

Greany, M. J. (2002). Comparisons of optic nerve imaging methods to distinguish normal eyes from those with glaucoma. *Investigative Ophthalmology & Visual Science*, *43*(1), 140–145. PMID:11773024

Hagiwara, Y., Koh, J. E. W., Tan, J. H., Bhandary, S. V., Laude, A., Ciaccio, E. J., Tong, L., & Acharya, U. R. (2018). Computer-aided diagnosis of glaucoma using fundus images: A review. *Computer Methods and Programs in Biomedicine*, *165*, 1–12. doi:10.1016/j.cmpb.2018.07.012 PMID:30337064

Huang, N. E., Shen, Z., Long, S. R., Wu, M. C., Shih, H. H., Zheng, Q., Yen, N.-C., Tung, C. C., & Liu, H. H. (1998). The empirical mode decomposition and the Hilbert spectrum for nonlinear and non-stationary time series analysis A: Mathematical physical and engineering sciences. *Processing of the Royal Society*, *454*(1971), 903–995. doi:10.1098/rspa.1998.0193

Kirar, B. S., & Agrawal, D. K. (2019). Computer aided diagnosis of glaucoma using discrete and empirical wavelet transform from fundus images. *IET Image Processing*, *13*(1), 73–82. doi:10.1049/iet-ipr.2018.5297

Lahmiri, S., & Shmual, S. (2017). Variational mode decomposition based approach for accurate classification of color fundus images with hemorrhages. *Optics & Laser Technology*, *96*, 243–248. doi:10.1016/j.optlastec.2017.05.012

Li, L., Xu, M., Liu, H., Li, Y., Wang, X., Jiang, L., Wang, Z., Fan, X., & Wang, N. (2020). A large-scale database and a CNN model for attention based glaucoma detection. *IEEE Transactions on Medical Imaging*, *39*(2), 413–424. doi:10.1109/TMI.2019.2927226 PMID:31283476

Li, M., Fei, Z., Zeng, M., Wu, F.-X., Li, Y., Pan, Y., & Wang, J. (2019). Automated ICD-9 Coding via A Deep Learning Approach. *IEEE/ACM Transactions on Computational Biology and Bioinformatics*, *16*(4), 1193–1202. doi:10.1109/TCBB.2018.2817488 PMID:29994157

Lim, T. C., Chattopadhyay, S., & Acharya, U. R. (2012). A survey and comparative study on the instruments for glaucoma detection. *Medical Engineering & Physics*, *34*(2), 129–139. doi:10.1016/j.medengphy.2011.07.030 PMID:21862378

Maheshwari, S., Pachori, R. B., & Acharya, U. R. (2017). Automated diagnosis of glaucoma using empirical wavelet transform and correntropy features extracted from fundus images. *IEEE Journal of Biomedical and Health Informatics*, *21*(3), 803–813. doi:10.1109/JBHI.2016.2544961 PMID:28113877

Mishra, V., Bajaj, V., Kumar, A., Sharma, D., & Singh, G. K. (2017). An Efficient Method for Analysis of EMG Signals using Improved Empirical Mode Decomposition. *AEÜ. International Journal of Electronics and Communications*, *72*(1), 200–209. doi:10.1016/j.aeue.2016.12.008

Naithani, P., Sihota, R., Sony, P., Dada, T., Gupta, V., Kondal, D., & Pandey, R. M. (2007). Evaluation of optical coherence tomography and Heidelberg retinal tomography parameters in detecting early and moderate glaucoma. *Investigative Ophthalmology & Visual Science*, *48*(7), 3138–3145. doi:10.1167/iovs.06-1407 PMID:17591883

Noronha, K. P., Acharya, U. R., Nayak, K. P., Martis, R. J., & Bhandary, S. V. (2014). Automated classification of glaucoma stages using higher order cumulant features. *Biomedical Signal Processing and Control*, *10*, 174–183. doi:10.1016/j.bspc.2013.11.006

Orlando, J. I., Fu, H., Barbosa Breda, J., van Keer, K., Bathula, D. R., Diaz-Pinto, A., Fang, R., Heng, P.-A., Kim, J., Lee, J. H., Lee, J., Li, X., Liu, P., Lu, S., Murugesan, B., Naranjo, V., Phaye, S. S. R., Shankaranarayana, S. M., Sikka, A., ... Bogunović, H. (2020). REFUGE Challenge: A unified framework for evaluating automated methods for glaucoma assessment from fundus photographs. *Medical Image Analysis*, *59*, 1–19. doi:10.1016/j.media.2019.101570 PMID:31630011

Pachiyappan, A., Das, U. N., Murthy, T. V. S. P., & Tatavarti, R. (2012). Automated diagnosis of diabetic retinopathy and glaucoma using fundus and OCT images. *Lipids in Health and Disease*, *11*(73), 1–10. doi:10.1186/1476-511X-11-73 PMID:22695250

Parashar, D., & Agrawal, D. K. (2020). Automated classification of glaucoma using retinal fundus images. *IEEE International Conference on Measurement, Instrumentation, Control and Automation (ICMICA)*, 1-6. 10.1109/ICMICA48462.2020.9242702

Parashar, D., & Agrawal, D. K. (2020). Automated classification of glaucoma stages using flexible analytic wavelet transform from retinal fundus images. *IEEE Sensors Journal*, *20*(21), 12885–12894. doi:10.1109/JSEN.2020.3001972

Parashar, D., & Agrawal, D. K. (2021). Automatic classification of glaucoma stages using two-dimensional tensor empirical wavelet transform. *IEEE Signal Processing Letters*, *28*, 66–70. doi:10.1109/LSP.2020.3045638

Parashar, D., & Agrawal, D. K. (2021). 2-D compact variational mode decomposition-based automatic classification of glaucoma stages from fundus images. *IEEE Transactions on Instrumentation and Measurement*, *70*, 1–10. doi:10.1109/TIM.2021.3071223

Pinto, A. (2019). Retinal Image Synthesis and Semi-Supervised Learning for Glaucoma Assessment. *IEEE Transactions on Medical Imaging*, *38*(9), 2211–2218. doi:10.1109/TMI.2019.2903434 PMID:30843823

Rewri, P., & Kakkar, M. (2014). Awareness, knowledge, and practice: A survey of glaucoma in north Indian rural residents. *Indian Journal of Ophthalmology*, *62*(4), 482–486. doi:10.4103/0301-4738.132105 PMID:24817749

Sharma, R., Sircar, P., Pachori, R. B., Bhandary, S., & Acharya, U. R. (2019). Automated glaucoma detection using center slice of higher order statistics. *Journal of Mechanics in Medicine and Biology*, *19*(1), 1–21. doi:10.1142/S0219519419400116

Stella Mary, M. C. V., Rajsingh, E. B., & Naik, G. R. (2016). Retinal fundus image analysis for diagnosis of glaucoma: A comprehensive survey. *IEEE Access: Practical Innovations, Open Solutions*, *4*, 4327–4354. doi:10.1109/ACCESS.2016.2596761

Sung, K. R., Kim, J. S., Wollstein, G., Folio, L., Kook, M. S., & Schuman, J. S. (2011). Imaging of the retinal nerve fiber layer with spectral domain optical coherence tomography for glaucoma diagnosis. *The British Journal of Ophthalmology*, *95*(7), 909–914. doi:10.1136/bjo.2010.186924 PMID:21030413

Yoshida, T. (2011). Two dimensional non-separable adaptive directional lifting structure of discrete wavelet transform. *IEEE International Conference on Acoustics, Speech and Signal Processing (ICASSP)*, 1529-1532. 10.1109/ICASSP.2011.5946785

Yousefi, S., Goldbaum, M. H., Balasubramanian, M., Medeiros, F. A., Zangwill, L. M., Liebmann, J. M., Girkin, C. A., Weinreb, R. N., & Bowd, C. (2014). Learning From Data: Recognizing Glaucomatous Defect Patterns and Detecting Progression From Visual Field Measurement. *IEEE Transactions on Biomedical Engineering*, *61*(7), 2112–2124. doi:10.1109/TBME.2014.2314714 PMID:24710816

Zosso, D., Dragomiretskiy, K., Bertozzi, A. L., & Weiss, P. S. (2017). Two-dimensional compact variational mode decomposition. *Journal of Mathematical Imaging and Vision*, *58*(2), 294–320. doi:10.100710851-017-0710-z

Chapter 14
Deep Learning–Based Approach to Detect Leukemia, Lymphoma, and Multiple Myeloma in Bone Marrow

Janasruti U.
Avinashilingam Institute for Home Science and Higher Education for Women, India

Kavya S.
Avinashilingam Institute for Home Science and Higher Education for Women, India

Merwin A.
Avinashilingam Institute for Home Science and Higher Education for Women, India

Vanithamani Rangasamy
Avinashilingam Institute for Home Science and Higher Education for Women, India

ABSTRACT

Bone marrow cancer is one of the life-threatening diseases which may cause death to many individuals. Leukemia, lymphoma, multiple myeloma, and other cancers that form in the blood-forming stem cells of the bone marrow constitute bone marrow cancer. Early detection can increase the chance for remission. Accurate and rapid segmentation techniques can assist physicians to identify diseases and provide better treatment at the right time. CAD systems can be useful for the early discovery of bone marrow cancer. It features the latest updated algorithm that combines deep learning with MATLAB for health assessment. This can assist in the early detection of leukemia, lymphoma, and multiple myeloma. For denoising histopathological images, new K-SVD and fast non-local mean filter algorithms are employed. For pre-processing, algorithms like multilayer perceptron and novel hybrid histogram-based soft covering rough k-means clustering techniques are employed. Three classifiers, namely R-CNN, ResNet 50, and LSTM, are used to classify, and the performance is compared based on the accuracy.

DOI: 10.4018/978-1-6684-3947-0.ch014

INTRODUCTION

For the last few years, Computer-Aided Diagnosis (CAD) has been increasing rapidly. Numerous machine learning algorithms and deep learning algorithms have been developed to identify different diseases, e.g., leukemia, lymphoma and multiple myeloma. Leukemia is a White Blood Cells (WBC) related illness affecting the bone marrow and/or blood. Lymphoma is a broad term for cancer that begins in cells of the lymph system, which is part of the body's germ-fighting network. Multiple myeloma is a cancer that forms in a type of WBC's called a plasma cell. There must be an accurate detection and classification system available to diagnose bone marrow cancer at early stage. Early detection of cancer seems to be the important factor in increasing the chance of cancer patient survival. Classification of cancer is one of the most challenging tasks in clinical finding and diagnosis. Bone tumors vary widely in their biological behaviour and require different management depending on their classification as benign, intermediate, or malignant, by the World Health Organization (WHO).

Ching-Wei wang et.al., (2021) Examined the Bone Marrow (BM) which is the essential step in both diagnosing and managing numerous hematologic disorders. BM Nucleated Differential Count (NDC) analysis, as part of BM examination, holds the most fundamental and crucial information. However, there are many challenges to perform automated BM NDC analysis on Whole-Slide Images (WSIs), including large dimensions of data to process, complicated cell types with subtle differences. Vyshnav M T et.al. (2020) developed Deep learning (DL) models that are in large-scale. ANN consisting of a multitude of interconnected parallel processing units called artificial neurons. Especially Convolutional Neural Nets (CNN) achieve outstanding results in image recognition. These capabilities can be used for computer vision purposes in the diagnosis of acute leukemia. The deep learning models were trained by monitoring the train and validation loss per epoch and the best model was selected based on the minimal loss for the validation data. From the comparison results obtained for both the models, it is observed that Mask RCNN has competing results than U-Net and it addresses most of the challenges existing in multiple myeloma segmentation.

RELATED WORK

Ching-Wei wang et.al., (2021) have presented the first study on fully automatic Bone Marrow Nucleated Differential Count (BM NDC) using WSIs with objective magnification, which can replace traditional manual counting relying on light microscopy and proposed an efficient and fully automatic hierarchical deep learning framework for BM NDC WSI analysis in seconds which consist of deep learning model for rapid localization of bone marrow particles and a patch based deep learning for integrating patch-based results and producing final outputs. Rohollah Moosavi Tayebi et. al., (2021) have developed the first ever end-to-end deep learning-based technology for automated bone marrow cytology. Starting with a bone marrow aspirate digital whole slide image, and the technology rapidly and automatically detects suitable regions for cytology, and subsequently identifies and classifies all bone marrow cells in each region. This collective cytomorphological information is captured in a novel representation called Histogram of Cell Types (HCT) quantifying bone marrow cell class probability distribution and acting as a cytological "patient fingerprint.

Eckardt et.al., (2021) Deep learning (DL) can process medical image data and provides data-driven class predictions and here the author have applied a multi-step DL approach to automatically segment

cells from bone marrow images, distinguish between AML samples and healthy controls with an Area Under the Receiver Operating Characteristic (AUROC) of 0.9699, and predict the mutation status of Nucleophosmin 1 (NPM1)—one of the most common mutations in AML—with an AUROC of 0.92 using only image data from bone marrow smears. Vyshnav M T et.al., (2020) have explored the effectiveness of deep learning-based object detection and segmentation algorithms such as mask CNN and U-Net for the detection of multiple myeloma. The manual polygon annotation of the current dataset is performed using VGG image annotation software. The deep learning models were trained by monitoring the train and validation loss per epoch and the best model was selected based on the minimal loss for the validation data.

D. Kumar et.al., (2020) have proposed a model eradicates the probability of errors in the manual process by employing deep learning techniques, namely CNN. The model, trained on cells images, first pre-processes the images and extracts the best features. This is followed by training the model with the optimized Dense Convolutional Neural Network framework and finally predicting the type of cancer present in the cells. The model was able to reproduce all the measurements correctly while it recollected the samples exactly 94 times out of 100. Maryam Bukhari et .al (2021) DCNN- Dense CNN is the used algorithm in Deep Learning. Microscopic images with two subsets Acute Lymphoblastic Leukemia (90 images), Multiple Myeloma (100 images). Accuracy-97.2%- Better than Decision Tree (95%), Random Forest (96%), Naive Bayes (82%). The datasets were small in size hence there is no broader study.

S. Patil Babaso et.al., (2020) have compared machine learning and deep learning techniques. The different machine learning algorithms used to diagnosis leukemia are Support Vector Machine, Nearest Neighbour, Neural Networks and Naive Bayes. Deep Learning algorithms which are used to classify leukemia into its sub-types are: CNN, VGG16, U-Net. Machine learning algorithm has an accuracy of 87% where as deep learning algorithm has achieved accuracy of 94%. Machine learning takes time to train and test a data when compared to deep learning.

Dongguang Li et.al., (2020) have collected the datasets from three different hospitals. Deep learning platform is used for high accuracy. Consisting of multiple Convolutional Neural Networks, to classify pathologic images by using smaller datasets. The diagnostic accuracy of AI models reaches a high level (close to 100%) suitable for clinical use. Luvashen Marimuthu et.al., (2021) Compares machine learning approaches, such as Artificial Neural Networks, Convolutional Neural Networks, random forests and support vector machines, for the diagnosis of multiple myeloma from gel strips and densitometer graphs. This revealed that convolutional neural network, specifically VGG16, was the most suitable approach for the detection of multiple myeloma. But the expected accuracy was not achieved. Feyisope R. Eweje et.al., (2021) have generated an image-based model using the EfficientNet-B0 architecture and a logistic regression model was trained using patient age, sex, and lesion location and the model achieved accuracy of 76%. The analysis was not sufficiently powered to absorb significance difference in classification.

Patrick Le ydon et.al., (2020) The system outlines a U-Net architecture with novel pre-processing techniques, based on the training data and the modification of sigmoid activation threshold selection to successfully segment bone marrow region. The proposed method achieved mean Dice coefficients of 0.979 $\pm$0.02, 0.965 $\pm$0.03, and 0.934 $\pm$0.06. Excellent results are obtained only with limited data. Roxane Licandro et.al., (2019) have proposed a cascaded architecture, consisting of two distinct configured U-Nets, first detects the bone regions and subsequently predicts lesions within bones in a patch-based way. The algorithm provides a full volumetric risk score map for the identification of early signatures of emerging lesions and for visualising high-risk locations. At the right distal femur, the proximal part of

the right femur as well as at the right and left trochanter major, local anomalies in the bone are visible, which falsely are predicted as lesion.

The datasets collected by Roxane Licandro et al., (2020) consist of 2820 Blood microscopic images which were pre-processed to remove and enhance the images which were contaminated with salt and pepper noise; then, features were extracted using a pre-trained Deep Convolutional Neural Network (AlexNet), which makes classifications according to numerous well-known classifiers. After pre-processing the images, AlexNet with well-known classifiers, such as DT, LD, SVM, and K-NN, are employed for classification is fine-tuned for both feature extraction and classification. Experiments were conducted on a dataset consisting of 2820 images confirming that the second model performs better than the first because of 100% classification accuracy. leukemia-free or leukemia-affected are only classified rather than its types. Haneen. T_Salahet et.al., (2021) have described the literature of ML utilization in the diagnosis of the four common types of leukemia: Acute Lymphocytic Leukaemia (ALL), Chronic Lymphocytic Leukemia (CLL), Acute Myeloid Leukaemia (AML), Chronic Myelogenous Leukaemia (CML). Accuracy of algorithms used ranged from 74% to 99.5%. Majority of studies had small and homogenous samples and used supervised learning for classification tasks.

Jothi G et.al., (2019) used hybrid clustering algorithm for leukemia nucleus image segmentation. Features extracted from segmented image are: gray level co-occurrence matrix. Color and shape-based features. Classification is done using deep learning algorithms. The Hybrid Histogram – based Soft Covering Rough K-means Clustering algorithm efficiently segments the nucleus than other prediction algorithms. Segmented image data are large and difficult to process. Nizar Ahmed et.al. In this study datasets were collected from two different sources namely ALL-IDB and The American Society of Hematology (ASH) Image Bank. ALL-IDB dataset provided annotated microscopic blood cell images. CNN architecture was designed for recognizing all subtypes of leukemia. The layers used were convolutional, maxpooling, flatten layer, fully connected layer. CNN model performance has 88.25% accuracy with multi-class classification of all subtypes. Cross validation in evaluation have not performed well. Syrykh, C et.al., (2020) Several deep CNNs were trained automatically to distinguish FL (follicular lymphoma) from benign FH (follicular hyperplasia) in lymph nodes on H&E digital slides. The CNN model, yields 84% accuracy. The experiment uses biased dataset.

Afshin bozorgpour et.al., (2019) have used Automatic deep learning method and two stage of deep learning was designed. STAGE: U-Net model was trained to segment nucleus from input STAGE 2: Trained deeplab3+ model using patches extracted from input images Multi scale technique is used to tackle the problem of cytoplasm boundary. The method ranked second on segpc2021 challenge for multiple myeloma cancer cell segmentation with 94.3% accuracy.

Image Datasets

The digital database of leukemia, lymphoma, and multiple myeloma is publically available. Bone marrow cancer digital database, which contains histopathological images from open access resources. It consisted of 3761 images which comprises images of Leukemia, Lymphoma, Multiple Myeloma in bone marrow. The 70% images are used for the training so called the training datasets and the rest 30% images are used for the testing and thus they are called the testing datasets. The datasets were obtained from the Kaggle.com an open-source network.[https://www.kaggle.com/andrewmvd/leukemiaclassification,https://www.kaggle.com/andrewmvd/multiple myeloma-classification].

The categorical classification is as follow;

- Normal images with 0% malignancy
- Leukemia,
- Lymphoma,
- Multiple myeloma.

The detailed description of the datasets is shown in *Figure 1*.
The sample images for each category are shown in *Figure 2*.

Figure 1. Pie chart of the dataset

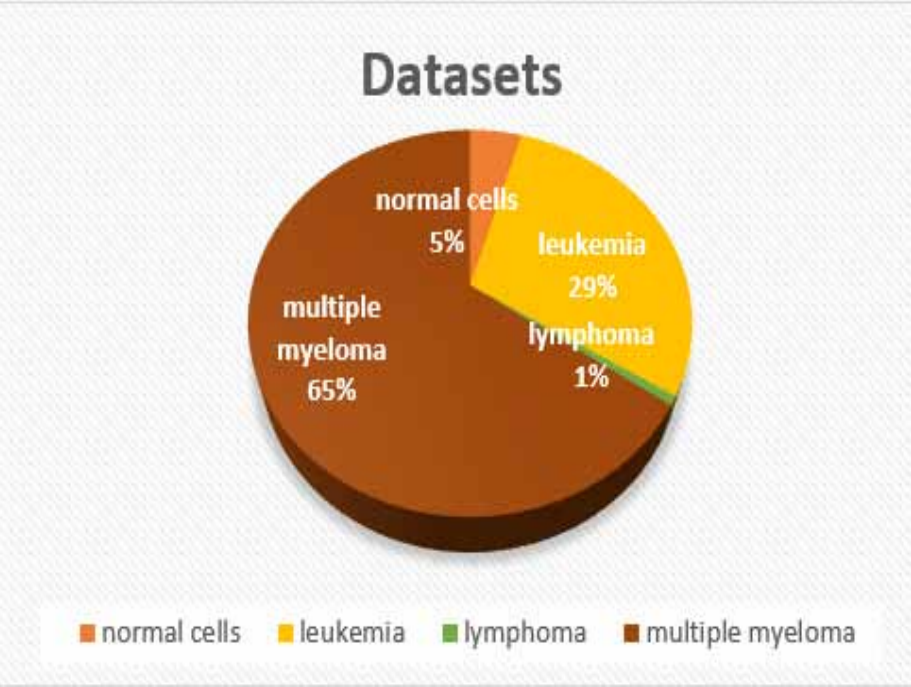

Figure 2. Sample Image from database (a) Normal (b) Multiple myeloma (c) Leukaemia (d) Lymphoma

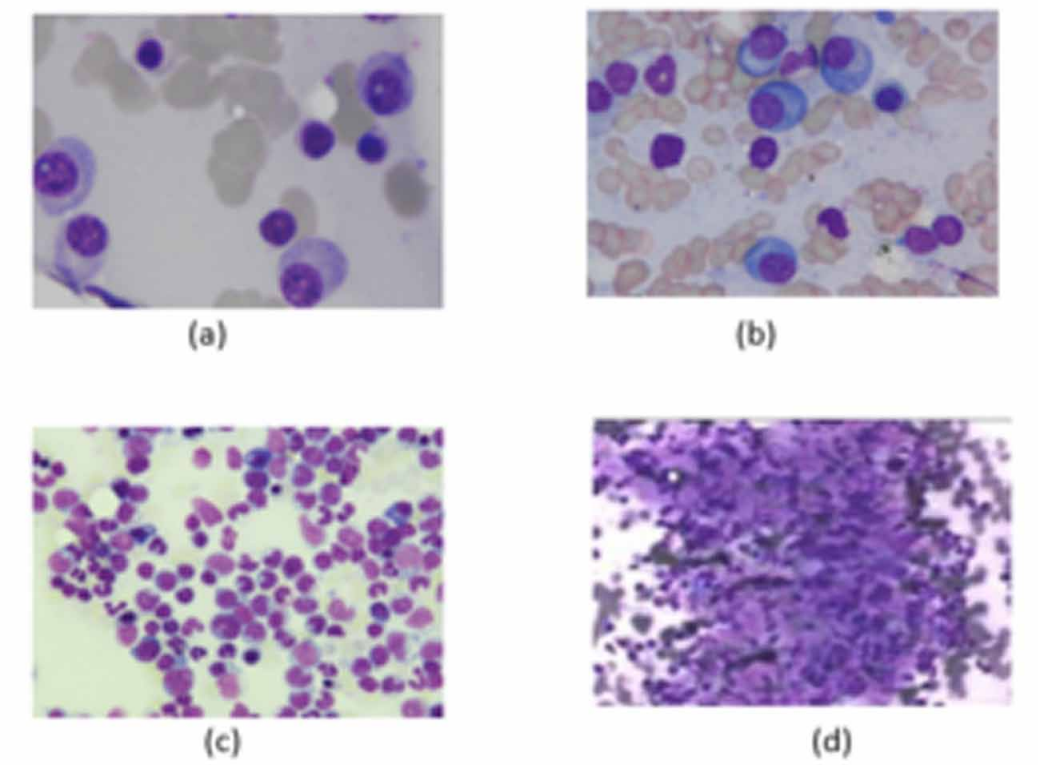

Deep learning techniques revolve around the use of models which have been trained and developed for one task and then used on another task. The proposed work presents the detection of Bone Marrow Cancer using Matlab software. That can be used for early detection of types of bone marrow cancer so that the life span of the patient can be increased. The images collected are leukemia, lymphoma, multiple myeloma which are segregated as testing and training sets. These images are pre-processed using filters, then the segmentation and feature extraction are done by using neural networks and finally they are classified as cancerous, non-cancerous and its types.

WORKFLOW

Figure 3. Workflow diagram to detect the bone marrow cancer using Deep Learning Techniques

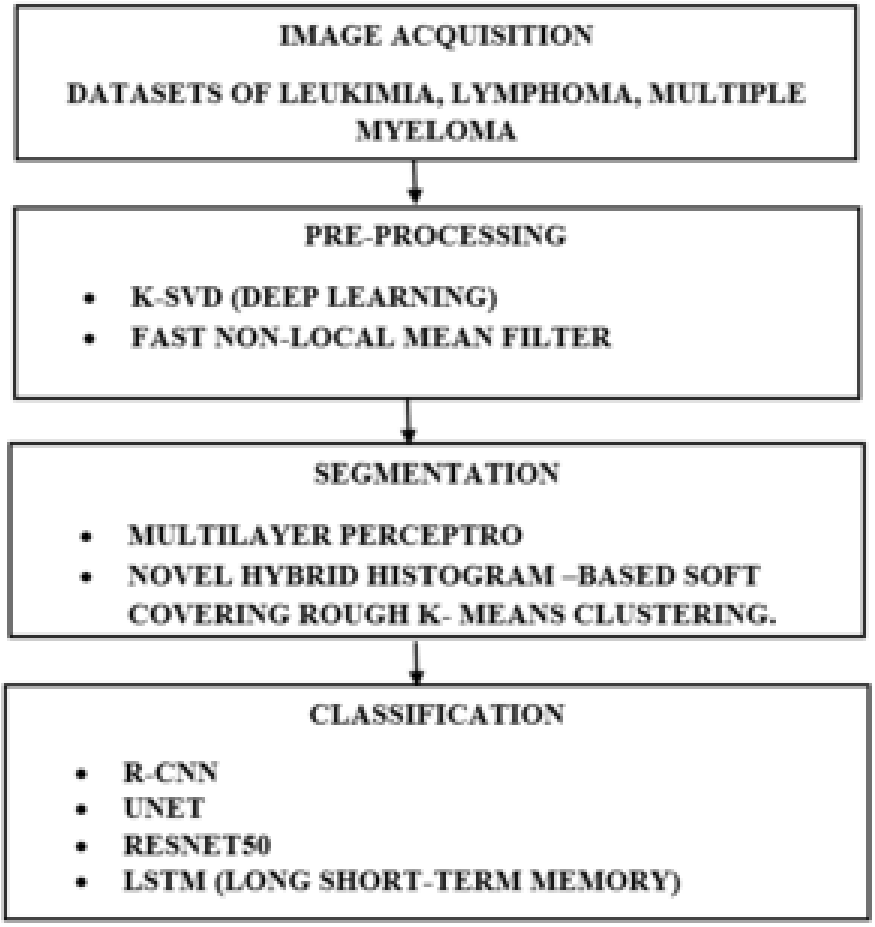

PRE-PROCESSING

The preprocessing of data is a common first step in the deep learning workflow to prepare raw data and transform it into a format that can be used by the network. For a network to be trained and make predictions on new data, the images must match the input size. The size of images needs to be adjusted to match the network, it can be rescaled or cropped according to the data. It is also possible to train the networks to be invariant to distortions in image data using augmenting. In the context of model training and inference, preprocessing is the process of formatting images before they are used for the training and inference process. Two algorithms were used for the preprocessing of the images they are K-SVD (K means singular value decomposition) and Fast Non local mean filter. They are used to remove the Gaussian noise which is present in the histopathological images.

K-SVD

It is a dictionary learning algorithm that uses a Singular Value Decomposition approach to create a dictionary for sparse representations. In general, K-SVD (K means singular value decomposition) is a generalization of k-means clustering. It is a method that works by iteratively alternating between sparse coding the input data based on the existing dictionary, and updating the atoms in the dictionary to better reflect the data. The below image describes the algorithm of K-SVD.

Step 1: Start
Step 2: From the original block se the initial dictionary value.
Step 3: Find the sparse coefficients using OMP algorithm.
Step 4: Thus, the output image is obtained as denoised image.

FAST NON-LOCAL MEAN FILTER

The Fast Non-Local Mean Filter takes the mean of all pixels in an image, weighted by the degree of similarity between each pixel and the target pixel. This result has greater post-filtering clarity, and less loss of detail in the image compared with local mean algorithms. Denoising with non-local means adds "method noise" (i.e., errors made during the process), which looks more like white noise, which is desirable because the denoised product is typically less disturbing when it is non-localized that was proposed by Buades, Antoni et.al (20–25 June 2018)

Given a discrete noisy image $v = \{v(i) \mid i \in I\}$, the estimated value NL[v](i), for a pixel i, is computed as a weighted average of all the pixels in the image,

$$NL[v](i) = j \in I \; w(i, j) \; v(j), \tag{1}$$

where the family of weights $\{w(i, j)\}$ j depends on the similarity between the pixels i and j, and satisfy the usual conditions $0 \leq w(i, j) \leq 1$ and j w (i, j) =1.

The similarity between two pixels i and j depends on the similarity of the intensity gray level vectors v(Ni) and v (Nj), where Nk denotes a square neighbourhood of fixed size and centered at a pixel k. This similarity is measured as a decreasing function of the weighted Euclidean distance, $v(Ni) - v(Nj)^2_{2, a}$ where a > 0 is the standard deviation of the Gaussian kernel. The application of the Euclidean distance to the noisy neighbourhoods raises the following equality

$$E\|v(Ni) - v(Nj)\|^2_{2, a} = \|u(Ni) - u(Nj)\|^2_{2, a} + 2\sigma 2. \tag{2}$$

This equality shows the robustness of the algorithm since in expectation the Euclidean distance conserves the order of similarity between pixels. The pixels with a similar grey level neighbourhood to v(Ni) have larger weights in the average. These weights are defined as, w (i, j) = 1 Z(i) e− $\|v(Ni)-v(Nj)\|^2_{2, ah}$2, where Z(i) is the normalizing constant Z(i) = j e− $\|v(Ni)-v(Ni)\|^2_{2, ah}$2 and the parameter h acts as a degree of filtering. It controls the decay of the exponential function and therefore the decay of the weights as a function of the Euclidean distances.

The NL-means not only compares the grey level in a single point but the geometrical configuration in a whole neighbourhood. This fact allows a more robust comparison than neighbourhood filters. Figure 1 illustrates this fact, the pixel q3 has the same grey level value of pixel p, but the neighbourhoods are much different and therefore the weight w (p, q3) is nearly zero.

EVALUATION METRICS

Table 1. Evaluation metrics for denoising the test images

Peak to signal ratio (PSNR)	$10\log_{10}(\text{peakval}^2)/\text{MSE}$
Mean Square Error (MSE)	$\frac{1}{MN}\sum_{n=0}^{M}\sum_{n=0}^{N}\left[\hat{g}\left(n,m\right)-g\left(n,m\right)\right]^2$
Signal to Noise Ratio (SNR)	$10\log_{10}\frac{\sum_0^{n_x-1}\sum_0^{n_y-1}\left[r\left(x,y\right)\right]^2}{\sum_0^{n_x-1}\sum_0^{n_y-1}\left[r\left(x,y\right)-t\left(x,y\right)\right]^2}$
Structure Similarity Index Measurement (SSIM)	$\frac{\left(2\mu_x\mu_y+c_1\right)\left(2\sigma_{xy}+c_2\right)}{\left(\mu_1^2+\mu_2^2+c_1\right)\left(\sigma_1^2+\sigma_2^2+c_2\right)}$

The two algorithms were compared in terms of the image quality evaluation metrics such as Signal to Noise Ratio (SNR), Peak Signal to Noise Ratio (PSNR), Mean Square Error (MSE) and Structural Similarity Index Measure (SSIM). SNR is defined as the ratio of the signal power and the noise power and is computed as equation (3). SNR is expressed in decibel.

$$10\log_{10}\frac{\sum_0^{n_x-1}\sum_0^{n_y-1}\left[r\left(x,y\right)\right]^2}{\sum_0^{n_x-1}\sum_0^{n_y-1}\left[r\left(x,y\right)-t\left(x,y\right)\right]^2} \tag{3}$$

Peak Signal to Noise Ratio (PSNR) (R.C. Gonzalez & R.E. Woods, 2008) is used to measure the difference between the original and denoised images of size M x N. It is estimated using equation (4) and is expressed in decibel (dB)

$$10\log_{10}(\textbf{peakval}^2) \textbf{ / MSE} \tag{4}$$

MSE is the Mean Squared Error and is given in equation (2). MSE is the Mean Square Error which represents the cumulative squared error between the denoised and the original image.it is the the average squared difference between the estimated values and the actual value.it is given in equation (5).

$$\frac{1}{\mathbf{MN}}\sum_{\mathbf{n}=0}^{\mathbf{M}}\sum_{\mathbf{n}=0}^{\mathbf{N}}\left[\hat{\mathbf{g}}\left(\mathbf{n},\mathbf{m}\right)-\mathbf{g}\left(\mathbf{n},\mathbf{m}\right)\right]^{2} \tag{5}$$

The Structural Similarity (SSIM) index is a method for measuring the similarity between two images and is calculated as in equation (6).

Figure 4. Evaluation matrices of pre-processing

TYPES OF BONE MARROW CANCER	MULTIPLE MYELOMA				LEUKEMIA				LYMPHOMA			
ALGORITHM	NLM	KSVD	NLM	KSVD	NLM	KSVD	NLM	KSVD	NLM	KSVD	NLM	KSVD
TEST IMAGES	1	1	2	2	1	1	2	2	1	1	2	2
PEAK SNR	31.57	33.94	30.035	33.81	27.179	30.89	28.71	30.93	32.41	34.22	33.17	35.74
SNR	28.55	30.86	29.16	30.25	26.99	29.99	27.04	28.96	27.33	30.13	28.07	30.63
MSE	0.0063	0.0002	0.0051	0.0001	0.0785	0.0004	0.0698	0.0001	0.0367	0.0003	0.0391	0.0002
SSIM	0.8346	0.9578	0.8288	0.9646	0.8074	0.9696	0.0794	0.9857	0.835	0.9584	0.8718	0.9949

The SNR, PSNR, MSE and SSIM values are listed in Table 1

From the table 1 it is observed that the SNR and PSNR values are higher in case of K-SVD when compared to NLM.The SSIM values ranges between 0 to 1 and from the SSIM values of both the filters in Table 2, it is inferred that the performance of KSVD is better. The value of MSE is also less in case of K-SVD compared to NLM filter. The quality evaluation metrics shows the salt and pepper noise suppression capability of K-SVD is good. The preprocessed images i.e., the denoised images are shown in figure 5,6, and 7.

TRAINING GRAPH

Figure 5. Training graph for pre-processing technique

Figure 6. Denoising results for leukaemia, (a)Test image 1, (b)Noisy image of test image 1, (c)Denoised image using NLM, (d)Denoised image using K-SVD, (e) Test image 2, (f)Noisy image of test image 2, (g)Denoised image using NLM, (h)Denoised image using K-SVD

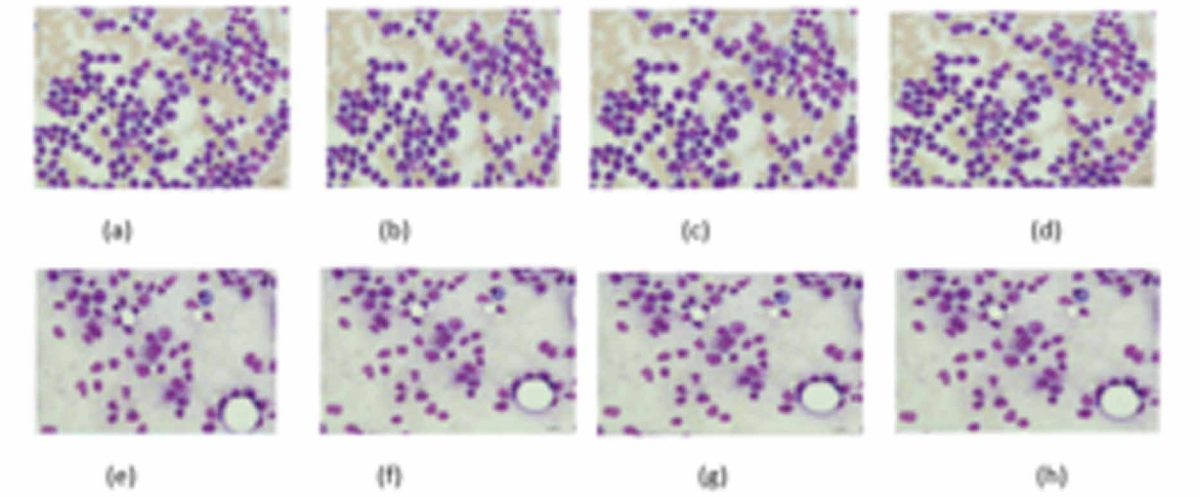

Figure 7. Denoising results for lymphoma (a)Test image 1, (b)Noisy image of test image 1, (c)Denoised image using NLM, (d)Denoised image using K-SVD, (e) Test image 2, (f)Noisy image of test image 2, (g)Denoised image using NLM, (h)Denoised image using K-SVD

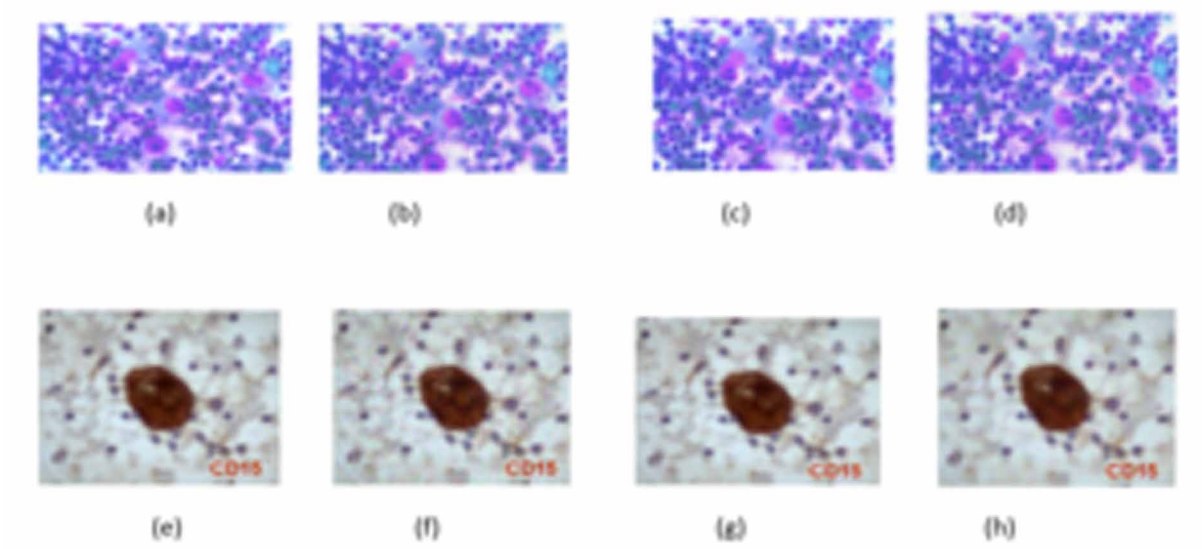

Figure 8. Denoising results for Multiple Myeloma (a)Test image 1, (b)Noisy image of test image 1, (c) Denoised image using NLM, (d)Denoised image using K-SVD, (e) Test image 2, (f)Noisy image of test image 2, (g)Denoised image using NLM, (h)Denoised image using K-SVD

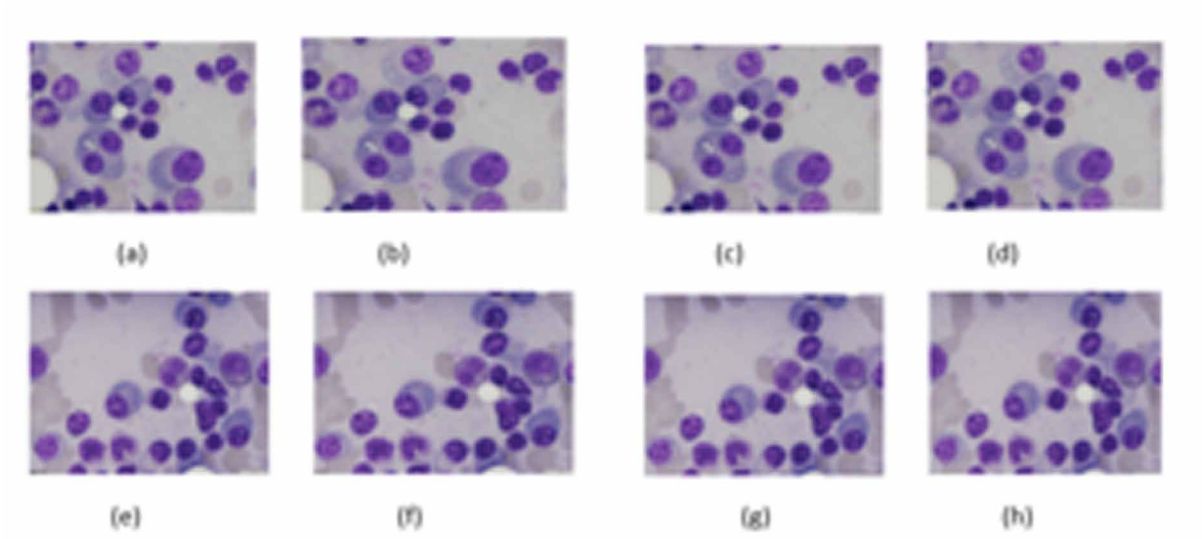

Figure 5 shows the training graph of preprocessing and Figure 6, Figure 7, Figure 8 shows the preprocessing done in the three types of datasets.

SEGMENTATION

Segmentation is a process that analyses the total pixel information of an image and groups related structures together. These similar patterns are not predefined, but rather random discrete structures within the images. This information is learned to identify similar patterns in other images for further classification purposes.

In this work, Multilayer perceptron, an RNN based algorithm and Novel Hybrid Histogram Based Soft Covering Rough K-means Clustering algorithm are used to segment the dataset.

MULTILAYER PERCEPTRON

Rumelhart et.al. Introduced the multilayer perceptron from the single-layer perceptron. As opposed to single-layer perceptron, multi-layer perceptron has an additional hidden layer. These hidden layers are responsible for the computation and operation of the input image and maintain it. The function of multilayer perceptron is like the neural network along with brain, where it is responsible not only for transferring data but also for learning. Aimi shaliah et.al.,2018 The Multilayer Perceptron neural network is a feed forward neural network with one or more hidden layers. Cybenko and Funahashi have proven that the MLP network with one hidden layer has the capability to approximate any continuous function up to certain accuracy. The classification performance of the MLP network will highly depend on the structure of the network and training algorithm

Figure 9. The architecture of multilayer perceptron

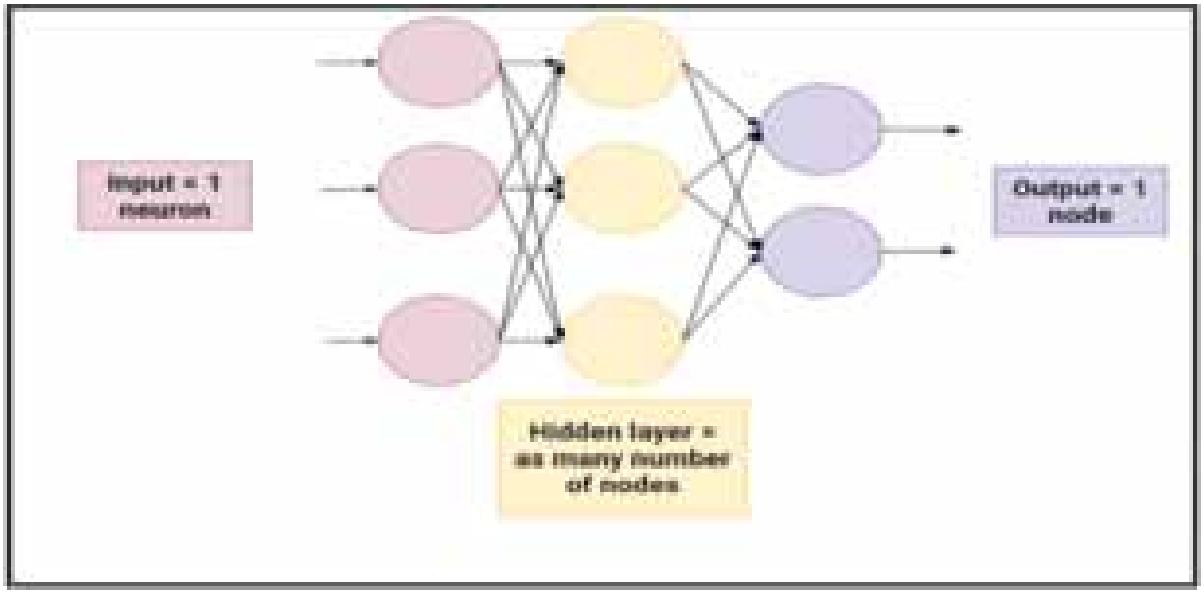

Figure 9 shows that, multilayer perceptron has three layers which include the input layer, the hidden layer, and the output layer. The input layer has one neuron responsible for providing one information. The final decision is made by one node in the output layer. The hidden layers would have just as many nodes for learning and decision-making. An input layer receives one neuron, which produces one output node, which is the output calculated by the hidden layer, based on the number of neurons in the input layer. The hidden layers would receive inputs from all neurons and the final outcome would be a single output from the vying layers.

NOVEL HYBRID HISTOGRAM BASED SOFT COVERING ROUGH K-MEANS CLUSTERING

Clusters are unidentified structures that form from common bases. When segmenting them together, clustering is done. K is the centroid that represents each group with a common structure. For reducing the sum of squared distance between all the points and the centroid, a K means clustering process is preferred.

Since the dataset consists of both soft and rough datasets, this clustering process is performed by combining both sets for a smooth clustering process. The K-means technique, a non-supervised learning method, is used to solve clustering problems. The K-means algorithm divides a set of unlabelled data into a number of clusters. They are grouped according to their similarity. The predefined K implies that if K is 2, we will have two clusters, if K is 3, we will have three clusters, and so on. With K-means clustering, you first determine the K centroid, and then allocate each data point to the cluster whose centroid is closest to the point's location. Iteratively calculating the centroid of the cluster and assigning each data point to it, K-means calculates the distance from the centroid until the number of distances from the centroid is minimized.

Figure 10. The architecture of novel hybrid based soft covering rough K-Means clustering

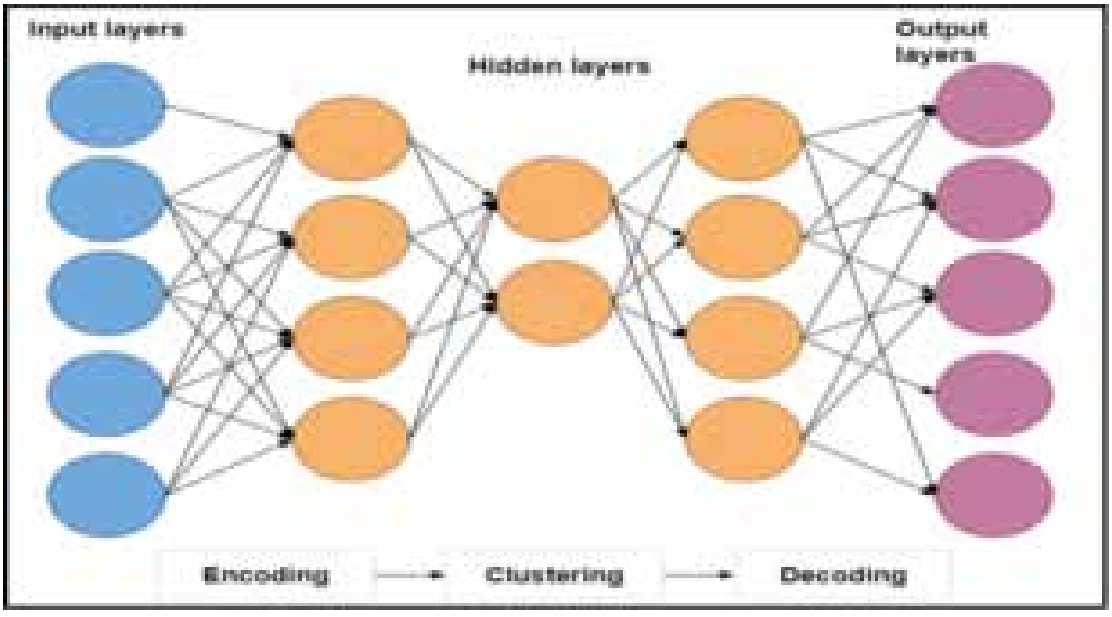

Figure 10 is the architecture of Novel Hybrid Based Soft Covering Rough K-Means Clustering. The value of K is determined with the peak value of the histogram image.

SEGMENTED IMAGES

Figure 11. Segmented results for leukaemia, (a)Test image 1, (b)MLP of test image 1, (c) Novel Hybrid Histogram Based Soft Covering Rough K-Means Clustering of test image 1 (d) Test Image 2 (e) MLP of test image 2 (f) Novel Hybrid Histogram Based Soft Covering Rough

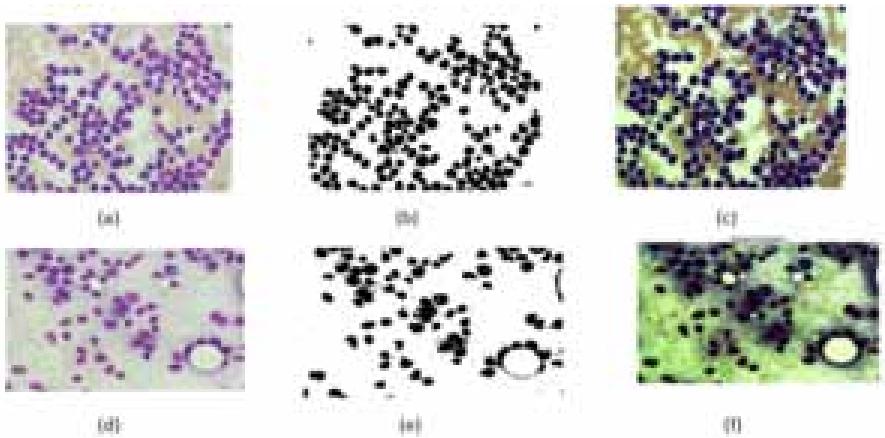

Figure 12. Segmented results for lymphoma, (a)Test image 1, (b)MLP of test image 1, (c) Novel Hybrid Histogram Based Soft Covering Rough K-Means Clustering of test image 1 (d) Test Image 2 (e) MLP of test image 2 (f) Novel Hybrid Histogram Based Soft Covering Rough

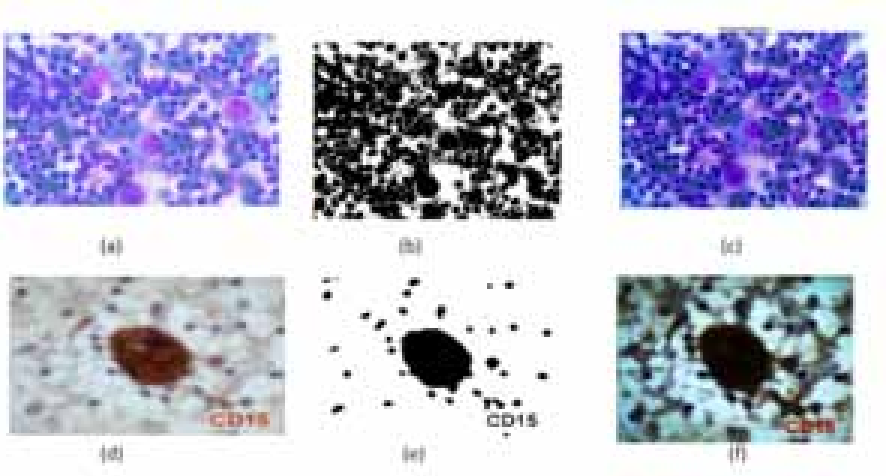

Figure 13. Segmented results for multiple myeloma, (a)Test image 1, (b)MLP of test image 1, (c) Novel Hybrid Histogram Based Soft Covering Rough K-Means Clustering of test image 1 (d) Test Image 2 (e) MLP of test image 2 (f) Novel Hybrid Histogram Based Soft Covering Rough K-Means Clustering

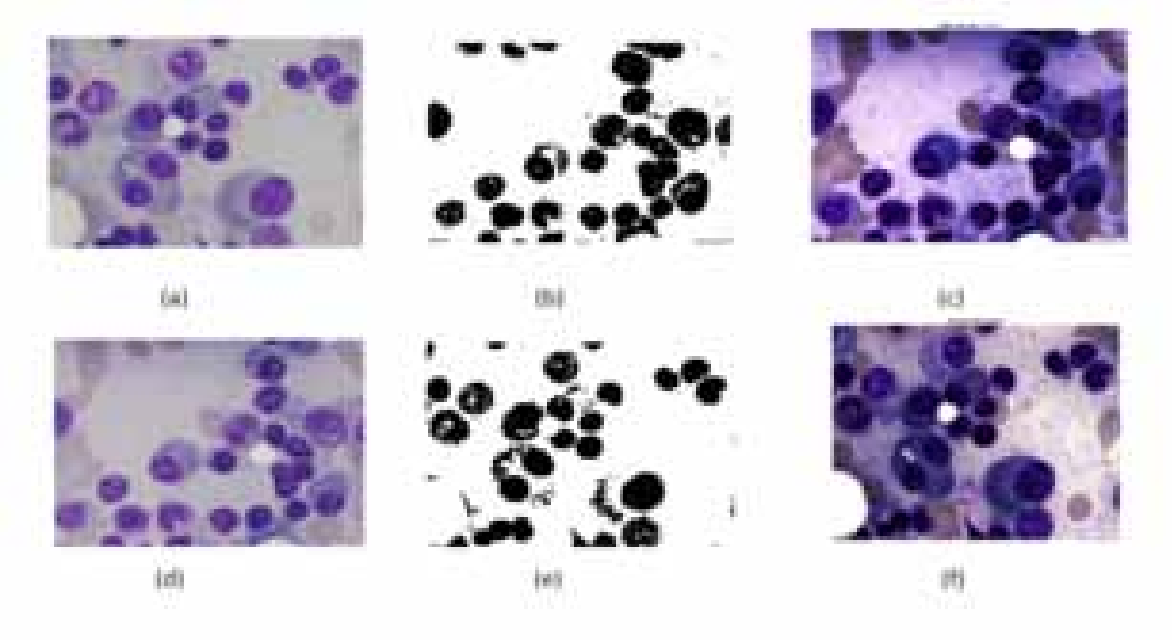

Figure 11, Figure 12 and Figure 13 shows the output obtained by Multilayer Perceptron and Novel Hybrid Histogram Based Soft Covering Rough K-Means Clustering for the dataset.

Figure 14. Comparison of classifiers (a) Jaccard and MCC (b) accuracy, specificity, sensitivity, F-measure, dice, precision

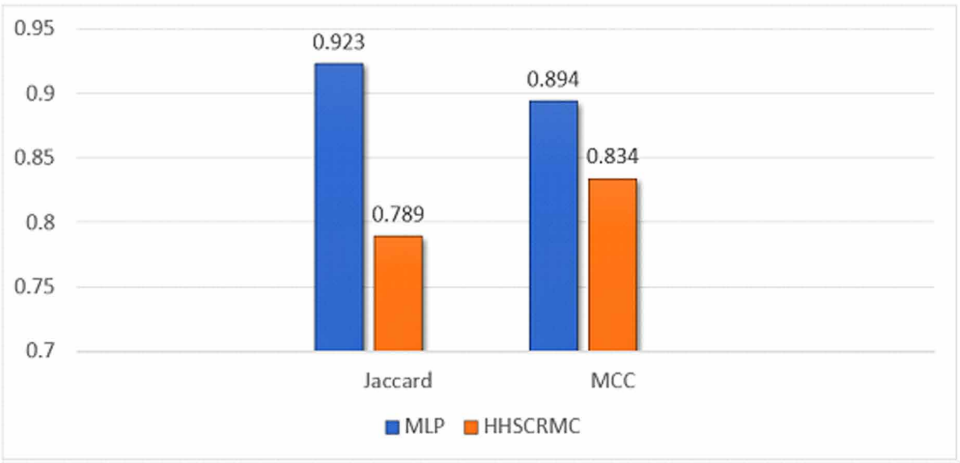

(a)

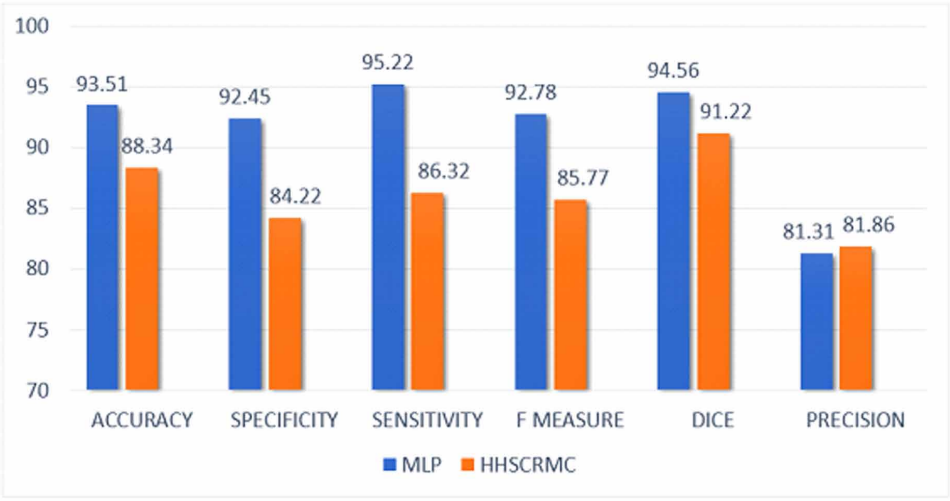

(b)

CLASSIFICATION

After segmenting the images, the data information from each image is used to segregate them into various classes. These classes are defined with various background. These classes are classified after training the image data.

With neural network, multiple classes are either predefined or they are classified with training. To classify the images, three types of classifiers are used in this project. They are Resnet50, Long Short-Term Memory, and finally R-CNN. Convolutional neural network (CNN) is the most popular neural network used for deep learning classification procedures owing to its variety of architecture and time-

saving algorithms. The CNN is built with ReLU (Rectification Linear Units), a pooling layer, and a fully connected layer. CNN is an advantage over other networks because it is most commonly used to transfer learning, which involves swapping out pre-trained architecture layers with the preferred layers. There are multiple types of CNN available through MathWorks, such as AlexNet, GoogleNet, ResNet.

ResNet50

ResNet50 is the residual neural network with 50 layers. These layers include convolutional regions and pooling regions. It is a deep convolutional neural network with shortcut connections that are used as basic convolutional connections. For a plain network, shortcut connections would result in a residual counter path. While normal residual layers may differ from the various layers that are included with the algorithm, there are common 34 residual layers. ResNet 50 shifts the 2-layer bottleneck block to a 3-layer bottleneck block, making it a 50-layer residual network architecture instead of the 34-layer architecture.

More 3-layer bottleneck blocks can be added to make more layers, like 101-layer ResNet or 152-layer ResNet architectures. In comparison with all the four available ResNet architectures, ResNet50, ResNet101, and ResNet152 train and classify better than ResNet34. Figure 15 explains the architecture of ResNet50.

Figure 15. Architecture of ResNet50

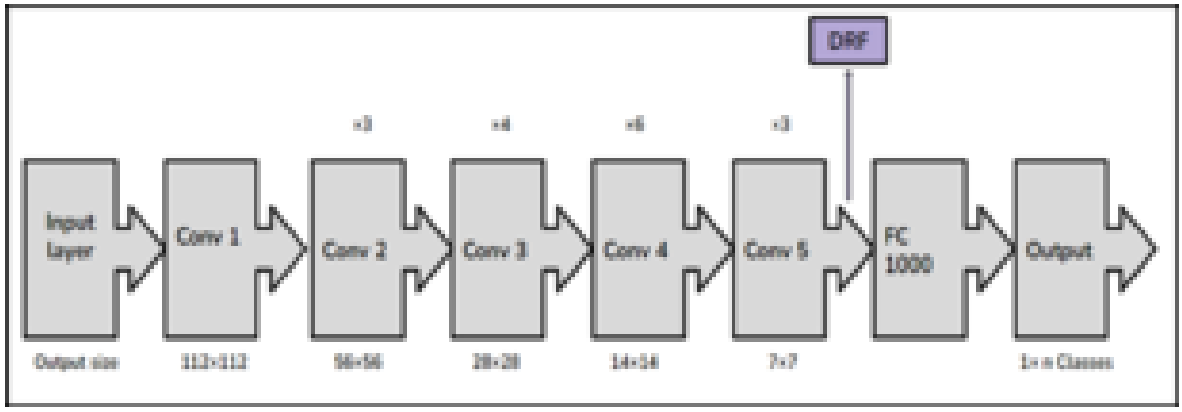

Long Short-Term Memory

LSTM is an algorithm based on RNN (recurrent neural networks). LSTM has a comparatively long memory compared to RNN classifiers which have a short memory. all the non-relevant data are discarded. This is because the architecture consists of multiple hidden layers.

Figure 16. Architecture of long short-term memory

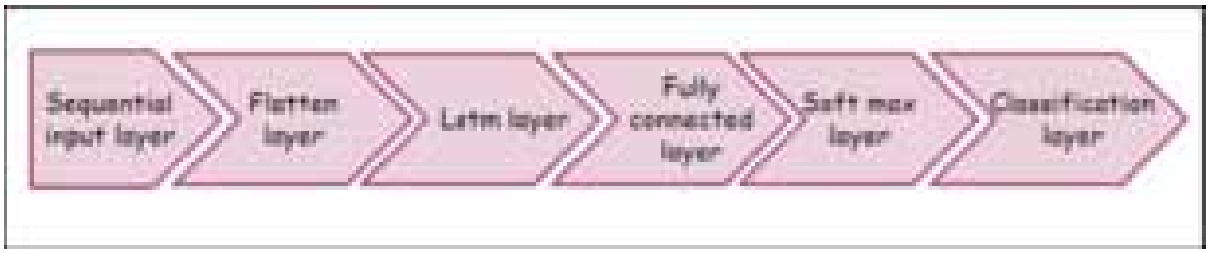

The architecture of LSTM consists of gates that allow for better memory. The architecture consists of input gate, output gate, memory cells, cell state and forget gate. Figure 16 explains the architecture of LSTM with the corresponding layers.

The RNN (Recurrent Neural Network) consists of cyclic networks that aid in the classification and sequence of input images. In recurrent neural networks, activations from a previous interval are used to guide prediction for the next interval. Data from these activations are stored as memory and used for more learning. Due to the excess memory block in the RNN, the LSTM architecture is suitable for long-term storage.

R-CNN

It is the Convolutional neural network that would have a special algorithm to find the region of interest. The regions of interest are those with certain requirements. There are regions of interest that are included in the classification process.

Figure 17. Architecture of R-CNN

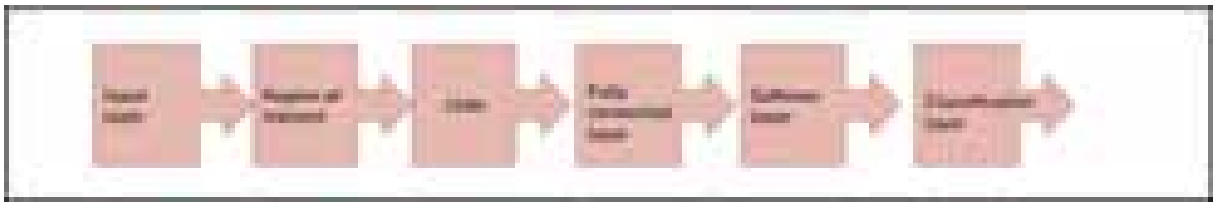

In R-CNN, layers from a pretrained network are usually replaced for image training. The Resnet 50 architecture is the architecture preferred here but with the last three layers being replaced with other layers for the training and classification process. Figure 17 explains the R-CNN architecture where the last three layers of CNN is replaced with other layers.

EVALUATION METRICS

Evaluation metrics provide a basis for knowing the performance of the algorithm and further improving the methodologies with time. Table 2 provides all the required formula for evaluation metrics.

True Positive: A true positive outcome occurs when both the outcome and the output show the expected positive outcome.

True Negative: An outcome that both results in a negative outcome and then results in a negative outcome is considered true Negative

False Positive: When the expected outcome is positive, but the obtained outcome is negative, it is False Positive.

False Negative: This occurs when the expected outcome is negative, and the actual outcome is positive.

Accuracy: To calculate this, divide the total number of true predictions by the total number of predictions. The accuracy calculation produces better results when a well-balanced set of classes is used, but with unbalanced classes, the numbers might fluctuate.

Precision*:* Precision is calculated based on Positive expected outcomes. It is the ratio of True Positive to the predicted number of Positive.

Sensitivity: The concept of sensitivity is also known as recall. It involves the calculation of how many true positives there are compared to the number of actual positives

F-Measure: It is the mean rate of both precision and sensitivity, and it reaches its maximum value when precision equals specificity.

Specificity: Basically, it is a ratio between the number of true negatives compared to the total number of negatives outcome

Jaccard: This is the calculation of the value that is common to both A and B to the values in both A and B

Dice: The calculation is based on the number of true positives divided by the number of predictions.

MCC: This is the Mathews correlation coefficient. Davidee et. Al proves that MCC is a more precise outcome.

Table 2. Formula of evaluation metrics

Accuracy	$\frac{TP+TN}{TP+TN+FP+FN}$
F-measure	$\frac{2\times precision\times recall}{precision+recall}$
Sensitivity	$\frac{TP}{TP+FN}$
Specificity	$\frac{TN}{FP+TN}$
Precision	$\frac{TP}{TP+FP}$
Jaccard	$\frac{A\cap B}{A\cup B}$
Dice	$\frac{2\times TP}{\left(TP+FP\right)+\left(TP+FN\right)}$
MCC	$\frac{\left(TP*TN-FP*FN\right)}{\left(\left(TP+FP\right)\left(TP+FN\right)\left(TN+FP\right)\left(TN+FN\right)\right)^{1/2}}$

Figure 18 shows a visual representation of the Evaluation metrics representing Positive and Negative events. Figure 19 shows the comparison of evaluation matrices of various classifiers.

Figure 18. Evaluation metrics

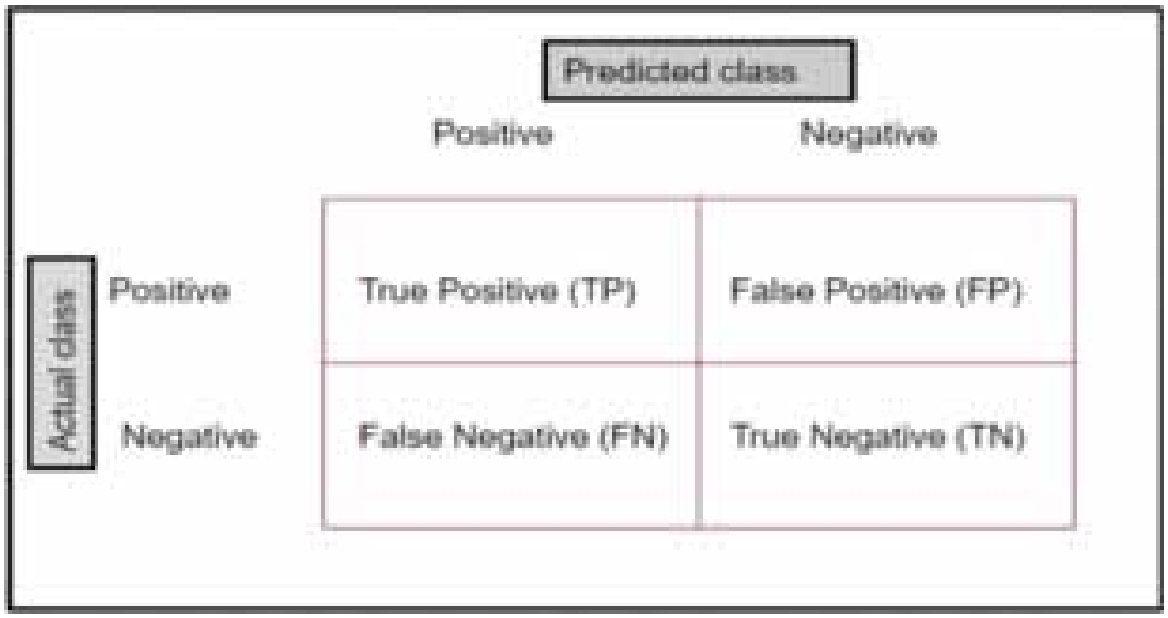

Figure 19. Comparison of the classifiers

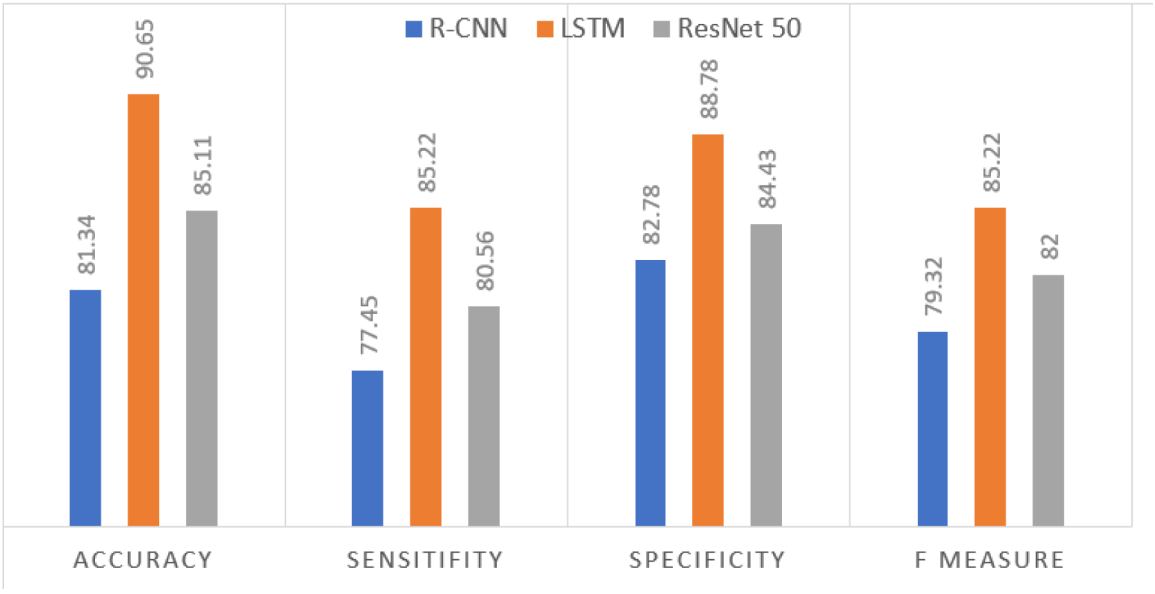

CONCLUSION

The bone marrow cancer was considered as a serious issue and can be cured if it is diagnosed at an

early stage. So, the computer aided method is proposed for the detection of leukemia, lymphoma and multiple myeloma. The image dataset comprises of leukemia, lymphoma, multiple myeloma and normal which consists of totally 3761 images. The 70% images are used for the training so called the training datasets and the rest 30% images are used for the testing and thus they are called the testing datasets. Image preprocessing has been successfully completed and the output has been taken which is effective. The preprocessing is done by using two different algorithms namely K-SVD (K means singular value decomposition) and Fast non-local mean filter. Step by step explanation for the algorithm is executed with formulas and methods. Among the two K-SVD (K means singular value decomposition) algorithm shows more accuracy. The segmentation is done by using multilayer perceptron and Novel hybrid histogram based soft covering rough k-means clustering. The architecture of the two-segmentation algorithm was explained. Among these two the multilayer perceptron algorithm shows more accuracy. The classification is done using RCNN, LSTM, Resnet-50 and explained along with their architecture. In comparison with that LSTM shows more accuracy.

FUTURE SCOPE

Implement real time images for the diagnosis of bone marrow cancer.

REFERENCES

Leyden, P., O'Connell, M., Greene, D., & Curran, K. (2019). Automatic bone marrow segmentation for PETCT imaging in multiple myeloma. *Physica Medica*.

Mosquera Orgueira, A., González Pérez, M. S., & Díaz Arias, J. Á. (2021). *Survival prediction and treatment optimization of multiple myeloma patients using machine-learning models based on clinical and gene expression data*. Leukaemia.

Meilˇa & Jordan. (2021). Multi-scale Regional Attention Deeplab3+: Multiple Myeloma Plasma Cells Segmentation in Microscopic Images. *Journal of Machine Learning Research*.

Zaid & Bes. (2021). *Multiple Myeloma Staging*. Med Space Journal.

Williams, Razzo, Caro, & Morga. (2019). Genetic Segmentation and Targeted Therapeutics for Multiple Myeloma. *Oncology Journal*.

Carvalodh. (2020). Machine-learning Algorithm Predicts Responses to Myeloma Treatments. *Myeloma Research*.

Vyshnav, S., & Gopalakrishnan, V., Menon, & Soman. (2020). Deep Learning Based Approach for Multiple Myeloma Detection. *11th International Conference on Computing, Communication and Networking Technologies (ICCCNT).*

Marimuthu, P. Punchoo, & Bhora. (2021). A Comparison of Machine Learning Techniques for Diagnosing Multiple Myeloma. Academic Press.

Syrykh, C., Abreu, A., Amara, N., & Siegfried, A. (2020). Accurate diagnosis of lymphoma on whole-slide histopathology images using deep learning. *Journal of NPJ Digit. Med, 3*(63), 354–380.

Bozorgpour, Azad, Showkatian, & Sulaiman. (2021). Multi-scale regional attention deeplab3+: Multiple Myeloma plasma cells segmentation in microscopic images. *Journal of Machine Learning Research, 6*(31), 234-245.

Eweje, F. R., Bao, B., Wu, J., Dalal, D., & Liao, W. (2021). Deep Learning for Classification of Bone Lesions on Routine MRI. EBiomedicine, 68(7), 103-402.

Loey, M., Naman, M., & Zayed, H. (2020). Deep Transfer Learning in Diagnosing Leukemia in Blood Cell. *Journal of Diagnostic*, *9*(29), 546–590. doi:10.3390/computers9020029

Salahet, Muhsen, Esalama, Owaidah, & Hashmi. (2019). Machine learning applications in the diagnosis of leukaemia: Current trends and future directions. *International Journal of Laboratory Haematology, 41*(6), 717-726.

Eckardt, J.-N., Bornhauser, M., Wendt, K., & Middeke, J. M. (2020). Application of machine learning in the management of acute myeloid leukemia. Current Practice and Future Prospects, 4(23), 79-90.

Ahmed, N., Yigit, A., Isik, Z., & Alpkocak, A. (2019). Identification of Leukemia Subtypes from Microscopic Images Using Convolutional Neural Network. *Journal of Diagnostic*, *9*(104), 128–234. doi:10.3390/diagnostics9030104 PMID:31450720

Sarker, S., Chowdhury, S., Laha, S., & Dey, D. (2019, April). use of non-local means filters to denoise image corrupted by salt and pepper noise. *International Journal (Toronto, Ont.)*, *3*(2).

Compilation of References

Abhinav, M. S., Kumar, M., Santhosh, J., Salhan, A., & Anand, S. (2009). Nadi Yantra: A Robust System Design to Capture the Signals from the Radial Artery for NonInvasive Diagnosis. *Journal of Biomedical Science and Engineering*, *2*(7).

Abo-Zahhad, M., Al-Ajlouni, A. F., Ahmed, S. M., & Schilling, R. J. (2013). A new algorithm for the compression of ECG signals based on mother wavelet parameterization and best-threshold levels selection. *Digital Signal Processing*, *23*(3), 1002–1011. doi:10.1016/j.dsp.2012.11.005

Accardo, A., Affinito, M., Carrozzi, M., & Bouquet, F. (1997). Use of the fractal dimension for the analysis of electroencephalographic time series. *Biological Cybernetics*, *77*(5), 339–350. doi:10.1007004220050394 PMID:9418215

Acharya, U. R., Chua, C. K., Lim, T. C., Dorithy, & Suri, J. S. (2009). Automatic identification of epileptic EEG signals using nonlinear parameters. *Journal of Mechanics in Medicine and Biology*, *9*(4), 539–553. doi:10.1142/S0219519409003152

Acharya, U. R., Dua, S., Du, X., Sree S, V., & Chua, C. K. (2011). Automated diagnosis of glaucoma using texture and higher order spectra features. *IEEE Transactions on Information Technology in Biomedicine*, *15*(3), 449–455. doi:10.1109/TITB.2011.2119322 PMID:21349793

Acharya, U. R., Fujita, H., Lih, O. S., Hagiwara, Y., Tan, J. H., & Adam, M. (2017). Automated detection of arrhythmias using different intervals of tachycardia ECG segments with convolutional neural network. *Information Sciences*, *405*, 81–90. doi:10.1016/j.ins.2017.04.012

Acharya, U. R., Fujita, H., Oh, S. L., Hagiwara, Y., Tan, J. H., & Adam, M. (2017). Application of deep convolutional neural network for automated detection of myocardial infarction using ECG signals. *Information Sciences*, *415*, 190–198.

Acharya, U. R., Fujita, H., Oh, S. L., Hagiwara, Y., Tan, J. H., Adam, M., & Tan, R. S. (2019). Deep convolutional neural network for the automated diagnosis of congestive heart failure using ECG signals. *Applied Intelligence*, *49*(1), 16–27.

Acharya, U. R., Joseph, K. P., Kannathal, N., Lim, C. M., & Suri, J. S. (2006). Heart rate vari- ability: A review. *Medical & Biological Engineering & Computing*, *44*(12), 1031–1051.

Acharya, U. R., Mookiah, M. R. K., Koh, J. E. W., Tan, J. H., Bhandary, S. V., Rao, A. K., Fujita, H., Hagiwara, Y., Chua, C. K., & Laude, A. (2016). Automated screening system for retinal health using bi-dimensional empirical mode decomposition and integrated index. *Computers in Biology and Medicine*, *75*(1), 54–62. doi:10.1016/j.compbiomed.2016.04.015 PMID:27253617

Acharya, U. R., Sree, S. V., Chattopadhyay, S., Yu, W., & Ang, P. C. A. (2011). Application of recurrence quantification analysis for the automated identification of epileptic EEG signals. *International Journal of Neural Systems*, *21*(3), 199–211. doi:10.1142/S0129065711002808 PMID:21656923

Acharya, U. R., Vinitha Sree, S., Swapna, G., Martis, R. J., & Suri, J. S. (2013). Automated EEG analysis of epilepsy: A review. *Knowledge-Based Systems*, *45*, 147–165. doi:10.1016/j.knosys.2013.02.014

Adamo, A., Grossi, G., Lanzarotti, R., & Lin, J. (2015). ECG compression retaining the best natural basis k-coefficients via sparse decomposition. *Biomedical Signal Processing and Control*, *15*, 11–17. doi:10.1016/j.bspc.2014.09.002

Afkhami, R. G., Azarnia, G., & Tinati, M. A. (2016). Cardiac arrhythmia classification using statistical and mixture modeling features of ECG signals. *Pattern Recognition Letters*, *70*, 45–51. doi:10.1016/j.patrec.2015.11.018

Agrawal, D. K., Kirar, B. S., & Pachori, R. B. (2019). Automated glaucoma detection using quasi-bivariate mode decomposition from fundus images. *IET Image Processing*, *13*(13), 2401–2408. doi:10.1049/iet-ipr.2019.0036

Ahmed, N., Yigit, A., Isik, Z., & Alpkocak, A. (2019). Identification of Leukemia Subtypes from Microscopic Images Using Convolutional Neural Network. *Journal of Diagnostic*, *9*(104), 128–234. doi:10.3390/diagnostics9030104 PMID:31450720

Akbari, H., & Esmaili, S. (2020). A Novel Geometrical Method for Discrimination of Normal, Interictal and Ictal EEG Signals. *Traitement Du Signal*, *37*(1), 59–68. doi:10.18280/ts.370108

Akcakaya, M., Peters, B., Moghadamfalahi, M., Mooney, A. R., Orhan, U., Oken, B., Erdogmus, D., & Fried-Oken, M. (2014). Noninvasive brain-computer interfaces for augmentative and alternative communication. *IEEE Reviews in Biomedical Engineering*, *7*, 31–49. doi:10.1109/RBME.2013.2295097 PMID:24802700

Akut, R. (2019). Wavelet based deep learning approach for epilepsy detection. *Health Information Science and Systems*, *7*(1), 1–9. doi:10.100713755-019-0069-1 PMID:31019680

Akyol, K. (2020). Stacking ensemble based deep neural networks modeling for effective epileptic seizure detection. *Expert Systems with Applications*, *148*, 113239. doi:10.1016/j.eswa.2020.113239

Al Madi, N. S., & Khan, J. I. (2016). Measuring learning performance and cognitive activity during multimodal comprehension. *2016 7th International Conference on Information and Communication Systems (ICICS)*, 50–55. 10.1109/IACS.2016.7476085

Al Madi, N., & Khan, J. I. (2019). Is a picture worth a thousand words? A computational investigation of the modality effect. *International Journal of Computational Science and Engineering, 19*(3), 440–451. doi:10.1504/IJCSE.2019.101351

Alamdari, N. T. (2016). *A morphological approach to identify respiratory phases of seismo- cardiogram*. The University of North Dakota.

Alivecor. (n.d.). *What is an ECG?* Retrieved from https://www.alivecor.com/education/ecg.html

Altunay, S., Telatar, Z., & Erogul, O. (2010). Epileptic EEG detection using the linear prediction error energy. *Expert Systems with Applications*, *37*(8), 5661–5665. doi:10.1016/j.eswa.2010.02.045

Alvarado, A. S., Lakshminarayan, C., & Principe, J. C. (2012). Time-based compression and classification of heartbeats. *IEEE Transactions on Biomedical Engineering*, *59*(6), 1641–1648. doi:10.1109/TBME.2012.2191407 PMID:22453601

Alvarado-González, M. (2016). P300 Detection Based on EEG Shape Features. Computational and Mathematical Methods in Medicine.

Andrzejak, R. G., Lehnertz, K., Mormann, F., Rieke, C., David, P., & Elger, C. E. (2001). Indications of nonlinear deterministic and finite-dimensional structures in time series of brain electrical activity: Dependence on recording region and brain state. *Physical Review E: Statistical Physics, Plasmas, Fluids, and Related Interdisciplinary Topics*, *64*(6), 8. doi:10.1103/PhysRevE.64.061907 PMID:11736210

Anmarkrud, Ø., Andresen, A., & Bråten, I. (2019). Cognitive Load and Working Memory in Multimedia Learning: Conceptual and Measurement Issues. *Educational Psychologist*, *54*(2), 1–23. doi:10.1080/00461520.2018.1554484

Annam, J. R., Kalyanapu, S. Ch. S., Somala, J., & Raju, S. B. (2020). Classification of ECG heartbeat arrhythmia: A review. *Procedia Computer Science*, *171*, 679–688.

Antonenko, P., Paas, F., Grabner, R., & van Gog, T. (2010). Using Electroencephalography to Measure Cognitive Load. *Educational Psychology Review*, *22*(4), 425–438. doi:10.100710648-010-9130-y

Anuragi, A., & Sisodia, D. S. (2020). Empirical wavelet transform based automated alcoholism detecting using EEG signal features. *Biomedical Signal Processing and Control*, *57*, 101777.

Anuragi, A., Sisodia, D. S., & Pachori, R. B. (2021). Automated FBSE-EWT based learning framework for detection of epileptic seizures using time-segmented EEG signals. *Computers in Biology and Medicine*, *136*, 104708. doi:10.1016/j.compbiomed.2021.104708 PMID:34358996

Arrouët. (2005). Open-ViBE: A Three Dimensional Platform for Real-Time Neuroscience. *Journal of Neurotherapy, 9*, 3-25.

Ashby, F. G. (2015). An Introduction to fMRI. In B. U. Forstmann & E.-J. Wagenmakers (Eds.), *An Introduction to Model-Based Cognitive Neuroscience* (pp. 91–112). Springer. doi:10.1007/978-1-4939-2236-9_5

Ashour, A. S., Dey, N., & Mohamed, W. S. (2016). Abdominal imaging in clinical applica- tions: Computer aided diagnosis approaches. In *Medical imaging in clinical applications* (pp. 3–17). Springer.

Axelberg, P. G., Gu, I. Y.-H., & Bollen, M. H. (2007). Support vector machine for classification of voltage disturbances. *IEEE Transactions on Power Delivery*, *22*(3), 1297–1303. doi:10.1109/TPWRD.2007.900065

Azad, M., Khaled, F., & Pavel, M. I. (2019). A novel approach to classify and convert 1D signal to 2D grayscale image implementing support vector machine and empirical mode decomposition algorithm. *International Journal of Advanced Research*, *7*(1), 328–335. doi:10.21474/IJAR01/8331

Balamurugan, B., Mullai, M., Soundararajan, S., Selvakanmani, S., & Arun, D. (2020). *Brain-computer interface for assessment of mental efforts in e-learning using the nonmarkovian queueing model. Computer Applications in Engineering Education*. Scopus. doi:10.1002/cae.22209

Balazsi, G. (1983). Relationship between baring of circumlunar vessels of the optic disc and glaucomatous visual field loss. *Canadian Journal of Ophthalmology*, *18*(7), 333–336. PMID:6671152

Bao, F. S. (2011). PyEEG: An open source python module for EEG/MEG feature extraction. Computational Intelligence and Neuroscience.

Bayram, I. (2013). An analytic wavelet transform with a flexible time-frequency covering. *IEEE Transactions on Signal Processing*, *61*(5), 1131–1142. doi:10.1109/TSP.2012.2232655

Beghi, E., Giussani, G., Abd-Allah, F., Abdela, J., Abdelalim, A., Abraha, H. N., Adib, M. G., Agrawal, S., Alahdab, F., Awasthi, A., Ayele, Y., Barboza, M. A., Belachew, A. B., Biadgo, B., Bijani, A., Bitew, H., Carvalho, F., Chaiah, Y., Daryani, A., ... Murray, C. J. L. (2019). Global, regional, and national burden of epilepsy, 1990–2016: A systematic analysis for the Global Burden of Disease Study 2016. *Lancet Neurology*, *18*(4), 357–375. doi:10.1016/S1474-4422(18)30454-X PMID:30773428

Bendjillali, R. I., Beladgham, M., Merit, K., & Taleb-Ahmed, A. (2019). Improved facial expression recognition based on DWT feature for deep CNN. *Electronics (Basel)*, *8*(3), 324. doi:10.3390/electronics8030324

Bernhardt, K. A., Poltavski, D., Petros, T., Ferraro, F. R., Jorgenson, T., Carlson, C., Drechsel, P., & Iseminger, C. (2019). The effects of dynamic workload and experience on commercially available EEG cognitive state metrics in a high-fidelity air traffic control environment. *Applied Ergonomics, 77*, 83–91. doi:10.1016/j.apergo.2019.01.008

Berntson, G. G., Quigley, K. S., & Lozano, D. (2007). Cardiovascular psychophysiology. Academic Press.

Bertamini, M. (2018). PsychoPy Is Fun. In Programming Visual Illusions for Everyone. Springer.

Bertolo, D., Dinet, J., & Vivian, R. (2014). Reducing cognitive workload during 3D geometry problem solving with an app on iPad. *2014 Science and Information Conference*, 896–900. 10.1109/SAI.2014.6918292

Bhattacharyya, A., Gupta, V., & Pachori, R. B. (2017). Automated identification of epileptic seizure EEG signals using empirical wavelet transform based Hilbert marginal spectrum. *2017 22nd International Conference on Digital Signal Processing (DSP)*, 1–5.

Bhattacharyya, A., Singh, L., & Pachori, R. B. (2018). Fourier–Bessel series expansion based empirical wavelet transform for analysis of non-stationary signals. *Digital Signal Processing: A Review Journal, 78*, 185–196. doi:10.1016/j.dsp.2018.02.020

Bhattacharyya, A., Tripathy, R. K., Garg, L., & Pachori, R. B. (2020). A novel multivariate-multiscale approach for computing EEG spectral and temporal complexity for human emotion recognition. *IEEE Sensors Journal*, *21*(3), 3579–3591. doi:10.1109/JSEN.2020.3027181

Bianchi, L. (2003). Introducing BF++: A C++ framework for cognitive bio-feedback systems design. *Methods of Information in Medicine*, *42*, 104–110.

Biju, K. S., Hakkim, H. A., & Jibukumar, M. G. (2017). Ictal EEG classification based on amplitude and frequency contours of IMFs. *Biocybernetics and Biomedical Engineering*, *37*(1), 172–183. doi:10.1016/j.bbe.2016.12.005

Bi, L. (2014). A speed and direction-based cursor control system with P300 and SSVEP. *Biomedical Signal Processing and Control*, *14*, 126–133.

Bin, G., Gao, X., Yan, Z., Hong, B., & Gao, S. (2009). An online multi-channel SSVEP-based brain-computer interface using a canonical correlation analysis method. *Journal of Neural Engineering*, *6*(4), 046002. doi:10.1088/1741-2560/6/4/046002 PMID:19494422

Birbaumer, N. (1999). Slow cortical potentials: Plasticity, operant control, and behavioral effects. *The Neuroscientist*, *5*, 74–78.

Boashash, B., Mesbah, M., & Colitz, P. (2003). Time-Frequency Detection of EEG Abnormalities. In B. Boashash (Ed.), *TIme-Frequency Signal Analysis and Processing: A Comprehensive Reference* (pp. 663–670). Elsevier Ltd. https://eprints.qut.edu.au/21351/https://espace.library.uq.edu.au/view/UQ:167080

Boateng, G., Sels, L., Kuppens, P., Lüscher, J., Scholz, U., & Kowatsch, T. (2020, April). *Emotion elicitation and capture among real couples in the lab. In 1st Momentary Emotion Elicitation & Capture workshop (MEEC 2020). ETH Zurich*. Department of Management, Technology, and Economics.

Boccippio, D. J., Koshak, W., Blakeslee, R., Driscoll, K., Mach, D., Buechler, D., Boeck, W., Christian, H. J., & Goodman, S. J. (2000). The Optical Transient Detector (OTD): Instrument characteristics and cross-sensor validation. *Journal of Atmospheric and Oceanic Technology*, *17*(4), 441–458.

Boucsein, W. (2012). *Electrodermal Activity* (2nd ed.). Springer.

Bozorgpour, Azad, Showkatian, & Sulaiman. (2021). Multi-scale regional attention deeplab3+: Multiple Myeloma plasma cells segmentation in microscopic images. *Journal of Machine Learning Research, 6*(31), 234-245.

Bradley, M. M., & Lang, P. J. (1994). Measuring emotion: The self-assessment manikin and the semantic differential. *Journal of Behavior Therapy and Experimental Psychiatry*, *25*(1), 49–59. doi:10.1016/0005-7916(94)90063-9 PMID:7962581

Brechet, L., Lucas, M.-F., Doncarli, C., & Farina, D. (2007). Compression of biomedical signals with mother wavelet optimization and best-basis wavelet packet selection. *IEEE Transactions on Biomedical Engineering*, *54*(12), 2186–2192. doi:10.1109/TBME.2007.896596 PMID:18075034

Bronzino, J. D. (2006). Biomedical signals: Origin and dynamic characteristics; frequency- domain analysis. In *Medical devices and systems* (pp. 27–48). CRC Press.

Bronzino, J. D. (Ed.). (2006). *Medical devices and systems*. CRC Press.

Burrus, C. S. (1997). *Introduction to wavelets and wavelet transforms: A primer*. Academic Press.

Butterworth, S. (1930). On the Theory of Filter Amplifiers. *Experimental Wireless and the Wireless Engineer*, *7*, 536–541.

Cacioppo, J. T., Tassinary, L. G., & Berntson, G. G. (Eds.), *Handbook of psychophysiology* (Vol. 3, pp. 182–210). Cambridge University Press.

Cao, X., Cheng, M., Xue, X., & Zhu, S. (2019). Effects of Lecture Video Types on Student Learning: An Analysis of Eye-Tracking and Electroencephalography Data. In F. Xhafa, S. Patnaik, & M. Tavana (Eds.), *Advances in Intelligent, Interactive Systems, and Applications* (pp. 498–505). Springer International Publishing. doi:10.1007/978-3-030-02804-6_66

Carvalodh. (2020). Machine-learning Algorithm Predicts Responses to Myeloma Treatments. *Myeloma Research*.

Casaccia, S., Sirevaag, E. J., Richter, E., O'Sullivan, J. A., Scalise, L., & Rohrbaugh, J. W. (2014, May). Decoding carotid pressure waveforms recorded by laser Doppler vibrometry: Effects of rebreathing. In *AIP Conference Proceedings* (Vol. 1600, No. 1, pp. 298–312). AIP.

Castro-Meneses, L. J., Kruger, J.-L., & Doherty, S. (2020). Validating theta power as an objective measure of cognitive load in educational video. *Educational Technology Research and Development, 68*(1), 181–202. doi:10.1007/s11423-019-09681-4

Cavazzana, L. (2012). *Integrating an EMG signal classifier and a hand rehabilitation device: Early signal recognition and real time performances*. Academic Press.

Cecotti, H., & Graser, A. (2011). Convolutional Neural Networks for P300 Detection with Application to Brain-Computer Interfaces. *IEEE Transactions on Pattern Analysis and Machine Intelligence*, *33*(3), 433–445.

Ceylan, R., Özbay, Y., & Karlik, B. (2009). A novel approach for classification of ECG arrhythmias: Type-2 fuzzy clustering neural network. *Expert Systems with Applications*, *36*(3), 6721–6726. doi:10.1016/j.eswa.2008.08.028

Chaiwisood, Wongkittisuksa, & Phukpattaranont. (2012). Comparison of Signal Quality between Electrocardiograms Measured from the Chest and the Wrist. *The 10th International PSU Engineering Conference*.

Chang, H.-C., Hung, I.-C., Chew, S. W., & Chen, N.-S. (2016). Yet Another Objective Approach for Measuring Cognitive Load Using EEG-Based Workload. *2016 IEEE 16th International Conference on Advanced Learning Technologies (ICALT)*, 501–502. 10.1109/ICALT.2016.145

Chaurasiya, R. K., Londhe, N. D., & Ghosh, S. (2015). An efficient P300 speller system for Brain-Computer Interface. *International Conference on Signal Processing, Computing and Control (ISPCC).*

Chaurasiya, R. K., Londhe, N. D., & Ghosh, S. (2016). Binary DE-Based Channel Selection and Weighted Ensemble of SVM Classification for Novel Brain–Computer Interface Using Devanagari Script-Based P300 Speller Paradigm. *International Journal of Human-Computer Interaction*, *32*(11), 861–877. doi:10.1080/10447318.2016.1203047

Chen, Weinberger, Sha, & Bengio. (2014). Marginalized Denoising Auto-encoders for Nonlinear Representations. *Proceedings of the 31st International Conference on Machine Learning, 32*(2), 1476-1484.

Chen, C., Hua, Z., Zhang, R., Liu, G., & Wen, W. (2020). Automated arrhythmia classification based on a combination network of CNN and LSTM. *Biomedical Signal Processing and Control*, *57*, 101819. doi:10.1016/j.bspc.2019.101819

Chen, G., Zhu, Y., Hong, Z., & Yang, Z. (2019). EmotionalGAN: generating ECG to enhance emotion state classification. *Proceedings of the 2019 International Conference on Artificial Intelligence and Computer Science*, 309-313. 10.1145/3349341.3349422

Chen, J., Wang, F., Zhang, Y., & Shi, X. (2008). ECG compression using uniform scalar dead-zone quantization and conditional entropy coding. *Medical Engineering & Physics*, *30*(4), 523–530. doi:10.1016/j.medengphy.2007.06.008 PMID:17693118

Chen, Z., Luo, J., Lin, K., Wu, J., Zhu, T., Xiang, X., & Meng, J. (2017). An energy-efficient ECG processor with weak-strong hybrid classifier for arrhythmia detection. *IEEE Transactions on Circuits and Wystems. II, Express Briefs*, *65*(7), 948–952. doi:10.1109/TCSII.2017.2747596

Cheyne, D. O. (2013). MEG studies of sensorimotor rhythms: A review. *Experimental Neurology*, *245*, 27–39.

Chicco, D., & Jurman, G. (2020). The advantages of the Matthews correlation coefficient (MCC) over F1 score and accuracy in binary classification evaluation. *BMC Genomics*, *21*(1), 6. doi:10.118612864-019-6413-7 PMID:31898477

Chowdary, M. K., Nguyen, T. N., & Hemanth, D. J. (2021). Deep learning-based facial emotion recognition for human–computer interaction applications. *Neural Computing & Applications*, 1–18. doi:10.100700521-021-06012-8

Chua, K. C., Chandran, V., Aeharya, R., & Lim, C. M. (2007). Higher order spectral (HOS) analysis of epileptic EEG signals. *Annual International Conference of the IEEE Engineering in Medicine and Biology - Proceedings*, 6495–6498. 10.1109/IEMBS.2007.4353847

Chung, C. Y., Chung, F. Y., Chu, Y. W., & Luo, C. H. (2013). Spatial feature extraction from wrist pulse signals. *1st International Conference on Orange Technologies Tainan*.

Cichocki, A. Z. (2009). Nonnegative Matrix and Tensor Factorizations - Applications to Exploratory Multi-way Data Analysis and Blind Source Separation. *IEEE Signal Processing Magazine*, 142–145.

Cimtay, Y., & Ekmekcioglu, E. (2020). Investigating the use of pretrained convolutional neural network on cross-subject and cross-dataset EEG emotion recognition. *Sensors (Basel)*, *20*(7), 2034. doi:10.339020072034 PMID:32260445

Claesen, M., De Smet, F., Suykens, J. A. K., & De Moor, B. (2014). EnsembleSVM: A Library for Ensemble Learning Using Support Vector Machines. *Journal of Machine Learning Research*, 141–145.

Clifford, G. D., Liu, C., Moody, B., Li-wei, H. L., Silva, I., Li, Q., . . . Mark, R. G. (2017, September). AF classification from a short single lead ECG recording: The PhysioNet/computing in cardiology challenge 2017. In 2017 Computing in Cardiology (CinC) (pp. 1-4). IEEE.

Congedo. (2011). *"Brain Invaders": A prototype of an open-source P300-based video game working with the OpenViBE platform*. Academic Press.

Cong, F., Phan, A. H., Zhao, Q., Huttunen-Scott, T., Kaartinen, J., Ristaniemi, T., Lyytinen, H., & Cichocki, A. (2012). Benefits of multi-domain feature of mismatch negativity extracted by non-negative tensor factorization from EEG collected by low-density array. *International Journal of Neural Systems*, *22*(06), 1250025. doi:10.1142/S0129065712500256 PMID:23186274

Conrad, C., & Bliemel, M. (2016). Psychophysiological Measures of Cognitive Absorption and Cognitive Load in E-Learning Applications. *ICIS 2016 Proceedings*. https://aisel.aisnet.org/icis2016/Human-ComputerInteraction/Presentations/9

Cooley, J. W., & Tukey, J. W. (1965). An algorithm for the machine calculation of complex Fourier series. *Mathematics of Computation*, *19*(90), 297–301. doi:10.1090/S0025-5718-1965-0178586-1

Cootes, T. F., Edwards, G. J., & Taylor, C. J. (2001). Active appearance models. *IEEE Transactions on Pattern Analysis and Machine Intelligence*, *23*(6), 681–685. doi:10.1109/34.927467

Correa, J. A. M., Abadi, M. K., Sebe, N., & Patras, I. (2018). Amigos: A dataset for affect, personality and mood research on individuals and groups. *IEEE Transactions on Affective Computing*.

Cortes, C., & Vapnik, V. (1995). Support-vector networks. *Machine Learning*, *20*(3), 273–297. doi:10.1007/BF00994018

Craik, A., He, Y., & Contreras-Vidal, J. L. (2019). Deep learning for electroencephalogram (EEG) classification tasks: A review. *Journal of Neural Engineering*, *16*(3), 031001. doi:10.1088/1741-2552/ab0ab5 PMID:30808014

Crk, I., & Kluthe, T. (2014). Toward using alpha and theta brain waves to quantify programmer expertise. *2014 36th Annual International Conference of the IEEE Engineering in Medicine and Biology Society*, 5373–5376. 10.1109/EMBC.2014.6944840

Cruz, A. (2017). Double ErrP detection for automatic error correction in an ERP-based BCI speller. *IEEE Transactions on Neural Systems and Rehabilitation Engineering*, *26*, 26–36.

Da He, D., & Sodini, C. G. (2014). A 58 nW ECG ASIC with motion-tolerant heartbeat timing extraction for wearable cardiovascular monitoring. *IEEE Transactions on Biomedical Circuits and Systems*, *9*(3), 370–376. PMID:25252285

Dalal, N., & Triggs, B. (2005). Histograms of oriented gradients for human detection. In *2005 IEEE Computer Society Conference on Computer Vision and Pattern Recognition (CVPR'05)* (Vol. 1, pp. 886-893). 10.1109/CVPR.2005.177

Dan, A., & Reiner, M. (2017). EEG-based cognitive load of processing events in 3D virtual worlds is lower than processing events in 2D displays. *International Journal of Psychophysiology, 122*, 75–84. doi:10.1016/j.ijpsycho.2016.08.013

Dan, A., & Reiner, M. (2017). Real Time EEG Based Measurements of Cognitive Load Indicates Mental States During Learning. *Journal of Educational Data Mining, 9*(2), 31–44. doi:10.5281/zenodo.3554719

Dan, A., & Reiner, M. (2018). Reduced mental load in learning a motor visual task with virtual 3D method. *Journal of Computer Assisted Learning*, *34*(1), 84–93. doi:10.1111/jcal.12216

Daneshfar, F., Kabudian, S. J., & Neekabadi, A. (2020). Speech emotion recognition using hybrid spectral-prosodic features of speech signal/glottal waveform, metaheuristic-based dimensionality reduction, and Gaussian elliptical basis function network classifier. *Applied Acoustics*, *166*, 107360. doi:10.1016/j.apacoust.2020.107360

Das, K., & Pachori, R. B. (2021). Schizophrenia detection technique using multivariate iterative filtering and multichannel EEG signals. *Biomedical Signal Processing and Control*, *67*, 102525. doi:10.1016/j.bspc.2021.102525

Daubechies, I. (1992). *Ten Lectures on Wavelets.* Academic Press.

Daubechies, I. (1992). *Ten lectures on wavelets*. Society for Industrial and Applied Mathematics.

Daubechies, I. (1988). Orthonormal bases of compactly supported wavelets. *Communications on Pure and Applied Mathematics*, *41*(7), 909–996. doi:10.1002/cpa.3160410705

Daubechies, I. (1992). *Ten Lectures on Wavelets*. Society for Industrial and Applied Mathematics. doi:10.1137/1.9781611970104

De Carolis, B., D'Errico, F., Macchiarulo, N., & Palestra, G. (2019). "Engaged Faces": Measuring and Monitoring Student Engagement from Face and Gaze Behavior. In *IEEE/WIC/ACM International Conference on Web Intelligence-Companion Volume* (pp. 80-85). 10.1145/3358695.3361748

de la O Serna, J. A., Paternina, M. R. A., Zamora-Mendez, A., Tripathy, R. K., & Pachori, R. B. (2020). EEG-Rhythm Specific Taylor–Fourier Filter Bank Implemented With O-Splines for the Detection of Epilepsy Using EEG Signals. *IEEE Sensors Journal*, *20*(12), 6542–6551. doi:10.1109/JSEN.2020.2976519

Deepu, C. J., & Lian, Y. (2014). A joint QRS detection and data compression scheme for wearable sensors. *IEEE Transactions on Biomedical Engineering*, *62*(1), 165–175. doi:10.1109/TBME.2014.2342879 PMID:25073164

Delorme & Makeig. (2014). EEGLAB: An open source toolbox for analysis of single-trial EEG dynamics including independent component analysis. *Journal of Neuroscience Methods, 134*, 9-21.

Delorme, A. (2010). MATLAB-Based Tools for BCI Research. In Brain-Computer Interfaces: Applying our Minds to Human-Computer Interaction. Springer London.

Delorme, A. (2011). EEGLAB, SIFT, NFT, BCILAB, and ERICA: New tools for advanced EEG processing. Computational Intelligence and Neuroscience.

Dervisevic, E., Pavljasevic, S., Dervisevic, A., & Kasumovic. (2016). Challenges in early glaucoma detection. *Medicinski Arhiv*, *70*(3), 203–207. doi:10.5455/medarh.2016.70.203-207 PMID:27594747

Dey, A. Mohammed, & Nguyen. (2019). Acoustic Sensors for Biomedical Applications. Academic Press.

Dey, N., & Ashour, A. S. (2017). *Direction of arrival estimation and localization of multi-speech sources*. Springer Science and Business Media.

Dey, N., Hassanien, A. E., Bhatt, C., Ashour, A., & Satapathy, S. C. (Eds.). (2018). *Internet of things and big data analytics toward next-generation intelligence*. Springer.

Díaz, D., Ramírez, R., & Hernández-Leo, D. (2015). The Effect of Using a Talking Head in Academic Videos: An EEG Study. *2015 IEEE 15th International Conference on Advanced Learning Technologies*, 367–369. 10.1109/ICALT.2015.89

Dickhaus, H., & Heinrich, H. (1996). Classifying biosignals with wavelet networks. *IEEE Engineering in Medicine and Biology Magazine*, *15*(5), 103–111.

Diker, A., Avci, E., Tanyildizi, E., & Gedikpinar, M. (2020). A novel ECG signal classification method using DEA-ELM. *Medical Hypotheses*, *136*, 109515.

Dissanayake, T., Rajapaksha, Y., Ragel, R., & Nawinne, I. (2019). An ensemble learning approach for electrocardiogram sensor based human emotion recognition. *Sensors (Basel)*, *19*(20), 4495. doi:10.339019204495 PMID:31623279

Dora, C., & Biswal, P. K. (2020). An improved algorithm for efficient ocular artifact suppression from frontal EEG electrodes using VMD. *Biocybernetics and Biomedical Engineering*, *40*(1), 148–161.

Dora, C., & Biswal, P. K. (2020). Correlation-based ECG artifact correction from single channel EEG using modified variational mode decomposition. *Computer Methods and Programs in Biomedicine*, *183*, 105092.

Dornhege. (2010). An introduction to brain-computer interfacing. The Berlin brain–computer interface: non-medical uses of BCI technology. *Frontiers in neuroscience*, *4*, 198. PMID:21165175

Doud, A. J. (2011). Continuous three-dimensional control of a virtual helicopter using a motor imagery based brain-computer interface. *PLoS One*, *6*, e26322.

Dragomiretskiy, K., & Zosso, D. (2015). Two-dimensional variational mode decomposition. In Energy Minimization Methods in Computer Vision and Pattern Recognition (Lecture Notes in Computer Science). Springer. doi:10.1007/978-3-319-14612-6_15

Dragomiretskiy, K., & Zosso, D. (2013). Variational mode decomposition. *IEEE Transactions on Signal Processing*, *62*(3), 531–544. doi:10.1109/TSP.2013.2288675

Dua, S., Acharya, U. R., Chowriappa, P., & Sree, S. V. (2012). Wavelet-Based Energy Features for Glaucomatous Image Classification. *IEEE Transactions on Information Technology in Biomedicine*, *16*(1), 80–87. doi:10.1109/TITB.2011.2176540 PMID:22113813

Ebrahimi, Z., Loni, M., Daneshtalab, M., & Gharehbaghi, A. (2020). A review on deep learning methods for ECG arrhythmia classification. *Expert Systems with Applications: X, 7*, 100033.

Eckardt, J.-N., Bornhauser, M., Wendt, K., & Middeke, J. M. (2020). Application of machine learning in the management of acute myeloid leukemia. Current Practice and Future Prospects, 4(23), 79-90.

Egger, M., Ley, M., & Hanke, S. (2019). Emotion recognition from physiological signal analysis: A review. *Electronic Notes in Theoretical Computer Science*, *343*, 35–55. doi:10.1016/j.entcs.2019.04.009

Eggins, B. R. (2008). *Chemical sensors and biosensors* (Vol. 28). Wiley.

Eldenfria, A., & Al-Samarraie, H. (2019). Towards an Online Continuous Adaptation Mechanism (OCAM) for Enhanced Engagement: An EEG Study. *International Journal of Human-Computer Interaction, 35*(20), 1960–1974. doi:10.1080/10447318.2019.1595303

Elhaj, F. A., Salim, N., Harris, A. R., Swee, T. T., & Ahmed, T. (2016). Arrhythmia recognition and classification using combined linear and nonlinear features of ECG signals. *Computer Methods and Programs in Biomedicine*, *127*, 52–63. doi:10.1016/j.cmpb.2015.12.024 PMID:27000289

Elsayed, N. (2017). Brain computer interface: EEG signal preprocessing issues and solutions. *International Journal of Computers and Applications*, *169*, 12–16.

Essock, E. A., Sinai, M. J., Fechtner, R. D., Srinivasan, N., & Bryant, D. F. (2000). Fourier analysis of nerve fiber layer measurements from scanning laser polarimetry in glaucoma: Emphasizing shape characteristics of the 'double-hump' pattern. *Journal of Glaucoma*, *9*(6), 444–452. doi:10.1097/00061198-200012000-00005 PMID:11131750

Estrada, E. F. (2010). *Computer-aided detection of sleep apnea and sleep stage classification using HRV and EEG signals*. The University of Texas at El Paso.

Eweje, F. R., Bao, B., Wu, J., Dalal, D., & Liao, W. (2021). Deep Learning for Classification of Bone Lesions on Routine MRI. EBiomedicine, 68(7), 103-402.

Fang, P., Peng, Y., Lin, W.-H., Wang, Y., Wang, S., & Zhang, X. (2021). Wrist Pulse Recording with a wearable Piezo resistor – Piezoelectric Compound Sensing system and Its Applications in Health Monitoring. *IEEE Sensors Journal*.

Farwell, L. A., & Donchin, E. (1988). Talking off the top of your head: Toward a mental prosthesis utilizing event-related brain potentials. *Electroencephalography and Clinical Neurophysiology*.

Faust, O., Shenfield, A., Kareem, M., San, T. R., Fujita, H., & Acharya, U. R. (2018). Automated detection of atrial fibrillation using long short-term memory network with RR interval signals. *Computers in Biology and Medicine*, *102*, 327–335.

Fay, C. (2013). Investigation into strategies for harvesting chemical based information using digital imaging and infra-red sensors for environmental and health applications (Doctoral dissertation). Dublin City University.

Fellman, R. L. (2011). Know the New Glaucoma Staging Codes. *American Academy of Ophthl., EyeNet Magazine*, 65-66. https://www.aao.org/eyenet/article/know-new-glaucoma-staging-codes

Ferdinando, H., Seppänen, T., & Alasaarela, E. (2016). Comparing features from ECG pattern and HRV analysis for emotion recognition system. *IEEE Conference on Computational Intelligence in Bioinformatics and Computational Biology (CIBCB)*, 1-6. 10.1109/CIBCB.2016.7758108

Fernandez Rojas, R., Debie, E., Fidock, J., Barlow, M., Kasmarik, K., Anavatti, S., Garratt, M., & Abbass, H. (2020). Electroencephalographic Workload Indicators During Teleoperation of an Unmanned Aerial Vehicle Shepherding a Swarm of Unmanned Ground Vehicles in Contested Environments. *Frontiers in Neuroscience, 14*. doi:10.3389/fnins.2020.00040

Fourier, J. (1878). *The analytical theory of heat*. The University Press.

Fu, L., Lu, B., Nie, B., Peng, Z., Liu, H., & Pi, X. (2020). Hybrid network with attention mechanism for detection and location of myocardial infarction based on 12-lead electrocardiogram signals. *Sensors (Basel)*, *20*(4), 1020.

Fumero, F. (2011). RIM-ONE: An open retinal image database for optic nerve evaluation. *24th IEEE Int. Symposium on Comput. Med. Syst. (CBMS),* 1-6.

Galambos, R. (1981). A 40-Hz auditory potential recorded from the human scalp. *Proceedings of the National Academy of Sciences of the United States of America*, *78*, 2643–2647.

Gao, X. (2003, June). A BCI-based environmental controller for the motion-disabled. *IEEE Transactions on Neural Systems and Rehabilitation Engineering*, *11*, 137–140.

Gao, Z., Wu, J., Zhou, J., & Jiang, W. (2012). Design of ECG Signal Acquisition and Processing System. *International Conference on Biomedical Engineering and Biotechnology.* 10.1109/iCBEB.2012.128

Garg, G., Singh, V., Gupta, J. R. P., & Mittal, A. P. (2012). Wrapper based wavelet feature optimization for EEG signals. *Biomedical Engineering Letters*, *2*(1), 24–37. doi:10.100713534-012-0044-0

Gautam, K. S., & Thangavel, S. K. (2021). Video analytics-based facial emotion recognition system for smart buildings. *International Journal of Computers and Applications*, *43*(9), 858–867. doi:10.1080/1206212X.2019.1642438

Gerlič, I., & Jaušovec, N. (2001). Differences in EEG power and coherence measures related to the type of presentation: Text versus multimedia. *Journal of Educational Computing Research, 25*(2), 177–195. doi:10.2190/YDWY-U3FJ-4LY4-LYND

Gholam-Hosseini & Nazeran. (1998). Detection an Extraction of the ECG signal Parameters. *Proceedings of the 20th Annual International Conference the IEEE Engineering in Medicine and Biology Society*, 20(1).

Ghosh-Dastidar, S., Adeli, H., & Dadmehr, N. (2008). Principal component analysis-enhanced cosine radial basis function neural network for robust epilepsy and seizure detection. *IEEE Transactions on Biomedical Engineering*, *55*(2), 512–518. doi:10.1109/TBME.2007.905490 PMID:18269986

Gilles, J. (2013). Empirical wavelet transform. *IEEE Transactions on Signal Processing*, *61*(16), 3999–4010. doi:10.1109/TSP.2013.2265222

Gilles, J., Tran, G., & Osher, S. (2014). 2D empirical transforms: Wavelets, ridgelets, and curvelets revisited. *SIAM Journal on Imaging Sciences*, *7*(1), 157–186. doi:10.1137/130923774

Gnawali, O., Yarvis, M., Heidemann, J., & Govindan, R. (2004, October). Interaction of retransmission, blacklisting, and routing metrics for reliability in sensor network routing. In *Sensor and Ad Hoc Communications and Networks, 2004. IEEE SECON 2004. 2004 First Annual IEEE Communications Society Conference on* (pp. 34–43). IEEE.

Goel, K. (2014). Home automation using SSVEP & eye-blink detection based brain-computer interface. *2014 IEEE International Conference on Systems, Man, and Cybernetics (SMC)*, 4035-4036.

Gokgoz, E., & Subasi, A. (2015). Comparison of decision tree algorithms for EMG signal classification using DWT. *Biomedical Signal Processing and Control*, *18*, 138–144. doi:10.1016/j.bspc.2014.12.005

Goldberger, A. L., Amaral, L. A., Glass, L., Hausdorff, J. M., Ivanov, P. C., Mark, R. G., ... Stanley, H. E. (2000). PhysioBank, PhysioToolkit, and PhysioNet: Components of a new research resource for complex physiologic signals. *Circulation*, *101*(23), e215–e220.

Gorodkin, J. (2004). Comparing two K-category assignments by a K-category correlation coefficient. *Computational Biology and Chemistry*, *28*(5–6), 367–374. doi:10.1016/j.compbiolchem.2004.09.006 PMID:15556477

Gospodinova, E., Gospodinov, M., Dey, N., Domuschiev, I., Ashour, A. S., Balas, S. V., Soni, Y., Jain, J. K., Meena, R. S., & Maheshwari, R. (2017, May). HRV analysis of young adults in pre-meal and post-meal stage. In *Recent Trends in Electronics*. Information.

Gourisaria, M. K., Harshvardhan, G. M., Agrawal, R., Patra, S. S., Rautaray, S. S., & Pandey, M. (2021). Arrhythmia Detection Using Deep Belief Network Extracted Features From ECG Signals. *International Journal of E-Health and Medical Communications*, *12*(6), 1–24. https://doi.org/10.4018/IJEHMC.20211101.oa9

Goyal, K., & Agarwal, R. (2017). Pulse based sensor design for wrist pulse signal analysis and health diagnosis. *Biomedical Research (Aligarh)*, *28*, 5187–5195.

Graf, R. F. (1999). *Modern dictionary of electronics*. Oxford Newnes.

Gramfort, A. (2010). OpenMEEG: Opensource software for quasistatic bioelectromagnetics. *Biomedical Engineering Online*, *9*, 45.

Greany, M. J. (2002). Comparisons of optic nerve imaging methods to distinguish normal eyes from those with glaucoma. *Investigative Ophthalmology & Visual Science*, *43*(1), 140–145. PMID:11773024

Gross, J. J., & Levenson, R. W. (1995). Emotion elicitation using films. *Cognition and Emotion*, *9*(1), 87–108. doi:10.1080/02699939508408966

Guidi, A., Gentili, C., Scilingo, E. P., & Vanello, N. (2019). Analysis of speech features and personality traits. *Biomedical Signal Processing and Control*, *51*, 1–7. doi:10.1016/j.bspc.2019.01.027

Guido, D. (2007). BioSig: An Open-Source Software Library for BCI Research. In Toward Brain-Computer Interfacing. MITP.

Güler, İ., & Übeylı˙, E. D.Güler. (2005). ECG beat classifier designed by combined neural network model. *Pattern Recognition*, *38*(2), 199–208. doi:10.1016/j.patcog.2004.06.009

Gupta, D., Bansal, P., & Choudhary, K. (2018). The state of the art of feature extraction techniques in speech recognition. *Speech and Language Processing For Human-Machine Communications*, 195-207.

Gupta, K., Lazarevic, J., Pai, Y. S., & Billinghurst, M. (2020). AffectivelyVR: Towards VR Personalized Emotion Recognition. *26th ACM Symposium on Virtual Reality Software and Technology*, 1-3.

Gupta, V., Chopda, M. D., & Pachori, R. B. (2018). Cross-subject emotion recognition using flexible analytic wavelet transform from EEG signals. *IEEE Sensors Journal*, *19*(6), 2266–2274. doi:10.1109/JSEN.2018.2883497

Gupta, V., & Pachori, R. B. (2019). Epileptic seizure identification using entropy of FBSE based EEG rhythms. *Biomedical Signal Processing and Control*, *53*, 101569. doi:10.1016/j.bspc.2019.101569

Gutiérrez-Gnecchi, J. A., Morfin-Magana, R., Lorias-Espinoza, D., del Carmen Tellez-Anguiano, A., Reyes-Archundia, E., Méndez-Patiño, A., & Castañeda-Miranda, R. (2017). DSP-based arrhythmia classification using wavelet transform and probabilistic neural network. *Biomedical Signal Processing and Control*, *32*, 44–56. doi:10.1016/j.bspc.2016.10.005

Hagiwara, Y., Koh, J. E. W., Tan, J. H., Bhandary, S. V., Laude, A., Ciaccio, E. J., Tong, L., & Acharya, U. R. (2018). Computer-aided diagnosis of glaucoma using fundus images: A review. *Computer Methods and Programs in Biomedicine*, *165*, 1–12. doi:10.1016/j.cmpb.2018.07.012 PMID:30337064

Hakvoort, G., Reuderink, B., & Obbink, M. (2011). *Comparison of PSDA and CCA detection methods in a SSVEP-based BCI-system.* Centre for Telematics and Information Technology (CTIT).

Hammad, M., Iliyasu, A. M., Subasi, A., Ho, E. S., & Abd El-Latif, A. A. (2020). A multitier deep learning model for arrhythmia detection. *IEEE Transactions on Instrumentation and Measurement*, *70*, 1–9.

Hannun, A. Y., Rajpurkar, P., Haghpanahi, M., Tison, G. H., Bourn, C., Turakhia, M. P., & Ng, A. Y. (2019). Cardiologist-level arrhythmia detection and classification in ambulatory electrocardiograms using a deep neural network. *Nature Medicine*, *25*(1), 65–69. doi:10.103841591-018-0268-3 PMID:30617320

Haqque, R. H. D., Djamal, E. C., & Wulandari, A. (2021). Emotion Recognition of EEG Signals Using Wavelet Filter and Convolutional Neural Networks. In *2021 8th International Conference on Advanced Informatics: Concepts, Theory and Applications (ICAICTA)* (pp. 1-6). 10.1109/ICAICTA53211.2021.9640279

Haseena, H. H., Mathew, A. T., & Paul, J. K. (2011). Fuzzy clustered probabilistic and multi layered feed forward neural networks for electrocardiogram arrhythmia classification. *Journal of Medical Systems*, *35*(2), 179–188. doi:10.100710916-009-9355-9 PMID:20703571

Hasnul, M. A., Alelyani, S., & Mohana, M. (2021). Electrocardiogram-Based Emotion Recognition Systems and Their Applications in Healthcare—A Review. *Sensors (Basel)*, *21*(15), 5015. doi:10.339021155015 PMID:34372252

Hassouneh, A., Mutawa, A. M., & Murugappan, M. (2020). Development of a real-time emotion recognition system using facial expressions and EEG based on machine learning and deep neural network methods. *Informatics in Medicine Unlocked*, *20*, 100372. doi:10.1016/j.imu.2020.100372

He, M., Nian, Y., Xu, L., Qiao, L., & Wang, W. (2020). Adaptive separation of respiratory and heartbeat signals among multiple people based on empirical wavelet transform using uwb radar. *Sensors (Basel)*, *20*(17), 4913.

Herold, M., Scepan, J., & Clarke, K. C. (2002). The use of remote sensing and landscape met- rics to describe structures and changes in urban land uses. *Environment & Planning A*, *34*(8), 1443–1458. doi:10.1068/a3496

Hilbert, S., McAssey, M., Bühner, M., Schwaferts, P., Gruber, M., Goerigk, S., & Taylor, P. C. J. (2019). Right hemisphere occipital rTMS impairs working memory in visualizers but not in verbalizers. *Scientific Reports*, *9*(1), 6307. doi:10.103841598-019-42733-6 PMID:31004125

Hoffmann, J., Mahmood, S., Fogou, P. S., George, N., Raha, S., Safi, S., . . . Hübner, M. (2020, September). A Survey on Machine Learning Approaches to ECG Processing. In 2020 Signal Processing: Algorithms, Architectures, Arrangements, and Applications (SPA) (pp. 36-41). IEEE.

Hosni, S. M. (2007). Classification of EEG signals using different feature extraction techniques for mental-task BCI. *2007 International Conference on Computer Engineering & Systems*, 220-226.

Hossain, M. S. (2011). ECG signal compression using energy compaction based thresholding of the wavelet coefficients. *Duet Journal, 1*(2).

Hotelling, H. (1936). Relations Between Two Sets of Variates. *Biometrika*, *28*(3-4), 321–377. doi:10.1093/biomet/28.3-4.321

Huang, N. E., Shen, Z., Long, S. R., Wu, M. C., Shih, H. H., Zheng, Q., . . . Liu, H. H. (1998). The empirical mode decomposition and the Hilbert spectrum for nonlinear and non-stationary time series analysis. *Proceedings of the Royal Society of London. Series A: Mathematical, Physical and Engineering Sciences, 454*(1971), 903-995. 10.1098/rspa.1998.0193

Huang, N. E. (2014). Introduction to the Hilbert–Huang transform and its related mathematical problems. In *Hilbert–Huang transform and its applications* (pp. 1–26). World Scientific. doi:10.1142/9789814508247_0001

Idaji, Shamsollahi, & Sardouie. (2017). Higher order spectral regression discriminant analysis (HOSRDA): A tensor feature reduction method for ERP detection. *Journal of Pattern Recognition.*

Ilakiyaselvan, N., Khan, A. N., & Shahina, A. (2020). Deep learning approach to detect seizure using reconstructed phase space images. *Journal of Biomedical Research*, *34*(3), 240–250. doi:10.7555/JBR.34.20190043 PMID:32561702

Ingale, A. B., & Chaudhari, D. S. (2012). Speech emotion recognition. *International Journal of Soft Computing and Engineering*, *2*(1), 235–238.

Jabid, T., Kabir, M. H., & Chae, O. (2010). Local directional pattern (LDP) for face recognition. *Digest of Technical Papers International Conference On Consumer Electronics (ICCE)*, 329-330.

Jalaleddine, S. M. S., Hutchens, C. G., Strattan, R. D., & Coberly, W. A. (1990). ECG data compression techniques-a unified approach. *IEEE Transactions on Biomedical Engineering*, *37*(4), 329–343. doi:10.1109/10.52340 PMID:2186997

Jenkins, S. D., & Brown, R. D. H. (2014). A correlational analysis of human cognitive activity using Infrared Thermography of the supraorbital region, frontal EEG and self-report of core affective state. *Proceedings of the 2014 International Conference on Quantitative InfraRed Thermography*. 10.21611/qirt.2014.131

Jeong, J., & Rogers, J. A. (2016). Epidermal mechano-acoustic sensing electronics for cardio- vascular diagnostics and human-machine interfaces. *Science Advances*, *2*(11), e1601185.

Jha, C. K., & Kolekar, M. H. (2016). Efficient ECG data compression and transmission algorithm for telemedicine. *2016 8th International Conference on Communication Systems and Networks (COMSNETS)*, 1–6.

Jha, C. K., & Kolekar, M. H. (2015). Performance analysis of ECG data compression using wavelet based hybrid transform method. *2015 International Conference on Microwave, Optical and Communication Engineering (ICMOCE)*, 138–141. 10.1109/ICMOCE.2015.7489709

Jha, C. K., & Kolekar, M. H. (2017). ECG data compression algorithm for tele-monitoring of cardiac patients. *International Journal of Telemedicine and Clinical Practices*, *2*(1), 31–41. doi:10.1504/IJTMCP.2017.082106

Jha, C. K., & Kolekar, M. H. (2018). Classification and compression of ECG signal for holter device. In *Biomedical signal and image processing in patient care* (pp. 46–63). IGI Global. doi:10.4018/978-1-5225-2829-6.ch004

Jha, C. K., & Kolekar, M. H. (2018). Electrocardiogram data compression using DCT based discrete orthogonal Stockwell transform. *Biomedical Signal Processing and Control*, *46*, 174–181. doi:10.1016/j.bspc.2018.06.009

Jha, C. K., & Kolekar, M. H. (2019a). Arrhythmia ECG beats classification using wavelet-based features and support vector machine classifier. In *Advanced Classification Techniques for Healthcare Analysis* (pp. 74–88). IGI Global. doi:10.4018/978-1-5225-7796-6.ch004

Jha, C. K., & Kolekar, M. H. (2019b). Diagnostic quality assured ECG signal compression with selection of appropriate mother wavelet for minimal distortion. *IET Science, Measurement & Technology*, *13*(4), 500–508. doi:10.1049/iet-smt.2018.5217

Jha, C. K., & Kolekar, M. H. (2020). Cardiac arrhythmia classification using tunable Q-wavelet transform based features and support vector machine classifier. *Biomedical Signal Processing and Control*, *59*, 101875. doi:10.1016/j.bspc.2020.101875

Jha, C. K., & Kolekar, M. H. (2021a). Electrocardiogram data compression techniques for cardiac healthcare systems: A methodological review. *IRBM*. Advance online publication. doi:10.1016/j.irbm.2021.06.007

Jha, C. K., & Kolekar, M. H. (2021b). Empirical mode decomposition and wavelet transform based ECG data compression scheme. *IRBM*, *42*(1), 65–72. doi:10.1016/j.irbm.2020.05.008

Jha, C. K., & Kolekar, M. H. (2021c). Tunable Q-wavelet based ECG data compression with validation using cardiac arrhythmia patterns. *Biomedical Signal Processing and Control*, *66*, 102464. doi:10.1016/j.bspc.2021.102464

Jiang, M., Gu, J., Li, Y., Wei, B., Zhang, J., Wang, Z., & Xia, L. (2021). HADLN: Hybrid attention-based deep learning network for automated arrhythmia classification. *Frontiers in Physiology*, 12.

Jian, H., & Tang, K.-T. (2014). Improving classification accuracy of SSVEP based BCI using RBF SVM with signal quality evaluation. *2014 International Symposium on Intelligent Signal Processing and Communication Systems (ISPACS)*, 302-306. 10.1109/ISPACS.2014.7024473

Jing, C., Liu, G., & Hao, M. (2009). The research on emotion recognition from ECG signal. *International Conference on Information Technology and Computer Science*, 1, 497-500. 10.1109/ITCS.2009.108

Jolliffe, I. T., & Cadima, J. (2016). Principal component analysis: a review and recent developments. *Philosophical Transactions. Series A, Mathematical, Physical, and Engineering Sciences, 374*(2065).

Jonnalagadda. (2018). *Sparse, Stacked and Variational Autoencoder*. https://medium.com/

Joshi, S., & Bajaj, P. (2012). Design & Development of Portable Vata, Pitta & Kapha [VPK] Pulse Detector to Find Prakriti of an Individual using Artificial Neural Network. *6th International Conference for Convergence in Technology (I2CT)*.

Jovanov, E. (1999). Perceptualization of biomedical data. An experimental environment for visualization and sonification of brain electrical activity. *IEEE Engineering in Medicine and Biology Magazine*, *18*, 50–55.

Juanes, J. A., Ruisoto, P., Obeso, J. A., Prats, A., & San-Molina, J. (2015). Computer-Based Visualization System for the Study of Deep Brain Structures Involved in Parkinson's Disease. *Journal of Medical Systems*, *39*(11), 151. doi:10.100710916-015-0348-6 PMID:26370536

Kabir, M. A., & Shahnaz, C. (2012). Denoising of ECG signals based on noise reduction algorithms in EMD and wavelet domains. *Biomedical Signal Processing and Control*, *7*(5), 481–489. doi:10.1016/j.bspc.2011.11.003

Kachenoura, A. (2007). ICA: A potential tool for BCI systems. *IEEE Signal Processing Magazine*, *25*, 57–68.

Kaiser, J. F. (1993). Some useful properties of Teager's energy operators. *IEEE International Conference on Acoustics, Speech, and Signal Processing*, 3, 149-152. 10.1109/ICASSP.1993.319457

Kalange, A.E., & Gangal, S.A. (2007). Piezoelectric sensor for human pulse detection. *Defense Sci Journals, 57*, 109-114.

Kalunga, E., Djouani, K., Hamam, Y., Chevallier, S., & Monacelli, E. (2013). *SSVEP enhancement based on Canonical Correlation Analysis to improve BCI performances. In IEEE AFRICON*. IEEE.

Kaniusas, E. (2012). Fundamentals of biosignals. In Biomedical signals and sensors I (pp. 1–26). Springer.

Kaniusas, E. (2015). Biomedical signals and sensors II. Springer.

Kaur, C., Bisht, A., Singh, P., & Joshi, G. (2021). EEG Signal denoising using hybrid approach of Variational Mode Decomposition and wavelets for depression. *Biomedical Signal Processing and Control*, *65*, 102337.

Khalaf, A. F., Owis, M. I., & Yassine, I. A. (2015). A novel technique for cardiac arrhythmia classification using spectral correlation and support vector machines. *Expert Systems with Applications*, *42*(21), 8361–8368. doi:10.1016/j.eswa.2015.06.046

Khan, K. A., P. P., S., Khan, Y. U., & Farooq, O. (2020). A hybrid Local Binary Pattern and wavelets based approach for EEG classification for diagnosing epilepsy. *Expert Systems with Applications*, *140*, 112895. doi:10.1016/j.eswa.2019.112895

Khateeb, M., Anwar, S. M., & Alnowami, M. (2021). Multi-Domain Feature Fusion for Emotion Classification Using DEAP Dataset. *IEEE Access: Practical Innovations, Open Solutions*, *9*, 12134–12142. doi:10.1109/ACCESS.2021.3051281

Kim, J. H., Poulose, A., & Han, D. S. (2021). The extensive usage of the facial image threshing machine for facial emotion recognition performance. *Sensors (Basel)*, *21*(6), 2026. doi:10.339021062026 PMID:33809352

Kirar, B. S., & Agrawal, D. K. (2019). Computer aided diagnosis of glaucoma using discrete and empirical wavelet transform from fundus images. *IET Image Processing*, *13*(1), 73–82. doi:10.1049/iet-ipr.2018.5297

Kohavi, R. (1995). A study of cross-validation and bootstrap for accuracy estimation and model selection. *Proceedings of the 14th International Joint Conference on Artificial Intelligence*, 2, 1137–1143.

Kołakowska, A., Landowska, A., Szwoch, M., Szwoch, W., & Wrobel, M. R. (2014). Emotion recognition and its applications. In *Human-Computer Systems Interaction: Backgrounds and Applications 3* (pp. 51–62). Springer.

Kolekar, M. H., Jha, C. K., & Kumar, P. (2021). ECG Data Compression Using Modified Run Length Encoding of Wavelet Coefficients for Holter Monitoring. *IRBM*. Advance online publication. doi:10.1016/j.irbm.2021.10.001

Kopsinis, Y., & McLaughlin, S. (2009). Development of EMD-based denoising methods inspired by wavelet thresholding. *IEEE Transactions on Signal Processing*, *57*(4), 1351–1362. doi:10.1109/TSP.2009.2013885

Korbach, A., Brünken, R., & Park, B. (2017). Measurement of cognitive load in multimedia learning: A comparison of different objective measures. *Instructional Science*, *45*(4), 515–536. doi:10.100711251-017-9413-5

Kothe, C. A., & Makeig, S. (2013). BCILAB: A platform for brain–computer interface development. *Journal of Neural Engineering*, *10*, 056014.

Kramme, R., Hoffmann, K. P., & Pozos, R. S. (Eds.). (2011). *Springer handbook of medical technology*. Springer Science & Business Media.

Krishna, P. K. M., & Ramaswamy, K. (2017). Single channel speech separation based on empirical mode decomposition and Hilbert transform. *IET Signal Processing*, *11*(5), 579–586. doi:10.1049/iet-spr.2016.0450

Kruger, J.-L., Hefer, E., & Matthew, G. (2013). Measuring the impact of subtitles on cognitive load: Eye tracking and dynamic audiovisual texts. *Proceedings of the 2013 Conference on Eye Tracking South Africa*, 62–66. 10.1145/2509315.2509331

Kruger, J.-L., Hefer, E., & Matthew, G. (2014). Attention distribution and cognitive load in a subtitled academic lecture: L1 vs. L2. *Journal of Eye Movement Research, 7*(5). https://www.scopus.com/inward/record.uri?eid=2-s2.0-84921875042&partnerID=40&md5=37f8408445395de5b8087cb794e90925

Kruger, J-L., & Doherty, S. (2016). *Measuring cognitive load in the presence of educational video: Towards a multimodal methodology*. doi:10.14742/ajet.3084

Krusienski, D. J. (2008). Toward enhanced P300 speller performance. *Journal of Neuroscience Methods*, *167*, 15–21.

Kshirsagar, G. B., & Londhe, N. D. (2020). Weighted Ensemble of Deep Convolution Neural Networks for Single-Trial Character Detection in Devanagari-Script-Based P300 Speller. *IEEE Transactions on Cognitive and Developmental Systems*, *12*(3), 551–560.

Kumar, R., Sundaram, M., & Arumugam, N. (2021). Facial emotion recognition using subband selective multilevel stationary wavelet gradient transform and fuzzy support vector machine. *The Visual Computer*, *37*(8), 2315–2329. doi:10.100700371-020-01988-1

Kundu, S., & Ari, S. (2018). P300 Detection Using Ensemble of SVM for Brain-Computer Interface Application. *9th International Conference on Computing, Communication and Networking Technologies (ICCCNT).*

Kundu, S., & Ari, S. (2019). P300 based character recognition using sparse autoencoder with ensemble of SVMs. *Biocybernetics and Biomedical Engineering*, *39*(4), 956–966. doi:10.1016/j.bbe.2019.08.001

Kwang-Sup Soh, Myeong-Hwa Lee, & Young-Zoon Yoon. (2000, November-December). Pulse type classification by varying contact pressure. *IEEE Engineering in Medicine and Biology Magazine*, *19*(6), 106–110. doi:10.1109/51.887253 PMID:11103713

Kybic, J. (2005). A common formalism for the Integral formulations of the forward EEG problem. *IEEE Transactions on Medical Imaging*, *24*, 12–28.

Lahmiri, S. (2014). Comparative study of ECG signal denoising by wavelet thresholding in empirical and variational mode decomposition domains. *Healthcare Technology Letters*, *1*(3), 104–109.

Lahmiri, S., & Shmual, S. (2017). Variational mode decomposition based approach for accurate classification of color fundus images with hemorrhages. *Optics & Laser Technology*, *96*, 243–248. doi:10.1016/j.optlastec.2017.05.012

Lakshmi. (2014). Survey on EEG signal processing methods. *International Journal of Advanced Research in Computer Science and Software Engineering, 4*.

Lang, P. J., Bradley, M. M., & Cuthbert, B. N. (1997). International affective picture system (IAPS): Technical manual and affective ratings. NIMH Center for the Study of Emotion and Attention, 1(39-58), 3.

Lee, H. (2014). Measuring cognitive load with electroencephalography and self-report: Focus on the effect of English-medium learning for Korean students. *Educational Psychology, 34*(7), 838–848. doi:10.1080/01443410.2013.860217

Lee, C. T., & Wei, L. Y. (1983). Spectrum analysis of human pulse. *IEEE Transactions on Biomedical Engineering*, *BME-30*(6), 348–352. doi:10.1109/TBME.1983.325136 PMID:6873965

Lee, S. H., Lim, J. S., Kim, J. K., Yang, J., & Lee, Y. (2014). Classification of normal and epileptic seizure EEG signals using wavelet transform, phase-space reconstruction, and Euclidean distance. *Computer Methods and Programs in Biomedicine*, *116*(1), 10–25. doi:10.1016/j.cmpb.2014.04.012 PMID:24837641

Lee, S., Kim, J., & Lee, M. (2011). A real-time ECG data compression and transmission algorithm for an e-health device. *IEEE Transactions on Biomedical Engineering*, *58*(9), 2448–2455. doi:10.1109/TBME.2011.2156794 PMID:21606020

Lehnertz, K., & Elger, C. E. (1995). Spatio-temporal dynamics of the primary epileptogenic area in temporal lobe epilepsy characterized by neuronal complexity loss. *Electroencephalography and Clinical Neurophysiology*, *95*(2), 108–117. doi:10.1016/0013-4694(95)00071-6 PMID:7649002

León-Carrion, J., Damas-López, J., Martín-Rodríguez, J. F., Domínguez-Roldán, J. M., Murillo-Cabezas, F., Barroso y Martin, J. M., & Domínguez-Morales, M. R. (2008). The hemodynamics of cognitive control: The level of concentration of oxygenated hemoglobin in the superior prefrontal cortex varies as a function of performance in a modified Stroop task. *Behavioural Brain Research*, *193*(2), 248–256. doi:10.1016/j.bbr.2008.06.013 PMID:18606191

Leppink, J., Paas, F., Van der Vleuten, C. P. M., Van Gog, T., & Van Merriënboer, J. J. G. (2013). Development of an instrument for measuring different types of cognitive load. *Behavior Research Methods*, *45*(4), 1058–1072. doi:10.375813428-013-0334-1 PMID:23572251

Leyden, P., O'Connell, M., Greene, D., & Curran, K. (2019). Automatic bone marrow segmentation for PETCT imaging in multiple myeloma. *Physica Medica*.

Liang, S.-F., Wang, H.-C., & Chang, W.-L. (2010). Combination of EEG Complexity and Spectral Analysis for Epilepsy Diagnosis and Seizure Detection. *EURASIP Journal on Advances in Signal Processing*, *15*(1), 853434. Advance online publication. doi:10.1155/2010/853434

Liao, S., Jain, A. K., & Li, S. Z. (2015). A fast and accurate unconstrained face detector. *IEEE Transactions on Pattern Analysis and Machine Intelligence*, *38*(2), 211–223. doi:10.1109/TPAMI.2015.2448075 PMID:26761729

Li, C., Zheng, C., & Tai, C. (1995). Detection of ECG characteristic points using wavelet transforms. *IEEE Transactions on Biomedical Engineering*, *42*(1), 21–28. doi:10.1109/10.362922 PMID:7851927

Li, H., Yuan, D., Ma, X., Cui, D., & Cao, L. (2017). Genetic algorithm for the optimization of features and neural networks in ECG signals classification. *Scientific Reports*, *7*(1), 1–12. doi:10.1038rep41011 PMID:28139677

Li, J., Qiu, T., Wen, C., Xie, K., & Wen, F. Q. (2018). Robust face recognition using the deep C2D-CNN model based on decision-level fusion. *Sensors (Basel)*, *18*(7), 2080. doi:10.339018072080 PMID:29958478

Li, K., Pan, W., Li, Y., Jiang, Q., & Liu, G. (2018). A method to detect sleep apnea based on deep neural network and hidden Markov model using single-lead ECG signal. *Neurocomputing*, *294*, 94–101.

Li, L., Xu, M., Liu, H., Li, Y., Wang, X., Jiang, L., Wang, Z., Fan, X., & Wang, N. (2020). A large-scale database and a CNN model for attention based glaucoma detection. *IEEE Transactions on Medical Imaging*, *39*(2), 413–424. doi:10.1109/TMI.2019.2927226 PMID:31283476

Li, M., Fei, Z., Zeng, M., Wu, F.-X., Li, Y., Pan, Y., & Wang, J. (2019). Automated ICD-9 Coding via A Deep Learning Approach. *IEEE/ACM Transactions on Computational Biology and Bioinformatics*, *16*(4), 1193–1202. doi:10.1109/TCBB.2018.2817488 PMID:29994157

Lim, T. C., Chattopadhyay, S., & Acharya, U. R. (2012). A survey and comparative study on the instruments for glaucoma detection. *Medical Engineering & Physics*, *34*(2), 129–139. doi:10.1016/j.medengphy.2011.07.030 PMID:21862378

Lin, Y. P., Wang, C. H., Jung, T. P., Wu, T. L., Jeng, S. K., Duann, J. R., & Chen, J. H. (2010). EEG-based emotion recognition in music listening. *IEEE Transactions on Biomedical Engineering*, *57*(7), 1798–1806. doi:10.1109/TBME.2010.2048568 PMID:20442037

Lin, Z. (2006). Frequency recognition based on canonical correlation analysis for SSVEP-based BCIs. *IEEE Transactions on Biomedical Engineering*, *53*, 2610–2614.

Lin, Z., Zhang, C., Wu, W., & Gao, X. (2007). Frequency recognition based on canonical correlation analysis for SSVEP-based BCIs. *IEEE Transactions on Biomedical Engineering*, *54*(6), 1172–1176. doi:10.1109/TBME.2006.889197 PMID:17549911

Li, S., Zhou, W., Yuan, Q., Geng, S., & Cai, D. (2013). Feature extraction and recognition of ictal EEG using EMD and SVM. *Computers in Biology and Medicine*, *43*(7), 807–816. doi:10.1016/j.compbiomed.2013.04.002 PMID:23746721

Liu, C., Wang, R., Li, L., Ding, G., Yang, J., & Li, P. (2020). Effects of encoding modes on memory of naturalistic events. *Journal of Neurolinguistics, 53*. doi:10.1016/j.jneuroling.2019.100863

Liu, C.-J., & Chiang, W.-W. (2014). Theory, Method And Practice Of Neuroscientific Findings In Science Education. *International Journal of Science and Mathematics Education*, *12*(3), 629–646. doi:10.100710763-013-9482-0

Liu, Wu, Gu, & Yu, Qi, & Li. (2017). Deep Learning Based on Batch Normalization for P300 Signal Detection. *Neurocomputing*, *275*, 288–297.

Liu, Y., Lin, Y., Jia, Z., Ma, Y., & Wang, J. (2020). Representation based on ordinal patterns for seizure detection in EEG signals. *Computers in Biology and Medicine*, *126*, 104033. doi:10.1016/j.compbiomed.2020.104033 PMID:33091826

Liu, Y., Yang, G., Li, M., & Yin, H. (2016). Variational mode decomposition denoising combined the detrended fluctuation analysis. *Signal Processing*, *125*, 349–364.

Li, W., Zhang, Z., & Song, A. (2021). Physiological-signal-based emotion recognition: An odyssey from methodology to philosophy. *Measurement*, *172*, 108747. doi:10.1016/j.measurement.2020.108747

Li, X., Li, X., Zheng, X., & Zhang, D. (2010). EMD-TEO based speech emotion recognition. In *Life System Modeling and Intelligent Computing* (pp. 180–189). Springer. doi:10.1007/978-3-642-15597-0_20

Li, Y. (2013). A hybrid BCI system combining P300 and SSVEP and its application to wheelchair control. *IEEE Transactions on Biomedical Engineering*, *60*, 3156–3166.

Li, Y., & Guan, C. (2008). Joint feature re-extraction and classification using an iterative semi-supervised support vector machine algorithm. *Machine Learning*, *71*(1), 33–53. doi:10.100710994-007-5039-1

Li, Y., Huang, J., Zhou, H., & Zhong, N. (2017). Human emotion recognition with electroencephalographic multidimensional features by hybrid deep neural networks. *Applied Sciences (Basel, Switzerland)*, *7*(10), 1060. doi:10.3390/app7101060

Li, Z., Tian, X., Shu, L., Xu, X., & Hu, B. (2017, August). Emotion recognition from EEG using RASM and LSTM. *In International Conference on Internet Multimedia Computing and Service* (pp. 310-318). Springer.

Llamedo, M., & Martínez, J. P. (2010). Heartbeat classification using feature selection driven by database generalization criteria. *IEEE Transactions on Biomedical Engineering*, *58*(3), 616–625. doi:10.1109/TBME.2010.2068048 PMID:20729162

Loey, M., Naman, M., & Zayed, H. (2020). Deep Transfer Learning in Diagnosing Leukemia in Blood Cell. *Journal of Diagnostic*, *9*(29), 546–590. doi:10.3390/computers9020029

Loftus, J. J., Jacobsen, M., & Wilson, T. D. (2017). Learning and assessment with images: A view of cognitive load through the lens of cerebral blood flow. *British Journal of Educational Technology, 48*(4), 1030–1046. doi:10.1111/bjet.12474

Loftus, J. J., Jacobsen, M., & Wilson, T. D. (2018). The relationship between spatial ability, cerebral blood flow and learning with dynamic images: A transcranial Doppler ultrasonography study. *Medical Teacher, 40*(2), 174–180. doi:10.1080/0142159X.2017.1395401

Loftus, J., Jacobsen, M., & Wilson, T. D. (2016). Spatial Ability Mitigates Cognitive Load during Learning with Dynamic Images: A Transcranial Doppler Ultrasonography Study. AERA Online Paper Repository.

Loni, M., Sinaei, S., Zoljodi, A., Daneshtalab, M., & Sjödin, M. (2020). DeepMaker: A multi-objective optimization framework for deep neural networks in embedded systems. *Microprocessors and Microsystems*, *73*, 102989.

Lotte, F. (2007). A review of classification algorithms for EEG-based brain–computer interfaces. *Journal of Neural Engineering*, *4*, R1.

Lotte, F., Congedo, M., Lécuyer, A., Lamarche, F., & Arnaldi, B. (2007). A review of classification algorithms for EEG-based brain-computer interfaces. *Journal of Neural Engineering*, *4*(2), R1–R13. doi:10.1088/1741-2560/4/2/R01 PMID:17409472

Lukáš & Pavel. (2017). Stacked Autoencoders for the P300 Component Detection. *Frontiers in Neuroscience.*

Luo, C. H., Chung, Y. F., Yeh, C. C., Si, X. C., Chang, C. C., Hu, C. S., & Chu, Y.-W. (2012). String like pulse quantification study by pulse wave in 3D pulse mapping. *Journal of Alternative and Complementary Medicine (New York, N.Y.)*, *18*(10), 924–931. doi:10.1089/acm.2012.0047 PMID:23057481

Luo, K., Li, J., Wang, Z., & Cuschieri, A. (2017). Patient-specific deep architectural model for ECG classification. *Journal of Healthcare Engineering*.

Luz, E. J. D. S., Schwartz, W. R., Cámara-Chávez, G., & Menotti, D. (2016). ECG-based heartbeat classification for arrhythmia detection: A survey. *Computer Methods and Programs in Biomedicine*, *127*, 144–164. doi:10.1016/j.cmpb.2015.12.008 PMID:26775139

Mac Ruairí, R., Keane, M. T., & Coleman, G. (2008, August). A wireless sensor network application requirements taxonomy. In *Sensor Technologies and Applications, 2008. SENSORCOMM'08. Second International Conference on* (pp. 209–216). IEEE.

Maćkiewicz, A., & Ratajczak, W. (1993). Principal components analysis (PCA). *Computers & Geosciences*, *19*(3), 303–342.

Maheshwari, S., Pachori, R. B., & Acharya, U. R. (2017). Automated diagnosis of glaucoma using empirical wavelet transform and correntropy features extracted from fundus images. *IEEE Journal of Biomedical and Health Informatics*, *21*(3), 803–813. doi:10.1109/JBHI.2016.2544961 PMID:28113877

Makary, M. M., & Kadah, Y. M. (2014). Improving P300 and SCP-based Brain computer interfacing by spectral subtraction denoising. *2nd Middle East Conference on Biomedical Engineering*, 228-231.

Makransky, G., Terkildsen, T. S., & Mayer, R. E. (2019a). Adding immersive virtual reality to a science lab simulation causes more presence but less learning. *Learning and Instruction*, *60*, 225–236. doi:10.1016/j.learninstruc.2017.12.007

Makransky, G., Terkildsen, T. S., & Mayer, R. E. (2019b). Role of subjective and objective measures of cognitive processing during learning in explaining the spatial contiguity effect. *Learning and Instruction*, *61*, 23–34. doi:10.1016/j.learninstruc.2018.12.001

Mamun, M., Al-Kadi, M., & Marufuzzaman, M. (2013). Effectiveness of wavelet denoising on electroencephalogram signals. *Journal of Applied Research and Technology*, *11*(1), 156–160. doi:10.1016/S1665-6423(13)71524-4

Manikandan, M. S., & Dandapat, S. (2014). Wavelet-based electrocardiogram signal compression methods and their performances: A prospective review. *Biomedical Signal Processing and Control*, *14*, 73–107. doi:10.1016/j.bspc.2014.07.002

Mantas, C. J., & Abellán, J. (2014). Credal-C4.5: Decision tree based on imprecise probabilities to classify noisy data. *Expert Systems with Applications*, *41*(10), 4625–4637. doi:10.1016/j.eswa.2014.01.017

Mao, K. Z., Tan, K.-C., & Ser, W. (2000). Probabilistic neural-network structure determination for pattern classification. *IEEE Transactions on Neural Networks*, *11*(4), 1009–1016. doi:10.1109/72.857781 PMID:18249828

Marimuthu, P. Punchoo, & Bhora. (2021). A Comparison of Machine Learning Techniques for Diagnosing Multiple Myeloma. Academic Press.

Marinho, L. B., Nascimento, N. M. M., Souza, J. W. M., Gurgel, M. V., Rebouças Filho, P. P., & de Albuquerque, V. H. C. (2019). A novel electrocardiogram feature extraction approach for cardiac arrhythmia classification. *Future Generation Computer Systems*, *97*, 564–577. doi:10.1016/j.future.2019.03.025

Mar, T., Zaunseder, S., Martínez, J. P., Llamedo, M., & Poll, R. (2011). Optimization of ECG classification by means of feature selection. *IEEE Transactions on Biomedical Engineering*, *58*(8), 2168–2177.

Martínez-Tejada, L. A., Puertas-González, A., Yoshimura, N., & Koike, Y. (2021). Exploring EEG Characteristics to Identify Emotional Reactions under Videogame Scenarios. *Brain Sciences*, *11*(3), 378. doi:10.3390/brainsci11030378 PMID:33809797

Ma, Y., & Cao, S. (2019). An improved robust threshold for variational mode decomposition based denoising in the frequency-offset domain. *Journal of Seismic Exploration*, *28*(3), 277–305.

Mazher, M., Abd Aziz, A., Malik, A. S., & Ullah Amin, H. (2017). An EEG-Based Cognitive Load Assessment in Multimedia Learning Using Feature Extraction and Partial Directed Coherence. *IEEE Access, 5*, 14819–14829. doi:10.1109/ACCESS.2017.2731784

Mazher, M., Aziz, A. A., & Malik, A. S. (2016). Evaluation of rehearsal effects of multimedia content based on EEG using machine learning algorithms. *2016 6th International Conference on Intelligent and Advanced Systems (ICIAS)*, 1–6. 10.1109/ICIAS.2016.7824134

Mazher, M., Aziz, A. A., Malik, A. S., & Qayyum, A. (2015a). A statistical analysis on learning and nonlearning mental states using EEG. *2015 IEEE Student Symposium in Biomedical Engineering Sciences (ISSBES)*, 36–40. 10.1109/ISSBES.2015.7435889

Mazher, M., Aziz, A. B. A., Malik, A. S., & Qayyum, A. (2015b). A comparison of brain regions based on EEG during multimedia learning cognitive activity. *2015 IEEE Student Symposium in Biomedical Engineering Sciences (ISSBES)*, 31–35. 10.1109/ISSBES.2015.7435888

McCraty, R. (2015). *Science of the heart: Exploring the role of the heart in human performance*. HeartMath Institute.

Meilˇa & Jordan. (2021). Multi-scale Regional Attention Deeplab3+: Multiple Myeloma Plasma Cells Segmentation in Microscopic Images. *Journal of Machine Learning Research*.

Melgani, F., & Bazi, Y. (2008). Classification of electrocardiogram signals with support vector machines and particle swarm optimization. *IEEE Transactions on Information Technology in Biomedicine*, *12*(5), 667–677. doi:10.1109/TITB.2008.923147 PMID:18779082

Melin, P., Amezcua, J., Valdez, F., & Castillo, O. (2014). A new neural network model based on the LVQ algorithm for multi-class classification of arrhythmias. *Information Sciences*, *279*, 483–497. doi:10.1016/j.ins.2014.04.003

Mert, A. (2016). ECG feature extraction based on the bandwidth properties of variational mode decomposition. *Physiological Measurement*, *37*(4), 530.

Mert, A., & Akan, A. (2018). Emotion recognition based on time–frequency distribution of EEG signals using multivariate synchrosqueezing transform. *Digital Signal Processing*, *81*, 106–115. doi:10.1016/j.dsp.2018.07.003

Mishra, V., Bajaj, V., Kumar, A., Sharma, D., & Singh, G. K. (2017). An Efficient Method for Analysis of EMG Signals using Improved Empirical Mode Decomposition. *AEÜ. International Journal of Electronics and Communications*, *72*(1), 200–209. doi:10.1016/j.aeue.2016.12.008

Moavenian, M., & Khorrami, H. (2010). A qualitative comparison of artificial neural networks and support vector machines in ECG arrhythmias classification. *Expert Systems with Applications*, *37*(4), 3088–3093. doi:10.1016/j.eswa.2009.09.021

Mondéjar-Guerra, V., Novo, J., Rouco, J., Penedo, M. G., & Ortega, M. (2019). Heartbeat classification fusing temporal and morphological information of ECGs via ensemble of classifiers. *Biomedical Signal Processing and Control*, *47*, 41–48. doi:10.1016/j.bspc.2018.08.007

Mondini, V., Mangia, A., Talevi, L., & Cappello, A. (2018). Sinc-Windowing and Multiple Correlation Coefficients Improve SSVEP Recognition Based on Canonical Correlation Analysis. *Computational Intelligence and Neuroscience*, *2018*, 1–11. doi:10.1155/2018/4278782 PMID:29849546

Moody, G. B. (2008, September). The physionet/computers in cardiology challenge 2008: T-wave alternans. In 2008 Computers in Cardiology (pp. 505-508). IEEE.

Moody, G. B., & Mark, R. G. (2001). The impact of the MIT-BIH arrhythmia database. *IEEE Engineering in Medicine and Biology Magazine*, *20*(3), 45–50. doi:10.1109/51.932724 PMID:11446209

Morlet, J., Arens, G., Fourgeau, E., & Giard, D. (1982). Wave propagation and sampling theory—Part II: Sampling theory and complex waves. *Geophysics*, *47*(2), 222–236. doi:10.1190/1.1441329

Mosquera Orgueira, A., González Pérez, M. S., & Díaz Arias, J. Á. (2021). *Survival prediction and treatment optimization of multiple myeloma patients using machine-learning models based on clinical and gene expression data*. Leukaemia.

Motinath, V. A., Jha, C. K., & Kolekar, M. H. (2016). A novel ECG data compression algorithm using best mother wavelet selection. *2016 International Conference on Advances in Computing, Communications and Informatics (ICACCI)*, 682–686. 10.1109/ICACCI.2016.7732125

Mühl, C., Allison, B., Nijholt, A., & Chanel, G. (2014). A survey of affective brain computer interfaces: Principles, state-of-the-art, and challenges. *Brain-Computer Interfaces*, *1*(2), 66–84. doi:10.1080/2326263X.2014.912881

Mukhopadhyay, S., & Ray, G. C. (1998). A new interpretation of nonlinear energy operator and its efficacy in spike detection. *IEEE Transactions on Biomedical Engineering*, *45*(2), 180–187. doi:10.1109/10.661266 PMID:9473841

Müller, K.-R. (2008). Machine learning for real-time single-trial EEG-analysis: From brain–computer interfacing to mental state monitoring. *Journal of Neuroscience Methods*, *167*, 82–90.

Muller-Putz, G. R., & Pfurtscheller, G. (2007). Control of an electrical prosthesis with an SSVEP-based BCI. *IEEE Transactions on Biomedical Engineering*, *55*, 361–364.

Müller-Putz, R. G., Scherer, R., Christian, B., & Gert, P. (2005). Steady-state visual evoked potential (SSVEP)-based communication: Impact of harmonic frequency components. *Journal of Neural Engineering*, *2*(4), 123–130. doi:10.1088/1741-2560/2/4/008 PMID:16317236

Mutlu-Bayraktar, D., Cosgun, V., & Altan, T. (2019). Cognitive load in multimedia learning environments: A systematic review. *Computers & Education*, *141*, 103618. doi:10.1016/j.compedu.2019.103618

Nagel, J. H. (2000). Biopotential amplifiers. In J. D. Bronzino (Ed.), *Biomedical engineering hand book* (2nd ed., pp. 70–71). Springer-Verlag.

Naithani, P., Sihota, R., Sony, P., Dada, T., Gupta, V., Kondal, D., & Pandey, R. M. (2007). Evaluation of optical coherence tomography and Heidelberg retinal tomography parameters in detecting early and moderate glaucoma. *Investigative Ophthalmology & Visual Science*, *48*(7), 3138–3145. doi:10.1167/iovs.06-1407 PMID:17591883

Nanyue, W., Youhua, Y., Dawei, H., Bin, X., Jia, L., Tongda, L., Liyuan, X., Zengyu, S., Yanping, C., & Jia, W. (2015). Pulse diagnosis signals analysis of fatty liver disease and cirrhosis patients by using machine learning. *TheScientificWorldJournal*.

Nicolas-Alonso, F. L., & Gomez-Gil, J. (2012). Brain computer interfaces, a review. *Sensors (Basel)*, *12*(2), 1211–1279. doi:10.3390120201211 PMID:22438708

Nishad, A., & Pachori, R. B. (2020). Classification of epileptic electroencephalogram signals using tunable-Q wavelet transform based filter-bank. *Journal of Ambient Intelligence and Humanized Computing*, 1–15. doi:10.100712652-020-01722-8

Noronha, K. P., Acharya, U. R., Nayak, K. P., Martis, R. J., & Bhandary, S. V. (2014). Automated classification of glaucoma stages using higher order cumulant features. *Biomedical Signal Processing and Control*, *10*, 174–183. doi:10.1016/j.bspc.2013.11.006

Oakley, A. (2012). Foreword. In D. Gough, S. Oliver, & J. Thomas (Eds.), *An Introduction to Systematic Reviews* (pp. 7–10). SAGE Publications.

Ojansivu, V., & Heikkilä, J. (2008). Blur insensitive texture classification using local phase quantization. In *International Conference On Image And Signal Processing*. Springer. 10.1007/978-3-540-69905-7_27

Okoye, G. C. (2008). Biomedical technology and health human life. *Biomedical Engineering*, ●●●, 1–12.

Olariu, T. (2016, August). Specialized software system for heart rate variability analysis: An implementation of nonlinear graphical methods. In *International workshop soft computing applications* (pp. 367–374). Springer.

Orlando, J. I., Fu, H., Barbosa Breda, J., van Keer, K., Bathula, D. R., Diaz-Pinto, A., Fang, R., Heng, P.-A., Kim, J., Lee, J. H., Lee, J., Li, X., Liu, P., Lu, S., Murugesan, B., Naranjo, V., Phaye, S. S. R., Shankaranarayana, S. M., Sikka, A., ... Bogunović, H. (2020). REFUGE Challenge: A unified framework for evaluating automated methods for glaucoma assessment from fundus photographs. *Medical Image Analysis*, *59*, 1–19. doi:10.1016/j.media.2019.101570 PMID:31630011

Ortiz De Guinea, A., Titah, R., & Léger, P.-M. (2013). Measure for Measure: A two study multi-trait multi-method investigation of construct validity in IS research. *Computers in Human Behavior, 29*(3), 833–844. doi:10.1016/j.chb.2012.12.009

Örün, Ö., & Akbulut, Y. (2019). Effect of multitasking, physical environment and electroencephalography use on cognitive load and retention. *Computers in Human Behavior*, *92*, 216–229. doi:10.1016/j.chb.2018.11.027

Osowski, S., & Linh, T. H. (2001). ECG beat recognition using fuzzy hybrid neural network. *IEEE Transactions on Biomedical Engineering*, *48*(11), 1265–1271. doi:10.1109/10.959322 PMID:11686625

Oung, Q. W., Muthusamy, H., Basah, S. N., Lee, H., & Vijean, V. (2018). Empirical wavelet transform based features for classification of Parkinson's disease severity. *Journal of Medical Systems*, *42*(2), 1–17.

Oweis, R. J., & Abdulhay, E. W. (2011). Seizure classification in EEG signals utilizing Hilbert-Huang transform. *Biomedical Engineering Online*, *10*(1), 1–15. doi:10.1186/1475-925X-10-38 PMID:21609459

Özbay, Y., & Tezel, G. (2010). A new method for classification of ECG arrhythmias using neural network with adaptive activation function. *Digital Signal Processing*, *20*(4), 1040–1049. doi:10.1016/j.dsp.2009.10.016

Paas, F., & Sweller, J. (2014). Implications of Cognitive Load Theory. In *The Cambridge Handbook of Multimedia Learning* (2nd ed., pp. 27–43). Cambridge University Press. doi:10.1017/CBO9781139547369.004

Paas, F., Tuovinen, J. E., Tabbers, H., & Van Gerven, P. W. (2003). Cognitive load measurement as a means to advance cognitive load theory. *Educational Psychologist*, *38*(1), 63–71. doi:10.1207/S15326985EP3801_8

Pachiyappan, A., Das, U. N., Murthy, T. V. S. P., & Tatavarti, R. (2012). Automated diagnosis of diabetic retinopathy and glaucoma using fundus and OCT images. *Lipids in Health and Disease*, *11*(73), 1–10. doi:10.1186/1476-511X-11-73 PMID:22695250

Palo, H. K., & Mohanty, M. N. (2018). Wavelet-based feature combination for recognition of emotions. *Ain Shams Engineering Journal*, *9*(4), 1799–1806. doi:10.1016/j.asej.2016.11.001

Pal, S., & Mitra, M. (2012). Empirical mode decomposition based ECG enhancement and QRS detection. *Computers in Biology and Medicine*, *42*(1), 83–92. doi:10.1016/j.compbiomed.2011.10.012 PMID:22119222

Panahi, F., Rashidi, S., & Sheikhani, A. (2021). Application of fractional Fourier transform in feature extraction from electrocardiogram and galvanic skin response for emotion recognition. *Biomedical Signal Processing and Control*, *69*, 102863. doi:10.1016/j.bspc.2021.102863

Pan, J., & Tompkins, W. J. (1985). A real-time QRS detection algorithm. *IEEE Transactions on Biomedical Engineering*, *32*(3), 230–236. doi:10.1109/TBME.1985.325532 PMID:3997178

Parashar, D., & Agrawal, D. (2021). 2-D Compact Variational Mode Decomposition-Based Automatic Classification of Glaucoma Stages From Fundus Images. *IEEE Transactions on Instrumentation and Measurement*, *70*, 1–10. doi:10.1109/TIM.2021.3071223

Parashar, D., & Agrawal, D. K. (2020). Automated classification of glaucoma stages using flexible analytic wavelet transform from retinal fundus images. *IEEE Sensors Journal*, *20*(21), 12885–12894. doi:10.1109/JSEN.2020.3001972

Parashar, D., & Agrawal, D. K. (2020). Automated classification of glaucoma using retinal fundus images. *IEEE International Conference on Measurement, Instrumentation, Control and Automation (ICMICA)*, 1-6. 10.1109/ICMICA48462.2020.9242702

Parashar, D., & Agrawal, D. K. (2021). Automatic classification of glaucoma stages using two-dimensional tensor empirical wavelet transform. *IEEE Signal Processing Letters*, *28*, 66–70. doi:10.1109/LSP.2020.3045638

Parikhrt, K., & Thakker, B. (2015). Wrist pulse classification system for healthy and unhealthy subjects. *International Journal of Computers and Applications*, *1*, 120–124.

Parvaneh, S., & Rubin, J. (2018, September). Electrocardiogram monitoring and interpretation: from traditional machine learning to deep learning, and their combination. In *2018 Computing in Cardiology Conference (CinC)* (Vol. 45, pp. 1-4). IEEE. 10.22489/CinC.2018.144

Parvaneh, S., Rubin, J., Babaeizadeh, S., & Xu-Wilson, M. (2019). Cardiac arrhythmia detection using deep learning: A review. *Journal of Electrocardiology*, *57*, S70–S74. doi:10.1016/j.jelectrocard.2019.08.004 PMID:31416598

Patro, Sahu, & Kumar. (2015). Normalization: A Preprocessing Stage. *International Advanced Research Journal in Science, Engineering and Technology.*

Penzel, T., Moody, G. B., Mark, R. G., Goldberger, A. L., & Peter, J. H. (2000, September). The apnea-ECG database. In Computers in Cardiology 2000. Vol. 27 (Cat. 00CH37163) (pp. 255-258). IEEE.

Perego, P. (2009). BCI++: A New Framework for Brain Computer Interface Application. SEDE, 37-41.

Philippot, P., Chapelle, G., & Blairy, S. (2002). Respiratory feedback in the generation of emotion. *Cognition and Emotion*, *16*(5), 605–627. doi:10.1080/02699930143000392

Picard, R. W., Vyzas, E., & Healey, J. (2001). Toward Machine Emotional Intelligence: Analysis of Affective Physiological State. *IEEE Transactions on Pattern Analysis and Machine Intelligence*, *23*(10), 1175–1191. doi:10.1109/34.954607

Pinto, A. (2019). Retinal Image Synthesis and Semi-Supervised Learning for Glaucoma Assessment. *IEEE Transactions on Medical Imaging*, *38*(9), 2211–2218. doi:10.1109/TMI.2019.2903434 PMID:30843823

Polat, K., & Güneş, S. (2007). Classification of epileptiform EEG using a hybrid system based on decision tree classifier and fast Fourier transform. *Applied Mathematics and Computation*, *187*(2), 1017–1026. doi:10.1016/j.amc.2006.09.022

Poornachandra, S. (2008). Wavelet-based denoising using subband dependent threshold for ECG signals. *Digital Signal Processing*, *18*(1), 49–55. doi:10.1016/j.dsp.2007.09.006

Prutchi, D., & Norris, M. (2005). *Design and development of medical electronic instrumenta- tion: A practical perspective of the design, construction, and test of medical devices*. Wiley.

Qayyum, A., Faye, I., Malik, A. S., & Mazher, M. (2018). Assessment of Cognitive Load using Multimedia Learning and Resting States with Deep Learning Perspective. *2018 IEEE-EMBS Conference on Biomedical Engineering and Sciences (IECBES)*, 600–605. 10.1109/IECBES.2018.8626702

Qayyum, A., Khan, M. K. A. A., Mazher, M., & Suresh, M. (2018). Classification of EEG Learning and Resting States using 1D-Convolutional Neural Network for Cognitive Load Assessment. *2018 IEEE Student Conference on Research and Development (SCOReD)*, 1–5. 10.1109/SCORED.2018.8711150

Qin, Q., Li, J., Zhang, L., Yue, Y., & Liu, C. (2017). Combining low-dimensional wavelet features and support vector machine for arrhythmia beat classification. *Scientific Reports*, *7*(1), 1–12. doi:10.103841598-017-06596-z PMID:28729684

Rahman, M. M., Bhuiyan, M. I. H., & Das, A. B. (2019). Classification of focal and non-focal EEG signals in VMD-DWT domain using ensemble stacking. *Biomedical Signal Processing and Control*, *50*, 72–82. doi:10.1016/j.bspc.2019.01.012

Rahul, J., & Sharma, L. D. (2022). Automatic cardiac arrhythmia classification based on hybrid 1-D CNN and Bi-LSTM model. *Biocybernetics and Biomedical Engineering*, *42*(1), 312–324. doi:10.1016/j.bbe.2022.02.006

Rajani, Nawsupe, & Wangikar. (2012). Automatic detection of pulse morphology patterns & cardiac risks. *Journal of Biomedical Science and Engineering*, *5*(6).

Rajesh, K. N., & Dhuli, R. (2018). Classification of imbalanced ECG beats using re-sampling techniques and AdaBoost ensemble classifier. *Biomedical Signal Processing and Control*, *41*, 242–254. doi:10.1016/j.bspc.2017.12.004

Rakotomamonjy, A., & Guigue, V. (2008). BCI Competition III: Dataset II- Ensemble of SVMs for BCI P300 Speller. *IEEE Transactions on Biomedical Engineering*, *55*(3), 1147–1154.

Rangayyan, R. M., & Reddy, N. P. (2002). Biomedical signal analysis: A case-study approach. *Annals of Biomedical Engineering*, *30*(7), 983–983. doi:10.1114/1.1509766

Rashid, M., Sulaiman, N., Mustafa, M., Khatun, S., & Bari, B. S. (2019). The Classification of EEG Signal Using Different Machine Learning Techniques for BCI Application. *Robot Intelligence Technology and Applications*, 207-221.

Ravi Kumar, M., & Srinivasa Rao, Y. (2019). Epileptic seizures classification in EEG signal based on semantic features and variational mode decomposition. *Cluster Computing*, *22*(S6), 13521–13531. doi:10.100710586-018-1995-4

Ray, G. C. (1994). An Algorithm to Separate Nonstationary Part of a Signal Using Mid-Prediction Filter. *IEEE Transactions on Signal Processing*, *42*(9), 2276–2279. doi:10.1109/78.317850

Regan, D. (1975). Recent advances in electrical recording from the human brain. Nature, 253, 401-407.

Reinerman-Jones, L., Barber, D. J., Szalma, J. L., & Hancock, P. A. (2017). Human interaction with robotic systems: Performance and workload evaluations. *Ergonomics, 60*(10), 1351–1368. doi:10.1080/00140139.2016.1254282

Rewri, P., & Kakkar, M. (2014). Awareness, knowledge, and practice: A survey of glaucoma in north Indian rural residents. *Indian Journal of Ophthalmology*, *62*(4), 482–486. doi:10.4103/0301-4738.132105 PMID:24817749

Reza, F.-R., Brendan, A., Christoph, G., Eric, S., Sonja, K., & Andrea, K. (2012). P300 brain computer interface: Current challenges and emerging trends. *Frontiers in Neuroengineering*.

Rhyner, H. H. (1998). *Ayurveda: The gentle health system*. Motilal Banarsidass Publishers Pvt. Ltd.

Rodrigues, F. M. S. (2015). *Establishing a framework for the development of multimodal virtual reality interfaces with applicability in education and clinical practice* (Doctoral dissertation).

Rodriguez-Mozaz, S., Marco, M. P., de Alda, M. J. L., & Barceló, D. (2004). Biosensors for environmental monitoring of endocrine disruptors: A review article. *Analytical and Bioanalytical Chemistry*, *378*(3), 588–598. doi:10.100700216-003-2385-0 PMID:14647938

Ronkainen, N. J., Halsall, H. B., & Heineman, W. R. (2010). *Electrochemical biosensors*. Academic Press.

Ronkainen, N. J., Halsall, H. B., & Heineman, W. R. (2010). Electrochemical biosensors. *Chemical Society Reviews*, *39*(5), 1747–1763. doi:10.1039/b714449k

Ross, A. J., & Sachdev, P. S. (2004). Magnetic resonance spectroscopy in cognitive research. *Brain Research. Brain Research Reviews*, *44*(2), 83–102. doi:10.1016/j.brainresrev.2003.11.001 PMID:15003387

Rößler, J., Sun, J., & Gloor, P. (2021). Reducing Videoconferencing Fatigue through Facial Emotion Recognition. *Future Internet*, *13*(5), 126. doi:10.3390/fi13050126

Rothrock, R. L., & Drummond, O. E. (2000, July). Performance metrics for multiple-sensor multiple-target tracking. In *Signal and Data Processing of Small Targets 2000* (Vol. 4048, pp. 521–532). International Society for Optics and Photonics. doi:10.1117/12.392004

Ruisoto Palomera, P., Juanes Méndez, J. A., & Prats Galino, A. (2014). Enhancing neuroanatomy education using computer-based instructional material. *Computers in Human Behavior*, *31*, 446–452. doi:10.1016/j.chb.2013.03.005

Sadhukhan, D., Pal, S., & Mitra, M. (2015). Electrocardiogram data compression using adaptive bit encoding of the discrete Fourier transforms coefficients. *IET Science, Measurement & Technology*, *9*(7), 866–874. doi:10.1049/iet-smt.2015.0013

Safieddine, D., Kachenoura, A., Albera, L., Birot, G., Karfoul, A., Pasnicu, A., Biraben, A., Wendling, F., Senhadji, L., & Merlet, I. (2012). Removal of muscle artifact from EEG data: Comparison between stochastic (ICA and CCA) and deterministic (EMD and wavelet-based) approaches. *EURASIP Journal on Advances in Signal Processing*, *2012*(1), 127.

Sahoo, S., Kanungo, B., Behera, S., & Sabut, S. (2017). Multiresolution wavelet transform based feature extraction and ECG classification to detect cardiac abnormalities. *Measurement*, *108*, 55–66. doi:10.1016/j.measurement.2017.05.022

Salahet, Muhsen, Esalama, Owaidah, & Hashmi. (2019). Machine learning applications in the diagnosis of leukaemia: Current trends and future directions. *International Journal of Laboratory Haematology, 41*(6), 717-726.

Salimpoor, V. N., Benovoy, M., Longo, G., Cooperstock, J. R., & Zatorre, R. J. (2009). The rewarding aspects of music listening are related to degree of emotional arousal. *PLoS One*, *4*, e7487.

Salovey, P., & Mayer, J. D. (1990). Emotional intelligence. *Imagination, Cognition and Personality*, *9*(3), 185–211. doi:10.2190/DUGG-P24E-52WK-6CDG

Sannino, G., & De Pietro, G. (2018). A deep learning approach for ECG-based heartbeat classification for arrhythmia detection. *Future Generation Computer Systems*, *86*, 446–455. doi:10.1016/j.future.2018.03.057

Saragih, J. M., Lucey, S., & Cohn, J. F. (2009). Face alignment through subspace constrained mean-shifts. In *2009 IEEE 12th International Conference on Computer Vision* (pp. 1034-1041). 10.1109/ICCV.2009.5459377

Sarin, M., Verma, A., Mehta, D. H., Shukla, P. K., & Verma, S. (2020). Automated Ocular Artifacts Identification and Removal from EEG Data Using Hybrid Machine Learning Methods. In *7th International Conference on Signal Processing and Integrated Networks (SPIN)* (pp. 1054-1059). Noida: IEEE. 10.1109/SPIN48934.2020.9071360

Sariyanidi, E., Gunes, H., & Cavallaro, A. (2014). Automatic analysis of facial affect: A survey of registration, representation, and recognition. *IEEE Transactions on Pattern Analysis and Machine Intelligence*, *37*(6), 1113–1133. doi:10.1109/TPAMI.2014.2366127 PMID:26357337

Sarker, S., Chowdhury, S., Laha, S., & Dey, D. (2019, April). use of non-local means filters to denoise image corrupted by salt and pepper noise. *International Journal (Toronto, Ont.)*, *3*(2).

Satti, A., Guan, C., Coyle, D., & Prasad, G. (2010). A Covariate Shift Minimisation Method to Alleviate Non-stationarity Effects for an Adaptive Brain-Computer Interface. *20th International Conference on Pattern Recognition.*

Schalk, G. (2004). BCI2000: A general-purpose brain-computer interface (BCI) system. *IEEE Transactions on Biomedical Engineering*, *51*, 1034–1043.

Schalk, G. (2009). Effective brain-computer interfacing using BCI2000. *2009 Annual International Conference of the IEEE Engineering in Medicine and Biology Society*, 5498-5501.

Scheller, F., Schubert, F., Pfeiffer, D., Hintsche, R., Dransfeld, I., Renneberg, R., Wollenberger, U., Riedel, K., Pavlova, M., Kuhn, M., Muller, H. G., Tan, P., Hoffmann, W., & Movitz, W. (1989). Research and development of biosensors. A review. *Analyst (London)*, *114*(6), 653–662. doi:10.1039/AN9891400653 PMID:2665569

Schlorhaufer, C., Behrends, M., Diekhaus, G., Keberle, M., & Weidemann, J. (2012). Implementation of a web-based, interactive polytrauma tutorial in computed tomography for radiology residents: How we do it. *European Journal of Radiology*, *81*(12), 3942–3946. doi:10.1016/j.ejrad.2012.07.006 PMID:22883533

Sejdić, E., Kalika, D., & Czarnek, N. (2013). An Analysis of Resting-State Functional Transcranial Doppler Recordings from Middle Cerebral Arteries. *PLoS One*, *8*(2), e55405. doi:10.1371/journal.pone.0055405 PMID:23405146

Selesnick, I. W. (2011). Wavelet transform with tunable Q-factor. *IEEE Transactions on Signal Processing*, *59*(8), 3560–3575. doi:10.1109/TSP.2011.2143711

Seo, D. W. (2016). Hybrid reality-based user experience and evaluation of a context-aware smart home. *Computers in Industry*, *76*, 11–23.

Sharan, R. V., & Berkovsky, S. (2020). Epileptic Seizure Detection Using Multi-Channel EEG Wavelet Power Spectra and 1-D Convolutional Neural Networks. *2020 42nd Annual International Conference of the IEEE Engineering in Medicine & Biology Society (EMBC)*, 545–548.

Sharma, S., & Kumar, G. (2012). Wavelet analysis based feature extraction for pattern classification from Single channel acquired EMG signal. *Elixir Online Journal, 50*, 320-1.

Sharma, L. N., Dandapat, S., & Mahanta, A. (2010). ECG signal denoising using higher order statistics in Wavelet subbands. *Biomedical Signal Processing and Control*, *5*(3), 214–222. doi:10.1016/j.bspc.2010.03.003

Sharma, R., Pachori, R. B., & Sircar, P. (2020). Seizures classification based on higher order statistics and deep neural network. *Biomedical Signal Processing and Control*, *59*, 101921. doi:10.1016/j.bspc.2020.101921

Sharma, R., Sircar, P., Pachori, R. B., Bhandary, S., & Acharya, U. R. (2019). Automated glaucoma detection using center slice of higher order statistics. *Journal of Mechanics in Medicine and Biology*, *19*(1), 1–21. doi:10.1142/S0219519419400116

Shen, Q., Qin, H., Wei, K., & Liu, G. (2021). Multiscale deep neural network for obstructive sleep apnea detection using RR interval from single-lead ECG signal. *IEEE Transactions on Instrumentation and Measurement*, *70*, 1–13. doi:10.1109/TIM.2021.3062414

Shopon, Mohammed, & Abedin. (2016). Bangla handwritten digit recognition using autoencoder and deep convolutional neural network. *International Workshop on Computational Intelligence*, 64-68. 10.1109/IWCI.2016.7860340

Shukla, P. K., Chaurasiya, R. K., & Verma, S. (2020). Single-Channel Region-Based Speller for Controlling Home Appliances. *International Journal of E-Health and Medical Communications*, *11*(4), 65–89. doi:10.4018/IJEHMC.2020100105

Silva, C., Pimentel, I. R., Andrade, A., Foreid, J. P., & Ducla-Soares, E. (1999). Correlation dimension maps of EEG from epileptic absences. *Brain Topography*, *11*(3), 201–209. doi:10.1023/A:1022281712161 PMID:10217444

Šimić, G., Tkalčić, M., Vukić, V., Mulc, D., Španić, E., Šagud, M., & ... & R Hof, P. (. (2021). Understanding Emotions: Origins and Roles of the Amygdala. *Biomolecules*, *11*(6), 823. doi:10.3390/biom11060823 PMID:34072960

Si-Mohammed, H. (2018). Towards BCI-based interfaces for augmented reality: Feasibility, design and evaluation. *IEEE Transactions on Visualization and Computer Graphics*.

Singh, O., & Sunkaria, R. K. (2015). Powerline interference reduction in ECG signals using empirical wavelet transform and adaptive filtering. *Journal of Medical Engineering & Technology*, *39*(1), 60–68.

Singh, O., & Sunkaria, R. K. (2017). ECG signal denoising via empirical wavelet transform. *Australasian Physical & Engineering Sciences in Medicine*, *40*(1), 219–229.

Singh, P., & Pradhan, G. (2018). Variational mode decomposition based ECG denoising using non-local means and wavelet domain filtering. *Australasian Physical & Engineering Sciences in Medicine*, *41*(4), 891–904.

Soleymani, S., Borzage, M., Noori, S., & Seri, I. (2012). Neonatal hemodynamics: Monitoring, data acquisition and analysis. *Expert Review of Medical Devices*, *9*(5), 501–511.

Sontakay, R. (2018). *Real-time signal analysis of the ECG signal for generating an artificial pulse for continuous flow blood pumps using virtual instrumentation* (Doctoral dissertation). California State University, Northridge.

Specht, D. F. (1990). Probabilistic neural networks. *Neural Networks*, *3*(1), 109–118. doi:10.1016/0893-6080(90)90049-Q PMID:18282828

Spüler, M., & Rosenstiel, W., & Bogdan, M. (2012). Principal component based covariate shift adaption to reduce non-stationarity in a MEG-based brain-computer interface. *EURASIP Journal on Advances in Signal Processing*.

Srinivasan, V., Eswaran, C., & Sriraam, A. N. (2005). Artificial neural network based epileptic detection using time-domain and frequency-domain features. *Journal of Medical Systems*, *29*(6), 647–660. doi:10.100710916-005-6133-1 PMID:16235818

Srinivasan, V., Eswaran, C., & Sriraam, N. (2007). Approximate entropy-based epileptic EEG detection using artificial neural networks. *IEEE Transactions on Information Technology in Biomedicine*, *11*(3), 288–295. doi:10.1109/TITB.2006.884369 PMID:17521078

Stella Mary, M. C. V., Rajsingh, E. B., & Naik, G. R. (2016). Retinal fundus image analysis for diagnosis of glaucoma: A comprehensive survey. *IEEE Access: Practical Innovations, Open Solutions*, *4*, 4327–4354. doi:10.1109/ACCESS.2016.2596761

Su, Z.Y., Wang, C.C., Wu, T., Wang, Y.T., & Tang, F.C. (2008). Instantaneous Frequency-Time analysis of physiology signals: The application of pregnant Women's Radia l Artery Pulse Signals. *Physica A: Statistical Mechanics and its Application, 387*, 485-494.

Suguna, G. C., & Veerabhadrappa, S. T. (2009). A review of wrist pulse analysis. *Biomedical Research*, *30*(4).

Sujadevi, V. G., Soman, K. P., & Vinayakumar, R. (2017, September). Real-time detection of atrial fibrillation from short time single lead ECG traces using recurrent neural networks. In *The International Symposium on Intelligent Systems Technologies and Applications* (pp. 212-221). Springer.

Suleiman, A.-B. R., & Fatehi, T. A.-H. (2007). Features extraction techniques of EEG signal for BCI applications. Faculty of Computer and Information Engineering Department College of Electronics Engineering, University of Mosul, Iraq.

Sung, K. R., Kim, J. S., Wollstein, G., Folio, L., Kook, M. S., & Schuman, J. S. (2011). Imaging of the retinal nerve fiber layer with spectral domain optical coherence tomography for glaucoma diagnosis. *The British Journal of Ophthalmology*, *95*(7), 909–914. doi:10.1136/bjo.2010.186924 PMID:21030413

Suykens, J. A., & Vandewalle, J. (1999). Least squares support vector machine classifiers. *Neural Processing Letters*, *9*(3), 293–300. doi:10.1023/A:1018628609742

Sweller, J. (2010). Element Interactivity and Intrinsic, Extraneous, and Germane Cognitive Load. *Educational Psychology Review*, *22*(2), 123–138. doi:10.100710648-010-9128-5

Sweller, J., Ayres, P., & Kalyuga, S. (2011). *Cognitive Load Theory*. Springer. doi:10.1007/978-1-4419-8126-4

Sweller, J., van Merriënboer, J. J. G., & Paas, F. (2019). Cognitive Architecture and Instructional Design: 20 Years Later. *Educational Psychology Review*, *31*(2), 261–292. doi:10.100710648-019-09465-5

Swiderski, B., Osowski, S., & Rysz, A. (2005). Lyapunov exponent of EEG signal for epileptic seizure characterization. *Proceedings of the 2005 European Conference on Circuit Theory and Design*, 153–156. 10.1109/ECCTD.2005.1523016

Syrykh, C., Abreu, A., Amara, N., & Siegfried, A. (2020). Accurate diagnosis of lymphoma on whole-slide histopathology images using deep learning. *Journal of NPJ Digit. Med, 3*(63), 354–380.

Szafir, D. J. (2010). *Non-Invasive BCI Through EEG* (Unpublished Undergraduate Honors Thesis). Boston College.

Tadel, F. (2011). Brainstorm: A User-Friendly Application for MEG/EEG Analysis. Computational Intelligence and Neuroscience.

Taji, B., Chan, A. D., & Shirmohammadi, S. (2017). False alarm reduction in atrial fibrillation detection using deep belief networks. *IEEE Transactions on Instrumentation and Measurement*, *67*(5), 1124–1131.

Talwar, T. S., & Matharu, S. S. (2016). Classification of SSVEP Based Brain Signals using Discrete Wavelet Transform. *International Journal for Research in Applied Science and Engineering Technology*, 421–426.

Tang, A. C. Y. (2012). Review of traditional Chinese medicine pulse diagnosis quantification. *Complementary Ther. Contemp. Healthcare*, *2012*, 61–80.

Tavakolian, K., Nasrabadi, A. M., & Rezaei, S. (2004, May). Selecting better EEG channels for classification of mental tasks. In *Circuits and Systems, 2004. ISCAS'04. Proceedings of the 2004 International Symposium on* (*Vol. 3*, pp. III–537). IEEE.

Tessy, E., Muhammed Shanir, P. P., & Manafuddin, S. (2017). Time domain analysis of epileptic EEG for seizure detection. *2016 International Conference on Next Generation Intelligent Systems, ICNGIS 2016*. 10.1109/ICNGIS.2016.7854034

Thakkar, S., & Thakker, B. (2015). Wrist pulse acquisition and recording system. *Communication on Applied Electronics.*, *1*(6), 20–24. doi:10.5120/cae-1568

Thakker, B., & Vyas, A. L. (2009). Outlier pulse detection and feature extraction for wrist pulse analysis. *International Conference on Biological Science and Technologies (ICBST 2009)*.

Thakker, B., & Vyasn, A. L. (n.d.). Wrist (pulse signal classification for health diagnosis. *4th International Conference on Biomedical Engineering and Informatics (BMEI)*. 10.1109/BMEI.2011.6098759

Thara & Premasudha. (2019). *Electroencephalogram analysis for Automatic Epileptic Seizure detection method using PyEEG*. Academic Press.

Thara, D. K., Premasudha, B. G., Nayak, R. S., Murthy, T. V., Prabhu, G. A., & Hanoon, N. (2021). Electroencephalogram for epileptic seizure detection using stacked bidirectional LSTM_GAP neural network. *Evolutionary Intelligence*, *14*(2), 823–833. doi:10.100712065-020-00459-9

Thulasidas, M., Guan, C., & Wu, J. (2006). Robust classification of EEG signal for brain-computer interface. *IEEE Transactions on Neural Systems and Rehabilitation Engineering*.

Townsend, G. (2010, July). A novel P300-based brain-computer interface stimulus presentation paradigm: Moving beyond rows and columns. *Clinical Neurophysiology*, *121*, 1109–1120.

Tsiouris, K., Pezoulas, V. C., Zervakis, M., Konitsiotis, S., Koutsouris, D. D., & Fotiadis, D. I. (2018). A Long Short-Term Memory deep learning network for the prediction of epileptic seizures using EEG signals. *Computers in Biology and Medicine*, *99*, 24–37. doi:10.1016/j.compbiomed.2018.05.019 PMID:29807250

Tuncer, T., Dogan, S., & Subasi, A. (2020). Surface EMG signal classification using ternary pattern and discrete wavelet transform based feature extraction for hand movement recognition. *Biomedical Signal Processing and Control*, *58*, 101872. doi:10.1016/j.bspc.2020.101872

Tuncer, T., Dogan, S., & Subasi, A. (2021). A new fractal pattern feature generation function based emotion recognition method using EEG. *Chaos, Solitons, and Fractals*, *144*, 110671. doi:10.1016/j.chaos.2021.110671

Tzallas, A. T., Tsipouras, M. G., & Fotiadis, D. I. (2007). Automatic seizure detection based on time-frequency analysis and artificial neural networks. *Computational Intelligence and Neuroscience*, *2007*(18), 1–13. doi:10.1155/2007/80510 PMID:18301712

Tzallas, A. T., Tsipouras, M. G., & Fotiadis, D. I. (2009). Epileptic seizure detection in EEGs using time–frequency analysis. *IEEE Transactions on Information Technology in Biomedicine*, *13*(5), 703–710. doi:10.1109/TITB.2009.2017939 PMID:19304486

Ullah, A., Tu, S., Mehmood, R. M., & Ehatisham-ul-haq, M. (2021). A hybrid deep CNN model for abnormal arrhythmia detection based on cardiac ECG signal. *Sensors (Basel)*, *21*(3), 951. doi:10.339021030951 PMID:33535397

Ullah, H., Uzair, M., Mahmood, A., Ullah, M., Khan, S. D., & Cheikh, F. A. (2019). Internal emotion classification using EEG signal with sparse discriminative ensemble. *IEEE Access: Practical Innovations, Open Solutions*, *7*, 40144–40153. doi:10.1109/ACCESS.2019.2904400

Unser, M. A. (1997, October). Ten good reasons for using spline wavelets. In *Wavelet Applications in Signal and Image Processing V* (Vol. 3169, pp. 422–431). International Society for Optics and Photonics. doi:10.1117/12.292801

Upadhyaya & Deva. (2003). *Nadi Vijnana: Ancient pulse science*. Chaukhamba Sanskrit Pratishthan.

Uthayakumar, R., & Easwaramoorthy, D. (2013). Epileptic seizure detection in eeg signals using multifractal analysis and wavelet transform. *Fractals*, *21*(2), 1350011. Advance online publication. doi:10.1142/S0218348X13500114

Uysal, M. P. (2016). Evaluation of learning environments for object-oriented programming: Measuring cognitive load with a novel measurement technique. *Interactive Learning Environments*, *24*(7), 1590–1609. doi:10.1080/10494820.2015.1041400

Vafaie, M. H., Ataei, M., & Koofigar, H. R. (2014). Heart diseases prediction based on ECG signals' classification using a genetic-fuzzy system and dynamical model of ECG signals. *Biomedical Signal Processing and Control*, *14*, 291–296. doi:10.1016/j.bspc.2014.08.010

Vaid, S. (2015). EEG signal analysis for BCI interface: A review. *2015 fifth international conference on advanced computing & communication technologies*, 143-147. 10.1109/ACCT.2015.72

Vangelis, P. O., Georgios, L., Kostantinos, G., Elisavet, C., Katerina, A., Spiros, N., & Ioannis, K. (2016). Comparative evaluation of state-of-the-art algorithms for SSVEP-based BCIs. *Clinical Orthopaedics and Related Research*.

Vasquez-Correa, J. C., Arias-Vergara, T., Orozco-Arroyave, J. R., Vargas-Bonilla, J. F., & Noeth, E. (2016, October). Wavelet-based time-frequency representations for automatic recognition of emotions from speech. In *Speech Communication; 12. ITG Symposium* (pp. 1-5). VDE.

Ventricular Ectopic Beats. (n.d.). *Gale Encyclopedia of Medicine*. Retrieved March 10 2022 from https://medical-dictionary.thefreedictionary.com/Ventricular+Ectopic+Beats

Vidaurre, C. (2011). BioSig: The free and open source software library for biomedical signal processing. Computational Intelligence and Neuroscience.

Viola, P. A., & Jones, M. J. (2001). Rapid object detection using a boosted cascade of simple features. *Proceedings of the 2001 IEEE Computer Society Conference on Computer Vision and Pattern Recognition*, *1*, I-I. 10.1109/CVPR.2001.990517

Vyshnav, S., & Gopalakrishnan, V., Menon, & Soman. (2020). Deep Learning Based Approach for Multiple Myeloma Detection. *11th International Conference on Computing, Communication and Networking Technologies (ICCCNT).*

Wadsworth. (2004). *B. C. I. Dataset (P300 Evoked Potentials), Data Acquired Using BCI2000's P3 Speller Paradigm*. http://www.bci2000.org

Walter, C., Schmidt, S., Rosenstiel, W., Gerjets, P., & Bogdan, M. (2013). Using Cross-Task Classification for Classifying Workload Levels in Complex Learning Tasks. *2013 Humaine Association Conference on Affective Computing and Intelligent Interaction*, 876–881. 10.1109/ACII.2013.164

Wang, C., Zou, J., Zhang, J., Wang, M., & Wang, R. (2010). Feature extraction and recognition of epileptiform activity in EEG by combining PCA with ApEn. *Cognitive Neurodynamics*, *4*(3), 233–240. doi:10.100711571-010-9120-2 PMID:21886676

Wang, F., Wu, S., Zhang, W., Xu, Z., Zhang, Y., Wu, C., & Coleman, S. (2020). Emotion recognition with convolutional neural network and EEG-based EFDMs. *Neuropsychologia*, *146*, 107506. doi:10.1016/j.neuropsychologia.2020.107506 PMID:32497532

Wang, G., Zhang, C., Liu, Y., Yang, H., Fu, D., Wang, H., & Zhang, P. (2019). A global and updatable ECG beat classification system based on recurrent neural networks and active learning. *Information Sciences*, *501*, 523–542.

Wang, J., Antonenko, P., Keil, A., & Dawson, K. (2020). *Converging Subjective and Psychophysiological Measures of Cognitive Load to Study the Effects of Instructor-Present Video. In Mind, Brain, and Education*. Scopus., doi:10.1111/mbe.12239

Wang, K., Xu, L., Li, Z., Zhang, D., Li, N., & Wang, S. (2003). Approximate entropy based pulse variability analysis. *16th IEEE Symposium Computer-Based Medical Systems*.

Wang, L., & Zhou, X. (2019). Detection of congestive heart failure based on LSTM-based deep network via short-term RR intervals. *Sensors (Basel)*, *19*(7), 1502.

Wang, X., Chen, Z., Luo, J., Meng, J., & Xu, Y. (2016). ECG compression based on combining of EMD and wavelet transform. *Electronics Letters*, *52*(19), 1588–1590. doi:10.1049/el.2016.2174

Wang, Y., Liu, F., Jiang, Z., He, S., & Mo, Q. (2017). Complex variational mode decomposition for signal processing applications. *Mechanical Systems and Signal Processing*, *86*, 75–85.

Wang, Z. (2019). Towards a hybrid BCI gaming paradigm based on motor imagery and SSVEP. *International Journal of Human-Computer Interaction*, *35*, 197–205.

Wasimuddin, M., Elleithy, K., Abuzneid, A. S., Faezipour, M., & Abuzaghleh, O. (2020). Stages-based ECG signal analysis from traditional signal processing to machine learning approaches: A survey. *IEEE Access: Practical Innovations, Open Solutions*, *8*, 177782–177803. doi:10.1109/ACCESS.2020.3026968

Watson, D., Clark, L. A., & Tellegen, A. (1988). Development and validation of brief measures of positive and negative affect: The PANAS scales. *Journal of Personality and Social Psychology*, *54*(6), 1063–1070. doi:10.1037/0022-3514.54.6.1063 PMID:3397865

Wei, C., Chen, L. L., Song, Z. Z., Lou, X. G., & Li, D. D. (2020). EEG-based emotion recognition using simple recurrent units network and ensemble learning. *Biomedical Signal Processing and Control*, *58*, 101756. doi:10.1016/j.bspc.2019.101756

Wei, L. Y., & Chow, P. (1985). Frequency distribution of human pulse spectra. *IEEE Transactions on Biomedical Engineering*, *BME-32*(3), 245–246. doi:10.1109/TBME.1985.325537 PMID:3997182

Whelan, R. R. (2007). Neuroimaging of cognitive load in instructional multimedia. *Educational Research Review, 2*(1), 1–12. doi:10.1016/j.edurev.2006.11.001

Williams, Razzo, Caro, & Morga. (2019). Genetic Segmentation and Targeted Therapeutics for Multiple Myeloma. *Oncology Journal*.

Wolpaw, J. R., Birbaumer, N., McFarland, D. J., Pfurtscheller, G., & Vaughan, T. M. (2002). Brain-computer interfaces for communication and control. *Clinical Neurophysiology*, *113*(6), 767–791. doi:10.1016/S1388-2457(02)00057-3 PMID:12048038

Wong, H. B., & Lim, G. H. (2011). Measures of diagnostic accuracy: Sensitivity, specificity, PPV and NPV. *Proceedings of Singapore Healthcare*, *20*(4), 316–318. doi:10.1177/201010581102000411

World Health Organization. (n.d.). *Cardiovascular Diseases*. Author.

Wu, C. H., Chang, H. C., Lee, P. L., Li, K. S., Sie, J. J., Sun, C. W., Yang, C.-Y., Li, P.-H., Deng, H.-T., & Shyu, K. K. (2011). Frequency recognition in an SSVEP-based brain computer interface using empirical mode decomposition and refined generalized zero-crossing. *Journal of Neuroscience Methods*, *196*(1), 170–181. doi:10.1016/j.jneumeth.2010.12.014 PMID:21194547

Wu, G., Liu, G., & Hao, M. (2010). The analysis of emotion recognition from GSR based on PSO. In *International Symposium on Intelligence Information Processing and Trusted Computing* (pp. 360-363). IEEE. 10.1109/IPTC.2010.60

Wu, Y., Shen, C., Cao, H., & Che, X. (2018). Improved morphological filter based on variational mode decomposition for MEMS gyroscope de-noising. *Micromachines*, *9*(5), 246.

Xiefeng, C., Wang, Y., Dai, S., Zhao, P., & Liu, Q. (2019). Heart sound signals can be used for emotion recognition. *Scientific Reports*, *9*(1), 1–11. doi:10.103841598-019-42826-2 PMID:31019217

Xu, D., & Erdogmuns, D. (2010). Renyi's entropy, divergence and their nonparametric estimators. In *Information Theoretic Learning* (pp. 47–102). Springer. doi:10.1007/978-1-4419-1570-2_2

Xue, J., Gu, X., & Ni, T. (2020). Auto-Weighted Multi-View Discriminative Metric Learning Method With Fisher Discriminative and Global Structure Constraints for Epilepsy EEG Signal Classification. *Frontiers in Neuroscience*, *14*, 586149. doi:10.3389/fnins.2020.586149 PMID:33132835

Xu, Q. (2009). Fuzzy support vector machine for classification of EEG signals using wavelet-based features. *Medical Engineering & Physics*, *31*, 858–865.

Xu, X., Liang, Y., He, P., & Yang, J. (2019). Adaptive motion artifact reduction based on empirical wavelet transform and wavelet thresholding for the non-contact ECG monitoring systems. *Sensors (Basel)*, *19*(13), 2916.

Xu, Y., Zhu, Q., Fan, Z., Qiu, M., Chen, Y., & Liu, H. (2013). Coarse to fine K nearest neighbor classifier. *Pattern Recognition Letters*, *34*(9), 980–986. doi:10.1016/j.patrec.2013.01.028

Yang, W., Makita, K., Nakao, T., Kanayama, N., Machizawa, M. G., Sasaoka, T., Sugata, A., Kobayashi, R., Hiramoto, R., Yamawaki, S., Iwanaga, M., & Miyatani, M. (2018). Affective auditory stimulus database: An expanded version of the International Affective Digitized Sounds (IADS-E). *Behavior Research Methods*, *50*(4), 1415–1429. doi:10.375813428-018-1027-6 PMID:29520632

Yang, Y., Yu, D., & Cheng, J. (2007). A fault diagnosis approach for roller bearing based on IMF envelope spectrum and SVM. *Measurement: Journal of the International Measurement Confederation*, *40*(9–10), 943–950. doi:10.1016/j.measurement.2006.10.010

Yang, Z., Yang, L., Qi, D., & Suen, C. Y. (2006). An EMD-based recognition method for Chinese fonts and styles. *Pattern Recognition Letters*, *27*.

Yildirim, O., Baloglu, U. B., Tan, R.-S., Ciaccio, E. J., & Acharya, U. R. (2019). A new approach for arrhythmia classification using deep coded features and LSTM networks. *Computer Methods and Programs in Biomedicine*, *176*, 121–133. doi:10.1016/j.cmpb.2019.05.004 PMID:31200900

Yin, E. (2015). A hybrid brain–computer interface based on the fusion of P300 and SSVEP scores. *IEEE Transactions on Neural Systems and Rehabilitation Engineering*, *23*, 693–701.

Yoshida, T. (2011). Two dimensional non-separable adaptive directional lifting structure of discrete wavelet transform. *IEEE International Conference on Acoustics, Speech and Signal Processing (ICASSP)*, 1529-1532. 10.1109/ICASSP.2011.5946785

Yousefi, S., Goldbaum, M. H., Balasubramanian, M., Medeiros, F. A., Zangwill, L. M., Liebmann, J. M., Girkin, C. A., Weinreb, R. N., & Bowd, C. (2014). Learning From Data: Recognizing Glaucomatous Defect Patterns and Detecting Progression From Visual Field Measurement. *IEEE Transactions on Biomedical Engineering*, *61*(7), 2112–2124. doi:10.1109/TBME.2014.2314714 PMID:24710816

Yu, S.-N., & Chen, Y.-H. (2007). Electrocardiogram beat classification based on wavelet transformation and probabilistic neural network. *Pattern Recognition Letters*, *28*(10), 1142–1150. doi:10.1016/j.patrec.2007.01.017

Yu, T., Yu, Z., Gu, Z., & Li, Y. (2015). Grouped Automatic Relevance Determination and Its Application in Channel Selection for P300 BCIs. *IEEE Transactions on Neural Systems and Rehabilitation Engineering*, *23*(6), 1068–1077.

Z, W., & D, Y. (2008). Frequency detection with stability coefficient for steady-state visual evoked potential (SSVEP)-based BCIs. *J Neural Eng*, 36-43.

Zahabi, M., Abdul Razak, A. M., Shortz, A. E., Mehta, R. K., & Manser, M. (2020). Evaluating advanced driver-assistance system trainings using driver performance, attention allocation, and neural efficiency measures. *Applied Ergonomics, 84*. doi:10.1016/j.apergo.2019.103036

Zaid & Bes. (2021). *Multiple Myeloma Staging*. Med Space Journal.

Zarei, A., Beheshti, H., & Asl, B. M. (2022). Detection of sleep apnea using deep neural networks and single-lead ECG signals. *Biomedical Signal Processing and Control*, *71*, 103125.

Zeng, W., Li, M., Yuan, C., Wang, Q., Liu, F., & Wang, Y. (2020). Identification of epileptic seizures in EEG signals using time-scale decomposition (ITD), discrete wavelet transform (DWT), phase space reconstruction (PSR) and neural networks. *Artificial Intelligence Review*, *53*(4), 3059–3088. doi:10.100710462-019-09755-y

Zhang, L. (2013). Low-cost circuit design of EEG signal acquisition for the brain-computer interface system. *2013 6th International Conference on Biomedical Engineering and Informatics*, 245-250.

Zhang, Y., Zhou, G., Zhao, Q., Onishi, A., Jin, J., Wang, X., & Cichocki, A. (2011). Multiway Canonical Correlation Analysis for Frequency Components Recognition in SSVEP-Based BCIs. *Neural Information Processing*, 287-295.

Zhang, D., Zuo, W., & Wang, P. (2019). *Comparision Between Pulse and ECG signal*. Computational Pulse Signal Analysis.

Zhang, K., Zhang, Z., Li, Z., & Qiao, Y. (2016). Joint face detection and alignment using multitask cascaded convolutional networks. *IEEE Signal Processing Letters*, *23*(10), 1499–1503. doi:10.1109/LSP.2016.2603342

Zhang, Q., Chen, X., Zhan, Q., Yang, T., & Xia, S. (2017). Respiration-based emotion recognition with deep learning. *Computers in Industry*, *92*, 84–90. doi:10.1016/j.compind.2017.04.005

Zhang, W., Wang, F., Jiang, Y., Xu, Z., Wu, S., & Zhang, Y. (2019). Cross-subject EEG-based emotion recognition with deep domain confusion. In *International Conference On Intelligent Robotics And Applications* (pp. 558-570). Springer. 10.1007/978-3-030-27526-6_49

Zhang, X. (2018). *Neutrosophic filters in pseudo-BCI algebras* (Vol. 8). International Journal for Uncertainty Quantification.

Zhang, X., & Liu, S. (2017). Understanding Reading Comprehension in Multi-display Presenting System: Visual Distribution and Cognitive Effect. In C. Stephanidis (Ed.), *HCI International 2017 – Posters' Extended Abstracts* (pp. 207–214). Springer International Publishing. doi:10.1007/978-3-319-58753-0_32

Zhang, Y. D., Yang, Z. J., Lu, H. M., Zhou, X. X., Phillips, P., Liu, Q. M., & Wang, S. H. (2016). Facial emotion recognition based on biorthogonal wavelet entropy, fuzzy support vector machine, and stratified cross validation. *IEEE Access: Practical Innovations, Open Solutions*, *4*, 8375–8385. doi:10.1109/ACCESS.2016.2628407

Zhang, Y., Zhou, G., Jin, J., Wang, X., & Cichocki, A. (2014). Frequency recognition in SSVEP-based BCI using multiset canonical correlation analysis. *International Journal of Neural Systems*, *24*(04), 1450013. doi:10.1142/S0129065714500130 PMID:24694168

Zhang, Y., Zhou, G., Jin, J., Wang, X., & Cichocki, A. (2015). SSVEP recognition using common feature analysis in brain-computer interface. *Journal of Neuroscience Methods*, *244*, 8–15. doi:10.1016/j.jneumeth.2014.03.012 PMID:24727656

Zhang, Z., Dong, J., Luo, X., Choi, K. S., & Wu, X. (2014). Heartbeat classification using disease-specific feature selection. *Computers in Biology and Medicine*, *46*, 79–89. doi:10.1016/j.compbiomed.2013.11.019 PMID:24529208

Zhang, Z., Zhang, Y., Yao, L., Song, H., & Kos, A. (2018). A sensor-based wrist pulse signal processing and lung cancer recognition. *Journal of Biomedical Informatics*, *79*, 107–116. doi:10.1016/j.jbi.2018.01.009 PMID:29428411

Zheng, W. (2016). Multichannel EEG-based emotion recognition via group sparse canonical correlation analysis. *IEEE Transactions on Cognitive and Developmental Systems*, *9*(3), 281–290. doi:10.1109/TCDS.2016.2587290

Zheng, W. L., & Lu, B. L. (2015). Investigating critical frequency bands and channels for EEG-based emotion recognition with deep neural networks. *IEEE Transactions on Autonomous Mental Development*, *7*(3), 162–175. doi:10.1109/TAMD.2015.2431497

Zhong, P., Wang, D., & Miao, C. (2020). EEG-based emotion recognition using regularized graph neural networks. *IEEE Transactions on Affective Computing*, 1. doi:10.1109/TAFFC.2020.2994159

Zhou, G., Wang, Y., & Cui, L. (2015). Biomedical sensor, device and measurement systems. In *Advances in Bioengineering*. InTech.

Zhou, Y., Xu, T., Cai, Y., Wu, X., & Dong, B. (2017). Monitoring Cognitive Workload in Online Videos Learning Through an EEG-Based Brain-Computer Interface. In P. Zaphiris & A. Ioannou (Eds.), *Learning and Collaboration Technologies. Novel Learning Ecosystems* (pp. 64–73). Springer International Publishing. doi:10.1007/978-3-319-58509-3_7

Zosso, D., Dragomiretskiy, K., Bertozzi, A. L., & Weiss, P. S. (2017). Two-dimensional compact variational mode decomposition. *Journal of Mathematical Imaging and Vision*, *58*(2), 294–320. doi:10.100710851-017-0710-z

About the Contributors

Rahul Kumar Chaurasiya received the B. Tech. degree from MANIT Bhopal in 2009, and the M.E. degree from the IISc Bangalore in 2011. He received his Ph.D. degree in 2017 NIT Raipur. He was a Senior Software Engineer with Brocade Communications Systems, Bangalore, in 2011-12. During 2013-19, he was Assistant Professor at the NIT, Raipur. He has served as Assistant Professor Grade-1 at MNIT Jaipur during 2019-20. Since 2020, he is with MANIT Bhopal as Assistant Professor Grade-1. His research area includes Machine Learning, Pattern Recognition, Brain-Computer Interfacing, Optimization, Biomedical Signal Processing. He has authored several research articles in aforementioned areas. He is currently supervising 4 PhD scholars and have supervised 08 M Techs and 50+ B Techs in his area of research.

Dheeraj Agrawal received the B. E. degree from RGTU Bhopal in 2001. He received the M.Tech. and PhD degrees from MANIT Bhopal in 2005 and 2011, respectively. He has more than 20 years of teaching experience and is currently working as Associate Professor at MANIT Bhopal. He is also working as nodal officer at Indian Institute of Information Technology Bhopal. His research area includes Machine Learning, Image processing, and Signal Processing. He has authored several research articles in aforementioned areas. He has supervised 03 PhD scholars and is currently supervising 03 PhD scholars in his area of research.

Ram Bilas Pachori received the B.E. degree with honours in ECE from RGTU, Bhopal, India in 2001, the M.Tech. and Ph.D. degrees in EE from Indian Institute of Technology (IIT) Kanpur, India in 2003 and 2008, respectively. He worked as a Postdoctoral Fellow at Charles Delaunay Institute, University of Technology of Troyes, Troyes, France during 2007-2008. He is presently working as a Professor at IIT Indore. He worked as a Visiting Scholar at Intelligent Systems Research Center, Ulster University, Northern Ireland, UK during December 2014. He is an Associate Editor of Electronics Letters, Biomedical Signal Processing and Control journal and an Editor of IETE Technical Review journal. He is a senior member of IEEE and a Fellow of IETE and IET. He has supervised 12 Ph.D., 20 M.Tech., and 37 B.Tech. students for their theses and projects.

* * *

Tugba Altan is a Research Assistant at the Department of Educational Sciences in the Faculty of Kahramanmaras Sutcu Imam University, Turkey. Her research focuses on the design and evaluation of multimedia learning environments such as textbooks and mobile apps in K-12 and teacher education,

integration of massively multiplayer online role-playing games into K-12 education, and the use of mobile technologies in teacher education.

Veysel Coskun received her Ph.D. in Computer Education and Instructional Technology Department from Marmara University in July 2018 and has been working as an assistant professor at Hatay Mustafa Kemal University. His research focuses on multimedia learning, instructional design, eye-tracking, and cognitive science.

Kritiprasanna Das received the B.Tech. and M.Tech. degree in Electronics and Communication Engineering and VLSI and Embedded Systems in 2016 and 2018, respectively, from West Bengal University of Technology and NIT Arunachal Pradesh. Currently, he is pursuing PhD in the Department of Electrical Engineering, IIT Indore. His research interests include biomedical signal processing, EEG, time-frequency analysis, and related area.

Chandan Kumar Jha is working as an Assistant Professor in the Department of Electronics and Communication Engineering at Indian Institute of Information Technology Bhagalpur. He completed his Ph.D. from IIT Patna in 2019. He has more than 2 years of teaching and research experience. He received his Master's degree with distinction in Electronics and Communication Engineering from Birla Institute of Technology Mesra in 2012. He obtained his Bachelor's Degree in Electronics and Communication Engineering from West Bengal University of Technology Kolkata in 2010. His research interests include biomedical signal & image processing, machine learning, deep learning. He has published many reputed international journals, conference papers, and book chapters.

Sibghatullah I. Khan received Bachelor of Engineering (B.E), Master of Engineering (M.E) and Ph. D degrees in Electronics and Telecommunication Engineering from SGB Amravati University, Amravati, India in 2007, 2012, and 2018, respectively. He served as an Assistant Professor at Department of Electronics and Telecommunication Engineering, BNCOE Pusad, India and SVPCET Nagpur during 2008-2017 and 2017-2018, respectively. Presently, he is Associate Professor at Department of Electronics and Communication Engineering in Sreenidhi Institute of Science and Technology, Hyderabad, India. His research interest includes Biomedical and Signal and Image Processing, Non-stationary Signal processing, Human-computer interaction, Artificial Intelligence and Machine learning for Telemedicine Applications. He is a life member of Indian Society of Technical Education (ISTE), Delhi, India. He has also served in the scientific committees of various national and international conferences. He has delivered talks and lectures in conferences, workshops, short term courses, and academic events organized by various institutes related to signal processing and machine learning.

Duygu Mutlu-Bayraktar received her Ph.D. in Computer Education and Instructional Technology Department from Marmara University in July 2014 and has been working as a research assistant at Istanbul University-Cerrahpasa. Her research interests include multimedia learning, instructional design, eye-tracking, cognitive science, and human-computer interaction.

Aditya Nalwaya received the B.E. and M.E. degree in Electronics and Communication in 2010 and 2013, respectively, from Rajiv Gandhi Proudyogiki Vishwavidyalaya, Bhopal. He worked as an assistance professor (2013-2021) in the Department of Electronics and Communication at Shri G. S. Institute of

Technology and Science, Indore. Currently, he is pursuing PhD in the Department of Electrical Engineering, IIT Indore. His research interests include biomedical signal processing, human emotion recognition, time-frequency analysis, and related area.

Ali Olamat received his Ph.D. degree in Biomedical Engineering from Istanbul University in 2019. He has been working as a post-doctoral student at Yildiz Teknik University. His research areas are brain-computer interface, signal processing, and machine learning techniques to biomedical signals.

Pinar Ozel received her Ph.D. degree in Biomedical Engineering from Istanbul University in 2019. She has been working as a research assistant at Nevsehir Haci Bektas Veli University. Her research areas are signal processing and machine learning techniques to biomedical signals.

Deepak Parashar received the B.E. degree in Electronics and Communication Engineering from Indira Gandhi Engineering College, Sagar, India in 2008, and the M.Tech. Degree in Microelectronics and VLSI Design from the SGSITS Indore, India, in 2011. Received PhD degree in Electronics and Communication Engineering with specialization in signal processing from Maulana Azad National Institute of Technology, Bhopal, India. He is currently an Assistant Professor in the Department of Electronics & Communication Engineering, IES College of Technology Bhopal, India. His research interests include biomedical signal processing, machine learning, and computer-aided medical diagnosis.

Neha Rathore received the B.E. degree in Electronics and Communication Engineering and the M.Tech. Degree in Digital communication. She is currently pursuing a PhD degree in Electronics and Communication Engineering with a specialization in signal and image processing from Maulana Azad National Institute of Technology, Bhopal, India. Her research interests include signal processing, Image processing and Neural networks.

Praveen Kumar Shukla currently serves as an assistant professor in the department of VIT Bhopal University in the school of electrical and electronics engineering (SEEE). Dr. Praveen Kumar Shukla is a Doctorate in Signal Processing from NIT Raipur. He has completed his M.Tech from the Dept. of Control and Automation, VIT University, Vellore and B.Tech in Electronics and Communication from Rajiv Gandhi Proudyogiki Vishwavidyalaya (RGPV) University Bhopal. He has published a patent and several research articles in peer-reviewed international journals, books chapters, and IEEE conference proceedings. He is a reviewer of many reputed journals namely, IEEE Journal of Biomedical and Health and Informatics, Computers in Biology and Medicine and other International Conferences. His research interests include Brain Computer Interfacing, Signal Processing, Computer vision, Machine Learning and Deep Learning.

Praveen Kumar Tyagi received the B.E. degree in Electronics and Communication Engineering from Dr. A.P.J. Abdul Kalam Technical University, Lucknow, India, and the M.Tech. Degree in Digital communication domain from the ABV IIITM Gwalior, India. He is currently pursuing a Ph.D. degree in Electronics and Communication Engineering with a specialization in signal processing from Maulana Azad National Institute of Technology, Bhopal, India. His research interests include biomedical signal processing, Image processing, machine learning, and deep learning algorithms.

Index

F

G

I

K

L

M

N

P

Q

R

S

T

V

W